Computationally Guided Rational Ligand Design of Novel Iridium(I) Complexes for Elevated Substrate Applicability in Hydrogen Isotope Exchange Processes

---

Gary J. Knox

PhD Thesis

2019

Author Declaration

This thesis is the result of the author's original research. It has been composed by the author and has not been previously submitted for examination which has led to the award of a degree.

The copyright of this thesis belongs to the author under the terms of the United Kingdom Copyrights Acts as qualified by University of Strathclyde Regulation 3.50. Due acknowledgment must always be made of the use of any material contained in, or derived from, this thesis.

Gary J. Knox

08/03/2019

Abstract

Using a computationally guided rational ligand design approach, a novel chelated NHC-P iridium(I) catalyst system has been identified for the directed hydrogen isotope exchange (HIE) of aryl sulfones. The catalyst design process was aided primarily through DFT binding energy calculations. The solvent scope of the reaction was studied, and the optimised conditions applied to the successful deuterium labelling of a broad range of 20 aryl sulfones. The catalyst system was also shown to be highly active in the HIE of aryl sulfones at sub-atmospheric pressures of deuterium. Additionally, the catalyst system was applied in the tritiation of aryl sulfones, affording tritiated samples of methylphenyl sulfone, as well as a GPR119 agonist, in high levels of specific activity.

This chelated catalyst system was then further refined for the labelling of highly substituted sulfonamides. A more focussed approach to the catalyst design process was taken at this stage, with a combination of binding energy calculations and binding mode analysis being used to guide the modification of the ligand. This resulted in a novel, chelated NHC-Py system, which proved to be highly active in the HIE of a broad range of highly substituted sulfonamides. A total of 22 sulfonamide substrates were synthesised, and labelled using this novel catalyst system. Additionally, this complex was shown to be highly effective in the deuteration of sulfoximines, for which the means of labelling are severely under met.

Finally, our studies in the labelling of aryl sulfones led us to the serendipitous discovery of ether-directed HIE. This process was investigated with our novel NHC-P catalyst system, and a substrate scope established. Additionally, a potential application in form of labelling natural products, and natural product-like molecules has been proposed, with a series of three natural product-like molecules having been synthesised for attempts towards labelling.

Acknowledgments

Firstly, I would like to extend my deepest gratitudes to Professor William J. Kerr for taking me on as a PhD student and creating an environment that has allowed me to develop as a chemist and person over the past few years. I am incredibly grateful for all of the opportunities you have given me.

I would also like to thank Dr David Lindsay for all your help and day-to-day input that you have offered (even with the carboxylates). I am also grateful to Dr Laura Paterson, for all your helpful suggestions and (sometimes inebriated) advice. The support of these two people, over the past few years, in directing my research has been absolutely invaluable.

I would like to thank the various members of the Kerr Group, past and present, that I have worked with throughout my time here. To Dr Richard Mudd and Dr Andrew Malcolm, for all the time spent helping me, and pushing me to become a better chemist. To Dr Philippa Owens, thank you for all your patient guidance throughout both my year in the group as an undergraduate student, as well as my time as a PhD student. I will always be grateful to you for all the time you generously spent, which led to me to becoming the chemist I am today. To Dr Renan Zorzatto, thank you for the ever-insightful chemistry discussion, as well as your constant enthusiasm for science. To Dr Petter Katai, thank you for all your encouragement and keeping a positive atmosphere, particularly with your practical jokes and michief. To Liam McLean, I am eternally grateful for all the thought-provoking discussions about chemistry (amoung various other topics), as well as all the great food! I couldn't have asked for a better lab-buddy and friend. I would also like to thank Adele Queen, despite the incredible amount of time you've spent trying to annoy and infuriate me, you have always been there for me to keep things positive and cheery. To Giorgia Kidd, your constant energy and cheery attitude has made life in the danger zone interesting, to say the least. Thank you for all your encouragement and

help keeping me sane, especially towards the end. Raymond Chung, your hilarious (often dark) jokes and remarks have always proven to be entertaining, and I will miss them greatly. I would like to thank Paul Shaw, not only for some great discussions around the ever-infuriating area of computational chemistry, but also the numerous rants and tirades which are always enjoyable. I would also like to thank Jemma MacLachlan, her time spent in the group was kept interesting with strange conversation and comical dancing. To Conor and Nathan (who's names I will never get right), thanks for the good laughs both in and out of the lab, I wish you all the best with the remainder of your PhD studies.

In addition to the Kerr group member who I've worked with every day over the past few years, I'd also like to extend my thanks to those from GSK who spent time with us. To Dr Jason Williams, thank you for all the hilarious, if questionable, conversation while you were here. I hope your sense of direction only improves as you get (even) older. To Blake Baker, I will always enjoy the many incredible stories you were kind enough to share. I wish you all the best with your music, as well as the short remainder of your PhD. To James Thompson, thank you for the fun times while you were here, as well as some truly impressive feats of food consumption! I would also like to thank Jack Eton Washington, despite not being an official Kerr-group member, you're definitely a great part of the 7th floor team, I will miss your quirky dress sense and mannerisms, as well as being such a good sport with HR.

Finally, I would like to thank my parents, as well as the rest of the family, for all of their patience, help, and support and support over the years. I will always be grateful for the sacrifices made for helping me get to where I am today.

Abbreviations

Ac – Acetyl

ADMET – Adsorption, Distribution, Metabolism, Excretion and Toxicology

Ar – Aryl

Avg – Average

BAr_F - Tetrakis[3,5-bis(trifluoromethyl)phenyl]borate

BINAP - Bis(diphenylphosphino)-1,1′-binaphthalene

Bn – Benzyl

BSSE – Basis Set Superposition Error

Cat – Catalyst

Ci - Curie

CNS – Central Nervous System

COD – Cyclooctadiene

CPU – Computer Processing Unit

Cy – Cyclohexyl

dba – Dibenzylideneacetone

DCE – Dichloroethane

DCM – Dichloromethane

DiPP – Di-*iso*-propylphenyl

DFT – Density Functional Theory

DG – Directing Group

DMAc – Dimethylacetamide

DMF – Dimethyl Formamide

DMSO – Dimethyl Sulfoxide

Et – Ethyl

eq – Equivalents

FDA – Food and Drug Administration

g – Gram(s)

h – Hour(s)

HBD – Hydrogen Bond Donor

HIE – Hydrogen Isotope Exchange

HRMS – High Resolution Mass Spectrometry

Hz – Hertz

IAd – 1,3-Bis(adamantly)imidazolylidene

IMes – 1,3-Dimesitylimidazolylidene

IPr - 1,3-Bis(2,6-di-*iso*-propylphenyl)imidazolylidene

^{i}Pr – *Iso*-propyl

IR – Infrared

kcal – Kilocalorie

M – Molar

mCPBA – *meta*-Chloro Perbenzoic Acid

Me – Methyl

Mes – Mesityl

min – Minute

mmHg – Millimetres of Mercury

mmi – Membered Metallocyclic Intermediate

mmol – Millimoles

mol – Moles

mol% – Mole Percent

MTBE – Methyl *tert*-Butyl Ether

MW – Molecular Weight

m/z – Mass to Charge Ratio

^{n}Bu – *n*-Butyl

NCE – New Chemical Entity

NHC – *N*-Heterocyclic Carbene

NHCP – *N*-Heterocyclic Carbene-Phosphine

NMR – Nuclear Magnetic Resonance

- **appt** – Apparent Triplet
- **bs** – Broad Singlet
- **d** – Doublet

dd – Doublet of Doublets

ddd – Doublet of Doublet of Doublets

J – Coupling Constant

m - Multiplet

ppm – Parts Per Million

sep – Septet

t – Triplet

td – Triplet of Doublets

***o*-Tol** – *ortho*-Tolyl

Ph – Phenyl

***p*TSA** – *para*-Toluene Sulfonic Acid

Py – Pyridyl

R – Substituent

r - Radius

R&D – Research and Development

rt – Room Temperature

S – Solvent Molecule

SIMes – 1,3-Dimesityl-4,5-dihydro Imidazolylidene

S^{Me}IMes - 1,3-Dimesityl-4,5-dimethyl-4,5-dihydro imidazolylidene

S_N1 – Unimolecular Nucleophilic Substitution

S_N2 – Bimolecular Nucleophilic Substitution

^{t}Bu – *tert*-Butyl

temp – Temperature

TEP – Tolman Electronic Parameter

tert – Tertiary

Tf – Triflyl

THF – Tetrahydrofuran

TLC – Thin Layer Chromatography

Tol – Toluene

TPSA – Topological Polar Surface Area

UV – Ultraviolet

%V_{Bur} – Percent Buried Volume

Contents

1. Introduction

1.1 Pharmaceutical Development & Drug Discovery

In 2012, the pharmaceutical industry saw the largest number of approved drugs by the Food and Drug Administration in 15 years.[1] A 33% increase in the average approval rate, constituting a total of 39 new chemical entities (NCEs), were approved, of which 20 were first-in-class. Of the drugs approved, 80% were first cycle approved, representing the highest first cycle approval rate ever reported.

While these statistics convey a positive outlook, the pharmaceutical industry is still faced with major difficulties in terms of the overwhelming attrition rate affecting major drug candidates, resulting in extensive costs in the development sector.[2,3] Additionally, the cost associated with research and development of new drug candidates only continues to grow.[4] In recent years, high throughput methods have been employed in order to improve the number of products reaching the market. In relation to this, it was thought that the use of combinatorial methods to produce vast libraries of potential candidates, coupled with efficient screening methods in order to evaluate these candidates, would increase the number of potential drugs at the discovery stage and result in a higher number of FDA approved drug molecules reaching patients.[5] While the number of drugs in the development pipeline has increased by 62% over the past decade, the average approval rate over the same period has dropped by around 25% when compared to the 1990s.[6] As a result of this, the research and development expenditure has more than doubled; **Figure 1.1** shows the total pharmaceutical expenditure in R&D since 1990, as produced by the European Federation of Pharmaceutical Industries and Associations, Pharmaceutical Research and Manufacturers of America, and Japan Pharmaceutical Manufactures Association (Note: units of currency for Europe = € million, USA = $ million, and Japan = ¥×100 million).[7]

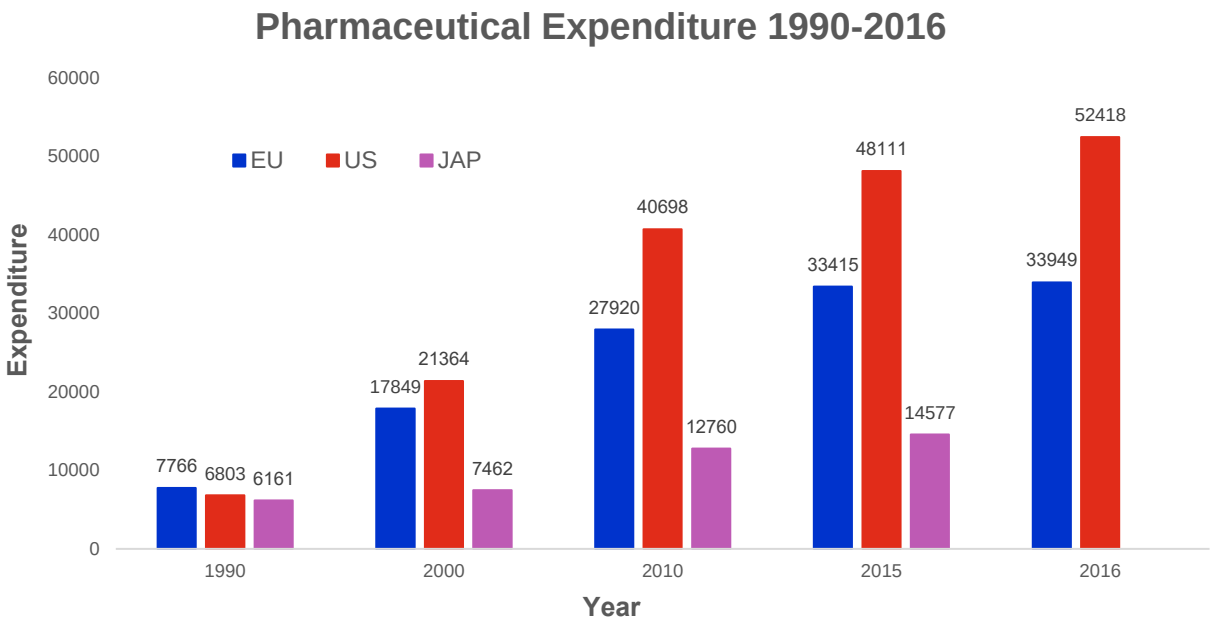

Figure 1.1

One way to reduce the enormous costs attributed to the drug discovery process is for medicinal chemists to address issues with the pharmacokinetic properties of a drug at early stages in the development process. Indeed, it is in preclinical stages that 90% of all NCEs fail. As a result, the absorption, distribution, metabolism, excretion and toxicological profile (ADMET) of a candidate is now investigated at a much earlier stage in the discovery process.[8] Absorption is the ability of the molecule to reach its intended target, commonly a specific receptor protein within a cell or on the surface of the cell membrane. Targeting drugs which can be administered orally, at the convenience of the patient, is highly attractive in the face of alternative modes of delivery (such as intravenous methods), despite the issues of bioavailability this brings. The likelihood that a drug will be able to reach its target is highly dependent on whether the drug is able to pass from the gastrointestinal tract into the bloodstream in order to be carried to the intended organ. This, in turn, is highly dependent on the physiochemical properties of the drug, namely its size, polarity, solubility, and lipophilicity.

Several models have been produced in order to evaluate these properties, for example, the "Lipinski rule of 5" which acts as a very general paradigm for estimating the potential of a drug to be bioavailable.[9 10] More extensive models such as the Pfizer central nervous system multi-parameter optimisation system take into account the calculated partition coefficient (ClogP, a model of lipophilicity), calculated distribution coefficient (ClogD, lipophilicity at pH 7.4), topological polar surface area (TPSA), molecular weight (MW), number of hydrogen bond donors (HBD), and the pK_a of the drug molecule.[11] This algorithm uses much tighter parameters in order to address the difficulties in accessing the central nervous system. However, despite the complexity of the models being produced, predicting the properties of a drug candidate remains difficult.

In the process of metabolising a drug, wherein it is chemically altered prior to its removal from the body, the concentration is reduced and therefore its efficacy affected. In addition to this, the process can produce bioactive metabolites. The metabolism of a drug can be broken down into three phases. In phase I, the compound is generally oxidised in order to make it more polar and less lipophilic, hindering its distribution. At this point, the molecule may be polar enough to be excreted. In phase II, the molecule is conjugated to a large molecule (for example, in glucuronidation) hindering its activity. Finally, if required, the molecule can be further modified, in phase III prior to its excretion. This is generally achieved through conjugation to small biomolecules such as acetylcysteine.

A key method of investigating the metabolic pathway of a drug is isotopic labelling. This process involves replacing an atom within the drug molecule with an uncommon isotope which can act as a tracer, for example replacing hydrogen with tritium (^{3}H, T), or carbon with heavier isotopes such as ^{14}C. These isotopes can be incorporated by building the final drug molecule from commercially available, pre-labelled starting materials; however, this method is time-consuming, expensive and, in the case of radioactive isotopes, it can generate large amounts of

radioactive waste and greatly increase the synthetic complexity of the processes involved. Alternatively, isotopes of hydrogen can be incorporated through hydrogen isotope exchange (HIE), allowing the label to be transferred to the molecule, usually in a single step and at a late stage in the overall synthesis. The clear advantages of this process have resulted in a significant amount of research being focused on the development of mild and efficient exchange processes that will ultimately be cost-saving to the pharmaceutical industry's drug development process.[12]

1.2 Hydrogen Isotope Exchange

Over the years, several methods for substituting one isotope of hydrogen for another have been developed, many of which take advantage of exchangeable positions or, for example, work through electrophilic aromatic substitution.[13,14,15,16] The simplest methods involve reacting the desired substrate under either acidic or basic conditions in the presence of a relatively cheap and easily accessed deuterated solvent such as D_2O or MeOD. **Scheme 1.1** shows an example wherein d_5-aniline hydrochloride **d-1** was prepared by heating aniline hydrochloride **1** under pressure in DCl/D_2O. This procedure was also applied to phenol and benzoic acid, successfully incorporating high levels of deuterium.[10]

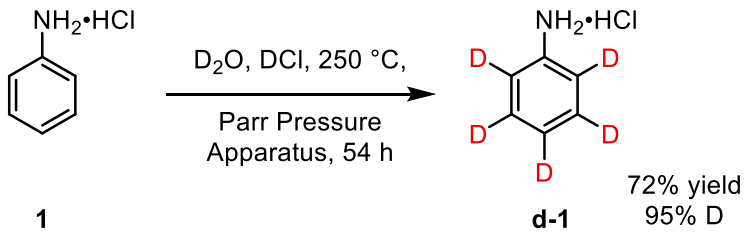

Scheme 1.1

In addition to the above, **Scheme 1.2** highlights a more complex example whereby basic conditions were used to incorporate deuterium at positions adjacent to the enone and ketone

functionality to form the corresponding bismethylenedioxy-protected d_8-cortisone **d-2**.[16] The authors state that labelled positions are determined by the acidity of the protons adjacent to the carbonyl groups.

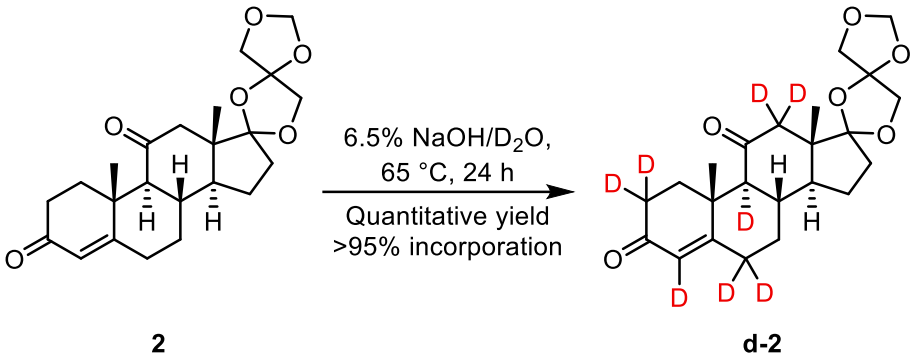

2 **d-2**

Scheme 1.2

1.3 Heterogeneous Catalysis in HIE

Due to the chemical similarity between deuterium and hydrogen (i.e. protium) gas, many methods of hydrogen isotope installation have been derived from hydrogenation methods. For example, **Scheme 1.3** shows the efficient deuteration of aryl lactone **3**, catalysed by palladium on carbon in D_2O, along with the concurrent decarboxylation, to yield the deuterated phenol.[17]

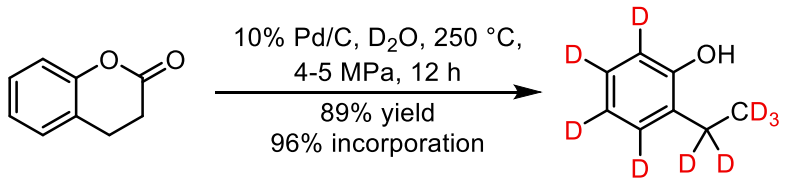

3 **d-4**

Scheme 1.3

In relation to the above example, the use of a heterogeneous catalyst has the added benefit of simple catalyst removal *via* filtration. However, a trait shared by the methods described so far

is the harsh conditions required for the exchange to proceed. Moreover, such methods display poor selectivity and exhibit very limited substrate scope.

An example of much milder conditions being used for the incorporation of deuterium was published by Lockley in 2006, wherein a series of three catalyst systems (rhodium black, ruthenium black, and 5% rhodium on alumina) were tested in the labelling of the α-positions of a range of nitrogen-containing heteroaromatics (**Scheme 1.4**). Despite low pressures of deuterium gas, and ambient temperatures, substrate degradation still proved problematic, such as in 4-acetylpyridine **5**, with rhodium black. Additionally, poor incorporation was observed in the presence of electron donating groups, as exhibited by the 2-methoxypyridine **6**. Various heterocyclic motifs were well tolerated, however, with quinolines **7** and **8**, phthalazine **9** and bipyridyl **10**, all showing moderate to good levels of isotope incorporation with at least one of the catalyst systems. Unfortunately, however, there was little rationale for which catalyst systems would perform best with each substrate. This highlights a significant problem with heterogeneous catalysis, in that the challenges associated with understanding these processes lead to poor understanding of the mechanisms involved and, as such, result in difficulty in predicting the behaviour of untested substrates.

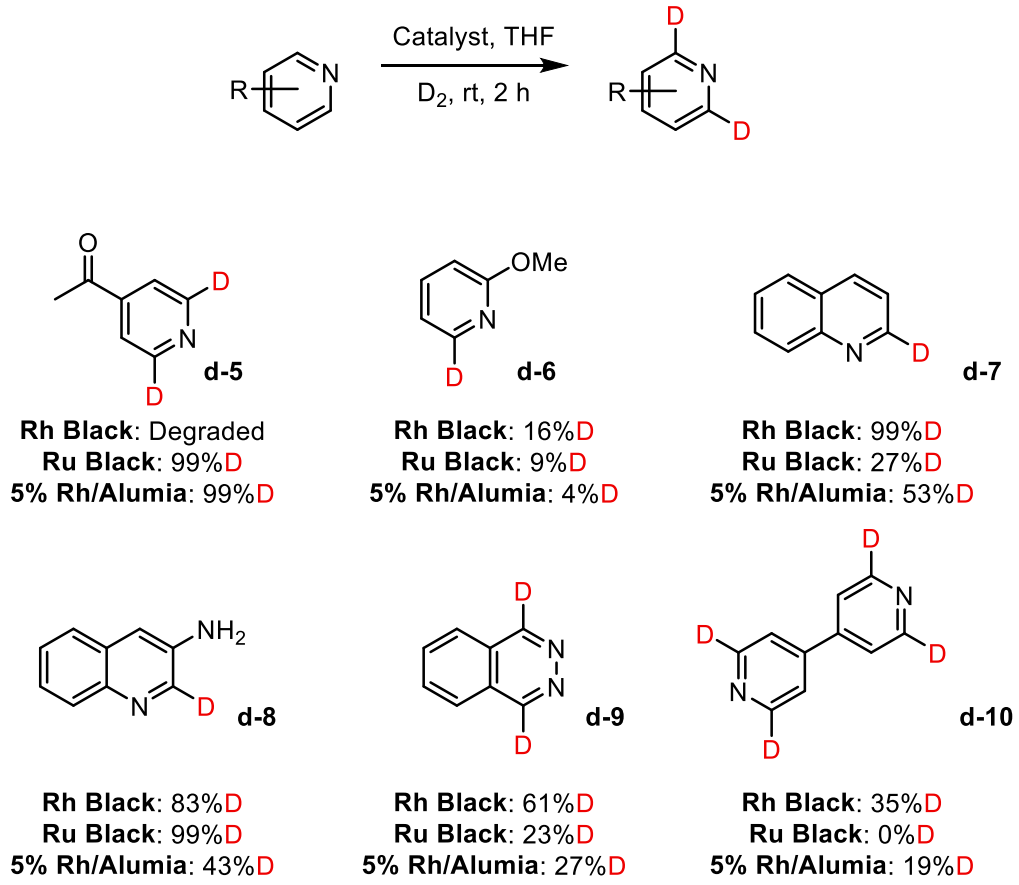

Scheme 1.4

1.4 Non-directed Homogeneous Catalysis

Homogeneous transition metal catalysts have become some of the most widely utilised tools in HIE, as well as in many chemical processes, and in many cases, they are able to address the issue of harsh reaction conditions and poor selectivity associated with heterogeneous catalysis. Generally, an inert C—H bond is converted to a C—D bond through a process known as C—H activation, wherein the metal catalyst inserts into the bond to be activated, forming a reactive metalated species (**Scheme 1.5**).

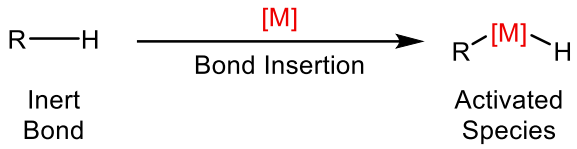

Scheme 1.5

The ability to directly functionalise a C—H bond is a powerful tool in synthesis, since it precludes the installation of a more reactive C—X moiety (X = halogen, or equivalent), thus reducing the number of steps required to reach the target and potentially opening up new disconnections. This is well exemplified by Corey's synthesis of (+)-austamide.[18] The original route, pioneered by Kishi in 1979, produced a racemic product in a total of 29 steps.[19] However, in 2002, Corey utilised C—H activation in a palladium-catalysed coupling reaction in order to cyclise indole **11** to give compound **12**. This allowed the natural product to be synthesised from tryptophan methyl ester, as a single enantiomer, in just 7 steps (**Scheme 1.6**).

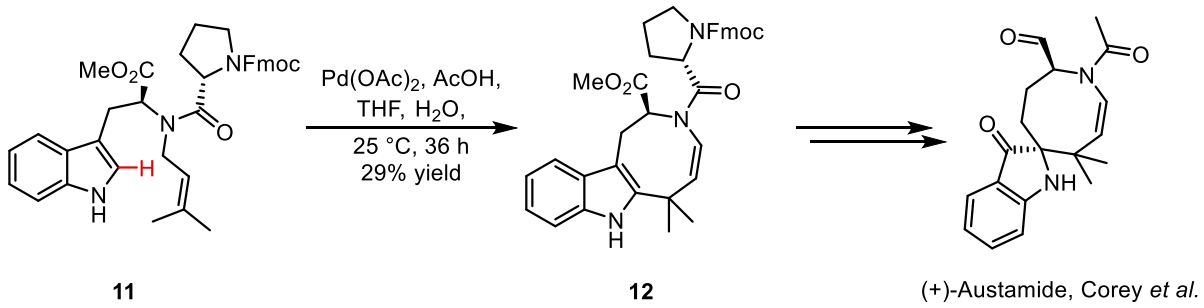

Scheme 1.6

Applications of non-directed homogeneous catalysis in the installation of deuterium labels have been investigated. Indeed, one prominent example is the use of $Ru_3(CO)_{12}$ in the labelling of nitrogen-containing heterocycles (**Scheme 1.7**), using deuterated *tert*-butanol as the source of the label.[20] This methodology allowed for good levels of incorporation across a series of indole- and pyridine derivatives. Electron-rich and electron-poor aromatic systems were well tolerated, however electron-withdrawing groups, such as in 5-nitroindole **14**, required the use of

microwave radiation to adequately label the desired positions. Pleasingly, the presence of aryl chlorides was well tolerated in pyrimidine **17**, as well as the free NH_2 group in pyridine **18**. Interesting to note is example **20**, with a 2-benzylamine substituent, where only moderate levels of incorporation were observed at the C6 position (22%), while significant amounts of incorporation (88%) were observed, presumably through a directed mechanism, into the benzylic position. In addition to this, the C5 position also exhibited moderate levels of isotope incorporation (55%). While the undirected mechanism still requires investigation, it is proposed that, in the case of the pyridine examples, coordination of the nitrogen atom promotes the adjacent C—H bond towards direct insertion.

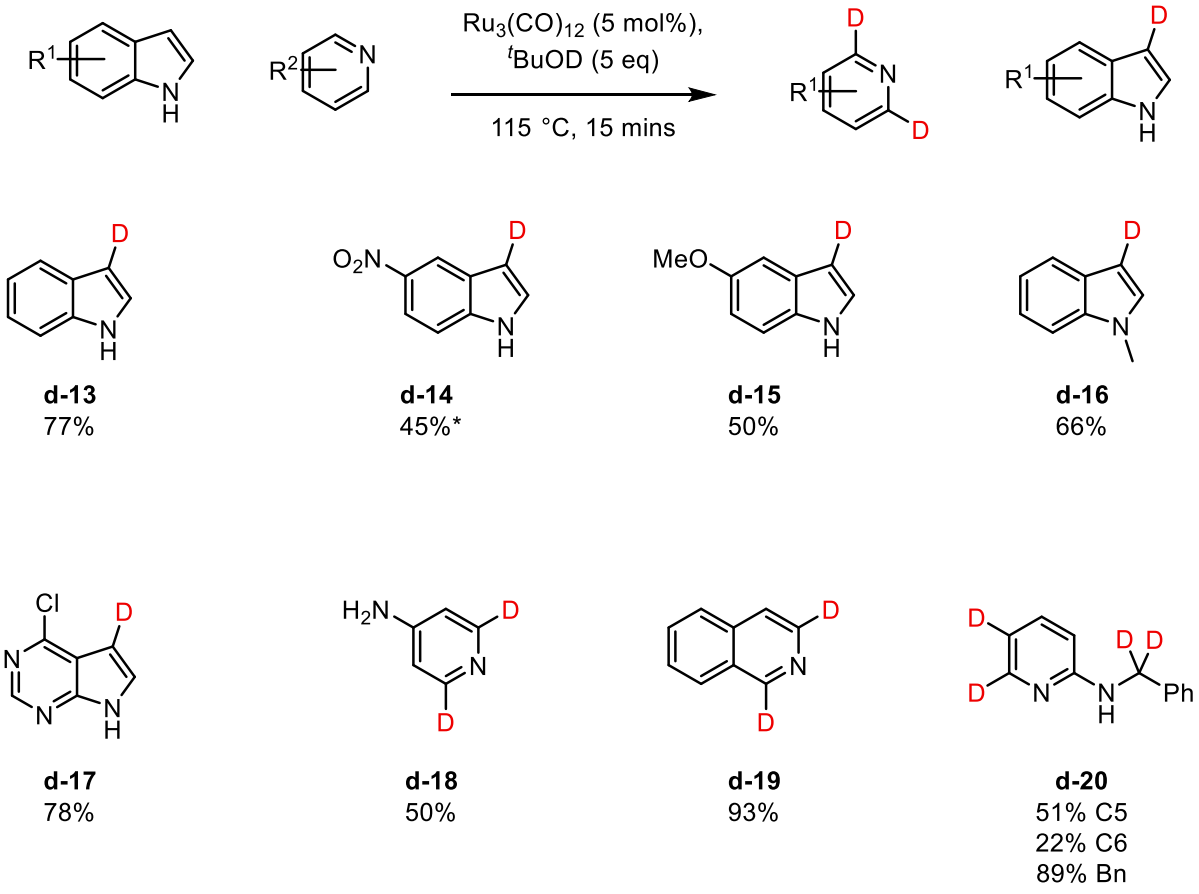

Scheme 1.7

A notable example in the area of non-directed isotope exchange is the use of iron pincer complex **21** in the labelling of pharmaceutically-relevant molecules under mild conditions, from the Chirik group.[21] Generally, the most accessible aryl C—H bonds are activated by this catalyst system, resulting in several positions being activated within the same molecule, and delivering labelled compounds with high deuterium incorporation, or specific activity. While the paper discusses the deuterium labelling of 22 simple aromatic and heteroaromatic substrates to good levels, the scope of applicable drug motifs displayed is the main focus of the work, and several are highlighted in **Scheme 1.8**. With respect to the deuterium labelling section, the levels of incorporation fluctuate significantly from one example to another, ranging from 10% to >98%. It is difficult to discern what factors drive the levels of incorporation in each of these cases. Nonetheless, the number of complex examples labelled to useable levels of incorporation is admirable. Additionally, with the five tritium labelling examples discussed within the paper, all relatively complex small molecule drug motifs, all levels of observed incorporation were over 15 Ci $mmol^{-1}$, which is suitable for a range of ADMET studies.

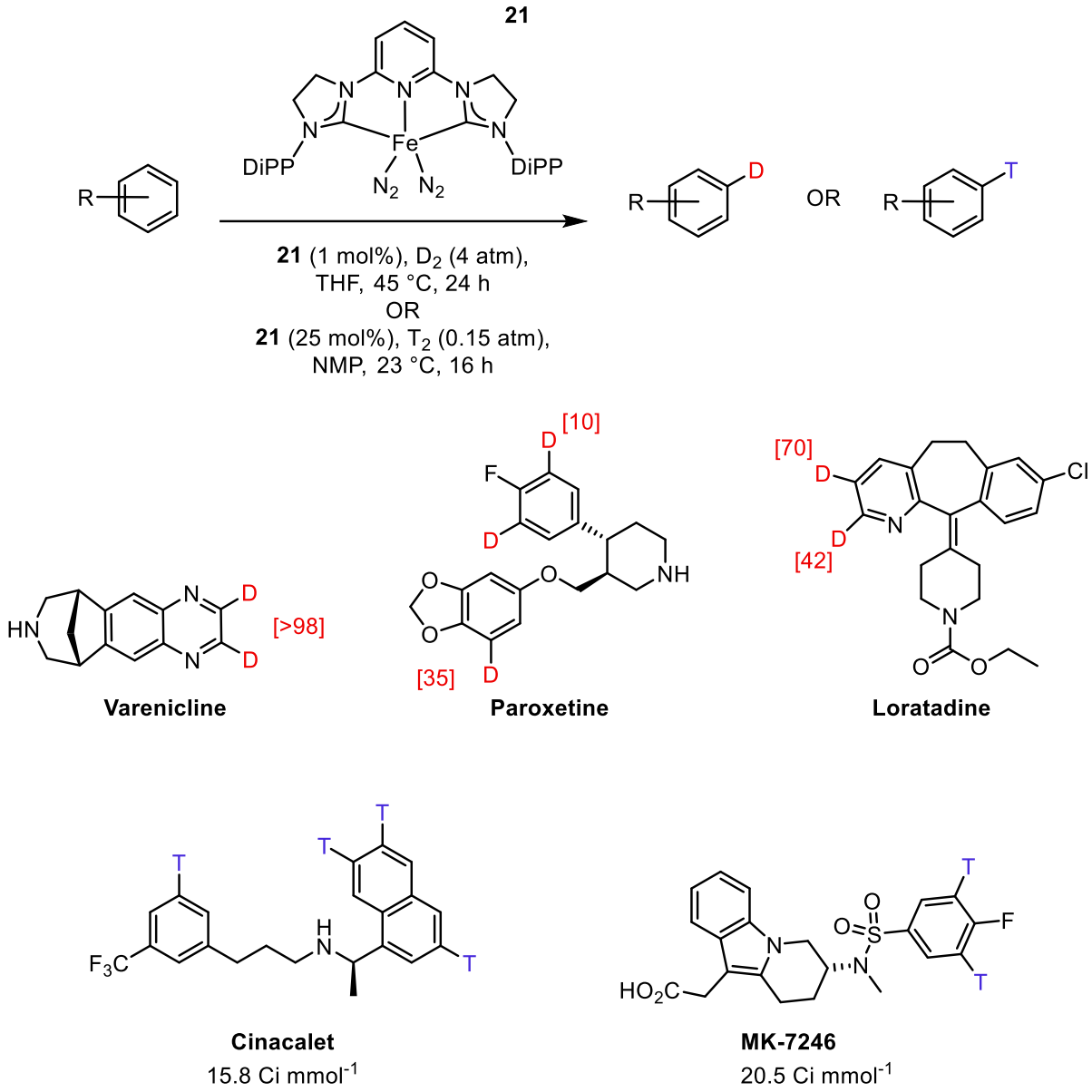

Scheme 1.8

Following on from this, the Chirik group next tackled the activation of benzylic C_{sp3}—H bonds for HIE, this time utilizing the cobalt diimine catalyst **22** (**Scheme 1.9**).[22] While the majority of substrates illustrated in the paper were simple alkylarenes, some functionality was shown to be tolerated. Electron-deficient and electron-rich aryl rings were tolerated (3-fluorotoluene **23** and 2-methylanisole **24**), as well as potentially reactive functional groups such as cyclopropane **25**, boronic ester **26**, and tertiary amine **27**. Interestingly, a number of substrates also showed activation of various C_{sp2}—H bonds, as highlighted in blue in molecules **25**, **27**, and **29**. Finally,

compound **30** proved to be a particularly interesting example, as it shows excellent levels of stereoretention at the chiral tertiary centre, despite significant levels of incorporation being observed at this site. In addition to this, good levels of diastereoselectivity were observed, with only very minor levels of incorporation (8%) being recorded at the more hindered face of the secondary benzylic position.

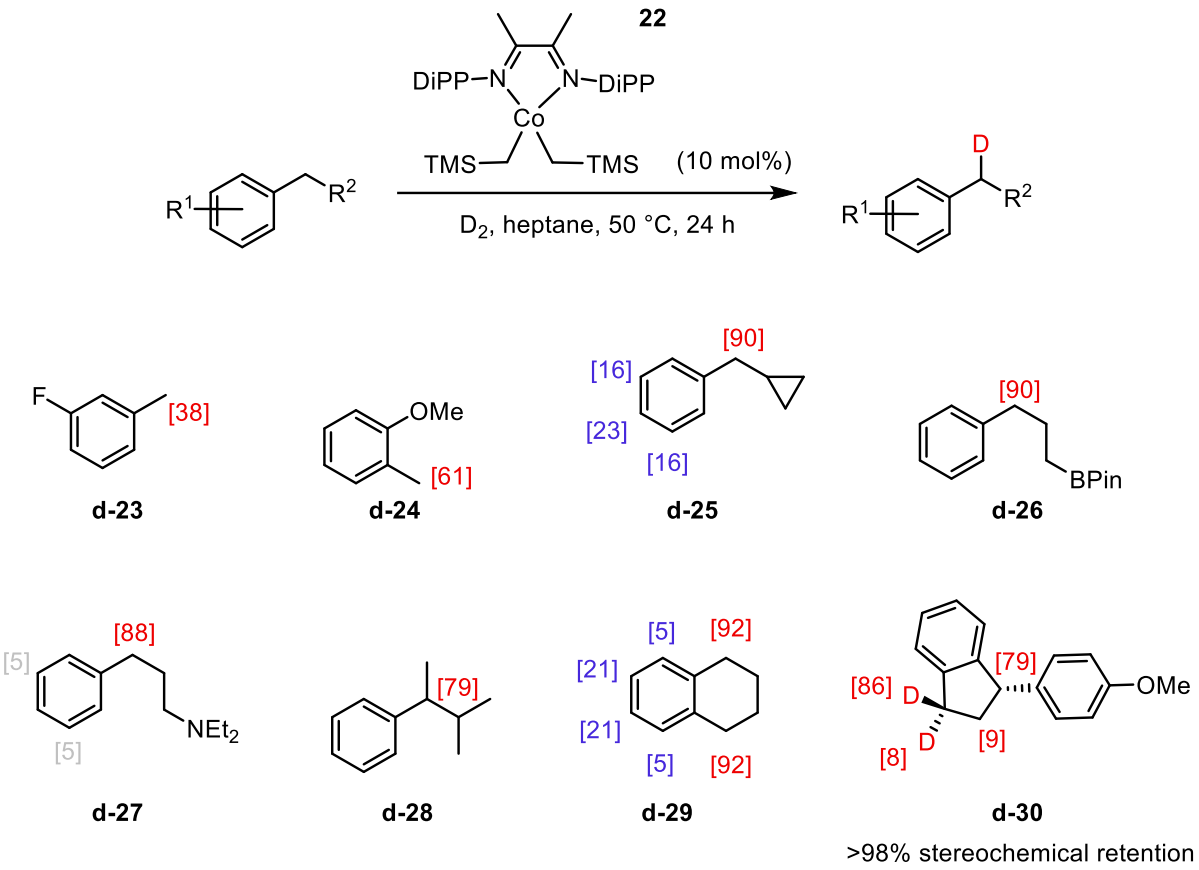

Scheme 1.9

1.5 Directed Homogeneous Hydrogen Isotope Exchange

In many instances, the ability to selectively incorporate a label into a specific site within a molecule is crucial. When utilizing C—H activation processes for labelling purposes, therefore, the ubiquity of these bonds is an obvious concern, with several positions in a molecule having the potential to be activated by a catalyst. In order to achieve selectivity in these

functionalisations, a nearby Lewis basic directing group (DG) is often exploited. This group binds to the metal catalyst, bringing the metal centre close enough to the desired C—H, potentially forming an agostic interaction, such that the activation occurs selectively (**Scheme 1.10**). What results from this activation process is a metallocycle, the formation of which reduces the overall energy of the C—H activation and functionalisation process. Due to the formation of less strained ring structures, this form of activation is generally *ortho*-selective when considering aromatic C—H activation, resulting from, typically, a 5- or 6-membered metallocyclic intermediate (5 mmi or 6 mmi).

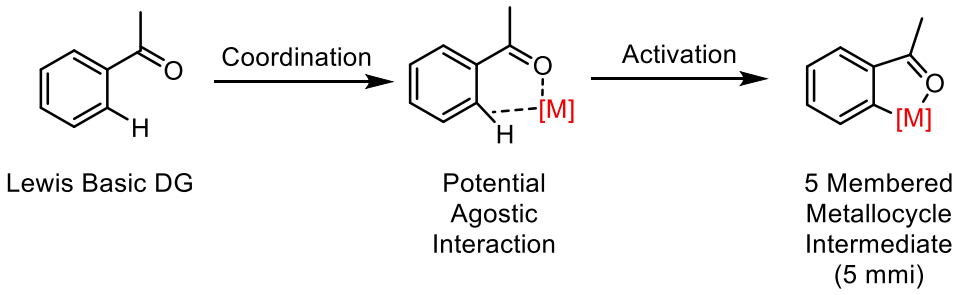

Scheme 1.10

One of the earliest examples of this type of activation being used to incorporate deuterium into an aromatic structure were reported by Lockley in 1984.[23] In this publication, Lockley demonstrated that rhodium trichloride trihydrate [$RhCl_3$•$3H_2O$] could be used to selectively *ortho*-label a range of aromatic substrates using a variation of directing groups, with D_2O as the deuterium source. **Scheme 1.11** shows the excellent levels of isotope incorporation obtained when employed across various carbonyl containing DGs. Both benzoic acid **31** and its sodium salt **32** exhibited impressive levels of incorporation, with similar values being reported for benzamide **33**. It was noted that introducing an *N*-substituent to the benzamide, in **34**, appeared to have little effect on the observed incorporation, however, increasing steric congestion further in the *N*,*N*-dimethyl variant, **35**, resulted in a significant loss in deuterium incorporation. Acetanilide **36** also displayed near quantitative incorporation, highlighting the

ability of the catalyst to label through a directing group which is further removed from the site of deuteration (through a 6 mmi). Unfortunately, when the system was applied to benzylamine **37**, an incorporation of only 34% was observed. Following these results, for several years, [$RhCl_3$•$3H_2O$] became a standard catalyst in labelling experiments and was used in the tritium labelling of a series of drugs.[24]

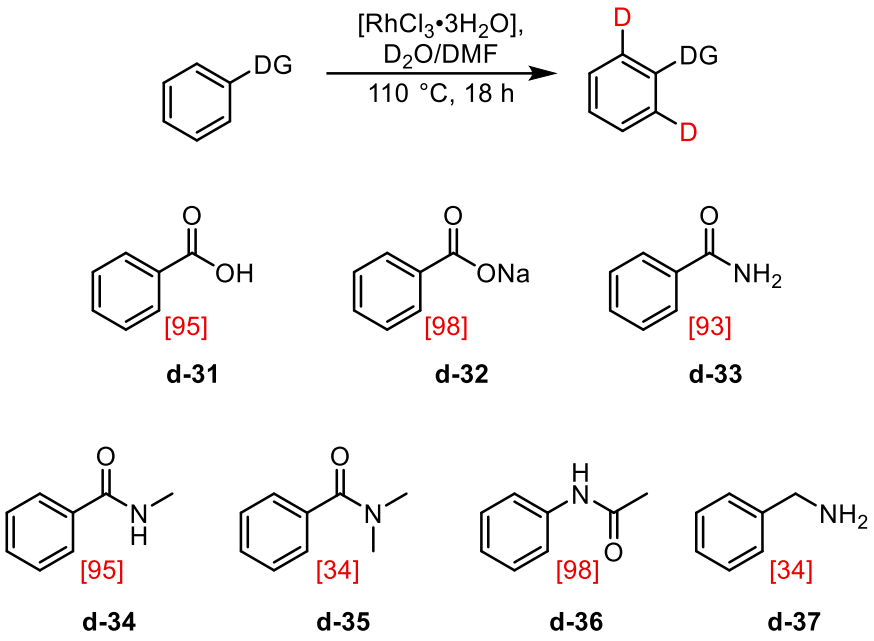

Scheme 1.11

One class of homogeneous catalyst which has shown excellent utility in the area of directed HIE are cationic iridium complexes.[25,26] Such catalyst systems have become ubiquitous through the area of HIE, and as such, have been the focus of much development, particularly in recent years. One such example of a markedly useful system is known as Crabtree's catalyst **38**. Despite the initial focus of the catalyst system on the hydrogenation of alkenes, its abundant applications in HIE led it to becoming a standard for labelling catalysts.[27] The first application of Crabtree's catalyst in isotope labelling was in 1995, when Hesk applied the catalyst to the labelling of a range of acetanilides.[28] Some examples have been highlighted in **Scheme 1.12**. Notably, a low catalyst loading of only 5 mol% was required to provide extremely high levels

of labelling. Electron-donating (**40**) and -withdrawing groups (**41**, **42**) were both well tolerated; in the case of the nitro containing substrate **42**, a very small amount of competing labelling was observed through this alternate directing group. The authors also noted that there was no evidence of C—X activation in the presence of a halogen (**41**). While the electronic character of the aryl ring appeared to have little effect on the incorporation, strongly coordinating substituents such as nitrile **43** and amino groups **44** hindered the reaction. The catalyst also appeared to be susceptible to steric effects of substituents in the *meta* position, as the *meta*-methyl **45** and trifluoromethyl **46** variants exhibited substantial selectivity for the less hindered *ortho* position on the aryl ring.

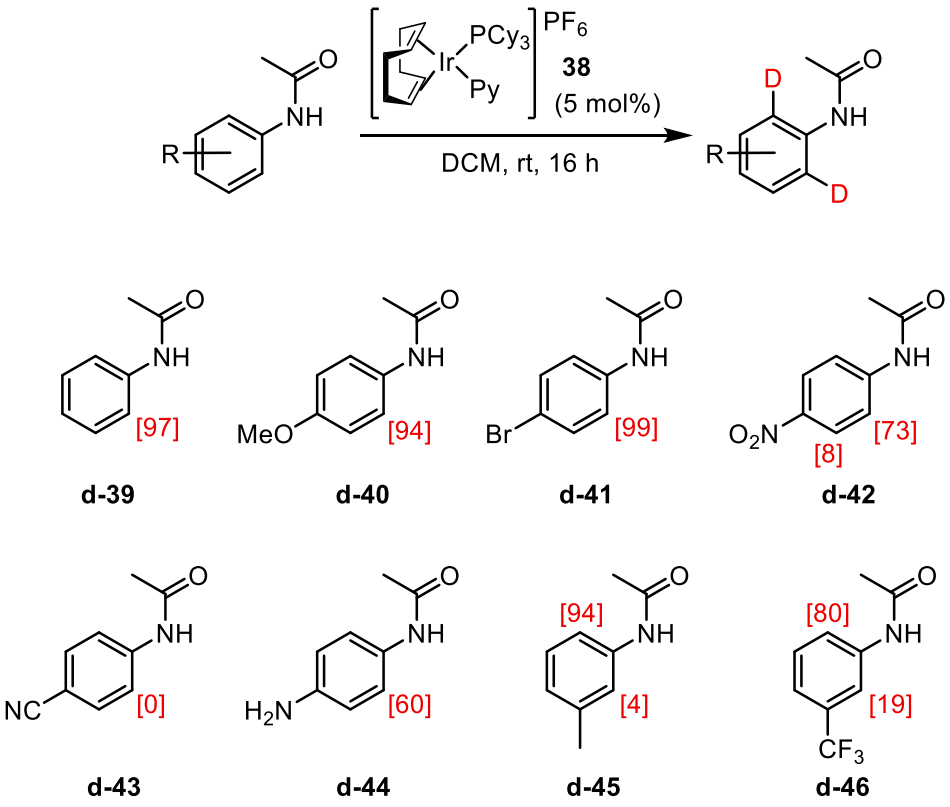

Scheme 1.12

From Hesk's report of such high activity, the use of Crabtree's catalyst in labelling reactions soon became widespread throughout the pharmaceutical industry. However, the promising results of Hesk did not translate into a wider range of substrates, with many reactions requiring

(super)stoichiometric loading. In 2001, Herbert investigated the HIE process across a wider range of carbonyl containing substrates using complex **38** (**Scheme 1.13**).[29] In this study, a minimum of 1 eq. of Crabtree's catalyst was used in each case in order to prevent catalyst deactivation by irreversible substrate binding. In addition to this, an extended reaction time of ninety hours was used in order to observe the maximum level of incorporation in each case. Generally, amide substrates worked well and an increase in the steric bulk around the nitrogen of the amide (primary amide **33** vs tertiary amide **35**) did not reduce the observed incorporation, implying that the catalyst binds through the oxygen of the amide to form a 5 mmi. There also appeared to be very little electronic influence in the case of tertiary amides, with *para*-methoxy **47** and *para*-nitro **48** giving identical levels of incorporation. Contrasting this, however, esters were found to be more sensitive to the electronic effects of other substituents on the aryl ring, for example electron poor ester **50** exhibited significantly reduced levels of incorporation, with respect to the electron rich example **49**. An interesting note made by Herbert was that, with respect to unsubstituted acetophenone **51**, a *para*-methoxy group in **52** hindered the reaction whereas the *para*-nitro group in **53** resulted in similar levels of incorporation. This inconsistency with previous results indicates a possibility for multiple mechanisms.

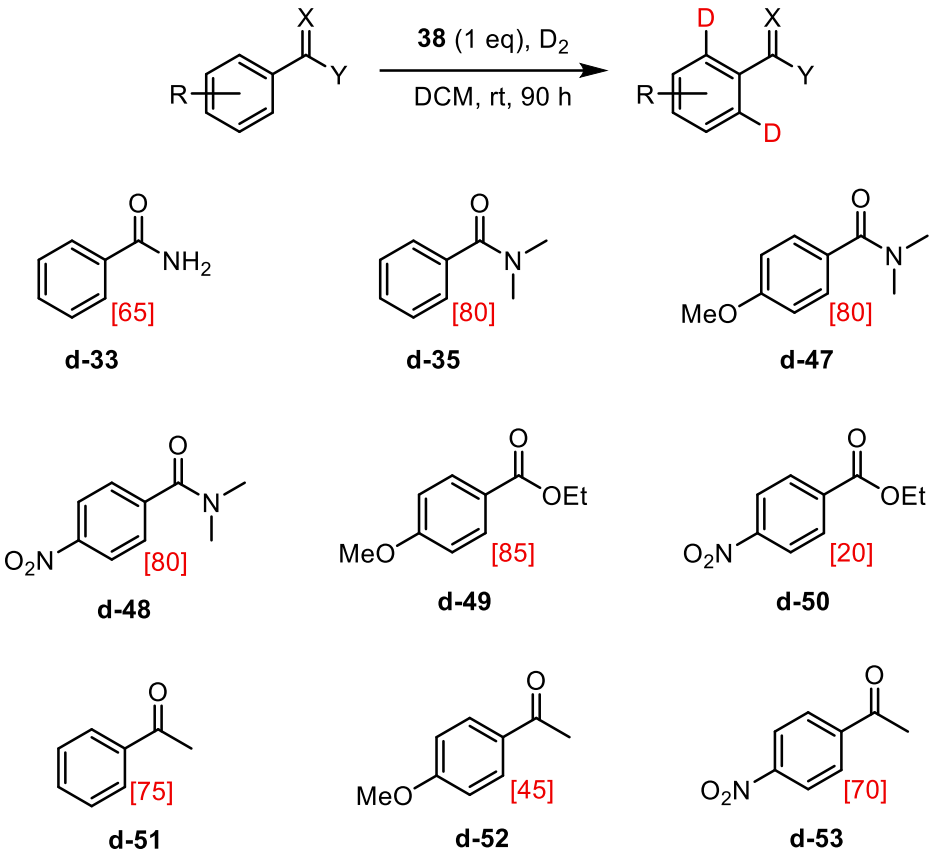

Scheme 1.13

The Kerr group has, over recent years, developed and studied a range of iridium catalysts incorporating both NHC and phosphine ligands, in an effort to combat the challenges presented in the use of Crabtree's catalyst. In 2008, a range of iridium catalysts equipped with bulky phosphine ligands, as well as the sterically encumbered IMes, was unveiled (**Scheme 1.14**).[30] The complexes could be synthesised by first taking $[Ir(COD)Cl]_2$ **54**, in the presence of sodium ethoxide, and introducing the NHC *in situ* through deprotonation of imidazolium salt **55**. This allowed the isolation of stable chlorocarbene complex **56**. The chloride could then be abstracted *via* silver hexafluorophosphate, and the resultant iridium complex trapped by the desired phosphine, delivering the iridium(I) precatalyst system. This practically convenient method requires no glove box manipulation, and afforded a series of previously unreported iridium complexes in very appreciable yields.

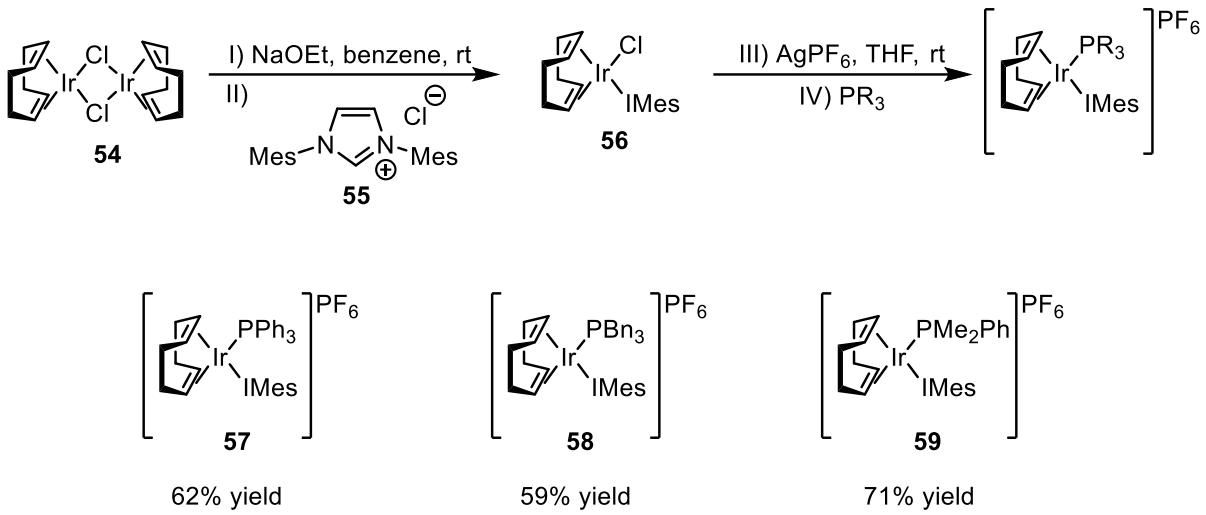

Scheme 1.14

These complexes were then tested against a series of substrates of varying difficulty in *ortho*-directed HIE reactions (**Scheme 1.15**). All three complexes exhibited excellent incorporation across a range of substrates under very mild conditions. Ketones, amides, and heterocyclic substrates all performed admirably. Interestingly, even the remarkably poor nitro directing group, in nitrobenzene **64**, resulted in excellent levels of incorporation with all three catalyst systems. Additionally, the group showed that the catalyst systems could also exploit functional groups which direct through a 6 mmi, with acetamide **39**.

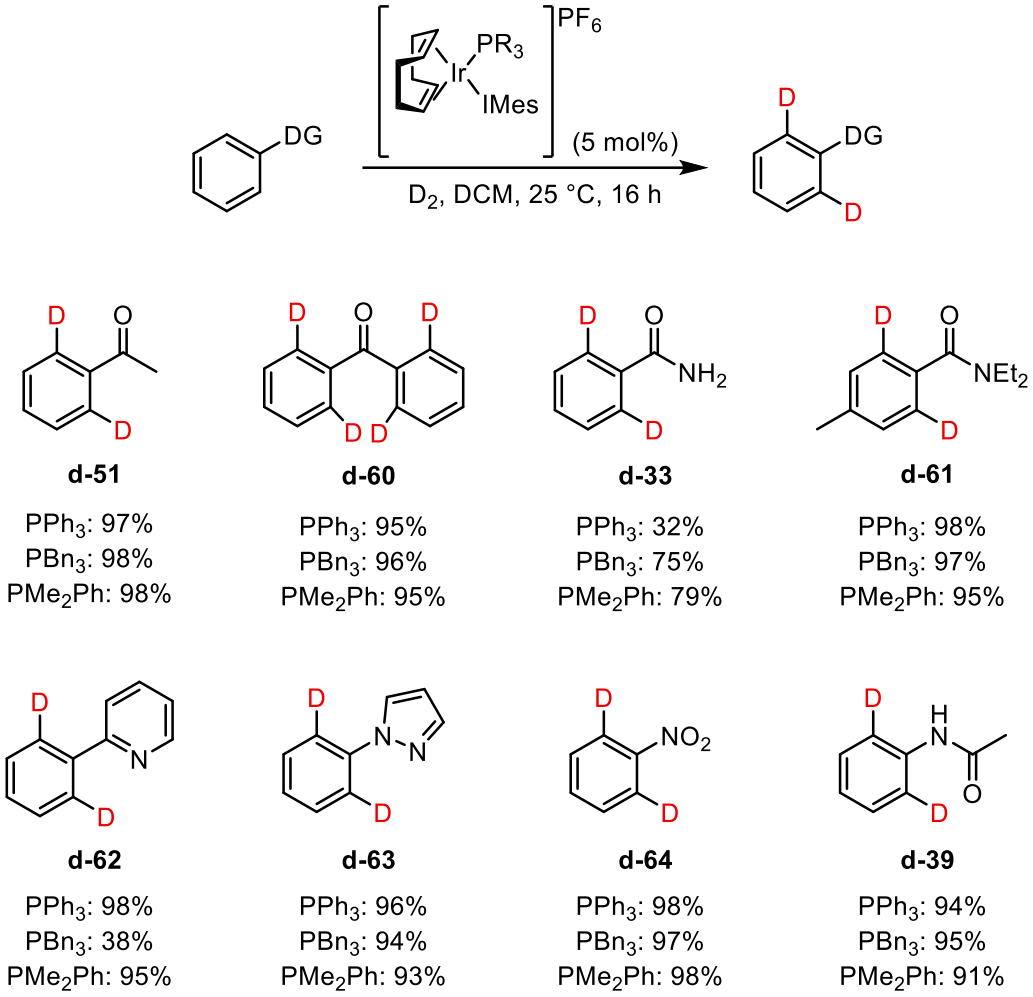

Scheme 1.15

Furthermore, within the same paper, Kerr demonstrated impressive selectivity for sites that were activated through a 5 mmi over a 6 mmi (**Scheme 1.16**). This was achieved with the labelling of benzanilide **65**, wherein reaction at the standard 5 mol% catalyst loading resulted in both sites being deuterated to an extremely high level. However, a drop in the catalyst loading to 0.5 mol% resulted in deuteration through a 5 mmi, only, with high selectivity.

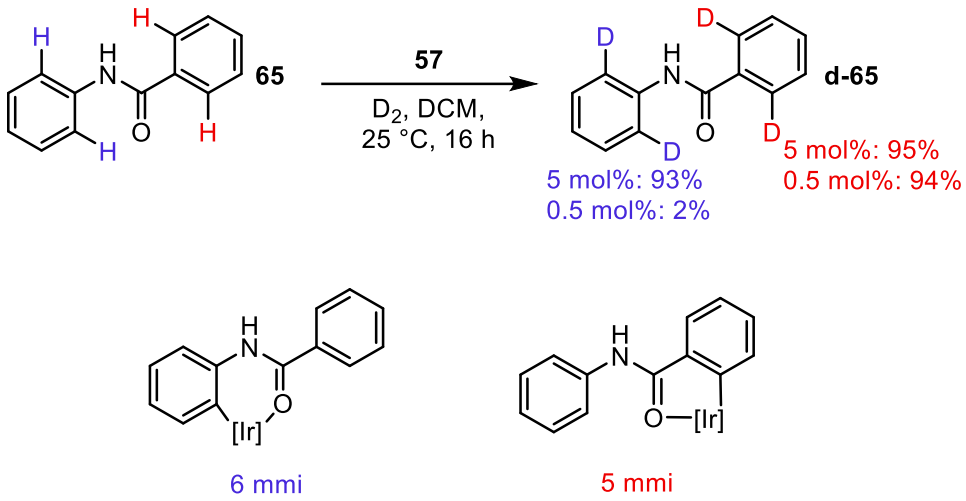

Scheme 1.16

This report was followed up in 2014, with further additions to the series of catalytically active systems. [31] Furthermore, the group also applied highly active iridium catalyst **57** to more complex marketed drug molecules (**Scheme 1.17**). The outstanding levels of deuterium incorporation in Perebron highlights the catalyst system's tolerance to tertiary amines. Labelling of Celecoxib with complex **57** showed good selectivity for labelling through the pyrazole motif, affording exceptional levels of incorporation. Interestingly, reacting Nilutamide with complex **57** for 1 h results in good selectivity for the nitro group, delivering an excellent 98% incorporation. Finally, application of **57** to the labelling of Niclosamide allowed several positions within the molecule to be exchanged, with good levels of incorporation across all four possible positions.

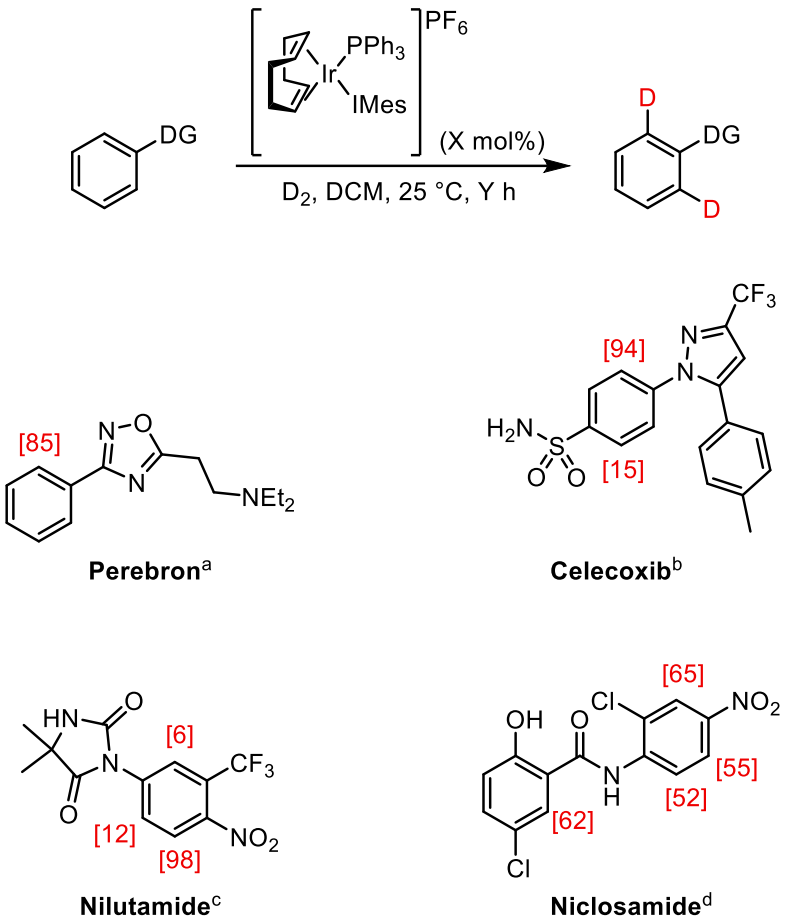

[a] 5 mol%, 16 h [b] 10 mol%, 1 h, [c] 2.5 mol%, 1 h, [d] 5 mol%, 1 h

Scheme 1.17

Within the same paper, the mechanism of the HIE process was investigated by a combination of NMR analysis and DFT calculations (**Scheme 1.18**, note that complexes remain cationic throughout the cycle). The mechanism proposed the formation of an iridium(III) dideuteride in the presence of D_2 gas, to which the substrate rapidly coordinates. The substrate is bound through the directing group (the carbonyl oxygen, in the case of acetophenone **51**, shown in **Scheme 1.18**), as well as forming an agostic interaction with the C—H bond to be activated. The system then undergoes a C—H activation step, approaching Ir(V) in the transition state, resulting in the formation of an Ir—C bond being formed in a *cis* arrangement with the resultant hydride. The dideuterium and hydride ligands can undergo H-D fluxionality in order to deliver a complex with a deuteride *cis* to the substrate. From here, C—D bond formation, followed by

substrate turnover, releases the labelled product. It was found that the C—H activation step was rate determining, being 3.5 kcal/mol higher than the C—D formation step.

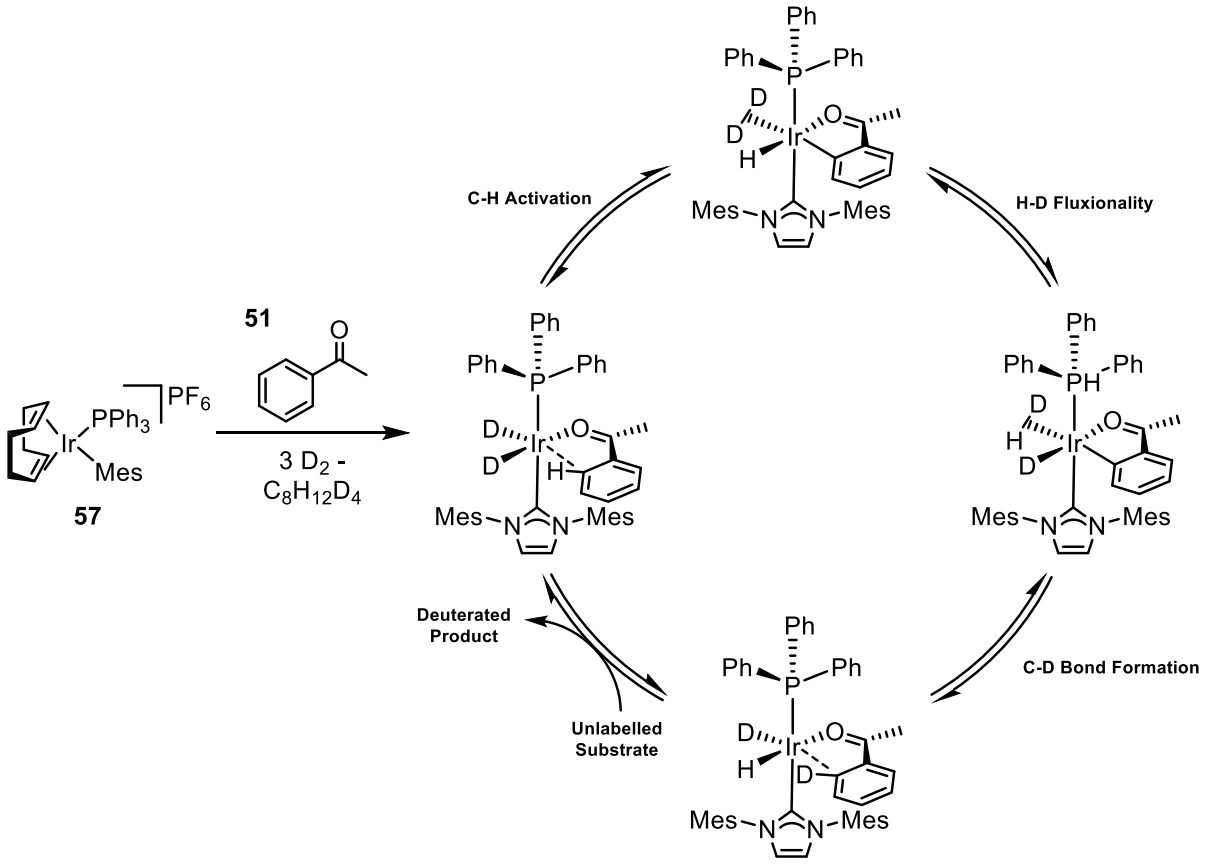

Scheme 1.18

Having established an excellent substrate applicability with these catalyst systems, the Kerr group then reported a more focused study on a particular directing group which had proven quite challenging, namely, the ester functionality (**Scheme 1.19**).[32] When the previously optimised reaction conditions were applied to a range of ester-containing molecules, it was found that the levels of deuterium incorporation varied significantly. On examining the aryl ring substituents, for example, it was seen that the electron-neutral ester **66a** and the electron-poor ester **66b** both exhibited moderate levels of incorporation, at 42% and 32% respectively. However, when electron-rich ester **66c** was applied, excellent levels of 89% deuterium incorporation were observed. The *O*-substituent of the ester directing group was also varied,

showing good levels of incorporation into *iso*-propyl ester **66d**. However, more challenging examples, such as the sterically hindered *tert*-butyl ester **66e**, and the electron-withdrawing trifluoroethyl ester **66f**, delivered only low levels of isotope incorporation. Interestingly, however, it was found that running the reactions at a slightly elevated temperature of 40 °C significantly improved the levels of observed deuterium incorporation in each of the examples tested.

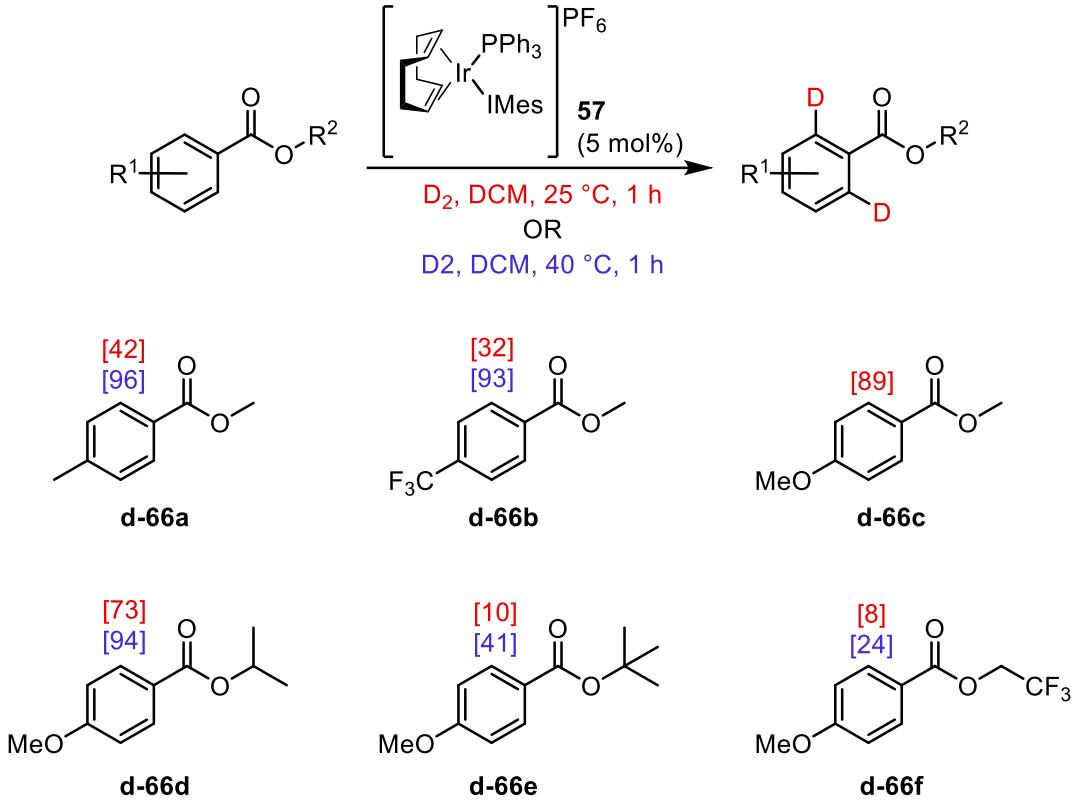

Scheme 1.19

Following this, the group also examined the applicability of these catalyst systems in the labelling of pharmaceutically relevant heterocycles.[33] As shown in **Scheme 1.20**, a series of heterocyclic directing groups were successfully targeted, such as imidazole **67a**, the partially saturated dihydrooxazole **67b**, isoxazole **67c**, and the sulfur-containing thiazole **67d.** All substrates demonstrated excellent levels of isotope incorporation under mild conditions and short reaction times. In addition to this, benzo-fused heterocycles, such as benzimidazole **67e**

and benzothiazole **67f** could also be labelled to good levels. Finally, the group also showcased the ability to exploit these functional groups in more complex drug-like examples, such as **67g**, with similarly high levels of isotope incorporation.

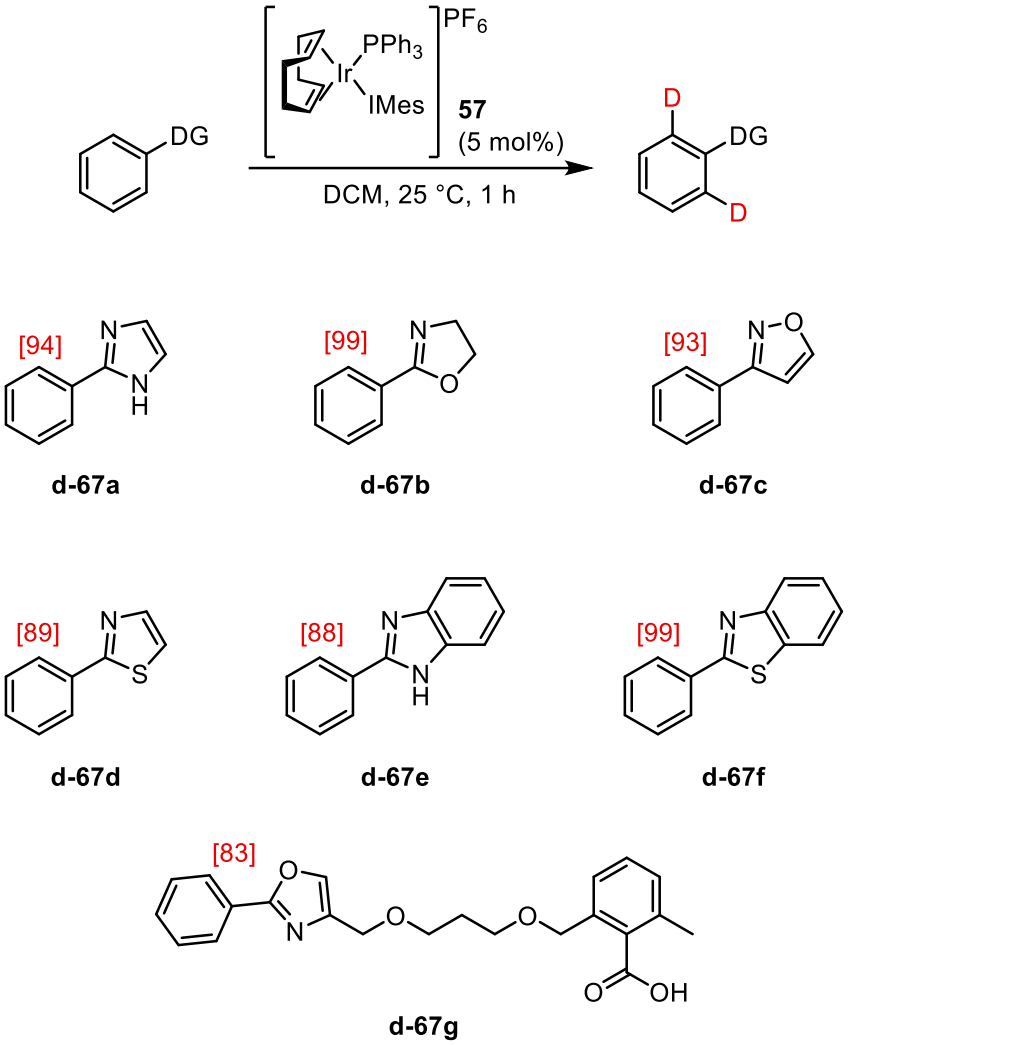

Scheme 1.20

In addition to the installation of isotopic labels on aromatic positions, the group also investigated the use of these catalyst systems to introduce deuterium at non-aromatic sp^2 centres within a molecule, specifically, the ß-position of α,ß-unsaturated systems.[34] Indeed, in order to label this class of substrates, careful consideration of the catalyst system was required in order to avoid competing alkene reduction. Fortunately, it was found that, the triphenylphosphine containing complex **57** was able to deliver excellent levels of

incorporation, with high selectivity. **Scheme 1.21** below shows some examples of the substrates which were deuterated using this methodology. The numbers in parentheses highlight the ratio of labelling to alkene reduction. Both electron-withdrawing and electron-donating substituents on the aryl ring, in **68a** and **68b**, were well tolerated, giving excellent incorporation into the ß-position. Additionally, the thiophene example **68c** highlighted the tolerance of such heterocyclic motifs. Larger alkyl substituents on the directing group, such as in *tert*-butyl example **68d**, delivered high levels of isotope incorporation, however, small amounts of alkene reduction were also observed. Finally, changing the directing group from a ketone, to an amide, in **69**, or even a nitro group, in **70**, also afforded outstanding levels of incorporation.

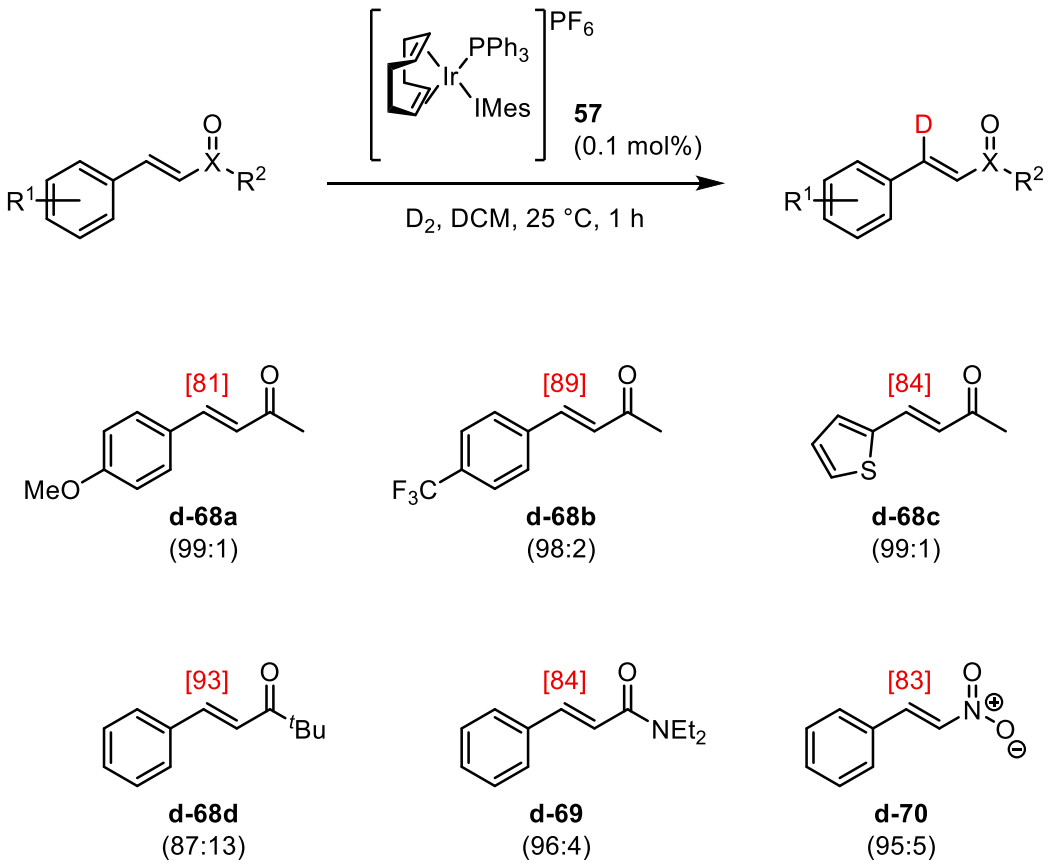

Scheme 1.21

In addition to the applications of these catalyst systems established by our own group, there are several reports of others using our developed catalyst systems in order to gain access to labelled drugs and drug-like compounds. One particularly notable example is the use of complex **59** in the synthesis of four tritiated drug molecules: t-ethylmelagatran, t-melagatran, t-ximelagatran, and t-hydroxymelagatran (**Scheme 1.22**).[35] Carbamate-protected amidine **71** was selected as an intermediate which could be successfully labelled and subsequently transformed into the desired tritiated targets. Previous use of Crabtree's catalyst (in stoichiometric levels) had yielded unsatisfactory levels of specific activity and radiochemical purity. In contrast to this, use of complex **59**, at only 10 mol% catalyst loading, furnished a sample of the labelled intermediate **t-71** in excellent levels of isotope incorporation and radiochemical purity, beyond the minimal requirements of the study. Through a short series of transformations, this intermediate allowed access to tritiated samples of the desired drug molecules.

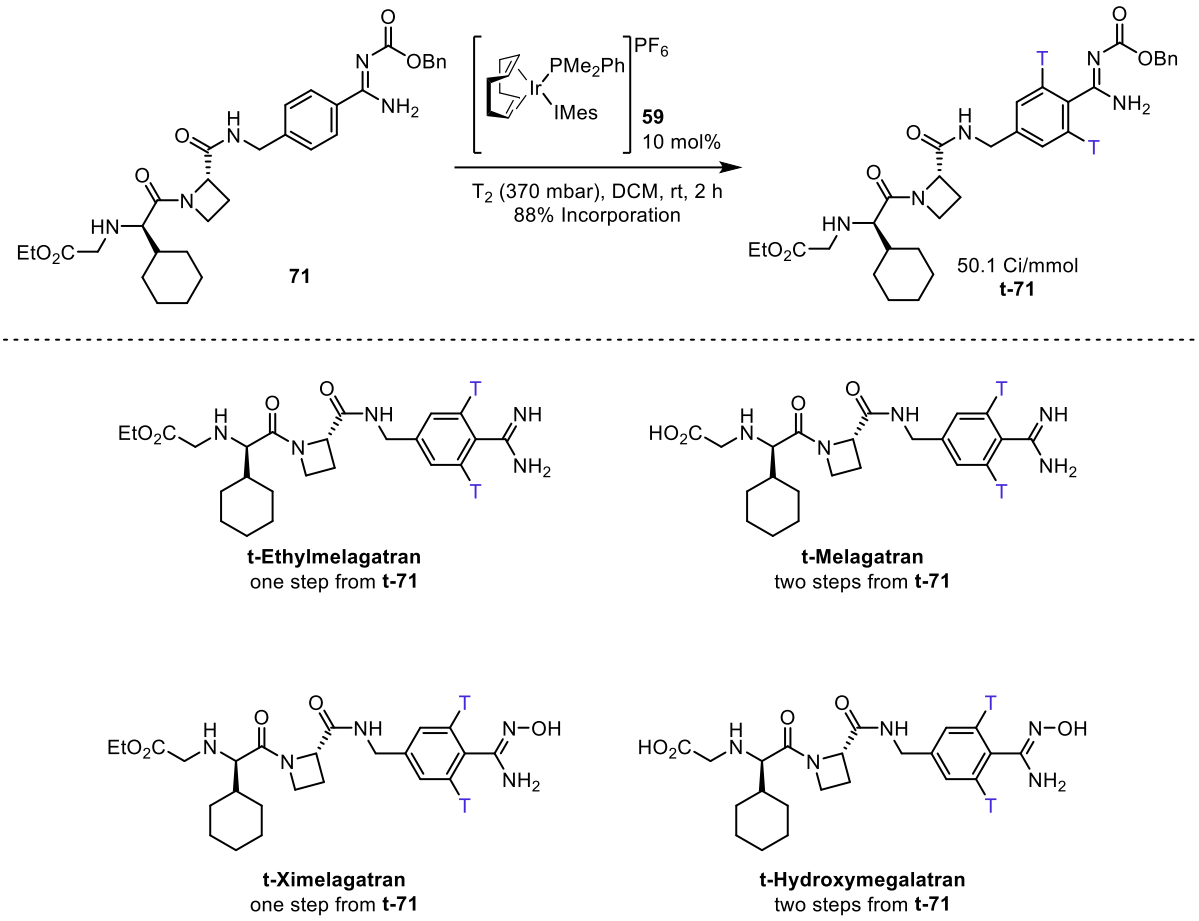

Scheme 1.22

Another noteworthy example of the application of complex **59** is in the synthesis of tritiated AZD5248, a highly potent cathepsin C inhibitor.[36] A tritiated sample of this drug candidate was required for preclinical metabolism studies, and the Kerr group catalysts proved outstanding in accessing such labelled molecules. While direct labelling of AZD5248 proved challenging, due to the presence of the strongly coordinating nitrile groups within the final molecule, intermediate **72** was selected as a suitable precursor. Using the amide directing group, in conjunction with complex **59**, a sample of **t-72** was afforded with good levels of specific activity at 13.3 Ci/mmol. This compound was then dehydrated by reaction with the Burgess reagent, and the Boc-protecting groups removed by stirring in formic acid. This sequence successfully afforded a radiolabelled sample of AZD5248 for the metabolic studies.

Indeed, the isotope group at AstraZeneca have showcased further excellent applications of our catalyst systems in the production of labelled drug molecules.[37,38]

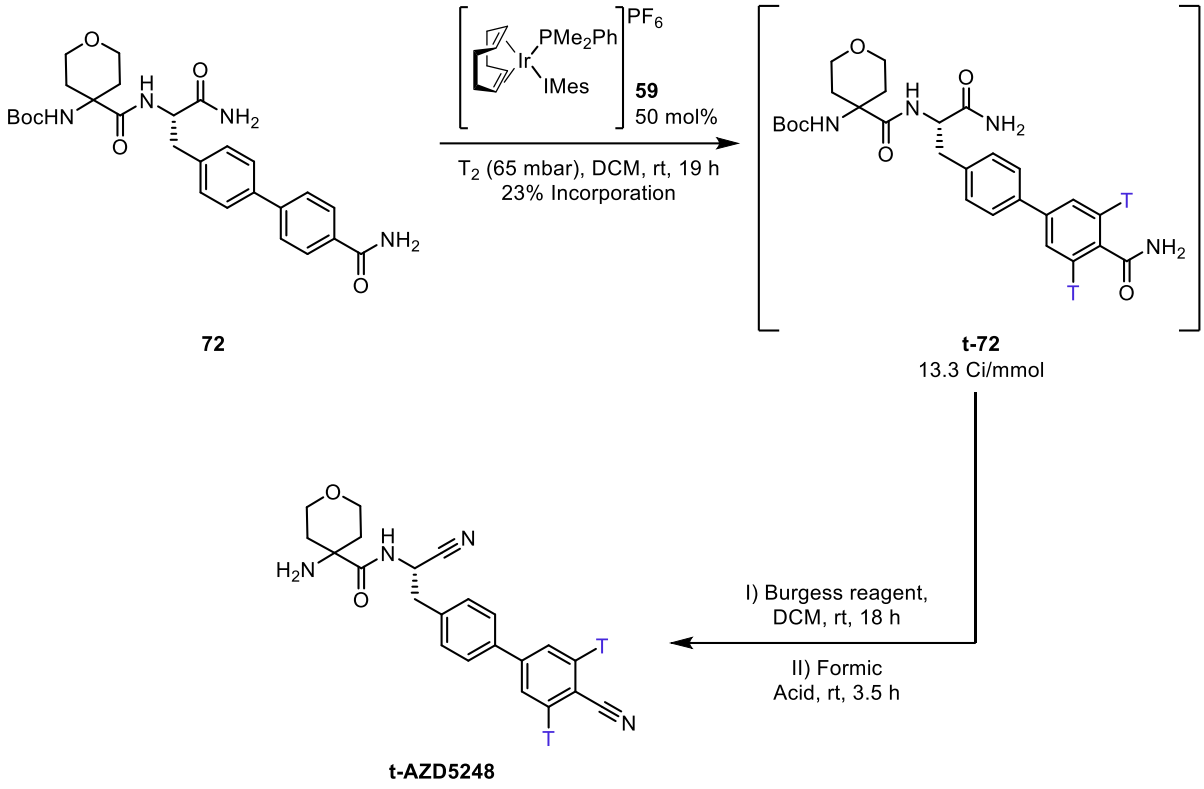

Scheme 1.23

A final example of application of this catalyst system comes from the Skrydstrup group.[39] This report detailed the use of a two-chamber reactor system for the *in situ* generation of hydrogen or deuterium gas in small quantities for single experiments, from the reaction of zinc metal and aqueous HCl or DCl. This two-chamber system allowed for safe and efficient access to pressurised gases in small quantities. While the report discussed many examples of this equipment in hydrogenation, and, indeed, deuterogenation, notable examples of HIE were also showcased. Using complex **57**, deuterated samples of olaparib, (an ovarian cancer treatment), and CX-546 (a schizophrenia treatment), were accessed directly, as shown in **Scheme 1.24**. Both drug molecules were labelled to impressive levels of isotope incorporation. In the case of CX-546, there was a distinction in the levels of deuterium incorporation between the two

available *ortho*-C—H sites. Following this, developments with this system have improved upon the method of deuterium gas production, further advancing the applicability of this equipment in directed HIE. [40]

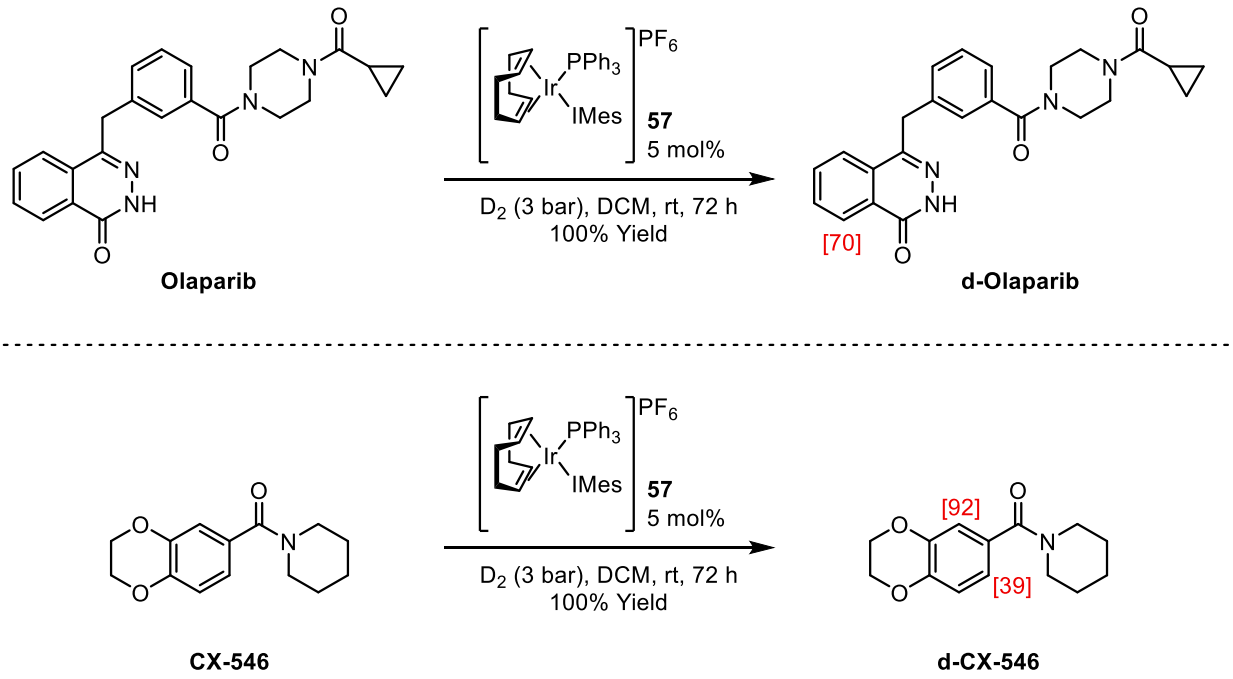

Scheme 1.24

In order to provide a more applicable catalyst system for the pharmaceutical industry, Kerr focused on establishing a range of non-chlorinated solvents within which the catalysts could be utilised.[41] Initial solvent screening appeared to be promising, with the PPh_3/IMes catalyst **57** labelling acetophenone at room temperature over 16 h in diethyl ether (Et_2O), *tert*-butyl methyl ether (MTBE), and 2-methyl tetrahydrofuran (2-Me THF). However, when moving to the more coordinating solvent acetone, the observed incorporation dropped to only 43%. In order to rationalise this, the binding enthalpies of the solvents were calculated (**Table 1.1**). It was found that in order for the reaction to proceed efficiently, the substrate must be able to efficiently bind to the catalyst centre. Thus, it was proposed that the Lewis basic solvent may compete with the substrate binding, and hinder the reaction. Examination of the enthalpy of displacement (ΔH_{exc}) showed that, in the case of acetone, the displacement was slightly

endothermic, whereas the displacement of the ethereal solvents and DCM was exothermic. It was concluded that this equilibrium was instrumental to the reaction rate.

Table 1.1

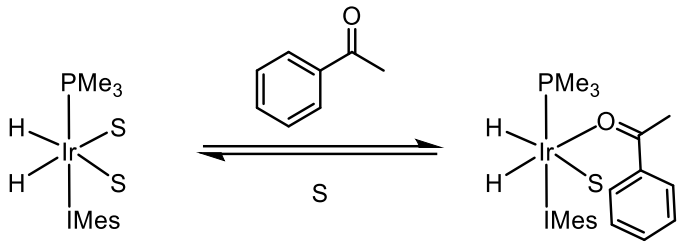

Entry	Solvent	ΔH_{exc}	Incorporation (%)[a]
1	DCM	-13.3	97
2	MTBE	-12.8	91
3	Et_2O	-7.3	94
4	2-Me THF	-3.7	95
5	Acetone	0.3	43

[a]Incorporation of deuterium into acetophenone

It was therefore suggested that 2-methyltetrahydrofuran would be a suitable, more industrially aligned solvent which is polar enough to dissolve a range of drug-like molecules, whilst still able to be readily displaced by a molecule of substrate. In order to showcase how useful this newfound understanding of the reaction process can be, the group further tuned the labelling conditions for Niclosamide (**Scheme 1.25**). Whilst only moderate levels of incorporation were observed, albeit across four positions, when applied in DCM, switching the solvent to 2-methyltetrahydrofuran resulted in a significant increase in the observed incorporation across almost all positions.

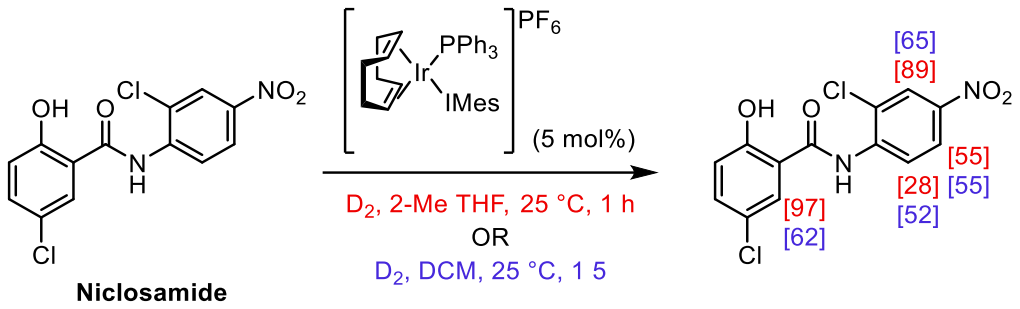

Scheme 1.25

Investigations within the Kerr group then turned to the catalyst counterion in order to further enhance the activity of the catalysts.[42] It had previously been shown by Pfaltz, in the area of hydrogenation, that switching to a large, non-coordinating anion such as tetrakis[3,5-bis(trifluoromethyl)phenyl]borate (BAr_F) can augment a catalyst's activity. As such, variants of catalyst **57** were synthesised, each with an anion of increasing steric bulk and decreasing coordinative ability (**Scheme 1.26**).

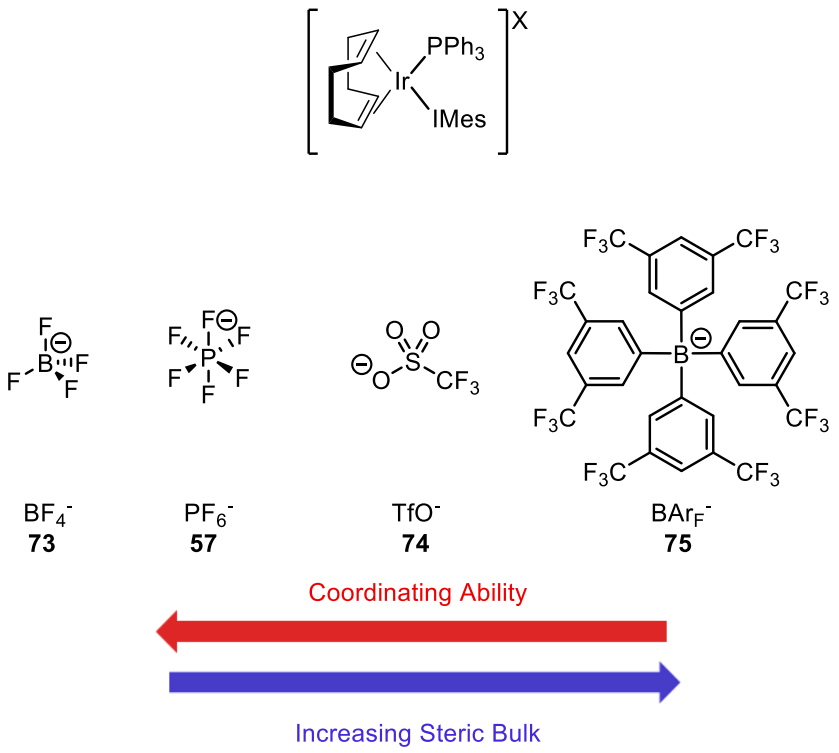

Scheme 1.26

Each complex was applied to the labelling of acetophenone and the rate of incorporation was measured for each reaction. It was noted that while all four complexes reached high amounts of incorporation, the triflate and BAr_F anions reached the maximum incorporation much faster. In addition to this, the BAr_F complex **75** and the PF_6 complex **57** were tested in a range of industrially aligned solvents, with the higher solubility of the BAr_F catalyst **75** allowing it to perform on a much wider range of solvents than the PF_6 variant **57**.

With this new catalyst system, supported by the BAr_F counterion, the group also reported a study which compared the reactivity of this complex to the previous generation, which utilised the PF_6 counterion.[43] The results of this study are highlighted in **Table 1.2** below. When labelling *para*-nitroacetophenone **53** in toluene, it can be seen that the PF_6 containing catalyst **57** delivers good levels of incorporation though both directing groups: 86% through the ketone, and 52% through the nitro group (**Entry 1**). However, when the BAr_F variant **75** is used, a much more selective delivery of deuterium is observed, highlighting the effect that the counterion has on catalyst electrophilicity as well as solubility (**Entry 2**). In considering ethyl 4-nitrobenzoate **50**, which exhibits only moderate levels of incorporation when using complex **57**, a significant increase in the observed isotope incorporation across both positions is noted when switching to complex **75** (**Entries 3** and **4**). Finally, when employing both catalyst systems in the labelling of Nilutamide, the BAr_F complex **75** again shows increased levels of selectivity, when compared to the PF_6 variant **57** (**Entries 5** and **6**). This highlights the importance of catalyst electronics and solubility even in more complex drug examples.

Table 1.2

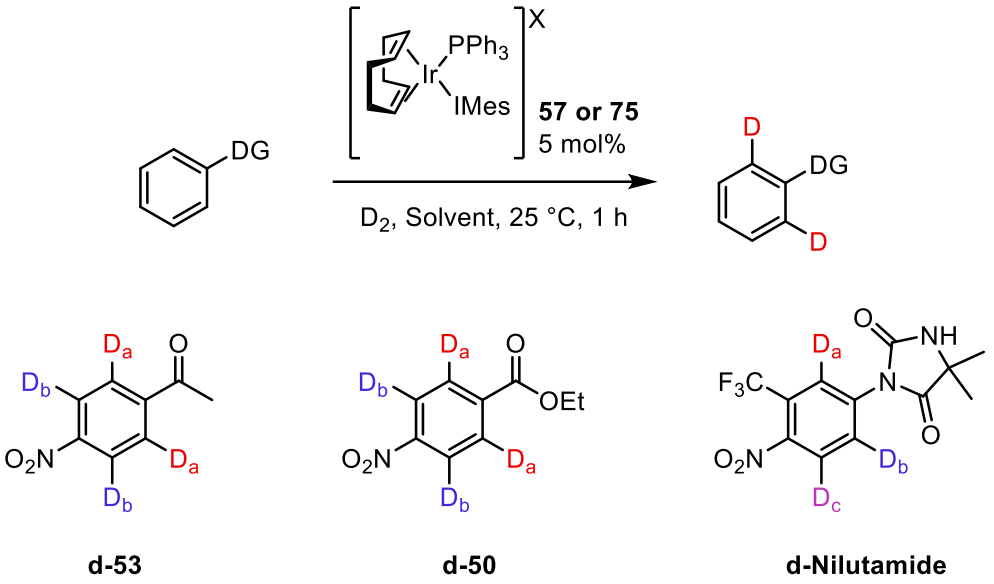

Entry	Substrate	X	Solvent	%D_a	%D_b	%D_c
1	**53**	PF_6	Toluene	86	52	-
2	**53**	BAr_F	Toluene	87	14	-
3	**50**	PF_6	DCM	29	41	-
4	**50**	BAr_F	DCM	52	66	-
5	Nilutamide	PF_6	DCM	5	11	99
6	Nlutamide	BAr_F	DCM	3	3	99

One particular class of pharmaceutically relevant heterocycles, however, which did not prove amenable to the standard labelling conditions applied in previous examples was the aryl tetrazole.[44] It was suggested, however, that a different mode of reactivity could possibly be exploited in this case, in order to utilise tetrazoles as directing groups for the installation of heavy isotopes of hydrogen. As such, the Kerr group developed a base-assisted protocol for the labelling of molecules containing aryl tetrazoles. Through careful consideration of base, temperature, and time, the newly optimised conditions, highlighted in **Scheme 1.27**, were

found. As seen with *para*-methyl substituted example **76a**, excellent levels of incorporation can be achieved through these conditions, at 85% D. Interestingly, when the methyl group is placed in the *meta*-position in example **76b**, a difference in incorporation is noted between the more hindered site, at 58% incorporation, and the less hindered site, at 83% incorporation. Additionally, moving the steric bulk of the methyl group to the *ortho*-position in **76c**, the level of isotope incorporation is not affected. Electron-donating groups in **76d**, and electron-withdrawing groups, in **76e**, are also well tolerated, both giving outstanding levels of incorporation. Interestingly, when the acidic proton of the tetrazole is replaced with a methyl group, as in **76f**, a significant level of incorporation is still observed. Finally, the group also showcased these labelling conditions in the production of a tritiated sample of antihypertensive drug Valsartan. By running the reaction under 1.5 Ci of tritium gas, a sample of this angiotensin receptor blocker was afforded with 15 Ci/mmol and in excellent radiochemical purity.

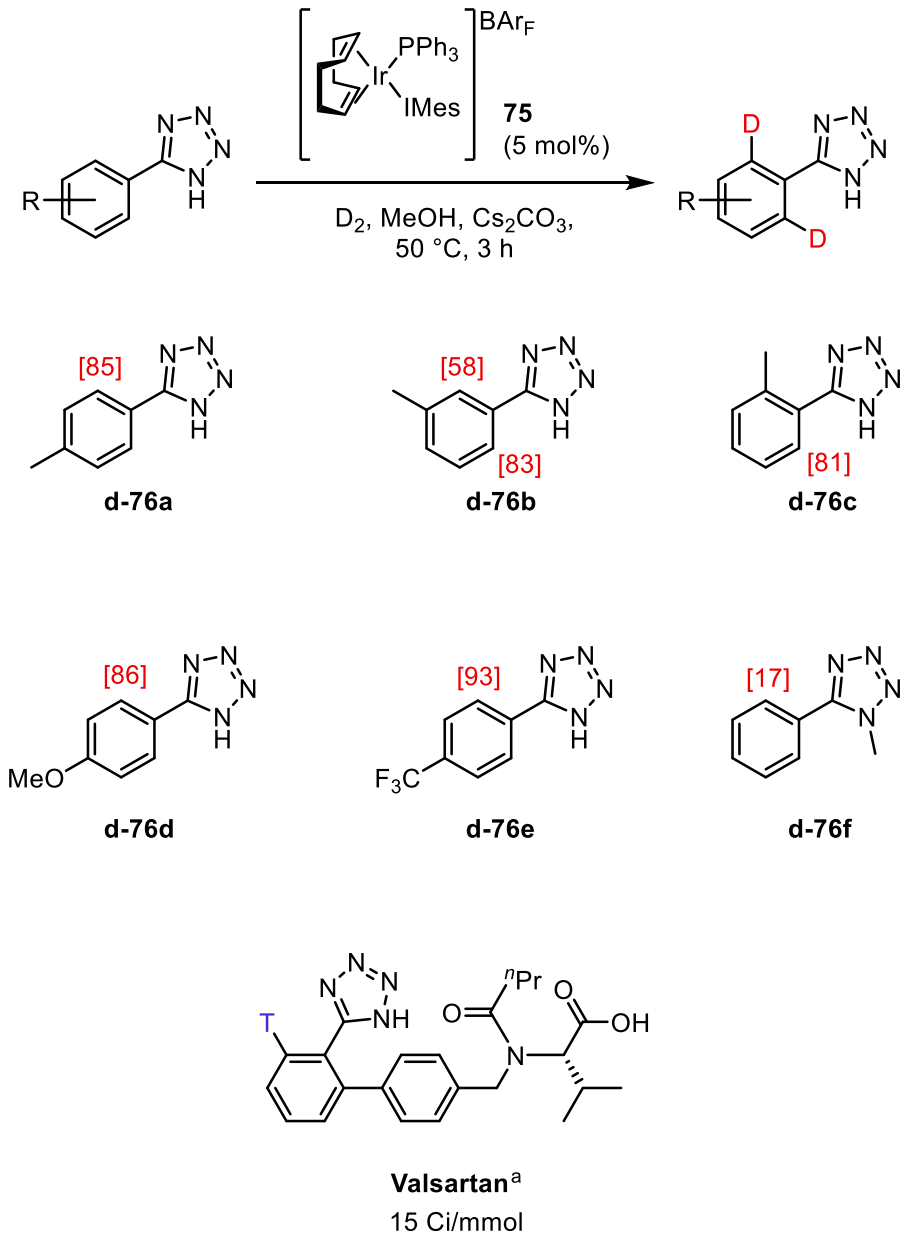

Scheme 1.27

Whilst the currently established Kerr group catalysts, bearing both phosphine and NHC ligands, have shown unprecedented scope in labelling reactions, there are some challenging motifs which were not accommodated for by this generation of catalysts, for example, primary sulfonamides, which are prevalent in many pharmaceuticals. At the time, however, the current Kerr group catalysts were unable to exploit this directing group to any great effect. **Scheme**

1.28 shows the limited levels of incorporation achieved by one of the most active NHC/phosphine type catalysts with benzenesulfonamide **77**.[45]

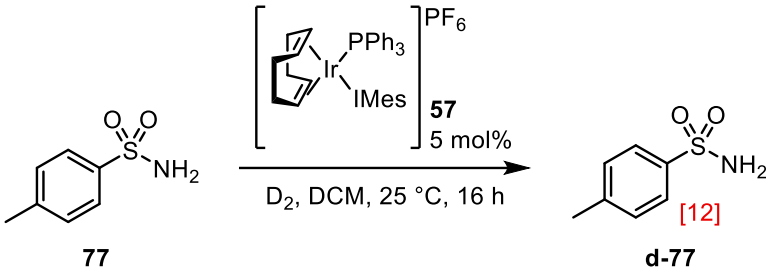

Scheme 1.28

With a mere twelve percent incorporation observed, it was hypothesised that the tetrahedral sulfonamide directing group was too sterically hindered to be effective. As such, it was proposed that a catalyst featuring a smaller ligand sphere, and a higher electron density, would favour the coordination of the sulfonamide-containing substrate and increase the rate of the C—H activation step. Pleasingly, employing the chlorocarbene complex **56** (a synthetic precursor to the NHC-phosphine catalysts) resulted in an impressive ninety percent incorporation (**Scheme 1.29**).[45] In order to optimise these parameters, the TEP and buried volume of various NHCs were investigated (*vide infra*). This resulted in a catalyst which incorporated up to ninety-six percent deuterium in only two hours. These results highlighted the dramatic change in activity which can be brought about by subtle changes in the catalyst parameters.

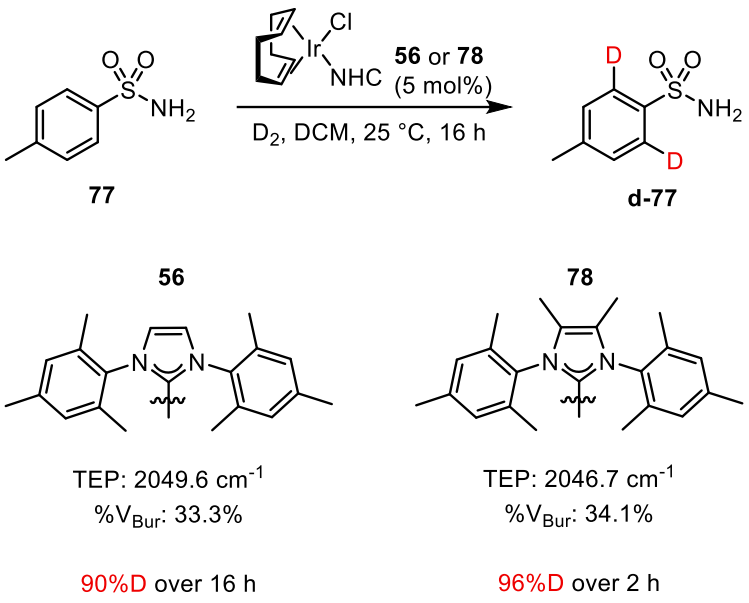

Scheme 1.29

This remarkable piece of methodology was underpinned by careful computational guidance, with the binding enthalpy (ΔH_{bind}) and enthalpy of C—H insertion (ΔH_{ins}) calculated in order to support the experimental observations (**Scheme 1.30**). Accordingly, it was found that the binding enthalpy of the benzenesulfonamide substrate was more exothermic for the cationic, phosphine containing catalysts than the smaller, neutral chloride complex. However, in contrast to this, the C—H activation, predicted to be the rate determining step, was more endothermic for the cationic, phosphine-containing catalyst.

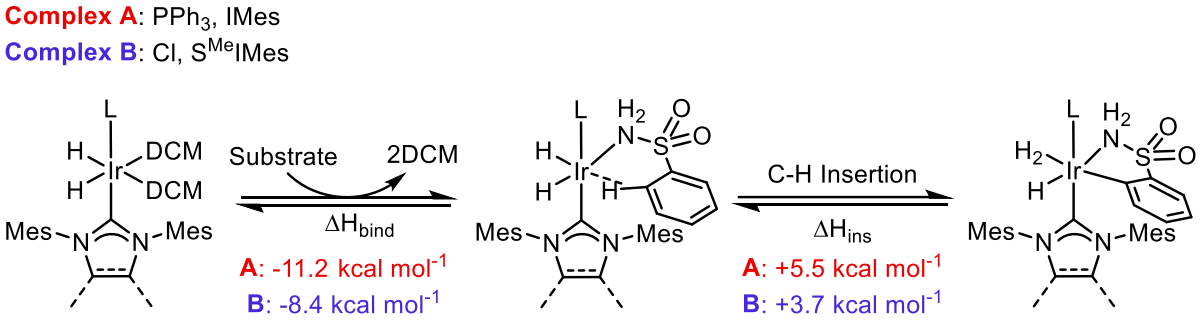

Scheme 1.30

Shortly after this publication, the Kerr group moved on to further showcase the catalytic utility of these iridium chlorocarbene systems.[46] While many of the catalyst systems discussed thus far have targeted aryl-selective labelling through exploitation of a directing group, the application of the chlorocarbene type catalysts to aryl aldehydes exhibits a very different mode of reactivity. Instead of activating the aryl C—H bonds in close proximity to the aldehyde functionality, it is, in fact, the formyl position which is preferentially activated, and thus labelled, *via* these neutral catalyst systems. Initially, the catalyst system was refined in order to tune the selectivity of this process, resulting in complex **78**. The substrate scope was next explored, which is highlighted in **Scheme 1.31**. The novel catalyst system exhibits remarkable selectivity for the formyl position, with excellent levels of deuterium being incorporated into benzaldehyde **79a**. Both electron-donating substituents (**79b**) and electron-withdrawing substituents (**79c**, **79d**) do little to hinder incorporation. Additionally, compound **79d** shows that the inclusion of an additional directing group does not result in a change in regioselectivity, as no labelling is observed through the nitro group. Substituents in the 3-position (**79e**-**79g**), and a naphthyl motif (**79h**) were also tolerated.

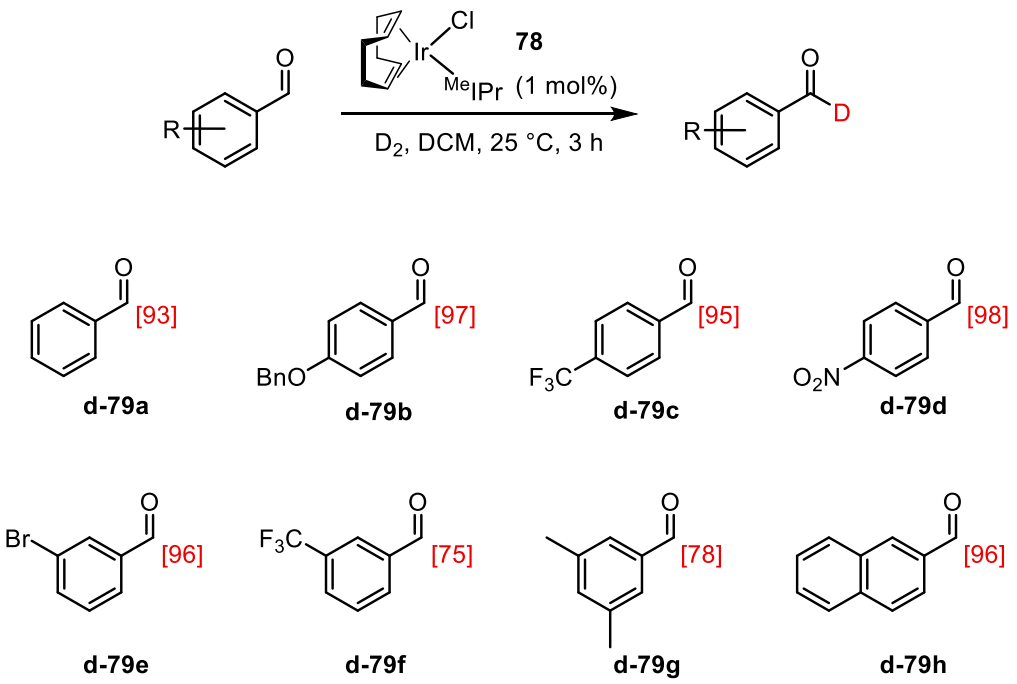

Scheme 1.31

In order to explain this change in reactivity, an alternate mechanism was proposed, supported by DFT calculations. Unlike the very bulky NHC/phosphine combination, the catalytically active iridium(III) deuteride species derived from the chlorocarbene precursor can adopt a conformation with the ligands in a *cis* configuration (**Scheme 1.32**). This configuration allows rapid activation of the formyl position, to give an iridium(V) complex, which can rearrange such that a deuteride ligand is *cis* to the activated substrate. Once again, C—D bond formation and substrate turn over will release the formyl-labelled substrate.

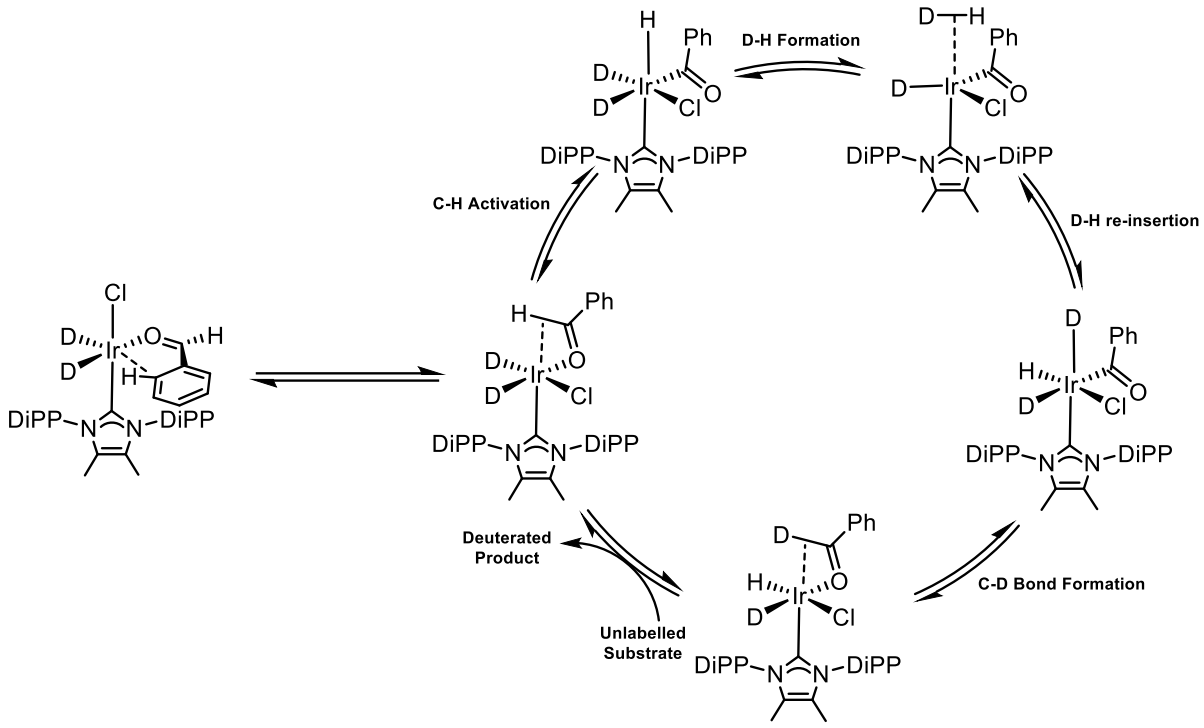

Scheme 1.32

Returning to the applications of the NHC/phosphine type catalysts, the Kerr group next showed the highly efficient, directed labelling of indole and pyrrole heterocycles (**Scheme 1.33**).[47] Utilising an acetyl directing group on the nitrogen of the heterocycle, it was shown that pyrrole **80** could be labelled to high levels. Additionally, when the directing group was changed to a benzoyl, in example **81**, good levels of selectivity for the pyrrole ring were observed. The introduction of a formyl group on the pyrrole ring in **82** did not alter the regioselectivity of the labelling. Unfortunately, however, moving to a carbamate directing group did not allow for useful levels of incorporation. *N*-Acetyl indole **84** could also be labelled to excellent levels, with no incorporation observed at the C7 position. Interestingly, the use of a directing group on the C3 position, in example **85**, also allows for outstanding levels of incorporation at C2, with minimal incorporation on both methyl groups of the Weinreb amide. Other sp^2 nitrogen centres are tolerated, as shown in 4-azaindole **86**. The indole motif also showed better levels of selectivity in the case of a benzoyl directing group in **87**. Finally, the group also showcased

the ability to remove the directing group in a facile manner, affording a sample of C2 deuterated free indole **d-88**.

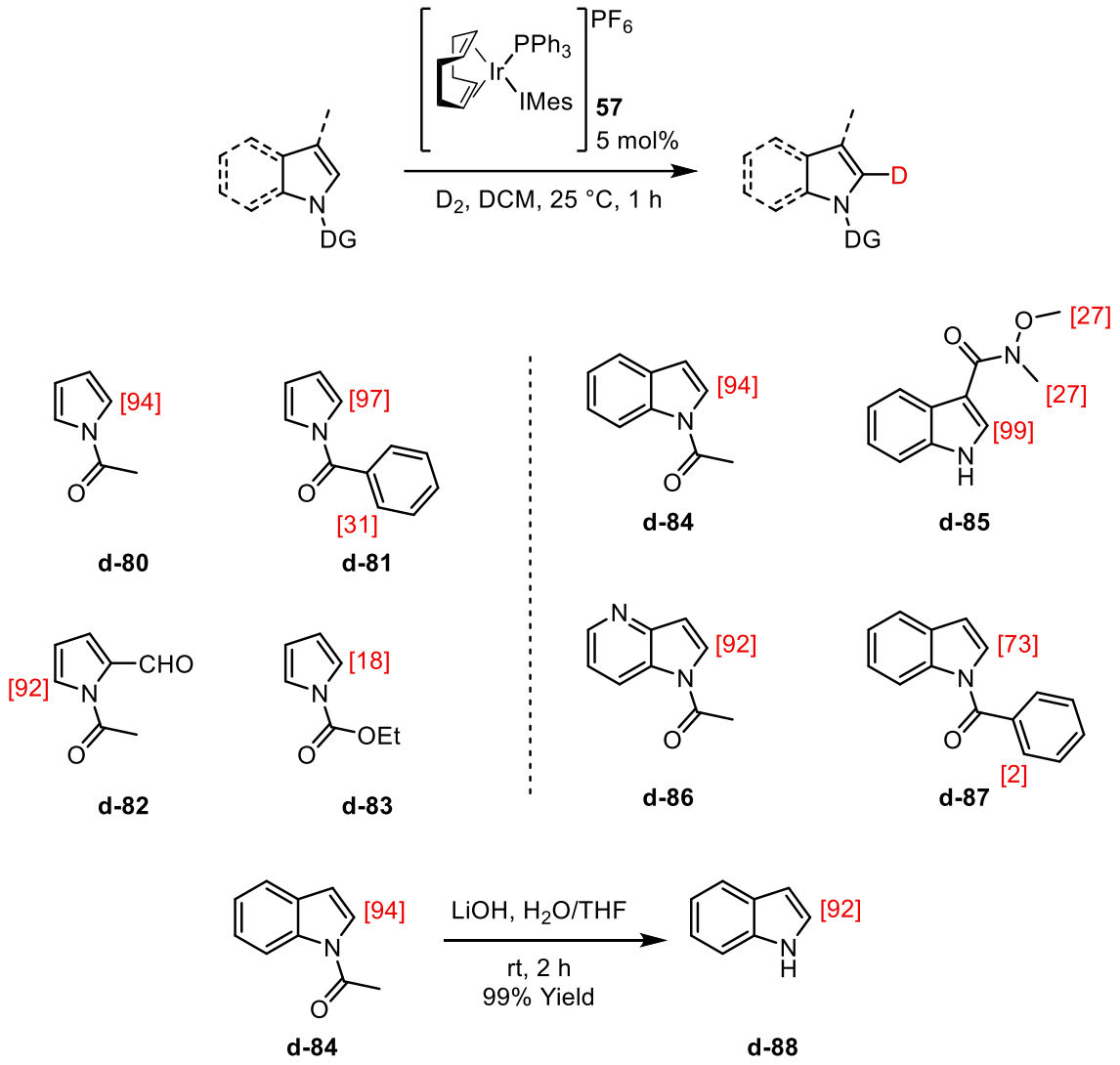

Scheme 1.33

With significant advancement in the area of aryl HIE having been accomplished, the group next turned its attention to the activation of C_{sp3}—H bonds.[48] In addition to the ubiquitous nature of C_{sp3}—H bonds in pharmaceuticals and bioactive natural products, the ability to activate such bonds as a means of functionalisation is highly sought after. As such, studies into the activation of these bonds from a HIE standpoint could provide highly valuable data in following investigations into C—H functionalisation. Pleasingly, when the highly active

[Ir(COD)(PPh_3)IMes]BAr_F **75** was applied to the labelling of a series of molecules, it was found that many of the systems could be activated and labelled to high levels of incorporation under very mild conditions and low catalyst loading (conditions A). Some of the more challenging examples did require a slight increase in catalyst loading and reaction time, but were successfully activated under comparatively mild conditions, nonetheless (conditions B). A sample of the compounds labelled in this study is shown in Scheme **1.34**. A range of cyclic substrates (morpholine **89**, piperidine **90**, and piperazine **91**) could be accessed, labelling to excellent levels. It was also shown in each of these cases that a range of heterocyclic directing groups could be utilized, even the smaller five-membered thiazole directing group in **92**. The size of the ring system being labelled had a strong effect on the levels of incorporation, but both seven- and five-membered rings (**93** and **94**) could be accessed. Lamentably, the four-membered azepane ring **95** proved too challenging, at this stage, exhibiting only 9% deuterium incorporation. It was also shown that acyclic substrates were also applicable to this process, as shown in example **96**. Finally, the group showcased the utility of this process by targeting three active pharmaceutical ingredients, mirtazapine, caffeine, and azaperone. All of these examples were labelled to >90% incorporation under very mild reaction conditions.

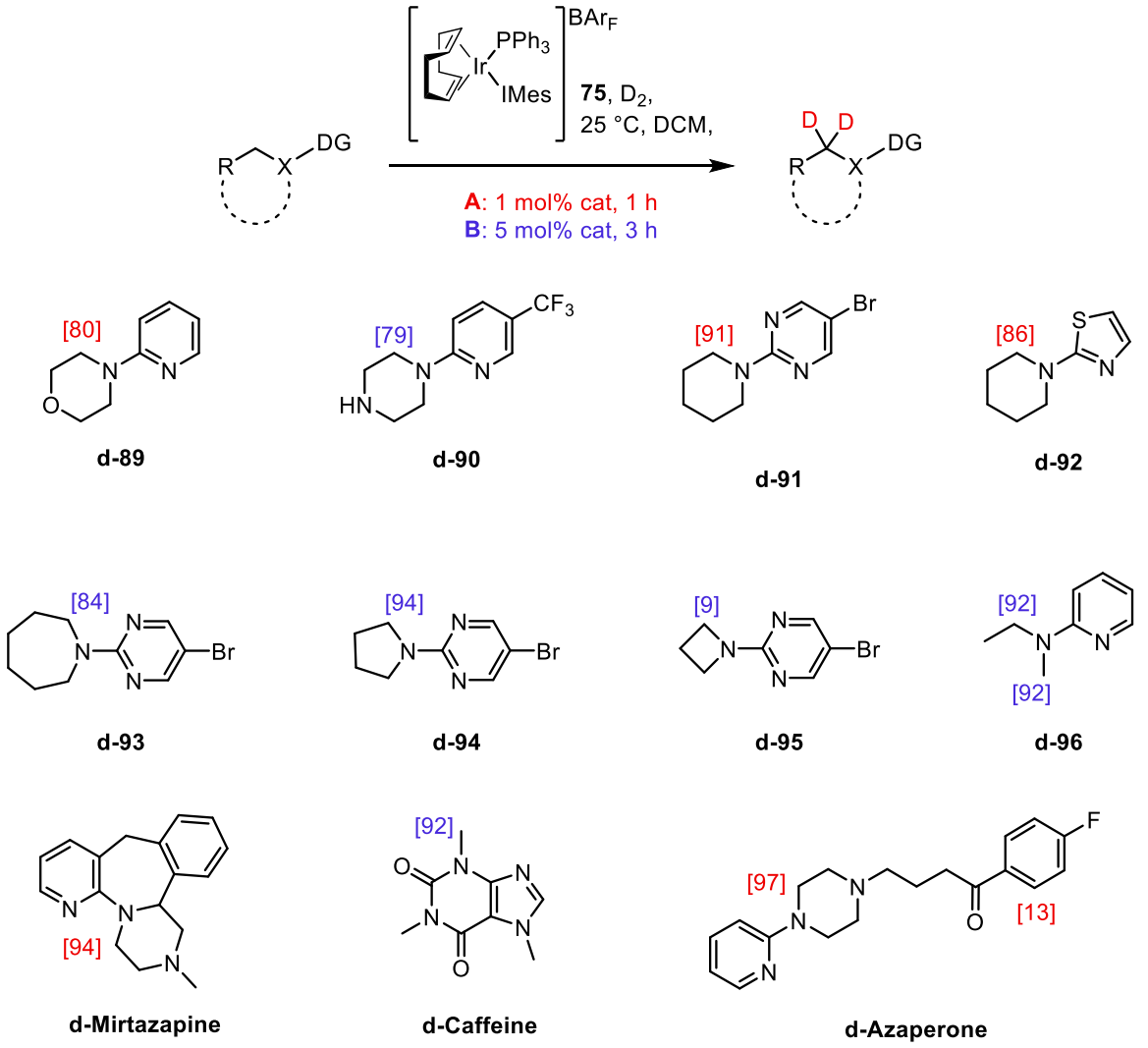

Scheme 1.34

Furthermore, it has been shown that the same catalyst system is proficient in labelling aliphatic amide structures, lending themselves to the generation of labelled amino acid and peptide structures (**Scheme 1.35**). [49] The challenging nature of these particular substrates required more forcing conditions, however, with a change in solvent to *iso*-propyl acetate at close to refluxing temperatures. When a single secondary centre is present, such as in protected glycine **97**, excellent levels of incorporation are observed. However, placing a relatively small substituent at this position, e.g. in protected alanine **98**, has a significant effect on the incorporation. Making this substituent any larger, for example an *iso*-propyl group in **99**, prevents any observable incorporation. It was also noted that disulfide structures were well tolerated, giving

high levels of deuterium incorporation, **100**. When multiple residues, and thus labelling positions, are present, it would appear that there are many factors which determine selectivity, and the extent to which selectivity is observed. Generally speaking, any secondary centres will be labelled over tertiary, but determining the selectivity between secondary centres within the same molecule remains challenging with the data at hand. Regardless, it was shown in this study that di-, tri- and even tetrapeptide structures could be labelled to excellent levels. It was also shown that the labelling is a stereoretentive process, and does not disturb the native chirality of the molecule.

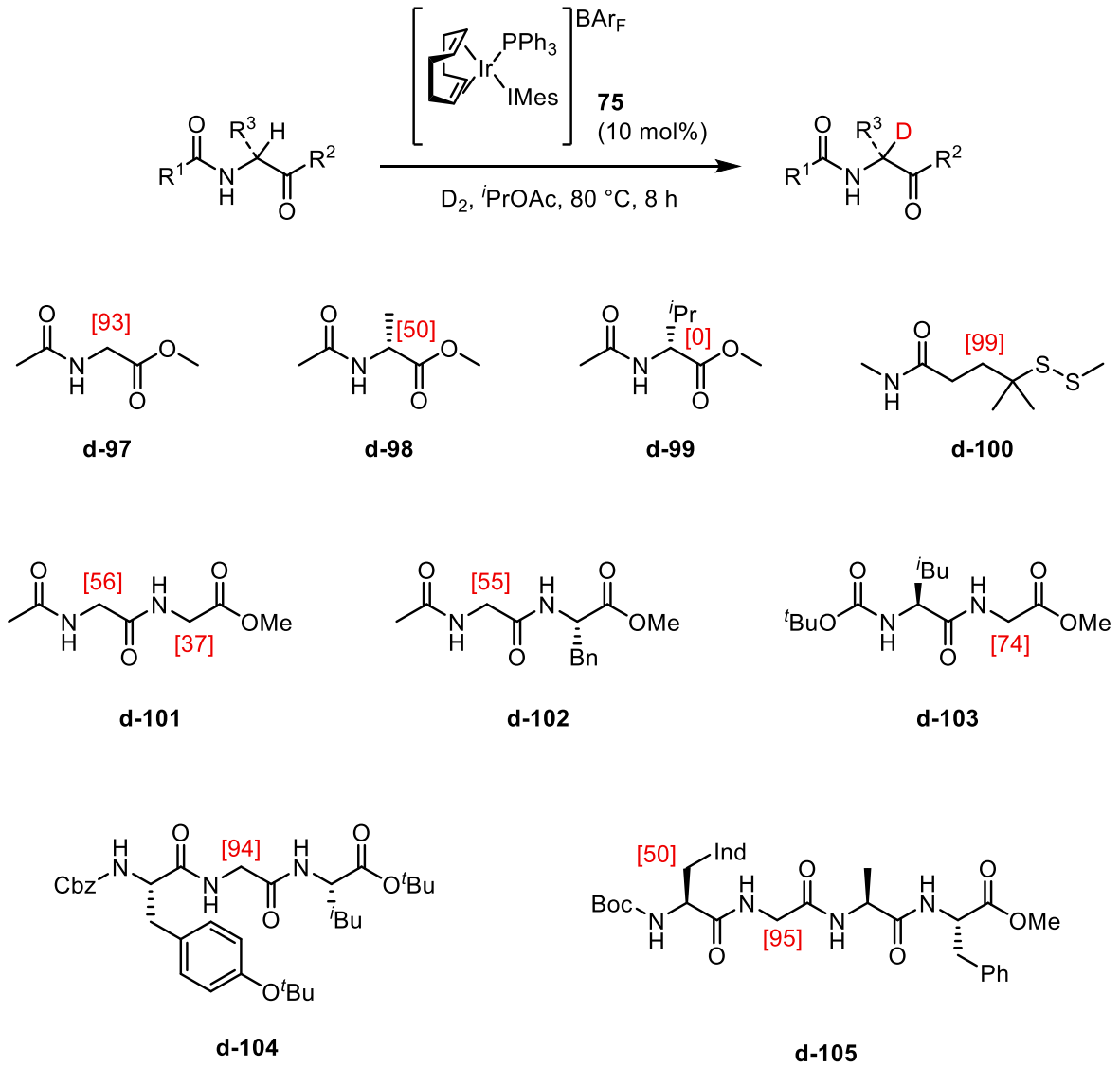

Scheme 1.35

1.6 Development of Chelated Catalyst Systems

More recently, many groups have also begun to focus on the development of iridium catalysts for hydrogen isotope exchange. As seen with Crabtree's catalyst, iridium complexes originally intended for hydrogenation are often also useful as catalysts for HIE. As such, many of the complexes more recently applied to HIE have their origins in hydrogenation, resulting in a trend towards the development of chelated exchange catalysts. The first notable example of a chelated hydrogenation catalyst being applied to HIE with the intention of improving upon Crabtree's system is the *P,N*-ligated catalysts developed by Pfaltz (**Scheme 1.36**). [50] With iridium-catalysed alkene hydrogenation being a highly developed area, a vast number of complexes were available for their catalyst screening, with a total of 15 catalyst systems being tested in total. Of this screen, the majority of catalyst systems were shown to be catalytically active in the HIE of relatively simple substrates, such as acetophenone. However, when applied to more challenging substrates, it was shown that complex **106** was the most active across a range of substrate classes. Generally, good levels of incorporation were observed across the board. It was noted that sulfone **108** could be labelled to a moderate level with complex **106**, but an alternate catalyst system was highlighted within the same paper which gave significantly higher levels of incorporation. Additionally, secondary sulfonamide substrate **109** could also be labelled, however, quite harsh reaction conditions were required in this case.

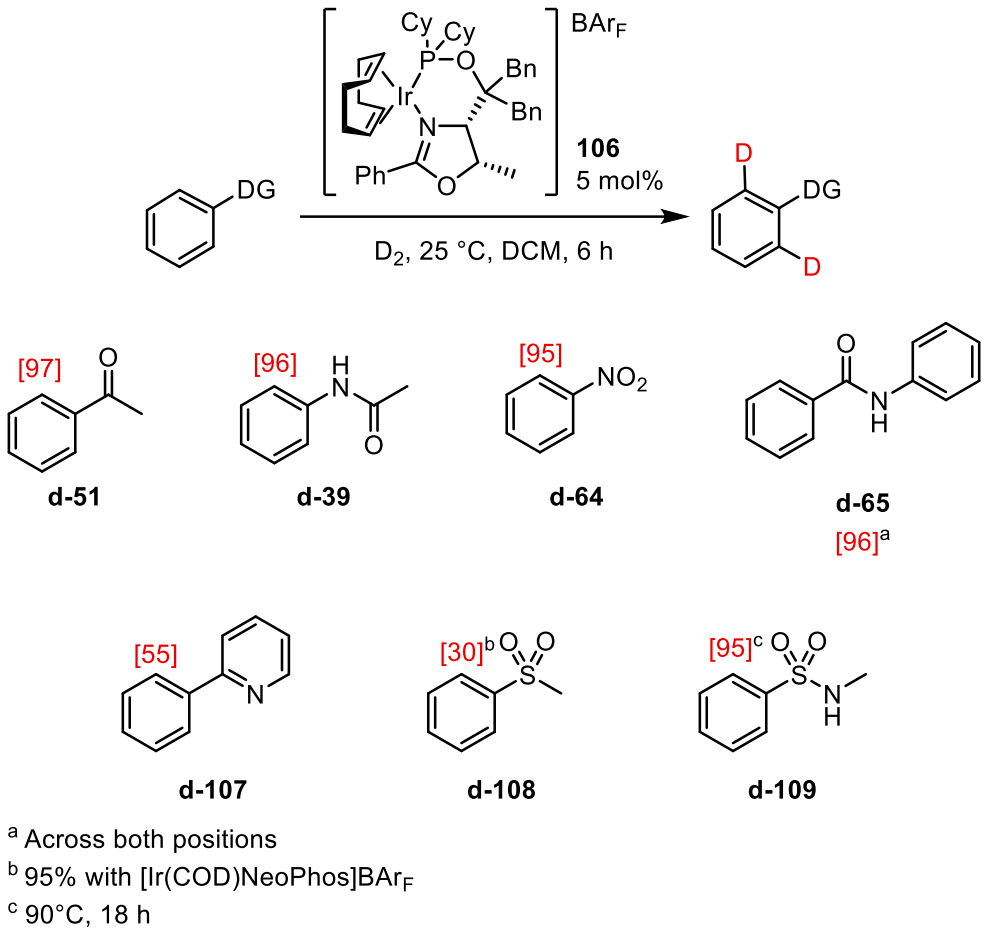

^{a} Across both positions
^{b} 95% with [Ir(COD)NeoPhos]BAr$_F$
^{c} 90°C, 18 h

Scheme 1.36

Given that complex **106** is normally applied to asymmetric hydrogenation, the ligand contains stereogenic centres to enable this, which are unnecessary when considering C—H activation of a planar aryl ring. As such, an achiral variant of this complex (**110**) was synthesised and also applied to a range of substrates under the previously optimised conditions, showing very similar levels of incorporation in most cases (**Scheme 1.37**).

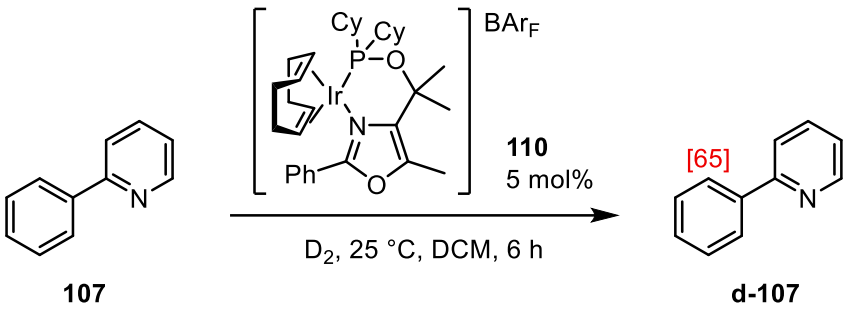

Scheme 1.37

Highly substituted sulfonamides are desirable targets for HIE processes. While primary sulfonamides have been labelled in an effective manner utilising the chlorocarbene motif developed by the Kerr group, substitution on the sulfonamide nitrogen still proves highly challenging.[45] In an attempt to address this, other groups have applied the chlorocarbene type complex, albeit an unoptimized variant, as well as the chelating NHC-oxazole system, known as the Burgess catalyst **111**, under harsh conditions to facilitate the labelling of hindered sulfonamides (**Scheme 1.38**).[51,52] Considering the incorporations delivered by chlorocarbene complex **56**, moderate to good levels of incorporation were observed across the series, with *N*-methylbenzene sulfonamide **109** matching the levels of isotope incorporation obtained using the Pfaltz system at 90 °C. Additionally, the larger *N*-phenyl substituent in example **112** was also well tolerated, delivering similar levels of deuteration. Unfortunately, no incorporation was observed in *N*-mesylaniline **113**. The tertiary amine in **114** also did not appear to hinder the observed incorporation, and both positions of the naphthyl ring in example **115** were labelled to high levels. Interestingly, while the ester motif in **116** was well tolerated, a small but significant amount of labelling on the methyl group of the ester was also observed. Finally, the indole motif in **117** was also well tolerated, with both the C2 and C3 positions of the indole ring being labelled to good levels. Moving on to discuss the performance of the Burgess system in the labelling of substituted sulfonamides, generally lower levels of incorporation were observed across the series, albeit under more mild conditions and at a lower catalyst loading.

N-Phenyl sulfonamide **112**, for example, exhibited only moderate levels of incorporation, compared to that delivered by chlorocarbene complex **56**. Additionally, the positions of the naphthyl ring in **115** showed a higher degree of selectivity, with the *peri*-position being labelled to only 13%, as well as a lower incorporation of 76% at the *ortho*-position. Interestingly, ester **116** was not tolerated, possibly due to strong chelation of the substrate to the more open, cationic catalyst sphere. While indole **117** was labelled by the Burgess system, only low levels were observed at the C2 (15%) and C3 (20%) positions. Interestingly, there was no deuterium delivered through a 6-mmi in either example **112** or **113**, highlighting the challenge of accessing such an intermediate with these directing groups.

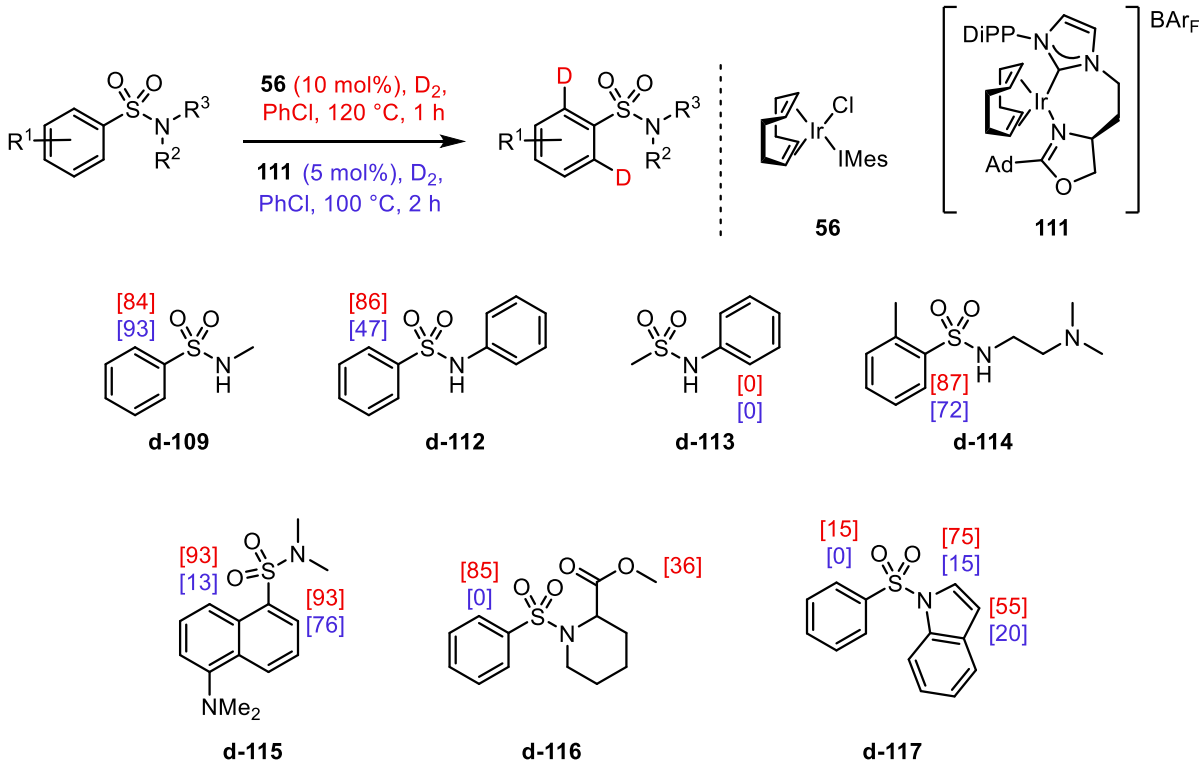

Scheme 1.38

With substrate scope established for this process, the group next moved on to use the chlorocarbene complex to produce a sample of tritiated Glibenclamide, a treatment for diabetes (**Scheme 1.39**).

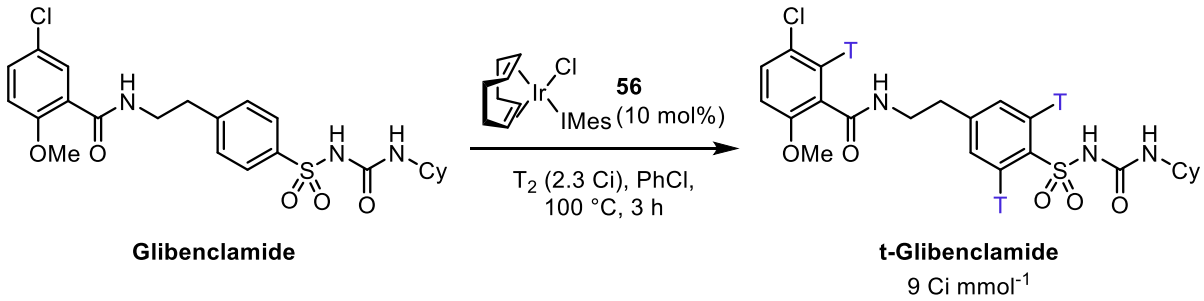

Glibenclamide **t-Glibenclamide**

9 Ci mmol^{-1}

Scheme 1.39

Following on from this, the utility of the Burgess catalyst system as a more general catalyst for HIE was also investigated. [53] Generally speaking, the catalyst proved competent in labelling a series of common functional groups, albeit at 10 mol%. Aldehydes, amides (5 and 6 mmi directing), pyridines, and a nitro group are all shown in **Scheme 1.40**, being labelled from good to excellent levels. Interestingly, sulfur-based directing groups, in **119** and in **69**, have also been shown to label to moderate levels.

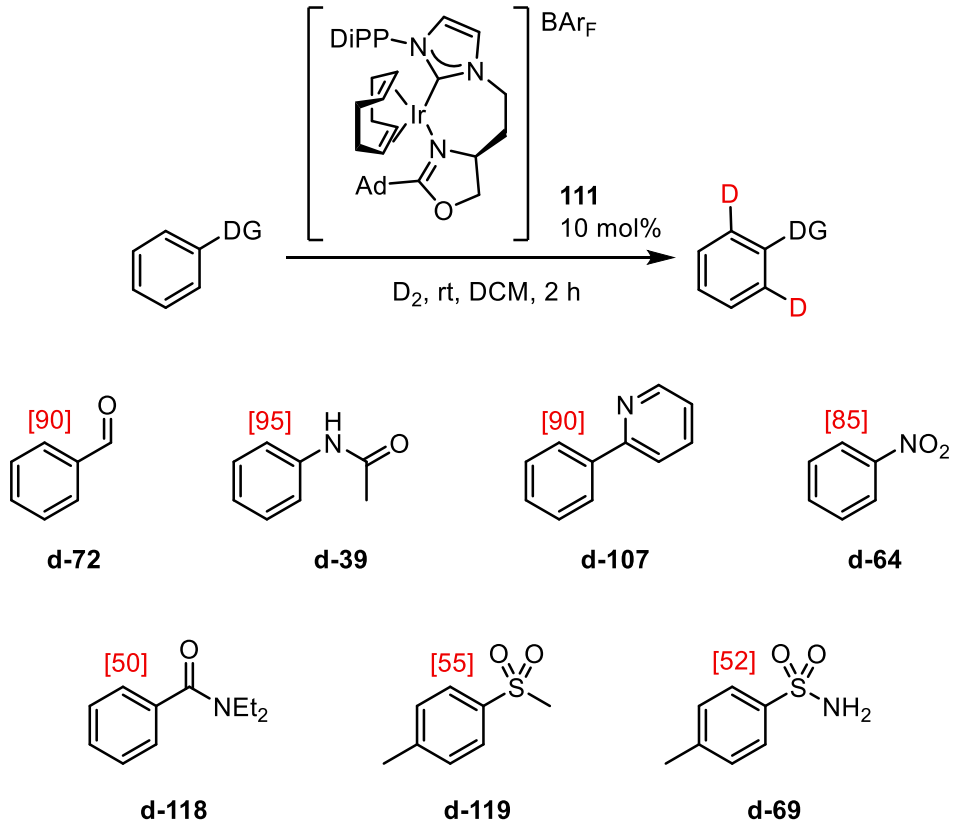

Scheme 1.40

The next notable catalyst motif for HIE is the highly electron rich *P,N*-complexes developed by the Tamm group.[54] This ligand set facilitated the labelling of a wide range of directing groups to high levels, as shown in **Scheme 1.41**. While ketones, heterocycles, and esters (**121**, **107**, and **122**, respectively) were shown to be suitable directing groups for this system, the most noteworthy results were of those which were able to use the Boc protecting group to direct labelling into the aryl rings of anilines (such as **123**) or heterocycles (**124**). The significant steric bulk of this group would usually render its use very challenging. However, the chelated system allows for excellent levels of incorporation under mild conditions. Of final note, is the observed labelling adjacent to methoxy groups, such as in **126**. When placed under more forcing conditions, and in the absence of other suitable directing groups, it appears that these aryl ethers can also facilitate the incorporation of deuterium. This, presumably, occurs through a different mechanism to the classical directed C—H activation mechanism; however no mechanistic proposals or investigations have been published at this point.

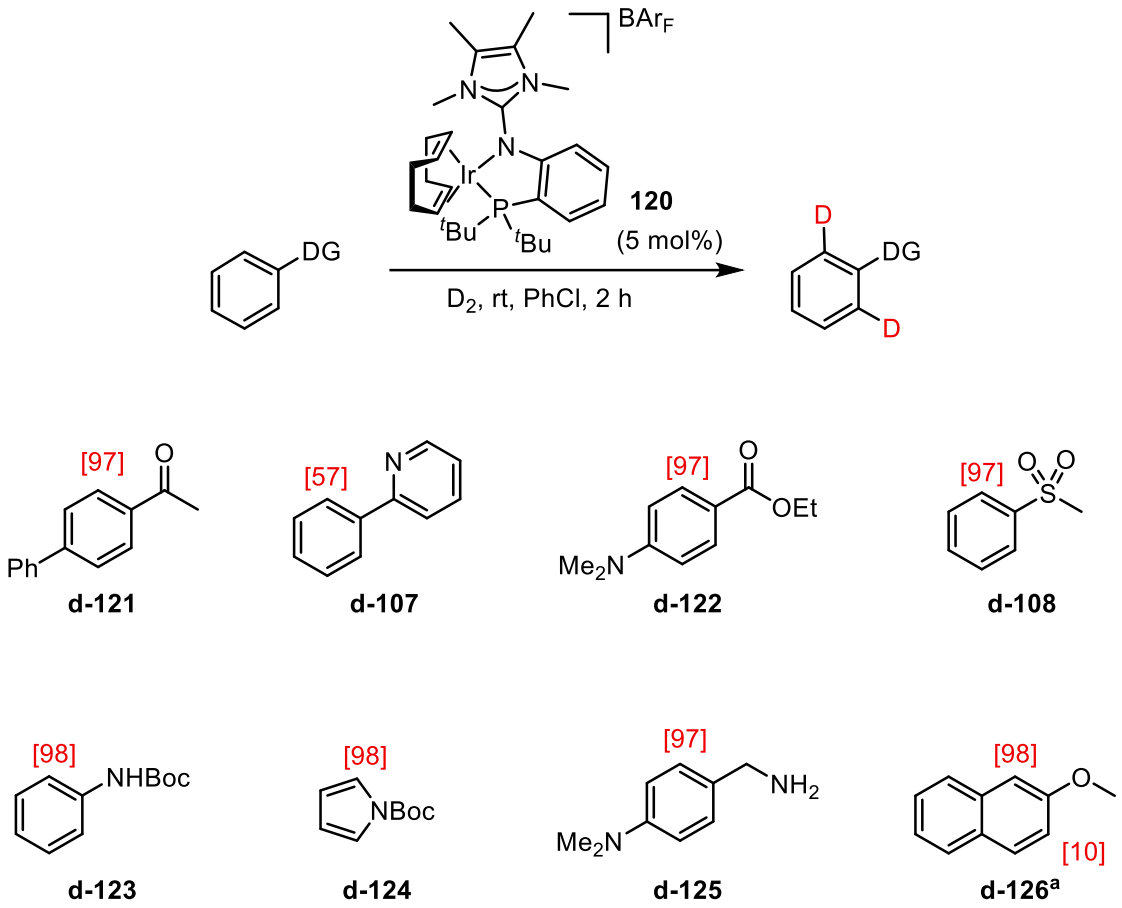

Scheme 1.41

Following on from this, the group also established the ability of the same catalyst system to label highly hindered sulfonamides, *N*-oxides and phosphonamides (**Scheme 1.42**).[55] Unlike the previous attempts to label hindered sulfonamides with complexes **56**, **106**, and **111**, the Tamm catalyst afforded high levels of incorporation into *N*-substituted and *N*,*N*-disubstituted sulfonamides under very mild conditions and low levels of catalyst loading. Additionally, excellent levels of incorporation were observed for the labelling of quinoline *N*-oxide derivative **129**, isoquinoline *N*-oxide **130**, and 4-methylpyridine *N*-oxide **131**. Finally, it was also shown that a range of substituents were tolerated in the labelling of phosphonamide, as shown in **132-134**.

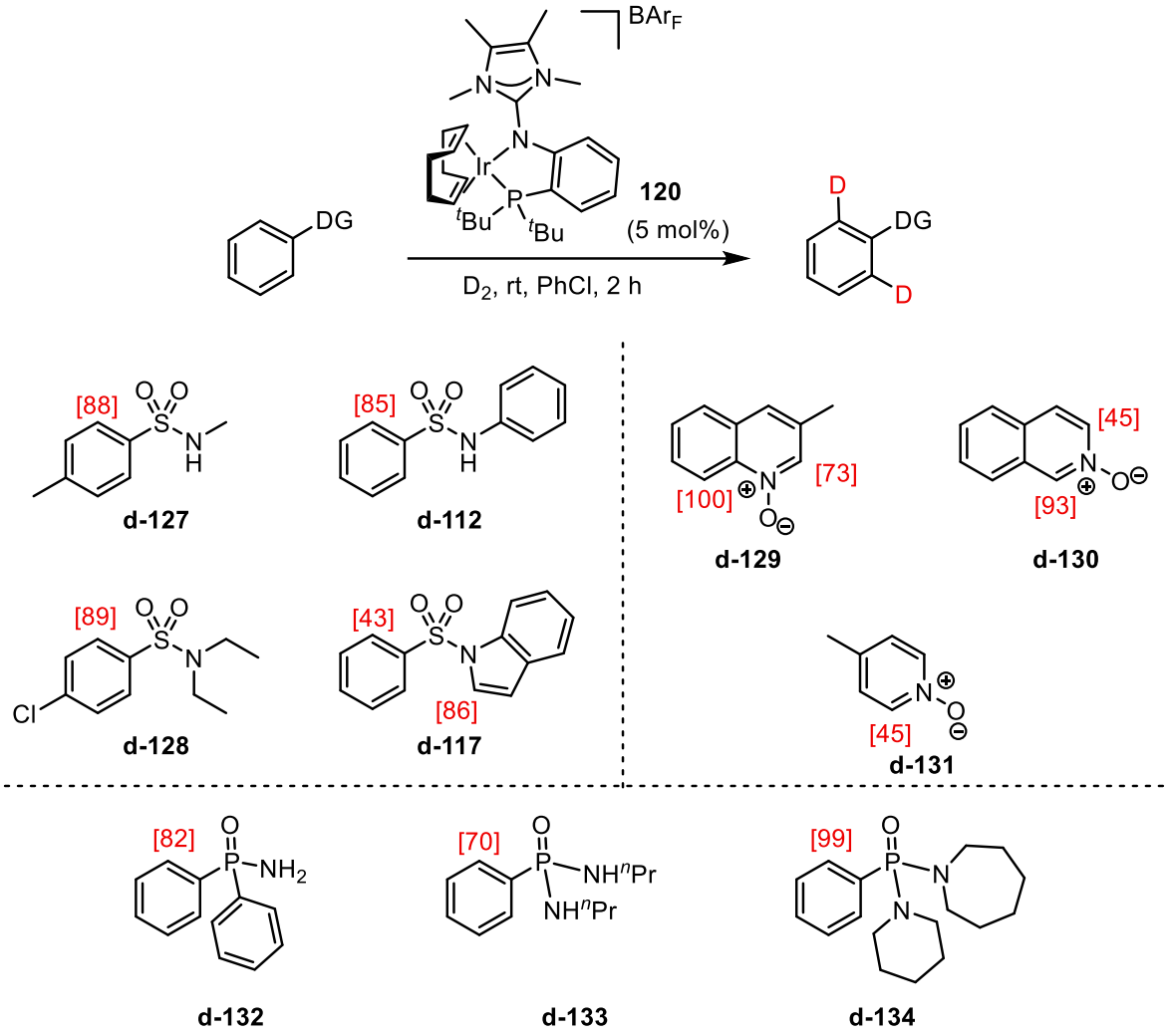

Scheme 1.42

It is clear from these recent examples that the development of iridium catalysts for HIE is progressing at an astounding rate. However, in order to further expand the utility lent by these catalysts, beyond the screening of complexes optimised for other processes, thorough knowledge of the catalyst system is required. Most notably, understanding of ligand effects and characteristics is a necessity, in order to effectively design and optimise a catalytic system. The following sections provide overviews on the use of phosphine and NHC ligands, as well as combining these ligand motifs.

1.7 Phosphine Ligands

Phosphine ligands have long been ubiquitous within organometallic chemistry, with the electronic and steric parameters of the ligand having a dramatic effect on the properties of a complex as well as its mode of catalysis.

With regards to electronic characterisation, phosphines are generally strong σ-donors, binding to the metal through the lone pair on phosphorus. However, phosphines also exhibit significant back donation from the metal centre into the σ* orbital of the P—R bond (**Figure 1.2**).[56]

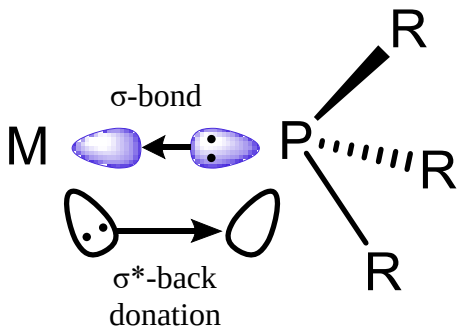

Figure 1.2

Consideration of such orbital interactions is particularly important when utilising phosphines in a complex, as the nature of the R groups can dictate the relative amount of σ-bonding and back donation exhibited by the ligand. In 1970, Tolman used nickel carbonyl complexes to parameterize the electronic impact of various phosphine ligands through the A_1 carbonyl stretching frequency.[57] Substituting $[Ni(CO)_4]$ with a phosphine ligand, to produce complexes of the form $[Ni(CO)_3L]$, results in a change of the electron density at the metal centre and therefore the back donation to the π* of the carbonyl ligands. **Table 1.1** gives examples of some common phosphine ligands, with the lowest frequency values corresponding to the most electron-rich ligands. This stretching frequency, termed the Tolman electronic parameter (TEP) has been measured for a number of phosphine ligands, allowing novel ligands to be compared in terms of their electron donating ability. As the bond strength between the carbon and oxygen

is varied, the change in stretching frequency, υ(CO), can be measured using infrared (IR) spectroscopy. This provides a reliable method for parameterizing the σ-donating nature of the phosphine ligand and has since been used as a standard method of ligand characterisation.

Table 1.1

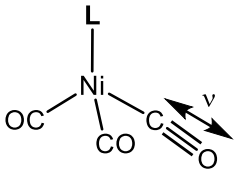

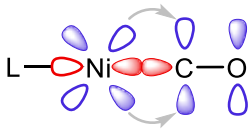

Entry	Phosphine	ν_{CO} (cm^{-1})
1	**P^tBu_3**	**2051.6**
2	**P^iPr_3**	**2059.2**
3	**PMe_3**	**2064.1**
4	**PPh_3**	**2068.9**
5	**$P(O^iPr)_3$**	**2075.9**
6	**$P(OPh)_3$**	**2085.3**

In order to investigate the steric influence of phosphine ligands, Tolman introduced the concept of the cone angle, θ (**Scheme 1.43**).[58] The phosphine substituents are "folded back" away from the metal and a cone is drawn from the vector projecting from the centre of the metal to the edge of the ligand. The angle between the centre of this cone and the edge is denoted θ.

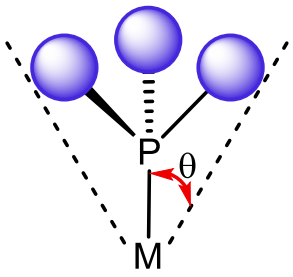

Scheme 1.43

Again, nickel carbonyl complexes were used in the validation of this method, wherein substitution with various phosphines with an increasing range of cone angles resulting in a reduced degree of substitution at the metal centre. For example, when the relatively small trimethyl phosphite was used, up to three phosphine ligands could be bound to the metal centre. However, when triphenylphosphine was used, with a cone angle of 145°, only two phosphine ligands were observed (**Table 1.2**). It should be noted, however, that while this parameter works well for most phosphines, it is a static value which does not account for flexibility within a ligand. For instance, tribenzylphosphine and ethyl di-*tert*-butyl phosphine may have the same cone angle, but the flexibility of the benzyl group, relative to the bulky *tert*-butyl, results in a very different steric environment.[59]

Table 1.2

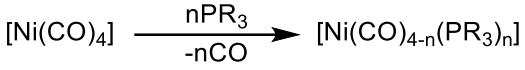

Entry	Ligand	Cone Angle (θ)	Degree of Substitution
1	$P(OMe)_3$	107	3.0
2	PMe_3	118	2.4
3	PPh_3	145	2.0
4	$P(Cy)_3$	179	1.5

The ability to simultaneously control both the steric and electronic parameters is extremely beneficial when designing a catalyst, with subtle changes likely having a drastic effect on the catalyst activity. For example, while tri-*iso*-propyl phosphite ($P(O^iPr)_3$ and tributylphosphine (P^nBu_3) have similar cone angles, the heteroatoms of $P(O^iPr)_3$ result in a ligand which imparts a very different electronic state to the metal centre.

1.8 NHC Ligands

Prior to the early 1990s, free *N*-heterocyclic carbenes (NHCs), i.e. those which were not coordinated to a metal centre, were considered too reactive and unstable to be isolated and unambiguously characterised. However, 1991 saw the first synthesis and isolation of the relatively stable NHC, 1,3-bisadamantylimidazole-2-ylidene (IAd) by Arduengo, *via* deprotonation of the corresponding imidazolium salt.[60] In the relatively short time since the initial isolation of IAd, the number of publications utilising NHCs as ligands in transition metal complexes has increased dramatically.

The carbene structure itself consists of a lone pair of electrons on carbon, which can exist either in the triplet state or relatively more stable singlet state (**Scheme 1.44**).

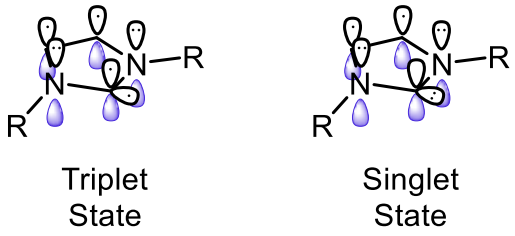

Scheme 1.44

In the triplet state, both electrons remain unpaired, residing in orthogonal p-orbitals on the carbenic carbon. In the singlet state, however, the electrons are paired in a single sp^2-orbital, leaving an orbital free, into which the adjacent heteroatoms can donate, stabilising the structure. A mixture of steric and electronic factors affects the stability of an NHC, as highlighted in **Figure 1.3**. The unsaturated backbone in IAd imparts aromaticity to the structure and has a stabilising effect, however this is not a necessity when synthesising a persistent carbene. The *N*-substituents play an especially large role in the stabilisation of the carbene, as well as tuning the electronic nature of the carbene. The cyclic nature is also important; the cyclic structure

favours the bent singlet state, whereas the ring size can push the *N*-substituents towards the carbenic carbon, further enhancing their effective stabilisation.

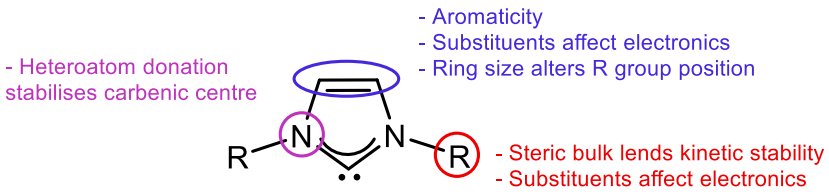

Figure 1.3

The use of NHCs as ligands in transition metal catalysis has been likened to phosphines and, indeed, there are significant similarities between the two ligand classes. As with the phosphine ligands, many attempts have been made to parameterize the various aspects of NHC binding.

In a similar manner to Tolman's study, Nolan used a set of [IrCl(CO)$_2$NHC] complexes to investigate the electronic character through the stretching frequency of the carbonyl ligands (**Table 1.3**).[61] It was discovered that the most poorly donating NHC imparted more electron density onto the metal centre than the most strongly donating phosphine. This was rationalised by the fact that NHCs are incredibly strong σ-donors. This, coupled with the fact that most NHCs exhibit a smaller amount of back-bonding (due to the nitrogen atom's ability to donate into the free p-orbital), means that the NHCs can push a higher amount of electron density onto the metal to which they are coordinated.

Table 1.3

Entry	Ligand	TEP (cm^{-1})
1	PPh_3	2068.9
2	PEt_3	2061.7
3	PCy_3	2056.4
4	IPr	2051.5
5	IMes	2050.7
6	IAd	2049.5

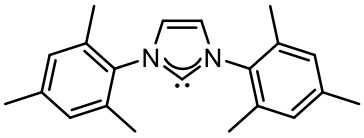

IMes
135

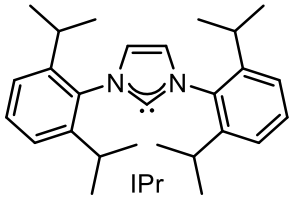

IPr
136

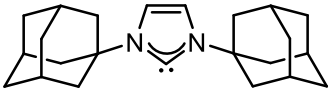

IAd
137

There have been criticisms in the use of the TEP for the characterisation of NHC ligands, however.[62] Most notable of these, is the fact that, while phosphine ligands give a good range of values for the TEP (typically ~30 cm^{-1}), NHC complexes will generally be restricted to a very tight range of ~10 cm^{-1} (**Scheme 1.45**). This unfortunately makes the technique less diagnostic for NHCs, as several changes to the structure of the ligand will result in only very minor changes, or indeed no change, to the TEP value measured. A second criticism is that the values measured are highly sensitive to the conditions in which the stretching frequencies are measured, leading to risk for introduction of error, and limiting the ability to compare results in a valid fashion. Unfortunately, this has led to several differing values being published for the same NHC, seemingly using the same method, as highlighted for SIMes **144** and 6-Mes **145** in **Scheme 1.38**.[63]

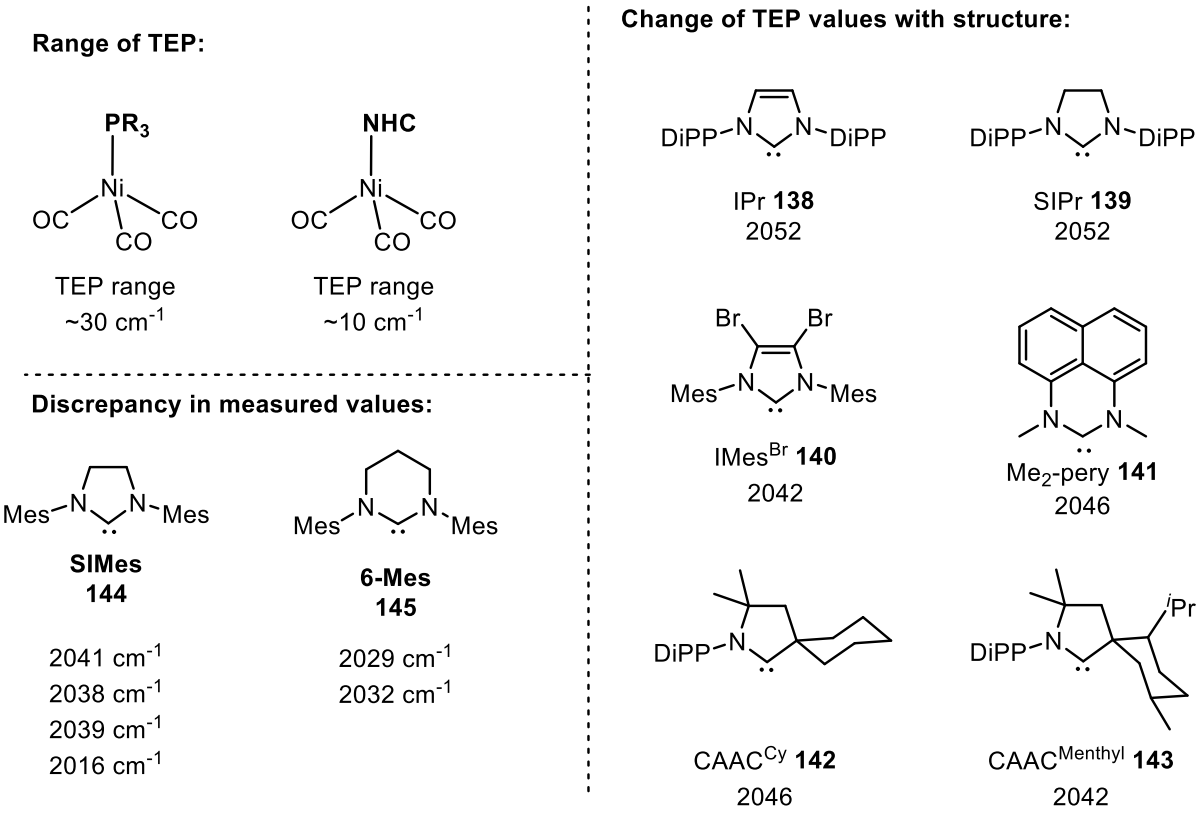

Scheme 1.45

In order to address these issues, the development of a more reliable method for the electronic quantification of NHCs has been the focus of many research groups. One of the most notable methods which has been unveiled in recent years is Huynh's electronic parameter (HEP).[64,65] This technique requires the formation of stable palladium(II) bis-NHC complexes, as shown in **Scheme 1.46**. One of these ligands, $^{i}Pr_2$-bimy **146**, is termed the reporter ligand, and it is the carbenic shift of this ligand in the ^{13}C NMR spectrum which is used to parameterize the electronic character of the NHC being investigated. The carbenic shift of an NHC is inversely proportional to the singlet-triplet gap. The transition of an electron from the σ-orbital to the unoccupied p-orbital has the strongest contribution to the paramagnetic shielding parameter, which in turn leads to a downfield shift. The binding of an NHC ligand to a metal centre reduces the probability of this transition, and thus results in a more upfield shift. If we now consider the *trans*-influence from the ligand being investigated, stronger donation from this ligand will

weaken the Pd—^{i}Pr$_2$-bimy bond, and thus return more "free NHC" character to the ^{i}Pr$_2$-bimy ligand, resulting in a more downfield shift. This process therefore allows for the relative parameterization of NHC ligands, provided they can form stable complexes with palladium(II) species.

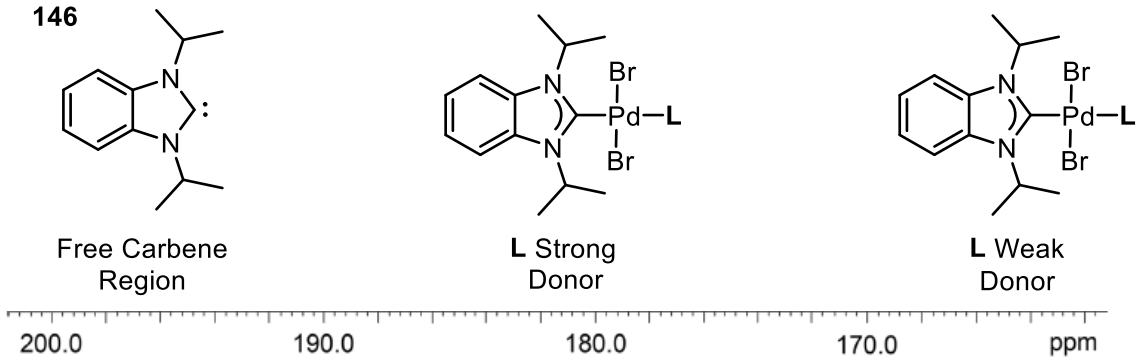

Scheme 1.46

Scheme 1.47 below shows some examples of HEP for several NHCs. It shows the significant changes in this parameter that are made with changing various aspects of the ligand. For instance, structures **147**-**150** show how the hybridisation of the backbone, as well as aromaticity and presence of a heteroatom, affects the HEP. Additionally, the substituents of the nitrogen atoms also have significant influence over the electronic character of the ligand, as shown with varying substitution from benzyl to mesityl groups in **151**, **152** and **135**. Finally, even subtle effects from very remote substitution can also be seen through this method, as shown in **153**-**155**. Indeed, there are several advantages this method brings to the process of electronic parameterization. Notably, the use of ^{13}C NMR spectroscopy means that the signals produced are sharp, cover a wide shift range, and can be easily referenced for reproducibility. Secondly, the accuracy of ^{13}C peaks is much greater than that of IR signals, generally ~0.02 ppm. Thus, subtle changes in shift (~0.1 ppm, or five times the standard deviation) can be taken as meaningful. [66]

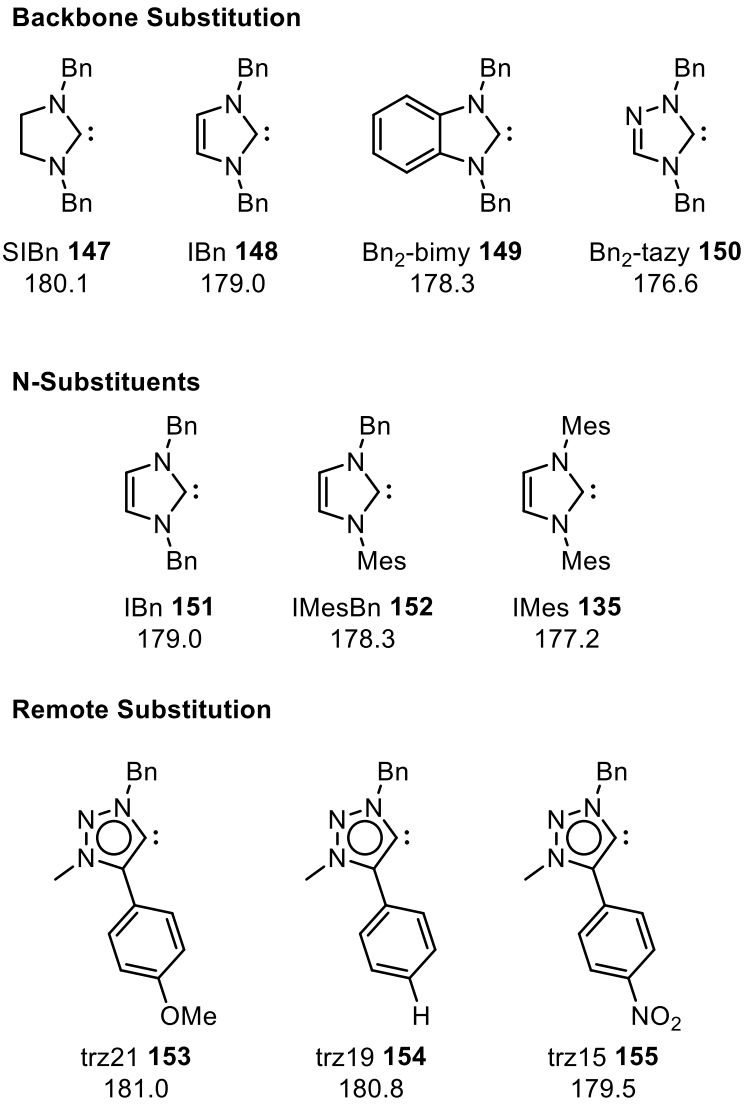

Scheme 1.47

A final note on the HEP, while TEP measurements use metal (nickel, rhodium, and iridium) carbonyl complexes which are prone for π-backbonding, this method makes use of much more electronegative palladium, which is much less prone to back donation, particularly so in the +2-oxidation state. As such, this method generally gives a good indication of σ-donation ability.

With this in mind, Ganter was able to utilise ^{77}Se nuclear magnetic resonance (NMR) in an attempt to investigate the π-acceptor properties of an NHC.[67,68] **Scheme 1.48** depicts the proposed binding motif for the selenide adducts used. Generally speaking, NHCs which are

primarily σ-donating will have character more similar to the resonance structure on the right, and exhibit a more upfield shift. Contrasting this, NHCs with significant π-acceptor abilities will have more character of that on the left-hand side and, as a result, have a more downfield signal.

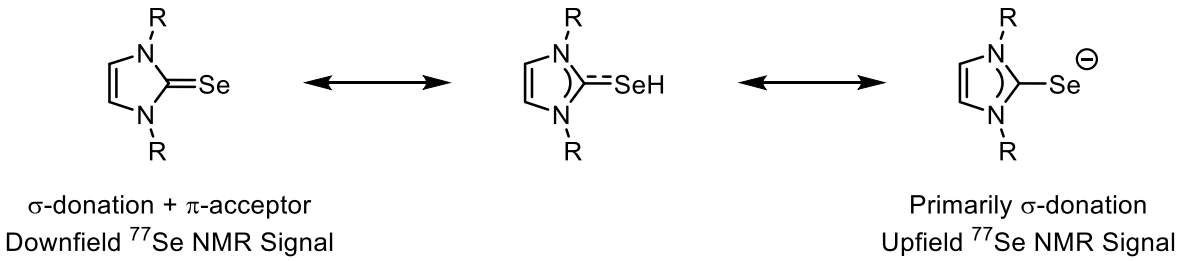

Scheme 1.48

A number of NHC-selenide adducts were synthesised using ligands which had already been thoroughly studied in the literature. Selenium NMR is known to encompass a range of around 800 parts per million (ppm) and is particularly sensitive. Having such a wide range is advantageous when attempting to parametrise a series, allowing for more confident assignment of the π-accepting nature. As **Scheme 1.49** shows, structures which are known to be strongly σ-donating such as IPr **156** exhibit a significantly low shift, whereas the strongly π-acidic variant, **158**, has a significantly higher shift of 856 ppm.

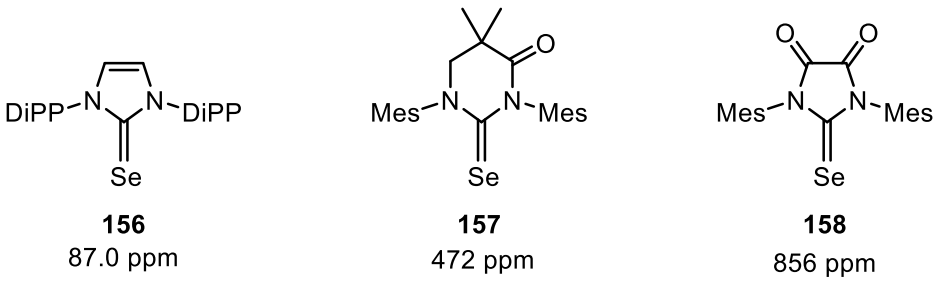

Scheme 1.49

As a final point on the use of selenourea NMR for characterisation of NHCs is that the overall shift of the adduct is inextricably tied to both the σ-donating and π-accepting properties of the

ligand, and as such cannot be used to inform about the π-acidity alone. Generally speaking, an established method that allows for the individual investigation of π-accepting ability of a ligand has not yet been achieved.

1.9 Combining Experimental and Computational methods

The very nature of reaction mechanisms presents several challenges which makes the study of a mechanism difficult, particularly in the case of homogeneous transition metal catalysed reactions. Catalytic cycles, consisting of various steps, each highly dependent on the conditions, coupled with the short-lived intermediates and catalytic species which are often difficult to detect, make unambiguous mechanistic conclusions difficult to draw. Detailed aspects of a reaction, such as solvent or additives can, if altered, give vast changes in the outcome of a reaction, serving only to add further complexity to the problem. In addition to this, many catalytic routes or competing pathways are often separated by small energy differences. It is in these instances where it may be beneficial to invoke the use of computational chemistry in order to gain insight into a system which may further understanding of the mechanism at hand.

The increase in computing power and continuous refinement of functionals that has occurred over the past four decades has allowed more complex systems to be confidently investigated using density functional theory (DFT) methods. In recent years, the use of such calculations by those investigating detailed reaction mechanisms has become somewhat of a staple, in many regards.[69] Indeed, DFT calculations have proven imperative in the development and understanding of a myriad of processes, offering insight which can strengthen or attempt to clarify the understanding gained from experimental data. While this use of computational reinforcement brings many advantages, great care must be taken when attempting to make use

of such methods, as the use of these techniques without careful consideration can be lead to highly misled conclusions.[70] Regardless, there are many who foresee the use of computational chemistry in aiding, or even leading, the rational design of novel catalyst systems for any given process. [71,72,73] Realistically, however, the current situation is that the use of computational guidance for catalyst design is, for the vast majority, rooted in previously established systems with a reservoir of mechanistic understanding behind them. Indeed, this removes a myriad of issues present at the start of such an investigation, thus accelerating the process, in that the many potential side-reactivities are less likely to require investigation, as well as giving a sensible starting position for the design process. With further development in this area, however, it is possible that this process may well become more streamlined and more accessible.

2. Previous & Proposed Work

The paradigm of rational ligand design is emerging as an incredibly powerful tool in the development of novel catalyst systems (*vide supra*). We sought to apply this approach to our current generation of catalyst systems in order to further advance their effectiveness and applicability in HIE processes. Initially, we chose to focus our efforts on facilitating the labelling of sulfur-based directing groups, specifically the aryl sulfone. At the time we embarked upon this endeavour, only a single example of an aryl sulfone being successfully labelled through iridium-catalysed directed, HIE was reported, that of the Muri and Pfaltz collaboration. [45,50] These substrates have thus proven highly challenging, and with such an unmet need for their use as labelling substrates, this appeared to be an ideal starting point for the rational design process to be applied to our catalyst systems.

Sulfones are prevalent in the pharmaceutical industry, with many commercialised drugs containing an aryl sulfone functional group. Sulfones are particularly ubiquitous in antibiotics, such as Dapsone and Dextrosulphenidiol (**Figure 2.1**). They are, however, also utilised in a range of other medicines, such as the non-steroidal anti-inflammatory Rofecoxib, or the retinoid, Sumarotene. The abundance of the sulfone functional group in the pharmaceutical industry makes the ability to exploit it as a directing group for *ortho*-directed HIE a particularly attractive goal.

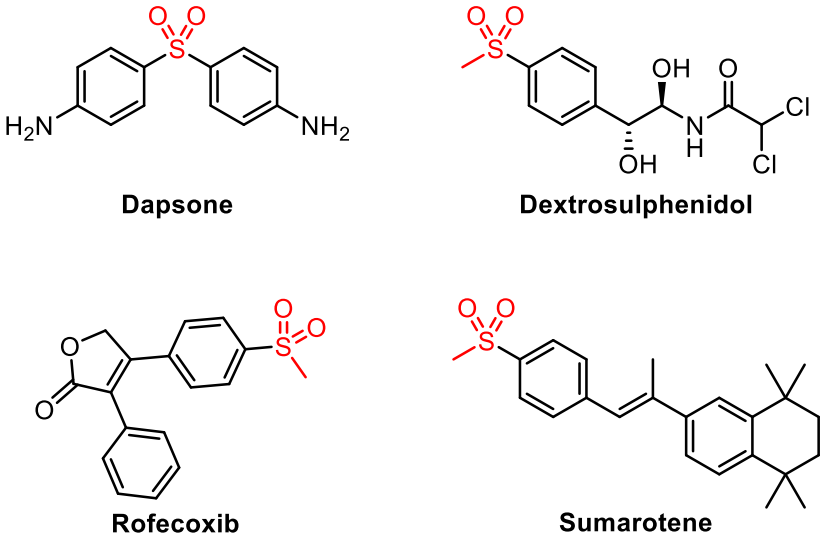

Figure 2.1

Examining in detail Muri and Pfaltz's investigation of the activity of iridium catalysts supported by the "PHOX" ligands in the HIE process, a total of 15 catalysts were selected for screening across 11 diverse substrates. Relatively simple examples such as acetophenone **51**, acetanilide **39** and phenyl benzamide **65** could be labelled to high levels with a wide range of catalysts under mild conditions and low catalyst loading (**Scheme 2.1a**). However, more difficult substrates such as phenyl pyridine **107** could only be labelled up to moderate levels of 70% with two specific catalysts. Little rationale was given to explain the efficacy, or lack thereof, in each case and the overall system is still poorly understood. Further still, when a selection of seven catalysts were applied to methylphenyl sulfone **108**, all but one exhibited low to moderate levels of incorporation (**Scheme 2.1b**). An impressive incorporation of 95% was achieved using ligand **165**, however, again, no rationale for the success of this ligand was ever given. As a result of the sporadic manner in which the catalysts were deployed, it is unclear which ligand characteristics are imperative to the high levels of incorporation. In addition to this, the substrate scope or robustness of the process was never established.

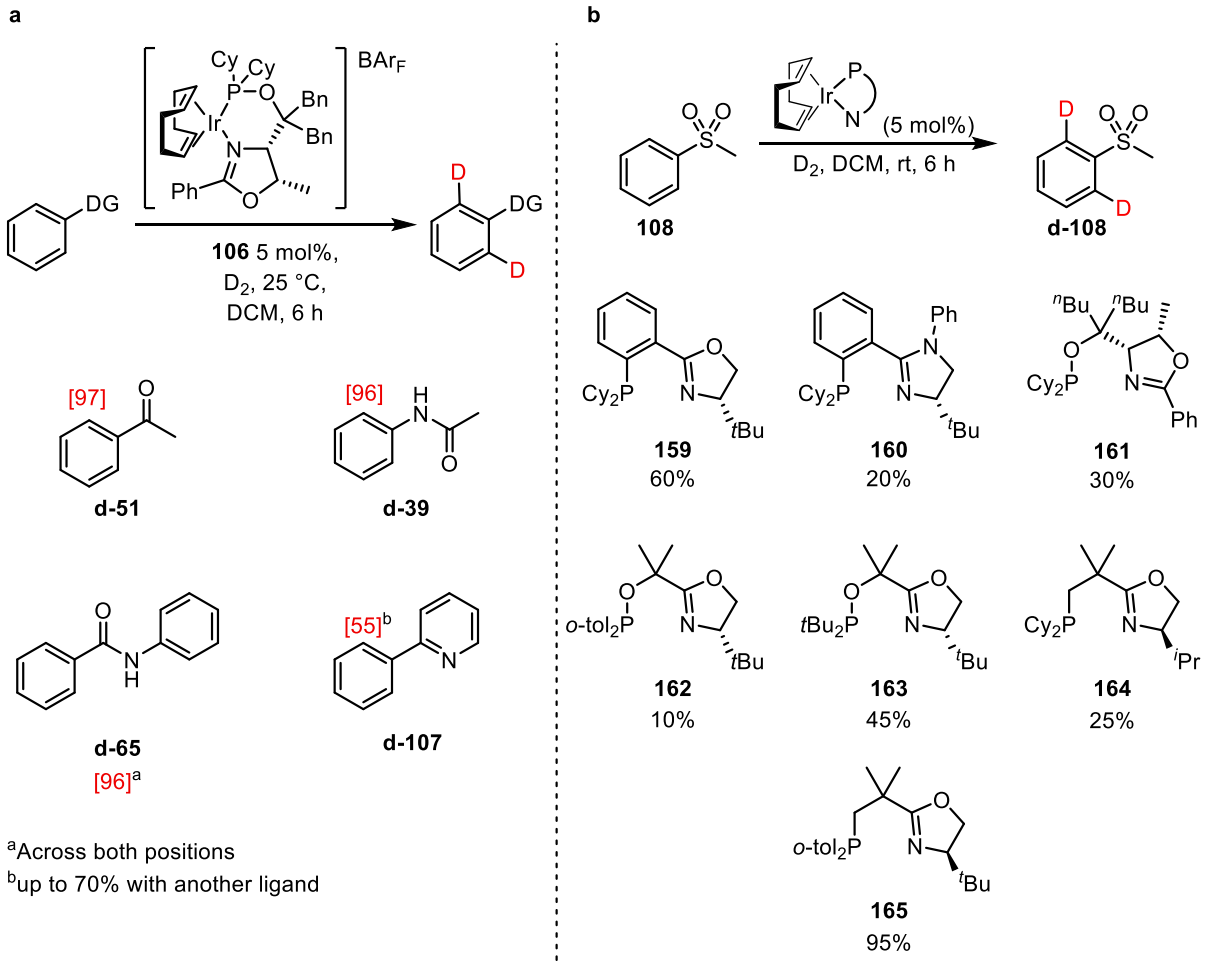

Scheme 2.1

Returning to the work of the Kerr group, our previous studies into the mechanism have shown that the C—H activation step is generally rate determining, but has a relatively low activation energy, leading us to believe that the low incorporation was a result of another aspect of the system.[31] Additionally, we know from our rationale in solvent choice that the ability of the substrate to displace solvent and to bind to the metal centre is crucial to the reaction, and not always guaranteed.[41] Bearing in mind that the current catalysts employed in our group result in a complex with very large phosphine and NHC ligands coordinated in a *trans* relationship, it was thought that the tetrahedral nature of the sulfone directing group results in a large amount of steric repulsion between the substrate and ligand (**Figure 2.2**). This inhibits substrate binding and, in turn, severely limits the observed incorporation. It was hypothesised that tethering the

NHC and phosphine ligands to form a single bidentate motif would reduce steric interaction with the substrate, facilitate binding, and deliver higher levels of incorporations.

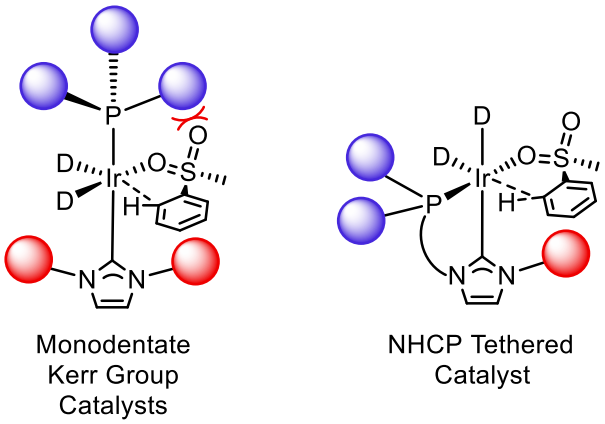

Figure 2.2

In order to validate this hypothesis *in silico*, we turned to calculating the binding energies of a small set of substrates to the catalytically relevant iridium(III) hydride species (**Scheme 2.2**).[74] The energy associated with binding of the model substrate was calculated using the basis set superposition error (BSSE) corrected counterpoise method described by Boys and Bernardi.[75] First, upon considering the binding energy between acetophenone **51** and "free" catalyst **166** in complex **167**, it was noted that a significantly negative, and therefore favourable, value of -23.1 kcal mol^{-1} was calculated. Contrasting this, however, when we consider the binding energy of our model sulfone **108**, a significantly less negative, and thus less favourable, value of only -15.3 kcal mol^{-1} is calculated.

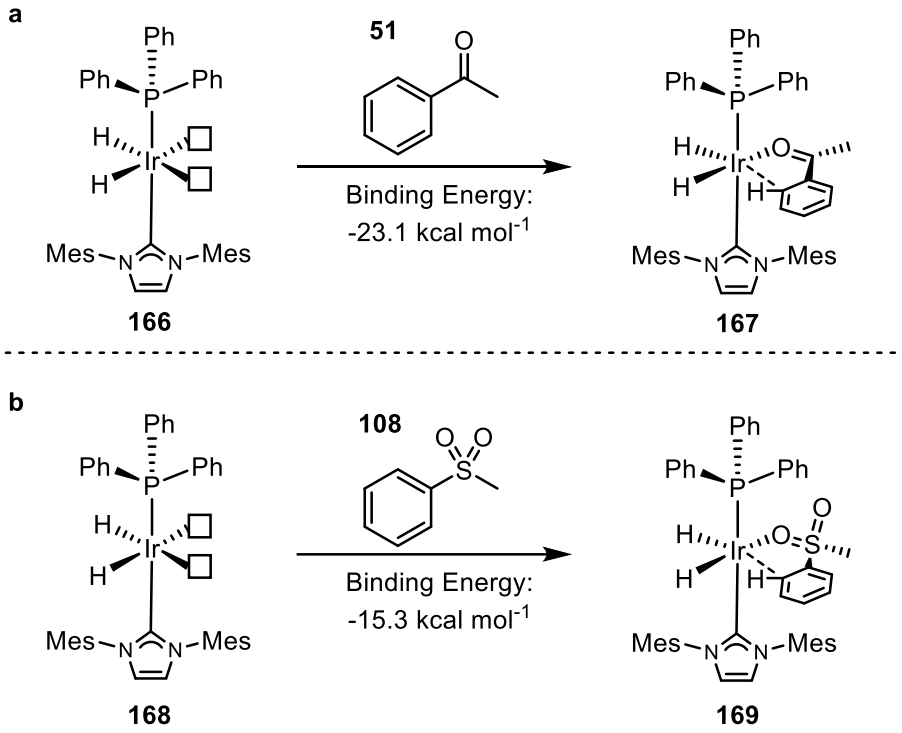

Scheme 2.2

With this information in hand, it was decided that the binding energy of **108** could be used as a screening parameter with which an *in silico* library of NHC-P chelated catalyst systems could be screened. This library consisted of 16 NHC-P ligand systems, focusing on altering the imidazole substituents, tether length between the ligating atoms, and the phosphine substituents (**Scheme 2.3**). Gratifyingly, all the entries in this screen gave more favourable binding energies for **108**, but also, most notably, gave a good range of binding energies across the series.

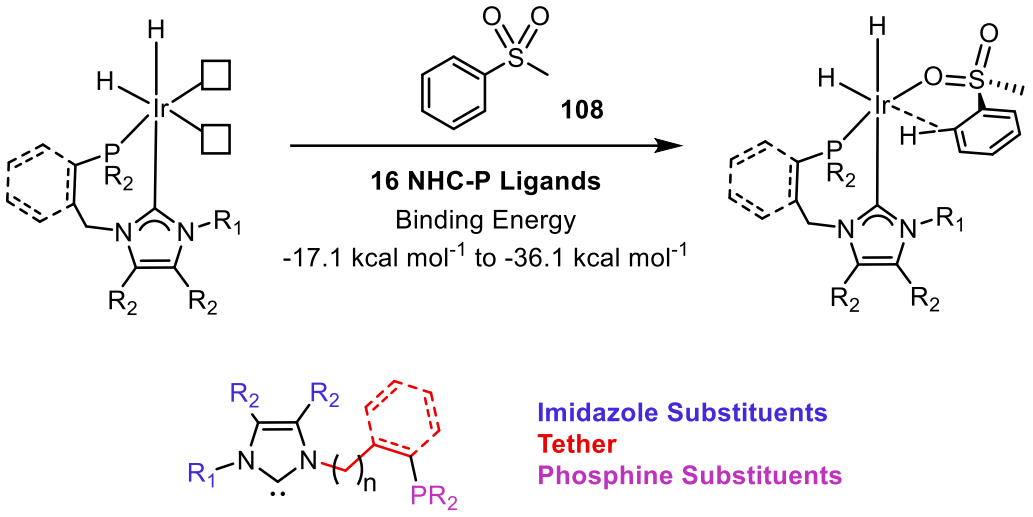

Scheme 2.3

As an initial proof of concept, two of these ligand systems were selected, and the corresponding iridium(I) precatalyst complexes were synthesised. These complexes were then applied to the labelling of methylphenyl sulfone **108** (**Scheme 2.4**). We were delighted to see a modest increase in the levels of deuterium incorporation in both cases, however, neither catalyst system delivered the levels of incorporation we desired. Nonetheless, these results showed that our catalyst development was indeed progressing in the right direction.

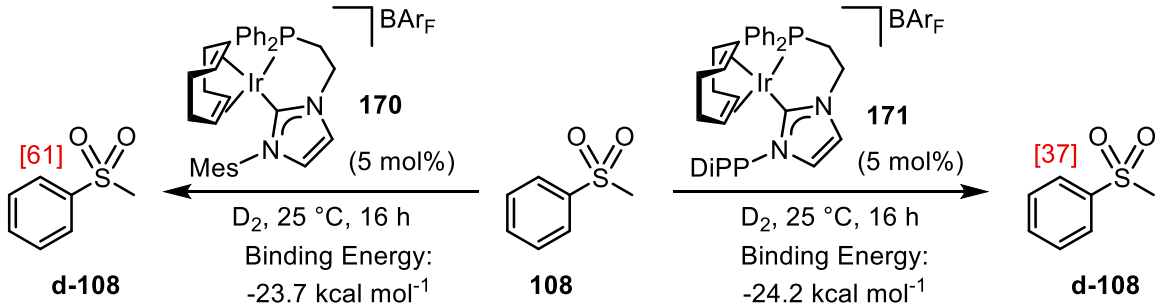

Scheme 2.4

With this in mind, an alternate catalyst system has been selected for synthesis as the first endeavour towards the refinement of a chelated catalyst system for such sulfur based directing groups (**Figure 2.3**). The selected catalyst systems make use of a benzyl tether, retaining the triarylphosphine structure, which we hope will benefit the ability of the complex to deliver high

levels of incorporation. Once synthesised, the selected catalysts will be applied in the labelling of methylphenyl sulfone **108**. From here, the most active catalyst system will be taken forward for further optimisation, if required. Once an optimal system has been established, the substrate scope will be explored, in order to determine the efficiency of the catalyst in a range of sterically and electronically varied examples.

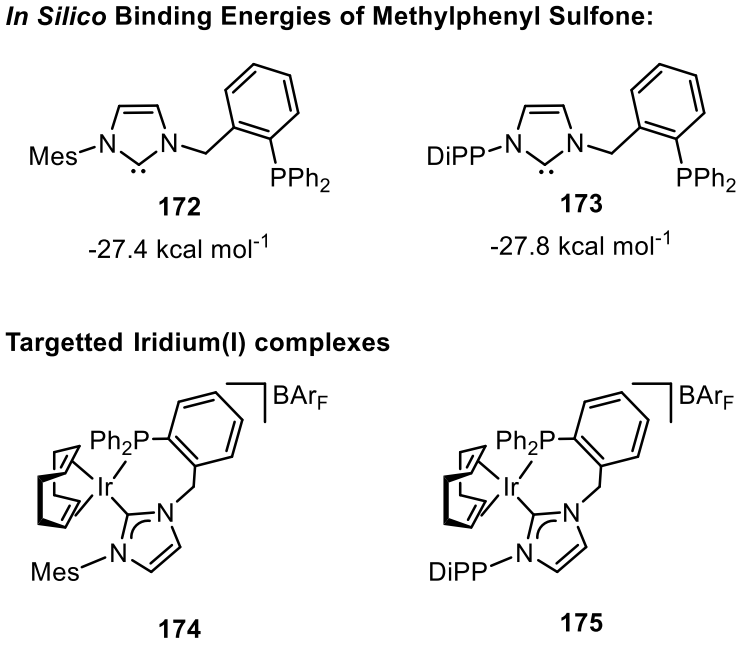

Figure 2.3

3. *in Silico* Parameterization & Ligand Screening for the Development of a Novel Chelated Iridium(I) Complex for HIE of Aryl Sulfones

3.1 Catalyst Synthesis & Characterisation

The desired catalyst systems can be synthesised from the corresponding imidazolium salts which, in turn, can be quickly accessed in a modular fashion from 2-(diphenylphosphanyl)benzyl chloride **176** and the appropriate *N*-aryl imidazole, as shown retrosynthetically in **Scheme 3.1**. Palladium catalyst systems supported by such ligands have previously been synthesised by Zhou *via* a similar method.[76]

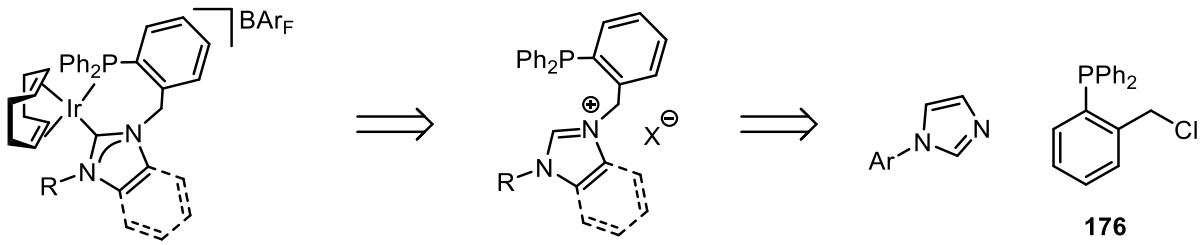

Scheme 3.1

As such, we embarked upon the synthesis of our desired catalyst systems, starting with the synthesis of the necessary imidazoles. Synthesis of the aryl imidazoles was achieved by a one-pot, multicomponent synthesis starting from the relevant aniline, glyoxal, formaldehyde, and ammonium acetate (**Table 3.1**). Both mesitylimidazole **179** and di-*iso*-propylphenyl imidazole **180** were synthesised, however the yields for the much more sterically encumbered di-*iso*-propyl variant were consistently reduced. Isolation of products from multicomponent reactions such as these are notoriously difficult, with several by-products requiring separation. It was found that isolating the products by column chromatography was possible, however, this was rather time consuming. Pleasingly, a significantly more efficient method of triturating the

product in boiling petroleum ether or hexanes was found, allowing isolation in comparable yields.

Table 3.1

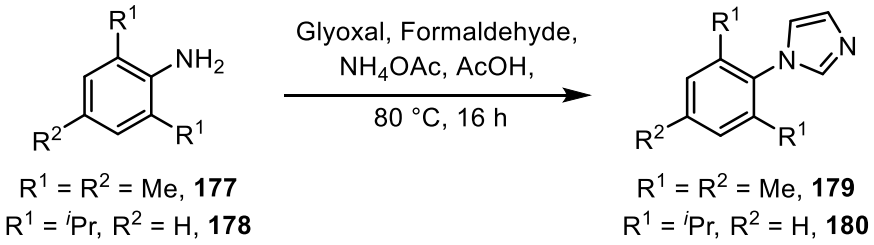

$R^1 = R^2 = Me$, **177**
$R^1 = {}^iPr$, $R^2 = H$, **178**

$R^1 = R^2 = Me$, **179**
$R^1 = {}^iPr$, $R^2 = H$, **180**

Entry	Product	Isolation Method	Yield (%)
1	**179**	Column	54
2		Trituration	66
3	**180**	Column	16
4		Trituration	20

With the relevant imidazoles in hand, we turned our attention to the phosphine moiety (**Scheme 3.2**). Benzyl bromide **181** was used to generate *N*,*N*-dimethylbenzyl amine **182** in an S_N2 reaction, which proceeded in high yield. This compound was then metallated, exploiting the dimethylamine group in a directed *ortho*-lithiation, yielding highly air-sensitive crystals which were immediately reacted with chlorodiphenyl phosphine to afford **183** in admirable yield. Indeed, phosphine **183** was resistant to oxidation such that it could be exposed to air and purified by column chromatography without any noticeable loss in yield, however storage of the compound requires an inert atmosphere as noticeable amounts of phosphine oxide were noted to have formed after 24 hours in air. The final step in forming **176** involved chlorination at the benzylic position. It was found that toluene could be used in place of the highly carcinogenic solvent, benzene, which was used in the original publication.[76] Gratifyingly, this

resulted in an excellent yield of **176** which could employed in the preparation of a series of benzylic ligands.

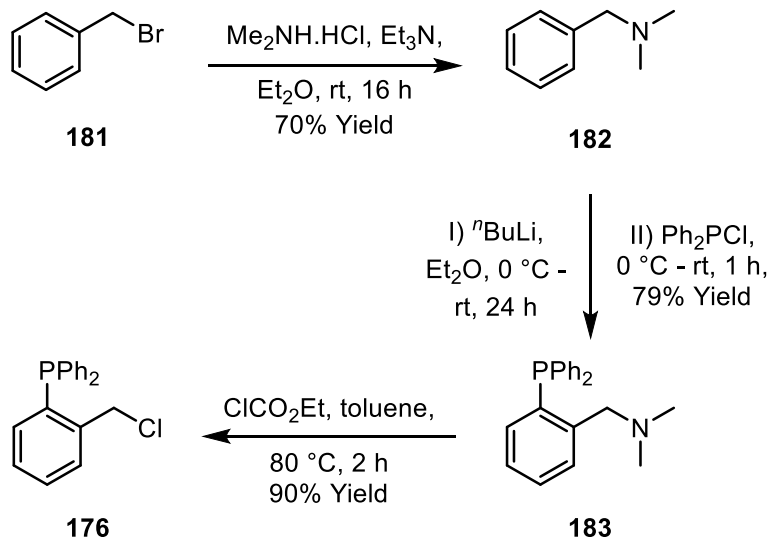

Scheme 3.2

The displacement of the benzylic chloride by mesityl imidazole **179** was reported by Zhou to take two days at reflux in ethanol. However, when the reaction mixture was analysed by TLC after two days it was found that it contained unreacted imidazole. The benzyl chloride **176** however, had been completely consumed. Indeed, the desired chloride salt proved difficult to remove from the crude mixture and as such, was not isolated. Instead, the crude mixture was stirred with sodium BAr_F in order to exchange the anion associated with the imidazolium salt. Not only did this install the desired anion, but the lipophilicity of **184** allowed significantly easier separation of the product from the unreacted imidazole as well as other side products of the displacement. This procedure afforded the novel imidazolium salt **184** in an appreciable 56% yield (**Scheme 3.3**). When attempting the same procedure with the larger di-*iso*-propylphenyl imidazole **176**, however, poor reactivity was observed. In order to address this, the solvent was changed to acetonitrile, and half an equivalent of potassium iodide was added.

This allowed the displacement to proceed in only two hours. The counterion was exchanged *via* the same method as **184**, affording the di-*iso*-propylphenyl salt **185** in 58% yield.

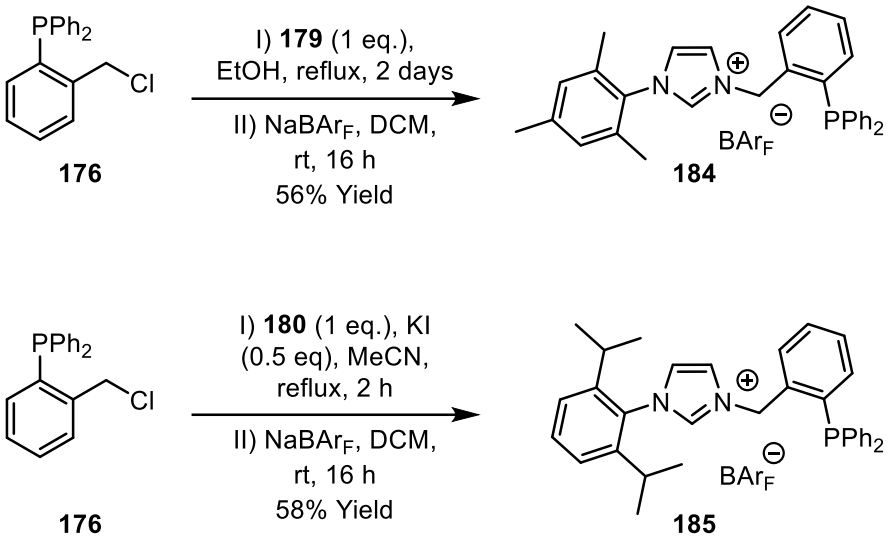

Scheme 3.3

With the ligands in hand, the full catalysts could be synthesised *via* deprotonation of the imidazolium salt in the presence of the iridium cyclooctadiene chloride dimer, **54**. The catalysts were isolated in generally good yields as bright red solids (**Table 3.2**). Indeed, it was noted that the reactions proceeded significantly better on larger scale, producing excellent yields on a 0.6 mmol scale.

Table 3.2

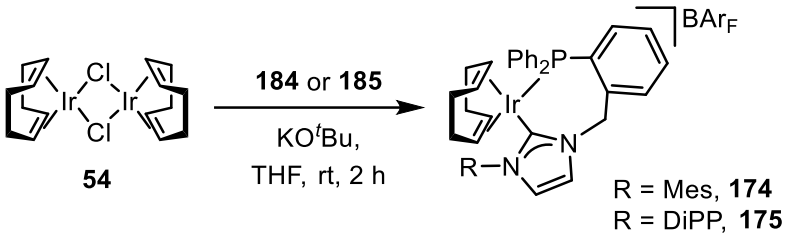

Entry	Complex	R	Scale (mmol)	Yield (%)
1	**174**	Mes	0.3	49
2			0.6	86
3	**175**	DiPP	0.3	73
4			0.6	91

Pleasingly, crystals of **175** could be grown from DCM and petroleum ether, and an x-ray crystal structure confirmed the solid state structure of our novel complex. **Figure 3.1** depicts the structure, with hydrogen atoms and the BAr_F anion omitted for clarity.

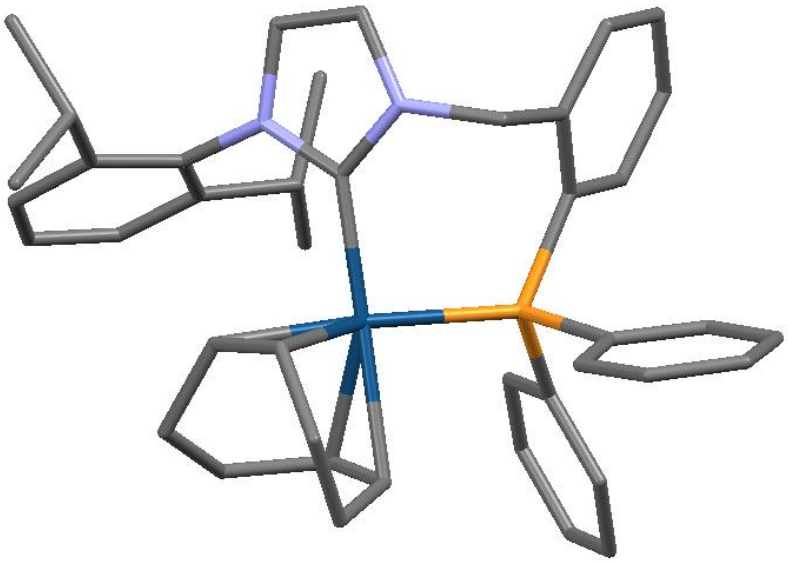

Figure 3.1

As discussed in *Section 2*, the complexes which have been synthesised were targeted based on the binding energies of catalytically relevant iridium(III) dihydrides. However, such species are highly reactive and, thus, not isolatable. Since obtaining a crystal structure of these iridium(III) dihydrides is unfeasible, making a direct comparison between the structures generated *in silico* and experimental data is not an option. Therefore, it was determined that the crystal structure of iridium(I) complex **175** could prove to be a useful tool in order to validate the computational methods. As such, the structure of **175** was optimised separately, in the absence of the BAr_F anion, and in the gas phase, in the same fashion as the dihydrides have been calculated. **Table 3.3** highlights some key values for both structures. Generally, the calculated values were in good agreement with the crystal structure data. Both structures suggest a distorted square planar structure. Pleasingly, the bond lengths between the iridium, phosphine and the carbenic carbon of the NHC in the calculated structure agreed well with those of the crystal structure, with differences of the order of 10^{-2} Å in each case. Notably, both structures show a significant twist in in the NHC, with respect to the xy plane defined by the other ligands. This can be easily illustrated by measuring the P-Ir-C-N dihedral angle, which shows a significant distortion at approximately 130°. This twist is required to accommodate the large, relatively inflexible 7-membered chelate.

Table 3.3

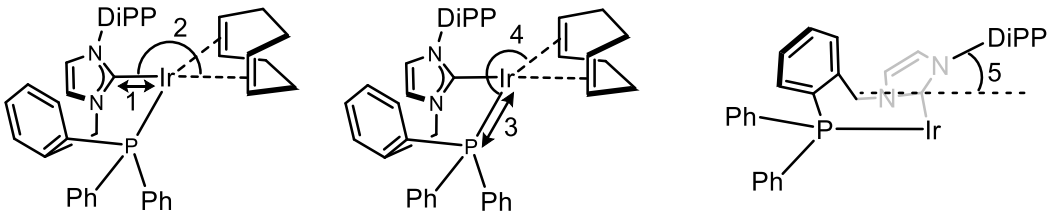

Entry	Dimension	Crystal Structure	Calculated Structure	Magnitude of Error (%)
1	Ir—C Bond Length	2.04858 Å	2.06582 Å	0.842
2	Ir—P Bond Length	2.31489 Å	2.37947 Å	2.79
3	C-Ir-Alkene Angle	160.8551°	161.1586°	0.189
4	P-Ir-Alkene Angle	158.004°	156.5759°	0.904
5	P-Ir-C-N Dihedral	132.5500°	135.6473°	2.34

Prior to continuing with the two novel complexes synthesised, we were interested in further diversifying our ligand set. It was noted that the computational screen performed previously (*vide supra*) did not investigate the effects of backbone substituent effects on the imidazole ring for the benzyl tethered systems. Accordingly, two further catalysts were selected wherein the backbone of the imidazole was modified in order to tune the properties of the NHC portion of the ligand. While these structures were not present in the initial computational screen, the binding energy of methylphenyl sulfone **108** was calculated in the same fashion. The corresponding imidazolium salts, as well as the binding energies associated with the

corresponding iridium(III) dihydride systems, are illustrated in **Scheme 3.4**. The versatility of the benzylic tether meant that the additional synthetic steps were limited to the generation of the imidazole.

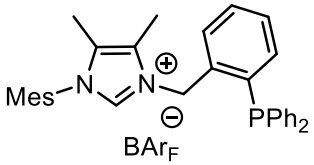

186

Binding Energy of Corresponding Ir(III) Dihydride: - 28.6 kcal mol^{-1}

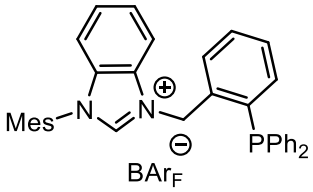

187

Binding Energy of Corresponding Ir(III) Dihydride: - 30.8 kcal mol^{-1}

Scheme 3.4

The dimethyl substituted imidazolium salt **186** was synthesised in a similar fashion to **184** and **185**, wherein a multicomponent reaction was used to generate the imidazole **188**, in 45% yield, followed by alkylation to install the phosphine moiety (**Scheme 3.5**). Once again, potassium iodide was used to facilitate the alkylation step, affording the imidazolium salt **185** in an excellent 82% yield. The catalyst synthesis proceeded in excellent yield on a small scale of 0.27 mmol, to give **189** in 91% yield.

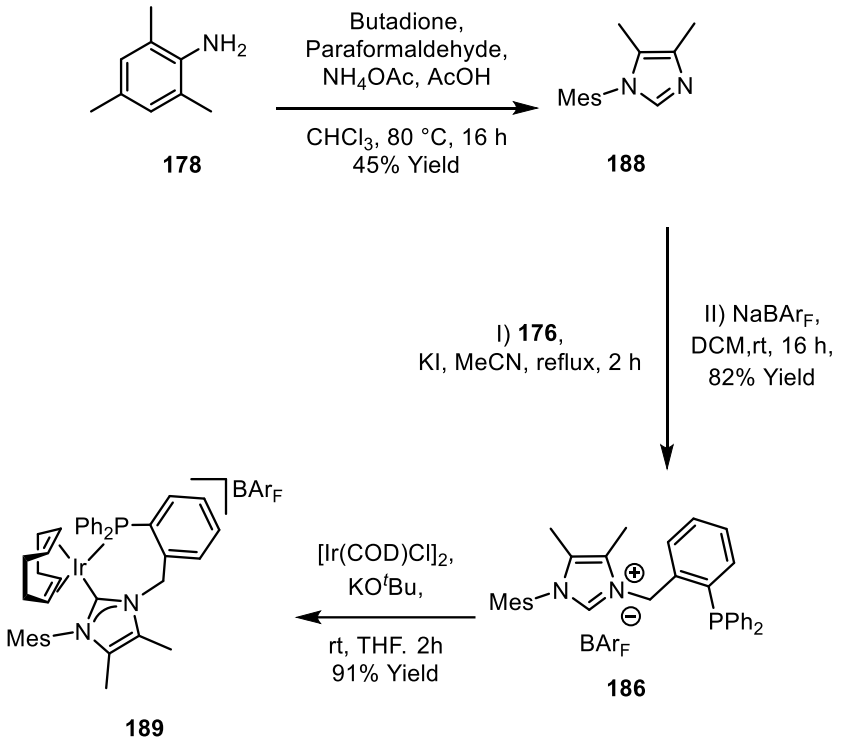

Scheme 3.5

The benzimidazole motif present in **187** required a more extensive synthesis, as a one-pot, multicomponent procedure to directly form *N*-mesityl benzimidazole is not possible. Following a recent procedure by Scheidt, which detailed the synthesis of *N*-mesityl benzimidazole **194** in four steps from 1,2-dibromobenzene **190**, the desired imidazole species was obtained in a very good overall yield (**Scheme 3.6**).[77] Reacting dibromobenzene **190** with mesitylamine in a Buchwald amination afforded **191** in a 70% yield. A successive Buchwald amination using benzophenone imine was then performed in order to install the second nitrogen moiety. Due to the steric bulk of the coupling partners, this reaction required 48 h to go completion. Pleasingly, however, the product **192** was obtained in a good 60% yield. From here, the imine was removed by acid catalysed methanolysis to yield the free aniline **193**. Satisfyingly, **193** could be cyclised to give the benzimidazole **194**, using trimethyl orthoformate, in an excellent 96% yield. Due to the reduced nucleophilicity of the benzimidazole, the alkylation step required longer reaction time, compared to previous imidazole alkylations, and only afforded the ligand **187** in a poor

31% yield. However, this step provided enough material for the following complexation step, which proceeded well to give complex **195** in a serviceable 58% yield.

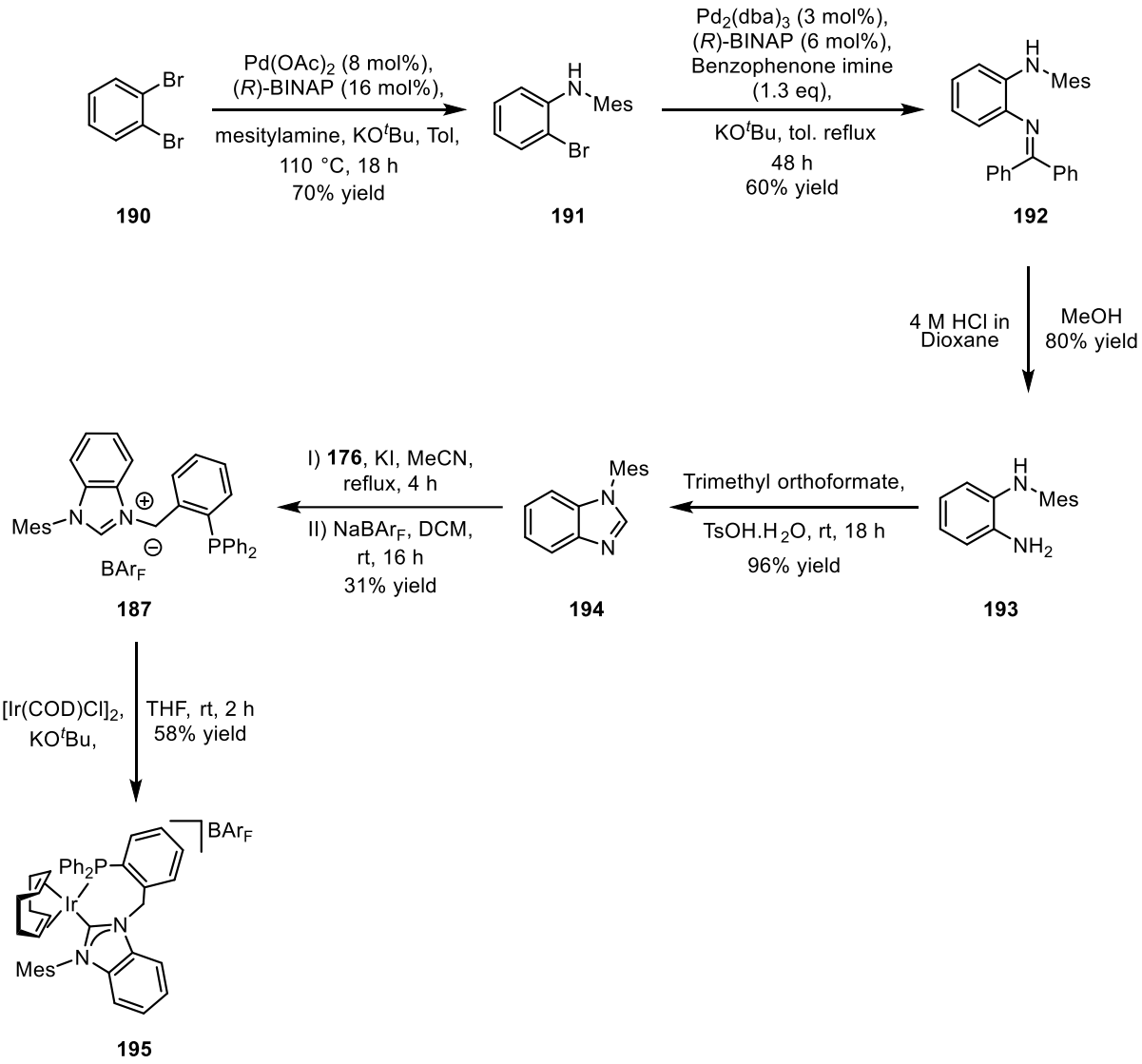

Scheme 3.6

With four NHC-P iridium(I) precatalysts in hand, electronic and steric characteristics of each complex were parameterized, in order to better understand the systems. A common method of characterising the electronics of a catalyst is through examination of the ^{1}H NMR spectrum of the corresponding iridium dihydrides.[78] As such, the hydride shifts of each of the benzylic tethered complexes were analysed. This was performed by dissolving the catalyst in deuterated acetonitrile, in an NMR tube, and passing hydrogen through the solution, hydrogenatively

removing the cyclooctadiene ligand and forming the corresponding dihydride species. A very strongly coordinating solvent, such as acetonitrile, is necessary to stabilise the hydride structures, which are too fluxional to observe in less coordinating solvents. The chemical shift and coupling of the resulting species can be compared to give information about the environment of the hydride. Once activated, the complexes can form 3 distinct isomers, in which the hydrides occupy a *cis* relationship, as shown in **Scheme 3.7**. Isomer **C**, in which the both hydrides are *trans* to the strongly σ-donating donating ligands, would be less stable than **A** and **B** and, as such, would not be expected to be present in significant quantities. The ^{31}P-^{1}H coupling can be used to deduce the which signals correspond to **A** and **B**, with a hydride *trans* to the phosphine exhibiting a significantly larger coupling than that of a hydride in a *cis* relationship.[78]

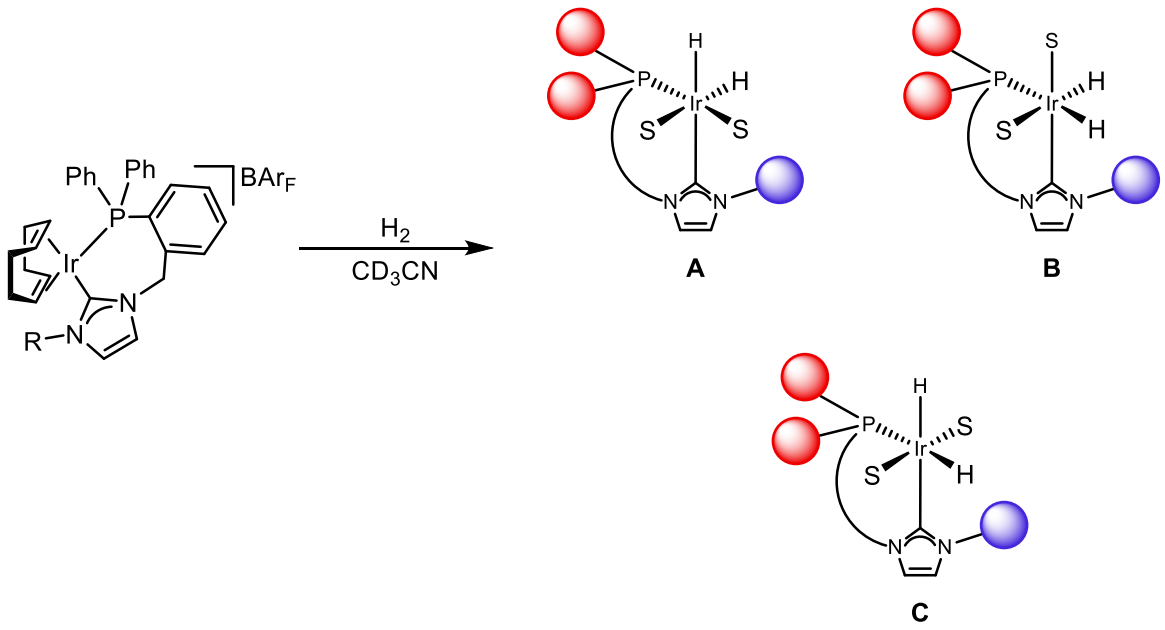

Scheme 3.7

Scheme 3.8 below details the results of these experiments. In general, it was noted that complexes of form **A** were formed in vast excess over those of form **B**. Indeed, the lowest estimated ratio of isomers **A**:**B** was 97:3 in the case of **175**. In the remaining complexes, levels

of **B** were too low to accurately estimate. The characteristically large $^{2}J_{HPtrans}$ could be measured and used to identify the presence of **175B**, however, due to the small concentration of the species, the smaller $^{2}J_{HPcis}$ coupling could not be reliably measured. Signals which are consistently around -20 to -22 ppm are characteristic of hydrides *trans* to labile ligands, such as acetonitrile. Generally, more σ-donating NHC-P ligands result in a more negative shift for the hydride occupying a *trans* relationship, allowing the σ-donating nature of the series to be analysed. Unsurprisingly, **175A** exhibited the lowest shift of the series, -12.82 ppm, proving to be significantly more σ-donating than the rest of the series. However, it was noted that substitution on the backbone of the NHC, in **189**, proved to have little effect on the hydride shift, with respect to the unsubstituted complex **174**, implying that this substitution had minimal effect on the σ-donating nature of the ligand. The benzimidazole variant, **195**, showed a significant change in hydride shift, implying that the additional aryl ring has a substantial effect on the ligand. The ^{31}P NMR spectrum of each of the hydride complexes was also analysed, however, no H-P coupling was observed in any case. This implies that, despite the strongly coordinating acetonitrile, the extended timescale required for the ^{31}P spectra to be generated means that the complexes are too fluxional for coupling to be observed. In addition to this, the sensitivity of ^{31}P NMR to geometrical effects means that little can be taken from the shift alone.

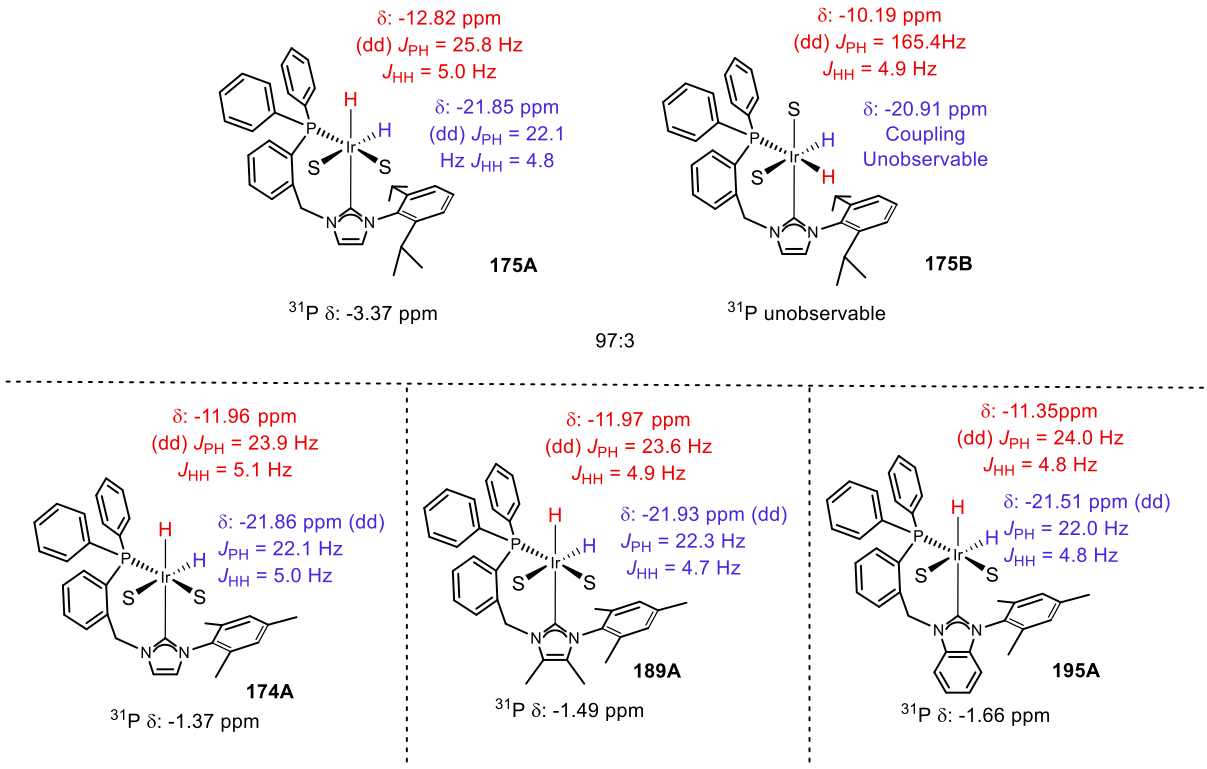

Scheme 3.8

It should be noted that this technique offers no information on the other aspects of the catalyst's electronic properties, such as the π-back donation, and, therefore, further investigation is required in order to fully understand the electronic nature of these systems.

Next, attention was turned to examining the steric influence of the ligands. Since the Tolman cone angle is best suited to analysing structures with C_3 symmetry, the steric parameters of the catalysts were next evaluated using $\%V_{Bur}$. This parameter was calculated using the SambVuca web-based application.[79] The coordinates used for the calculations were taken from optimised structures of catalytically relevant sulfone-bound iridium hydrides, wherein the atoms belonging to the sulfone were removed. The main concern with using this method of analysing the steric influence of the ligand is that the software does not recognise the iridium centre. As such, approximations have to be made in placing a putative sphere at the "centre" of the complex based on the coordinates of the ligating atom. This process is illustrated, along with

the calculated data in **Table 3.4**. The $\%V_{Bur}$ was also calculated for the ethyl-tethered catalyst systems previously synthesised.

Table 3.4

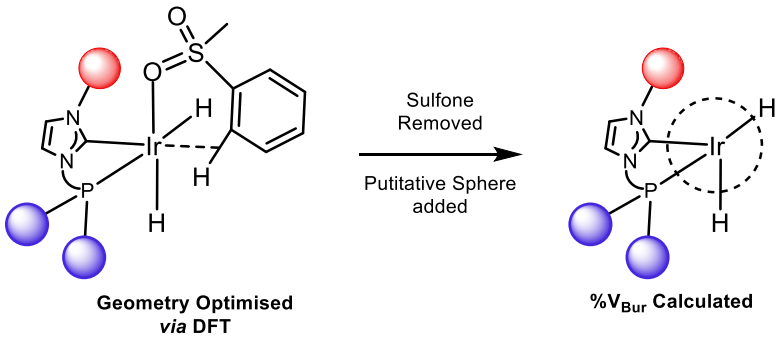

Entry	Catalyst	%V$_{Bur(NHC)}$	%V$_{Bur(P)}$
1	Mes-Im-Et-PPh_2 **170**	50.1	47.4
2	DiPP-Im-Et-PPh_2 **171**	51.0	46.6
3	Mes-Im-Bn-PPh_2 **174**	52.6	52.2
4	DiPP-Im-Bn-PPh_2 **175**	53.4	55.2
5	Mes-^{Me}Im-Et-PPh_2 **189**	52.8	52.2
6	Mes-ArIm-Et-PPh_2 **195**	52.9	50.9

It should be noted that, while the difference in $\%V_{Bur}$ is only over a range of around 3%, it has already been shown that small changes in this parameter have significant effects on catalyst activity.[45] Since the application used to measure this parameter was designed for monodentate systems, two sets of data are presented: one measured from the perspective of the carbenic carbon, and the other from that of the phosphine. Both of these give information about the respective ligating centres. It can be seen from the data that, when compared to the ethyl tethered systems, the new benzylic catalysts exhibit a higher $\%V_{Bur}$. This occurs due to the increased ring size of the benzylic ligands, which forces the phosphine farther from the NHC,

thus encompassing more of the ligand sphere. In moving from the mesityl-substituted **174** to the di-*iso*-propylphenyl **175**, a significant increase in $\%V_{Bur}$ is observed, resulting in **175** having the highest $\%V_{Bur}$ of the series. As expected, substitution on the backbone of the NHC, **189** and **195**, results in an increase in $\%V_{Bur}$ with respect to the NHC, as the aryl substituent is pushed towards the iridium centre.While there is still much information about the catalysts which has not yet been elucidated, the methods applied so far have given insight into the individual characteristics of each complex.

Since only single proof of concept reactions were attempted for each of the ethylene tethered catalysts, it was decided that these systems would also be synthesised and used in the initial catalyst screening.[74] **Scheme 3.9** below outlines the general route towards these two complexes, with full details given in *Section 8*. Mesitylimidazole **179**, or di-*iso*-propylphenylimidazole **180**, were alkylated with bromoethanol to give the corresponding imidazolium salts **196** and **197**. Following this, the free hydroxyl group of these imidazolium salts could be converted to alkyl bromides through reaction with phosphorus tribromide, affording imidazolium salts **198** and **199**. Following this, the bromide, in each case, could be displaced in an S_N2 reaction using potassium diphenylphosphide in a solution of DMSO. In the same step, the counterion was exchanged using $NaBAr_F$, which aided in the isolation of imidazolium salts **200** and **201** (*vide supra*). With the respective ligands in hand, we were able to synthesise the full NHC-P complexes, **170** and **171**, by deprotonating the imidazolium salt with potassium *tert*-butoxide in the presence of $[Ir(COD)Cl]_2$.

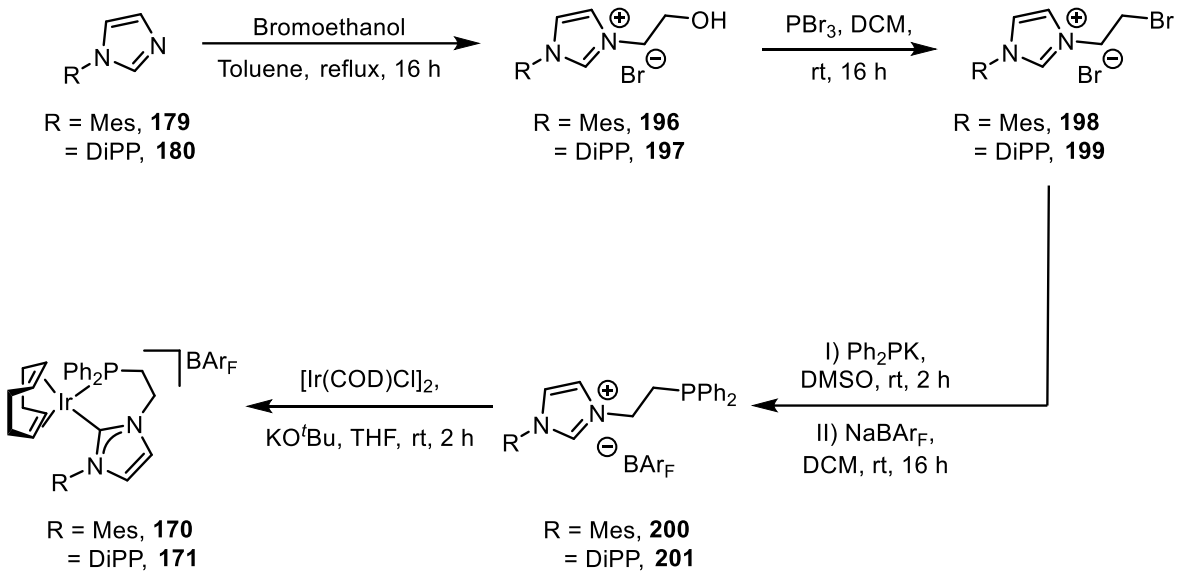

Scheme 3.9

3.2 Catalyst Screening, Reaction Optimisation, and Substrate Scope

With a total of six NHC-P complexes having been prepared, we turned our attention to applying these in the labelling of aryl sulfones. **Table 3.5** below details the results of the labelling reactions with the six chelated NHC-P iridium(I) complexes with our model substrate, methylphenyl sulfone **108**.

Table 3.5

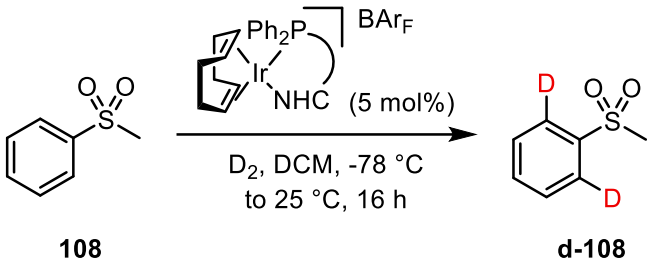

Entry	Catalyst	Solvent	Run 1 (%)	Run 2 (%)	Run 3 (%)	Avg (%)
1	**170**	DCM	34	37	35	35
2	**171**	DCM	16	9	10	12
3	**174**	DCM	22	19	29	23
4	**175**	DCM	44	38	46	43
5	**189**	DCM	12	15	13	13
6	**195**	DCM	37	33	39	36

Upon application of our new NHC-P complexes, almost all gave higher levels of incorporation, when compared to those of the monodentate system. However, none of the catalyst systems were able to incorporate deuterium to the levels we desired. **Figure 3.2** below compares the calculated binding energy of the NHC-P systems, as well as monodentate systems **56** and **57**, with the experimental incorporations.[45,74] This shows that while there is a general increase in the level of incorporation with increasing binding energy, the correlation is fairly poor, indicating that another aspect of the reaction is likely responsible for the limited levels of isotope incorporation.

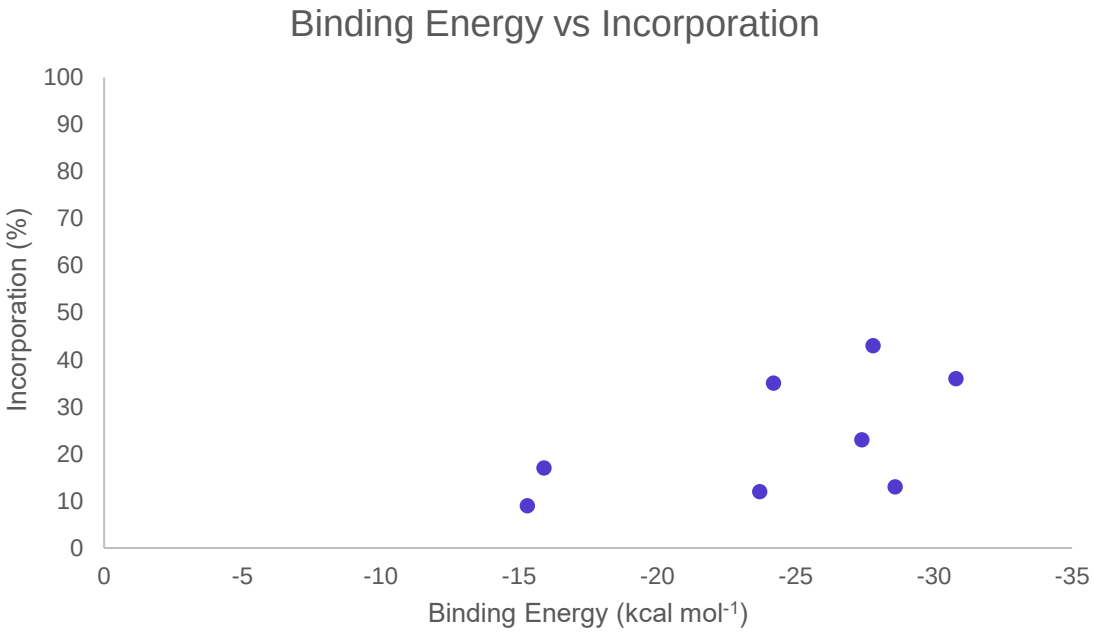

Figure 3.2

It was noted that the catalyst which exhibited the highest levels of incorporation, **175**, was highlighted as having both the more σ-donating NHC as well as the largest $\%V_{Bur}$. This can be rationalised by considering the conformation of the complex. The initial computational investigations of this system found the most favourable binding motif and lowest energy complex for the dihydride species **202** is as illustrated in **Scheme 3.10**. In this species, the agostic interaction occupies a *trans* relationship to the NHC portion of the ligand. Therefore, a more σ-donating NHC would result in facilitation of the C—H activation process, with respect to the less σ-donating ligands, through the *trans* effect. This would increase the rate of the C—H activation and therefore result in an overall higher level of incorporation. There is also the possibility that the higher levels of incorporation were due to a steric effect, owing to the larger $\%V_{Bur}$. Initially, it may be difficult to rationalise an increase in $\%V_{Bur}$ being beneficial, as one would expect a poorer binding of the substrate and hence poorer labelling. However, what the gas phase models do not consider is that the kinetic stability of a larger catalyst is likely to be greater. This results in a catalyst which is active for longer periods of time, and can therefore

incorporate more deuterium. In order to determine whether or not our new catalyst system was competent in C—H activation, we calculated the barrier to this process, also shown in **Scheme 3.10**. This barrier proved to be exceptionally low at 14.5 kcal mol^{-1}, indicating that the activation process should be rapid at room temperature. We did not foresee any other steps in the catalytic cycle being rate-limiting, and, thus, believed that the reason for the limited levels of incorporation lay in off-cycle processes.

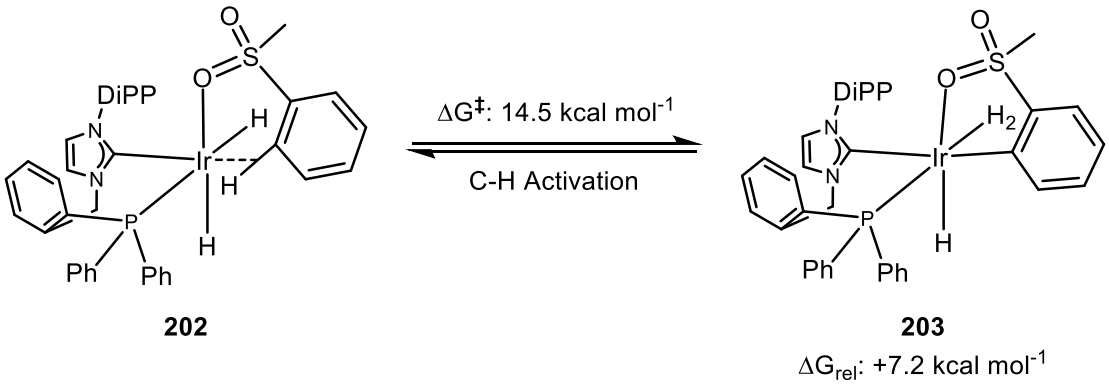

202 **203**

ΔG_{rel}: +7.2 kcal mol^{-1}

Scheme 3.10

Having previously observed how important the role of solvent choice is in the success of these reactions, it was decided that the most active catalyst of the series, **175**, would be brought forward for a solvent screen (**Figure 3.3**). To our delight, upon moving from the relatively poorly performing DCM to ethereal and aromatic solvents, a dramatic increase in the levels of incorporation was observed.

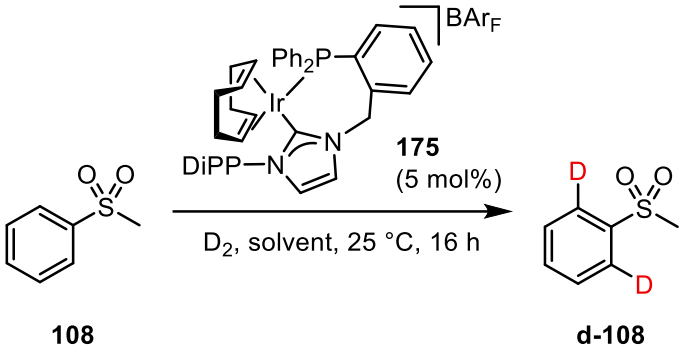

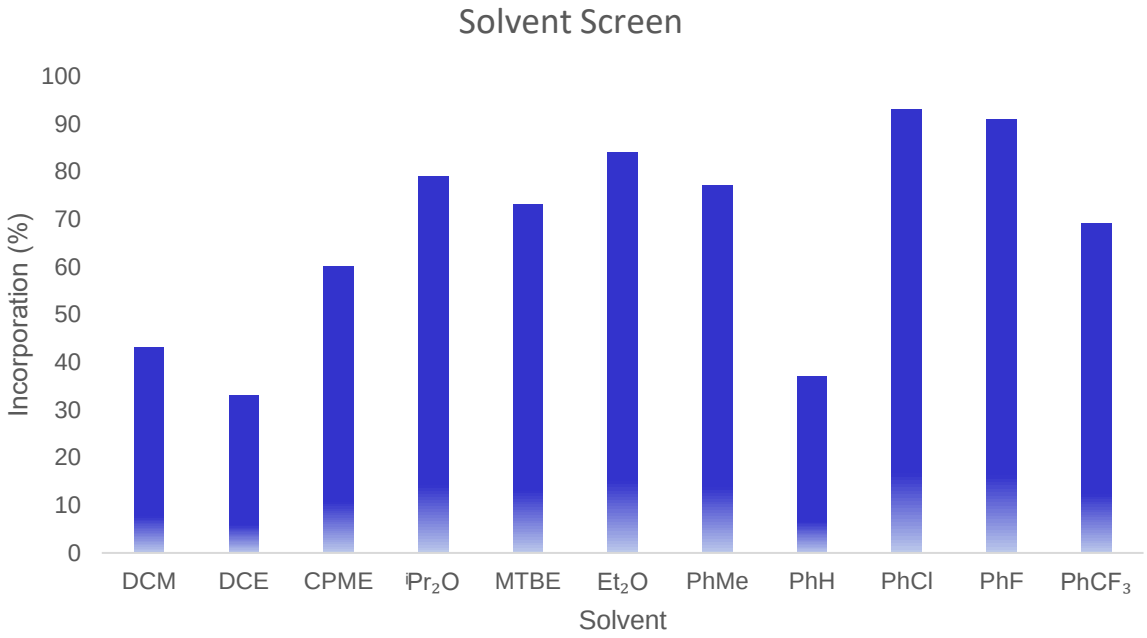

Figure 3.3

In general, the majority of tested solvents incorporated to good to excellent levels, with the exception of DCM, DCE and benzene. However, there is no clear rationale for why the incorporation was so limited in these solvents. **Table 3.6** below shows the calculated enthalpy of displacement for two molecules of five selected solvents with **108**. Unfortunately, there appears to be no simple explanation as to why some of these solvents (DCM, benzene) perform so poorly, while others (diethyl ether, chlorobenzene, fluorobenzene) allow high levels of incorporation. While we were elated with the performance of the complex across a wide range

of solvents, further investigation into determining a clear rationale behind solvent applicability is obviously required.

Table 3.6

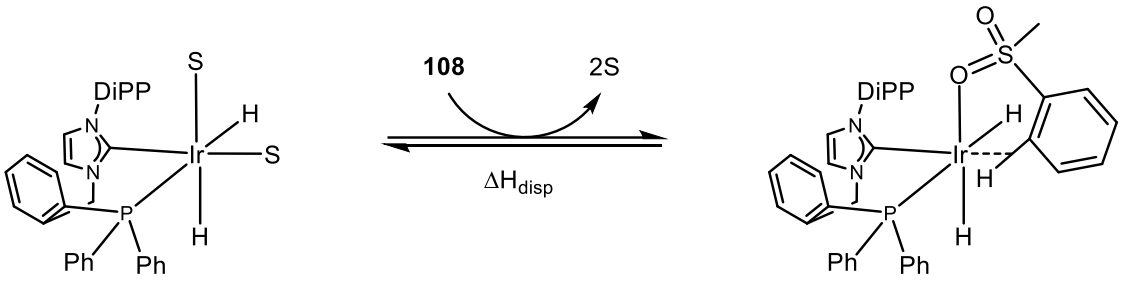

202

Entry	Solvent	ΔH_{disp} (kcal mol^{-1})
1	DCM	-1.28
2	Diethyl Ether	+14.1
3	Benzene	-3.49
4	Chlorobenzene	-9.90
5	Fluorobenzene	-4.74

One potential reason for the discrepancy in the performance of the catalyst system in various solvents, is that certain solvent systems are less likely to prevent, or indeed may even facilitate, the decomposition of the active catalyst. One very brief investigation into this possibility is outlined in **Figure 3.4**. A solution of **108** and complex **175** (1 eq) in either DCM or chlorobenzene were placed in an NMR tube. Deuterium gas was bubbled through the solutions for 5 minutes, until catalyst activation was complete. The solutions were then analysed by ^{2}H NMR spectroscopy. In chlorobenzene, the reaction appears to proceed quite smoothly, with the major signals corresponding to deuterated cyclooctane, and deuterated **108**. The reaction performed in DCM, however, exhibited several peaks in the aryl region. It is possible that this

could indicate the presence of side reactivity when using DCM as a solvent. This initial insight is, however, undoubtedly crude and can only be used as a starting point for a much more thorough investigation in this area.

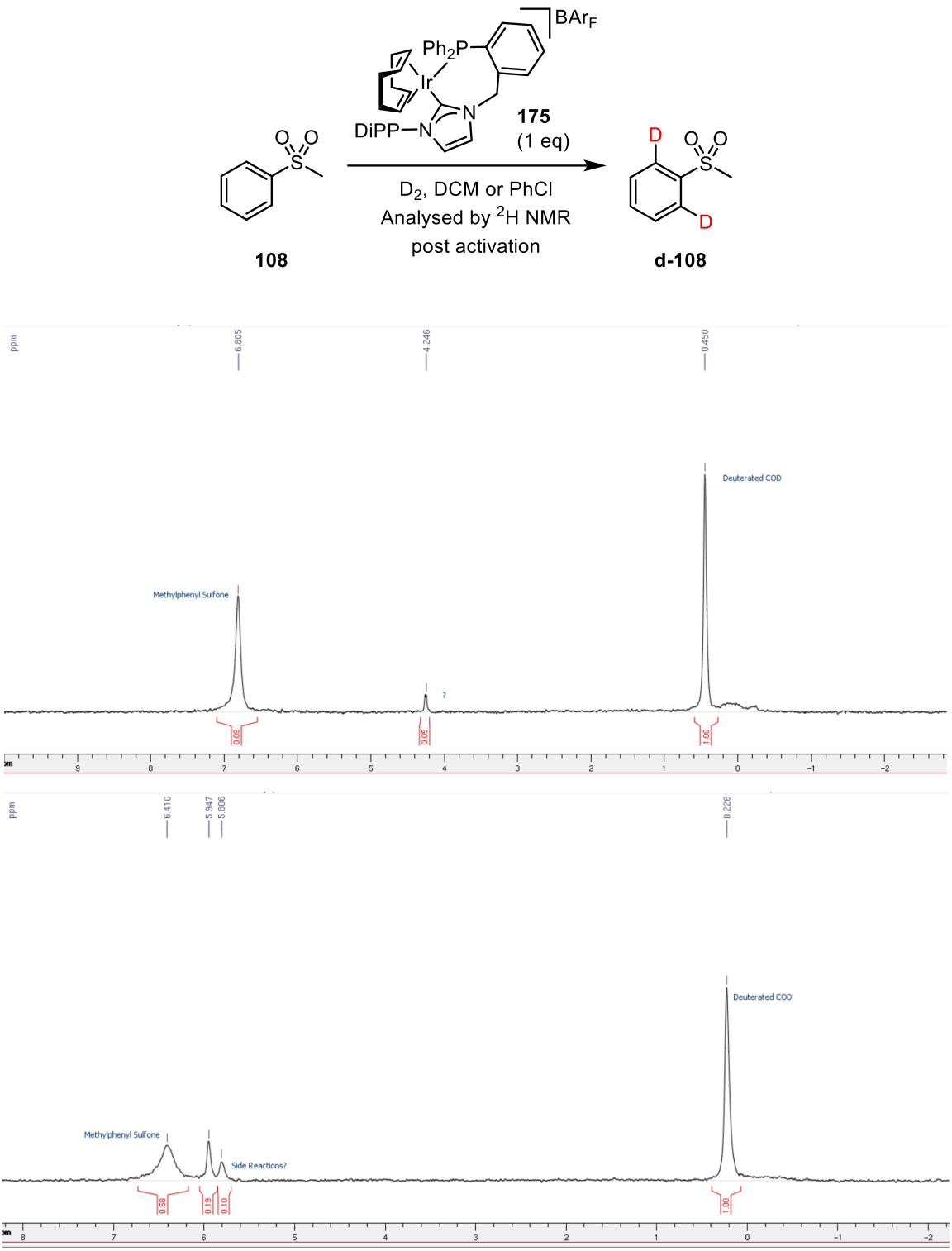

Figure 3.4

In light of the solvent screen, chlorobenzene was taken forth as the optimum solvent, with an overall incorporation of 92%, using just 5 mol% of iridium catalyst **175** over 16 h. Next, a short series of experiments was performed in order to establish whether the catalyst loading could be reduced and still retain the same level of deuteration (**Table 3.7)**. Indeed, it was noted that a reduction of catalyst loading resulted in lower incorporations, and, therefore, a loading of 5 mol% was used in future experiments.

Table 3.7

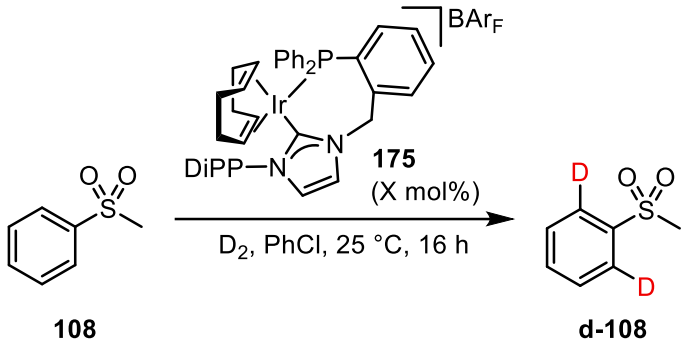

Entry	X (mol%)	Avg. (%)
1	5	91
2	3	77
3	1	59
4	0.5	33

With a system in hand that was labelling to high levels using low catalyst loading, a rate study was next performed in order to establish how quickly the exchange process reached completion. This was achieved by taking aliquots of a single reaction at set time points and quenching with diethyl ether to prevent further reaction. Gratifyingly, the labelling of methylphenyl sulfone **108** was shown to reach completion in less than one hour. **Figure 3.5** below depicts the data in terms of incorporation (%) and in the concentration of the non-

deuterated substrate ([S_H]) It can be seen that, initially, when the concentration of non-deuterated **108** is much greater than that of the deuterated substrate **d-108** ([S_D]), the reaction proceeds linearly, inferring pseudo-first order kinetics. However, as more deuterated substrate is produced, competitive binding and activation by S_D inhibits the rate and the reaction begins to slow significantly. Analysing the initial rate therefore informs about the reaction rate without the complication of product binding. In this case, the measured rate was shown to be 0.0264 M s^{-1}.

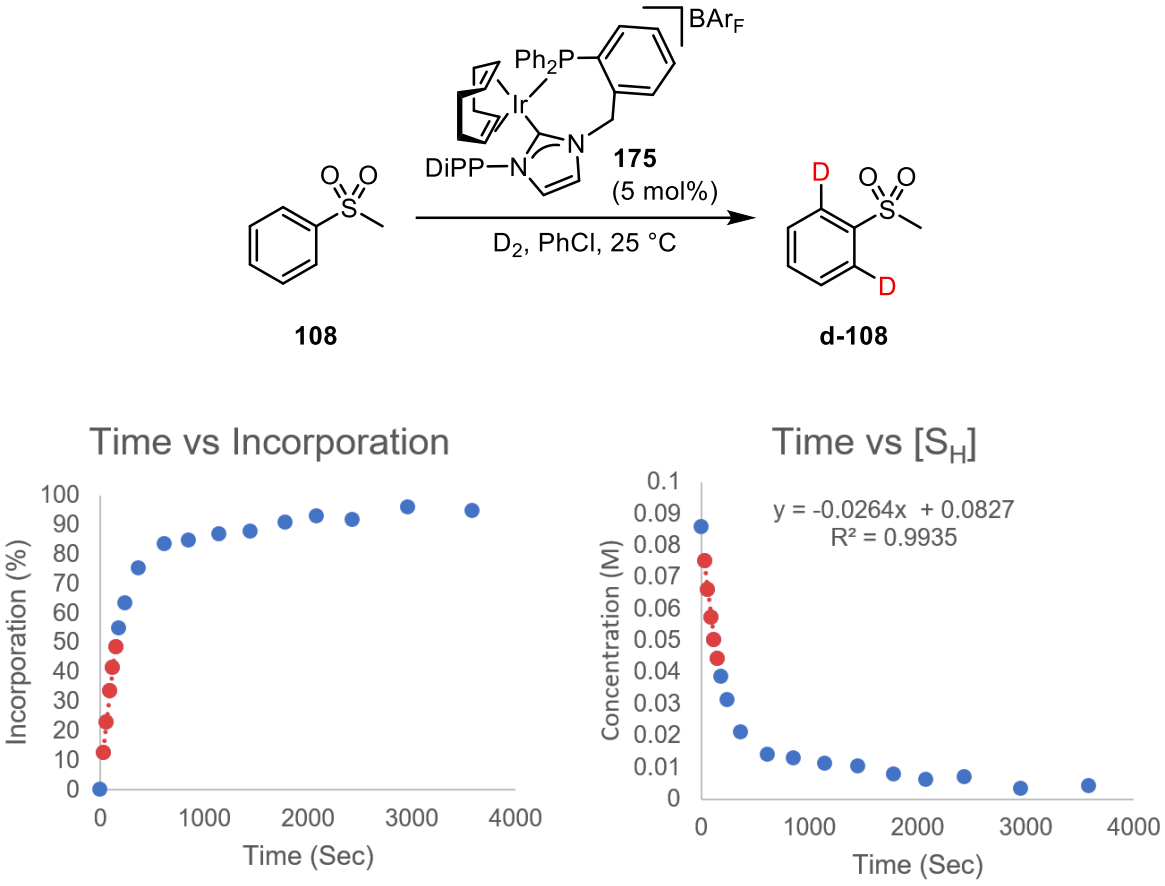

Figure 3.5

With the results of these experiments, the optimal reaction conditions were taken to be 5 mol% catalyst loading of **175** under a deuterium atmosphere at room temperature for one hour. These conditions were then taken and applied to a wider range of substrates to fully assess the robustness of our newly developed system.

3.3 Substrate Scope

Delighted with the activity of our newly discovered catalyst system, we aimed to investigate the effectiveness of the system across a range of sulfone-containing substrates. A total of nineteen substrates were targeted for this investigation, encompassing a diverse range of sulfones. See *Section 8* for details of substrate synthesis. Overall, excellent levels of deuterium incorporation were observed throughout the series of sulfones tested. Both electron-donating and electron-withdrawing substituents in the *ortho* (**108b**-**108d**) and *meta* (**108e**-**108h**) positions of the aryl ring were well tolerated, leading to high levels of incorporation. Notably, *meta*-trifluoromethyl substrate **108g** exhibits almost no incorporation at the considerably hindered position between both substituents, but displays excellent levels of deuterium incorporation at the less hindered position *ortho* to the sulfone. With less sterically encumbered *meta* substituents (**108f** and **108h**), both positions *ortho* to the sulfone are labelled to a high extent. A range of electronically distinct *para* substituents are also well tolerated (**108i**-**108l**). In the case of *para*-nitro substrate **108m**, this directing group mildly outcompetes the sulfone, but does not prevent an appreciable level of isotope incorporation through sulfone-directed HIE. Furthermore, restricting the orientation of the sulfone, in cyclic substrate **108o**, did not result in a decrease in the excellent levels of incorporation generally observed. We next turned our attention to the effects of increasing the steric bulk around the sulfone group, with substrates **108p**-**108r**. While a small decrease in the levels of incorporated deuterium were observed in diphenyl sulfone **108p** and *iso*propyl phenyl sulfone **108q** (65% and 66%, respectively), an excellent incorporation of 80% was observed with the extremely bulky *tert*-butyl phenyl sulfone **108r**. We also investigated labeling of benzyl methyl sulfone **108s**, where the sulfone would direct labelling *via* a 6-mmi, which is considerably less favoured than the more common 5-mmi. Nonetheless, appreciable levels of incorporation were still observed in this more challenging substrate under the very mild standard conditions with a low catalyst

loading of 5 mol%. Interestingly, when we examined acetal-containing **108t** under the reaction conditions, not only were excellent levels of incorporation observed through the sulfone, but a significant level of acetal-directed incorporation (26%) was also detected. Within our group's extensive studies on aryl HIE, this is the first example of acetal-directed labelling. It was decided that this labelling process would be investigated in more detail (S*ection 5.0*, *vide infra*).

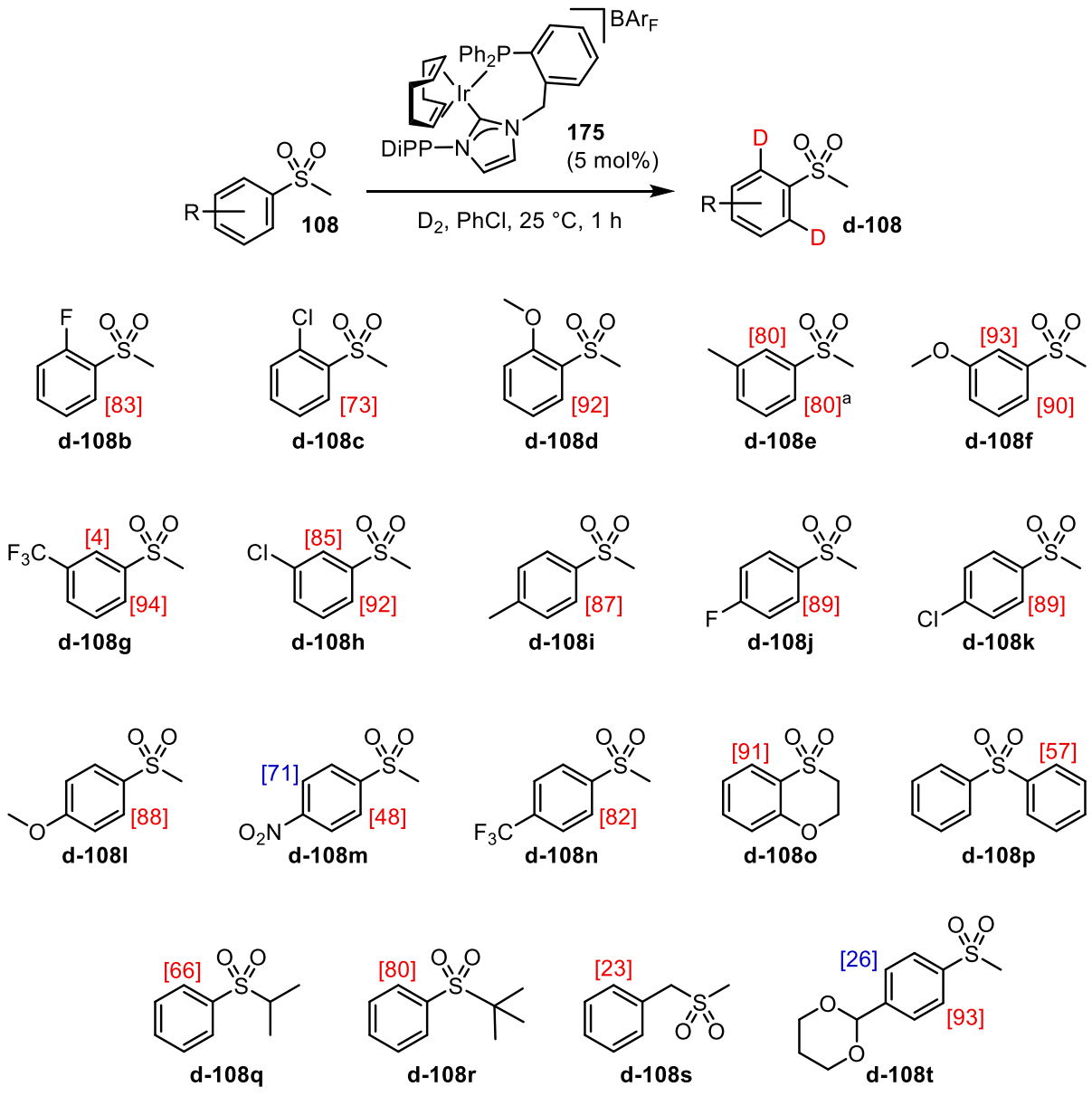

[a] Incorporation averaged across both positions.

Scheme 3.11

3.4 Sub-atmospheric HIE & Applications in Tritiation Chemistry

Having demonstrated a chelated NHC-P complex which could label aryl sulfones to excellent levels at low catalyst loading and under extremely mild conditions, we opted to further investigate the utility of the catalyst system to isotope chemists within the pharmaceutical industry, who may wish to use this newly developed methodology in order to produce labelled sulfone-containing compounds for ADMET studies. It is common in such industrial groups to make use of a TRITEC manifold for delivery of the deuterium/tritium source at sub-atmospheric pressures. Due to the obvious hazard associated with working with radioactive isotopes, these manifolds allow for safe and efficient delivery of the desired gas into the reaction mixture, as well as retrieval of any excess tritium (generally by reabsorption into a secondary uranium bed). In order to limit the amount of radioactive waste produced by the process of generating labelled material, as well as limiting unnecessary exposure, it is common to also use these manifolds to produce a deuterated sample of the desired molecule using such a manifold, prior to attempting a tritiation reaction. We were fortunate, therefore, to have access to the equipment necessary to conduct the following studies through collaboration with the industrial isotope chemists at the AstraZeneca site in Mölndal, Sweden. As such, we moved on to apply our newly developed system in the labelling of methylphenyl sulfone **108**, using such a manifold, under realistic radiolabelling conditions: sub-atmospheric pressures of deuterium gas, employing micromolar amounts of substrate. **Table 3.8** below shows the results of our initial foray into this area. Directly applying our previously optimised conditions to the labelling of **108** at ~200 mbar, we were elated to see modest levels of incorporation still being achieved by the system at low catalyst loading (Entries 1 and 2). Pleasingly, it was found that raising the pressure to ~400 mbar increased the observed incorporation significantly (Entries 3 and 4). Finally, modifying the catalyst loading to 7.5 mol% returned the levels of incorporation observed at 1 atm of deuterium gas (Entries 5 and 6).

Table 3.8

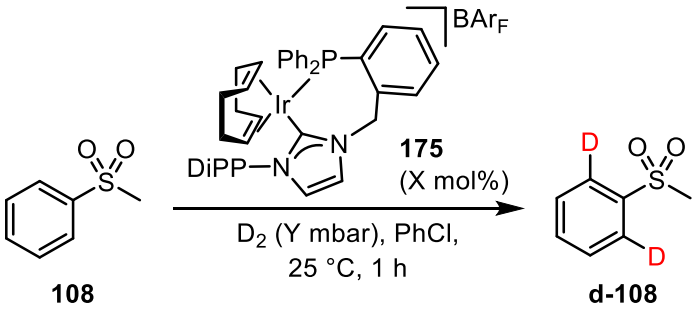

Entry	Loading (mol%)	Pressure (mbar)	Incorporation (%)
1	5.0	203	40
2	5.0	208	45
3	5.0	400	80
4	5.0	408	78
5	7.5	405	90
6	7.5	405	92

Delighted with our initial observations, we next moved to altering the pressure of the reaction at a fixed level of catalyst loading **Figure 3.6**. Interestingly, it appears that in the region of 150-400 mbar, there is a linear dependence of the observed levels of deuterium incorporation with pressure. Reducing the pressure below 150 mbar resulted in only very minor levels of deuterium being incorporated, however, it was shown that even at 5 mol% catalyst loading, high levels of incorporation could be achieved at pressures of 400 mbar and above.

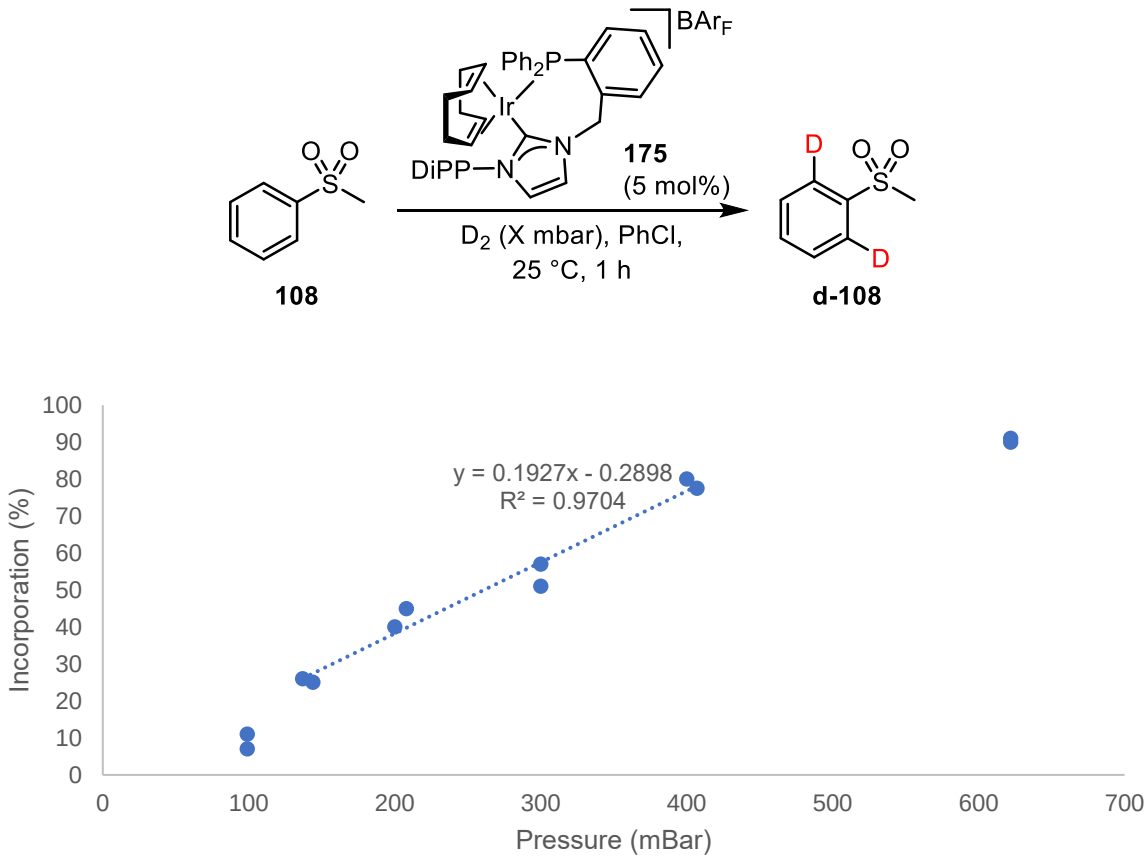

Figure 3.6

In many instances, however, it would be preferable to run labelling reactions at relatively low pressures. As such, we decided to investigate the effects of catalyst loading at a lower fixed pressure of ~200 mbar, the results of which are summarised in **Table 3.9**. Pleasingly, even at low pressures of 200 mbar, a slight increase in catalyst loading to 7.5 mol% (**Entries 3** and **4**) led to excellent levels of incorporation, similar to those obtained at atmospheric pressures. Raising the catalyst loading further, to 10 mol% (**Entries 5** and **6**) did not increase the levels of incorporation farther beyond this.

Table 3.9

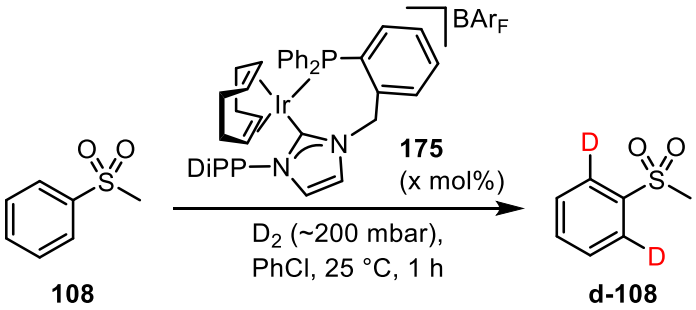

Entry	Pressure	Loading	%D
1	200	5.0 mol%	40
2	200	5.0 mol%	45
3	207	7.5 mol%	86
4	207	7.5 mol%	87
5	213	10 mol%	92
6	213	10 mol%	88

With newly optimised conditions for conducting isotopic labelling at reduced pressures in hand, we next focused on testing the catalyst system in a tritiation reaction. Using 7.5 mol% catalyst loading of **175**, and 411 mbar of tritium gas, we were delighted to deliver a sample of tritiated **108** with a high level of specific activity at 51.3 Ci mmol^{-1} (corresponding to an 89% incorporation) and an excellent radiochemical purity (**Scheme 3.12**).

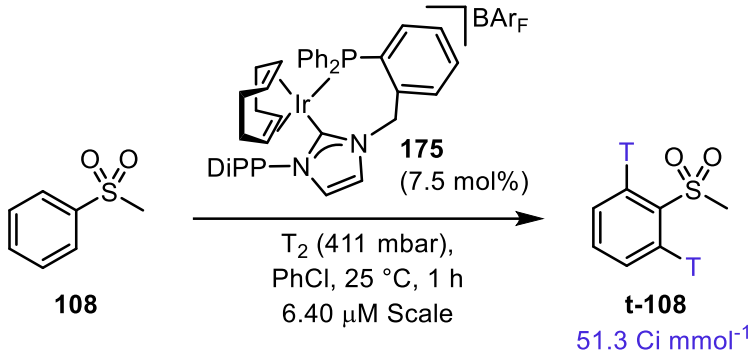

Scheme 3.12

In addition to the tritiation of methylphenyl sulfone, we also targetted the tritium labelling of a more complex example. Aryl sulfone **205** (**Scheme 3.13**) is a potent GPR119 agonist, investigated by AstraZeneca.[80] The selective tritium labelling of such an example would be an excellent opportunity to showcase the utility of our newly developed catalyst system. However, it was clear that direct labelling would be extremely challenging, owing to the high density of strongly Lewis basic heteroatoms within the molecule, and likely to proceed with poor levels of selectivity. Thus, we opted to apply our catalyst system, instead, to sulfone **108u**, forming the tritiated benzyl bromide motif **t-108u**, which could be used in an *in situ* alkylation reaction with pyrimidine alcohol fragment **204**. This sequence was highly successful, delivering a tritiated sample of **t-205** with a good level of specific activity, and excellent radiochemical purity.

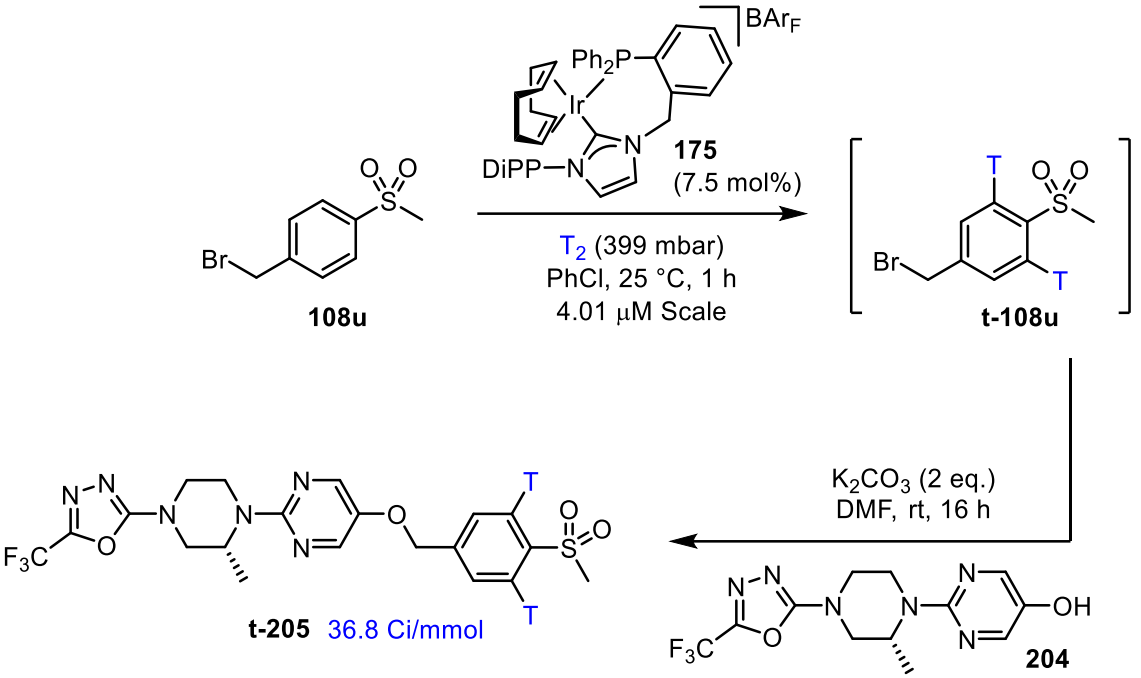
BAr$_F$
Ph$_2$P
Ir
N
DiPP–N
175
(7.5 mol%)
T$_2$ (399 mbar)
PhCl, 25 °C, 1 h
4.01 μM Scale
Br
108u
T
Br
T
t-108u
K$_2$CO$_3$ (2 eq.)
DMF, rt, 16 h
F$_3$C
t-205 36.8 Ci/mmol
OH
204

Scheme 3.13

4. Combining Solid Angle Analysis with Binding Energy Calculations for Further Refinement of a Chelated Iridium Catalyst system

4.1 Initial Screening for Labelling of Highly Substituted Sulfonamides

In Section 3, we demonstrated the power of computationally assisted rational ligands design to rapidly advance the discovery of active catalyst systems. In order to build upon these studies, therefore, we next turned our attention to investigating other substrate classes which could be labelled with the novel NHC-P iridium complex. Indeed, it was proposed that the more accessible catalyst sphere would allow us to pursue the labelling of hindered sulfonamide systems. At the time we embarked on this investigation, we had already seen that the chlorocarbene type catalysts, which had been successful for primary sulfonamides. However, these systems were not reactive enough to allow labelling of more hindered systems, incorporating only 8 %D into sulfonamide **127** (**Scheme 4.1**).[45]

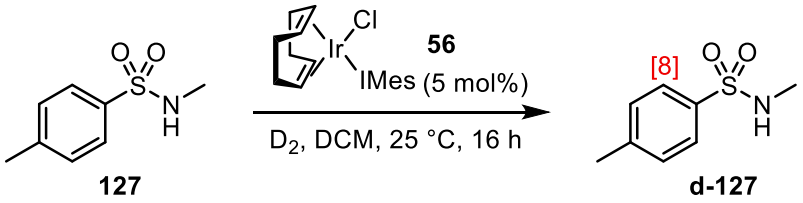

Scheme 4.1

While the chlorocarbene complexes have been shown to be excellent catalyst systems which cater well to the labelling of primary sulfonamides, the ability to also access systems with substitution on the nitrogen of the sulfonamide is highly desirable, as compounds containing *N*-substituted sulfonamides have myriad uses in the pharmaceutical industry (**Figure 4.1**). This motif appears in a broad range of drug molecules, such as the antibiotic Sulfanitran, and the pulmonary arterial hypertension treatment, Sildenafil. Highly-substituted sulfonamides can

also be found in the anticonvulsant, Sultiame, and the HIV inhibitor, Amprenavir. Indeed, in addition to developing new methods for HIE for pharmaceutical and academic groups, we are interested in this area for the further development of C—H activation processes. While there are a few instances of using sulfonamides as directing groups in direct C—H functionalisation, the examples are few in number, and this area is still far from developed. It is hoped that the information derived from this study might support other studies within this area.[81,82,83,84,85]

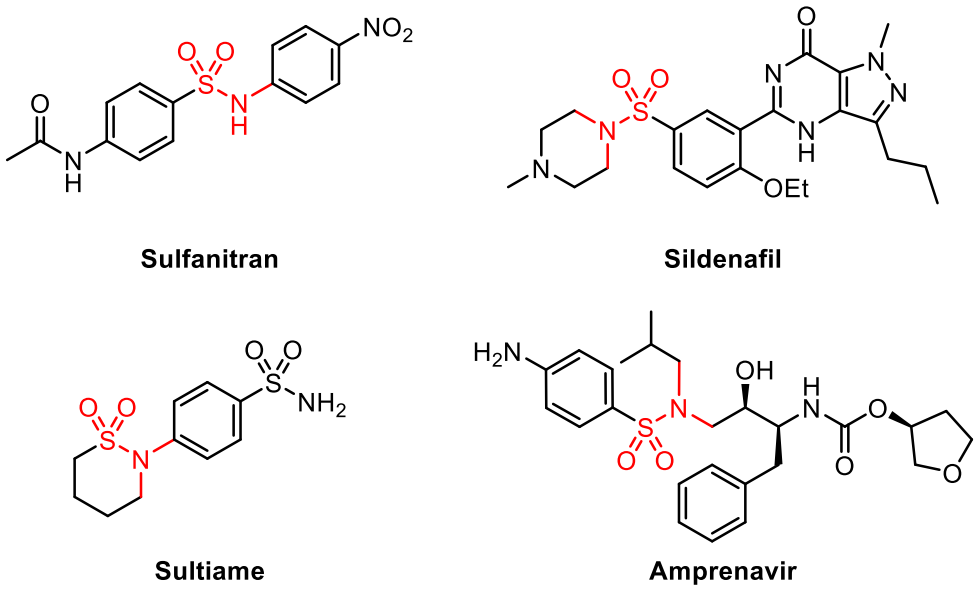

Figure 4.1

To investigate the proposal that our newly developed catalyst system would also be sufficiently reactive to take advantage of these weakly directing, hindered functional groups, we initially applied complex **175** to the labelling of *N*-methyltoluene sulfonamide **127**, as well as the significantly more challenging *N*,*N*-dimethyltoluene sulfonamide **206**, opting to initially apply long reaction times of 16 hours in order to observe the full reactivity of the catalyst system (**Scheme 4.2**). Indeed, in our initial application of substituted sulfonamide **127**, we observed excellent levels of incorporation, matching those previously observed with the sulfone substrates,which is a stark contrast the level of reactivity exhibited by the chlorocarbene type catalyst. When moving to the even more challenging *N*,*N*-disubstituted sulfonamide **206**, we

were elated to observe moderate amounts (56%) of deuterium being incorporated into the aryl ring. While this was an extremely encouraging result, we had envisioned a catalyst system which could incorporate higher levels of deuterium not only into **127** and **206**, but even more challenging substrate structures. Therefore, we next looked into further tuning our chelated catalyst system.

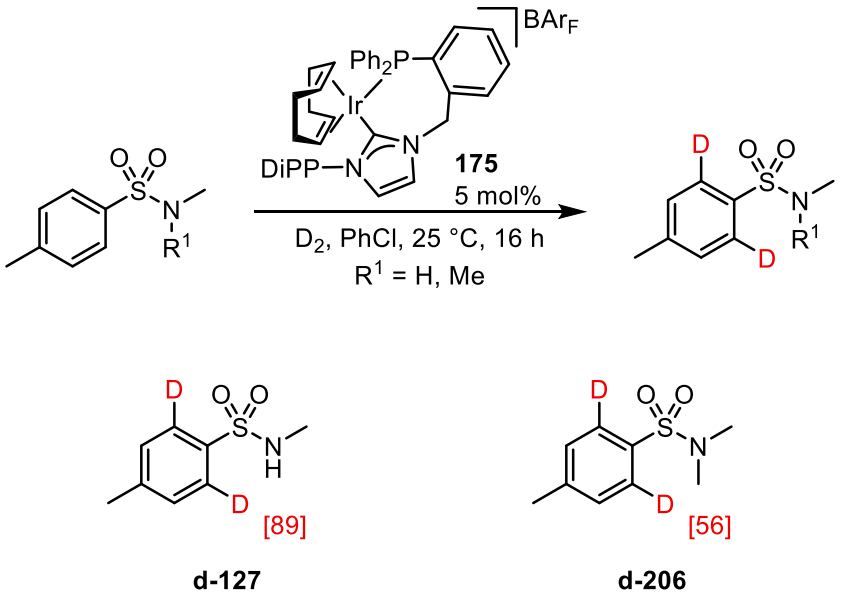

Scheme 4.2

Our first step in moving towards an improved catalyst system was to turn to an *in silico* investigation of the iridium(III) dihydride complexes believed to be the active species. As shown in **Scheme 4.3a**, the conformation in which the substrate is bound through nitrogen is, as expected, marginally more stable compared to that of the oxygen bound conformer. We decided, therefore, to focus our investigations on the nitrogen bound conformers, hoping to generate a catalyst system that could accommodate a bulky group directly bound to the iridium centre. Secondly, we calculated the respective binding energies of *N*-methylbenzene sulfonamide and *N*,*N*-dimethylbenzene sulfonamide in structures **207** and **209**. It was noted that the *N*-substituted example **207** retained good levels of binding energy, similar to that of the sulfone, which are in line the observed levels of deuterium incorporation with analogous

substrate **127**. However, with complex **209** the calculated binding energy was observed to drop considerably (**Scheme 4.3b**). Taking what we learned from the investigation of sulfone labelling, we wished to alter the catalyst system in order to better accommodate such groups in the HIE process. However, in this instance, we elected to move away from a screening of a large set of *in silico* catalyst structures, and instead opted for a more focused adjustment of the system.

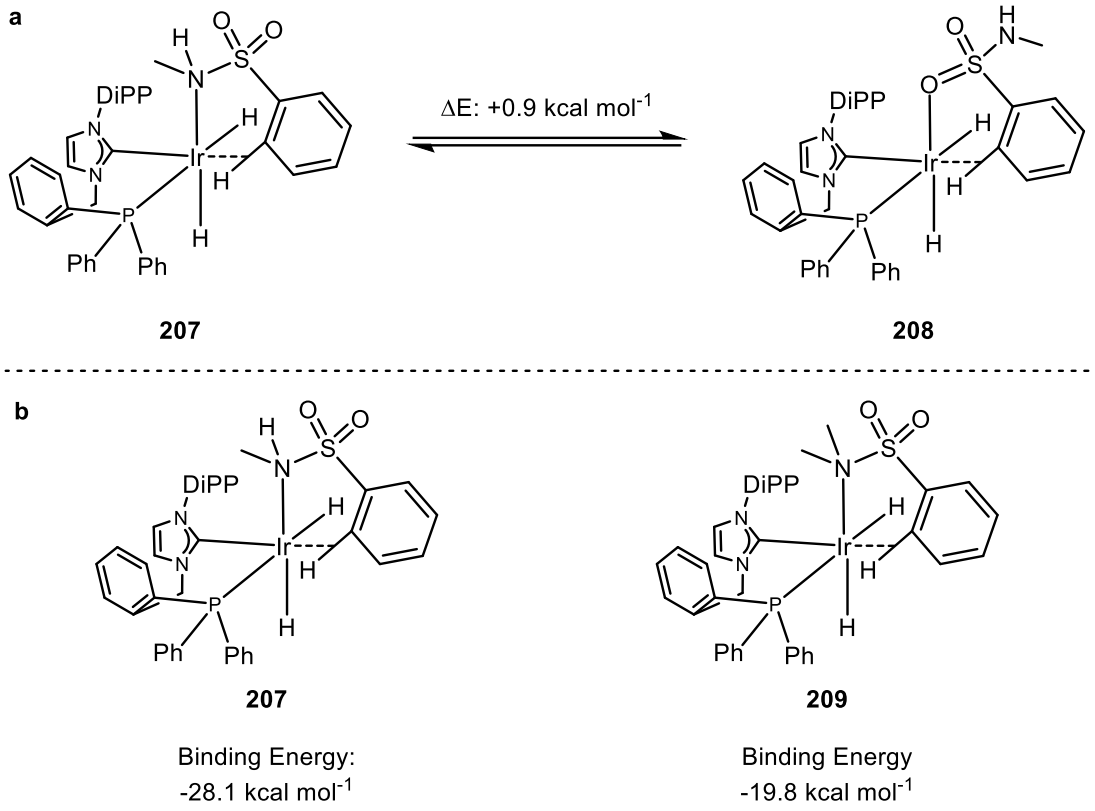

Scheme 4.3

In order to determine which aspect of the catalyst would best be altered to give a more active HIE complex, and believing the cause of poor binding energy to be steric in nature, we hoped to use a method which could advise us on the steric interactions and binding motifs of the respective complex systems. As discussed previously, one of the most common methods for investigating the steric environment of a metal complex is the $\%V_{Bur}$. However, one issue with this method of quantification is that, although it is highly effective in the region close to the

metal centre of the catalyst, we have recently established that overall binding efficiency of a molecule is heavily influenced by extended interactions between the overall catalyst system and substrate.[86] Thus, we instead turned to analysing the solid angles of the catalyst complexes.[87] The concept of a solid angle Ω (**Figure 4.2**), as a mathematical parameter to define areas on the surface of a sphere is relatively simple, and can be defined by:

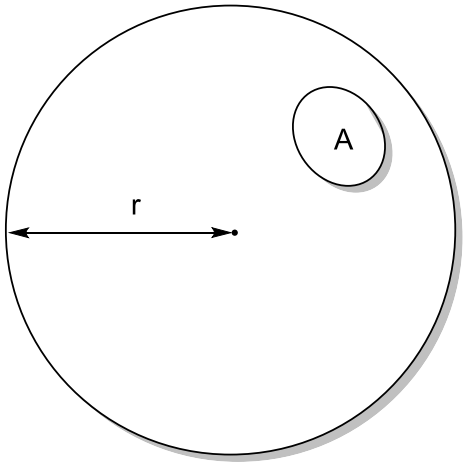

$$\Omega = \frac{A}{r^2}$$

Figure 4.2

Where r is the radius of the sphere on which surface area A has been selected. In terms of parameterizing ligand interactions however, if we place the metal centre of the desired complex at the centre of the sphere and supposed a light shone from this centre, the 'shadow' cast on the hypothetical sphere by the ligands around the metal would have a defined area which can be measured and converted into a solid angle by the above equation. This type of analysis has been shown to be valuable in a series of methodologies throughout organometallic chemistry.[88,89,90,91,92,93,94] Thus, the DFT optimised structures **202**, **207**, and **209** were subjected to solid angle analysis using SolidG, software which allows for a streamlined method for measuring the solid angles, among other parameters, of metal complexes. From the data generated in this program, the application SolidAngleGL8 can be used to visualise the information, as shown in **Figure 4.3**. In the visualisations given, the solid angles corresponding to the atoms of the NHC-P ligand are shown in blue, while that of the substrate, in each case, is shown in red.

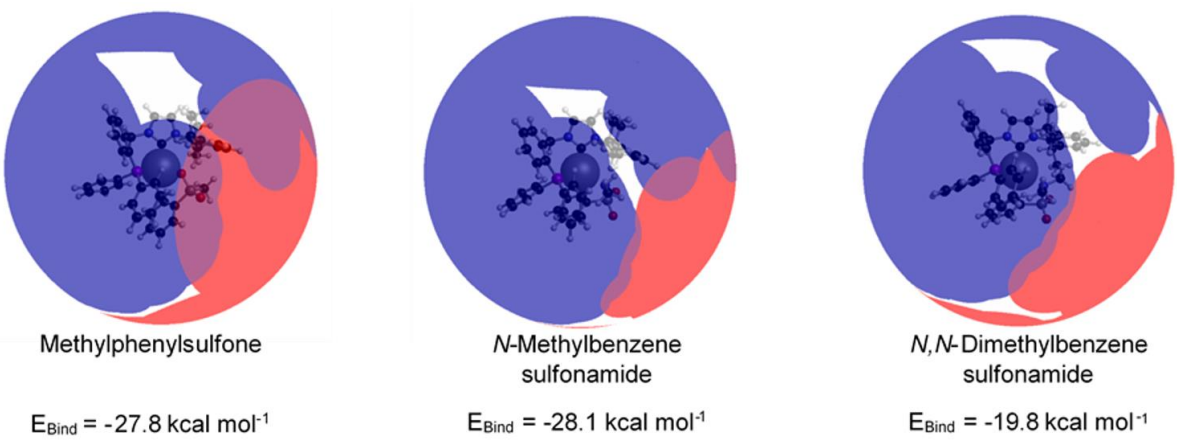

Figure 4.3

Table 4.1 highlights the information derived from this analysis, as well as the Ir—X bond lengths in each case. In analysing the solid angles, a series of parameters can be derived. The total occupation of the metal ligand sphere, represented as a percentage, is shown as SumGL. The overlap in solid angle of the two ligands is represented by Gγ. It is imperative to note that this value is not automatically a direct indication of steric encumbrance, as many overlaps in 3D space can be stabilizing (π-π stacking, C—H-π interactions etc.), destabilizing (steric repulsion, columbic repulsion), or even neutral. However, what can be derived from this parameter is information on how the system in question is bound. Furthermore, this parameter has been decomposed into the contributions to this value from the phosphine and NHC portions of the ligand, $G\gamma_{Phos}$ and $G\gamma_{NHC}$, respectively.

Table 4.1

Entry	Substrate	SumGL (%)	Gγ (%)	$G\gamma_{Phos}$ (%)	$G\gamma_{NHC}$ (%)	Ir—X (Å)
1	**108**	82.83	4.40	1.12	3.29	2.331
2	**127**	86.41	2.64	0.34	2.30	2.400
3	**206**	85.24	0.90	0.37	0.53	2.576

In moving from the relatively unhindered sulfone **108**, to the more hindered *N*-methylsulfonamide **127**, a significant increase in the Ir—X bond length is observed. While the SumGL shows a clear increase, the level of overlap between the solid angle of the ligand and substrate (Gγ) experiences a notable decrease. Examining this in more detail, it can be seen that the substantial steric bulk of the phosphine forces a distortion in the binding motif of the substrate. This is evidenced by the reduction of overlap between the phosphine portion of the ligand, and the substrate (1.12% with **108**, 0.34% with **127**), with respect to the more modest decrease experienced by the NHC portion (3.29% with **108**, 2.30% with **127**). Despite these influences, however, the increased Lewis basicity of the nitrogen atom ensures that a favourable binding energy of -28.1 kcal mol^{-1} is retained. Considering the even more bulky *N*,*N*-dimethylbenzenesulfonamide **206**, the Ir—X bond length increases further still, causing an overall decrease in SumGL, despite the increased steric bulk of the substrate. Significant steric clash with the phosphine portion of the ligand causes further distortion of the substrate binding motif, leading to a reduced Gγ of 0.9%, and an overall reduction in substrate binding energy to -19.8 kcal mol^{-1}. From this combination of computationally derived parameters, it was hypothesized that reducing the steric demand of the phosphine portion of the NHC-P ligand could lead to a more accessible catalyst system that can accommodate more hindered sulfonamide substrates. This is highly fortuitous: since the difficulties associated with handling and synthesizing phosphines (particularly those small in nature) require not inconsiderable effort, we viewed this as an opportunity to arrive at a system with a more efficient synthetic route. Additionally, phosphine building blocks towards such hypothetical ligands can often be expensive, or require long synthetic routes to acquire, strengthening our preference for other Lewis basic groups.

Our first consideration as a sterically less encumbered replacement for the phosphine moiety was a phenoxide, similar to those showcased by Duckett.[95] It was thought that perhaps a neutral

chelated system might be able to act as a chelated analogue of the neutral chlorocarbene catalysts which previously proved successful with primary sulfonamides (**Figure 4.4**). Unfortunately, however, it was found that, while this motif presented a significantly less encumbered ligand sphere, the catalyst was now electronically less predisposed towards substrate binding, owing to the significantly more electron-rich metal centre, when compared to that of cationic complexes such as **207**. Thus, poor binding energies were observed, even with the relatively strongly binding *N*-methylbenzene sulfonamide substrate in **210**. An attempt was made to modify the electronics of the system, by placing a nitro group in the *para*-position of the phenoxide in **211**, however this did not raise the binding energy to acceptable levels.

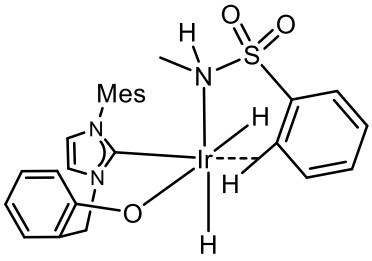

210
Binding Energy: -20.7 kcal mol^{-1}

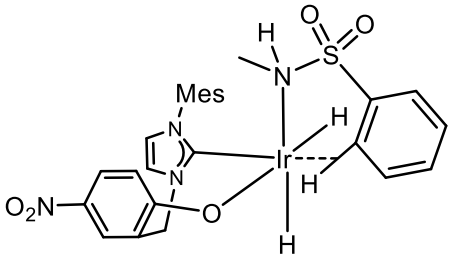

211
Binding Energy: -24.2 kcal mol^{-1}

Figure 4.4

In light of this, it was decided that a cationic complex would be best, in order to retain a good electronic disposition towards substrate binding. Our next suggestion was to replace the large triarylphosphine with a pyridine group. This type of structure would retain the cationic nature at iridium, whilst also incorporating a much smaller Lewis basic group as the ligand. To reiterate, a favourable binding energy of -28.7 kcal mol^{-1} was calculated with methylphenyl sulfone NHC-P complex **202**, which was matched by that of *N*-methylbenzene sulfonamide complex NHC-P **207**. Increasing the steric bulk around the substrate resulted in a drop in binding energy to only -19.8 kcal mol^{-1} in **209** (summarised in **Figure 4.5a**). Understandably, we were delighted to see that, not only was an excellent binding energy value of -27.8 kcal

mol^{-1} calculated for the NHC-Py complex bearing *N*-methylbenzene sulfonamide in **212**, but that an almost identical value was calculated for the analogous NHC-Py complex bearing *N*,*N*-dimethylbenzene sulfonamide **213**. Interestingly, the binding energy of this new NHC-Py catalyst motif with methylphenyl sulfone sees a reduced binding energy of only -23.8 kcal mol^{-1} (complex **214** compared with **202**). This is likely due to the fact that in moving from an NHC-P motif to an NHC-Py motif, we have removed a significant π-acceptor, leaving the iridium centre more electron rich than it was previously, and thus less electronically disposed to substrate binding.

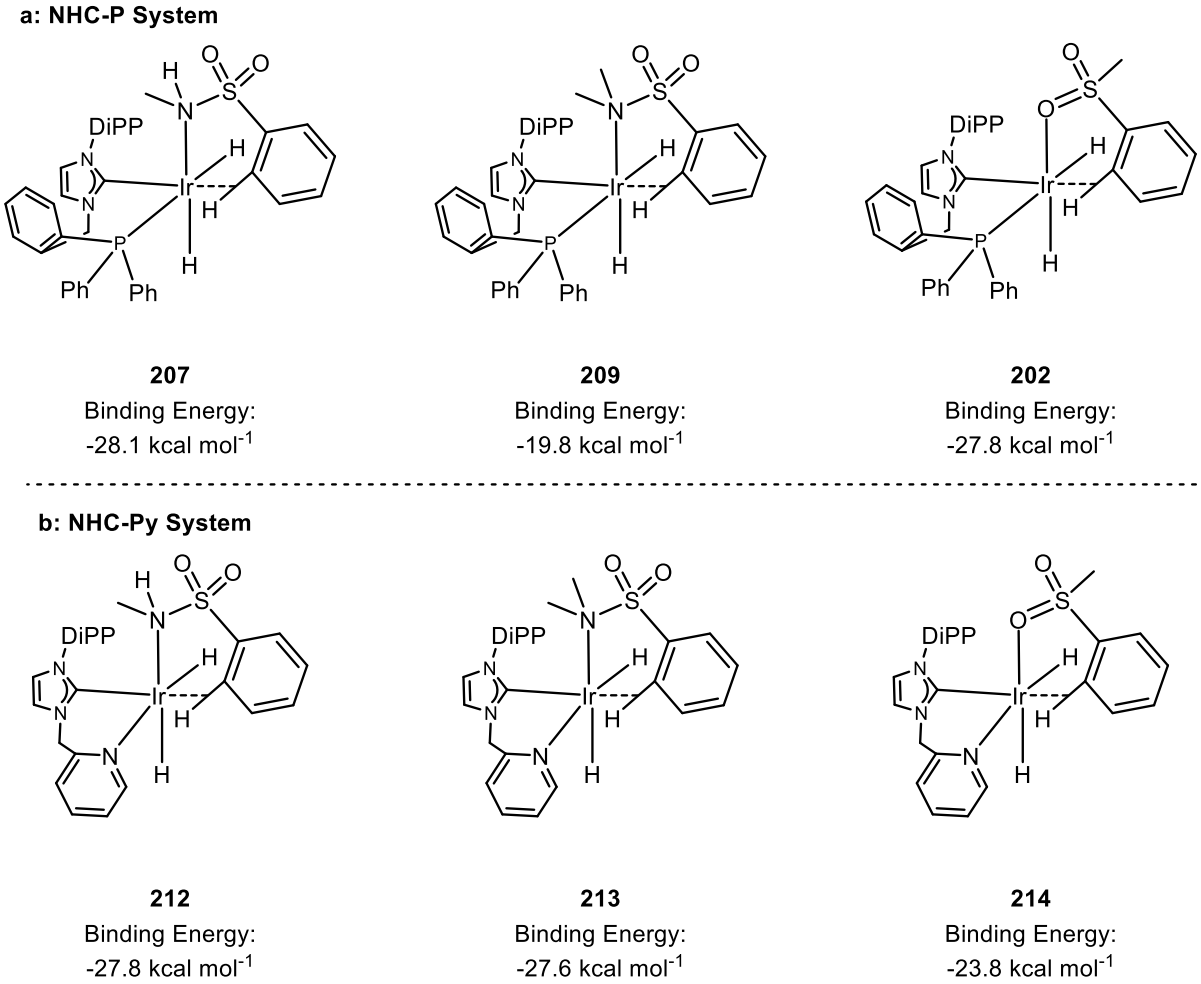

Figure 4.5

As an additional comparison to the steric influences of both these catalysts, complexes **212**, **213**, and **214** were subjected to the same solid angle analysis. Changing the catalyst structure in this way has left us with overall reduced values for the solid angle data, rendering direct comparison difficult. However, what does lend useful information is the change in Gγ values across each substrate class, as shown in **Figure 4.6**. As previously noted, with the NHC-P system we see a dramatic change in this value between each of the three substrates. However, when examining the NHC-Py system, a much more consistent binding motif is observed, reflected by the more consistent Gγ value across the three substrate classes.

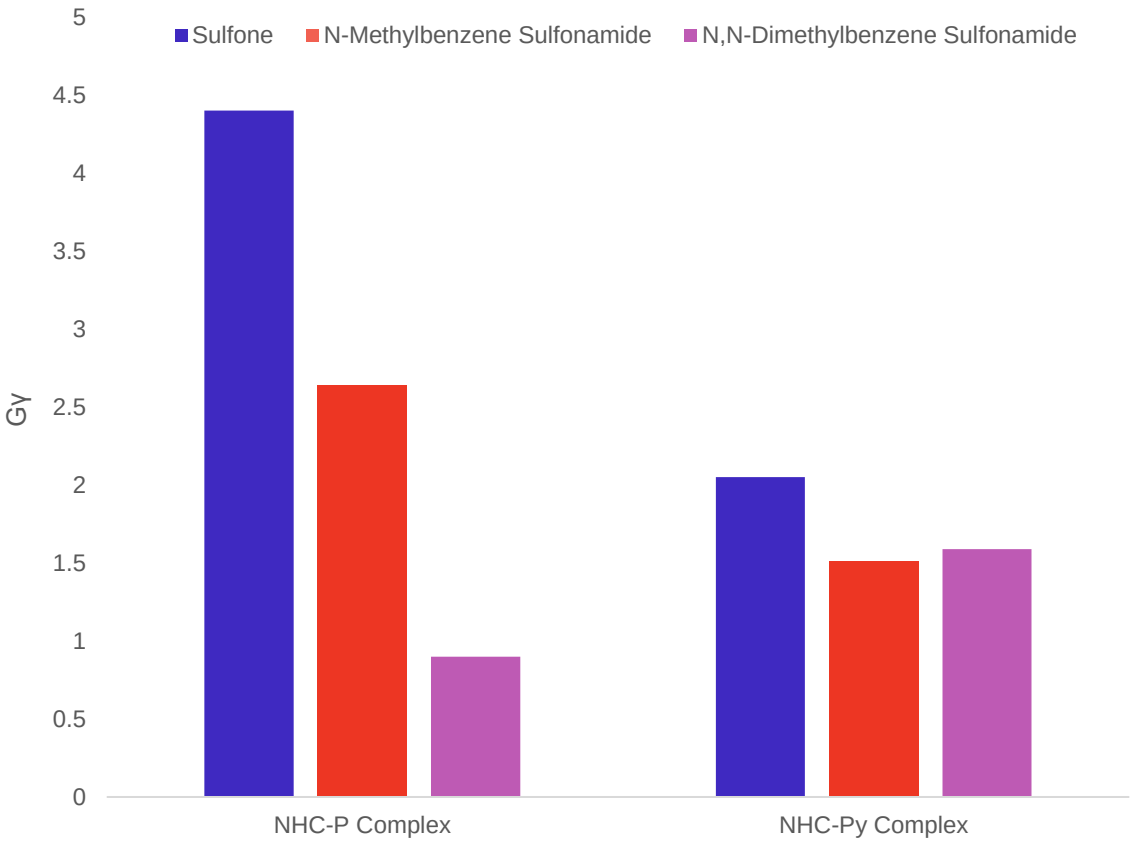

Figure 4.6

This NHC-Py complex, at first look, appears to be a promising candidate. In order to progress this candidate catalyst further, the next focus was to ensure that such a complex would be able to undergo the C—H activation process in a facile manner, in order to apply it in HIE under

mild conditions. The kinetic barrier for the NHC-P system for activating the *ortho* C—H bond was calculated to be 14.5 kcal mol^{-1} (*vide supra*). Similar values would be required with our new NHC-Py system, in order to ensure good reactivity. **Figure 4.7** below shows a comparison of the calculated energy barriers in each case. It was found that the C—H activation process for the NHC-Py system with *N*,*N*-dimethylbenzene sulfonamide bound complex **213**, through transition state **216** giving dihydrogen complex **217**, is reasonably close to that previously calculated for the activation of sulfone bound complex **202**. This led us to believe that activation should still be a facile process in this new system. One particularly interesting difference between the two calculated activation processes, however, is that the resultant dihydrogen complex for the NHC-Py system **217** is much more destabilised with respect to the dihydride complex, in contrast to complex **203**. Thus, one would expect the reverse reaction (C—H bond formation, or analogously, C—D bond formation) to be rapid. However, we did not foresee this to be problematic.

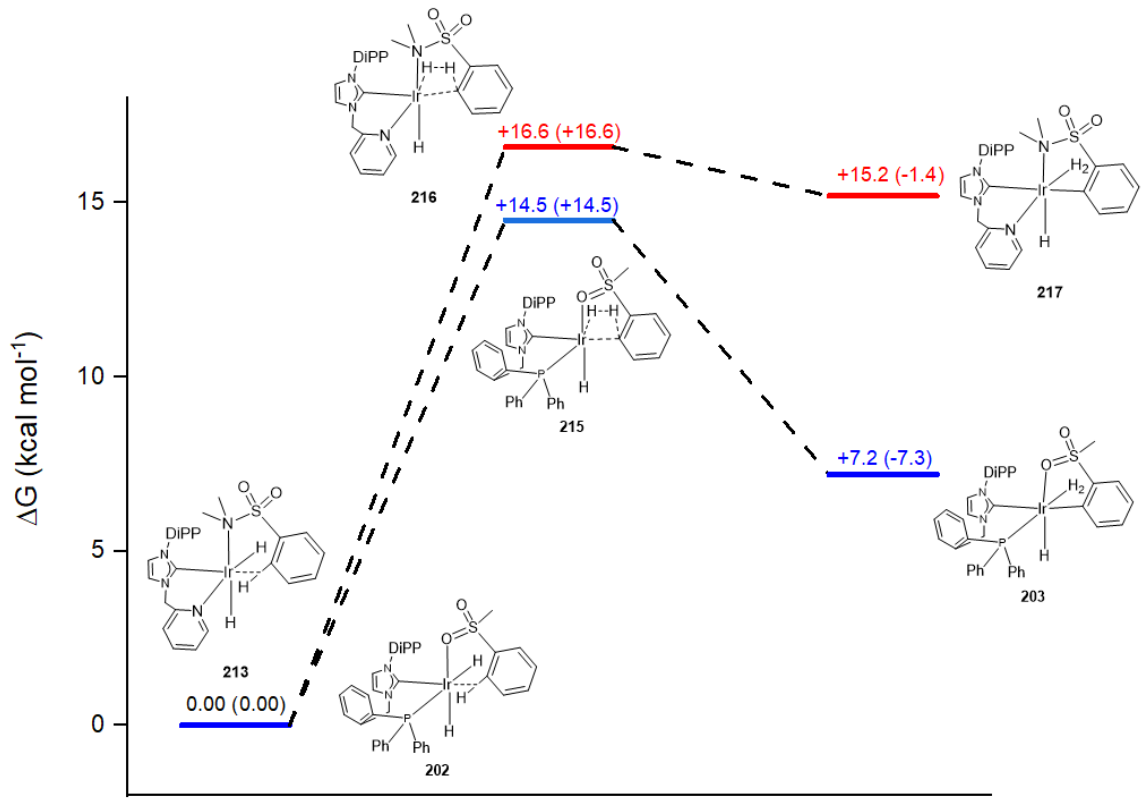

Figure 4.7

With a promising computational profile in front of us, we next moved to synthesising the corresponding iridium(I) precatalyst complex **218** for testing in the HIE of hindered sulfonamides. It was anticipated that the relevant complex could be accessed, from the corresponding imidazolium salt **219**, which in turn could be afforded readily *via* alkylation of di-i*so*-propylphenyl imidazole **180**. This is shown retrosynthetically in **Scheme 4.3**.

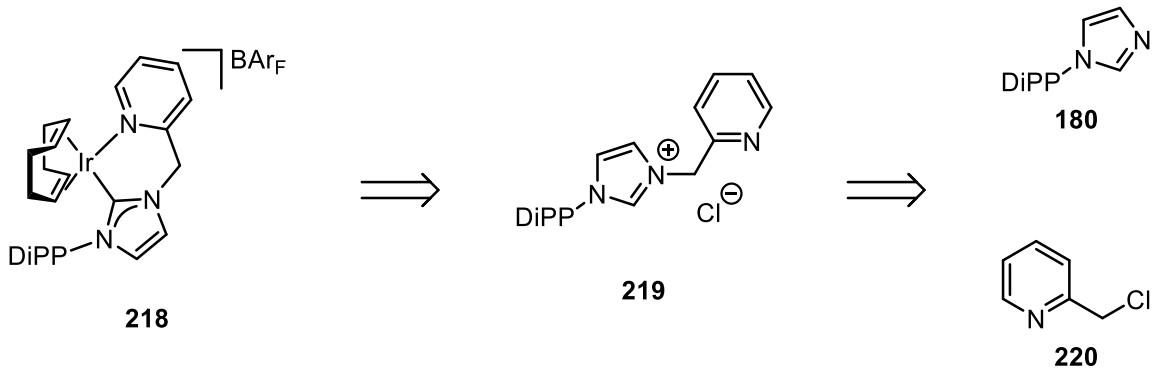

Scheme 4.4

Moving on to the forward synthesis, chloromethylpyridine **220** could be synthesised from pyridinemethanol **221** (**Scheme 4.5**). Unfortunately, it was found that this compound degraded even upon storage in the freezer and under argon, and, therefore, it was synthesised and used immediately. This product **220** could then be used in a neat alkylation reaction to afford **219** in a reasonable 49% yield. It is likely that this reaction could be further optimised, however, in its current form, it provided useable amounts of **219** in a timely fashion. Attempts to complex this imidazolium salt to $[Ir(COD)Cl]_2$ with the methods previously applied (*vide supra*), using potassium *tert*-butoxide as a base, gave complex mixtures. This is potentially due to the acidic centre at the methylene position which is produced upon binding to a metal centre.[96] Fortunately however, it was found that first forming the corresponding silver carbene and then transmetallation to iridium, followed by halide abstraction with $NaBAr_F$, afforded the desired complex **218** in good yields. One important note is that the silver species must be thoroughly purified prior to the transmetallation step, as stability issues were experienced in batches

wherein the silver complex was taken on without purification. The impurity which causes this degradation has proven extremely challenging to identify.

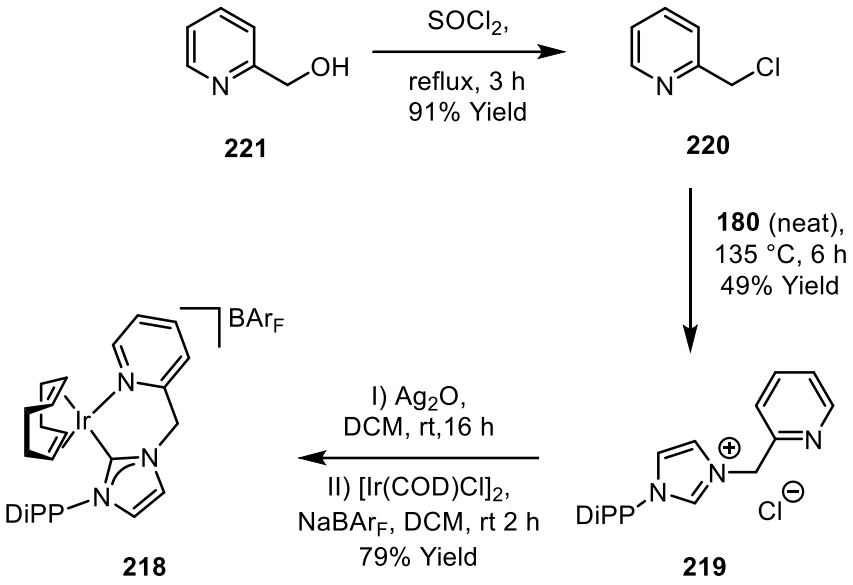

Scheme 4.5

Finally, we were also able to obtain an x-ray crystal structure of **218**, confirming its structure (**Figure 4.8**, see *Appendix* for full details).

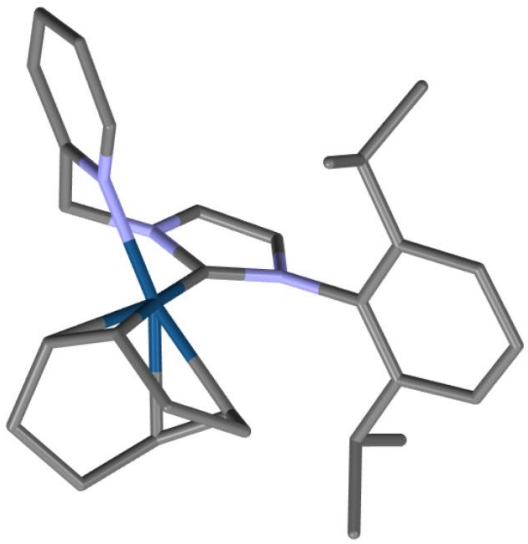

Figure 4.8

With the novel complexes in hand, we sought to also characterise the electronics of the system, by again observing the iridium(III) dihydride species in the ^{1}H NMR spectrum (**Scheme 4.6**). One interesting note that was made when performing the experiment was that, while the NHC-P complexes activate rapidly when exposed to deuterium gas, these NHC-Py systems appear to activate more slowly, with the colour change taking place over a duration of ~2 hours. Nonetheless, the data could be collected with ease, as it appears that the iridium(III) hydride species that form are exceptionally stable, remaining stable, in deuterated acetonitrile, in an NMR tube at room temperature overnight. This is in sharp contrast to the chelated NHC-P and monodentate NHC/phosphine catalyst systems, where the dihydride complexes would degrade over the course of a few hours. Additionally, the standard region of the ^{1}H NMR spectrum was exceptionally clear and could be analysed with ease. Once again, with a chelated system, there is the risk for several isomeric complexes to be formed in solution. Fortunately, only one species appears to form, with a single set of signals which can be attributed to one of two isomeric complexes, **222a** or **222b**.

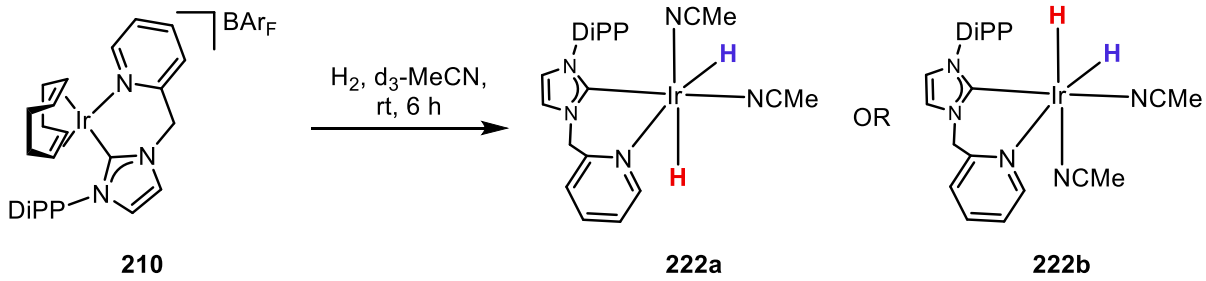

210 **222a** **222b**

Scheme 4.6

4.2 Application of Novel NHC-Py Type Catalyst in the Labelling of Highly Substituted Sulfonamides

With the novel NHC-Py iridium(I) precatalyst complex in hand, we immediately applied this in the labelling of *N*,*N*-dimethylsulfonamide **206** (**Scheme 4.7**). Again, reaction times of 16 hours were used to ensure the full reactivity of the complex could be observed. We were delighted to see a marked increase in the levels of incorporation, returning to the levels previously observed with the sulfone labelling. Furthermore, the reaction could also be performed with a reduced reaction time of six hours, giving very similar levels of incorporation.

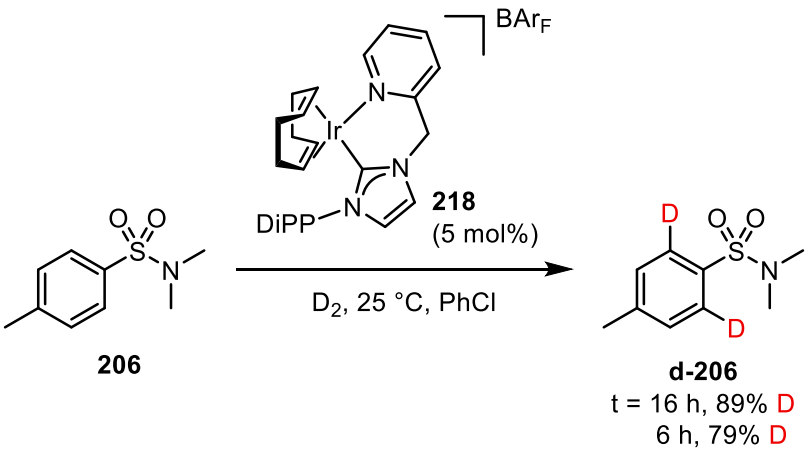

Scheme 4.7

Delighted with this initial result, we wished to further examine the scope of labelled sulfonamides encompassed by this complex. In order to support this endeavour, a series of 21 sulfonamide substrates were synthesised (see *Section 8* for full details of substrate synthesis) Firstly, we examined the scope of *N*-substituted sulfonamides (**Scheme 4.8**). *N*-methyltoluenesulfonamide **127** gave similar levels of isotope incorporation to the bulkier *N*,*N*-disubstituted analogue **206**. With the methyl substituent in the *meta*- position, high levels of labelling were maintained at both positions of incorporation, with an average of 94%. Increased steric bulk around the nitrogen atom, with *N*-cyclopropyl analogue **223c** and *N*-*tert*-butyl derivative **223d**, was well tolerated, with both substrates giving high levels of incorporation.

N-methylnaphthylsulfonamide **223e** showed a significant difference between the 2- and 8-positions; with 97% incorporation at the 2-position, through a 5-membered metallacyclic intermediate (5-mmi), and 50% at the 8-position through a 6-mmi. *N*-benzyl substituted example **223f**, however, showed little discrimination between the two aryl labelling positions, with 81% at the aryl sulfonamide and 87% at the *N*-benzyl *ortho*- positions. In studying the *N*-phenyl derivates **223g** and **223i**, it was noted that gently warming the reaction to 40 °C was required for consistent levels of labelling, with excellent levels of isotope incorporation observed in both. While 4-methoxy-*N*-(4-trifluorophenyl)benzenesulfonamide **223h** did not require heating for consistent labelling, a moderate drop in incorporation at the more electron poor ring was nonetheless noted.

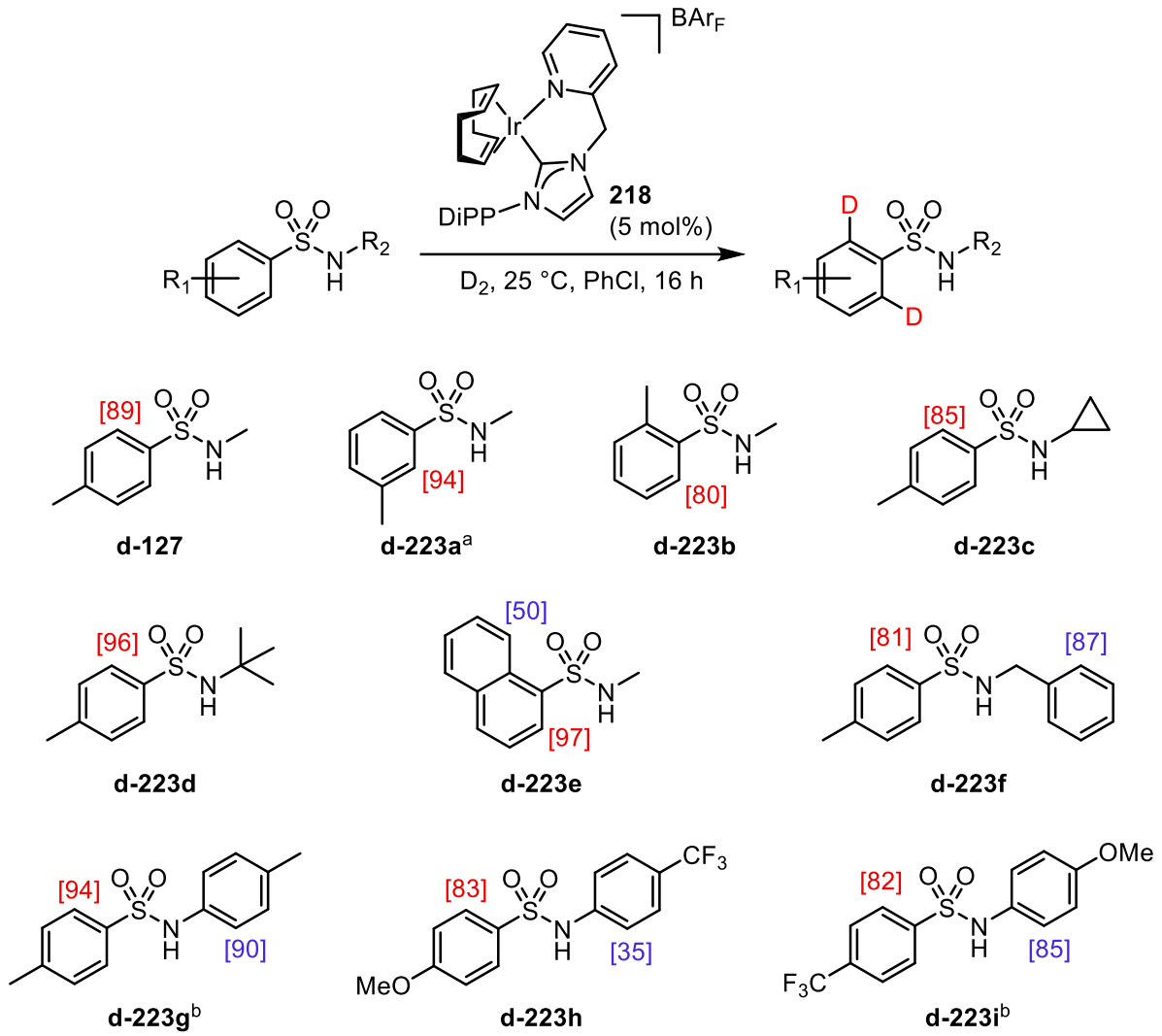

[a]Incorporation given as an average over both positions
[b]Reaction performed at 40 °C

Scheme 4.8

Next, the scope of labelling with *N*,*N*-disubstituted sulfonamides was examined (**Scheme 4.9**). Electron-rich sulfonamide **223j** showed high levels of isotope incorporation at 93%. Electron poor **223k** showed a slight drop to 72%, albeit with gentle heating to 40 °C to maintain consistency. Increasing the steric bulk of the system further still with *N*-tolyl-*N*-*iso*-propyl substrate **223l** does not hinder incorporation, with exceptionally high levels of deuterium incorporation observed. *N*-Tosyl tetrahydroquinoline **223m** incorporated high levels of deuterium into both aryl rings, while *N*-methanesulfonyl tetrahydroquinoline **223n** also

incorporated excellent levels of deuterium into the remaining aryl ring. *N*-Tosyl piperidine **223o** was well tolerated, with 91% incorporation. The successful labelling of *N*-tosyl pyrazole **223p** was observed, albeit with complete selectivity for the tosyl moiety, directed by the superior Lewis basicity of the pyrazole nitrogen. In contrast to this, in the isomeric *N*-tosyl imidazole **223q**, where the nitrogen atom can still complex but can no longer direct labelling, no incorporation was observed. Next, *N*-tosyl indole **223r** was investigated. Despite a total of three potential positions for directed deuterium incorporation, the system showed good selectivity for the 2- and 7-positions of the indole ring, incorporating excellent levels of deuterium into both.

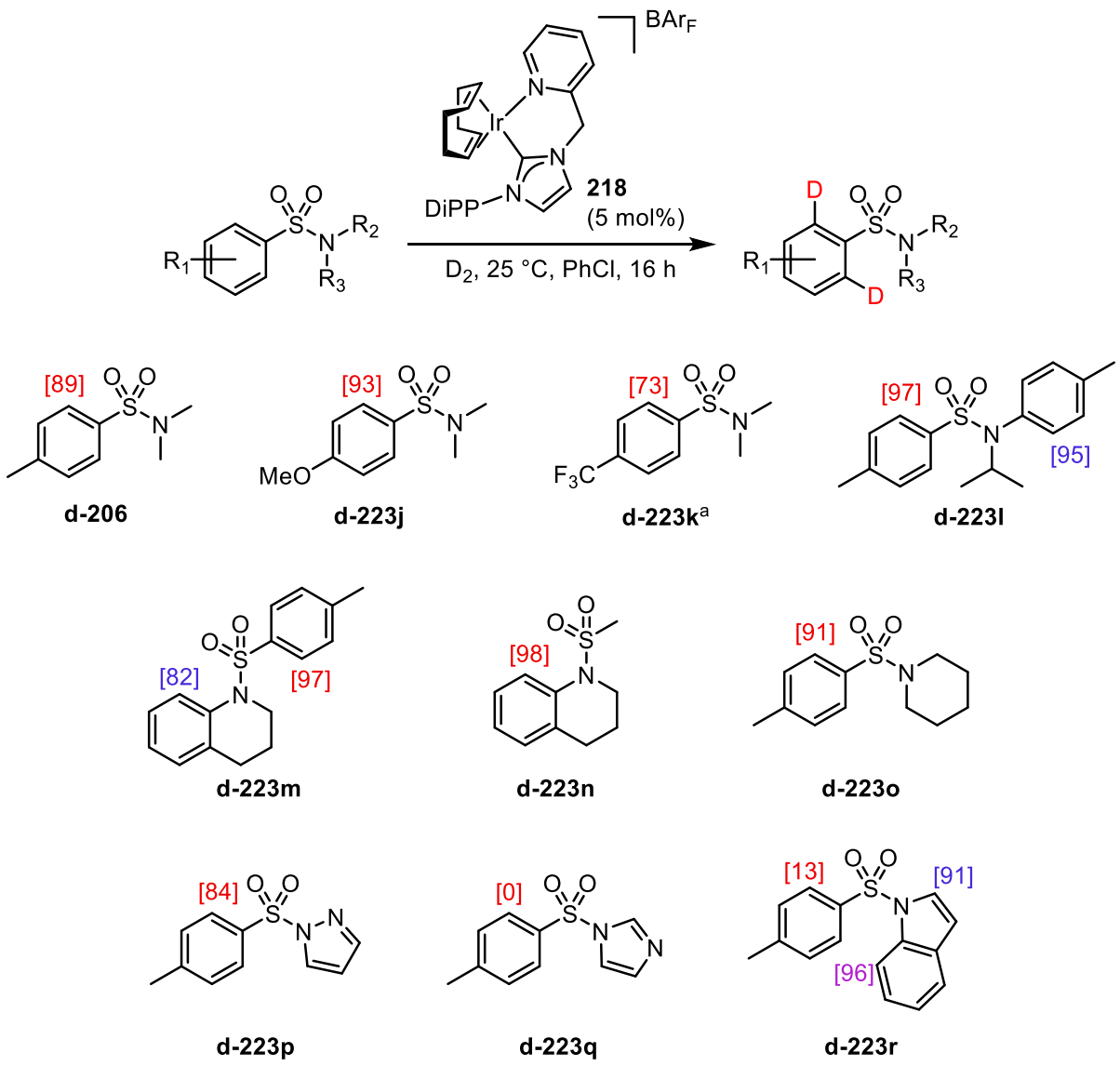

[a]Reaction run at 40 °C

Scheme 4.9

Delighted with the substrate scope established thus far, we finally turned to examining the effect of competing intramolecular directing groups with this catalyst system (**Scheme 4.10**). Firstly, methyl-(4-nitrobenzene)sulfonamide **223s** showed high levels of incorporation, through both directing groups, with no discrimination between the two, albeit at 40 °C. Next, we moved to examine other competent directing groups, ester **223t** and amide **223u**. Both showed excellent levels of incorporation into the respective substrates, however, sulfonamide directed labelling was significantly reduced. While in these cases, the labelling is delivered by

the more powerful directing group, it is promising to see that this NHC-Py catalyst system is an effective catalyst for HIE processes directed by other functional groups.

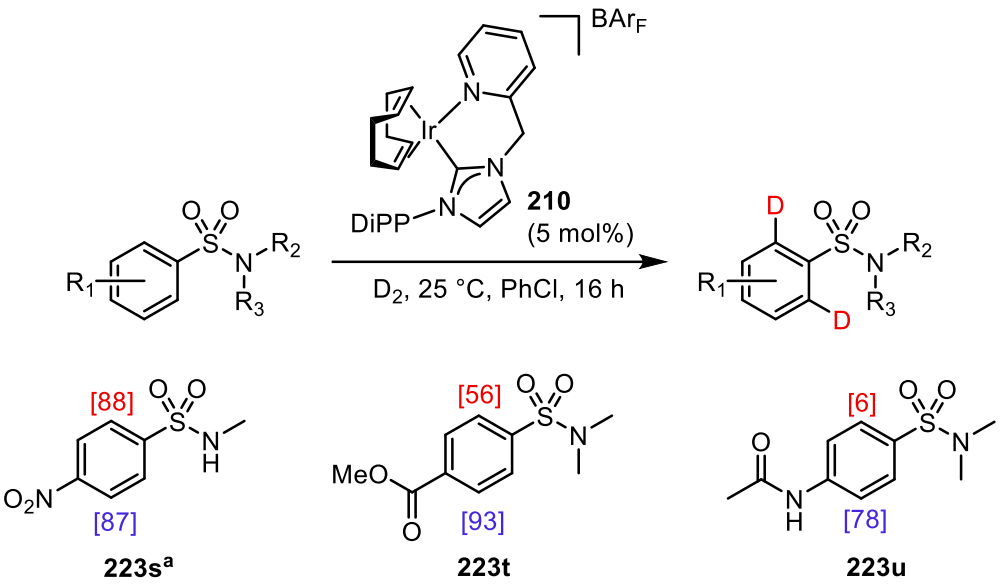

[a]Reaction run at 40 °C

Scheme 4.10

4.3 Understanding NHC-Py Reactivity with Computational Support

We were pleased with the established substrate scope of HIE of highly substituted sulfonamides using our newly developed NHC-Py catalyst system. The catalyst system is highly active, delivering a wide range of labelled sulfonamide substrates to excellent levels of incorporation under mild conditions. As mentioned in *Section 1*, since undertaking this work, other groups have also showcased the ability of other iridium catalysts systems for the directed HIE of substituted sulfonamides. Most notable of these is the application of the Tamm catalyst which, similarly to our system, appears to be able to deliver labelled sulfonamides under mild conditions.[55] However, despite the similarities with our system, we believe both of these catalyst systems to be highly complementary. **Scheme 4.11** below shows some key comparisons between the results of each study into the labelling of sulfonamides. Firstly, a

comparison between **112** and **223g**, we can see that the Tamm system is proficient in activating a substrate primarily through a 5 mmi, as no incorporation was reported on the *N*-phenyl group. Contrasting this, our own NHC-Py system is highly proficient in labelling both positions. It also appears that each catalyst system is capable of activating both sites on a naphthyl substituted compound, such as in **216** and **223e**. Initially, it appears as though there may be a difference in selectivity here also, however the electronic effect of the NMe_2 group, as well as the substitution on the sulfonamide, cannot be discounted and further investigation would be required prior to drawing any further conclusions. The indole examples, **224** and **223r**, are particularly interesting. Using the Tamm catalyst, it appears there is some selectivity for activating the C2 position, with significant competition on the phenyl ring. With our NHC-Py catalyst, however, there is good selectivity for labelling on the indole with only 13% incorporation on the phenyl ring. In addition to this, our catalyst systems also allow activation of the C7 position of the indole, which is labelled to an excellent level of 96%. Through these initial comparisons, it can be seen that both of these catalyst systems could potentially have distinct uses throughout the labelling community. Indeed, in many instances, selectively labelling one position reliably is required in order to analyse specific metabolites within the realms of an ADMET study; however oftentimes, incorporating significantly higher levels of a label is more favourable, such as in the generation of mass spectrometry standards, or tritium-based experiments which require high levels of specific activity.

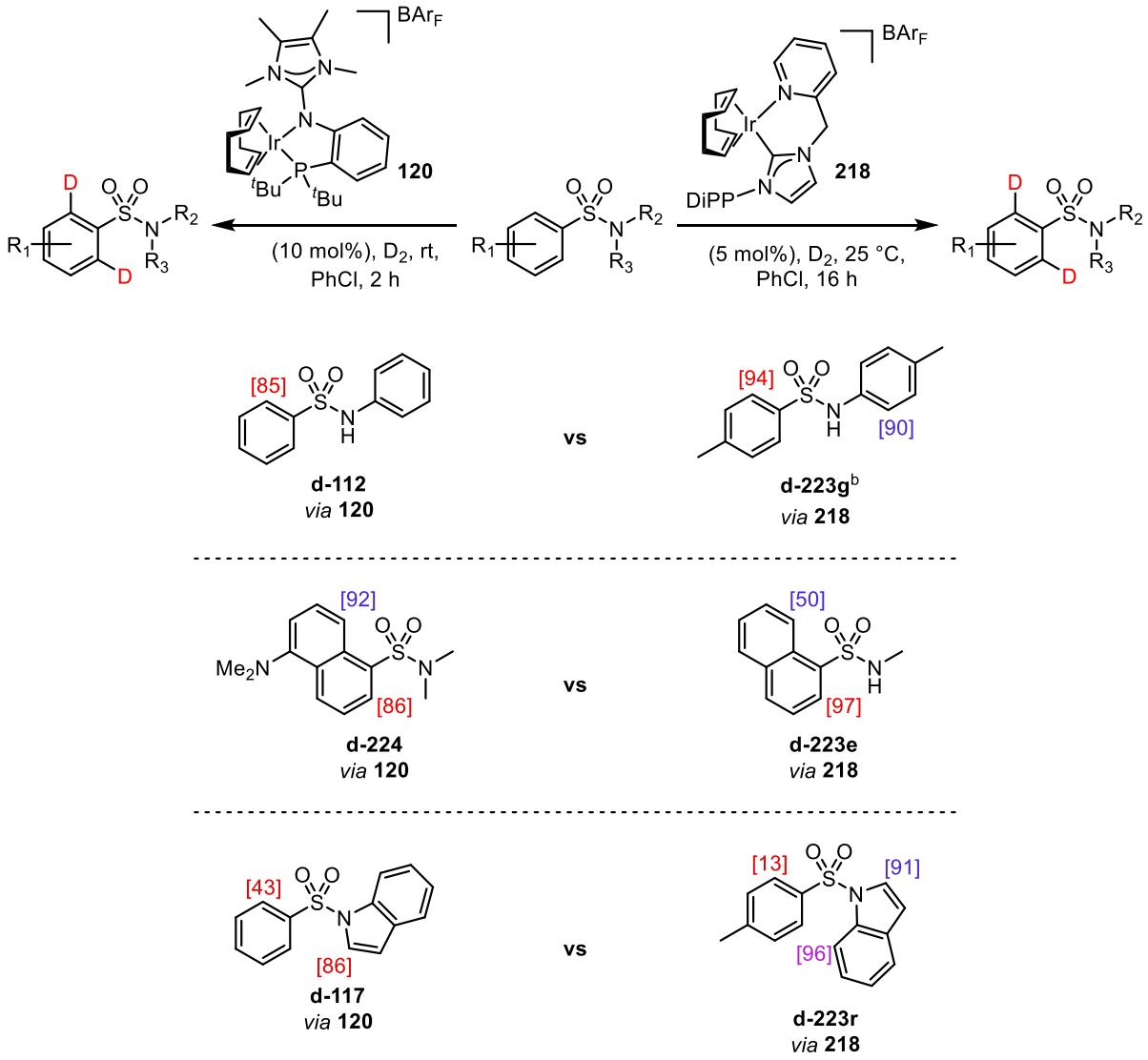

Scheme 4.11

In observing the ability of our NHC-Py catalyst system to activate C—H bonds through both a 5- and a 6-mmi, we initiated a short study in the interest of gaining a better understanding of the reactivity of our system. As mentioned previously, the monodentate catalyst systems of type **57** (shown again in **Scheme 4.12**) also have the ability to activate both sites within a molecule such as benzanilide **65**.[41] However, we were able to gain selectivity between the sites simply by lowering the catalyst loading to 0.5 mol%. Thus, we reasoned that by running a reaction with our NHC-Py system under reduced catalyst loadings, a similar selectivity might be observed. Thus, we decided to take **223g** as a model substrate, which incorporates excellent

levels of deuterium into both positions at 5 mol% catalyst loading. When this was performed at a reduced loading of 1 mol%, we did indeed see a reduced level of incorporation through a 6-mmi, however, quite surprisingly, the level of deuterium incorporated through a 5-mmi also dropped to the same level. This curious observation has led us to believe that there is a potential for both of these positions to be activated at similar rates.

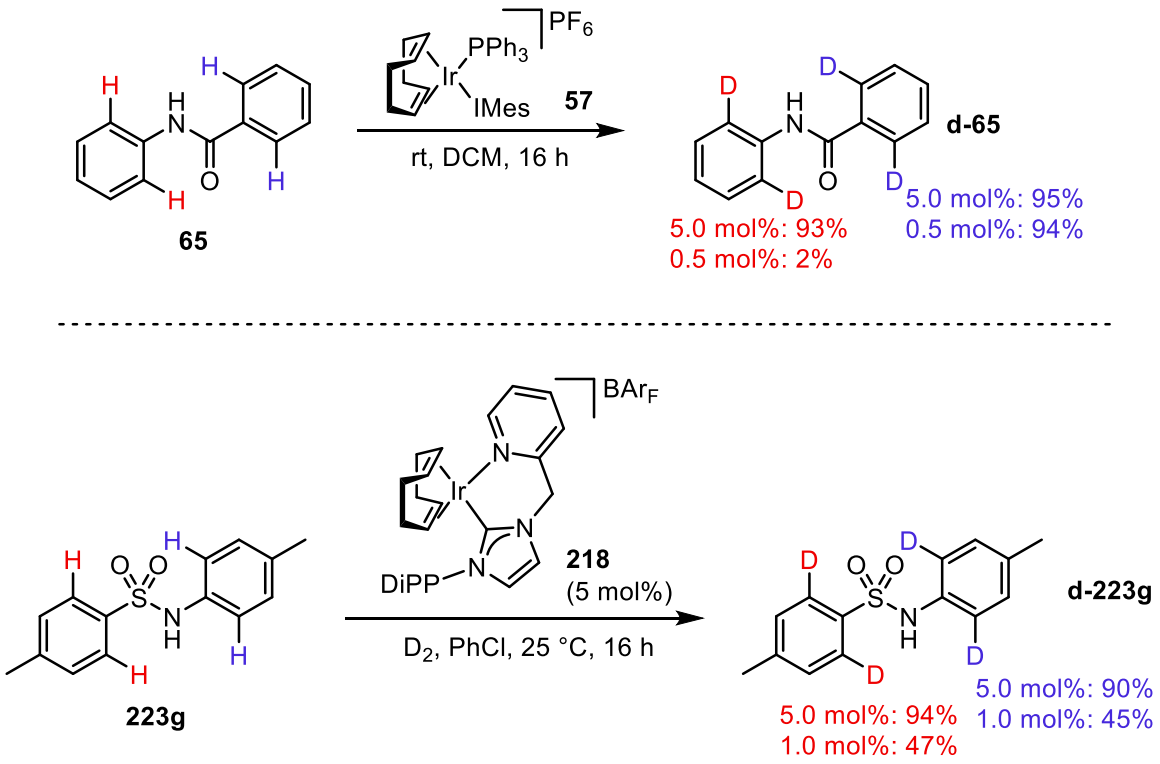

Scheme 4.12

In order to address this hypothesis, we once again turned to DFT calculations. Initially, we examined the various binding conformers of the analogous *N*-phenylbenzene sulfonamide to the corresponding NHC-Py iridium(III) hydride species, in complexes **225a-c** (**Figure 4.9**). While complex **225a**, which forms an agostic interaction prior to forming a 5-mmi, has a binding energy in the region expected, according to our previous calculations during catalyst design, the oxygen directed analogue **225b**, has a significantly lowered binding energy. Surprisingly, however, the oxygen bound species which would activate the C—H bond to form a 6-mmi, complex **225c**, has a very similar binding energy to that of **225a**.

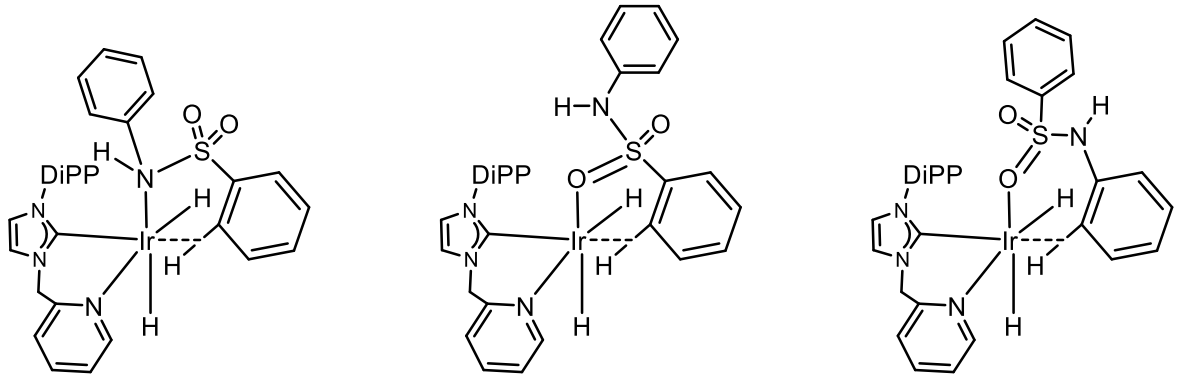

***N*-Bound, 5 mmi 225a**
Binding Energy:
-27.7 kcal mol^{-1}

***O*-Bound, 5 mmi 225b**
Binding Energy:
-22.4 kcal mol^{-1}

***O*-Bound, 6 mmi 225c**
Binding Energy:
-26.4 kcal mol^{-1}

Figure 4.9

In observing this, we next turned to investigating the kinetic energy barrier to C—H activation and formation of the corresponding dihydrogen complex in each case. This is shown in **Figure 4.10**. What is seen is that the barrier to activation of a C—H bond is relatively low in all cases (11.4 kcal mol^{-1}, 12.1 kcal mol^{-1}, and 16.3 kcal mol^{-1}, respectively). As expected, the barrier to forming a 6-mmi has the highest barrier at 16.3 kcal mol^{-1}, with that of the *N*-bound 5-mmi being marginally smaller at only 12.1 kcal mol^{-1}. However, what is surprising is the relative free energies of the dihydride structures, wherein the *O*-bound **225c** appears to be the most stable of the three, by at least 4.79 kcal mol^{-1}.

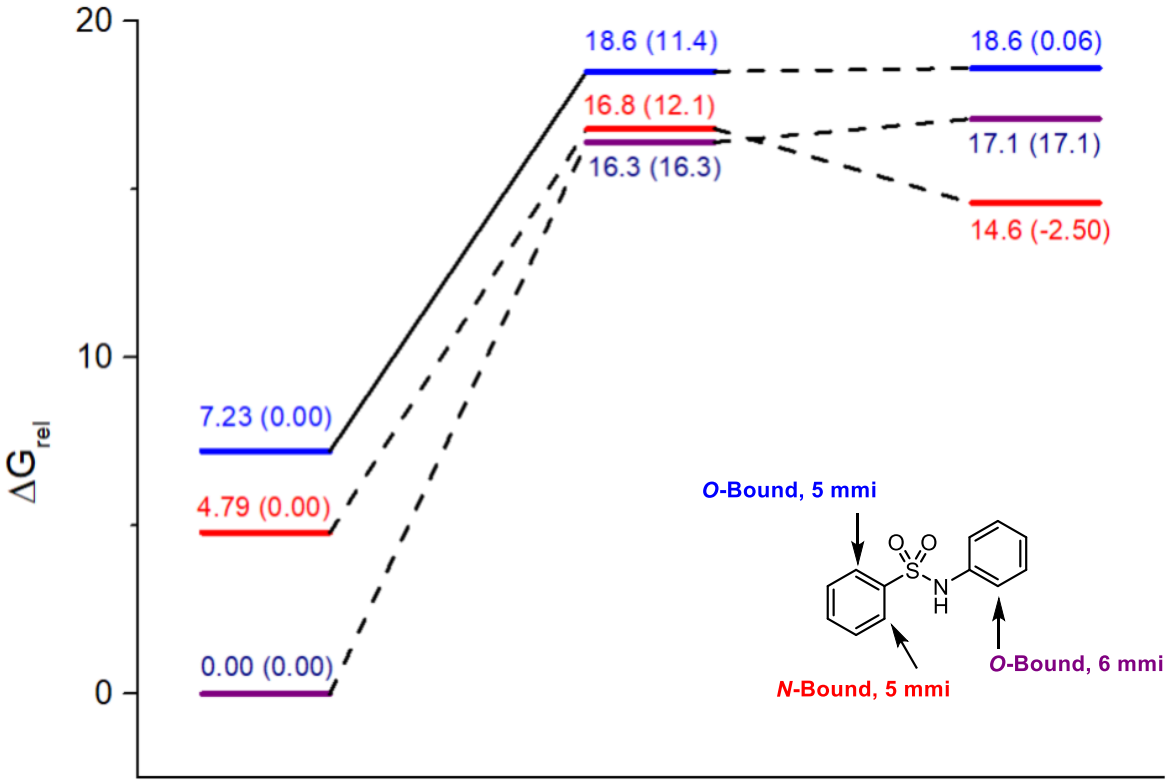

Figure 4.10

In order to gain more insight, we next selected a substrate with multiple points of activation, but which also showed selectivity between the sites, namely *N*-tosyl indole **223r**. This substrate showed excellent levels of selectivity between the C2/C7 positions of the indole to that of the tolyl ring. As such, we subjected the analogous sulfonamide **117** to the same *in silico* investigation, generating complexes **226a-c** (**Scheme 4.13**). It should be noted that no agostic complexes where the nitrogen of the indole is bound to the iridium centre could be found. We therefore believe that the oxygen atoms are solely responsible for incorporation in this example.

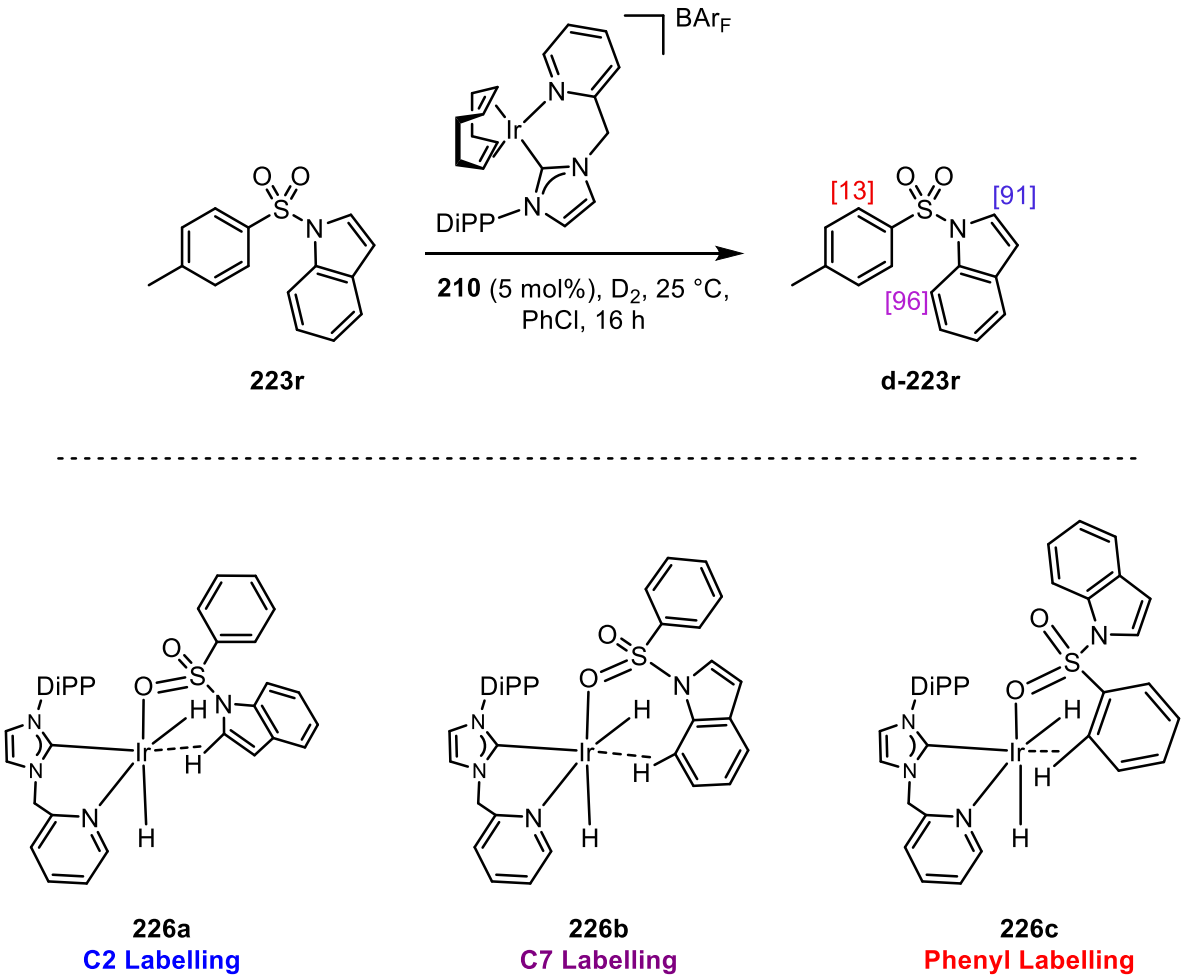

Scheme 4.13

The relative energies of these complexes, as well as the barrier of activation to the corresponding dihydrogen complex were compared (**Figure 4.11**). Surprisingly, it appears that the activation of the benzene ring, in which we observed very little incorporation, actually exhibits the lowest barrier to activation, at only 4.98 kcal mol^{-1}. However, it would appear that the free energy of the dihydride complex **226c** is significantly higher than **226a** and **226b**, indicating that very little of this species would actually be present in solution. Contrasting this, the difference in energy between **226a** and **226b** is much smaller.

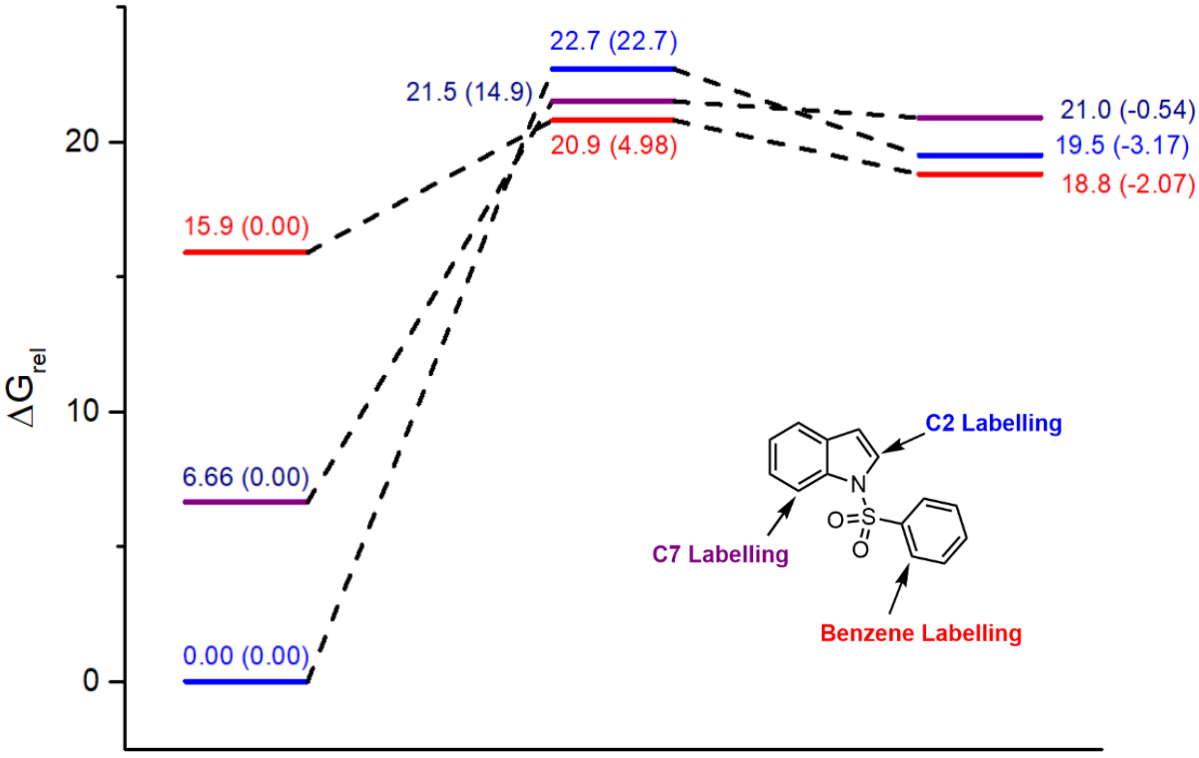

Figure 4.11

While investigating the labelling of heterocyclic aromatic compounds using the monodentate complexes, it was shown that the site selectivity observed was determined by the relative barriers to C—H activation.[47] However, it appears that this is no longer the case when applying the chelated NHC-Py system. We hypothesise, therefore, that, owing to the high proficiency in these systems to activate C—H bonds, the observed selectivity in these systems is a result of the relative free energies of the corresponding dihydride complexes. In order to further support this hypothesis, confident rate data for these systems would have to be acquired. Additionally, it should be noted that these calculations were completed using the same level of theory which was used for the catalyst design and screening processes in the previous section. This combination of method and basis set prioritises efficiency in the calculation of transition metal complexes, which we chose to allow us reasonable accuracy at low computational cost. However, if we wished to attain quantitative information for the comparison of rate data, a higher, more accurate, level of theory should possibly be considered.

4.4 Applying NHC-Py Systems to the Labelling of Other Pharmaceutically Relevant Sulfur Based Functional Groups

Confident that we had developed catalyst systems proficient in the labelling of aryl sulfones and highly substituted sulfonamides, we next turned our attention to other sulfur based groups which are prevalent throughout the pharmaceutical industry. One particular functional group which has gained much focus in recent years is the sulfoximine. [97,98,99] Indeed, many advanced clinical candidates that make use of a sulfoximine group have already been put forward. A series of such molecules are highlighted in **Figure 4.12**. The kinase inhibitor, BAY 10000394, is currently in Phase II trials, and incorporates an S-cyclopropane group on the sulfoximine.[100] Suloxifen was proposed as an antiasthmatic before clinical trials were terminated, and takes advantage of an *N*-alkyl substituted sulfoximine.[101] Meanwhile the ATR inhibitor, AZD6738, has been proposed as an anticancer treatment, and is currently also in Phase II trials.[102] Finally, the kinase inhibitor BAY 114572 is in Phase I clinical trials. Furthermore, each of these compounds contains an aryl ring which one could imagine being labelled through exploiting the sulfoximine in directed HIE.

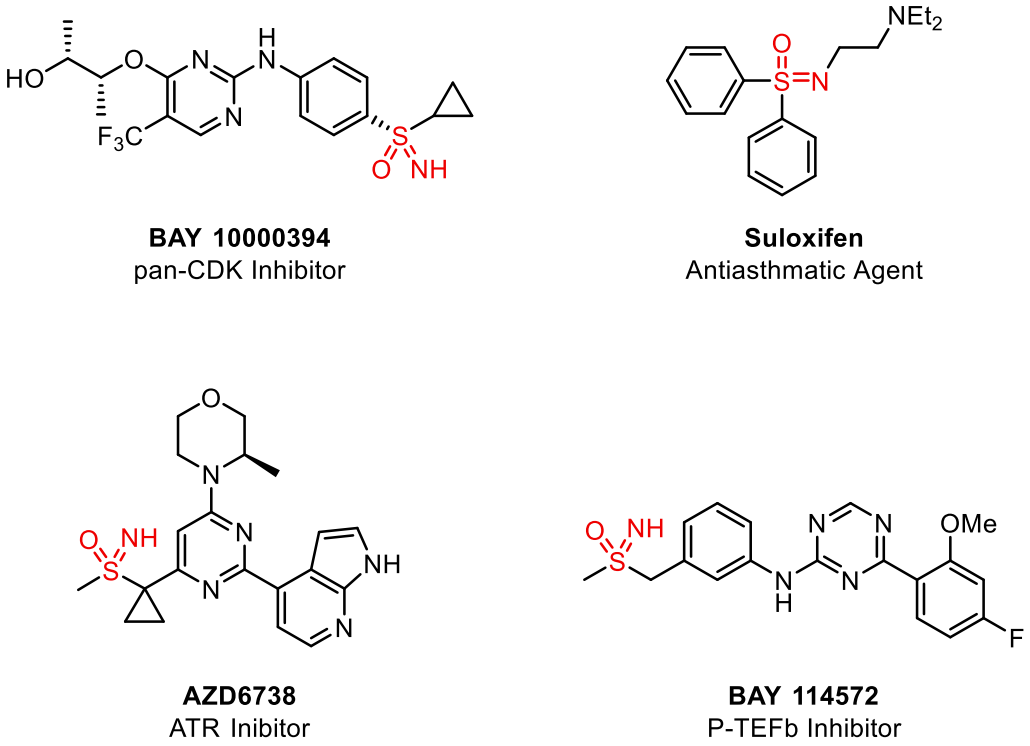

Figure 4.12

We hoped to apply our new NHC-Py catalyst system to the labelling of a simple model sulfoximine, reasoning that the structural similarity to that of a sulfonamide should allow us to access such structures with minimal optimisation. In applying the same conditions used for the labelling of highly hindered sulfonamides, we were delighted to see good levels of incorporation at 73% (**Scheme 4.14**). In order to rationalise the slight drop in incorporation, with respect to the excellent levels observed in the sulfonamide substrate scope, we calculated the binding energy of sulfoximine **227** to the NHC-Py iridium(III) dihydride complex in **228**. Here, we observed an exceptionally high binding energy of -36.6 kcal mol^{-1}. Indeed, it would appear that the significantly stronger binding ability of this group limits catalyst turnover, and in this way results in a lower incorporation.

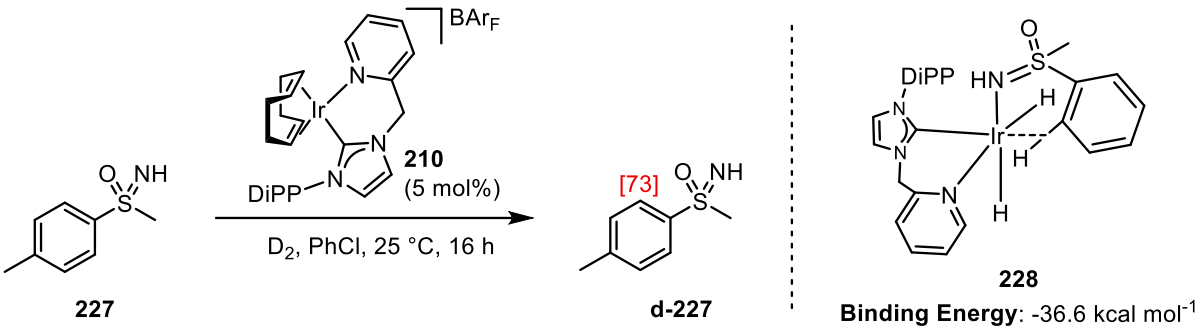

Scheme 4.14

With this in mind, we next investigated the *N*-ethyl variant of this compound **229**, predicting that the more hindered nitrogen would have a reduced binding energy and give higher levels of isotope incorporation (**Scheme 4.15**). We were elated to see this was the case, with a significantly improved 97% incorporation being observed. Surprisingly, however, deuteration of the *S*-methyl group of this compound was also observed, to lower but significant levels of 12% incorporation.

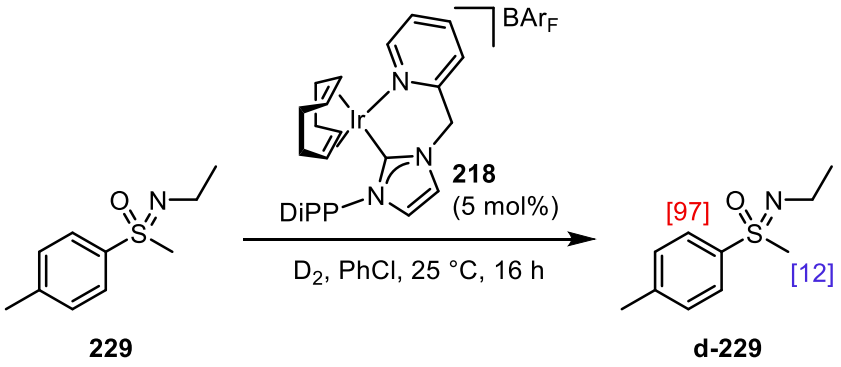

Scheme 4.15

Curious about this unexpected result, we also conducted a rate study (**Figure 4.13**). It appears that, despite the long reaction time of 16 h used for the labelling of these sulfoximines, the deuteration of the aryl ring reaches the desired levels in about four hours. Additionally, the incorporation observed at the *S*-methyl group reached its maximum level very quickly, and remained fairly constant across the study.

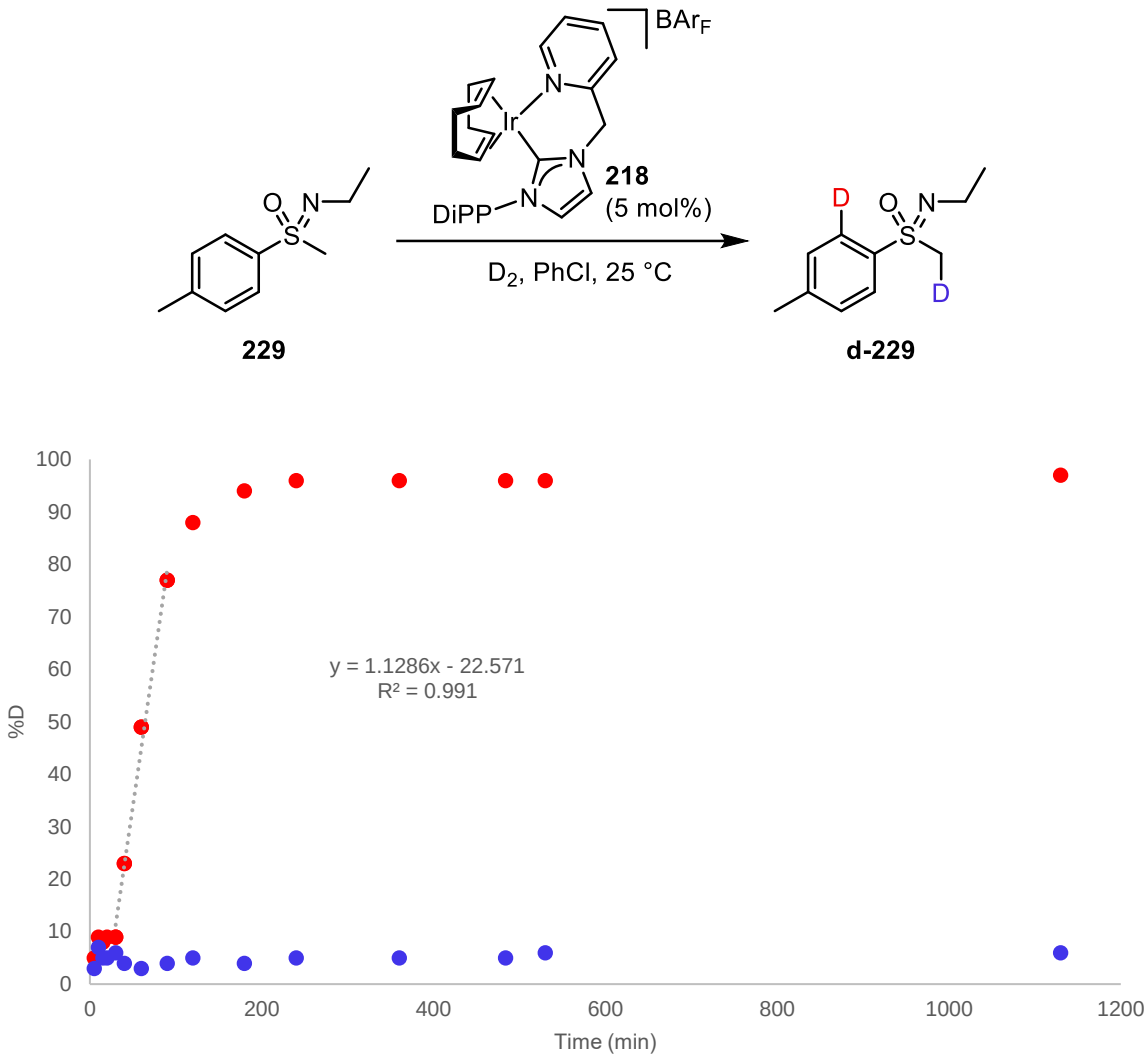

Figure 4.13

We were curious to discover whether this unexpected labelling also occurred with other catalyst motifs. Therefore, we also applied monodentate NHC/phosphine type catalyst **75** to the labelling of **227** and **229** (**Scheme 4.16**). It was expected that, much like the sulfonamides, the aryl positions would not be deuterated, while the *S*-methyl group, depending on the mechanism, may retain the observed levels of incorporation. Again, we were surprised by the results of these experiments. Not only was the deuteration on the S-methyl group significantly increased in both cases (24% for **227** and 51% for **229**), but the aryl ring in each case was also labelled to excellent levels.

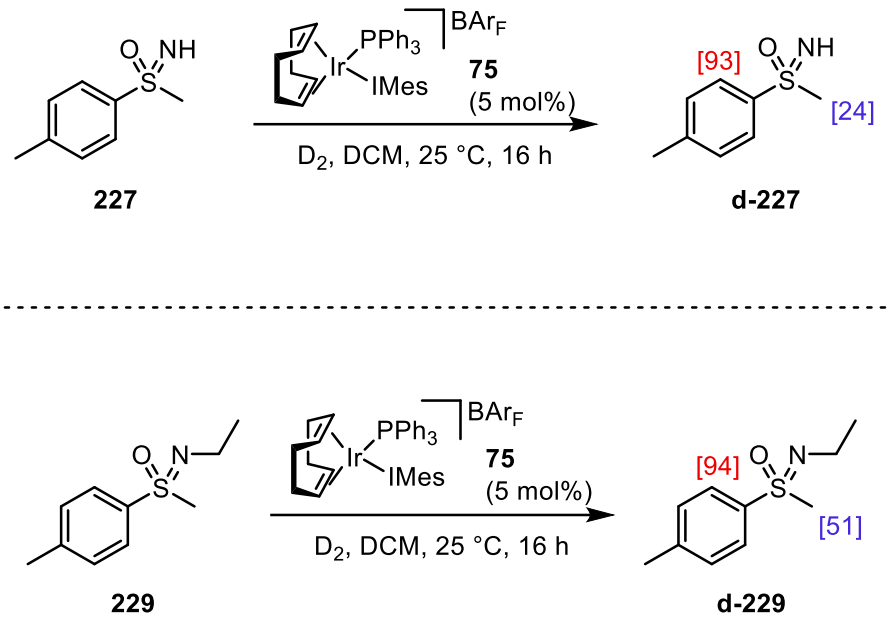

Scheme 4.16

Whilst we were delighted to learn that several catalyst generations could be used to label these sulfoximine substrates, we wished to understand the difference in the ability of the monodentate systems to exploit these tetrahedral sulfur-based groups in directed HIE. Initially, we calculated the respective binding energies of a sulfonamide and sulfoximine to the monodentate catalyst system, as shown in **Figure 4.14**. There appears to be a significant discrepancy between the values, with the sulfonamide in complex **230** giving a binding energy of only -22.7 kcal mol^{-1}. The sulfoximine binding energy, in complex **231**, however, is calculated to be -28.4 kcal mol^{-1}. This difference in binding energy highlights the effect that the geometry not only of the directing group as a whole, but specifically that of the bound atom, can have on the binding energy of the substrate. In the monodentate systems, only a small region around the iridium centre is available for substrate binding, due to the significant steric influence of the phosphine and NHC ligands. Using a tertiary nitrogen atom results in significant amount of steric clash. A planar nitrogen, such as that in the sulfoximine example, experiences less steric repulsion and results in better binding energies. However, the calculated binding energy for **230** is still in line with what we would expect for good levels of

incorporation (see acetophenone, *vide supra*). Thus it is possible that another aspect of the reaction system is responsible for the lack of incorporation. Furthermore, a more thorough investigation to account for the electronic effects of this structural change would also be highly valuable.

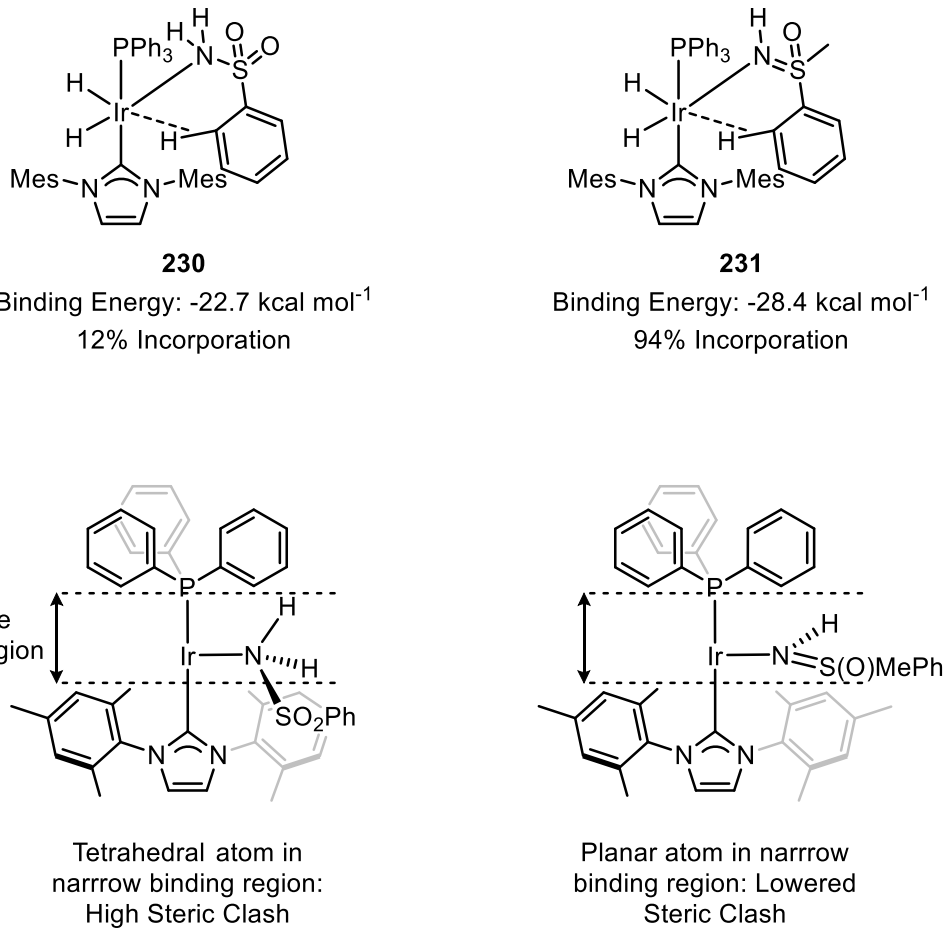

Figure 4.14

Thus, we have established that several catalyst systems designed within our group are highly proficient in the labelling of sulfoximines, highly desirable targets in medicinal chemistry. Further work is required to understand both the ability of the monodentate catalyst system to exploit these directing groups, as well as the source of the unexpected labelling of the *S*-methyl group.

5. Investigating Alternate Applications of Chelated Iridium Catalysts Within HIE

5.1 Initial Screening of Chelated Systems in Ether Labelling

While establishing the scope of our NHC-P chelating catalyst system **175** in the labelling of sulfones, we investigated substrate **108t**, which possesses an acetal group in the *para*-position. While we were delighted to see excellent deuterium incorporation of 93% through the sulfone, quite unexpectedly, we also noted a significant 26% incorporation being directed by the acetal.

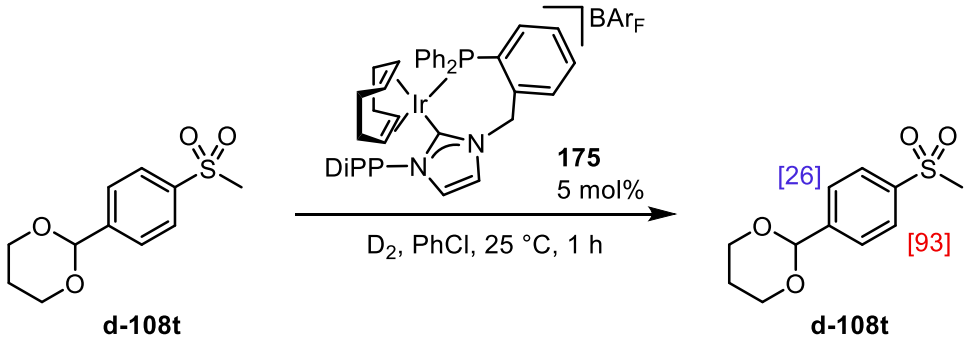

Scheme 5.1

This being the first instance of incorporation through such a group in our iridium catalysts, we wished to understand why the monodentate NHC/phosphine systems had not shown the ability to label these types of molecules. **Figure 5.1** below shows the corresponding monodentate and chelate complexes with a model acetal substrate, 2-phenyl-1,3-dioxane. It appears that, in the monodentate system, a low binding energy of only 14.9 kcal mol^{-1} is found. Contrasting this, when the same substrate is bound in the chelated system in **232**, a much improved binding energy of -29.9 kcal mol^{-1} is calculated. We believe this, again, to be the influence of the geometry of the bound atom. While carbonyl groups have proven to be highly effective directing groups for HIE using these catalyst systems, when considering acetals or ethers, the presence of extended substitution, as well as extraneous lone pairs around the oxygen,

significantly hinders the substrate's ability to bind to the metal centre. The more accessible catalyst sphere offered by the chelated system however, attenuates this effect.

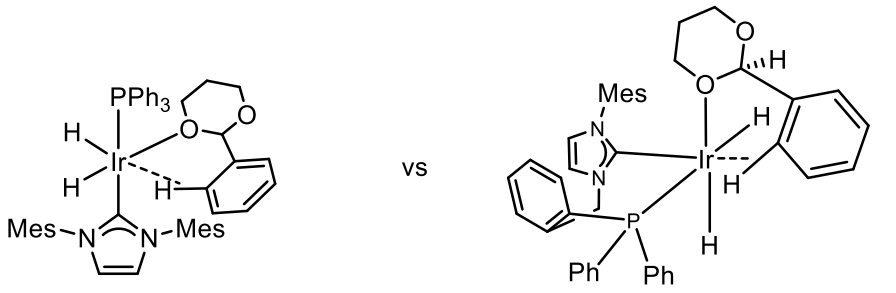

232
Binding Energy = -14.9 kcal mol^{-1}

233
Binding Energy = -29.9 kcal mol^{-1}

Figure 5.1

Confident that our chelated NHC-P system **175** would be an excellent catalyst for the labelling of ether substrates, we turned to optimising the system using a model substrate, 2-tolyl tetrahydrofuran **234** (**Table 5.1**). See *Section 8* for the full details of the synthesis of **234**, as well as the other ether substrates used in this section. In applying our catalyst system to the labelling of **234** over 16 hours, we were elated to see an excellent level of 96% incorporation. Furthermore, reducing the reaction time to one hour did not impede observed levels of isotope incorporation. We were also able to reduce the catalyst loading to only 2.5 mol% and still see excellent levels of incorporation, but to ensure that even more challenging ether substrates could be included, we decided to retain a catalyst loading of 5 mol% as our optimised conditions. It was noted, however, that MTBE, a solvent which performed admirably with sulfones, was a poor solvent for this substrate class, likely owing to its ether functionality, which could compete with the substrate in binding to the metal centre.

Table 5.1

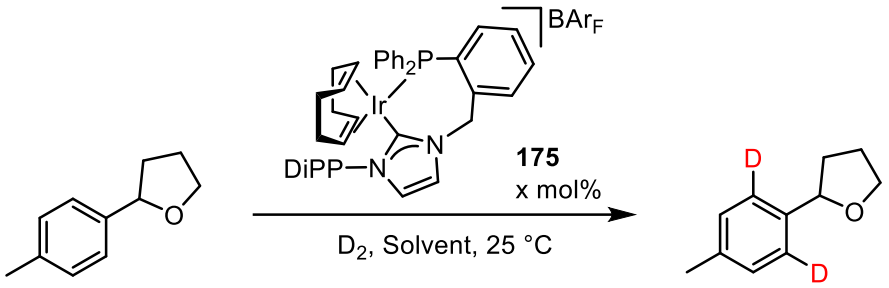

234 **d-234**

Entry	Solvent	Time (h)	Catalyst Loading (mol%)	Incorporation (%)
1	PhCl	16	5.0	96
2	PhCl	1	5.0	94
3	PhCl	1	2.5	90
4	MTBE	1	5.0	30

With optimised conditions in hand, we next turned to investigating the substrate scope of this labelling reaction. A series of 10 substrates was selected for investigation, as shown in **Scheme 5.2**. The acyclic ether **235a** incorporated excellent levels of deuteration at 95%. Additional substitution at the benzylic position, as in **235b** was also well tolerated, with exceptional levels of 92% incorporation. Unfortunately, however, increasing this steric bulk further, in the *gem*-dimethyl example **235c**, we observed no incorporation. A cyclic motif bearing an exocyclic ether moiety in six-membered **235d**, and seven-membered **235e**, was also tolerated, giving good levels of isotope incorporation. Surprisingly, increasing the steric bulk around the ether, had little impact on the observed levels of incorporation, with good levels of 72% being observed in **235f**. We were elated to see that an acyclic ether could also direct labelling through a 6-mmi, as shown in compound **227g**, albeit with a moderate incorporation of 46%. Finally, we were also curious to establish whether a free alcohol was tolerated as a directing group, in

235h. We were delighted to confirm this to be the case, with an outstanding level of deuteration being observed in this example. Interestingly, significant levels of incorporation were also observed at the benzylic position, presumably through a transfer hydrogenation mechanism. We were also curious to determine if a protected alcohol would also undergo this labelling process. As such, we applied TIPS protected **235i** to the labelling conditions. Interestingly, we observed a reduced level of incorporation on the aryl ring, as well as a complete absence of labelling at the benzylic position. However, in conjunction with this, we also observed complete removal of the silyl protecting group. This curious result implies that the cleavage of the Si—O bond occurs after the activation and subsequent labelling of the aryl positions within the molecule, as the benzylic position remains undeuterated. Finally, placing a methyl group at the benzylic position of the free alcohol in **235j** allowed excellent levels of incorporation at the aryl position with a slight drop in benzylic labelling.

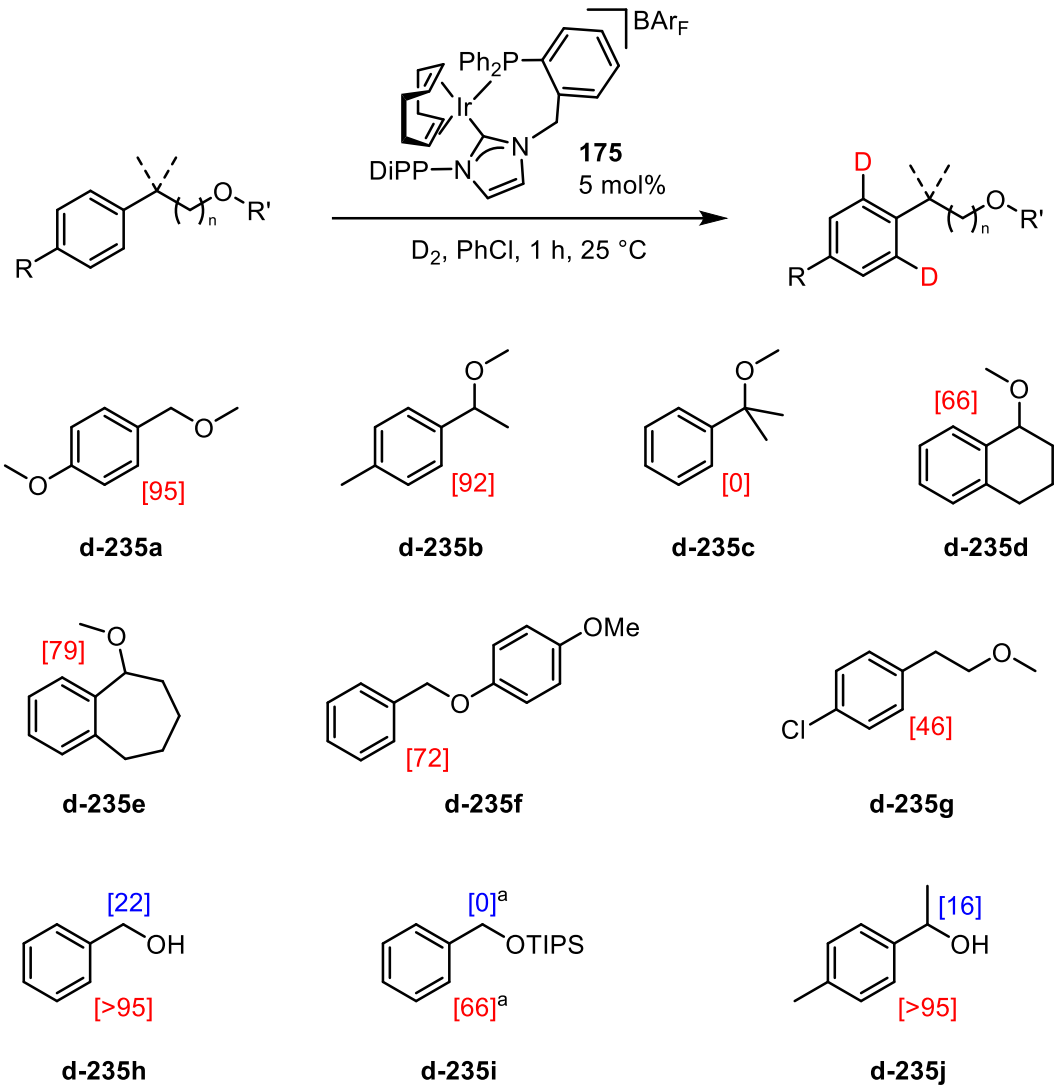

Scheme 5.2

5.2 Potential Applications in Natural Product Labelling

At this point, we began to consider the potential applications of our serendipitous discovery of this ether directed HIE. In most cases, the catalyst systems developed in our group are done so with the interest of facilitating the production of deuterated pharmaceuticals. However, within this area, benzylic and homobenzylic ether moieties are less prevalent than many of the other directing groups already established in directed HIE. Some examples of medicinally relevant

molecules containing such functionality are highlighted in **Figure 5.2**. Indeed, compounds of type **236** have been highlighted as potential broad-spectrum psychotropic agents.[103] Additionally, PA-824 has been shown to have excellent potency in the treatment of tuberculosis. [104] Finally, Omarigliptin, possessing an aryl tetrahydropyran core, is a known DPP-4 inhibitor, which was recently approved for the treatment of type II diabetes.[105] While there are certainly many pharmaceutically relevant compounds which contain this functionality, oftentimes this functionality is accompanied by much more powerful directing groups, and as such, exploiting ethers for the installation of a label may not be possible in those cases. Indeed, it may often be necessary to adopt a strategy similar to that of our own method to generate a sample of labelled GPR119 agonist **t-205** (*vide supra*), wherein the labelled functionality is installed through a chemical transformation post-HIE.

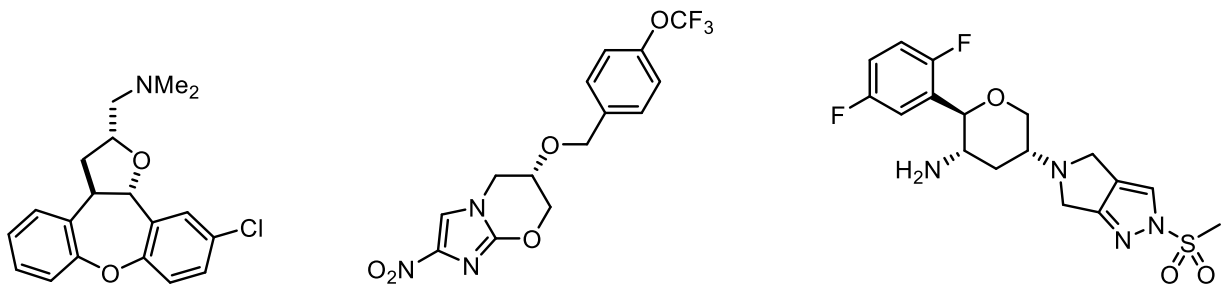

Figure 5.2

We wondered, therefore, if there was an area where this methodology could prove more valuable. Our attention turned to the labelling of natural products, and natural product-like molecules.[106,107,108,109] Indeed, when considering the field of natural products, there is often a distinct lack of heteroatom-containing functionality, and in many cases ethers and alcohols are the main points of functionality within a molecule. One particular class of natural products which attracted our attention was that of lignans.[110,111] Lignans are an incredibly large and diverse class of natural products, initially reported in 1980, which have great potential in

medicinal chemistry, owing to their potent bioactivities in many areas.[112,113,114] Indeed, it is owing to this biological activity that many groups have an interest in producing labelled variants of these natural products in order to better study their properties. This is no small undertaking, as, in many cases, a combination of the scarcity of material and complexity of the substrates can make production of labelled material highly challenging. Some have made use of deuterated reductants in order to obtain labelled lignans for studying. One example of this is shown in **Scheme 5.3**, with the synthesis of deuterated enterolactone and enterodiol.[115] Anhydride **237** could be reduced using sodium borodeuteride, in order to install the label, giving the deuterated lactone **d-238**. Vacuum pyrolysis of this material furnished **d-239** in good yields. A conjugate addition of the thioether **241**, and trapping of the resultant anion with benzyl iodide **242**, afforded the desired core structure **d-240** in 90% yield. From here, global deprotection using Raney nickel afforded the desired deuterated lignan in quantitative yield. From here, lithium aluminium deuteride could be used to convert this species into enterodiol, while concomitantly installing a further two deuterium atoms. Additionally, the measured level of protium in the final sample was measured to only be 0.7% across the four labelled positions.

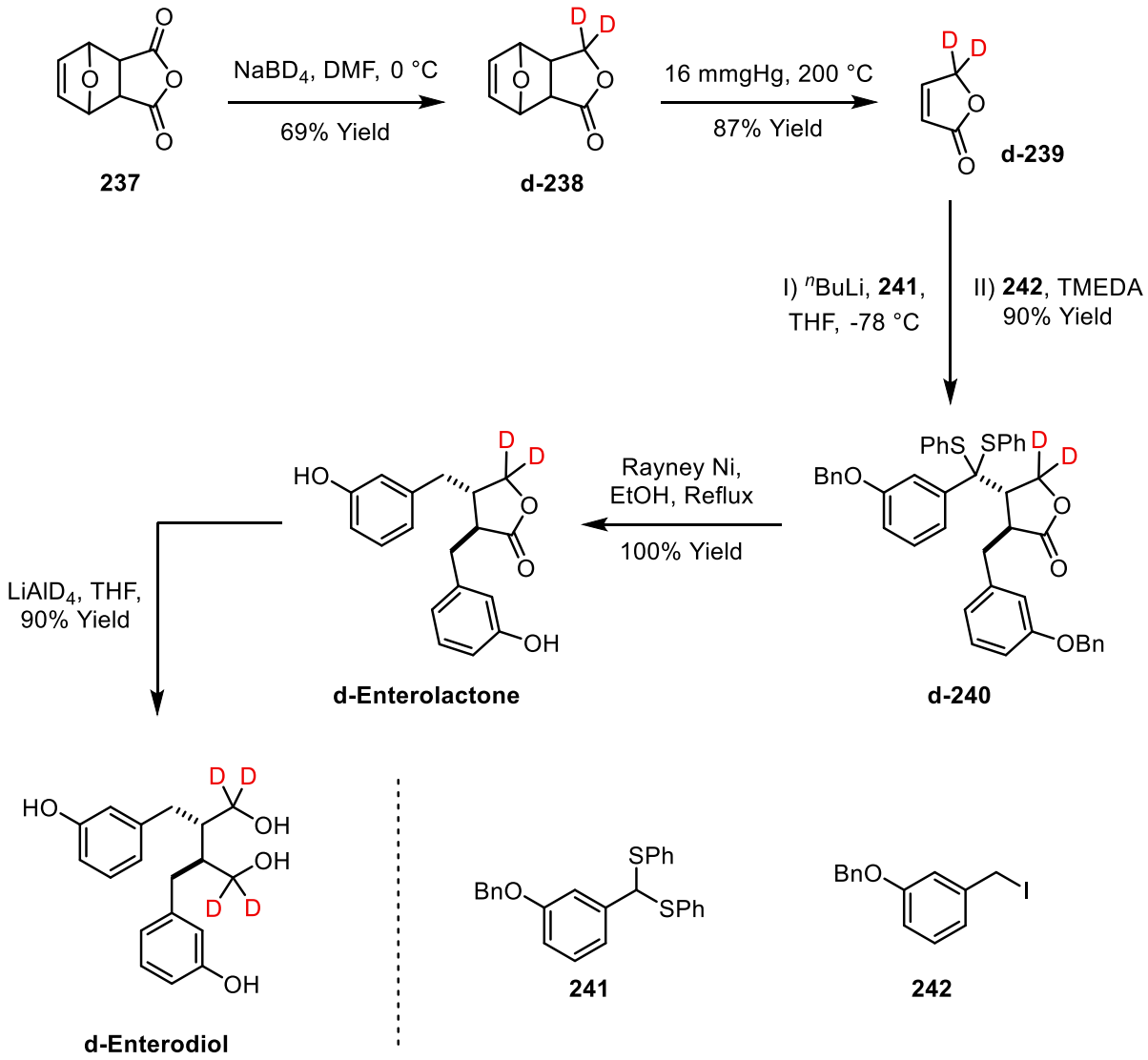

Scheme 5.3

While this is an impressive synthesis of a deuterated natural product, which suitably served the purpose of the study, performing a labelled synthesis for each compound of interest is a challenging and time-consuming endeavour. As such, some groups have turned to methods for directly labelling bioactive lignans; specifically, taking advantage of electron-rich aromatic ring systems for installation of a label through electrophilic aromatic substitution. For example, a perdeuterated sample of genistein was prepared, using a mixture of D_3PO_4•BF_3 in deuterated water over the course of three days (**Scheme 5.4**).[116] This method successfully gave a fully deuterated product, however, selective labelling of the pendant phenyl ring was required.

Fortunately, a selective deuteration pattern could be achieved by re-exchanging the positions on the more active aryl ring, affording a sample of D_4-genistein, in 91% yield over both steps.

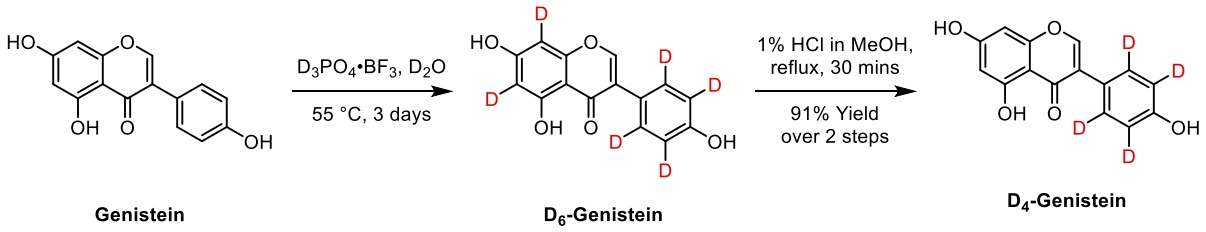

Scheme 5.4

This work was followed-up by applying the same methodology to produce a series of labelled lignan samples of the general structure shown in **Scheme 5.5**.[117] A range of seven lignan structures in total were labelled, all in good yields. While this method has shown to be effective in the production of labelled lignans, there are some challenges which have yet to be addressed. The lack of control with this method of labelling means that the number of labels installed, as well as which sites will be labelled, are difficult to predetermine. Indeed, the regiochemistry is entirely controlled by the electronics of the system, and requires electron-rich aromatic rings to proceed. While all of the examples shown here have good isolated yields, it is not guaranteed that the relatively harsh conditions applied will be tolerated with other structures, owing to the complexity of some bioactive lignan structures. Finally, the labelling reagent is made *in situ*, but requires the use of boron trifluoride gas, which makes its use impractical for those unequipped to deal with such reagents.

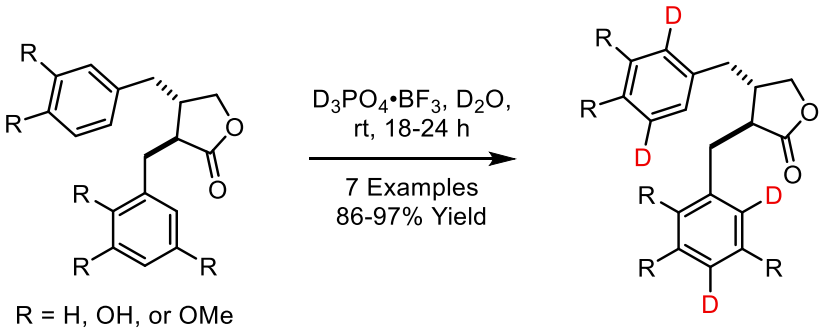

Scheme 5.5

In light of these issues, we surmised that our directed HIE methodology might offer a different method through which labelled lignans could be accessed. With this in mind, we selected three naturally occurring lignan molecules, with notable bioactivity, as shown in **Figure 5.3**. Eudesmine is a furofuran lignan which was been isolated from many plant families, most notably from Rutaceae.[118] It has shown extensive biological activity in many areas, including cytotoxicity; antibacterial activity; antifungal activity; tumour necrosis factor-alpha production; and vascular reactivity. [119,120,121,122,123] The neolignan cedrusin methyl ether was isolated from *Eucommia ulmoides*.[124] This compound has been found to be both cytotoxic and to have effects on nerve growth factor induction.[125,126] Although not a lignan itself, medicarpin is a member of the closely related pterocarpin family. Interestingly, it can be isolated as a racemate from *Dalbergia odorifera*, as (+)-medicarpin from *Arachis hypogea*, or as (-)-medicarpin from *Medicago sativa*.[127,128,129] (-)-Medicarpin has been shown to have potent antineuroinflammatory effects, as well as nitric oxide production inhibition.[130,131]

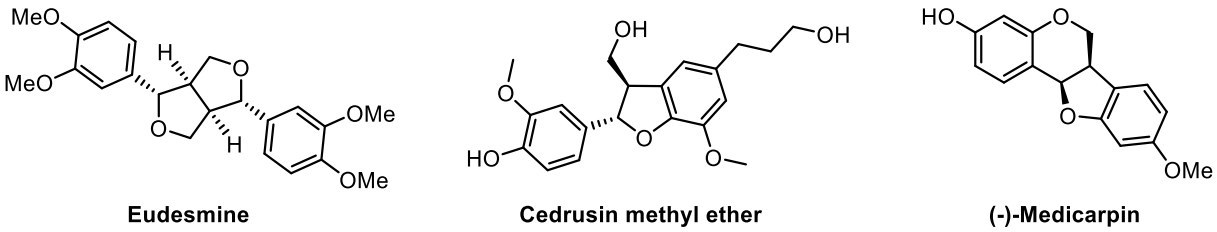

Eudesmine **Cedrusin methyl ether** **(-)-Medicarpin**

Figure 5.3

One could imagine the installation of a deuterium or tritium label into each of these compounds, as directed by an ether or alcohol functional group, which would otherwise be very challenging to access. With these biologically active natural products in mind, we sought to challenge our HIE methodology by applying our chelated NHC-P catalyst to synthetically tractable racemic forms of these compounds.

5.3 Synthesis Towards Natural Product-like Substrates for HIE

The first compound we targeted was (±)-eudesmin. The route selected was similar to that applied by Lancefield and Westwood, and is shown retrosynthetically in **Scheme 5.6**.[132] The desired lignan could be afforded from the methylation of related lignan (±)-pinoresinol. The furofuran core could be accessed rapidly from allylic alcohol **243**, which, in turn, could be generated from the 1,2-reduction of ester **244**. This ester could be furnished from vanillin **245** through a Knoevenagel condensation and esterification, giving **246**.

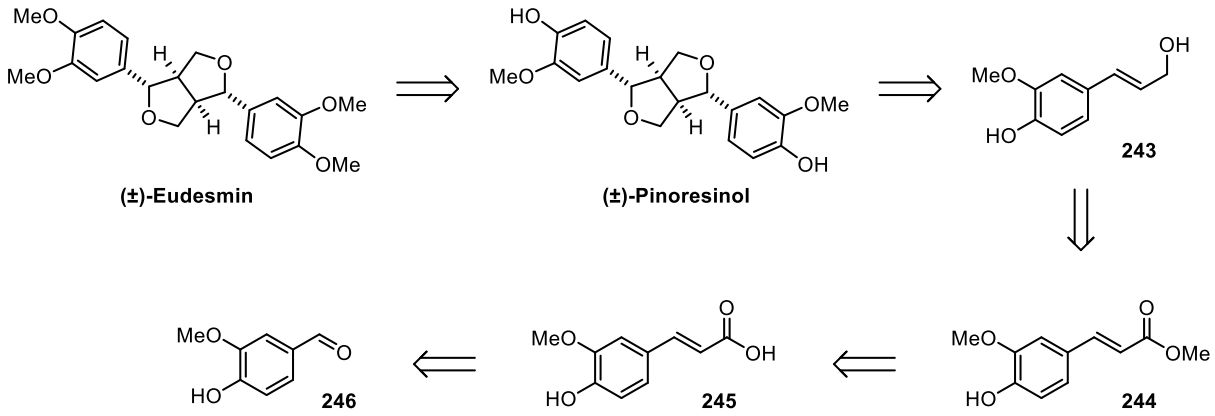

Scheme 5.6

With a route selected, we embarked upon the forward synthesis of our first racemic substrate (**Scheme 5.7**). The route to allylic alcohol **243** proceeded smoothly, with the Knoevenagel reaction yielding 64% of ferulic acid **245** in 64% yield on a 197 mmol scale. This could be converted to methyl ferulate **244** in quantitative yields, using thionyl chloride in methanol. It was then found that toluene was the best solvent for the reduction step, affording us the desired allylic alcohol **243** in 87% yield on a 38 mmol scale.

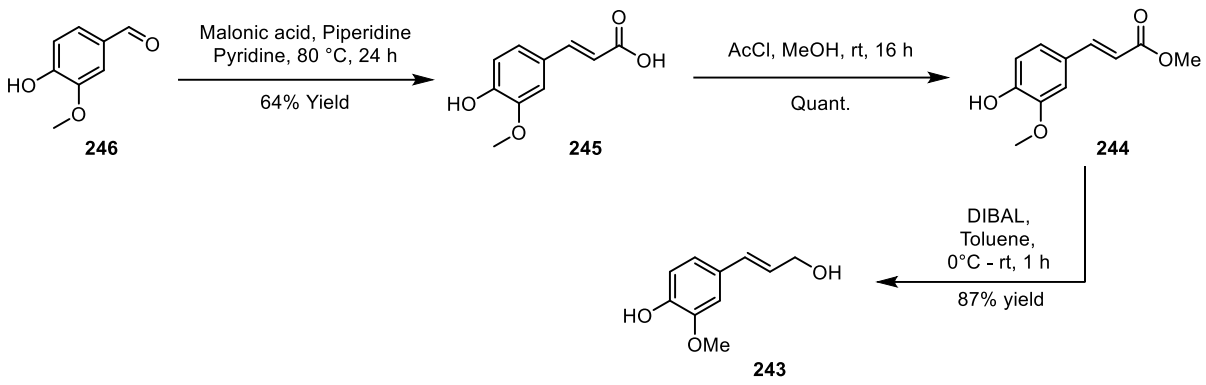

Scheme 5.7

With allylic alcohol **243** in hand, we next attempted the iron-mediated oxidative cyclisation to give to give pinoresinol (**Table 5.2**). This method is highly effective in building up the furofuran core from simple starting materials, however the yields are notoriously low, owing to poor regioselectivity. Nonetheless, we were able to isolate useable amounts of (±)-pinoresinol from the reaction mixture. It should be noted that we also observed by-product **247** in all cases, which was isolated in 18% yield in **Entry 2**; this by-product may be useful in the synthesis of another substrate.

Table 5.2

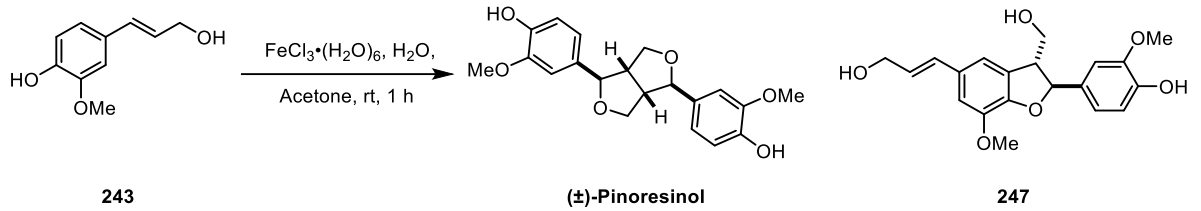

Entry	Scale (mmol)	(±) Pinoresinol	247
1	9.98	23% Yield	Not Isolated
2	24.9	17% Yield	18% Yield
3	61.9	21% Yield	Not Isolated

Finally, we looked to the methylation step to form our desired substrate, (±)-eudesmin (**Scheme 5.8**). The methylation of (±)-pinoresinol proved sluggish, requiring several equivalents of methyl iodide and a relatively long reaction time of 48 hours. Nonetheless, we were delighted to obtain a sample of (±)-eudesmin for our labelling studies in a very good yield.

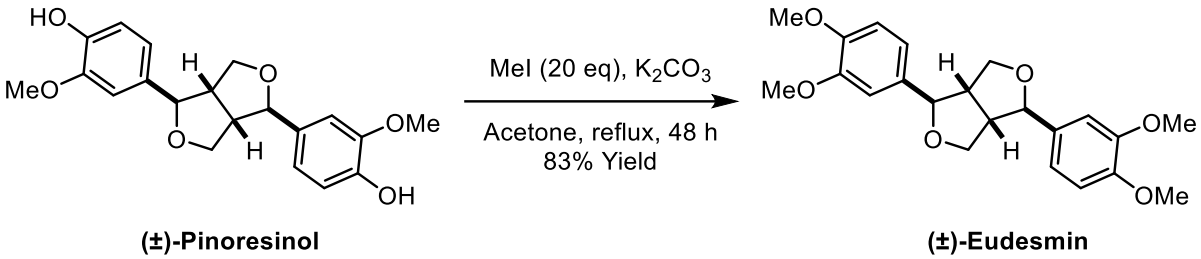

(±)-Pinoresinol **(±)-Eudesmin**

Scheme 5.8

We next turned our attention to the synthesis of (±)-cedrusin methyl ether. In observing small amounts of **247** being generated in the oxidative cyclisation of allylic alcohol **243** (**Table 5.2**), it was thought that this species could be reduced in the presence of palladium to gain efficient access to (±)-cedrusin methyl ether. Unfortunately, when this was attempted, as shown in **Scheme 5.9**, only degradation was observed, and we quickly focused on another method to access this compound.

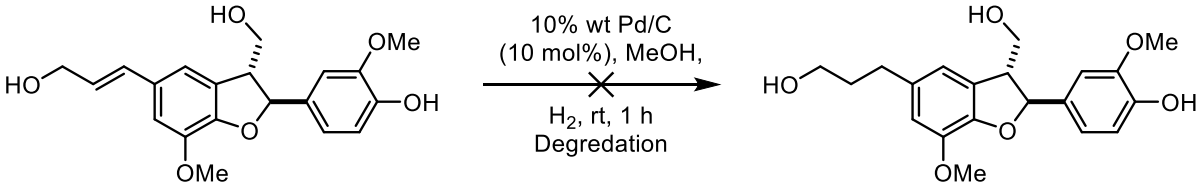

247 **(±)-Cedrusin methyl ether**

Scheme 5.9

Rather than performing the oxidative cyclisation with allylic alcohol **243**, which gives a poorly regioselective reaction with many products formed, methyl ferulate **244** is known to undergo a silver mediated cyclisation to give **248** in higher yields.[133] In our hands, this cyclisation reaction worked moderately well, giving us our best yield at 30% (**Scheme 5.10**). The α,ß-unsaturated

ester **248** could then be reduced in the presence of palladium on carbon, under mild conditions and in excellent yields. Gratifyingly, a final reduction step using lithium aluminium hydride proceeded smoothly to afford us a sample of (±)-cedrusin methyl ether.

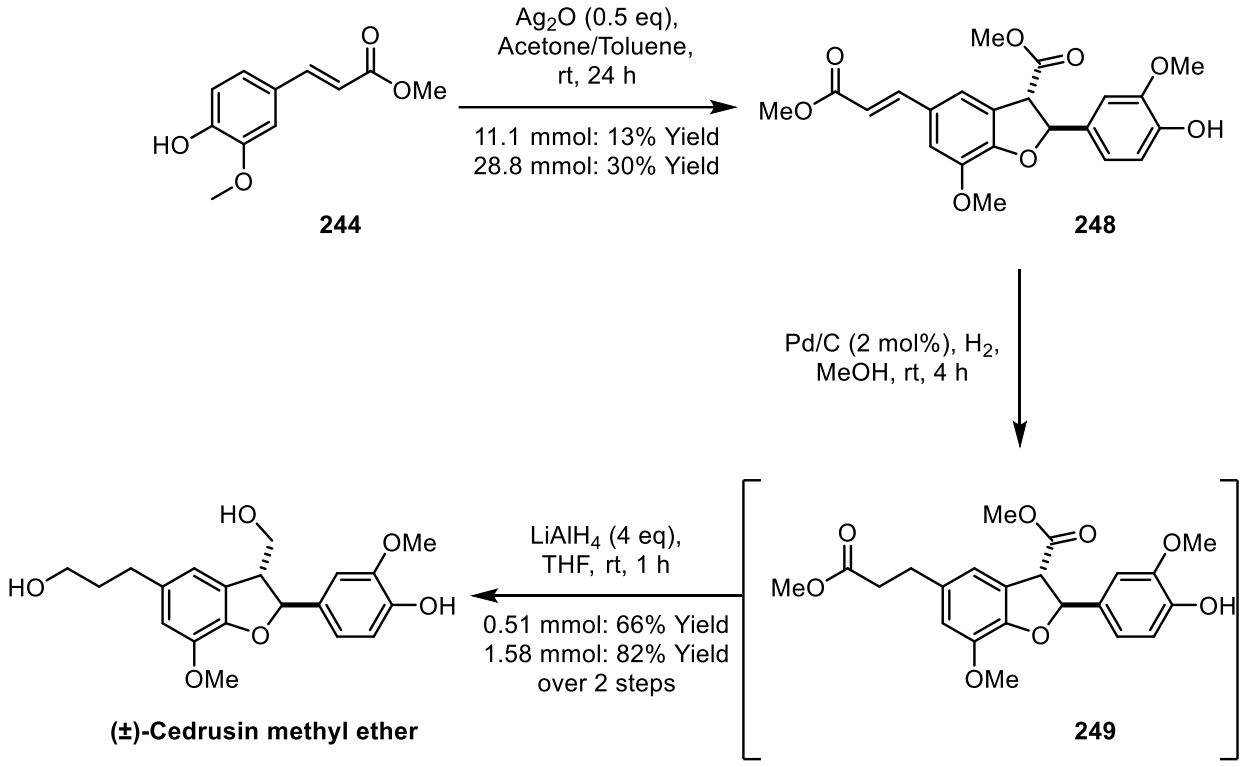

Scheme 5.10

With two out of the three substrates synthesised, we focused our efforts on synthesising the final target, (±)-medicarpin.[134] **Scheme 5.11** below highlights the synthesis. Commercial phenylacetic acid derivative **250** could be reacted with resorcinol and methane sulfonyl chloride to afford chromen-4-one **251** in reasonable yields. This could then be selectively demethylated in the presence of anhydrous aluminium chloride, however a large excess of this reagent was required. Nonetheless, the demethylated product **252** was isolated in good yield. The final cyclisation could be mediated by sodium borohydride, giving a sample of (±)-medicarpin in good yields.

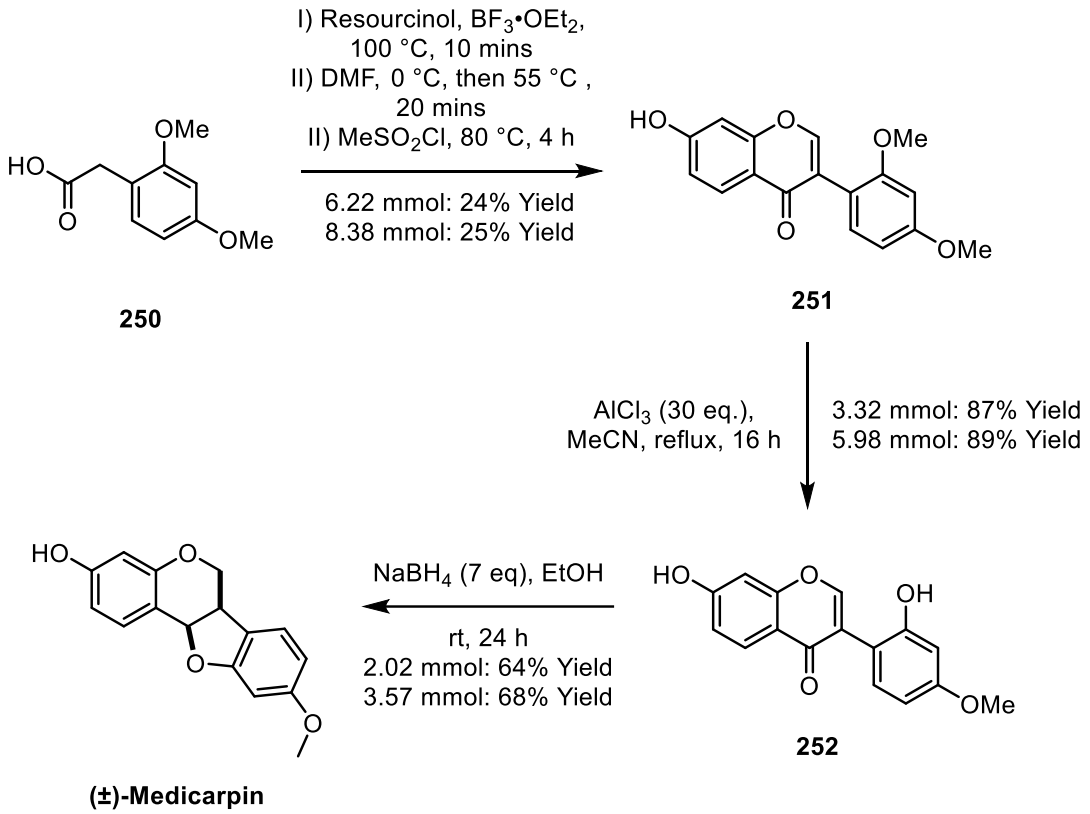

Scheme 5.11

Delighted to have samples of all three desired natural product-like compounds in hand, we then turned to applying our chelated NHC-P system **175** to the deuteration of these compounds.

5.4 Attempts to Label Natural Product-like Compounds Using a Chelated NHC-P catalyst System

We first attempted to apply our previously optimised reaction conditions to the labelling of (±)-eudesmin, as shown in **Table 5.3**. We were delighted to see excellent levels of incorporation under the reaction conditions applied to our simple ether substrates. Lamentably, however, the catalyst system also degraded the substrate to quite significant levels. What was returned on first attempts was an inseparable mixture of what we believe to be (±)-d-eudesmine and the ring cleavage product, **d-253**. Reducing the concentration of the reaction did help to reduce the

amount of this by-product formed, with little effect on the labelling, however this outcome was still not satisfactory. Additionally, cooling the reaction mixture to -10 °C (**Entry 3**), did appear to prevent any side reactivity, no labelling was apparent. Conditions between these two temperatures may allow us to use this catalyst system to label (±)-eudesmin in a clean, and effective manner.

Table 5.3

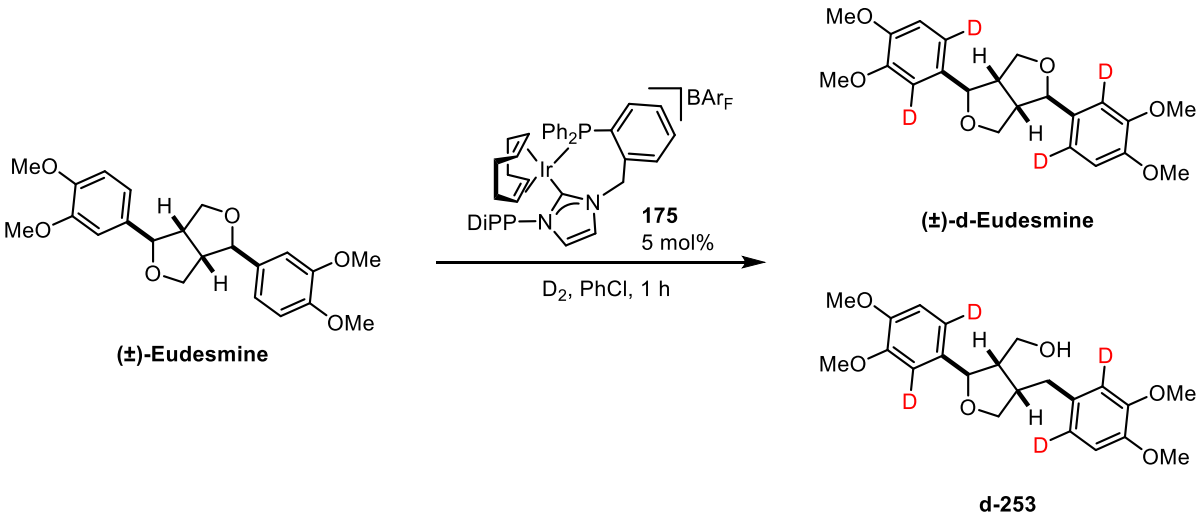

Entry	Conc. (mM)	Temp (°C)	%D	(±)-d-Eudesmine : d-253
1	86	25	92	1.70 : 1.00
2	8.6	25	93	3.55 : 1.00
3	8.6	-10	0	100 : 0

Next, we turned our attention to the labelling of (±)-cedrusin methyl ether. Once again, applying our previously optimised reaction conditions to this substrate, what we observed was a complete lack of reactivity, even with an extended reaction time of 16 hours (**Scheme 5.12**).

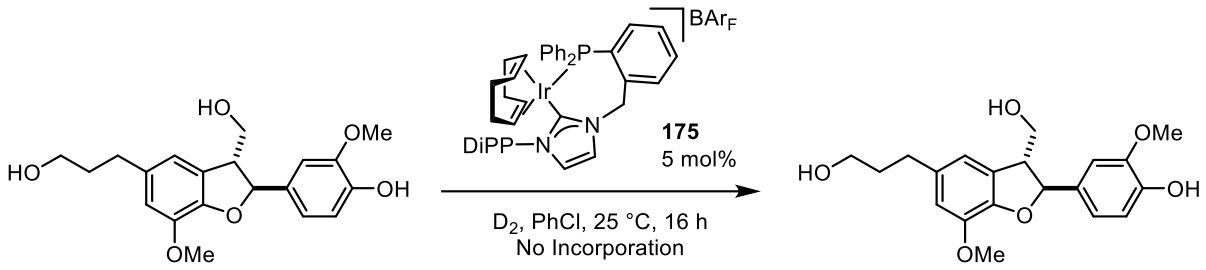

Scheme 5.12

Curious about the lack of reactivity with this compound, having seen that free alcohols were tolerated in the substrate scope (*vide supra*), we turned to DFT calculations for some potential insight into the ground state energies of the species in solution. As previously, we focused on the dihydride structures **254a-c**, as shown in **Scheme 5.13**. Of the three binding motifs that we calculated, the alcohol bound in a chelated fashion with an agostic interaction to the available proton on the dihydrobenzofuran structure **254b** was significantly more stable than **254a** and **254c**. It should be noted that, due to the large, planar nature of the substrate, the usual binding motif for **254a** could not be adopted, and as such the structure in which the hydride ligands are isomeric to the standard conformation was used. This structure still appears to be viable, with only a small increase in energy upon activating to the dihydrogen complex **255a**. Additionally, unproductive chelate **254c** is also accessible, being only +6.02 kcal mol^{-1} more unstable than **254b**. Interestingly, despite **254b** being the most stable of the three, the activation to dihydrogen complex **255b** showed an increase in energy to +27.5 kcal mol^{-1}, indicating that it is unlikely to form in solution at room temperature. Thus, observing this data, we hoped that, with some encouragement, the system would be able to access structure **254a** and selectively label the pendant phenyl ring.

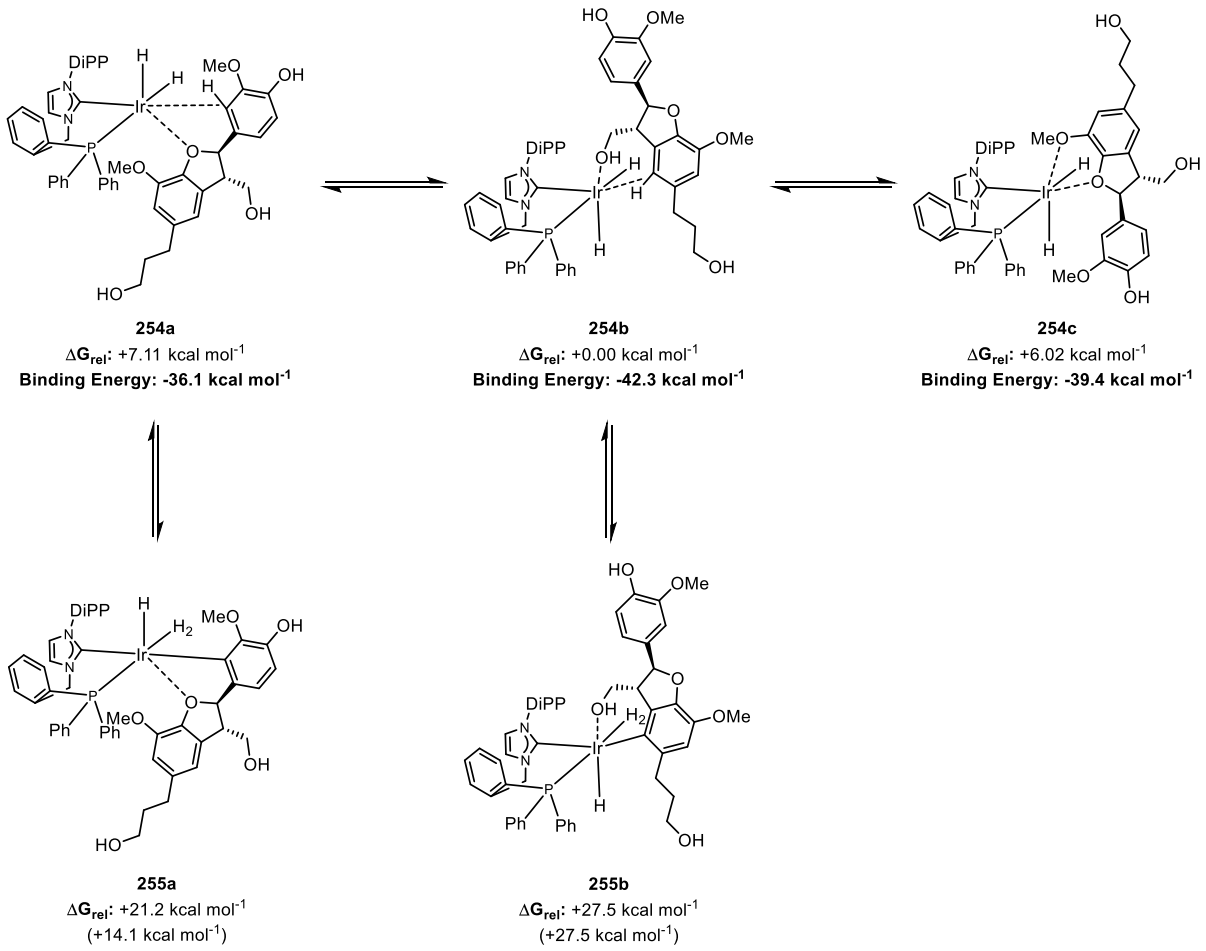

Scheme 5.13

Thus, we decided to apply our catalyst system at elevated temperatures (**Table 5.4**). Unfortunately, when applied at higher temperatures for an extended reaction time of 16 h, complete degradation of the substrate was observed, both at 90 °C, and at a lower temperature of 50 °C. Interestingly, when applied at 50 °C for one hour, a small but significant amount of incorporation was observed directed by the alcohol. We were elated to see this result, as it highlights the possibility for further tuning the reaction conditions in order to achieve improved incorporations with no degradation. Considering the complexity of this substrate, it is not entirely unsurprising that the short computational investigation was initially misleading, as a combination of a large substrate with many points of functionality, coupled with a highly

fluxional iridium hydride system will likely require more thorough investigation to fully understand.

Table 5.4

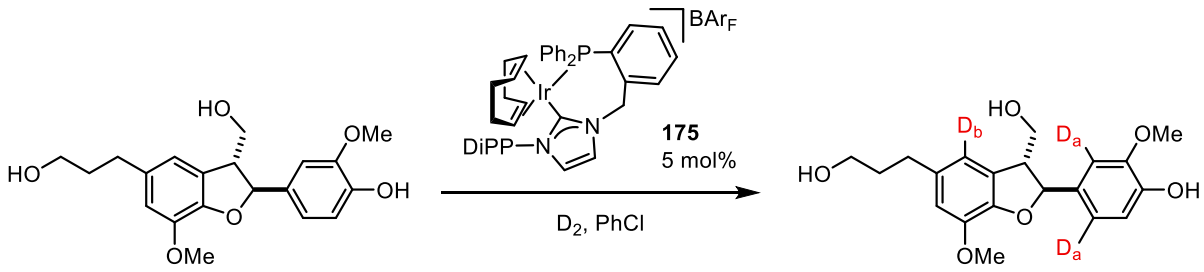

Entry	Temp. (°C)	Time (h)	Results
1	90	16	Degradation
2	50	16	Degradation
3	50	1	25% Incorporation at D_b

Finally, we attempted to label our sample of (±)-medicarpin using this catalyst system (**Table 5.5**). Upon our first attempt to label the substrate, we noted that the lack of solubility of the substrate in chlorobenzene was problematic, returning clean starting material with no incorporation. Finding a solvent system in which the substrate was soluble proved challenging. A short solubility screen showed that the compound was only reasonably soluble in mixtures of alcoholic solvents, or highly polar solvents. It was decided that a mixture of an alcohol and chlorobenzene, or neat 2-methyltetrahydrofuran would be the most likely candidates for a successful labelling. Unfortunately, a 20% ^{t}BuOH in chlorobenzene mixture proved unsuccessful, and, thus, we turned to 2-methyltetrahydrofuran. Despite solubilising the system well, no incorporation was observed during a reaction time of one hour. Surprisingly, leaving the reaction overnight, or heating for one hour when using 2-methyltetrahydrofuran, resulted in complete degradation of the sample.

Table 5.5

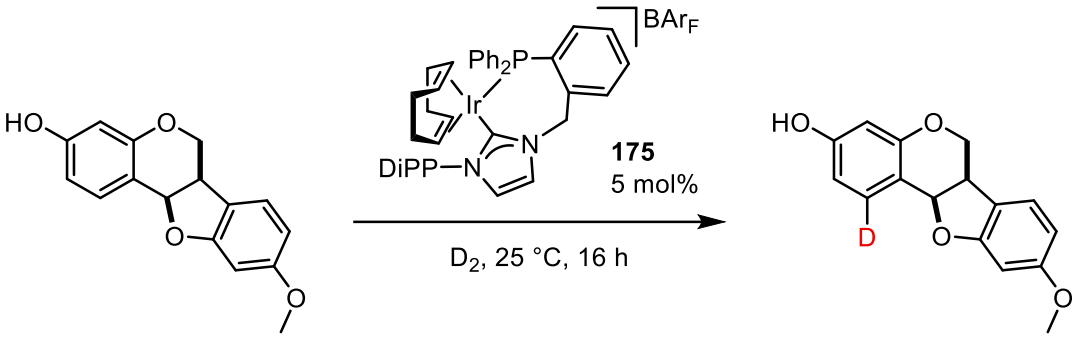

(±)-Medicarpin **(±)-d-Medicarpin**

Entry	Solvent System	Temp. (°C)	Time (h)	Result
1	PhCl	25	16	No Incorporation
2	20% tBuOH/PhCl	25	16	No Incorporation
3	2-MeTHF	25	1	No Incorporation
4	2-MeTHF	60	16	Degradation
5	2-MeTHF	60	1	Degradation

We also analysed the proposed reaction intermediates *in silico*, as before, in order to ensure substrate binding was not the cause of our lack of reactivity (**Scheme 5.14**). The calculated binding energy of medicarpin is highly favourable, but should still allow substrate turnover to occur. Additionally, the kinetic barrier to form the activated species **257**, is reasonable and would be expected to occur at room temperature. These values indicate that the lack of reactivity in chlorobenzene is likely due to insolubility of the substrate. Finally, analysing the enthalpy of solvent displacement in 2-methyltetrahydrofuran, we can see that the complexation of medicarpin shows an increase of 21.0 kcal mol^{-1}, indicating that this displacement is highly unlikely in solution. Thus, in order to achieve labelling of this compound, a solvent system is required which can solubilise the compound, whilst not outcompeting the substrate for binding

to the catalyst centre. This may well be solved by performing the reaction in a solvent in which (±)-medicarpin is sparingly soluble, but at slightly elevated temperatures so as to not degrade the sample.

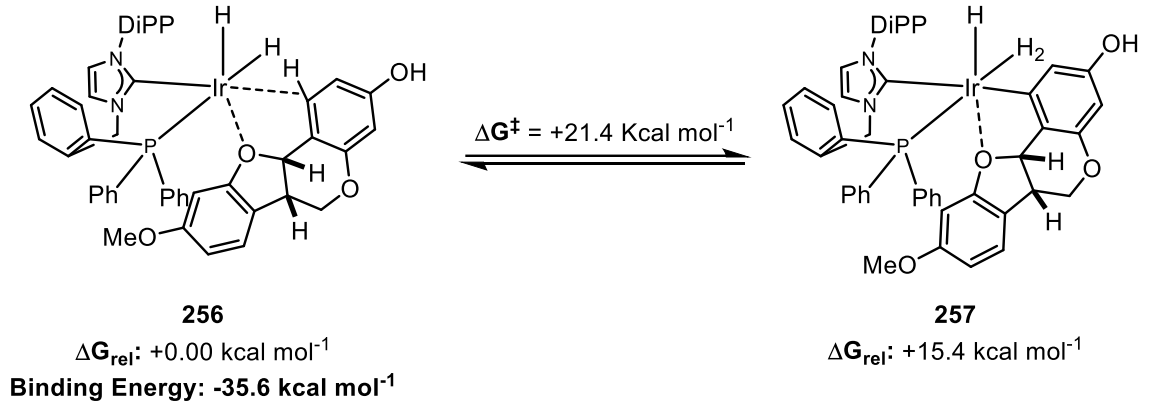

256

ΔG_{rel}: +0.00 kcal mol^{-1}

Binding Energy: -35.6 kcal mol^{-1}

257

ΔG_{rel}: +15.4 kcal mol^{-1}

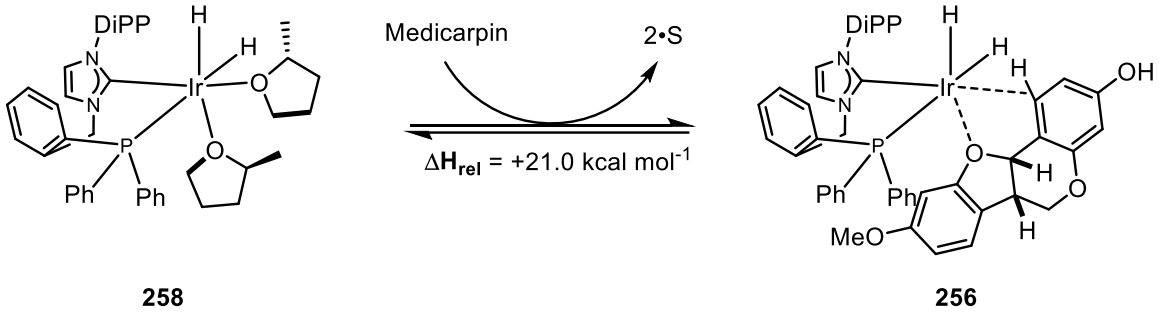

258

256

Scheme 5.14

6. Conclusions

Using a computationally guided rational ligand design approach, novel catalyst systems for directed HIE processes have been developed and applied to a range of challenging directing groups.

Initially, an *in silico* screening method utilising binding energy as a screening parameter, was used to identify potentially effective catalyst systems (**Scheme 6.1**).

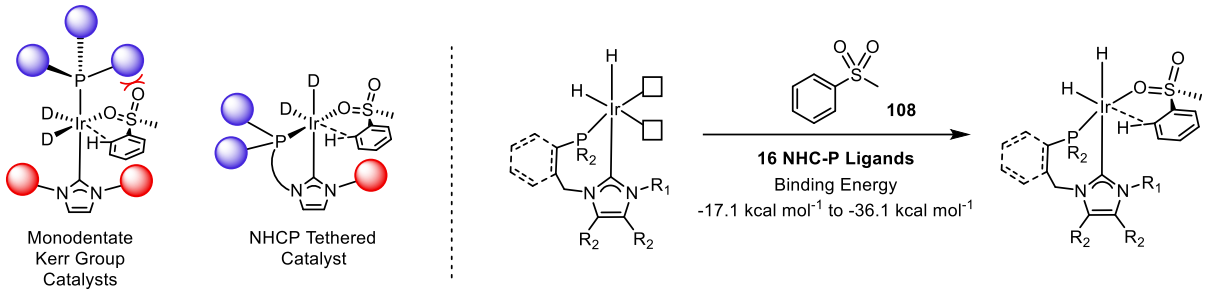

Scheme 6.1

When applied to the labelling of methylphenyl sulfone, novel NHC-P complex **175** showed excellent activity, giving good levels of incorporation in a wide range of aryl and ethereal solvents. Thus far, more investigation into how the various solvent attributes affect the reaction mechanism is certainly required. Nonetheless, outstanding levels of isotope incorporation were observed with chlorobenzene, which was taken forward to study the scope of the reaction. We were delighted to see the catalyst system successfully applied to 20 varied sulfone systems, delivering high levels of deuterium labelling in the majority of cases (**Scheme 6.2**).

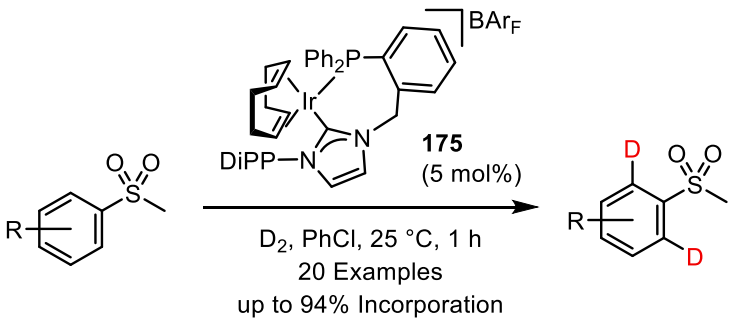

Scheme 6.2

Furthermore, we were able to apply this catalyst system under conditions better suited to isotope chemists within the pharmaceutical industry, making use of the TRITEC manifold system to perform these labelling experiments under reduced pressure of deuterium. Transferring the methodology from our atmospheric experiments to such sub-atmospheric conditions was highly successful, requiring minimal alteration of the reaction conditions to retain the excellent levels of isotope incorporation seen previously (**Scheme 6.3a**). In addition to this, we were elated to showcase the utility of the catalyst in tritiation reactions, affording a sample of methylphenyl sulfone with exceptional specific activity. Finally, in labelling sulfone **108u** using our newly optimised reaction conditions, followed by an alkylation reaction, we were able to deliver a tritiated sample of GPR119 agonist **205** with good levels of specific activity (**Scheme 6.3b**).

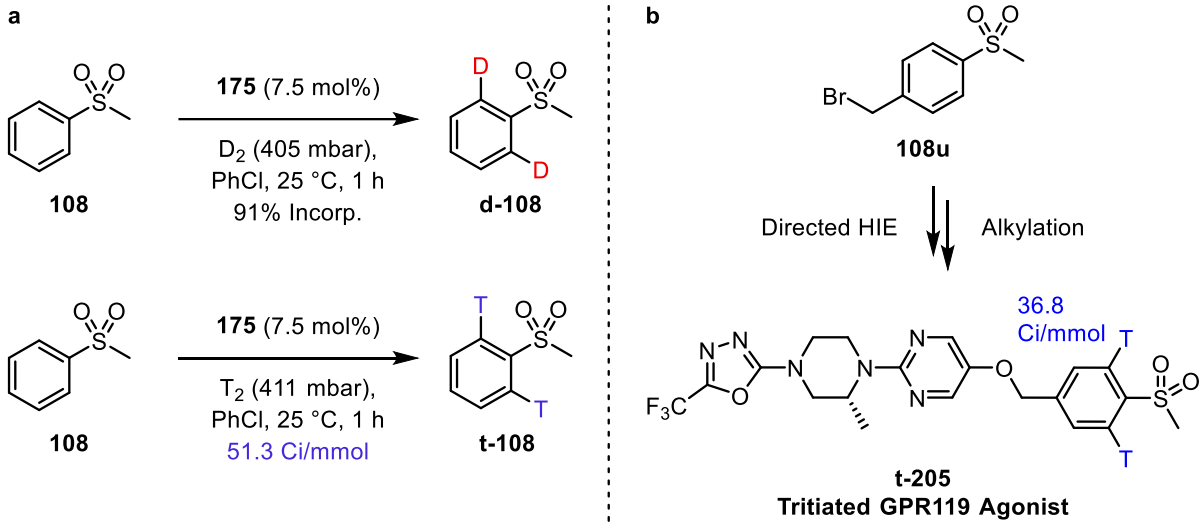

Scheme 6.3

Confident that we'd developed a catalyst system which could effectively cater to the production of labelled sulfones, we turned to applying the novel complex to the labelling of other known challenging directing groups, namely substituted sulfonamides. We were delighted, in our initial investigation, to see excellent levels of incorporation being delivered into *N*-methyltoluene sulfonamide **127**. However, levels of incorporation with the even more

challenging *N*,*N*-dimethyltoluene sulfonamide **206** were less than satisfactory, and as such, we moved to further modifying our catalyst system (**Scheme 6.4a**). Instead of applying a screening method to improving the activity of our catalyst system, we opted for a more focused approach. Indeed, our use of solid angle analysis and consideration of the catalyst binding motif allowed us to identify that the bulky phosphine moiety was preventing efficient substrate binding with significantly hindered sulfonamide substrates (**Scheme 6.4b**). This led us to the NHC-Py catalyst motif exhibited by **218** (**Scheme 6.4c**). With an improved binding motif, we hoped that such a catalyst system might deliver higher levels of incorporation into both secondary and tertiary sulfonamides, which was further supported by binding energy calculations as well as a low kinetic barrier to C—H activation.

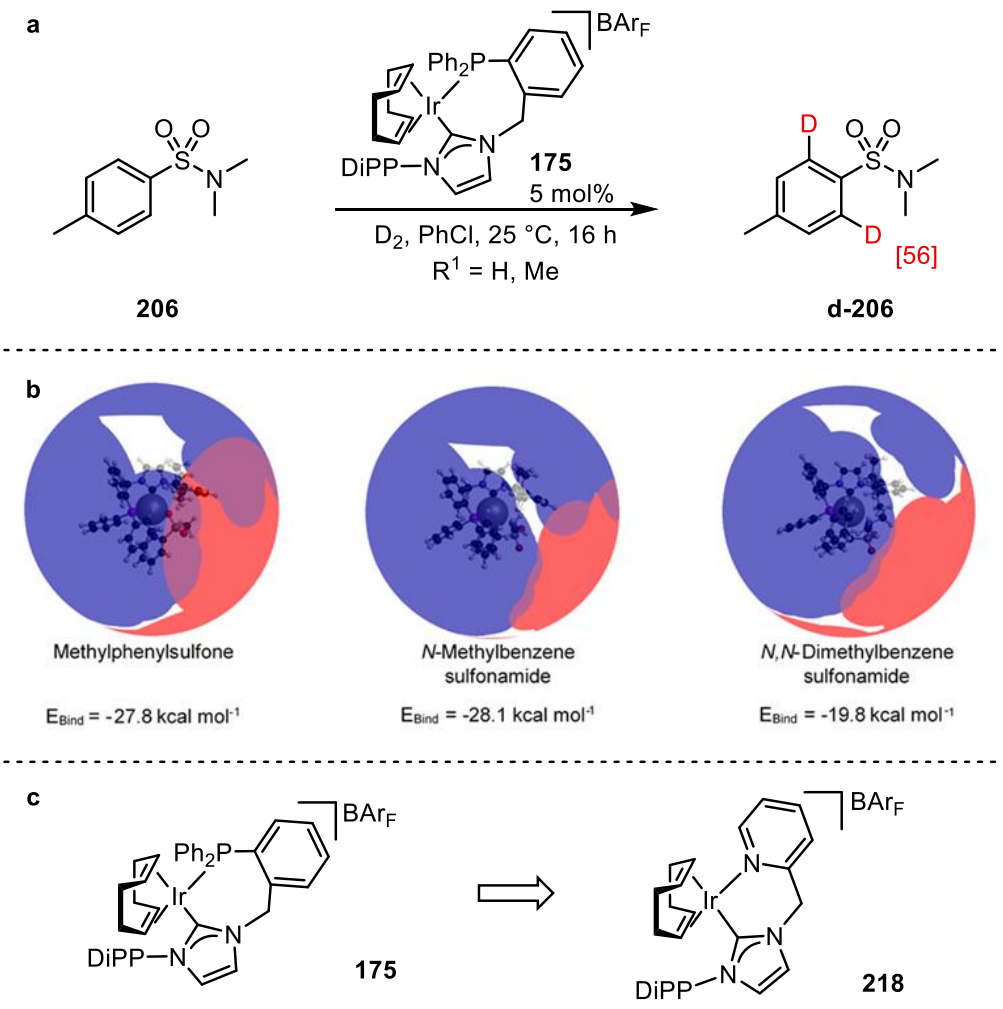

Scheme 6.4

With a promising computational profile in front of us, the synthesis of complex **218** was undertaken. The NHC-Py iridium(I) precatalyst complex could be accessed in a fast and efficient manner. Once synthesised, we quickly applied the complex to the labelling of a range of sulfonamides (**Scheme 6.5**). In doing so, we were delighted to see a marked increase in the incorporation delivered into **206**. Additionally, the complex was also extremely adept in the HIE of a range of sulfonamide substrates, with a total of 19 being successfully labelled.

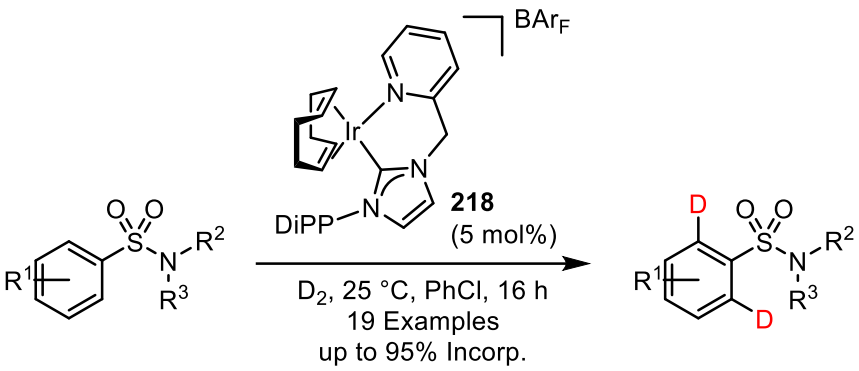

Scheme 6.5

It is hoped that this body of work, as a study on catalyst design guided by computational parameterization, will provide a foundation for the ongoing studies in C—H activation and functionalisation, as well as future catalyst development processes.

Finally, during the investigation of sulfone labelling, we serendipitously came across the HIE of ethereal and alcoholic substrates. The novel NHC-P catalyst system **175** proved to be highly effective with this substrate class, with good level of labelling being successfully afforded across ten examples (**Scheme 6.6a**). In addition to this, steps towards applying this catalyst system in the labelling of natural products and natural product-like molecules has also been undertaken. Within this study, a selection of three synthetically accessible natural product-like molecules have been generated, and initial attempts at deuterium labelling have been undertaken (**Scheme 6.6b**). The deuteration of natural products and natural product-like molecules is an area of great unmet need, in which the application of directed HIE could be of

significant value. The complexity and sensitivity of these targets presents an exciting challenge for our catalyst systems, which we believe will only further our understanding of these complexes.

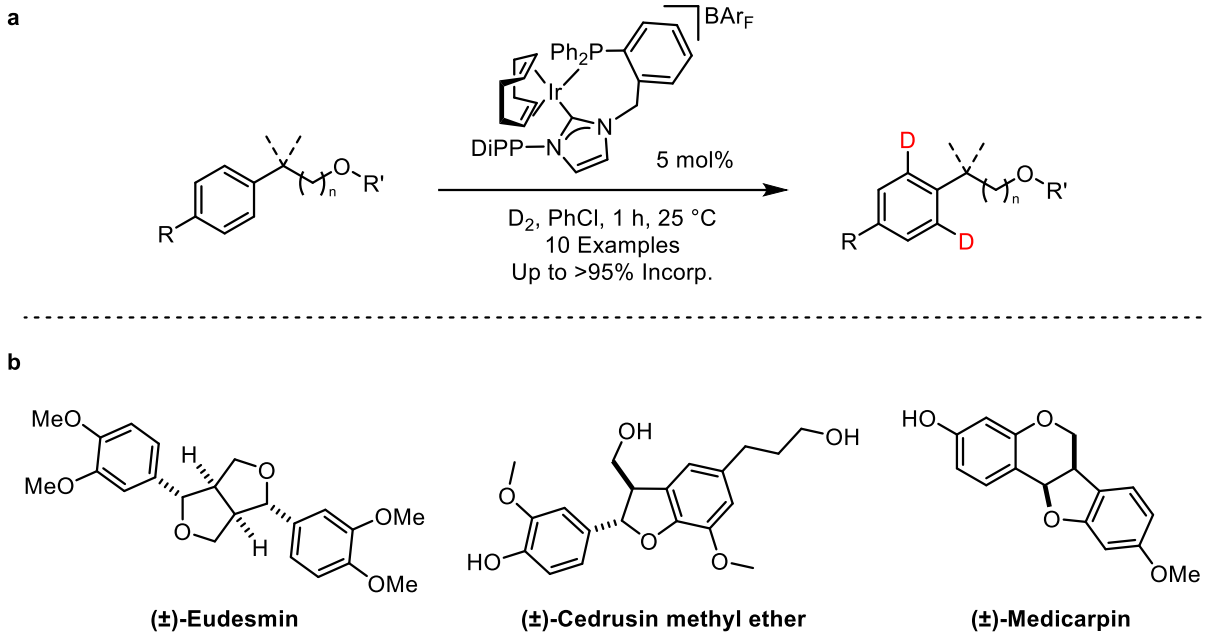

Scheme 6.6

7. Future Work

With this study, we have shown how a strong mechanistic understanding of our catalyst system has allowed us to successfully and efficiently develop novel catalyst systems for HIE processes. However, in venturing forward with these new chelate catalyst systems, a more thorough understanding of their nature becomes more vital as their utility becomes more apparent. As such, one of the most important aspects of the reaction which appears to have great influence over the success of the exchange process, is the choice in solvent. While in our own investigations of the sulfones, it was noted that several solvents afforded excellent levels of incorporation, while others did not. No clear rationale was established for these cases. In order to truly design a functioning catalyst system, an understanding of several factors must be attained: how the solvent used can affect the activity of the catalyst; how the solvent interactions with the complex/substrates affect kinetic barriers; and how the solvent can affect the degradation of the catalyst systems. Undeniably, investigation into the degradation of these catalyst systems would also be highly valuable. Furthermore, a more solid understanding of the kinetics involved with the systems discussed herein are of high priority, particularly in supporting further computational guidance, and ensuring the methods used for our calculations are reasonable. Indeed, in line with the computationally calculated barriers, some investigations not discussed within this report have led us to believe that the rate limiting process in some of these reactions is now the mass transport limit of deuterium within the system. Further investigation to confirm this would be highly desirable.

In furthering the group's interest in the development of C_{sp3}—H activation, we have also considered the ability of our new chelating catalysts to activate such bonds. The beginnings of an *in silico* investigation on this matter has been undertaken, and are highlighted in **Scheme 7.1**, examining the relevant iridium(III) dihydride species. Of an initial screen of binding conformations of *N*-mesyl piperidine to our NHC-Py catalyst, complex **249** (with an agostic

interaction with the axial proton) was found to be most stable. Gratifyingly, when the barrier to C— H activation was calculated, only a moderate increase to 22.0 kcal $mmol^{-1}$ (compared to the 16.6 kcal mol^{-1} for activation of **205**) was observed, implying that this intermediate should be accessible. However, what we did not anticipate, was an unproductive chelate between the nitrogen and oxygen of the sulfonamide being significantly more stable than that of the most favourable agostic interaction, by 8.93 kcal mol^{-1}. Troubled by this, we also investigated this possibility for *N*,*N*-dimethylbenzene sulfonamide and were surprised to find this structure was also more stable than the corresponding agostic interaction by 4.62 kcal mol^{-1}. This information could have interesting consequences when attempting to gain an understanding of the behaviour of such directing groups. Finally, we also looked into the relative ground state energies for the agostic interaction **253** and *N*,*O*-chelate **254** for the NHC-P system. Unsurprisingly, the more Lewis acidic metal centre favoured this unproductive chelate even more so. This indicates that the more electron-rich NHC-Py catalyst system may prove to be the best starting point for further developing a catalyst system which can effectively activate C_{sp3}—H bonds using a sulfonamide directing group.

a Kinetic Barrier to C_{sp3}-H Activation

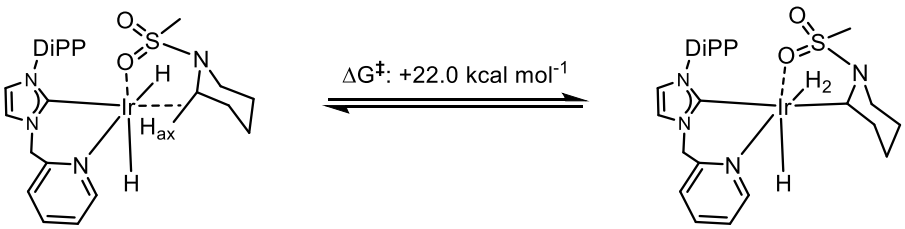

259
ΔG_{rel}: +0.00 kcal mol^{-1}

260
ΔG_{rel}: +21.9 kcal mol^{-1}

---

b Potentially Problematic Chelate

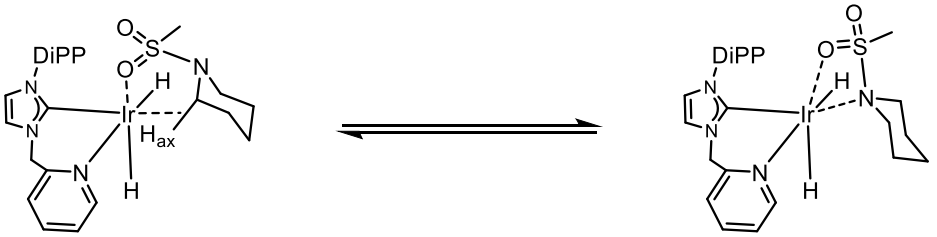

259
ΔG_{rel}: +0.00 kcal mol^{-1}

261
ΔG_{rel}: -8.93 kcal mol^{-1}

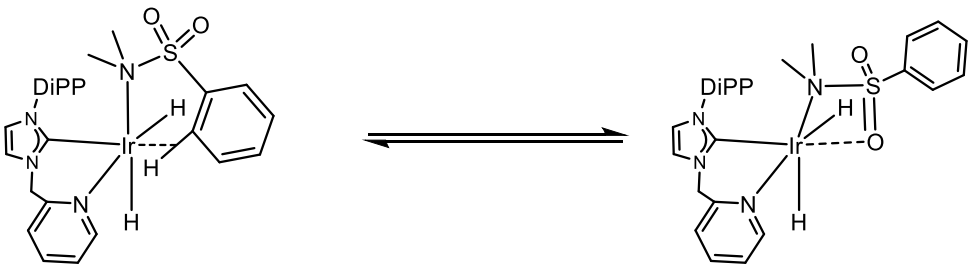

213
ΔG_{rel}: +0.00 kcal mol^{-1}

262
ΔG_{rel}: -4.62 kcal mol^{-1}

---

c NHC-P Complex

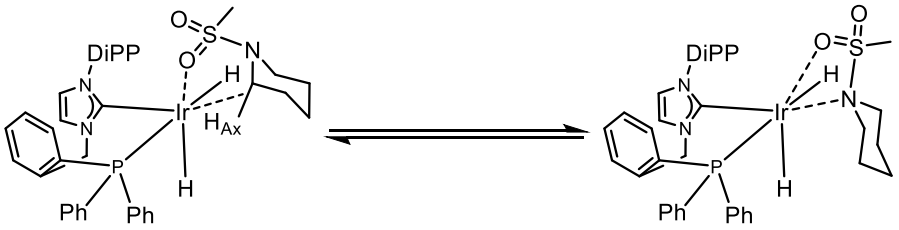

263
ΔG_{rel}: 0.00 kcal mol^{-1}

264
ΔG_{rel}: -10.9 kcal mol^{-1}

Scheme 7.1

Nonetheless, the beginning of an investigation into the C_{sp3}—H of sulfonamides has commenced, and it is hoped that this information will aid future investigation in this area.

In our short investigation of the sulfoximines, we were delighted to see these highly desirable groups deliver excellent amounts of incorporation, not only with our novel NHC-Py catalyst system, but also with the classical monodentate NHC/phosphine motif. Indeed, a more thorough investigation into the variations of sulfoximines which can be labelled would be beneficial, as their use in the pharmaceutical industry continues to grow. **Figure 7.1** shows some potentially interesting sulfoximine substitution patterns which could be investigated in **245-258**. Additionally, of course, the unexpected *S*-methyl labelling described within this work also requires significant mechanistic investigation. In understanding how the deuteration of this position takes place, we might be able more effectively exploit or, if necessary, avoid this process.

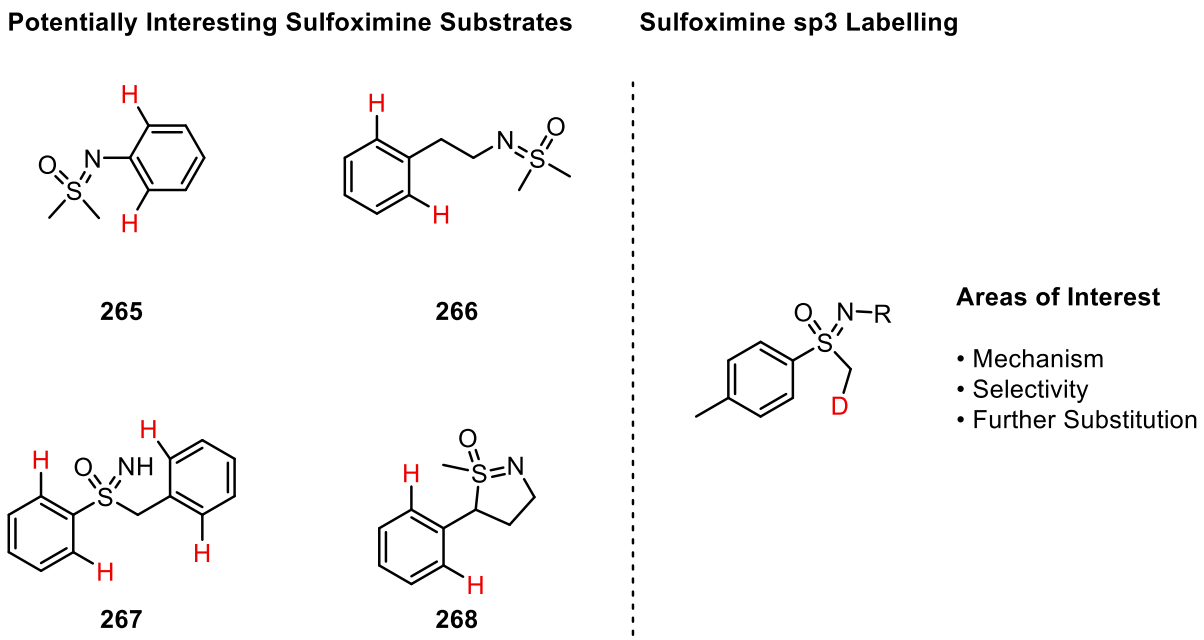

Figure 7.1

Finally, from our discovery of the ether directed labelling, we had hoped to apply our NHC-P catalyst system to the labelling of natural product-like molecules. This objective has yet to be

realised, however, with routes to the desired compounds now established in-house, it is hoped that further investigation into this area will allow us to deliver good levels of isotope incorporation into these complex examples. Furthermore, our initial focus on C_{sp2}—H activation in this area has us limited to natural product classes containing aryl rings in proximity to ethereal/alcohol functionality, of which there are indeed many. However, we hoped that further developments within the activation of C_{sp3}—H bonds will allow us to access an even wider range of natural product classes.

8. Experimental

8.1 General Considerations

All reagents were obtained from commercial suppliers (Alfa Aesar, Sigma Aldrich, Apollo Scientific or Strem) and used without further purification, unless stated. Purification was carried out according to standard laboratory methods.[135]

Tetrahydrofuran was purified by heating to reflux over sodium wire, using benzophenone ketyl as an indicator, before distilling under nitrogen. All other solvents were purified by heating to reflux over calcium hydride, before distilling under argon. Petroleum ether refers to ether in the boiling point range of 40-60 °C.

Thin layer chromatography was carried out using Camlab silica plates coated with fluorescent indicator UV254. These were analysed using a Mineralight UVGL-25 lamp or developed using vanillin or KMnO4 solution. Flash column chromatography was carried out using Prolabo silica gel (230-400 mesh).

IR spectra were obtained on a Shimadzu IR Affinity-1 Spectrophotometer machine and are reported in cm^{-1} unless stated otherwise.

^{1}H, ^{13}C, ^{11}B, ^{19}F, and ^{31}P spectra were recorded on a Bruker DPX 400 spectrometer at 400 MHz, 101 MHz, 128 MHz, 376 MHz, and 162 MHz, respectively. Chemical shifts are reported in ppm. Coupling constants are reported in Hz and refer to $^{3}J_{HH}$ interactions unless stated otherwise.

High resolution mass spectrometry was carried out at the EPSRC National Mass Spectrometry Facility, University of Wales, Swansea.

8.2 List of General Procedures

General Procedure A – Complexation of NHC-P Ligands

To a flame-dried Schlenk tube was added $[Ir(COD)Cl]_2$ (0.5 eq) and the respective ligand (1.00 eq). The mixture was then dissolved in THF and KO^{t}Bu (1.00 eq) was added. The reaction mixture was stirred at room temperature for 2 h, after which the solvent was removed *in vacuo*. The resulting residue was purified by column chromatography, eluting with 1:1 petroleum ether:DCM. The resulting oil was then triturated with petroleum ether, yielding the iridium complex as a red solid.

General Procedure B – Oxidation of Thioethers for Synthesis of Sulfone Substrates

To a 100 mL round-bottom flask was added the respective thioether (1.00 eq) and DCM. The solution was then cooled to 0 °C and *m*CPBA (3.00 eq) was added. The reaction mixture was stirred at room temperature for 16 h, at which point, a saturated solution of aqueous sodium bicarbonate solution was added, and the mixture transferred to a separating funnel. The aqueous layer was separated, and the organic phase was washed with water and separated. The organic phase was collected, dried, and concentrated *in vacuo* to yield the crude product. The crude product was purified by column chromatography, eluting with diethyl ether. The residue was then recrystallized from petroleum ether/diethyl ether to yield the desired sulfone as a white solid.

General Procedure C – Thiophenol Methylation and Oxidation for Synthesis of Sulfone Substrates

To a 100 mL round-bottom flask was added the respective thiophenol (1.00 eq) and ethanol. To this mixture was added NaOH (1.20 eq) and the suspension was stirred for 10 min. Methyl iodide (1.20 eq) was added and the reaction mixture stirred at room temperature for 2 h. The reaction mixture was then diluted with DCM, transferred to a separating funnel and washed

with distilled water. The organic phase was collected, dried, and concentrated *in vacuo*. The residue was re-dissolved in 1:1 acetone:water and Oxone® (3.00 eq) was added. The reaction mixture was stirred at room temperature for 16 h. The reaction mixture was then diluted with DCM and transferred to a separating funnel, then washed with distilled water. The organic phase was collected, dried, and concentrated *in vacuo*. The residue was purified by column chromatography, eluting with diethyl ether. The resulting solid was then recrystallized from petroleum ether/diethyl ether to yield the sulfone as a white solid.

General Procedure D – Sulfone Labelling - Catalyst Screen

Reactions were performed using a Radley's 12-chamber carousel. Each of the carousel tubes were dried overnight in an oven at 180 °C and allowed to cool under vacuum. Each tube was charged with methylphenyl sulfone (33.6 mg, 0.215 mmol) and the relevant catalyst (5 mol%). Each mixture was dissolved in DCM (2.50 mL) and the solutions were cooled to -78 °C. The atmosphere was exchanged with three vacuum/D_2 cycles and the tubes were then sealed and immediately placed in a heating block pre-heated to 25 °C. The reaction mixtures were stirred for 16 h, after which time the solvent was removed *in vacuo*. Petroleum ether was added to the residues and the mixtures were sonicated for 30 s, at which point the solvent was removed by pipette and reduced by blowing with compressed air, to give the crude product. The level of incorporation was determined by ^{1}H NMR spectroscopic analysis, with the integrals of the labelled positions measured against a peak corresponding to a position where labelling was not expected. The level of deuteration was then calculated using Equation **1**:

$$Deuteration\ (\%) = 100 - [100 \times \left(\frac{Residual\ Integral}{Expected\ Integral}\right)] \quad \mathbf{1}$$

General Procedure E – Sulfone Labelling - Solvent Screen

Reactions were all performed using a Radley's 12-chamber carousel. Each of the carousel tubes were dried overnight in an oven at 180 °C and allowed to cool under vacuum. Each tube was

charged with methylphenyl sulfone (33.6 mg, 0.215 mmol) and complex **175** (16.7 mg, 0.01 mmol, 5 mol%). Each mixture was then dissolved in the relevant solvent (2.50 mL) and the solutions were cooled to -78 °C. The atmosphere was exchanged with three vacuum/D_2 cycles and the tubes were sealed and immediately placed in a heating block pre-heated to 25 °C. The reactions were stirred for 16 h, after which time the solvent was removed *in vacuo*. Petroleum ether was added to the residues and the mixture was sonicated for 30 s, at which point the solvent was removed by pipette and reduced by blowing with compressed air, to give the crude product. The level of incorporation was determined by ^{1}H NMR spectroscopic analysis, with the integrals of the labelled positions measured against a peak corresponding to a position where labelling was not expected. The level of deuteration was then calculated as described in *General Procedure D*.

General Procedure F – Sulfone Labelling - Catalyst Loading Study

Reactions were all performed using a Radley's 12-chamber carousel. Each of the carousel tubes were dried overnight in an oven at 180 °C and allowed to cool under vacuum. Each tube was charged with methylphenyl sulfone (33.6 mg, 0.215 mmol) and complex **175**. Each mixture was dissolved in chlorobenzene (2.50 mL) and the solutions cooled to -78 °C. The atmosphere was exchanged with three vacuum/D_2 cycles and the tubes sealed and immediately placed in a heating block pre-heated to 25 °C. The reactions were stirred for 16 h, after which time the solvent was removed *in vacuo*. Petroleum ether was added to the residues and the mixture was sonicated for 30 s, at which point the solvent was removed by pipette and reduced by blowing with compressed air, to give the crude product. The level of incorporation was determined by ^{1}H NMR spectroscopic analysis, with the integrals of the labelled positions measured against a peak corresponding to a position where labelling was not expected. The level of deuteration was then calculated as described in *General Procedure D*.

General Procedure G – Sulfone Labelling - Substrate Scope

Reactions were all performed using a Radley's 12-chamber carousel. Each of the carousel tubes were dried overnight in an oven at 180 °C and allowed to cool under vacuum. Each tube was charged with the relevant substrate (0.215 mmol) and complex **175** (17.0 mg, 0.01 mmol, 5 mol%). The mixture was dissolved in chlorobenzene (2.50 mL). The tubes were placed in a heating block pre-heated to 25 °C and the atmosphere was exchanged with 3 vacuum/D_2 cycles, with the system then being isolated upon the third influx of deuterium. The tubes were then sealed, and the reactions were stirred for 1 h. The gaseous atmosphere was removed and each reaction mixture was loaded directly onto silica. The solvent was eluted with petroleum ether and the substrate eluted with diethyl ether. The level of incorporation was determined by ^{1}H NMR spectroscopic analysis, with the integrals of the labelled positions measured against a peak corresponding to a position where labelling was not expected. The level of deuteration was then calculated as described in *General Procedure D.*

General Procedure H – Synthesis of Sulfonamide Substrates

A solution of the relevant amine (1.00 eq) and triethylamine (1.50 eq) in DCM was cooled to 0 °C. The corresponding sulfonyl chloride (1.10 eq) was added in a single portion, and the reaction mixture stirred at room temperature overnight. The reaction mixture was then transferred to a separation funnel and washed with water. The organic layer was dried over sodium sulfate, filtered, and then concentrated *in vacuo*. The residue was purified by column chromatography.

General Procedure I – Sulfonamide Substrate Labelling at 25 °C

To a three-necked 100 mL round-bottom flask, fitted with two stopcocks, was added substrate (0.215 mmol, 1.00 eq) and complex **218** (16.0 mg, 0.0108 mmol, 5 mol%). The mixture was dissolved in chlorobenzene (2.5 mL) and the flask placed in a heating block, pre-set to 25 °C.

The atmosphere in the flask was exchanged *via* three vacuum/D_2 cycles, with the system then being isolated upon the third influx of deuterium. The reaction mixture was then stirred at 25 °C for 16 h, unless stated otherwise. The reaction mixture was then loaded directly onto a silica column, the chlorobenzene eluted with petroleum ether, and the deuterated product eluted with Et_2O and concentrated *in vacuo*. The level of deuteration was then calculated as described in *General Procedure D*.

General Procedure J – Sulfonamide Substrate Labelling at 40 °C

To a three-necked 100 mL round-bottom flask, fitted with two stopcocks, was added substrate (0.215 mmol, 1.00 eq) and precatalyst **218** (16.0 mg, 0.0108 mmol, 5 mol%). The mixture was dissolved in chlorobenzene (2.5 mL). The atmosphere in the flask was exchanged with three vacuum/D_2 cycles, with the system then being isolated upon the third influx of deuterium. The flask was immediately placed in a heating block, pre-set to 40 °C, and the reaction mixture was stirred at this temperature for 16 h. The reaction mixture was allowed to cool and then loaded directly into a silica column, eluting the chlorobenzene with petroleum ether. The deuterated product was eluted with Et_2O and concentrated *in vacuo*. The level of deuteration was then calculated as described in *General Procedure D*.

General Procedure K – Ether Substrate Labelling

To a three-necked 100 mL round-bottom flask, fitted with two stopcocks, was added substrate (0.215 mmol, 1.00 eq) and complex **175** (18.0 mg, 0.0108 mmol, 5 mol%). The mixture was dissolved in chlorobenzene (2.5 mL) and the flask placed in a heating block, pre-set to 25 °C. The atmosphere in the flask was exchanged *via* three vacuum/D_2 cycles, with the system then being isolated upon the third influx of deuterium. The reaction mixture was then stirred at 25 °C for 1 h, unless stated otherwise. The reaction mixture was then loaded directly onto a silica

column, the chlorobenzene eluted with petroleum ether, and the deuterated product eluted with Et_2O and concentrated *in vacuo*. The level of deuteration was then calculated as described in *General Procedure D.*

General Procedure L–- Attempts Towards Deuterium Labelled (±)-Eudesmin

To a three-necked 100 mL round-bottom flask, fitted with two stopcocks, was added (±)-Eudesmin (1.00 eq) and complex **175** (5 mol%). The mixture was dissolved in chlorobenzene (2.5 mL) and the flask placed either in a heating block, pre-set to 25 °C (**Table 5.3 Entries 1** and **2**), or an ice-methanol bath (**Table 5.3 Entry 3)**. The atmosphere in the flask was exchanged *via* three vacuum/D_2 cycles, with the system then being isolated upon the third influx of deuterium. The reaction mixture was then stirred at the stated temperature for 1 h, unless stated otherwise. The reaction mixture was then loaded directly onto a silica column and the chlorobenzene eluted with petroleum ether. The catalyst residues were removed by one column volume of DCM, and the deuterated product eluted with 50% acetone/petroleum ether and concentrated *in vacuo*. The level of deuteration was then calculated as described in *General Procedure D.*

8.3 Synthesis of NHC-P Catalysts

8.3.1 Synthesis of 1-mesityl-1H-imidazole and 1-(2,6-di-iso-propylphenyl)-1H-imidazole

1-Mesityl-1H-imidazole **179**[136]

To a 500 mL three neck round-bottom flask equipped with a condenser and an addition funnel was added glyoxal (40% wt. in water, 16.3 mL, 142 mmol, 1.10 eq), formaldehyde (37% wt. in water, 10.8 mL, 145 mmol, 1.10 eq) and acetic acid (35.0 mL). The mixture was then heated to 80 °C. In a separate conical flask was added NH_4OAc (10.9 g, 140 mmol, 1.10 eq), 2,4,6-trimethylaniline (18.3 mL, 130 mml, 1.00 eq), acetic acid (35 mL) and water (3.0 mL) and the mixture was stirred until a viscous solution formed. This viscous solution was transferred to the addition funnel and slowly added over 10 min. The reaction mixture was then stirred at 80 °C for 16 h, after which time it was cooled to room temperature and transferred to a dropping funnel. The reaction mixture was then slowly added to an excess amount of saturated aqueous sodium bicarbonate solution, with very vigorous stirring. Once quenched, the aqueous suspension could be purified through methods (a) or (b), detailed below.

Table 3.1, Entry 1

(a) The suspension was transferred to a separating funnel and washed several times with DCM. The organic phases were collected, dried, and concentrated *in vacuo*. The residue was loaded onto silica and purified by column chromatography, eluting with 0-10% MeOH/DCM. Mesityl imidazole **179** (13.1 g, 70.3 mmol, 54% yield) was afforded as a brown solid.

Table 3.1, Entry 2

(b) The suspension was then filtered and the filter cake washed with water and allowed to dry in air. The filtrand was transferred to a beaker and petroleum ether added. The suspension was heated to boiling and the hot solution decanted. This process was repeated until the petroleum ether remained clear upon boiling, at which point the remaining solid residue was discarded. The decanted liquid was concentrated *in vacuo* to yield mesityl imidazole **179** (15.9 g, 85.3 mmol, 66% yield) as a brown solid.

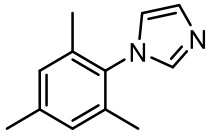

179

Melting Point: 106-108 °C (lit:[136]: 112-118 °C).

IR (neat, cm^{-1}): 3114, 3093, 2974, 2950, 2920, 1805, 1643, 1598, 1498.

^{1}H NMR (400 MHz, $CDCl_3$): δ 7.41 (t, ^{4}J = 0.9 Hz, 1H, NCHN), 7.21 (t, J = 0.9 Hz, 1H, ImH), 6.94 (s, 2H, ArH), 6.87 (t, J = 0.9 Hz, 1H, ImH), 2.32 (s, 3H, ArMe), 1.96 (s, 6H, ArMe).

^{13}C NMR (101 MHz, $CDCl_3$): δ 138.8, 137.5, 135.4, 133.4, 129.6, 129.0, 120.0, 21.0, 17.3.

1-(2,6-Di-iso-propylphenyl)-1H-imidazole **180**[137]

To a 250 mL three-neck round-bottom flask equipped with a condenser and an addition funnel was added glyoxal (40% wt. in water, 3.40 mL, 30.0 mmol, 1.10 eq), formaldehyde (37% wt. in water, 2.80 mL, 30.0 mmol, 1.10 eq) and acetic acid (15.0 mL). The reaction mixture was heated to 80 °C. In a separate conical flask was added NH_4OAc (2.30 g, 30.0 mmol, 1.10 eq), 2,6-di-*iso*-propyl aniline (5.00 mL, 27.0 mml, 1.00 eq), acetic acid (15.0 mL) and water (1.00 mL) and the resulting mixture was stirred until a viscous solution formed. This viscous solution

was then transferred to the addition funnel and added slowly over 10 min. The reaction mixture was then stirred at 80 °C for 16 h, after which time it was cooled to room temperature and transferred to a dropping funnel. The mixture was then slowly added to an excess amount of aqueous saturated sodium bicarbonate solution, with very vigorous stirring. Once quenched, the dark biphasic liquid could be purified through methods (a) or (b), stated below.

Table 3.1, Entry 3

(a) The mixture was transferred to a separating funnel and washed several times with DCM. The organic phases were collected, dried, and concentrated *in vacuo*. The residue was loaded onto silica and purified by column chromatography, eluting with 0-10% MeOH/DCM. 2,6-di-*iso*-propylphenyl imidazole **180** (1.01 g, 4.42 mmol, 16% yield) was afforded as a brown solid.

Table 3.1, Entry 4

(b) The mixture was transferred to a separating funnel and washed several times with DCM. The organic phases were collected, dried, and concentrated *in vacuo*. Petroleum ether was added to the resulting brown oil and heated to boil. At this point, the coloured solution was decanted whilst hot and this process was repeated until the hot solution remained clear upon boiling. The petroleum ether solution was concentrated *in vacuo* to yield di-*iso*-propylphenyl imidazole **180** (1.20 g, 5.40 mmol, 20% yield) as a brown solid.

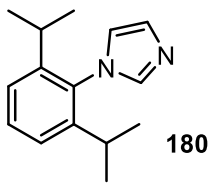

180

Melting Point: 121-123 °C (lit:[137] 123-125 °C).

^{1}H NMR (400 MHz, $CDCl_3$): δ 7.49 (t, ^4J = 0.9 Hz, 1H, NCHN), 7.42 (*t*, *J* = 7.6 Hz, 1H, ImH) 7.26-7.23 (m, 3H, ArH), 6.92 (t, *J* = 0.9 Hz, 1H, ImH), 2.36 (sep, *J* = 6.9 Hz, 2H, CH), 1.11 (d, *J* = 6.9 Hz, 12H, $CH(CH_3)_2$).

^{13}C NMR (101 MHz, $CDCl_3$): δ 146.7, 138.7, 132.7, 130.0, 129.6, 124.0, 121.7, 28.3, 24.6, 24.5.

*8.3.2 Towards (2-(Chloromethyl)phenyl)diphenylphosphane (**Scheme 3.2**)*

N,N-Dimethylbenzylamine **182**[138]

To a 250 mL round-bottom flask was added benzyl bromide **179** (3.6 mL, 30.0 mmol, 1.00 eq), dimethylamine hydrochloride (9.78 g, 120 mmol, 4.00 eq) and Et_2O (100 mL). To this was added triethylamine (23.0 mL, 165 mmol, 5.50 eq) and the reaction mixture stirred at room temperature for 16 h. The reaction mixture was then transferred to a separating funnel and washed several times with water. The organic phase was separated, dried, and concentrated *in vacuo*, yielding *N,N*-dimethylbenzylamine **182** (2.83 g, 21.0 mmol, 70% yield) as a colourless oil, which was taken on to the next step without further purification.

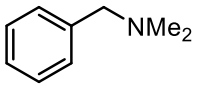

182

IR (neat, cm^{-1}): 2964, 2925, 1260, 1093, 1021, 800.

^{1}H NMR (400 MHz, $CDCl_3$): δ 7.38-7.25 (m, 5H, ArH), 3.44 (s, 2H, CH_2), 2.26 (s, 6H, CH_3).

^{13}C NMR (101 MHz, $CDCl_3$): δ 139.0, 129.3, 128.4, 127.2, 64.6, 45.6.

1-(2-(Diphenylphosphanyl)phenyl)-N,N-dimethylmethanamine **181**[139,140]

A flame-dried, 3-neck, 250 mL round-bottom flask was placed under inert an atmosphere and then charged with *N*,*N*-dimethylbenzylamine **182** (2.50 g, 18.5 mmol, 1.00 eq) and Et_2O (60.0 mL). The solution was cooled to 0 °C and ^{n}BuLi (2.5 M in hexanes, 8.90 mL, 22.2 mmol, 1.20 eq) was added, dropwise. The reaction mixture was then allowed to stir for 24 h at room temperature, after which the reaction was again cooled to 0 °C. Chlorodiphenylphosphine (3.98 mL, 2.22 mmol, 1.20 eq) was added, dropwise, and the reaction mixture stirred at room temperature for 1 h. The reaction mixture was then quenched by the addition of MeOH (1 mL) and the mixture transferred into a separating funnel. The product was extracted into an aqueous solution of HCl (2 M) and separated from the organic phase. The aqueous phase was then basified by addition of NaOH, and the resulting suspension was then transferred to a separating funnel and extracted into DCM. The organic phases were combined, dried, and concentrated *in vacuo*. The residue was then loaded onto silica and purified by column chromatography, eluting with 50% EtOAc/Hexane to afford 1-(2-(diphenylphosphanyl)phenyl)-*N*,*N*-dimethylmethanamine **183** (4.67 g, 14.6 mmol, 79% yield) as a colourless oil, which was stored under inert atmosphere to prevent any oxidation.

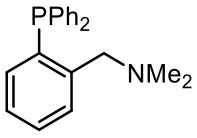

183

IR (neat, cm^{-1}): 3053, 2962, 1469, 1431, 1261.

^{1}H NMR (400 MHz, $CDCl_3$): δ 7.47 (dd, *J* = 7.1 Hz, $^4J_{H\text{-}P}$ = 4.2 Hz, 1H, ArH), 7.35-7.23 (m, 11H, ArH), 7.16 (t, *J* = 7.5 Hz, 1H, ArH), 6.94-6.88 (m, 1H, ArH), 3.62 (s, 2H, CH_2), 2.06 (s, 6H, Me).

^{13}C NMR (101 MHz, $CDCl_3$): δ 144.2 (d, $^1J_{C\text{-}P}$ = 23.5 Hz), 138.0 (d, $^2J_{C\text{-}P}$ = 10.2 Hz), 136.9 (d, $^2J_{C\text{-}P}$ = 14.6 Hz), 134.0, 138.8, 129.2 (d, $^3J_{C\text{-}P}$ = 4.4 Hz), 128.7, 128.5, 128.4, 127.2, 62.4 (d, $^3J_{C\text{-}P}$ = 15.8 Hz), 44.8.

^{31}P NMR (162 MHz, $CDCl_3$): δ -15.26 (s).

(2-(Chloromethyl)phenyl)diphenylphosphane **176**[139]

To a 100 mL round-bottom flask equipped with a condenser was added 1-(2-(diphenylphosphanyl)phenyl)-*N*,*N*-dimethylmethanamine **183** (1.50 g, 4.70 mmol, 1.00 eq) and toluene (12.0 mL). To this was added ethyl chloroformate (0.540 mL, 5.60 mmol, 1.20 eq) and the reaction mixture heated to 80 °C for 2 h. The reaction mixture was then cooled to room temperature and concentrated *in vacuo*. The residue was then loaded onto silica and purified by column chromatography, eluting with DCM. (2-(chloromethyl)phenyl)diphenylphosphane (1.31 g, 4.22 mmol, 90% yield) was afforded as a white, air stable solid.

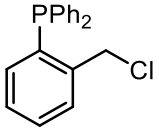

176

Melting Point: 147-149 °C.

IR (neat, cm^{-1}): 3053, 2962, 1469, 1431, 1261.

^{1}H NMR (400 MHz, $CDCl_3$): δ 7.55 (ddd, *J* = 7.6 Hz, $^4J_{H\text{-}P}$ = 4.5 Hz, ^4J = 1.1 Hz, 1H, ArH), 7.42-7.22 (m, 12H, ArH), 6.98 (ddd, J = 7.7 Hz, $^4J_{H\text{-}P}$ = 4.3 Hz, ^4J = 1.1 Hz, 1H, ArH), 4.91 (d, $^4J_{H\text{-}P}$ = 1.9 Hz, 2H, CH_2).

^{13}C NMR (101 MHz, $CDCl_3$): δ 142.0 (d, $^1J_{C\text{-}P}$ = 24.7 Hz), 136.6 (d, $^2J_{C\text{-}P}$ = 14.7 Hz), 136.4 (d, $^2J_{C\text{-}P}$ = 9.1 Hz), 134.3, 134.0 (d, $^1J_{C\text{-}P}$ = 19.9 Hz), 130.1 (d, $^3J_{C\text{-}P}$ = 4.5 Hz), 129.7, 129.0, 128.8, 128.7, 44.9 (d, $^3J_{C\text{-}P}$ = 30.2 Hz).

^{31}P NMR (162 MHz, $CDCl_3$): δ -16.90 (s).

HRMS (Positive ESI): m/z calculated for $[M+H]^+$ $C_{19}H_{17}ClP^+$: 311.0757; found:.311.0756.

*8.3.3 Alkylation to Form Imidazolium Salts **184** and **185** (**Scheme 3.3**)*

3-(2-(Diphenylphosphanyl)benzyl)-1-mesityl imidazolium BAr_F **184**

To a 50 mL round-bottom flask equipped with a condenser was added mesitylimidazole **179** (0.298 g, 1.60 mmol, 1.00 eq), (2-(chloromethyl)phenyl)diphenylphosphane **176** (0.500 g, 1.60 mmol, 1.00 eq) and EtOH (10.0 mL), and the solution placed under an inert atmosphere. The reaction mixture was then heated to reflux for 48 h, then cooled to room temperature and concentrated *in vacuo*. The residue was redissolved in DCM (10.0 mL) and $NaBAr_F$ (1.41 g, 1.60 mmol, 1.00 eq) was added. The reaction was placed under an inert atmosphere and allowed to stir at room temperature overnight. The suspension was then transferred to a separating funnel and washed with water. The organic phase was collected, dried, and concentrated *in vacuo*. The residue was loaded onto silica and purified by column chromatography, eluting with 50% DCM/petroleum ether. 3-(2-(Diphenylphosphanyl)benzyl)-1-mesitylimidazolium BAr_F **184** (1.19 g, 0.896 mmol, 56% yield) was afforded as a pale brown solid.

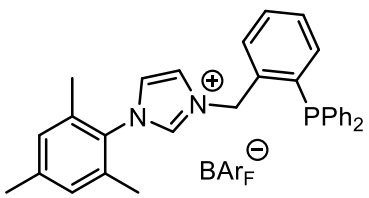

184

Melting Point: 116-118 °C.

IR (neat, cm^{-1}): 1352, 1276, 1159, 1111.

^{1}H NMR (400 MHz, $CDCl_3$): δ 8.02 (s, 1H, Im ArH), 7.72 (bs, 8H, BAr_F ArH), 7.52 (s, 4H, BAr_F ArH), 7.46-7.35 (m, 8H, ArH), 7.30 (s, 1H, ArH), 7.23-7.06 (m, 7H, ArH), 7.01 (s, 2H, ArH), 5.51 (s, 2H, CH_2), 2.34 (s, 3H, ArMe), 1.88 (s, 6H, ArMe).

^{13}C NMR (101 MHz, $CDCl_3$): δ 161.9 (q, $^{1}J_{B\text{-}C}$ = 50.1 Hz), 142.9, 138.0 (d, $J_{C\text{-}P}$ = 16.1 Hz), 135.7, 135.0, 134.6, 134.4, 133.9, 133.8 (d, $J_{C\text{-}P}$ = 20.0 Hz), 131.3 (d, $J_{C\text{-}P}$ = 74.4 Hz), 131.2, 130.4, 130.2, 130.0, 129.9, 129.4 (d, $J_{C\text{-}P}$ = 7.8 Hz), 129.1 (q, $^{2}J_{C\text{-}F}$ = 30.7 Hz), 124.7 (q, $^{1}J_{C\text{-}F}$ = 270.4 Hz), 124.6, 123.2, 117.0, 53.6 (d, $^{3}J_{C\text{-}P}$ = 21.1 Hz), 21.1, 17.2.

^{31}P NMR (162 MHz, $CDCl_3$): δ -15.9 (s).

^{11}B NMR (128 MHz, $CDCl_3$): δ -6.77 (s)

^{19}F NMR (376 MHz, $CDCl_3$): δ -62.4 (s)

HRMS (Positive ESI): m/z calculated for $[M]^+$ $C_{31}H_{30}N_2P^+$: 461.2141; found: 461.2134.

1-(2,6-Di-iso-propylphenyl)-3-(2-(diphenylphosphanyl)benzyl)imidazolium BAr_F **185**

To a 50 mL round-bottom flask equipped with a condenser was added 1-(2,6-di-*iso*-propylphenyl) imidazole **180** (0.250 g, 1.10 mmol, 1.00 eq), (2-(chloromethyl)phenyl)diphenylphosphane **176** (0.342 g, 1.10 mmol, 1.00 eq) and potassium iodide (0.091 g, 0.55 mmol, 0.50 eq). The mixture was suspended in acetonitrile (8.00 mL). The reaction was heated to reflux for 2 h, after which point it was cooled and passed through a silica plug, eluting with DCM. The filtrate was then concentrated *in vacuo*. The residue was then redissolved in DCM (10.0 mL), $NaBAr_F$ (0.984 g, 1.10 mmol, 1.00 eq) was added and the

reaction mixture stirred at room temperature overnight. The suspension was concentrated *in vacuo*, the residue loaded onto silica and purified by column chromatography, eluting with 50% DCM/petroleum ether. 1-(2,6-Di-*iso*-propylphenyl)-3-(2-(diphenylphosphanyl)benzyl) imidazolium BAr_F **185** (0.870 g, 0.638 mmol, 58% yield) was obtained as a pale brown solid.

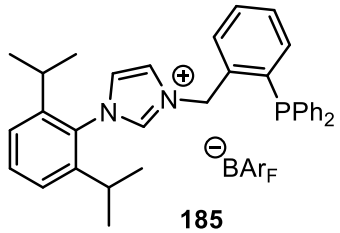

185

Melting Point: 186-188 °C.

IR (neat, cm^{-1}): 2968, 1352, 1274, 1159, 1116.

^{1}H NMR (400 MHz, $CDCl_3$): δ 8.18 (s, 1H, Im ArH), 7.71 (bs, 8H, BAr_F ArH), 7.68-7.41 (m, 19H, BAr_F ArH +ArH), 7.36-7.15 (m, 2H, ArH), 7.21-7.13 (m, 2H, ArH), 5.59 (s, 2H, CH_2), 2.15 (sep, J = 7.0 Hz, 2H, CH), 1.12 (d, J = 7.0 Hz, 12H, CH_3).

^{13}C NMR (101 MHz, $CDCl_3$): δ 161.9 (q, $^1J_{B\text{-}C}$ = 49.3 Hz), 145.2, 137.8, 135.6, 135.0, 133.8 (d, $J_{C\text{-}P}$ = 19.8 Hz), 133.0, 131.7, 131.3, 130.5 (d, $J_{C\text{-}P}$ = 62.7 Hz), 130.3, 129.5 (d, $J_{C\text{-}P}$ = 7.7 Hz), 129.1 (q, $^2J_{C\text{-}F}$ = 32.9 Hz), 125.8, 125.6, 125.3, 124.9, 124.8 (q, $^1J_{C\text{-}F}$ = 271.1 Hz), 122.9, 122.2, 117.7, 53.8 (d, $^3J_{C\text{-}P}$ = 21.3 Hz), 29.0, 24.2.

^{31}P NMR (162 MHz, $CDCl_3$): δ -16.2 (s).

^{11}B NMR (128 MHz, $CDCl_3$): δ -6.65 (s).

^{19}F NMR (376 MHz, $CDCl_3$): δ -62.4 (s).

HRMS (Positive ESI): m/z calculated for $[M]^+$ $C_{34}H_{36}N_2P^+$: 503.2611. Found: 503.2597.

*8.3.4 Synthesis of Complexes **174** and **175** (**Table 3.2**)*

η^4–Cycloocta-1,5-diene(3-(2-(diphenylphosphanyl)benzyl)-1-mesityl imidazole-2-ylidene)iridium BAr_F **174**

Prepared according to *General Procedure A*. Data are presented as (a) amount of $[Ir(COD)Cl]_2$, (b) amount of 3-(2-(diphenylphosphanyl)benzyl)-1-mesitylimidazolium BAr_F **184**, (c) volume of THF, and (d) amount of potassium *tert*-butoxide, and (e) yield.

Table 3.2, Entry 1

(a) 0.101 g, 0.150 mmol, (b) 0.397 g, 0.300 mmol, (c) 10.0 mL, (d) 0.034 g, 0.300 mmol, and (e) 0.238 g, 0.147 mmol, 49% yield.

Table 3.2, Entry 2

(a) 0.202 g, 0.300 mmol, (b) 0.794 g, 0.600 mmol, (c) 20.0 mL, (d) 0.067 g, 0.600 mmol, and (e) 0.835 g, 0.514 mmol, 86% yield.

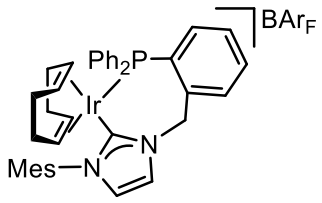

174

Melting Point: 200-202 °C.

IR (neat, cm^{-1}): 2972, 1354, 1278, 1157, 1114.

^{1}H NMR (400 MHz, $CDCl_3$): δ 7.74 (bs, 8H, BAr_F ArH), 7.66-7.59 (m, 2H, ArH), 7.58-7.50 (m, 7H, BAr_F ArH + ArH), 7.48-7.33 (m, 8H, ArH), 7.32-7.25 (m, 1H, ArH), 7.14 (d, ^3J = 2.0 Hz, 1H, ArH), 6.96 (s, 1H, ArH), 6.91 (s, 1H, ArH), 6.83 (d, ^3J = 2.0 Hz, 1H, ArH), 6.68 (d, $^2J_{HH}$ = 14.5 Hz, 1H, CH_2), 5.28-5.22 (m, 1H, COD CH), 4.74 (d, ^2J = 14.5 Hz, 1H, CH_2), 3.77-3.71 (m, 1H, COD CH), 3.68-3.60 (m, 1H, COD CH), 3.51-3.43 (m, 1H, COD CH), 2.33 (s,

3H, CH_3), 2.11-1.79 (m, 7H, ArMe + 2COD CH_2), 1.57 (s, 3H, ArMe), 1.54-1.54 (m, 2H, COD CH_2), 1.37-1.26 (m, 2H, COD CH_2).

^{13}C NMR (101 MHz, $CDCl_3$): δ 170.9 (d, $^2J_{C\text{-}P}$ = 9.6 Hz), 161.9 (q, $^1J_{C\text{-}B}$ = 50.7 Hz), 140.7 (d, $J_{C\text{-}P}$ = 12.4 Hz), 140.2, 135.7, 135.3 (d, $J_{C\text{-}P}$ = 24.9 Hz), 135.0, 134.6, 134.0 (d, $J_{C\text{-}P}$ = 10.8 Hz), 133.5 (d, $J_{C\text{-}P}$ = 10.1 Hz), 132.2, 131.8, 131.5, 130.5 (d, $J_{C\text{-}P}$ = 7.0 Hz), 130.0 (d, $J_{C\text{-}P}$ = 6.2 Hz), 129.5, 129.3 (d, $J_{C\text{-}P}$ = 27.4 Hz), 129.1 (q, $^2J_{C\text{-}F}$ = 29.4 Hz), 129.0, 126.9, 124.8 (q, $^1J_{C\text{-}F}$ = 273.1 Hz), 120.7, 117.7, 87.9 (d, $J_{C\text{-}P}$ = 9.2 Hz), 82.8, 82.0 (d, $^2J_{C\text{-}P}$ = 14.4 Hz), 77.6, 54.4 (d, $^3J_{C\text{-}P}$ = 9.9 Hz), 36.1, 34.0, 28.3, 27.6, 21.0, 19.0, 18.0.

^{31}P NMR (162 MHz, $CDCl_3$): δ 2.55 (s).

^{11}B NMR (128 MHz, $CDCl_3$): δ -6.65 (s).

^{19}F NMR (376 MHz, $CDCl_3$): δ -62.4 (s).

HRMS (Positive ESI): m/z calculated for $[M]^+$ $C_{39}H_{41}N_2P^+$: 761.2633; found:761.2638.

η^4–Cycloocta-1,5-diene(1-(2,6-di-iso-propylphenyl)-3-(2-(diphenylphosphanyl)benzyl) imidazole-2-ylidene)iridium BAr_F **175**

Prepared according to *General Procedure A*. The data presented as: (a) amount of $[Ir(COD)Cl]_2$, (b) amount of 1-(2,6-di-*iso*-propylphenyl)-3-(2-(diphenylphosphanyl)benzyl) imidazolium BAr_F **185**, (c) volume of THF, and (d) amount of potassium *tert*-butoxide, and (e) yield.

Table 3.2, Entry 3

(a) 1.01 g, 0.150 mmol, (b) 0.410 g, 0.300 mmol, (c) 10.0 mL, (d) 0.034 g, 0.300 mmol, and (e) 0.365 g, 0.219 mmol, 73% yield.

Table 3.2, Entry 4

(a) 0.202 g, 0.300 mmol, (b) 0.820 g, 0.600 mmol, (c) 20.0 mL, (d) 0.067 g, 0.600 mmol, and (e) 0.910 g, 0.546 mmol, 91% yield.

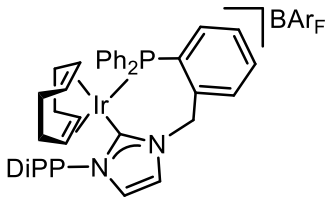

175

Melting Point: 186-188 °C.

IR (neat, cm^{-1}): 2972, 2375, 2328, 1610, 1354, 1274.

^{1}H NMR (400 MHz, $CDCl_3$): δ 7.90-7.82 (m, 2H, ArH), 7.69 (bs, 8H, BAr_F ArH), 7.54-7.40 (m, 10H, BAr_F ArH + ArH), 7.39-7.26 (m, 9H, ArH), 7.13 (d, ^3J = 2.0 Hz, 1H, ArH), 6.95 (d, ^3J = 2.0 Hz, 1H, ArH), 6.24 (d, ^2J = 14.5 Hz, 1H, CH_2), 5.52-5.45 (m, 1H, COD CH), 4.57 (d, ^2J = 14.5 Hz, 1H, CH_2), 3.78-3.70 (m, 1H, COD CH), 3.40-3.29 (m, 2H, COD CH), 3.16 (sep, J = 6.7 Hz, 1H, CH), 2.52-2.38 (m, 2H, COD CH_2), 2.21 (sep, J = 6.7 Hz, 1H, CH), 2.03-1.79 (m, 4H, 2 COD CH_2), 1.75-1.62 (m, 2H, COD CH_2), 1.23 (d, J = 6.7Hz, 3H, CH_3), 1.19 (d, J = 6.7Hz, 3H, CH_3), 1.14 (d, J = 6.7Hz, 3H, CH_3), 0.48 (d, J = 6.7Hz, 3H, CH_3).

^{13}C NMR (101 MHz, $CDCl_3$): δ 171.3 (d, $^2J_{C\text{-}P}$ = 10.1 Hz), 162.0 (q, $^1J_{B\text{-}C}$ = 50.6 Hz), 145.1 (d, $J_{C\text{-}P}$ = 109.1 Hz), 140.5 (d, $J_{C\text{-}P}$ = 11.9 Hz), 136.2, 135.0, 133.4, 133.1 (d, $J_{C\text{-}P}$ = 11.0 Hz), 132.7, 132.0, 131.7, 130.8, 130.4 (d, $J_{C\text{-}P}$ = 7.3 Hz), 130.2, 129.9 (d, $J_{C\text{-}P}$ = 7.3 Hz), 129.4, 129.1 (q, $^2J_{C\text{-}F}$ = 29.8 Hz), 128.2, 125.3, 124.7 (q, $^1J_{C\text{-}F}$ = 271.6 Hz), 123.8, 120.5, 117.7, 87.5 (d, $J_{C\text{-}P}$ = 7.2 Hz), 87.0, 79.4 (d, $^2J_{C\text{-}P}$ = 19.5 Hz), 76.8, 53.7 (d, $^3J_{C\text{-}P}$ = 12.3 Hz), 37.4, 34.7, 31.4, 28.6, 27.2, 26.7, 26.1, 23.8, 23.4, 22.2.

^{31}P NMR (162 MHz, $CDCl_3$): δ 3.92 (s).

^{11}B NMR (128 MHz, $CDCl_3$): δ -6.79 (s).

^{19}F NMR (376 MHz, $CDCl_3$): δ -62.4 (s).

HRMS (Positive ESI): m/z calculated for $C_{36}H_{41}N_2O_2PIr^+$ $[M + 2OMe]^+$ = 757.2906; found: 757.2899, corresponding to complex with COD displaced by two MeO^- anions:

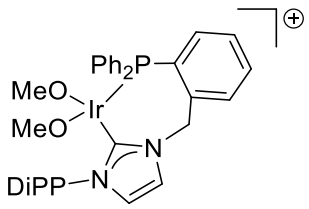

*8.3.5 Towards η^4–Cycloocta-1,5-diene(3-(2-(diphenylphosphanyl)benzyl)-1-mesityl-4,5-dimethyl imidazole-2-ylidene)iridium BAr_F (**Scheme 3.5**)*

1-Mesityl-4,5-dimethylimidazole **188**[141]

To a 250 mL, 3-neck round-bottom flask equipped with a condenser was added butadione (2.20 mL, 25.0 mmol, 1.0 eq), mesityl amine (4.20 mL, 30.0 mmol, 1.20 eq), NH_4OAc (1.90 g, 25.0 mmol, 1.0 eq) and paraformaldehyde (0.76 g, 25.0 mmol, 1.0 eq). The mixture was dissolved in chloroform (50.0 mL) and acetic acid (1.50 mL, 25.0 mmol, 1 eq) was added. The reaction mixture was stirred at 80 °C for 16 h, then cooled to room temperature and transferred to a dropping funnel. The reaction mixture was then slowly added to an excess amount of saturated aqueous sodium bicarbonate solution, with very vigorous stirring. The resulting mixture was then transferred to a separating funnel and extracted into DCM. The combined organic phases were collected, dried and concentrated *in vacuo*. The residue was loaded onto silica and purified by column chromatography, eluting with 0-50% EtOAc/petroleum ether. 1-Mesityl-4,5-dimethylimidazole **188** (2.42 g, 11.3 mmol, 45% yield) was afforded as a brown solid.

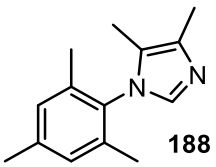

188

Melting Point: 137-138 °C (lit:[141] 130-131 °C).

IR (neat, cm^{-1}): 3101, 2980, 1589, 1490, 1473, 1384, 1224.

^{1}H NMR (400 MHz, $CDCl_3$): δ 7.22 (s, 1H, NCHN), 6.94 (s, 2H, ArH), 2.32 (s, 3H, CH_3), 2.22 (s, 3H, CH_3), 1.91 (s, 6H, CH_3), 1.82 (s, 3H, CH_3).

^{13}C NMR (101 MHz, $CDCl_3$): δ 138.9, 136.3, 134.6, 133.9, 132.7, 129.1, 122.9, 21.2, 17.6, 13.1, 8.4.

3-(2-(Diphenylphosphanyl)benzyl)-1-mesityl-4,5-dimethyl imidazolium BAr_F **186**

To a 50 mL round-bottom flask equipped with a condenser was added 1-mesityl-4,5-dimethylimidazole **188** (0.827 g, 3.86 mmol, 1.00 eq), (2-(chloromethyl)phenyl)diphenylphosphane **176** (1.12 g, 3.86 mmol, 1.00 eq) and potassium iodide (0.320 g, 1.93 mmol, 0.50 eq). The reaction mixture was dissolved in MeCN and heated to reflux for 2 h. The reaction mixture was then cooled to room temperature and concentrated *in vacuo*. The residue was dissolved in DCM and passed through a silica plug. The filtrate was diluted with DCM (10.0 mL) and $NaBAr_F$ (3.42 g, 3.86 mmol, 1.00 eq) was then added. The suspension was placed under an inert atmosphere and the reaction mixture stirred at room temperature overnight. The suspension was concentrated *in vacuo* and loaded onto silica. The product was purified by column chromatography, eluting with 50% DCM/petroleum ether. 3-(2-(Diphenylphosphanyl)benzyl)-1-mesityl-4,5-dimethyl imidazolium BAr_F **186** (4.30 g, 3.17 mmol, 82% yield) was obtained as a pale brown solid.

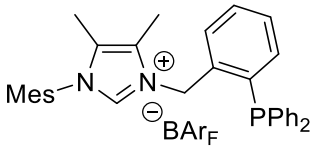

186

Melting Point: 74-76 °C.

IR (neat, cm^{-1}): 2968, 1318, 1279, 1173, 1199.

^{1}H NMR (400 MHz, CDCl$_3$): δ 7.71 (bs, 8H, BAr$_F$ ArH),7.63 (s, 1H, ArH), 7.52 (s, 4H, BAr$_F$ ArH), 7.48-7.35 (m, 8H, ArH), 7.24-7.14 (m, 5H, ArH), 7.09-7.04 (m, 1H, ArH), 7.02 (s, 2H, ArH), 5.29 (s, 2H, CH_2), 2.36 (s, 3H, ArMe), 2.24 (s, 3H, ArMe), 1.94 (s, 3H, ArMe), 1.84 (s, 6H, ArMe).

^{13}C NMR (101 MHz, CDCl$_3$): δ 161.2 (q, $^1J_{B\text{-}C}$ = 50.1 Hz), 142.0, 137.2 (d, $J_{C\text{-}P}$ = 15.6 Hz), 134.6, 134.3, 133.7, 133.4, 133.3, 133.1, 133.0, 131.9, 130.4, 129.9, 129.7, 129.5, 128.8, 128.7, 128.4 (q, $^2J_{C\text{-}F}$ = 31.2 Hz), 127.6, 124.0 (q, $^1J_{C\text{-}F}$ = 272.8 Hz), 116.9, 49.8 (d, $^3J_{C\text{-}P}$ = 22.0 Hz), 20.4, 16.5, 8.23, 7.5.

^{31}P NMR (162 MHz, CDCl$_3$): δ -15.9 (s).

^{11}B NMR (128 MHz, CDCl$_3$): δ -6.77 (s).

^{19}F NMR (376 MHz, CDCl$_3$): δ -62.4 (s).

HRMS (Positive ESI): m/z calculated for $[M]^+$ $C_{33}H_{34}N_2P^+$: 489.2454; found: 489.2426.

η^4–Cycloocta-1,5-diene(3-(2-(diphenylphosphanyl)benzyl)-1-mesityl 4,5-dimethyl imidazole-2-ylidene)iridium BAr$_F$ **189**

Prepared according to *General Procedure A*. Data presented as (a) amount of $[Ir(COD)Cl]_2$, (b) amount of 3-(2-(diphenylphosphanyl)benzyl)-1-mesityl-4,5-dimethyl imidazolium BAr_F **186**, (c) volume of THF, (d) amount of potassium *tert*-butoxide and (e) yield.

(a) 0.336 g, 0.500 mmol, 0.50 eq, (b) 1.35 g, 1.00 mmol, 1.00 eq, (c) 10.0 mL, (d) 0.113 g, 1.00 mmol, 1.00 eq, and (e) 1.50 g, 0.908 mmol, 91% yield.

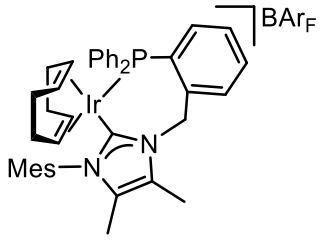

189

Melting Point: 82-84 °C.

IR (neat, cm^{-1}): 2978, 2357, 2331, 1608, 1352, 1273.

^{1}H NMR (400 MHz, $CDCl_3$): δ 7.71 (bs, 8H, BAr_F ArH), 7.61-7.47 (m, 10H, BAr_F ArH + ArH), 7.38-7.29 (m, 4H, ArH), 7.21-7.13 (m, 4H, ArH), 6.90 (s, 1H, ArH), 6.79 (s, 1H, ArH), 5.00-4.90 (m, 2H CH_2), 4.11-4.01 (m, 1H, COD CH), 3.66-3.50 (m, 3H, 3 COD CH), 2.30 (s, 3H, ArMe), 2.22 (s, 3H, ArMe), 2.12-1.88 (m, 4H, COD CH_2), 1.82 (s, 3H, ArMe), 1.70-1.49 (m, 7H, ArMe + COD CH_2), 0.89 (s, 3H, ArMe).

^{13}C NMR (101 MHz, $CDCl_3$): δ 167.1 (d, $^1J_{C\text{-}P}$ = 11.0 Hz), 161.7 (q, $^1J_{B\text{-}C}$ = 50.0 Hz), 140.6 (d, $J_{C\text{-}P}$ = 12.6 Hz), 139.9 ,138.6, 136.1, 135.6, 134.8, 133.9 (d, $J_{C\text{-}P}$ = 9.3 Hz), 132.6, 132.4 (d, $J_{C\text{-}P}$ = 10.8 Hz), 131.7 (d, $J_{C\text{-}P}$ = 17.0 Hz), 131.4, 130.9, 130.6, 130.5, 130.4, 129.8, 129.5, 128.9 (q, $^2J_{C\text{-}F}$ = 31.1 Hz), 128.4, 128.3, 125.3, 124.6 (q, $^1J_{C\text{-}F}$ = 273.3 Hz), 117.5, 87.4 (d, $J_{C\text{-}P}$ = 14.5 Hz), 85.5 (d, $^2J_{C\text{-}P}$ = 12.4 Hz), 77.7, 76.4, 65.8, 52.2 (d, $J_{C\text{-}P}$ = 8.3 Hz), 34.3, 32.9, 29.1, 28.6, 20.9, 17.4, 16.4, 15.2, 9.4, 8.6.

^{31}P NMR (162 MHz, $CDCl_3$): δ 2.39 (s).

^{11}B NMR (128 MHz, $CDCl_3$): δ -7.01 (s).

^{19}F NMR (376 MHz, $CDCl_3$): δ -61.9 (s).

HRMS (Positive ESI): m/z calculated for $C_{33}H_{33}N_2PIr^+$ $[M\text{-}COD]^+$ = 679.1847; found: 679.1841, corresponding to complex with COD decoordinated:

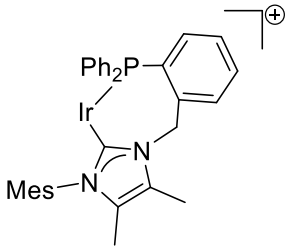

*8.3.6 Towards η^4–Cycloocta-1,5-diene(3-(2-(diphenylphosphanyl)benzyl)-1-mesityl benzimidazole-2-ylidene)iridium BAr_F (**Scheme 3.6**)*

N-(2-bromophenyl)-2,4,6-trimethylaniline **191**[77]

A flame-dried Schlenk tube equipped with a cold finger was placed under an inert atmosphere and then charged with $Pd(OAc)_2$ (0.149 g, 0.660 mmol, 8 mol%), (*R*)-BINAP (0.880 g 1.33 mmol, 16 mol%) and toluene (17.0 mL). The reaction mixture was heated to 60 °C for 10 minutes, at which point dibromobenzene (1.96 mL, 8.30 mmol, 1.00 eq), mesitylamine (1.50 mL, 10.0 mmol, 1.20 eq) and potassium *tert*-butoxide (1.20 g, 10.6 mmol, 1.28 eq) were added. The reaction mixture was heated to reflux and stirred for 18 h. The reaction mixture was then cooled to room temperature and filtered through Celite, washing with DCM. The filtrate was concentrated *in vacuo* and the residue dry loaded onto silica. The product was purified by column chromatography, eluting with 0-30% DCM/petroleum ether, affording *N*-(2-bromophenyl)-2,4,6-trimethylaniline **191** (16.9 g, 5.81 mmol, 70% yield) as a colourless oil.

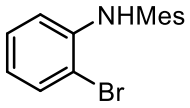

191

IR (neat, cm^{-1}): 3388, 2916, 1595, 1595, 1498, 1450.

^{1}H NMR (400 MHz, $CDCl_3$): δ 7.45 (dd, *J* = 7.9 Hz, 1.5 Hz, 1H, ArH), 6.99 (ddd, *J* = 8.5 Hz, *J* = 7.0 Hz, *J* = 1.0 Hz, 1H, ArH), 6.93 (s, 2H, ArH), 6.56 (ddd, *J* = 7.8 Hz,, *J* = 7.2 Hz, *J* = 1.4 Hz, 1H, ArH), 6.13 (dd, *J* = 8.1 Hz, 1.5 Hz, 1H, ArH), 5.61 (bs, 1H, NH) 2.29 (s, 3H, ArMe), 2.14 (s, 6H, ArMe).

^{13}C NMR (101 MHz, $CDCl_3$): δ 143.9, 136.7, 136.4, 135.1, 132.7, 129.5, 128.6, 118.6, 112.7, 109.6, 21.2, 18.3.

HRMS (Positive ESI): m/z calculated for $[M+H]^+$ $C_{15}H_{17}N^{79}Br$: 290.054; found: 290.054. Calculated for $[M+H]^+$ $C_{15}H_{17}N^{81}Br$: 292.052; found 292.052

N-(2-((diphenylmethylene)amino)phenyl)-2,4,6-trimethylaniline **192**[77]

A flame-dried Schlenk tube equipped with a cold finger was placed under an inert atmosphere and then charged with $Pd_2(dba)_3$ (0.271 g, 0.296 mmol, 3 mol%), (*R*)-BINAP (0.368 g, 0.591 mmol, 6 mol%), *N*-(2-bromophenyl)-2,4,6-trimethylaniline **191** (2.86 g, 9.86 mmol, 1.00 eq), benzophenone imine (2.15 mL, 12.8 mmol, 1.30 eq) and potassium *tert*-butoxide (1.44 g, 12.8 mmol, 1.30 eq). The mixture was suspended in toluene (35.0 mL) and heated to reflux for 48 h. The reaction mixture was then cooled to room temperature and filtered through Celite, washing with DCM. The filtrate was concentrated *in vacuo* and the residue purified by trituration with methanol. *N*-(2-((diphenylmethylene)amino)phenyl)-2,4,6-trimethylaniline **192** (2.29 g, 5.86 mmol, 60% yield) was afforded as a bright yellow solid.

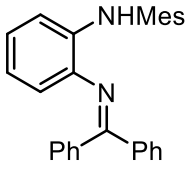

192

Melting Point: 147-149 °C.

IR (neat, cm^{-1}): 2970, 1589, 1487, 1274.

^{1}H NMR (400 MHz, $CDCl_3$): δ 7.84-7.80 (m, 2H, ArH), 7.48-7.43 (m, 1H, ArH), 7.42-7.37 (m, 2H, ArH), 7.34-7.30 (m, 3H, ArH), 7.25-7.21 (m, 2H, ArH), 6.92 (s, 2H, ArH), 6.71 (td, *J* = 7.5 Hz, 1.5 Hz, 1H, ArH), 6.33 (td, *J* = 7.5 Hz, 1.5 Hz, 1H, ArH), 6.21 (dd, *J* = 7.7 Hz, 1.4 Hz, 1H, ArH), 6.11 (dd, *J* = 7.7 Hz, 1.4 Hz, 1H, ArH), 5.58 (s, 1H, NH), 2.29 (s, 3H, ArMe), 2.22 (s, 6H, ArMe).

^{13}C NMR (101 MHz, $CDCl_3$): δ 168.2, 140.5, 139.8, 136.7, 136.5, 136.3, 136.1, 135.2, 130.6, 129.3, 129.1, 128.8, 128.2, 128.1, 124.9, 119.4, 116.6, 110.8, 20.9, 18.2.

HRMS (Positive ESI): m/z calculated for $[M+H]^+$ $C_{28}H_{27}N_2$: 391.217; found: 391.217.

N^1-Mesitylbenzene-1,2-diamine **193**[77]

A 100 mL round-bottom flask was charged with *N*-(2-((diphenylmethylene)amino)phenyl)-2,4,6-trimethylaniline **192** (2.00 g, 5.12 mmol, 1.00 eq) and MeOH (13.0 mL). To this was added HCl in dioxane (4 M, 2.00 mL, 4 eq) and the reaction mixture stirred at room temperature overnight. The reaction was concentrated *in vacuo* and the residue dissolved in EtOAc, transferred to a separating funnel and washed with saturated aqueous sodium bicarbonate solution until neutralised. The organic phase was separated, dried, and concentrated *in vacuo*. The residue was loaded onto silica and purified by column chromatography, eluting with 10-

25% Et_2O/petroleum ether. N^1-mesitylbenzene-1,2-diamine **193** (0.919 g, 4.06 mmol, 80% yield) was afforded as a dark oil.

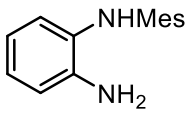

193

IR (neat, cm^{-1}): 2968, 1352, 1274, 1118.

^{1}H NMR (400 MHz, $CDCl_3$): δ 6.90 (s, 2H, ArH), 6.78-6.69 (m, 2H, ArH), 6.62 (td, J = 7.4 Hz, ^4J = 1.8 Hz, 1H, ArH), 6.22 (dd, J = 7.5 Hz, J = 1.5 Hz, 1H, ArH), 4.74 (s, 1H, NH), 3.60 (s, 2H, NH_2) 2.28 (s, 3H, ArMe), 2.11 (s, 6H, ArMe).

^{13}C NMR (101 MHz, $CDCl_3$): δ 130.6, 129.5, 129.3, 129.1, 128.8, 128.2, 124.9, 119.3, 116.6, 110.8, 20.9, 18.2.

HRMS (Positive ESI): m/z calculated for $[M+H]^+$ $C_{15}H_{19}N_2$: 227.154, found: 227.154.

1-Mesitylbenzimidazole **194**[77]

A 100 mL round-bottom flask was charged with N^1-mesitylbenzene-1,2-diamine **193** (0.600 g, 2.65 mmol, 1.00 eq) and $TsOH.H_2O$ (0.252 g, 1.33 mmol, 0.5 eq). The mixture was dissolved in trimethyl orthoformate (10.0 mL) and stirred at room temperature for 18 h. The solution was diluted with EtOAc, transferred to a separating funnel and washed with saturated aqueous sodium bicarbonate solution. The organic phase was collected, dried, and concentrated *in vacuo*. The residue was loaded onto silica and purified by column chromatography, eluting with 5% MeOH/DCM. 1-Mesitylbenzimidazole **194** (0.601 g, 2.54 mmol, 96% yield) was afforded as a pale brown oil.

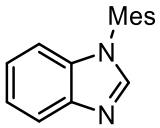

194

IR (neat, cm^{-1}): 2952, 1284, 1265, 1154.

^{1}H NMR (400 MHz, $CDCl_3$): δ 7.88 (d, *J* = 8.1 Hz, 1H, ArH), 7.85 (s, 1H, ArH), 7.30 (ddd, *J* = 7.8 Hz, *J* = 7.7 Hz, $^{4}J_{HH}$ = 1.3 Hz, 1H, ArH), .7.24 (ddd, *J* = 7.4 Hz, *J* = 7.4 Hz, $^{4}J_{HH}$ = 0.9 Hz, 1H, ArH), 7.05-6.98 (m, 3H, ArH), 2.37 (s, 3H, $ArCH_3$), 1.91 (s, 6H, $ArCH_3$).

^{13}C NMR (101 MHz, $CDCl_3$): δ 143.5, 143.1, 139.4, 136.5, 134.2, 131.2, 129.5, 123.6, 122.3, 120.4, 110.3, 21.2, 17.5.

HRMS (Positive ESI): m/z calculated for $[M+H]^+$ $C_{16}H_{17}N_2$: 237.139; found: 237.139.

3-(2-(Diphenylphosphanyl)benzyl)-1-mesitylbenzimidazolium BAr_F **187**

To a 50 mL round-bottom flask equipped with a condenser was added 1-mesitylbenzimidazole **194** (0.500 g, 2.12 mmol, 1.00 eq), (2-(chloromethyl)phenyl)diphenylphosphane **176** (0.725 g, 2.33 mmol, 1.10 eq) and potassium iodide (0.176 g, 1.06 mmol, 0.50 eq). The reaction mixture was dissolved in MeCN (10.0 mL) and heated to reflux for 4 h, then cooled to room temperature and concentrated *in vacuo*. The residue was dissolved in DCM and passed through a silica plug. The filtrate was diluted with DCM (15.0 mL) and $NaBAr_F$ (1.88 g, 2.12 mmol. 1.00 eq) was added. The suspension was placed under an inert atmosphere and the reaction mixture stirred at room temperature overnight. The reaction was then concentrated *in vacuo* and the residue loaded onto silica. The product was purified by column chromatography, eluting with 50% DCM/petroleum ether. 3-(2-(diphenylphosphanyl)benzyl)-1-mesitylbenzimidazolium BAr_F **187** (0.910 g, 0.662 mmol, 31% yield) was obtained as a pale brown solid.

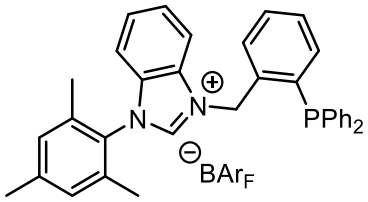

187

Melting Point: 48-54 °C.

IR (neat, cm^{-1}): 1352, 1274, 1159, 1116.

^{1}H NMR (400 MHz, $CDCl_3$): δ 8.24 (s, 1H, ArH), 7.74-7.62 (m, 11H, BAr_F ArH + ArH), 7.48 (s, 4H, BAr_F ArH), 7.45-7.28 (m, 11H, ArH), 7.18-7.12 (m, 3H, ArH), 7.10-7.05 (m, 3H, ArH), 5.70 (s, 2H, CH_2), 2.39 (s, 3H, ArMe), 1.82 (s, 6H, ArMe).

^{13}C NMR (101 MHz, $CDCl_3$): δ 161.9 (q, $^{1}J_{C\text{-}B}$ = 48.5 Hz), 143.1, 139.4, 138.3, 135.5, 135.0, 133.9 (d, $J_{C\text{-}P}$ = 19.4 Hz), 133.6, 132.2, 132.0, 131.5, 131.2, 130.8, 130.6, 130.5, 130.0, 129.4, 129.3, 129.0 (q, $^{2}J_{C\text{-}F}$ = 30.5 Hz), 128.7, 127.3, 126.1, 123.4, 120.7 (d, $^{1}J_{C\text{-}F}$ = 274.1 Hz) 117.7, 113.8, 51.2 (d, $^{3}J_{C\text{-}P}$ = 19.8 Hz), 21.2, 17.2.

^{31}P NMR (162 MHz, $CDCl_3$): δ -16.2 (s).

^{11}B NMR (128 MHz, $CDCl_3$): δ -6.77 (s).

^{19}F NMR (376 MHz, $CDCl_3$): δ -62.4 (s).

HRMS (Positive ESI): m/z calculated for $[M]^+$ $C_{35}H_{32}N_2P$: 511.2298; found: 511.2312.

η^4–Cycloocta-1,5-diene(3-(2-(diphenylphosphanyl)benzyl)-1-mesityl benzimidazole-2-ylidene)iridium BAr_F **195**

Prepared according to *General Procedure A*. Data presented as (a) amount of $[Ir(COD)Cl]_2$, (b) amount of 3-(2-(diphenylphosphanyl)benzyl)-1-mesityl benzimidazolium BAr_F, (c) volume of THF, (d) amount of potassium *tert*-butoxide and (e) yield.

(a) 0.121 g, 0.180 mmol, 0.50 eq, (b) 0.500 g, 0.360 mmol, 1.00 eq, (c) 5.0 mL, (d) 0.040 g, 0.360 mmol, 1.00 eq, and (e) 0.350 g, 0.209 mmol, 58% yield.

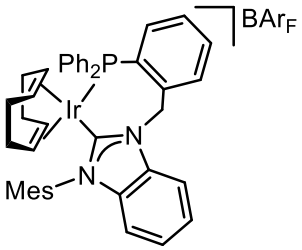

195

Melting Point: 80-82 °C.

IR (neat, cm^{-1}): 2980, 2358, 2341, 1352, 1273.

^{1}H NMR (400 MHz, CDCl$_3$): δ 7.71 (bs, 8H, BAr$_F$ ArH), 7.66-7.58 (m, 2H, ArH), 7.57-7.30 (m, 17H, BAr$_F$ ArH + ArH), 7.26-7.19 (m, 2H, ArH), 7.15 (d, $^2J_{HH}$ = 14.5 Hz, 1H, CH$_2$), 7.01 (s, 1H, ArH), 6.92 (s, 1H, ArH), 6.75 (d, J = 7.9 Hz, 1H, ArH), 5.31 (d, $^2J_{HH}$ = 14.5 Hz, 1H, CH$_2$), 5.23-5.16 (m, 1H, COD CH), 4.11-4.01 (m, 1H, COD CH), 3.96-3.89 (m, 1H, COD CH), 3.74-3.66 (m, 1H, COD CH), 2.37 (s, 3H, CH$_3$), 2.20-2.10 (m, 2H, COD CH$_2$), 2.03-1.92 (m, 2H, COD CH$_2$), 1.80 (s, 3H, ArMe), 1.68-1.58 (m, 2H, COD CH$_2$), 1.41-1.27 (m, 2H, COD CH$_2$), 1.24 (s, 3H, ArMe).

^{13}C NMR (101 MHz, CDCl$_3$): δ 180.7 (d, $^2J_{C\text{-}P}$ = 8.8 Hz), 162.0 (q, $^1J_{B\text{-}C}$ = 50.4 Hz), 140.7, 139.8 (d, $J_{C\text{-}P}$ = 15.2 Hz), 137.1, 136.7 (d, $J_{C\text{-}P}$ = 12.9 Hz), 135.8, 135.1, 134.0 (d, $J_{C\text{-}P}$ = 12.2 Hz), 133.2 (d, $J_{C\text{-}P}$ = 10.5 Hz), 132.7, 132.1 (d, $J_{C\text{-}P}$ = 9.0 Hz), 131.6, 131.4, 131.1, 130.3, 130.0, 129.7, 129.1 (d, $^2J_{C\text{-}F}$ = 30.9 Hz), 125.0 (d, $J_{C\text{-}P}$ = 7.0 Hz), 124.8 (d, $^1J_{C\text{-}F}$ = 271.0 Hz), 117.7, 112.1, 110.7, 87.7 (d, $^2J_{C\text{-}P}$ = 9.2 Hz), 83.9 (d, $^2J_{C\text{-}P}$ = 12.2 Hz), 82.8, 80.7, 52.0 (d, $^3J_{C\text{-}P}$ = 9.3 Hz), 35.4, 33.7, 28.7, 28.0, 21.1, 18.0.

^{31}P NMR (162 MHz, CDCl$_3$): δ 2.27 (s).

^{11}B NMR (128 MHz, CDCl$_3$): δ -6.89 (s).

^{19}F NMR (376 MHz, $CDCl_3$): δ -61.9 (s).

HRMS (Positive ESI): m/z calculated for $[M\text{-}COD+O]^+$ $C_{35}H_{31}N_2OP^+$: 719.1797; found 719.1801, corresponding to **193** with COD decoordinated and the phosphine oxidised to the corresponding phosphine oxide:

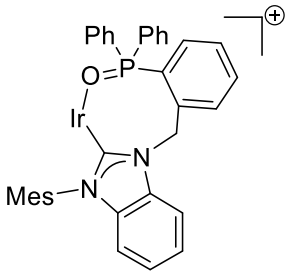

*8.4 Electronic Parameterization of NHC-P Complexes by Hydride NMR (**Scheme 3.8**)*

For each of the four benzylic NHC-P complexes (**174**, **175**, **189**, and **195**), the hydride NMR spectra of the corresponding activated iridium(III) species were recorded. Approximately 10 mg of the complex was weighed into a vial, and dissolved in an d_3-acetonitrile (0.5 mL). The solution was transferred to an NMR tube, capped with a pierceable septum. A needle, fitted to a balloon of hydrogen gas, as well as a regulatory needle was inserted into the tube. The gas was carefully bubbled through the solution for 5 minutes, at which time the hydride region of the spectrum was recorded, as well as the ^{31}P NMR spectrum. The shifts recorded, as well as the structures attributed to each signal, are shown in **Scheme 8.1** below.

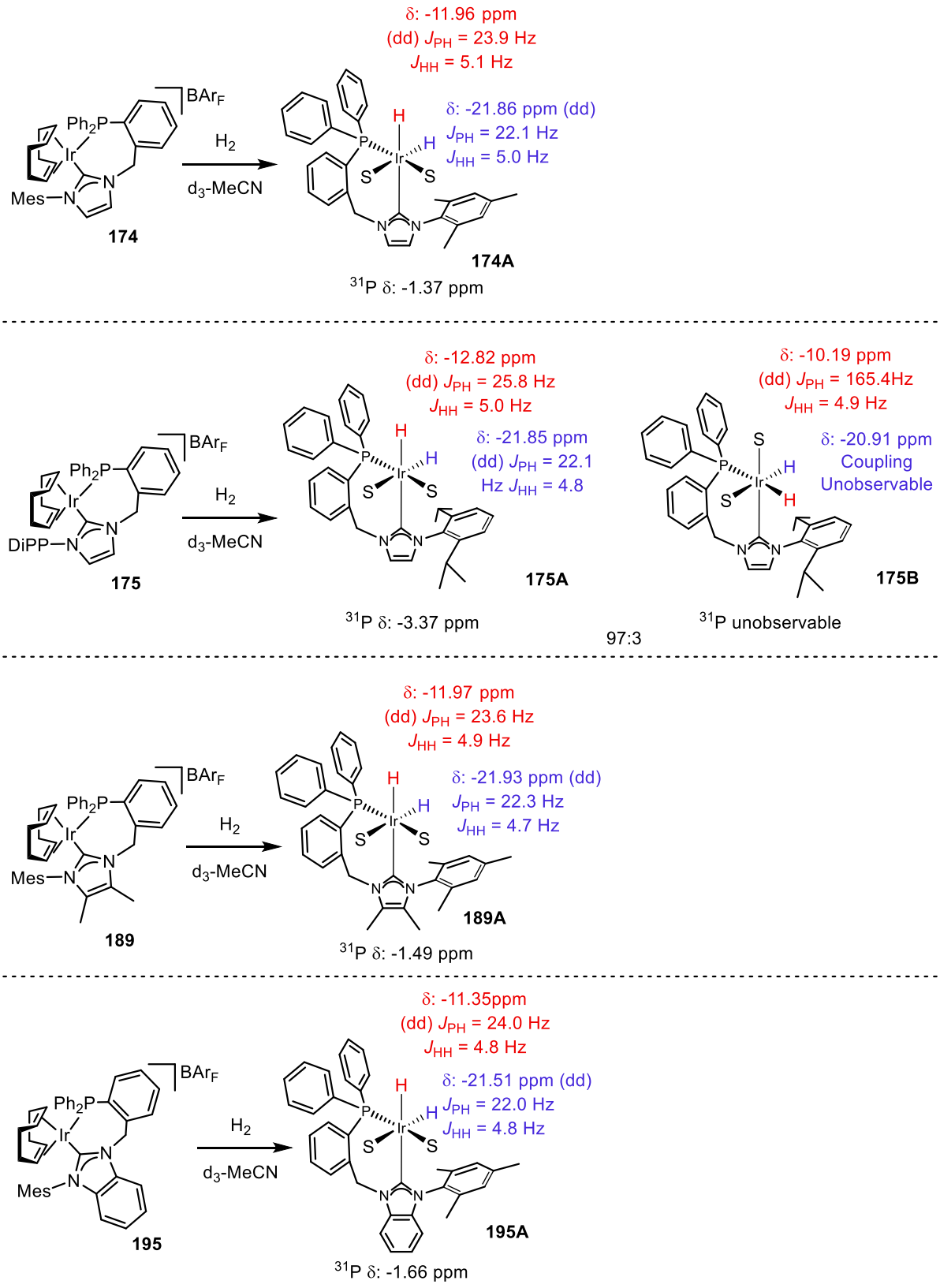
δ: -11.96 ppm
(dd) J_{PH} = 23.9 Hz
J_{HH} = 5.1 Hz
δ: -21.86 ppm (dd)
J_{PH} = 22.1 Hz
J_{HH} = 5.0 Hz
BAr$_F$
H_2
d$_3$-MeCN
Ph$_2$P
Ir
Mes
DiPP
174
174A
^{31}P δ: -1.37 ppm
δ: -12.82 ppm
(dd) J_{PH} = 25.8 Hz
J_{HH} = 5.0 Hz
δ: -21.85 ppm
(dd) J_{PH} = 22.1
Hz J_{HH} = 4.8
175
175A
^{31}P δ: -3.37 ppm
δ: -10.19 ppm
(dd) J_{PH} = 165.4Hz
J_{HH} = 4.9 Hz
δ: -20.91 ppm
Coupling
Unobservable
175B
^{31}P unobservable
97:3
δ: -11.97 ppm
(dd) J_{PH} = 23.6 Hz
J_{HH} = 4.9 Hz
δ: -21.93 ppm (dd)
J_{PH} = 22.3 Hz
J_{HH} = 4.7 Hz
189
189A
^{31}P δ: -1.49 ppm
δ: -11.35ppm
(dd) J_{PH} = 24.0 Hz
J_{HH} = 4.8 Hz
δ: -21.51 ppm (dd)
J_{PH} = 22.0 Hz
J_{HH} = 4.8 Hz
195
195A
^{31}P δ: -1.66 ppm

Scheme 8.1

*8.5 Towards Ethyl-Tethered NHC-P Catalyst systems (**Scheme 3.9**)*

*8.5.1 Towards η^4–cycloocta-1,5-diene(3-(2-(diphenylphosphanyl)ethyl)-1-mesityl imidazole-2-ylidene)iridium BAr_F **170***

3-(2-Hydroxyethyl)-1-mesitylimidazolium bromide **196**[142]

To a 100 mL round-bottom flask was added mesityl imidazole **179** (5.0 g, 26.8 mmol). The brown solid was dissolved in toluene (80 mL) and 2-bromoethanol (2.4 mL, 33.5 mmol, 1.25 eq) added. The reaction mixture was heated to reflux for 16 h, after which time the reaction mixture was cooled to 0 °C and the resulting precipitate was allowed to settle. The solvent was carefully removed by pipette and the product washed with diethyl ether, yielding 3-(2-hydroxyethyl)-1-mesitylimidazolium bromide **196** (5.45 g, 17.5 mmol, 65% yield) as an off-white solid.

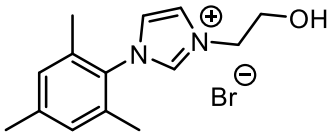

196

Melting Point: 160-162 °C (lit:[142] 164-166 °C).

IR (neat, cm^{-1}): 3301, 3063, 3032, 1600, 1567, 1463, 1453, 1050.

^{1}H NMR (400 MHz, DMSO-d_6): δ 9.39 (t, ^4J = 1.2 Hz, 1H, NCHN), 8.05 (t, J = 1.2 Hz, 1H, ImH), 7.92 (t, J = 1.2 Hz, 1H, ImH), 7.14 (s, 2H. ArH), 5.25 (bs, 1H, OH), 4.33 (t, J = 5.0 Hz, 2H, CH_2), 3.81 (t, J = 5.0 Hz, 2H, CH_2), 2.33 (s, 3H, ArMe), 2.02 (s, 6H, ArMe).

^{13}C NMR (101 MHz, DMSO-d_6): δ 141.5, 137.9, 134.5, 130.8, 130.0, 124.1, 123.0, 60.3, 52.4, 21.2, 17.8

3-(2-Bromoethyl)-1-mesitylimidazolium bromide **198**[143]

To a 100 mL round-bottom flask was added 3-(2-hydroxyethyl)-1-mesitylimidazolium bromide **196** (1.50 g, 4.82 mmol, 1.00 eq) and DCM (25 mL). The solution was cooled to 0 °C and PBr_3 (0.42 mL, 4.17 mmol, 0.87 eq) was added, dropwise. The reaction mixture was stirred at room temperature for 16 h, at which point the solution was cooled to 0 °C and quenched with a saturated aqueous solution of sodium bicarbonate. The mixture was transferred to a separating funnel and the aqueous phase extracted with three times with DCM. The combined organic phases were collected, dried, and concentrated *in vacuo* to yield 3-(2-bromoethyl)-1-mesityl imidazolium bromide **198** (1.50 g, 4.00 mmol, 83% yield) as an off-white solid.

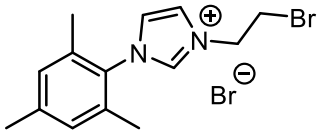

198

Melting Point: 160-162 °C (lit:[143] 164-166 °C).

IR (neat, cm^{-1}): 3116.9, 3062.9, 2959.2, 2158.3, 2029.1, 1604.7, 1546.9.

^{1}H NMR (400 MHz, $CDCl_3$): δ 10.32 (t, ^4J = 1.7 Hz, 1H, NCHN), 7.97 (t, J = 1.7 Hz, 1H, ImH), 7.17 (t, J = 1.7 Hz, 1H, ImH) 7.05 (s, 2H, ArH), 5.28 (t, J = 5.5 Hz, 2H, CH_2), 4.09 (t, J = 5.5 Hz, 2H, CH_2Br), 2.38 (s, 3H ArMe), 2.13 (s, 6H, ArMe).

^{13}C NMR (101 MHz, $CDCl_3$): δ 143.7, 136.4, 136.2, 134.9, 132.4, 129.3, 118.4, 112.4, 109.4, 21.0, 18.1.

3-(2-(Diphenylphosphanyl)ethyl)-1-mesitylimidazolium BAr_F **200**

A flame-dried 10 mL round-bottom flask was placed under an inert atmosphere *via* three vacuum/argon cycles and then charged with potassium *tert*-butoxide (0.224 g, 2.00 mmol, 1.00 eq) and DMSO (3.0 mL). To this was added diphenylphosphine (0.34 mL, 2.10 mmol, 1.05 eq)

and the reaction mixture stirred for 1 h. A separate flame-dried 10 mL round-bottom flask was placed under an inert atmosphere with three vacuum/argon cycles and then charged with 3-(2-bromoethyl)-1-mesitylimidazolium bromide **198** (0.750 g, 2.00 mmol, 1.00 eq) and DMSO (3.0 mL). The DMSO solution of potassium diphenylphosphide was then added dropwise, *via* syringe, over 15 min and then stirred for 2 h. Water (30 mL) was then added to the reaction mixture and the product extracted into DCM. The organic phase was separated, and placed under inert atmosphere with 5 vacuum/argon cycles then $NaBAr_F$ (1.95 g, 2.20 mmol, 1.10 eq) was added. The reaction mixture was allowed to stir at room temperature for 16 h, and was then concentrated *in vacuo*, and the residue loaded onto silica. The product was purified by column chromatography, eluting with 50% DCM/petroleum ether, to yield 3-(2-(diphenylphosphanyl)ethyl)-1-mesitylimidazolium BAr_F **200** (1.70 g, 1.35 mmol, 67% yield) as a tan solid.

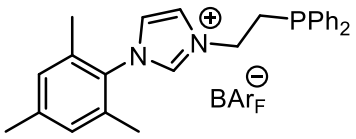

200

Melting Point: 116-118 °C.

IR (neat, cm^{-1}): 3123, 3072, 2980, 1610, 1546, 1483, 1435, 1355, 1275, 1121.

^{1}H NMR (400 MHz, $CDCl_3$): δ 8.08 (s, 1H, NCHN), 7.69 (bs, 8H, BAr_F ArH), 7.51 (s, 4H, BAr_F ArH), 7.51-7.44 (m, 10H, ArH), 7.35 (t, *J* = 1.8 Hz, 1H, ArH), 7.15 (t, *J* = 1.8 Hz, 1H, ArH), 7.04 (s, 2H, ArH), 4.29 (dt, $^2J_{H\text{-}P}$ = 11.4 Hz, *J* = 6.8 Hz, 2H, PCH_2), 2.62 (t, *J* = 6.8 Hz, 2H, CH_2), 2.36 (s, 3H, ArMe), 1.94 (s, 6H, ArMe).

^{13}C NMR (101 MHz, $CDCl_3$): δ 161.9 (q, $^1J_{B\text{-}C}$ = 50.0 Hz), 135.4, 135.0, 133.9, 132.8, 132.6, 130.6, 130.5, 130.4, 129.8, 129.6, 129.5, 129.1 (q, $^2J_{C\text{-}F}$ = 32.4 Hz), 124.7 (q, $^1J_{C\text{-}F}$ = 271.8 Hz), 117.7, 51.9, 29.0, 21.3, 17.1.

^{31}P NMR (162 MHz, $CDCl_3$): δ -25.8 (s).

^{11}B NMR (128 MHz, $CDCl_3$): δ -6.65 (s).

^{19}F NMR (376 MHz, $CDCl_3$): δ -62.4 (s).

HRMS (Positive ESI): m/z calculated for[M]+ $C_{26}H_{28}N_2P$: 399.1985; found: 399.1990.

η^4–Cycloocta-1,5-diene(3-(2-(diphenylphosphanyl)ethyl)-1-mesitylimidazole-2-ylidene)iridium BAr_F **170**

Prepared according to *General Procedure A*. Data presented as: (a) amount of $[Ir(COD)Cl]_2$, (b) amount of 3-(2-(diphenylphosphanyl)ethyl)-1-mesitylimidazolium BAr_F **200**, (c) volume of THF, (d) amount of potassium *tert*-butoxide and (e) yield.

(a) 0.161 g, 0.240 mmol, 0.50 eq, (b) 0.606 g, 0.480 mmol, 1.00 eq, (c) 4.50 mL, (d) 0.056 g, 0.500 mmol, 1.05 eq, and (e) 0.517 g, 0.331 mmol, 69% yield.

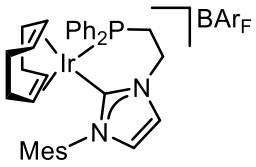

170

Melting Point: >150 °C (dec.).

IR (neat, cm^{-1}): 2958, 2928, 2081, 2029, 1611, 1437, 1410, 1354, 1273, 1117.

^{1}H NMR (400 MHz, $CDCl_3$): δ 7.73 (bs, 8H, BAr_F ArH), 7.53 (s, 4H, BAr_F ArH), 7.51-7.42 (m, 6H, ArH), 7.39-7.31 (m, 4H, ArH), 6.96 (s, 2H, Mes ArH), 6.95 (d, *J* = 2.0 Hz, 1H, ArH), 6.77 (d, *J* = 2.0 Hz, 1H, ArH), 4.62-4.50 (m, 2H, PCH_2), 4.39 (bs, 2H, Alkenyl CH), 3.59 (d

$^{2}J_{H\text{-}P}$ = 3.4 Hz, 2H, COD CH), 2.54-2.44 (m, 2H, CH_2), 2.35 (s, 3H, ArMe), 2.00-1.77 (m, 14H, ArMe + COD CH_2).

^{13}C NMR (101 MHz, $CDCl_3$): δ 161.9 (*q*, $^{1}J_{B\text{-}C$ = 50.2 Hz), 140.5, 135.1, 135.0, 134.9, 132.8 (*d*, $J_{C\text{-}P}$ = 9.9 Hz), 131.9, 131.4 (d, $J_{C\text{-}P}$ = 51.3 Hz), 129.5 (*d*, $J_{C\text{-}P}$ = 8.0 Hz), 129.3, 129.1 (*q*, $^{2}J_{C\text{-}F}$ = 31.2 Hz), 124.8 (q, $^{1}J_{C\text{-}F}$ = 273. Hz), 124.7, 122.0, 117.7, 89.6 (*d*, $^{2}J_{C\text{-}P}$ = 11.9 Hz), 78.6, 66.1, 50.7, 31.3 (*d*, $J_{C\text{-}P}$ = 36.8 Hz), 25.5 (*d*, $J_{C\text{-}P}$ = 36.5 Hz), 21.1, 18.6.

^{31}P NMR (162 MHz, $CDCl_3$): δ 10.2 (s).

^{11}B NMR (128 MHz, $CDCl_3$): δ -6.65 (s).

^{19}F NMR (376 MHz, $CDCl_3$): δ -62.4 (s).

HRMS (Positive ESI): Complete fragmentation observed, no satisfactory method of analysis has thus far been found.

8.5.2 Towards η^4–Cycloocta-1,5-diene(1-(2,6-di-iso-propylphenyl)-3-(2-(diphenylphosphanyl)ethyl)imidazole-2-ylidene)iridium BAr_F ***171***

1-(2,6-di-iso-propylphenyl)-3-(2-hydroxyethyl)imidazolium bromide **197**[144]

To a 100 mL round-bottom flask was added 1-(2,6-di-*i*so-propylphenyl)imidazole **180** (0.600 g, 2.63 mmol). The brown solid was dissolved in toluene (10.0 mL) and 2-bromoethanol (0.20 mL, 2.89 mmol, 1.25 eq) was added. The reaction mixture was heated to reflux for 16 h then cooled to 0 °C, and the resulting precipitate was allowed to settle. The solvent was carefully removed by pipette and the product washed with diethyl ether, yielding 1-(2,6-di-*iso*-propylphenyl)-3-(2-hydroxyethyl)imidazolium bromide **197** (0.773 g, 2.19 mmol, 83% yield) as an off-white solid

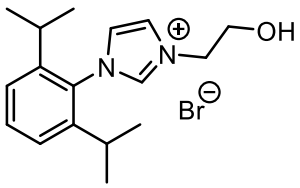

197

Melting Point:160-162 °C.

IR (neat, cm^{-1}): 3281, 3048, 2963, 2868, 1660, 1543, 1460, 1442.

^{1}H NMR (400 MHz, DMSO-d$_6$): δ 9.56 (s, 1H, NCHN), 8.13 (s, 1H, ImH), 8.08 (s, 1H, ImH), 7.62 (t, *J* = 7.7 Hz, 1H, ImH), 7.45 (s, 1H, ArH), 7.43 (s, 1H, ArH), 4.37 (t, *J* = 5.0 Hz, 2H, NCH_2), 3.81 (t, *J* = 5.0 Hz, 2H, CH_2OH), 2.28 (sep, *J* = 6.5 Hz, 2H, CH), 1.13 (d, J = 6.5 Hz, 12H, CH_3).

^{13}C NMR (101 MHz, DMSO-d$_6$): δ 145.2, 138.1, 131.3, 130.5, 124.9, 124.3, 123.4, 58.9, 52.0, 27.9, 23.8, 23.7.

3-(2-bromoethyl)-1-(2,6-di-iso-propylphenyl)imidazolium bromide **199**[144]

To a 100 mL round-bottom flask was added 1-(2,6-di-*iso*-propylphenyl)-3-(2-hydroxyethyl)imidazolium bromide **197** (0.400 g, 1.13 mmol, 1.00 eq) and DCM (5.00 mL). The solution was cooled to 0 °C and PBr_3 (0.110 mL, 1.13 mmol, 1.00 eq) was added, dropwise. The reaction mixture was stirred at room temperature for 16 h, at which point the solution was cooled to 0 °C and quenched with a saturated aqueous solution of sodium bicarbonate. The mixture was transferred to a separating funnel and the aqueous layer extracted three times with DCM. The combined organic phases were collected, dried, and concentrated *in vacuo* to yield 1-(2,6-di-*iso*-propylphenyl)-3-(2-bromoethyl)imidazolium bromide **199** (0.27 g, 0.64 mmol, 57% yield) as an off-white solid.

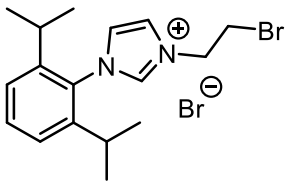

199

Melting Point: 149-152°C.

IR (neat, cm^{-1}): 3420, 3022, 2970, 1607, 1547, 1485, 1444, 1203.

^{1}H NMR (400 MHz, $CDCl_3$): δ 9.69 (s, 1H, NCHN), 8.20 (s, 1H, ImH), 8.16 (s, 1H, ImH), 7.64 (t, *J* = 7.8 Hz, 1H, ArH), 7.48 (s, 1H, ArH), 7.46 (s, 1H, ArH), 4.74 (t, *J* = 5.6 Hz, 2H, NCH_2), 4.09 (t, *J* = 5.6 Hz, 2H, CH_2Br), 2.31 (sep, *J* = 6.8 Hz, 2H, CH), 1.15 (d, *J* = 6.8 Hz, 12H, CH_3).

^{13}C NMR (101 MHz, $CDCl_3$): δ 145.1, 138.3, 131.5, 130.3, 125.4, 124.4, 123.1, 50.7, 32.2, 28.0, 23.9, 23.7.

1-(2,6-Di-iso-propylphenyl)-3-(2-(diphenylphosphanyl)ethyl)imidazolium BAr_F **201**

A flame-dried 10 mL round-bottom flask was placed under inert an atmosphere and then charged with potassium *tert*-butoxide (0.539 g, 4.80 mol, 1.00 eq) and DMSO (8.0 mL). To this was added diphenylphosphine (0.89 mL, 4.81 mmol, 1.05 eq) and the reaction stirred for 1 h. A separate flame-dried 10 mL round-bottom flask was placed under an inert atmosphere and then charged with 3-(2-bromoethyl)-1-(2,6-di-*iso*-propylphenyl)imidazolium bromide **199** (2.00 g, 4.80 mmol 1.00 eq,) and DMSO (8.0 mL). The DMSO solution of potassium diphenylphosphide was then added dropwise over 15 min and the reaction was was then stirred for 2 h. A large excess of water was then added to the reaction and the product extracted into DCM. The organic phase was separated and placed under an inert atmosphere then $NaBAr_F$ (4.20 g, 4.80 mmol, 1.00 eq) was added. The reaction mixture was allowed to stir at room

temperature for 16 h, at which point the solution was concentrated *in vacuo*, and the residue loaded onto silica. The product was purified by column chromatography, eluting with 50% DCM/petroleum ether, to yield 1-(2,6-di-*iso*-propylphenyl)-3-(2-(diphenylphosphanyl)ethyl) imidazolium BAr_F **201** (5.10 g, 3.89 mmol, 81% yield) as a tan solid.

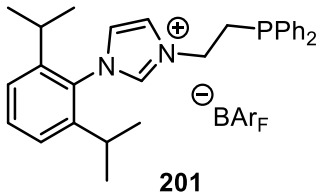

201

Melting Point: 170-172 °C.

IR (neat, cm^{-1}): 2968.4, 1352.1, 1273.0, 1159.2, 1114.8.

^{1}H NMR (400 MHz, $CDCl_3$): δ 8.16 (s, 1H, NCHN), 7.69 (bs, 8H, BAr_F ArH), 7.61 (t, J = 7.7 Hz, 1H, ArH), 7.51 (s, 4H, BAr_F ArH), 7.45-7.34 (m, 11H, ArH), 7.31 (s, 1H, ArH), 7.27-7.25 (m, 2H, ArH), 4.30 (dt, $^2J_{H\text{-}P}$ = 11.9 Hz, J = 7.0 Hz, 2H, PCH_2), 2.61 (t, J = 6.9 Hz, 2H, CH_2), 2.23 (sep, J = 6.9 Hz, 2H, CH), 1.17 (d, J = 6.8 Hz, 6H, ArMe), 1.14 (d, J = 6.8 Hz, 6H, ArMe).

^{13}C NMR (101 MHz, $CDCl_3$): δ 161.9 (q, $^1J_{C\text{-}B}$ = 50.1 Hz), 145.3, 135.2, 135.1, 134.5 (d, $J_{C\text{-}P}$ = 9.3 Hz), 133.1, 132.7 (d, $J_{C\text{-}P}$ = 19.4 Hz), 130.5, 129.5 (d, $J_{C\text{-}P}$ = 7.5 Hz), 129.1 (q, $^2J_{C\text{-}F}$ = 29.6 Hz), 126.2, 125.3, 124.8 (q, $^1J_{C\text{-}F}$ = 273.5 Hz), 122.9, 117.7, 48.6 (d, $^2J_{C\text{-}P}$ = 19.3 Hz), 29.3 (d, $^1J_{C\text{-}P}$ = 15.0 Hz), 29.0, 24.3, 24.2.

^{31}P NMR (162 MHz, CDCl3): δ -26.8 (s).

^{11}B NMR (128 MHz, $CDCl_3$): δ -6.77 (s).

^{19}F NMR (376 MHz, $CDCl_3$): δ -62.3 (s).

HRMS (Positive ESI): m/z calculated for$[M]^+$ $C_{29}H_{34}N_2P$: 441.2454; found: 441.2453.

η^4–Cycloocta-1,5-diene(1-(2,6-di-iso-propylphenyl)-3-(2-(diphenylphosphanyl)ethyl) imidazole-2-ylidene)iridium BAr_F **171**

Prepared according to *General Procedure A*. Data presented as (a) amount of $[Ir(COD)Cl]_2$, (b) amount of 1-(2,6-di-*iso*-propylphenyl)-3-(2-(diphenylphosphanyl)ethyl) imidazolium BAr_F **41**, (c) volume of THF, (d) amount of potassium *tert*-butoxide, and (e) yield.

(a) 0.300 g, 0.450 mmol, 0.50 eq, (b) 1.16 g, 0.900 mmol, 1.00 eq, (c) 10.0 mL, (d) 0.101 g, 0.900 mmol, 1.00 eq, and (e) 0.679 g, 0.423 mmol, 47% yield

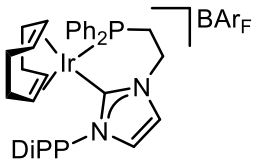

171

Melting Point: 158-160 °C.

IR (neat, cm^{-1}): 2968, 1611, 1464, 1435, 1354, 1275, 1121.

^{1}H NMR (400 MHz, $CDCl_3$): δ 7.69 (bs, 8H, BAr_F ArH), 7.52-7.42 (m, 11H, BAr_F ArH + ArH), 7.38-7.31 (m, 4H, ArH), 6.96 (d, *J* = 2.0 Hz, 1H, ArH), 6.86 (d, *J* = 2.0 Hz, 1H, ArH), 4.45-4.42 (m, 2H, PCH_2), 4.31 (bs, 2H, COD CH), 3.77-3.70 (bs, 2H, COD CH), 2.49 (sep, *J* = 6.7 Hz, 2H, CH), 2.44-2.37 (m, 2H, CH_2), 1.94-1.70 (m, 8H, COD $4CH_2$), 1.14 (d, *J* = 6.6 Hz, 6 H, CH_3), 0.85 (d, *J* = 6.6 Hz, 6H, CH_3).

^{13}C NMR (101 MHz, $CDCl_3$): δ 161.7 ($^1J_{C\text{-}B}$ = 50.0 Hz), 145.6, 135.1, 132.5, 132.4, 132.0, 131.9, 131.5, 129.6 ($J_{C\text{-}P}$ = 10.0 Hz), 129.2 ($^2J_{C\text{-}F}$ = 32.0 Hz), 126.6, 124.8 ($^1J_{C\text{-}F}$ = 273.7 Hz), 124.7, 121.6, 117.7, 87.4 ($^2J_{C\text{-}P}$ = 11.0 Hz), 80.2, 50.0, 31.4 ($^1J_{C\text{-}P}$ = 45.0 Hz), 29.2, 25.4, 22.8.

^{31}P NMR (162 MHz, $CDCl_3$): δ 8.98 (s).

^{11}B NMR (128 MHz, $CDCl_3$): δ -6.77 (s).

^{19}F NMR (376 MHz, $CDCl_3$): δ -62.4 (s).

HRMS (Positive ESI): m/z calculated for$[M]^+$ $C_{32}H_{12}BF_{24}$: 863.0660; found:863.0623.

8.6 Catalyst Screening and Reaction Optimisation of Methylphenyl Sulfone Labelling

*8.6.1 NHC-P Catalysed Labelling of Methylphenyl Sulfone – Catalyst Screen (**Table 3.5**)*

Following *General Procedure D*, substrate **108** (33.6 mg, 0.215 mmol, 1 eq) was labelled using precatalyst **170** (15.6 mg, 0.01 mmol, 5 mol%), **171** (16.0 mg, 0.01 mmol, 5 mol%), **174** (16.2 mg, 0.01, 5 mol%), **175** (16.5 mg, 0.01 mmol, 5 mol%), **189** (16.7 mg, 0.01 mmol, 5 mol%), **195** (16.7 mg, 0.01 mmol, 5 mol%) or in DCM. Deuterium incorporation data are displayed in **Table 8.1**.

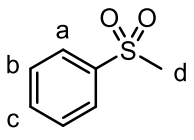

108

^{1}H NMR (400 MHz, $CDCl_3$): δ 7.97-7.90 (m, 2H, H^a), 7.68-7.62 (m, 1H, H^c), 7.60-7.53 (m, 2H, H^b), 3.03 (s, 3H, H^d). [145]

Labelling expected against signal at 7.97-7.90 ppm, measured against signal at 3.03 ppm.

Table 8.1

Entry	Catalyst	Solvent	Run 1 (%)	Run 2 (%)	Run 3 (%)	Avg (%)
1	**170**	DCM	34	37	35	35
2	**171**	DCM	16	9	10	12
3	**174**	DCM	22	19	29	23
4	**175**	DCM	44	38	46	43
5	**189**	DCM	12	15	13	13
6	**195**	DCM	37	33	39	36

*8.6.2 NHC-P Catalysed Labelling of Methylphenyl Sulfone – Solvent Screen (**Figure 3.3**)*

Following *General Procedure E*, data is summarised in **Table 8.2**.

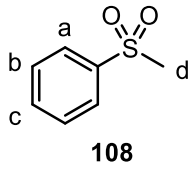

108

^{1}H NMR (400 MHz, $CDCl_3$): δ 7.97-7.90 (m, 2H, H^a), 7.68-7.62 (m, 1H, H^c), 7.60-7.53 (m, 2H, H^b), 3.03 (s, 3H, H^d). [145]

Labelling expected against signal at 7.97-7.90 ppm, measured against signal at 3.03 ppm.

Table 8.2

Entry	Solvent	Run 1 (%)	Run 2 (%)	Run 3 (%)	Avg. (%)
1	DCM	44	38	46	43
2	DCE	32	33	33	33
3	CPME	66	60	55	60
4	$^{i}Pr_2O$	75	83	79	79
5	MTBE	72	76	72	73
6	Et_2O	85	89	87	84
7	PhMe	73	76	82	77
8	PhH	43	35	34	37
9	PhCl	96	88	96	93
10	PhF	89	90	93	91
11	$PhCF_3$	68	70	69	69

*8.6.3 Solvent Behaviour Stoichiometric Experiments (PhCl vs DCM, **Figure 3.4**)*

A vial was charged with **175** (33.3 mg, 0.02 mmol, 1 eq) and **108** (3.10 mg, 0.02 mmol, 1 eq) were dissolved either in DCM or chlorobenzene (0.50 mL). The solutions were transferred to an NMR tube, equipped with a pierceable septum. D_2 gas was bubbled through each solution for 5 mins, at which point the ^{2}H NMR spectra were recorded. The results obtained by this method are reported in **Figure 3.5** in the *Section 3.2*.

*8.6.4 NHC-P Catalysed Labelling of Methylphenyl Sulfone – Catalyst Loading Study (**Table 3.7**)*

Following *General Procedure F*, data is summarised in **Table 8.3**.

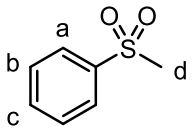

108

^{1}H NMR (400 MHz, $CDCl_3$): δ 7.97-7.90 (m, 2H, H^a), 7.68-7.62 (m, 1H, H^c), 7.60-7.53 (m, 2H, H^b), 3.03 (s, 3H, H^d). [145]

Labelling expected against signal at 7.97-7.90 ppm, measured against signal at 3.03 ppm.

Table 8.3

Entry	Amount of 175	Run 1 (%)	Run 2 (%)	Run 3 (%)	Avg (%)
1	17.0 mg, 0.01 mmol, 5 mol%	88	92	93	91
2	11.0 mg, 0.006 mmol, 3 mol%	77	78	75	77
3	3.6 mg, 0.002 mmol, 1 mol%	57	58	62	59
4	1.7 mg, 0.001 mmol, 0.5 mol%	30	37	31	33

*8.6.5 NHC-P Catalysed Labelling of Methylphenyl Sulfone – Rate Study (**Figure 3.5**)*

A flame-dried, two-neck 250 mL round-bottom flask fitted with a stopcock was placed under an inert atmosphere. The flask was charged with methylphenyl sulfone **108** (134.2 mg, 0.860 mmol, 1 eq) and complex **175** (71.6 mg, 0.043 mmol, 5 mol%). The mixture was dissolved in chlorobenzene (10.0 mL) and the flask was placed in an oil bath preheated to 25 °C. The atmosphere was exchanged *via* two vacuum/D_2 cycles and the timer started. Aliquots of 0.3 mL were withdrawn at each time point and injected into a vial containing diethyl ether (2.0 mL). Each solution was then concentrated *in vacuo* and 1.0 mL petroleum ether added. The

resulting suspensions were sonicated for 10 s and the solution separated from the solids by pipette. Each solution as concentrated *in vacuo* and the residues analysed by ^{1}H NMR spectroscopy. The incorporations were calculated as described in *General Procedure D*. The data are presented in **Table 8.4**.

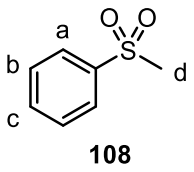

108

^{1}H NMR (400 MHz, $CDCl_3$): δ 7.97-7.90 (m, 2H, H^a), 7.68-7.62 (m, 1H, H^c), 7.60-7.53 (m, 2H, H^b), 3.03 (s, 3H, H^d). [145]

Labelling expected against signal at 7.97-7.90 ppm, measured against signal at 3.03 ppm.

Table 8.4

Time (Sec)	Incorporation (%)	Concentration SM (moles dm^{-3})
0	0.0	0.0860
32	12.5	0.0753
61	23.0	0.0662
93	33.5	0.0572
120	41.5	0.0503
150	48.5	0.0443
181	55.0	0.0387
241	63.5	0.0314
366	75.5	0.0211
616	83.5	0.0142
855	85.0	0.0129
1145	87.0	0.0112
1449	88.0	0.0103
1781	91.0	0.00774
2081	93.0	0.00602
2432	92.0	0.00688
2959	96.0	0.00344
3581	95.0	0.00430

8.7 Substrate Scope of NHC-P Catalysed Labelling of Aryl Sulfones

8.7.1 Substrate Synthesis

(2-Methoxyphenyl) methyl sulfone **108d**[146]

Prepared according to *General Procedure B*. Data presented as: (a) amount of 2-methoxythioanisole, (b) volume of DCM, (c) amount of *m*CPBA, and (d) yield.

(a) 0.34 mL, 2.00 mmol, 1.00 eq, (b) 10.0 mL, (c) 1.04 g, 6.00 mmol, 3.00 eq, and (d) 0.235 g, 0.630 mmol, 63% yield.

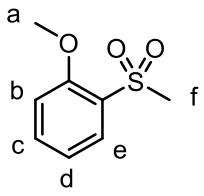

108d

Melting Point: 88-90 °C (lit:[146] 91-93 °C).

IR (neat, cm^{-1}): 3099, 2995, 1591, 1577, 1481, 1278.

^{1}H NMR (400 MHz, $CDCl_3$): δ 8.01 (dd, J = 7.9 Hz, $^{4}J_{HH}$ = 1.8 Hz, 1H, H^e), 7.62 (ddd, J = 8.5 Hz, J = 7.5 Hz, $^{4}J_{HH}$ = 1.6 Hz, 1H, H^c), 7.14 (td, J = 7.5 Hz, $^{4}J_{HH}$ = 0.9 Hz, 1H, H^d), 7.08 (d, J = 7.9 Hz, 1H, H^b), 4.03 (s, 3H, H^a), 3.24 (s, 3H, H^f).

^{13}C NMR (101 MHz, $CDCl_3$): δ 157.4, 135.7, 129.9, 128.6, 120.9, 112.5, 56.5, 43.1.

(3-Methylphenyl) methyl sulfone **108e**[147]

Prepared according to *General Procedure B*. Data presented as: (a) amount of (3-methylphenyl) methyl thioether, (b) volume of DCM, (c) amount of *m*CPBA, and (d) yield.

(a) 1.0 g, 7.20 mmol, 1.00 eq, (b) 15.0 mL, (c) 13.3 g, 21.6 mmol, 3.00 eq, and (d) 1.10 g, 6.46 mmol, 90% yield.

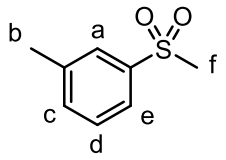

108e

IR (neat, cm^{-1}): 3018, 2926, 1598, 1477, 1411, 1311, 1294, 1222, 1139.

^{1}H NMR (400 MHz, $CDCl_3$): δ 7.78-7.71 (m, 2H, H^a, H^e), 7.50-7.42 (m, 2H, H^c, H^d), 3.05 (s, 3H, H^f), 2.46 (s, 3H, H^b).

^{13}C NMR (101 MHz, $CDCl_3$): δ140.6, 139.8, 134.6, 129.4, 127.8, 124.6, 44.6, 21.5.

(3-Methoxyphenyl) methyl sulfone **108f**[147]

Prepared according to *General Procedure C*. Data presented as: (a) amount of 3-Methoxythiophenol, (b) volume of ethanol, (c) amount of NaOH, (d) amount of methyl iodide, (e) volume of 1:1 acetone/H_2O, (f) amount of Oxone®, and (g) yield.

(a) 3.00 g, 19.3 mmol, 1.00 eq, (b) 30.0 mL, (c) 0.928 g, 23.2 mmol, 1.20 eq, (d) 1.50 mL, 23.2 mmol, 1.20 eq, (e) 30.0 mL, (f) 35.6 g, 57.9 mmol, 3.00 eq, and (g) 3.23 g, 17.4mmol, 90% yield

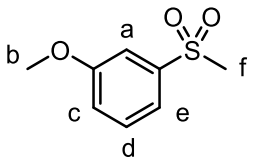

108f

Melting Point: 44-46 °C (lit:[148] 47 °C).

IR (neat, cm^{-1}): 3097, 3014, 2962, 2360, 2331, 1593, 1481, 1292.

^{1}H NMR (400 MHz, $CDCl_3$): δ 7.51 (dt, *J* = 7.9 Hz, $^{4}J_{HH}$ = 1.4 Hz, 1H, H^e), 7.46 (t, *J* = 7.9 Hz, 1H, H^d), 7.42 (t, $^{4}J_{HH}$ = 2.4 Hz, 1H, H^a), 7.15 (ddd, *J* = 7.8 Hz, $^{4}J_{HH}$ = 2.4 Hz, $^{4}J_{HH}$ = 1.0 Hz, 1H, H^c), 3.86 (s, 3H, H^b), 3.03 (s, 3H, H^f).

^{13}C NMR (101 MHz, $CDCl_3$): δ 160.3, 142.0, 130.7, 120.4, 119.7, 112.0, 56.0, 44.6.

(3-Trifluoromethylphenyl) methyl sulfone **108g**[147]

Prepared according to *General Procedure C*. Data presented as: (a) amount of 3-trifluoromethylthiophenol, (b) volume of ethanol, (c) amount of NaOH, (d) amount of methyl iodide, (e) volume of 1:1 acetone/H_2O, (f) amount of Oxone®, and (g) yield.

(a) 3.00 mL, 12.8 mmol, 1.00 eq, (b) 20.0 mL, (c) 0.615 g, 15.4 mmol, 1.20 eq, (d) 1.00 mL, 15.4 mmol, 1.20 eq, (e) 20.0 mL, (f) 23.6 g, 38.4 mmol, 3.00 eq, and, (g) 1.55 g, 6.91 mmol, 54% yield.

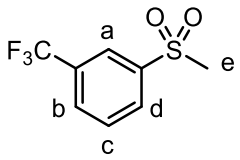

108g

Melting Point: 59-61 °C (lit:[149] 60-62 °C)

IR (neat, cm^{-1}): 3099, 3016, 2926, 2360.

^{1}H NMR (400 MHz, $CDCl_3$): δ 8.14 (s, 1H, H^a), 7.91 (d, *J* = 7.4 Hz, 1H, H^d), 7.73 (d, *J* = 7.4 Hz, 1H, H^b), 7.73 (t, *J* = 7.4 Hz, 1H, H^c), 3.08 (s, 3H, H^e).

^{13}C NMR (101 MHz, $CDCl_3$): δ 142.0, 133.3 (q, $^{2}J_{C\text{-}F}$ = 132.4 Hz), 131.0, 130.7, 130.5, 124.8, 123.3 (q, $^{1}J_{C\text{-}F}$ = 271.3 Hz), 44.6.

^{19}F NMR (376 MHz, $CDCl_3$): δ -62.9 (s).

(3-Chlorophenyl) methyl sulfone **108h**[150]

Prepared according to *General Procedure B*. Data presented as: (a) amount of 3-chlorothioanisole, (b) volume of DCM, (c) amount of *m*CPBA, and (d) yield.

(a) 2.00 g, 10.5 mmol, 1.00 eq, (b) 15.0 mL, (c) 5.44 g, 31.5 mmol, 3.00 eq, and (d) 1.12 g, 5.88 mmol, 56% yield

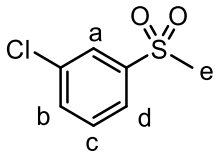

108h

Melting Point: 105-105 °C (lit:[151] 104-106 °C).

IR (neat, cm^{-1}): 3076, 3014, 2922, 2358, 2339, 1579, 1404, 1292.

^{1}H NMR (400 MHz, $CDCl_3$): δ 7.93 (t, ^4J = 1.8 Hz, 1H, H^a), 7.82 (ddd, J = 7.7 Hz, ^4J = 1.9 Hz, ^4J = 0.8 Hz, 1H, H^d), 7.62 (ddd, J = 7.7 Hz, ^4J = 2.1 Hz, ^4J = 1.0 Hz, 1H, H^b), 7.51 (t, J = 8.0 Hz, 1H, H^c), 3.05 (s, 3H, H^e).

^{13}C NMR (101 MHz, $CDCl_3$): δ 142.8, 135.9, 134.1, 131.0, 127.8, 125.7, 44.7.

(4-Methoxyphenyl) methyl sulfone **108l**[147]

Prepared according to *General Procedure B*. Data presented as: (a) amount of 4-Methoxythioanisole, (b) volume of DCM, (c) amount of *m*CPBA, and (d) yield.

(a) 1.50 g, 8.10 mmol, 1.00 eq, (b) 25.0 mL111, (c) 4.22 g, 24.4 mmol, 3.00 eq, and (d) 1.45 g, 7.78 mmol, 96% yield.

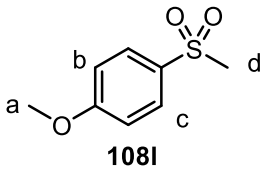

108l

Melting Point: 120-122 °C (lit:[152] 122-122°C).

IR (neat, cm^{-1}): 1591, 1314, 1291.

^{1}H NMR (400 MHz, $CDCl_3$): δ 7.86 (d, *J* = 8.7 Hz, 2H, H^c), 7.01 (d, *J* = 8.7 Hz, 2H, H^b), 3.87 (s, 3H, H^a), 3.01 (s, 3H, H^d).

^{13}C NMR (101 MHz, $CDCl_3$): δ 163.9, 132.6, 129.8, 114.7, 55.9, 45.0.

(4-Nitrophenyl) methyl sulfone **108m**[153]

Prepared according to *General Procedure C*. Data presented as: (a) amount of 4-nitrothiophenol, (b) volume of ethanol, (c) amount of NaOH, (d) amount of methyl iodide, (e) volume of 1:1 acetone/H_2O, (f) amount of Oxone®, and (g) yield.

(a) 3.00 g, 19.3 mmol, 1.00 eq, (b) 30.0 mL, (c) 0.928 g, 23.2 mmol, 1.20 eq, (d) 1.50 mL, 23.2 mmol, 1.20 eq, (e) 30.0 mL, (f) 42.8 g, 69.6 mmol, 3.00 eq, and (g) 2.52 g, 12.5 mmol, 65% yield.

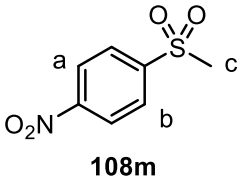

108m

Melting Point: 135-137 °C (lit:[153] 140-142 °C).

IR (neat, cm^{-1}): 3103, 3008, 1602, 1521, 1346, 1300.

^{1}H NMR (400 MHz, $CDCl_3$): δ 8.45 (d, *J* = 9.0 Hz, 2H, H^a), 8.18 (d, *J* = 9.0 Hz, 2H H^b), 3.14 (s, 3H, H^c).

^{13}C NMR (101 MHz, $CDCl_3$) δ 151.1, 146.2, 129.2, 124.9, 44.5.

(4-Trifluoromethylphenyl) methyl sulfone **108n**[147]

Prepared according to *General Procedure C*. Data presented as: (a) amount of 4-trifluoromethylthiophenol, (b) volume of ethanol, (c) amount of NaOH d) amount of methyl iodide, (e) volume of 1:1 acetone/H_2O, (f) amount of Oxone®, and (g) yield.

(a) 0.626 g, 3.51 mmol, 1.00 eq, (b) 10.0 mL, (c) 0.168 g, 4.21 mmol, 1.20 eq, (d) 0.30 mL, 4.21 mmol, 1.20 eq, (e) 10.0 mL, (f) 6.84 g, 10.5 mmol, 3.00 eq, and (g) 0.527 g, 2.35 mmol, 67% yield.

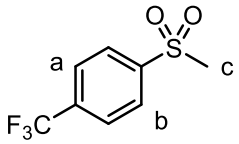

108n

Melting Point: 101-103 °C (lit:[154] 109-110°C).

IR (neat, cm^{-1}): 3003, 2920, 1402, 1311, 1292, 1141.

^{1}H NMR (400 MHz, $CDCl_3$): δ 8.13 (d, *J* = 8.5 Hz, 2H, H^a), 7.88 (d, *J* = 8.5 Hz, 2H, H^b), 3.12 (s, 3H, H^c).

^{13}C NMR (101 MHz, $CDCl_3$): δ 144.2, 135.7, 128.3 (q, J_{C-F} = 32.8 Hz),, 126.8, 123.3, (q, J_{C-F} = 274.1 Hz), 44.6.

^{19}F NMR (376 MHz, $CDCl_3$): δ -63.3 (s).

HRMS (Positive ESI): m/z calculated for $[M]^+$ $C_8H_7F_3SO_2$: 225.0197; found: 225.0196.

2,3-Dihydrobenzooxathiine 4,4-dioxide **108o**[155]

A 500 mL round-bottom flask equipped with a reflux condenser was charged with 2-hydroxythioanisole (3.00 mL, 29.8 mmol, 1.00 eq), 1,2-dibromoethane (2.60 mL, 29.8 mL, 1.00 eq) and potassium carbonate (8.25 g, 59.7 mmol, 2.00 eq). The mixture was suspended in acetone (200 mL) and the reaction mixture heated to reflux for 16 h, then cooled to room temperature and concentrated *in vacuo*. The residue was suspended in EtOAc and transferred to a separating funnel. The suspension was washed with water and the organic phase collected, dried, and concentrated *in vacuo*. The residue was loaded onto silica and purified by column chromatography, eluting with 50% Et_2O/petroleum ether. 2,3-Dihydro-1,4-benzoxathiine (2.27 g, 14.9 mmol, 50% yield) was obtained as a pale yellow oil. To a 100 mL round-bottom flask was added 2,3-dihydro-1,4-benzoxathiine (2.00 g, 13.1 mmol, 1.00 eq) and Oxone® (24.2 g, 39.3 mmol, 3.00 eq). The mixture was suspended in 1:1 acetone:water (30.0 mL) and the reaction mixture stirred at room temperature overnight. The mixture was diluted in DCM and transferred to a separating funnel. The organic phase was collected, dried (Na_2SO_4), and concentrated *in vacuo*. The residue was loaded onto silica and purified by column chromatography, eluting with Et_2O. 2,3-Dihydrobenzooxathiine 4,4-dioxide (1.50 g, 8.14 mmol, 62% yield) was obtained as a white solid.

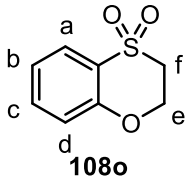

108o

Melting Point: 69-71 °C (lit:[155] 70-72°C).

IR (neat, cm^{-1}): 3003, 2953, 1597, 1573, 1471, 1440, 1386.

^{1}H NMR (400 MHz, $CDCl_3$): δ 7.83 (dd, *J* = 7.8 Hz, ^{4}J =1.8 Hz, 1H, H^a), 7.48 (ddd, *J* = 8.6 Hz, *J* = 7.0 Hz, ^{4}J = 1.6 Hz, H^b), 7.16 (ddd, *J* = 8.6 Hz, *J* = 7.0 Hz, ^{4}J = 1.6 Hz, 1H, H^c), 7.01 (dd, *J* = 7.8 Hz, ^{4}J = 1.8 Hz, 1H, H^d), 4.89-4.82 (m, 2H, H^e), 3.56-3.51 (m, 2H, H^f).

^{13}C NMR (101 MHz, $CDCl_3$): δ 153.4, 133.9, 125.7, 123.6, 121.7, 118.3, 64.6, 49.4.

HRMS (Positive ESI): m/z calculated for $[M]^+$ $C_8H_8SO_3$: 185.0272; found: 185.0270.

iso-Propyl phenyl sulfone **108q**[156]

To a 100 mL round-bottom flask was added thiophenol (1.02 mL, 10.0 mmol, 1.00 eq) and ethanol (20.0 mL). To this was added NaOH (0.480 g, 12.0 mmol, 1.20 eq) and the reaction mixture stirred at room temperature for 10 min. To this was added 2-iodopropane (1.10 mL, 11.0 mmol, 1.10 eq) and the reaction mixture stirred at room temperature for 2 h. The reaction mixture was then diluted with water and DCM, and transferred to a separating funnel. The organic phase was collected, dried, and concentrated *in vacuo*. *Iso*-Propyl phenyl sulfide (1.37 g, 9.00 mmol, 90% yield) was isolated, without further purification, as a colourless oil. To a 100 mL round-bottom flask was added *iso*-propyl phenyl sulfide (1.00 g, 6.57 mmol, 1.00 eq) and Oxone® (12.1 g, 19.7 mmol, 3.00 eq). The mixture was suspended in 1:1 acetone:water (30 mL) and stirred at room temperature overnight. The reaction mixture was then diluted with DCM and water, and then transferred to a separating funnel. The organic phase was collected, dried and concentrated *in vacuo*. The residue was loaded onto silica and purified by column chromatography, eluting with Et_2O. *iso*-Propyl phenyl sulfone **108q** (1.04 g, 5.65 mmol, 86% yield) was obtained as a colourless oil.

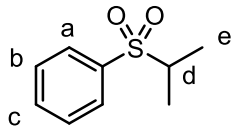

108q

IR (neat, cm^{-1}): 3059, 2978, 1444, 1301, 1261.

^{1}H NMR (400 MHz, $CDCl_3$): δ 7.93-7.89 (m, 2H, H^a), 7.71-7.65 (m, 1H, H^c), 7.62-7.56 (m, 2H, H^b), 3.12 (sep, *J* = 7.0 Hz, 1H, H^d) 1.32 (d, *J* = 7.0 Hz, 6H, H^e).

^{13}C NMR (101 MHz, $CDCl_3$): δ 137.1, 133.8, 129.2, 129.1, 55.7, 15.8.

tert-Butyl phenyl sulfone **108r**[156]

To a 250 mL round-bottom flask was added thiophenol (5.70 mL, 55.9 mmol, 1.00 eq), acetic acid (70.0 mL) and *tert*-butanol (6.40 mL, 67.4 mmol, 1.2 eq). The reaction mixture was cooled to 0 °C before acetic anhydride (6.00 mL, 63.5 mmol, 1.10 eq) and perchloric acid (70% wt. in water, 4.60 mL, 51.3 mmol, 0.90 eq) were added. The reaction mixture was stirred at room temperature for 4 h, at which point the reaction mixture was diluted with water, transferred to a separating funnel and extracted into Et_2O. The organic phase was separated then washed with saturated aqueous sodium bicarbonate solution, dried and concentrated *in vacuo*. The residue was then loaded onto silica and purified by column chromatography, eluting with petroleum ether. *tert*-Butyl phenyl sulfide (9.17 g, 55.1 mmol, 99% yield) was obtained as a colourless oil. To a 100 mL round-bottom flask was added *tert*-butyl phenyl sulfide (2.00 g, 12.0 mmol, 1.00 eq) and Oxone® (22.2 g, 24.0 mmol, 3.00 eq). The mixture was suspended in 1:1 acetone:water (15.0 mL) and stirred at room temperature overnight. The reaction mixture was diluted with water and DCM, then transferred to a separating funnel. The organic phase was collected, dried, and concentrated *in vacuo*. The residue was loaded onto silica and purified by

column chromatography, eluting with Et_2O. *tert*-Butyl phenyl sulfone (1.95 g, 9.83 mmol, 82% yield) was obtained as a white solid.

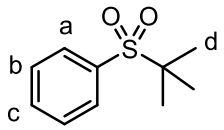

108r

Melting Point: 97-98 °C (lit[156]: 93-95 °C).

IR (neat, cm^{-1}): 3059, 2980, 1488, 1278, 1130.

^{1}H NMR (400 MHz, $CDCl_3$): δ 7.89-7.84 (m, 2H, H^a), 7.66-7.60 (m, 1H, H^c), 7.57-7.50 (m, 2H, H^b), 1.33 (s, 9H, H^d).

^{13}C NMR (101 MHz, $CDCl_3$): δ 135.6, 133.7, 130.6, 128.9, 60.0, 23.8.

HRMS (Positive ESI): m/z calculated for $[M]^+$ $C_{10}H_{14}SO_2$: 199.0793; found: 199.0791.

Benzyl methyl sulfone **108s**[157]

To a 100 mL round-bottom flask was added benzyl mercaptan (5.00 mL, 42.6 mmol, 1.00 eq) and ethanol (40.0 mL). To this was added NaOH (2.00 g, 51.1 mmol, 1.20 eq) and the reaction mixture stirred at room temperature for 20 min. To this was added methyl iodide (3.20 mL, 51.1 mmol, 1.20 eq) and the reaction mixture stirred at room temperature for 2 h. The reaction mixture was diluted with water and DCM, and transferred to a separating funnel. The organic phase was then separated, dried, and concentrated *in vacuo*. The residue was transferred to a 100 mL round-bottom flask, and dissolved in a 1:1 acetone:water mixture (20.0 mL). Oxone® (17.8 g, 29.0 mmol, 3.00 eq) was added and the reaction mixture stirred at room temperature overnight. The mixture was diluted with water and DCM and transferred to a separating funnel. The organic phase was separated, dried, and concentrated *in vacuo*. The residue was loaded

onto silica and purified by column chromatography, eluting with Et_2O. Benzyl methyl sulfone **4s** (1.90 g, 11.2 mmol, 73% yield) was obtained as a white solid.

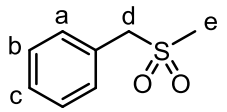

108s

Melting Point: 123-126 °C (lit:[158]124-126 °C).

IR (neat, cm^{-1}): 3047, 2978, 1458, 1300.

^{1}H NMR (400 MHz, $CDCl_3$) δ 7.44 (s, 5H, H^a, H^b, H^c), 4.27 (s, 2H, H^d), 2.77 (s, 3H, H^e).

^{13}C NMR (101 MHz, $CDCl_3$) δ 130.0, 128.7, 127.0, 60.9, 38.5.

2-(4-(Methylsulfonyl)phenyl)-1,3-dioxane **108t**[159]

To a 100 mL round-bottom flask, equipped with a Dean-Stark apparatus, was added 4-(methylsulfonyl)benzaldehyde (3.00 g, 16.2 mmol, 1.00 eq), 1,3-propanediol (3.51 mL, 48.9 mmol, .3.00 eq) and *p*-toluenesulfonic acid (0.279 g, 1.62 mmol, 0.10 eq). The mixture was heated to reflux for 48 h, at which point the reaction was cooled and diluted with a saturated solution of aqueous sodium bicarbonate (200 mL). The suspension was washed three times with EtOAc. The organic layers were combined, dried over sodium sulfate, filtered, and concentrated *in vacuo*. The resulting off-white solid was purified by boiling in diethyl ether, allowing to cool, then filter. The filter cake was washed with ice cold diethyl ether, and dried to afford 2-(4-(methylsulfonyl)phenyl)-1,3-dioxane (3.02 g, 12.5 mmol 77% yield) as a white solid.

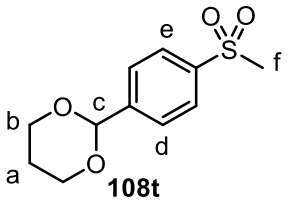

108t

Melting Point: In Progress

IR (neat, cm^{-1}): In Progress

^{1}H NMR (400 MHz, CDCl$_3$) δ 7.93 (d, *J* = 8.4 Hz, 2H, H^{e}), 7.68 (d, *J* = 8.4 Hz, 2H, H^{d}), 5.55 (s, 1H, H^{c}), 4.31-4.24 (m, 2H, H^{b}), 4.04-3.95 (m, 2H, H^{b}), 3.00 (s, 3H, H^{f}), 2.28-2.14 (m, 1H, H^{a}), 1.50-1.43 (m, 1H, H^{a}).

^{13}C NMR (101 MHz, CDCl$_3$) δ 144.5, 140.8, 127.5, 127.3, 100.2, 67.6, 44.6, 25.7.

*8.7.2 Aryl Sulfone Labelling (**Scheme 3.11**)*

All reactions were run as described in *General Procedure G*. Data are reported as: (a) amount of substrate, and (b) Incorporation.

(2-Fluorophenyl) methyl sulfone **108b**[160]

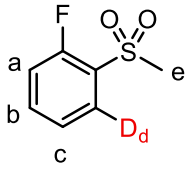

d-108b

^{1}H NMR (400 MHz, CDCl$_3$): δ 8.01 (ddd, *J* = 7.6 Hz, $^{4}J_{H-F}$ = 7.6 Hz, $^{4}J_{HH}$ = 1.4 Hz, 1H, H^{d}), 7.72-7.65 (m, 1H, H^{a}), 7.38 (ddd, *J* = 7.6 Hz, $^{4}J_{H-F}$ = 7.6 Hz, ^{4}J = 1.4 Hz, 1H, H^{c}), 7.32-7.26 (m, 1H, H^{b}), 3.26 (s, 3H, H^{e})

Incorporation expected at δ 8.01 ppm. Determined against integral at δ 3.26 ppm.

Run 1

(a) 37.5 mg, (b) 84%

Run 2

(a) 37.5 mg, (b) 82%

Run 3

(a) 37.5 mg, (b) 82%

Average Incorporation = 83%

(2-Chlorophenyl) methyl sulfone **108c**[145]

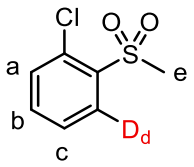

d-108c

^{1}H NMR (400 MHz, $CDCl_3$): δ 8.18 (d, *J* = 8.0 Hz, 1H, H^a), 7.63-7.57 (m, 2H, H^d, H^b), 7.53-7.48 (m, 1H, H^c), 3.30 (s, 3H, H^e).

Incorporation expected from δ 7.63-7.57 ppm. Determined against integral at δ 3.30 ppm.

Run 1

(a) 41.0 mg, (b) 75%

Run 2

(a) 41.0 mg, (b) 73%

Run 3

(a) 41.0 mg, (b) 70%

Average Incorporation = 73%

(2-Methoxyphenyl) methyl sulfone **108d**

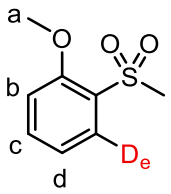

d-108d

^{1}H NMR (400 MHz, $CDCl_3$): δ 8.01 (dd, *J* = 7.9 Hz, $^4J_{HH}$ = 1.8 Hz, 1H, H^e), 7.62 (ddd, *J* = 8.5 Hz, *J* = 7.5 Hz, $^4J_{HH}$ = 1.6 Hz, 1H, H^c), 7.14 (td, *J* = 7.5 Hz, $^4J_{HH}$ = 0.9 Hz, 1H, H^d), 7.08 (d, *J* = 7.9 Hz, 1H, H^b), 4.03 (s, 3H, H^a), 3.24 (s, 3H, H^f).

Incorporation expected at δ 8.01 ppm. Determined against integral at δ 4.03 ppm.

Run 1

(a) 40.0 mg, (b) 91%

Run 2

(a) 40.0 mg, (b) 93%

Run 3

(a) 40.0 mg, (b) 93%

Average Incorporation = 92%

(3-Methylphenyl) methyl sulfone **108e**

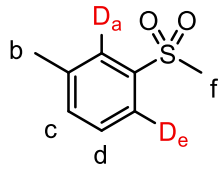

d-108e

^{1}H NMR (400 MHz, $CDCl_3$): δ 7.78-7.71 (m, 2H, H^a, H^e), 7.50-7.42 (m, 2H, H^c, H^d), 3.05 (s, 3H, H^f), 2.46 (s, 3H, H^b).

Incorporation expected at δ 7.78-7.71 ppm. Determined against integral at δ 2.46 ppm. Positions a and e overlap in a range of NMR solvents.

Run 1

(a) 36.0 mg (b) 77%, averaged across both positions.

Run 2

(a) 36.0 mg (b) 82%, averaged across both positions.

Run 3

(a) 36.0 mg (b) 81%, averaged across both positions.

Average incorporation = 80%, across both positions.

(3-Methoxyphenyl) methyl sulfone **108f**

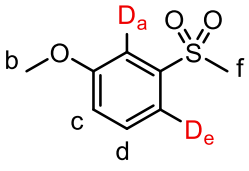

d-108f

^{1}H NMR (400 MHz, $CDCl_3$): δ 7.51 (dt, *J* = 7.9 Hz, $^4J_{HH}$ = 1.4 Hz, 1H, H^e), 7.46 (t, *J* = 7.9 Hz, 1H, H^d), 7.42 (t, $^4J_{HH}$ = 2.4 Hz, 1H, H^a), 7.15 (ddd, *J* = 7.8 Hz, $^4J_{HH}$ = 2.4 Hz, $^4J_{HH}$ = 1.0 Hz, 1H, H^c), 3.86 (s, 3H, H^b), 3.03 (s, 3H, H^f).

Incorporation expected at δ 7.51 ppm and δ 7.42 ppm. Determined against integral at δ 3.03 ppm.

Run 1

(a) 40.0 mg, (b) D_a = 92%, D_e = 89%

Run 2

(a) 40.0 mg, (b) D_a = 95%, D_e = 90%

Run 3

(a) 40.0 mg, (b) D_a = 92%, D_e = 90%

Average Incorporation = D_a = 93%, De = 90%.

(3-Trifluoromethylphenyl) methyl sulfone **108g**

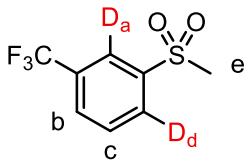

d-108g

^{1}H NMR (400 MHz, $CDCl_3$): δ 8.14 (s, 1H, H^a), 7.91 (d, *J* = 7.4 Hz, 1H, H^d), 7.73 (d, *J* = 7.4 Hz, 1H, H^b), 7.73 (t, *J* = 7.4 Hz, 1H, H^c), 3.08 (s, 3H, H^e).

Incorporation expected at δ 8.14 ppm and δ 7.91 ppm. Determined against integral at δ 3.08 ppm.

Run 1

(a) 48.2 mg, (b) D_a = 3%, D_d =93%

Run 2

(a) 48.2 mg, (b) D_a =4%, D_d =96%

Run 3

(a) 48.2 mg, (b) D_a =4%, D_d =93%

Average Incorporation = D_a =4%, D_d = 94%.

(3-Chlorophenyl) methyl sulfone **108h**

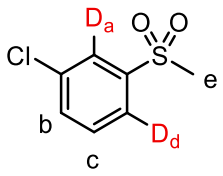

d-108h

^{1}H NMR (400 MHz, $CDCl_3$): δ 7.93 (t, ^4J = 1.8 Hz, 1H, H^a), 7.82 (ddd, J = 7.7 Hz, ^4J = 1.9 Hz, ^4J = 0.8 Hz, 1H, H^d), 7.62 (ddd, J = 7.7 Hz, ^4J = 2.1 Hz, ^4J = 1.0 Hz, 1H, H^b), 7.51 (t, J = 8.0 Hz, 1H, H^c), 3.05 (s, 3H, H^e).

Incorporation expected at δ 7.93 ppm and δ 7.82 ppm. Determined against integral at δ 3.05 ppm.

Run 1

(a) 41.0 mg, (b) D_a = 86%, D_d = 93%

Run 2

(a) 41.0 mg, (b) D_a = 86%, D_d = 92%

Run 3

(a) 41.0 mg, (b) D_a = 84%, D_d = 92%

Average Incorporation = D_a = 85%, D_d = 92%.

(4-Methylphenyl) methyl sulfone **108i**[145]

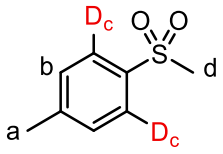

d-108i

^{1}H NMR (400 MHz, $CDCl_3$): δ 7.85 (d, *J* = 8.0 Hz, 2H, H^c), 7.39 (d, *J* = 8.0 Hz, 2H, H^b), 3.06 (s, 3H, H^d), 2.48 (s, 3H, H^a).

Incorporation expected at δ 7.85. Determined against integral at δ 3.06 ppm.

Run 1

(a) 36.0 mg, (b) 86%

Run 2

(a) 36.0 mg, (b) 88%

Run 3

(a) 36.0 mg, (b) 87%

Average Incorporation = 87%

(4-Fluorophenyl) methyl sulfone **108j**[161]

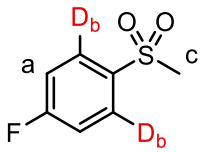

d-108j

^{1}H NMR (400 MHz, $CDCl_3$): δ 8.03-7.97 (m, 2H, H^b), 7.31-7.25 (m, 2H, H^a), 3.08 (s, 3H, H^c).

Incorporation expected at δ 8.03-7.97 ppm. Determined against integral at δ 3.08 ppm.

Run 1

(a) 37.5 mg, (b) 88%

Run 2

(a) 37.5 mg, (b) 90%

Run 3

(a) 37.5 mg, (b) 90%

Average Incorporation = 89%

(4-Chlorophenyl) methyl sulfone **108k**[145]

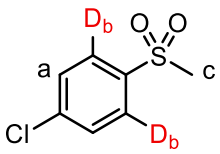

d-108k

^{1}H NMR (400 MHz, $CDCl_3$): δ 7.92 (d, *J* = 8.5 Hz, 2H, H^b), 7.58 (d, *J* = 8.5 Hz, 2H, H^a), 3.08 (s, 3H, H^c).

Incorporation expected at δ 7.92 ppm. Determined against integral at δ 3.08 ppm.

Run 1

(a) 41.0 mg, (b) 91%

Run 2

(a) 41.0 mg, (b) 88%

Run 3

(a) 41.0 mg, (b) 87%

Average Incorporation = 89%

(4-Methoxyphenyl) methyl sulfone **108l**

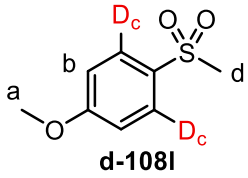

d-108l

^{1}H NMR (400 MHz, $CDCl_3$): δ 7.86 (d, *J* = 8.7 Hz, 2H, H^c), 7.01 (d, *J* = 8.7 Hz, 2H, H^b), 3.87 (s, 3H, H^a), 3.01 (s, 3H, H^d).

Incorporation expected at δ 7.86 ppm. Determined against integral at δ 3.01 ppm.

Run 1

(a) 40.0 mg, (b) 91%

Run 2

(a) 40.0 mg, (b) 82%

Run 3

(a) 40.0 mg, (b) 92%

Average Incorporation = 88%

(4-Nitrophenyl) methyl sulfone **108m**

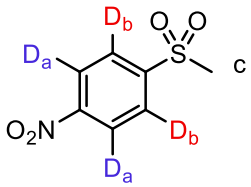

d-108m

^{1}H NMR (400 MHz, $CDCl_3$): δ 8.45 (d, *J* = 9.0 Hz, 2H, H^a), 8.18 (d, *J* = 9.0 Hz, 2H H^b), 3.14 (s, 3H, H^c).

Incorporation expected at δ 8.18 ppm for sulfone directed labelling (D_b). Determined against integral at δ 3.14 ppm.

Incorporation expected at δ 8.45 ppm for NO_2 directed labelling (D_a). Determined against integral at δ 3.14 ppm.

Run 1

(a) 43.3 mg, (b) D_a = 63%, D_b = 42%

Run 2

(a) 43.3 mg, (b) D_a = 73%, D_b = 50%

Run 3

(a) 43.3 mg, (b) D_a = 74%, D_b = 51%

Average Incorporation = D_a = 71%, D_b = 48%.

(4-Trifluoromethylphenyl) methyl sulfone **108n**

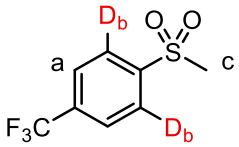

d-108n

^{1}H NMR (400 MHz, $CDCl_3$): δ 8.13 (d, *J* = 8.5 Hz, 2H, H^a), 7.88 (d, *J* = 8.5 Hz, 2H, H^b), 3.12 (s, 3H, H^c).

Incorporation expected at δ 7.88 ppm. Determined against integral at δ 3.12 ppm.

Run 1

(a) 48.2 mg, (b) 82%

Run 2

(a) 48.2 mg, (b) 82%

Run 3

(a) 48.2 mg, (b) 81%

Average Incorporation = 82%

2,3-Dihydrobenzooxathiine 4,4-dioxide **108o**

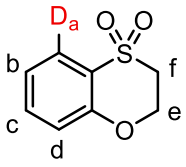

108o

^{1}H NMR (400 MHz, $CDCl_3$) δ 7.83 (dd, *J* = 7.8 Hz, ^4J =1.8 Hz, 1H, H^a), 7.48 (ddd, *J* = 8.6 Hz, *J* = 7.0 Hz, ^4J = 1.6 Hz, H^b), 7.16 (ddd, *J* = 8.6 Hz, *J* = 7.0 Hz, ^4J = 1.6 Hz, 1H, H^c), 7.01 (dd, *J* = 7.8 Hz, ^4J = 1.8 Hz, 1H, H^d), 4.89-4.82 (m, 2H, H^e), 3.56-3.51 (m, 2H, H^f).

Incorporation expected at 7.83 ppm. Determined against integral at δ 4.89-4.82 ppm.

Run 1

(a) 39.6 mg, (b) 91%

Run 2

(a) 39.6 mg, (b) 92%

Run 3

(a) 39.6 mg, (b) 91%

Average Incorporation = 91%

Phenyl sulfone **108p**[145]

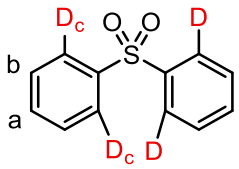

d-108p

^{1}H NMR (400 MHz, $CDCl_3$): δ 7.98 (d, *J* = 8.7 Hz, 4H, H^c), 7.62-7.57 (m, 2H, H^a), 7.56-7.50 (m, 4H, H^b).

Incorporation expected at δ 7.98 ppm. Determined against integral at δ 7.62-7.57 ppm.

Run 1

(a) 46.9 mg, (b) 55%

Run 2

(a) 46.9 mg, (b) 57%

Run 3

(a) 46.9 mg, (b) 60%

Average Incorporation = 57%

iso-Propyl phenyl sulfone **108q**

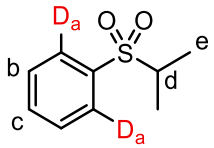

d-108q

^{1}H NMR (400 MHz, $CDCl_3$): δ 7.93-7.89 (m, 2H, H^a), 7.71-7.65 (m, 1H, H^c), 7.62-7.56 (m, 2H, H^b), 3.12 (sep, *J* = 7.0 Hz, 1H, H^d) 1.32 (d, *J* = 7.0 Hz, 6H, H^e).

Incorporation expected at δ 7.93-7.89 ppm. Determined against integral at δ 1.32 ppm.

Run 1

(a) 39.6 mg, (b) 70%

Run 2

(a) 39.6 mg, (b) 64%

Run 3

(a) 39.6 mg, (b) 65%

Average Incorporation = 66%

tert-Butyl phenyl sulfone **108r**

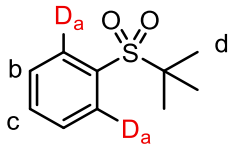

d-108r

^{1}H NMR (400 MHz, $CDCl_3$): δ 7.89-7.84 (m, 2H, H^a), 7.66-7.60 (m, 1H, H^c), 7.57-7.50 (m, 2H, H^b), 1.33 (s, 9H, H^d).

Incorporation expected at δ 7.89-7.84 ppm. Determined against integral at δ 1.33 ppm.

Run 1

(a) 42.6 mg, (b) 76%

Run 2

(a) 42.6 mg, (b) 83%

Run 3

(a) 42.6 mg, (b) 82%

Average Incorporation = 80%

Benzyl methyl sulfone **108s**

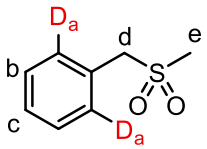

d-108s

^{1}H NMR (400 MHz, $CDCl_3$): δ 7.44 (s, 5H, H^a, H^b, H^c), 4.27 (s, 2H, H^d), 2.77 (s, 3H, H^e).

^{13}C NMR (101 MHz, $CDCl_3$) δ 130.0, 128.7, 127.0, 60.9, 38.5

Incorporation expected at δ 7.44 ppm. Determined against integral at δ 2.77 ppm.

Run 1

(a) 36.6 mg, (b) 22%

Run 2

(a) 36.6 mg, (b) 24%

Run 3

(a) 36.6 mg, (b) 23%

Average Incorporation = 23%

2-(4-(Methylsulfonyl)phenyl)-1,3-dioxane **108t**

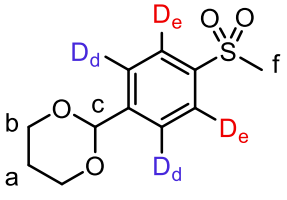

d-108t

^{1}H NMR (400 MHz, $CDCl_3$) δ 7.93 (d, *J* = 8.4 Hz, 2H, H^e), 7.68 (d, *J* = 8.4 Hz, 2H, H^d), 5.55 (s, 1H, H^c), 4.31-4.24 (m, 2H, H^b), 4.04-3.95 (m, 2H, H^b), 3.00 (s, 3H, H^f), 2.28-2.14 (m, 1H, H^a), 1.50-1.43 (m, 1H, H^a).

Incorporation expected at δ 7.93 ppm for sulfone directed labelling (D_e). Determined against integral at δ 3.00 ppm.

Incorporation expected at δ 7.68 ppm for acetal directed labelling (D_d). Determined against integral at δ 3.00 ppm.

Run 1

(a) 52.1 mg, (b) D_d = 27% D_e = 95%

Run 2

(a) 52.1 mg, (b) D_d = 24% D_e = 91%

Average Incorporation = D_d = 26%, D_e = 93%

8.8 Reduced Pressure Deuterium Labelling Studies

*Initial Investigation (**Table 3.8**)*

Reduced pressure deuteration studies were performed using an RC Tritec manifold, connected directly to a vacuum pump and D_2 cylinder. Methylphenyl sulfone **108** (1.000 mg, 6.40 μmol, 1 eq) and complex **175** were weighed, and transferred into a 5 mL flask as a solution in PhCl (2 × 0.3 mL). The flask was attached to the manifold and cooled to -78 °C. The atmosphere was evacuated, and the volume immediately above the flask isolated from the rest of the manifold. The reaction mixture was allowed to heat to room temperature, degassing the solution. This process was repeated twice. Upon evacuating the flask on the third time, D_2 gas

was added, and adjusted to the reported pressure. The reaction mixture was then allowed to stir at room temperature for 1 h. At this time, an aliquot was taken, and the deuterium incorporation analyzed by ^{1}H NMR spectroscopy. The incorporations were calculated as described in *General Procedure D*. Results are summarised in **Table 8.5**.

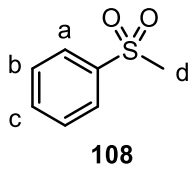

108

^{1}H NMR (400 MHz, $CDCl_3$): δ 7.97-7.90 (m, 2H, H^a), 7.68-7.62 (m, 1H, H^c), 7.60-7.53 (m, 2H, H^b), 3.03 (s, 3H, H^d). [145]

Labelling expected against signal at δ 7.97-7.90 ppm, measured against signal at δ 3.03 ppm.

Table 8.5

Entry	Loading	Pressure (mbar)	Incorporation (%)
1	0.533 mg, 0.32 μmol, 5.0 mol%	203	40
2	0.533 mg, 0.32 μmol, 5.0 mol%	208	45
3	0.533 mg, 0.32 μmol, 5.0 mol%	400	80
4	0.533 mg, 0.32 μmol, 5.0 mol%	408	78
5	0.800 mg, 0.48 μmol, 7.5 mol%	405	90
6	0.800 mg, 0.48 μmol, 7.5 mol%	405	92

*Effect of Varying Pressure at Constant Catalyst Loading (**Figure 3.6**)*

Reduced pressure deuteration studies were performed using an RC Tritec manifold, connected directly to a vacuum pump and D_2 cylinder. Methylphenyl sulfone **108** (1.000 mg, 6.40 μmol, 1 eq) and complex **175** (0.800 mg, 0.48 μmol, 7.5 mol%) were weighed, and transferred into a

5 mL flask as a solution in PhCl (2 × 0.3 mL). The flask was attached to the manifold and cooled to -78 °C. The atmosphere was evacuated, and the volume immediately above the flask isolated from the rest of the manifold. The reaction mixture was allowed to heat to room temperature, degassing the solution. This process was repeated twice. Upon evacuating the flask on the third time, D_2 gas was added, and adjusted to the correct pressure. The reaction mixture was then allowed to stir at room temperature for 1 h. At this time, an aliquot was taken, and the deuterium incorporation analyzed by ^{1}H NMR spectroscopy. The incorporations were calculated as described in *General Procedure D*. Results are summarised in **Table 8.6**.

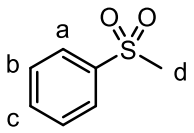

108

^{1}H NMR (400 MHz, $CDCl_3$): δ 7.97-7.90 (m, 2H, H^a), 7.68-7.62 (m, 1H, H^c), 7.60-7.53 (m, 2H, H^b), 3.03 (s, 3H, H^d). [145]

Labelling expected against signal at δ 7.97-7.90 ppm, measured against signal at δ 3.03 ppm.

Table 8.6

Entry	Pressure (mbar)	%D
1	99	7
2	99	11
3	144	25
4	137	26
5	200	40
6	208	45
7	300	51
8	300	57
9	400	80
10	407	78
11	622	91
12	622	90

*Effect of Catalyst Loading at Fixed Pressure (**Table 3.9**)*

Reduced pressure deuteration studies were performed using an RC Tritec manifold, connected directly to a vacuum pump and D_2 cylinder. Methylphenyl sulfone **108** (1.000 mg, 6.40 μmol, 1 eq) and complex **175** were weighed, and transferred into a 5 mL flask as a solution in PhCl (2 × 0.3 mL). The flask was attached to the manifold and cooled with liquid nitrogen. The atmosphere was evacuated, and the volume immediately above the flask isolated from the rest of the manifold. The reaction mixture was allowed to heat to room temperature, degassing the solution. This process was twice repeated. Upon evacuating the flask on the third time, D_2 gas was added, and adjusted to ~200 mbar. The reaction was allowed to stir at room temperature for 1 h. At this time, an aliquot was taken, and the deuterium content analysed by ^{1}H NMR

spectroscopy. The incorporations were calculated as described in *General Procedure D*. Results are summarised in **Table 8.7**.

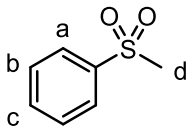

108

^{1}H NMR (400 MHz, $CDCl_3$): δ 7.97-7.90 (m, 2H, H^a), 7.68-7.62 (m, 1H, H^c), 7.60-7.53 (m, 2H, H^b), 3.03 (s, 3H, H^d). [145]

Labelling expected against signal at δ 7.97-7.90 ppm, measured against signal at δ 3.03 ppm.

Table 8.7

Entry	Pressure	Loading	%D
1	200	0.533 mg, 0.32 μmol, 5.0 mol%	40
2	200	0.533 mg, 0.32 μmol, 5.0 mol%	45
3	207	0.800 mg, 0.48 μmol, 7.5 mol%	86
4	207	0.800 mg, 0.48 μmol, 7.5 mol%	87
5	213	1.07 mg, 0.64 μmol, 10 mol%	92
6	213	1.07 mg, 0.64 μmol, 10 mol%	88

8.9 Aryl Sulfone Labelling Studies with Tritium

*Tritiation of Methphenyl Sulfone **108** (**Scheme 3.12**)*

The tritiation reaction was performed using an RC Tritec manifold. Methylphenyl sulfone **108** (1.000 mg, 6.40 μmol, 1 eq) and complex **175** (0.800 mg, 0.48 μmol, 7.5 mol%) were weighed, and transferred into a 5 mL flask as a solution in PhCl (2 × 0.3 mL). The flask was attached to the manifold and cooled with liquid nitrogen. The atmosphere was evacuated, and the volume

immediately above the flask isolated from the rest of the manifold. The reaction mixture was allowed to heat to room temperature, degassing the solution. This process was twice repeated. Upon evacuating the flask on the third time, 405 mbar of tritium gas was introduced. The reaction mixture was allowed to stir at room temperature for 1 h. The reaction mixture was again cooled with liquid nitrogen, and the remaining tritium gas was recovered onto a secondary uranium bed. Methanol (1 mL) was added to the reaction, and then removed *in vacuo*. This process was repeated three times. The reaction mixture was allowed to warm to room temperature and the chlorobenzene removed *in vacuo*. The residue was purified by HPLC, and the pure fractions combined to give the tritiated product **t-108**, which was stored as a solution in ethanol, and analysed by ^{1}H and ^{3}H NMR spectroscopy and GCMS. The specific activity of the product was found to be 51.3 Ci/mmol by GCMS.

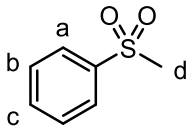

108

^{1}H NMR (500 MHz, MeOD): δ 7.77-7.73 (m, 2H, H^{a}), 7.69-7.64 (m, 1H, H^{c}), 7.63-7.48 (m, 2H, ArH) 3.15 (s, 3H, H^{d}).

^{3}H NMR (500 MHz, MeOD): δ 8.03 (d, $^{3}J_{T\text{-}H}$ = 8.1 Hz).

^{3}H{^{1}H} NMR (500 MHz, MeOD): δ 8.03.

*Synthesis of a Tritium Labelled GPR119 Agonist **t-205** (**Scheme 3.13**)*

The reaction was performed using an RC Tritec manifold. Sulfone **108t** (1.000 mg, 4.01 μmol, 1 eq) and complex **175** (0.502 mg, 0.30 μmol, 7.5 mol%) were weighed, and transferred into a 5 mL flask as a solution in PhCl (2 × 0.3 mL). The flask was attached to the manifold and

cooled with liquid nitrogen. The atmosphere was evacuated, and the volume immediately above the flask isolated from the rest of the manifold. The reaction mixture was allowed to heat to room temperature, degassing the solution. This process was twice repeated. Upon evacuating the flask on the third time, 399 mbar of tritium gas was introduced. The reaction mixture was allowed to stir at room temperature for 1 h. The reaction mixture was then cooled with liquid nitrogen, and the remaining tritium gas was recovered onto a secondary uranium bed. Methanol (1 mL) was added to the reaction, and then removed *in vacuo*. This process was repeated three times. The reaction mixture was allowed to warm to room temperature and the chlorobenzene removed *in vacuo*. (*R*)-2-(2-Methyl-4-(5-(trifluoromethyl)-1,3,4-oxadiazol-2-yl)piperazin-1-yl)pyrimidin-5-ol **204** (1.320 mg, 4.01 μmol, 1.00 eq), potassium carbonate (1.101 mg, 8.02 μmol, 2.00 eq) and DMF (1 mL) were added, and the reaction mixture stirred at room temperature overnight. The product was purified by HPLC, and the pure fractions combined to give the tritiated product, which was stored as a solution in ethanol, and analysed by ^{1}H and ^{3}H NMR spectroscopy and LCMS. The specific activity of the compound was found to be 36.8 Ci/mmol by LCMS.[162]

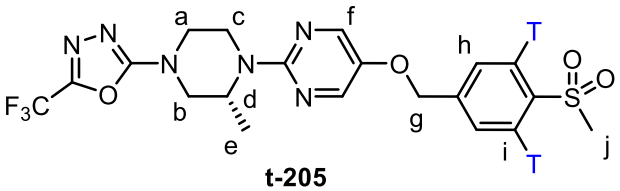

t-205

^{1}H NMR (500 MHz, MeOD): δ 8.24 (s, 2H, H^{f}), 7.99 (d, *J* = 8.6 Hz, 2H, H^{i}), 7.72 (d, *J* = 8.6 Hz, 2H, H^{h}), 5.23 (s, 2H, H^{g}) 5.01-4.94 (m, 2H, CH_2), 4.55-4.50 (m, 1H, H^{d}), 4.04-3.99 (m, 1H, alkylCH), 3.89-3.86 (m, 1H, alkylCH), 3.52-3.47 (m, 2H, alkylCH_2), 3.13 (s, 3H, H^{j}), 1.23 (d, *J* = 6.6 Hz, 3H, H^{e}).

^{3}H NMR (500 MHz, MeOD): δ 8.05 (d, $^{3}J_{T\text{-}H}$ = 9.2 Hz).

^{3}H{^{1}H} NMR (500 MHz, MeOD): δ 8.05.

*8.10 Initial Attempts at Sulfonamide Labelling with NHC-P Type Catalyst (**Scheme 4.2**)*

N-Methyl-p-toluenesulfonamide **127**[163]

To a 100 mL round-bottom flask, fitted with two stopcocks, was added *N*-methyl-*p*-toluenesulfonamide **127** (39.8 mg, 0.215 mmol, 1.00 eq) and complex **175** (18.0 mg, 0.108 mmol, 5 mol%). The mixture was dissolved in chlorobenzene (2.5 mL) and the flask placed in a heating block, pre-set to 25 °C. The atmosphere in the flask was exchanged with three vacuum/D_2 cycles, with the system being isolated upon the third influx of deuterium. The reaction was stirred at 25 °C for 16 h. The reaction mixture was loaded directly into a silica column, and the chlorobenzene eluted with petroleum ether. The deuterated product was eluted with Et_2O and concentrated *in vacuo*. The extent of deuteration was assessed by ^{1}H NMR spectroscopy. The incorporations were calculated as described in *General Procedure D*.

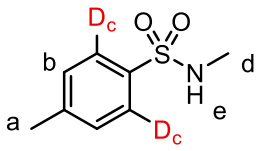

d-127

^{1}H NMR (400 MHz, $CDCl_3$): δ 7.73 (d, *J* = 8.1 Hz, 2H. H^c), 7.30 (d, *J* = 8.1 Hz, 2H, H^d), 4.34 (bs, 1H, H^e), 2.63 (s, 3H, H^d), 2.41 (s, 3H, H^a).

Run 1

(a) 87% Incorporation

Run 2

(a) 87% Incorporation

Run 3

(a) 94% Incorporation

Average Incorporation = 89%

Labelling expected against signal at δ 7.73 ppm, measured against signal at δ 2.41 ppm.

N,N-Dimethyl-p-toluenesulfonamide **206**[164]

To a 100 mL round-bottom flask, fitted with two stopcocks, was added *N*-methyl-p-toluenesulfonamide **206** (42.8 mg, 0.215 mmol, 1.00 eq) and complex **175** (18.0 mg, 0.108 mmol, 5 mol%). The mixture was dissolved in chlorobenzene (2.5 mL) and the flask placed in a heating block, pre-set to 25 °C. The atmosphere in the flask was exchanged with three vacuum/D_2 cycles, with the system being isolated upon the third influx of deuterium. The reaction was stirred at 25 °C for 16 h. The reaction mixture was loaded directly into a silica column, and the chlorobenzene eluted with petroleum ether. The deuterated product was eluted with Et_2O and concentrated *in vacuo*. The extent of deuteration was assessed by ^{1}H NMR spectroscopy. The incorporations were calculated as described in *General Procedure D*.

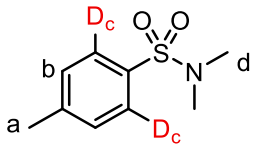

d-206

^{1}H NMR (400 MHz, $CDCl_3$): δ 7.64 (d, *J* = 8.3 Hz, 2H, H^c), 7.31 (d, *J* = 8.3 Hz, 2H, H^b), 2.67 (s, 6H, H^d), 2.41 (s, 3H, H^a).

Run 1

(a) 61% Incorporation

Run 2

(a) 55% Incorporation

Run 3

(a) 53% Incorporation

Average Incorporation = 56%

Labelling expected against signal at δ 7.64 ppm, measured against signal at δ 2.41 ppm.

*8.11 Towards η^4–Cycloocta-1,5-diene(1-(2,6-di-iso-propylphenyl)-3-(2-(pyridin-2'-lmethyl) imidazole-2-ylidene)iridium BAr_F (**Scheme 4.5**)*

Chloromethylpyridine **220**[165]

A 100 mL round-bottom flask was charged with thionyl chloride (18.0 mL), and cooled to 0 °C. Pyridinemethanol **221** (5.0 mL, 51.7 mmol) was added, slowly. Once the addition was complete, the reaction was heated to reflux and stirred for 3 h. The reaction was cooled to room temperature and the solvent removed *in vacuo*. The residue was dissolved in DCM, and slowly basified with a saturated solution of aqueous sodium bicarbonate. The mixture was transferred to a separating funnel and the layers separated. The aqueous layer was washed twice with DCM. The organic layers were combined, dried over sodium sulfate, filtered, and concentrated *in vacuo*. Due to the instability of the product, it was found that immediate use in the following step was best. Chloromethylpyridine **220** (6.03 g, 47.3 mmol, 91% yield) was isolated as a colourless liquid. The crude product was used without any further purification.

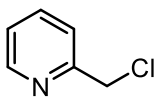

220

IR (neat, cm^{-1}): In Progress.

^{1}H NMR (400 MHz, $CDCl_3$): δ 8.56 (d, *J* = 5.0 Hz, 1H, ArH), 7.70 (td, *J* = 7.8 Hz, $^{4}J_{HH}$ = 1.7 Hz, 1H, ArH), 7.45 (d, *J* = 7.7 Hz, 1H, ArH), 7.24-7.19 (m, 1H, ArH), 4.66 (s, 2H, CH_2).

^{13}C NMR (101 MHz, $CDCl_3$) δ 156.6, 149.2, 137.2, 123.1, 122.9, 46.7.

1-(2,6-Di-iso-propylphenyl)-3-(pyridin-2-ylmethyl)-1H-imidazol-3-ium chloride **219**

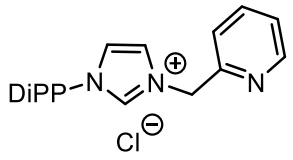

219

To a 20 mL microwave tube was added **180** (1.79 g, 7.82 mmol, 1.00 eq) and chloromethylpyridine **220** (1.30 g, 10.2 mmol, 1.00 eq). The tube was sealed and heated to 135 °C for 6 h. The resulting dark solid was cooled and dissolved in DCM and passed through a short column of Celite. The filtrate was then washed three times with distilled water. The aqueous layer was concentrated *in vacuo*, leaving a dark oil. The oil was re-dissolved in minimum amounts of DCM and precipitated with the addition of Et_2O, affording 1-(2,6-di-*iso*-propylphenyl)-3-(pyridin-2-ylmethyl)-1H-imidazol-3-ium chloride **219** (1.37g, 3.84 mmol, 49% yield) as an off-white solid.

Melting Point: decomposed above 138 °C.

IR (neat, cm^{-1}): 2964, 2926, 2868, 1589, 1556, 1541, 1467, 1438, 1361, 1257, 1193.

^{1}H NMR (400 MHz, $CDCl_3$): δ 10.44 (s, 1H, ArH), 8.52 (dd, *J* = 5.0 Hz, $^{4}J_{HH}$ = 1.5 Hz, 1H, ArH), 8.30 (s, 1H, ArH), 8.15 (d, *J* = 7.2 Hz, 1H, ArH), 7.81 (ddd, *J* = *J* = 7.5 Hz, $^{4}J_{HH}$ = 1.5 Hz, 1H, ArH), 7.51 (t, *J* = 7.5 Hz, 1H, ArH), 7.36-7.27 (m, 3H, ArH), 7.08 (s, 1H, ArH), 6.28

(s, 2H, CH_2), 2.27 (sep, *J* = 7.0 Hz, 2H, CH), 1.20 (d, *J* = 7.0 Hz, 6H, CH_3), 1.11 (d, *J* = 7.0 Hz, 6H, CH_3).

^{13}C NMR (101 MHz, $CDCl_3$) δ 152.1, 148.4, 144.9, 138.5, 137.9, 131.4, 129.4, 124.6, 124.2, 123.7, 123.4, 122.8, 53.0, 28.2, 23.8, 23.7.

HRMS (Positive ESI): m/z calculated for $[M]^+$ $C_{21}H_{26}N_3^+$ = 320.2121.; found: 320.2119.

η^4–Cycloocta-1,5-diene(1-(2,6-di-iso-propylphenyl)-3-(2-(pyridin-2'-lmethyl) imidazole-2-ylidene)iridium BAr_F **218**

To a flame-dried Schlenk tube was added **219** (0.600 g, 1.69 mmol, 1.00 eq) and silver oxide (0.235 g, 1.01 mmol, 0.60 eq). The mixture was suspended in DCM (20 mL) and stirred at room temperature for 16 h, protected from light. The reaction was filtered, under inert atmosphere, through Celite, washing with a further 10 mL of DCM. The filtrate was then concentrated *in vacuo*. To the residue was added Et_2O (20 mL) and DCM (1 mL), with vigorous stirring. The resulting precipitate was allowed to settle, and the pale solution removed *via* syringe. This process was repeated until the supernatant remained colourless, at which point the resulting solid was dried under high vacuum. The solid was dissolved in DCM (10 mL) and transferred *via* syringe into a separate Schlenk tube containing a solution of $[Ir(COD)Cl]_2$ (0.571 g, 0.85 mmol, 0.50 eq) in DCM (10 mL). $NaBAr_F$ (1.50 g, 1.69, 1.00 eq) was added and the reaction stirred at room temperature for 2 h. The red suspension was filtered through Celite and concentrated *in vacuo*. The residue was purified by column chromatography, eluting with 50% DCM in petroleum ether, affording η^4–cycloocta-1,5-diene(1-(2,6-di-*iso*-propylphenyl)-3-(2-(pyridin-2'-lmethyl) imidazole-2-ylidene)iridium BAr_F **218** (1.97 g, 1.33 mmol, 79% yield) as a red solid.

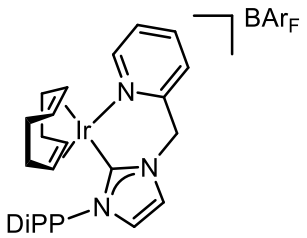

218

Melting Point: 64-66 °C

IR (neat, cm^{-1}): 2980, 2887, 1354, 1274, 1118.

^{1}H NMR (400 MHz, $CDCl_3$, 246 K): δ 8.43 (d, *J* = 5.1 Hz, 1H, ArH), 8.69 (s, 8H, BAr_F ArH), 7.64-7.58 (m, 1H, ArH), 7.53-7.54 (m, 5H, BAr_F ArH + ArH overlap), 7.45-7.30 (m, 2H, ArH), 7.29-7.24 (m, 2H, ArH),7.09 (s, 1H, ArH), 6.89 (s, 1H, ArH), 5.74 (d, $^2J_{HH}$ = 14.5 Hz, 1H, methylene CH), 4.96 (d, $^2J_{HH}$ = 14.5 Hz, 1H, methylene CH), 4.06-3.93 (m, 2H, COD CH), 3.86-3.78 (m, 1H, COD CH), 3.07-2.97 (m, 1H, COD CH), 2.43-2.31 (m, 1H, C**H**$(CH_3)_2$), 2.17-1.78 (m, 6H, COD CH_2 + C**H**$(CH_3)_2$ overlap), 1.60-1.52 (m, 1H, COD CH_2), 1.51-1.34 (m , 4H, COD CH_2 + CH_3 overlap), 1.20-1.06 (m, 6H, 2 CH_3 overlap), 0.90-0.76 (m, 4H, COD CH_2 + CH_3 overlap).

^{13}C NMR (101 MHz, $CDCl_3$) δ 174.8, 161.9 (J_{BC} = 50.0 Hz), 151.9, 151.6, 146.2, 145.6, 140.2, 135.0, 133.7, 131.1, 129.2 (J_{FC} = 30.8 Hz), 126.7, 125.5, 124.9 (J_{FC} = 272.8 Hz), 124.8, 124.7, 124.4, 120.9, 117.6, 86.6, 82.9, 65.9, 64.5, 55.8, 34.3, 31.5, 31.3, 28.9, 28.6, 27.9, 26.3, 26.1, 24.2, 22.9.

HRMS: m/z calculated for = $[M]^+$ $C_{29}H_{37}N_3Ir$ = 621.2643; found: 621.2630.

*8.12 Electronic Parameterization of Novel NHC-Py Complex (**Scheme 4.6**)*

To a flame-dried, three-necked 25 mL round-bottom flask, fitted with two stopcocks, was added η4–cycloocta-1,5-diene(1-(2,6-di-*iso*-propylphenyl)-3-(2-(pyridin-2'-lmethyl)

imidazole-2-ylidene)iridium BAr_F **218** (20 mg, 13.5 mmol) and d_3-acetonitrile (1.00 mL). The solution was cooled to -78 °C, and the atmosphere in the flask was exchanged *via* three vacuum/hydrogen cycles. In this case, the reaction mixture was left open to the hydrogen balloon for the duration of the experiment. The flask was moved to a heating block, pre-set to 25 °C, and stirred for 6 h. At this point, a 0.5 mL aliquot was taken and the hydride region of the NMR analysed. The remainder of the reaction mixture was left to stir under hydrogen for a further 18 h, at which point another 0.5 mL aliquot was taken, showing no change had occurred. Both the standard and hydride regions of the ^{1}H NMR spectrum were remarkably clear. With the data at hand, we attribute the corresponding shifts to one of two isomeric complexes, **214a** or **214b**.

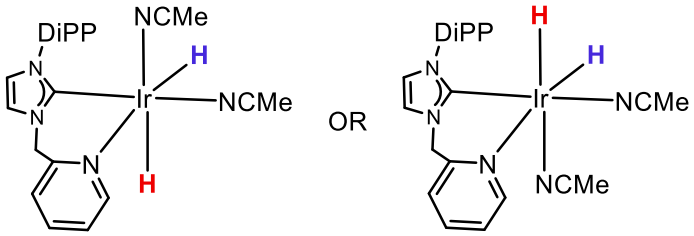

214a **214b**

-21.6 ppm, $^2J_{HH}$ = 7.5 Hz
-21.9 ppm, $^2J_{HH}$ = 7.5 Hz

^{1}H NMR (400 MHz, $CDCl_3$): δ 8.94 (d, *J* = 5.5 Hz, 1H, ArH), 7.99 (td, *J* = 7.7 Hz, $^4J_{HH}$ = 1.6 Hz, 1H, ArH), 7.74-7.69 (m, 8H, BAr_F ArH), 7.69-7.66 (m, 4H, BAr_F ArH), 7.55-7.39 (m, 3H, ArH), 7.38 (d, *J* = 2.0 Hz, 1H, Im ArH), 7.36-7.24 (m, 2H, ArH), 7.09 (d, *J* = 2.0 Hz, 1H, Im ArH), 5.47 (d, $^2J_{HH}$ = 16.0 Hz, 1H, methylene CH), 5.23 (d, $^2J_{HH}$ = 16.0 Hz, 1H, methylene CH), 2.44 (sep, *J* = 7.0 Hz, 1H, C**H**$(CH_3)_2$), 1.27 (d, *J* = 7.0 Hz, 3H, CH_3), 1.17 (d, *J* = 7.0 Hz, 3H, CH_3), 1.06 (d, *J* = 7.0 Hz, 3H, CH_3), 0.97 (d, *J* = 7.0 Hz, 3H, CH_3), -21.6 (d, $^2J_{HH}$ = 7.0 Hz, 1H, Ir—H), -21.9 (d, $^2J_{HH}$ = 7.0 Hz, 1H, Ir—H).

8.13 Labelling of Highly Substituted Sulfonamides with an NHC-Py Type Complex

*8.13.1 Initial Screening with NHC-Py Complex (**Scheme 4.7**)*

All reactions were run as described in *General Procedure I*, for the specified time. Data are reported as: (a) amount of substrate, and (b) Incorporation.

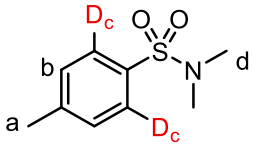

d-206

^{1}H NMR (400 MHz, $CDCl_3$): δ 7.64 (d, *J* = 8.3 Hz, 2H, H^c), 7.31 (d, *J* = 8.3 Hz, 2H, H^b), 2.67 (s, 6H, H^d), 2.41 (s, 3H, H^a).

16 hours

Run 1

(a) 42.8 mg, (b) 87%

Run 2

(a) 42.8 mg, (b) 89%

Run 3

(a) 42.8 mg, (b) 90%

Average Incorporation = 89%

Labelling expected against signal at δ 7.64 ppm, measured against signal at δ 2.41 ppm.

6 hours

Run 1

(a) 42.8 mg, (b) 83%

Run 2

(a) 42.8 mg, (b) 76%

Run 3

(a) 42.8 mg, (b) 79%

Average Incorporation = 79%

Labelling expected against signal at δ 7.64 ppm, measured against signal at δ 2.41 ppm.

8.13.2 Sulfonamide Substrate Synthesis

N-Methyl-p-toluenesulfonamide **127**[163]

Prepared according to *General Procedure H*, with 33% methylamine in ethanol (3.60 mL, 28.8 mmol) and *p*-toluenesulfonyl chloride (6.08 g, 31.9 mmol). Purified by column chromatography, eluting with 50% DCM in petroleum ether, isolated as a white solid (4.10 g, 85% yield).

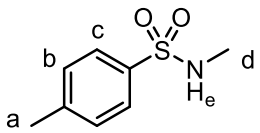

127

Melting Point: 69-71 °C (lit:[163] 70-71 °C)

IR (neat, cm^{-1}): 3265, 1595, 1450, 1408, 1315, 1305, 1228, 1153.s

^{1}H NMR (400 MHz, $CDCl_3$): δ 7.73 (d, *J* = 8.1 Hz, 2H. H^c), 7.30 (d, *J* = 8.1 Hz, 2H, H^d), 4.34 (bs, 1H, H^e), 2.63 (s, 3H, H^d), 2.41 (s, 3H, H^a).

^{13}C NMR (101 MHz, $CDCl_3$) δ 142.9, 135.2, 129.2, 126.8, 28.7, 20.9.

N,N-Dimethyl-p-toluenesulfonamide **206**[164]

Prepared according to *General Procedure H*, with 40% dimethylamine in ethanol (3.70 mL, 28.8 mmol) and *p*-toluenesulfonyl chloride (6.08 g, 31.9 mmol). Purified by column chromatography, eluting with 50% DCM in petroleum ether, isolated as a white solid (4.67 g, 89% yield).

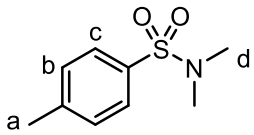

206

Melting Point:79-82 °C (lit:[166] 79-81 °C)

IR (neat, cm^{-1}): 3300, 1527, 1450, 1330, 1307, 1157, 1089.

^{1}H NMR (400 MHz, $CDCl_3$): δ 7.64 (d, *J* = 8.3 Hz, 2H, H^c), 7.31 (d, *J* = 8.3 Hz, 2H, H^b), 2.67 (s, 6H, H^d), 2.41 (s, 3H, H^a).

^{13}C NMR (101 MHz, $CDCl_3$) δ 143.4, 132.5, 129.6, 127.8, 37.9, 21.5.

N-Methyl-m-toluenesulfonamide **223a**[163]

Prepared according to *General Procedure H*, with 33% methylamine in ethanol (0.75 mL, 5.99 mmol) and *m*-toluenesulfonyl chloride (1.00 mL, 6.59 mmol). Purified by column chromatography, eluting with 50% DCM in petroleum ether, isolated as a colourless oil (1.11 g, quantitative yield).

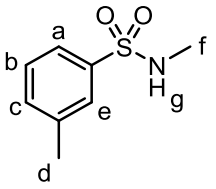

223a

IR (neat, cm^{-1}): 3284, 2924, 1475, 1409, 1319, 1301, 1219, 1149.

^{1}H NMR (400 MHz, CDCl$_3$): δ 7.67-7.61 (m, 2H, H^{a} + H^{e}), 7.42-7.34 (m, 2H, H^{b} + H^{c}), 4.39 (bs, 1H, H^{g}), 2.64 (s, 3H, H^{f}), 2.41 (s, 3H, H^{d}).

^{13}C NMR (101 MHz, CDCl$_3$) δ 139.3, 138.5, 133.5, 128.9, 127.5, 124.3, 29.3, 21.3.

N-Methyl-o-toluenesulfonamide **223b**[167]

Prepared according to *General Procedure H*, with 33% methylamine in ethanol (0.47 mL, 3.75 mmol) and *o*-toluenesulfonyl chloride (0.60 mL, 4.13 mmol). Purified by column chromatography, eluting with 50% DCM in petroleum ether, isolated as a white solid (0.629 g, quantitative yield).

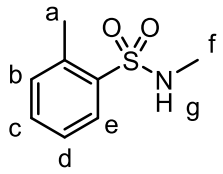

223b

Melting Point:70-72 °C (lit:[168] 70-72 °C)

IR (neat, cm^{-1}): 3290, 2964, 2360, 1469, 1456, 1406, 1303, 1155.

^{1}H NMR (400 MHz, CDCl$_3$): δ7.97-7.92 (m, 1H, H^{e}), 7.47-7.41 (m, 1H, H^{d}), 7.34-7.28 (m, 2H, H^{b} +H^{c}), 4.43 (bs, 1H, H^{g}) 2.64-2.60 (m, 6H, H^{a} + H^{f}).

^{13}C NMR (101 MHz, CDCl$_3$) δ 137.4, 137.1, 133.1, 132.8, 130.1, 126.4, 29.3, 20.5.

N-Cyclopropyl-p-toluenesulfonamide **223c**[169]

Prepared according to *General Procedure H*, with cyclopropylamine (1.00 mL, 21.3 mmol) and *p*-toluenesulfonyl chloride (4.46 g, 23.4 mmol). Purified by column chromatography, eluting with 30% DCM in petroleum ether, isolated as a white solid (4.33 g, 96% yield).

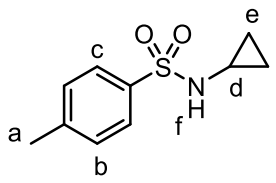

223c

Melting Point: 72-73 °C (lit:[170] 72-74 °C)

IR (neat, cm^{-1}): 3273, 2974, 2360, 1408, 1361, 1313, 1301, 1157.

^{1}H NMR (400 MHz, $CDCl_3$): δ 7.77 (d, *J* = 8.3 Hz, 2H, H^c), 7.30 (d, *J* = 8.3 Hz, 2H, H^b), 4.74 (bs, 1H, H^f), 2.42 (s, 3H, H^a), 2.22 (sep, *J* = 3.3 Hz, 1H, H^d), 0.62-0.54 (m, 4H, H^e).

^{13}C NMR (101 MHz, $CDCl_3$) δ 143.5, 136.7, 129.6, 127.5, 24.3, 21.5, 6.1.

N-tert-Butyl-p-toluenesulfonamide **223d**[171]

Prepared according to *General Procedure H*, with *tert*-butylamine (0.500 g, 6.84 mmol) and *p*-toluenesulfonyl chloride (4.46 g, 7.52 mmol). Purified by column chromatography, eluting with 30% DCM in petroleum ether, isolated as a white solid (1.37 g, 80% yield).

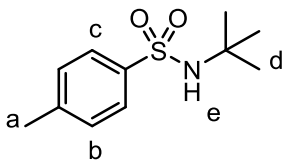

223d

Melting Point: 115-117 °C (lit:[172] 117-118 °C)

IR (neat, cm^{-1}): 3259, 2968, 2360, 1390, 1298, 1286, 1134, 1093.

^{1}H NMR (400 MHz, $CDCl_3$): δ 7.76 (d, *J* = 8.4 Hz, 2H, H^c), 7.25 (d, *J* = 8.4 Hz, 2H, H^b), 4.71 (bs, 1H, H^e), 2.39 (s, 3H, H^a), 1.19 (s, 9H, H^d).

^{13}C NMR (101 MHz, $CDCl_3$) δ 142.7, 140.5, 129.4, 126.9, 54.5, 30.1, 21.5.

N-Methylnapthalene-1-sulfonamide **223e**

Prepared according to *General Procedure H*, with 33% methylamine in ethanol (0.85 mL, 4.41 mmol) and 1-napthalenesulfonyl chloride (1.10 g, 4.85 mmol). Purified by column chromatography, eluting with 70% DCM in petroleum ether, isolated as a white solid (0.85 g, 87% yield).

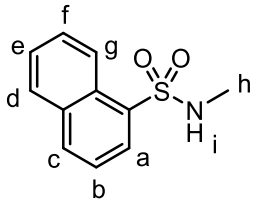

223e

Melting Point: 136-138 °C.

IR (neat, cm^{-1}): 3278, 2970, 2360, 1506, 1408, 1309, 1161, 1120.

^{1}H NMR (400 MHz, $CDCl_3$): δ 8.68 (d, *J* = 8.5 Hz, 1H, H^g), 8.30 (dd, *J* = 7.4 Hz, $^{4}J_{HH}$ = 1.0 Hz, 1H, H^a), 8.11 (d, *J* = 7.9 Hz, 1H, H^c), 7.99 (d, *J* = 8.1 Hz, 1H, H^d), 7.73-7.56 (m, 3H, H^b + H^e + H^f), 4.55 (bs, 1H, H^i), 2.62 (d, *J* = 5.5 Hz, 3H, H^h).

^{13}C NMR (101 MHz, $CDCl_3$) δ 134.3, 133.5, 130.0, 129.1, 129.0, 128.3, 126.9, 124.3, 124.1, 29.4. (Overlapping peaks at 134.3 ppm).

HRMS: m/z calculated for $[M+Na]^+$ $C_{11}H_{11}NO_2SNa^+$: 244.0403; found: 244.0401.

N-Benzyl-p-toluenesulfonamide **223f**[173]

Prepared according to *General Procedure H*, with benzylamine (1.50 mL, 14.3 mmol) and *p*-toluenesulfonyl chloride (2.99 g, 15.7 mmol). Purified by column chromatography, eluting with 50% DCM in petroleum ether, isolated as a white solid (3.33 g, 89% yield).

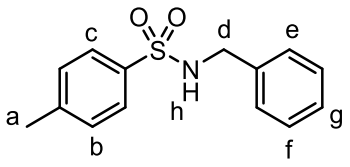

223f

Melting Point: 113-114 °C (lit:[173] 114-116 °C)

IR (neat, cm^{-1}): 3263, 2980, 2883, 2360, 1381, 1319, 1303, 1159.

^{1}H NMR (400 MHz, $CDCl_3$): δ 7.75 (d, *J* = 8.0 Hz, 2H, H^c), 7.31-7.24 (m, 5H, H^b + H^g + H^f), 7.18 (d, *J* = 8.0 Hz, 2H, H^e), 4.54 (bs, 1H, H^h), 4.11 (d, *J* = 6.2 Hz, 2H, H^d), 2.42 (s, 3H, H^a).

^{13}C NMR (101 MHz, $CDCl_3$) δ 143.5, 136.9, 136.3, 129.7, 128.7, 127.9, 127.8, 127.2, 47.3, 21.5.

4-Methyl-N-(p-tolyl)benzenesulfonamide **223g**[174]

Prepared according to *General Procedure H*, with *p*-toluidine (1.50 g, 14.0 mmol) and *p*-toluenesulfonyl chloride (2.94 g, 15.4 mmol). Purified by column chromatography, eluting with 50% DCM in petroleum ether, isolated as a white solid (2.89 g, 79% yield).

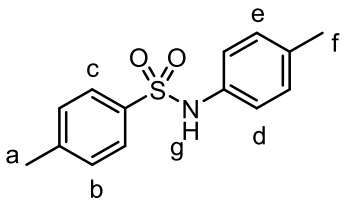

223g

Melting Point: 114-116 °C (lit:[174] 114-116 °C)

IR (neat, cm^{-1}): 3230, 1508, 1392, 1330, 1300, 1274, 1157.

^{1}H NMR (400 MHz, $CDCl_3$): δ 7.60 (d, *J* = 8.1 Hz, 2H, H^c), 7.19 (d, *J* = 8.1 Hz, 2H, H^b), 7.01 (d, *J* = 8.5 Hz, 2H, H^c), 6.92 (d, *J* = 8.5 Hz, 2H, H^d), 6.41 (bs, 1H, H^g), 2.36 (s, 3H, H^a), 2.25 (s, 3H, H^f).

^{13}C NMR (101 MHz, $CDCl_3$) δ 143.7, 136.1, 135.3, 133.8, 129.8, 129.6, 127.3, 122.2, 21.5, 20.8.

4-Methoxy-N-(4-(trifluoromethyl)phenyl)benzenesulfonamide **223h**

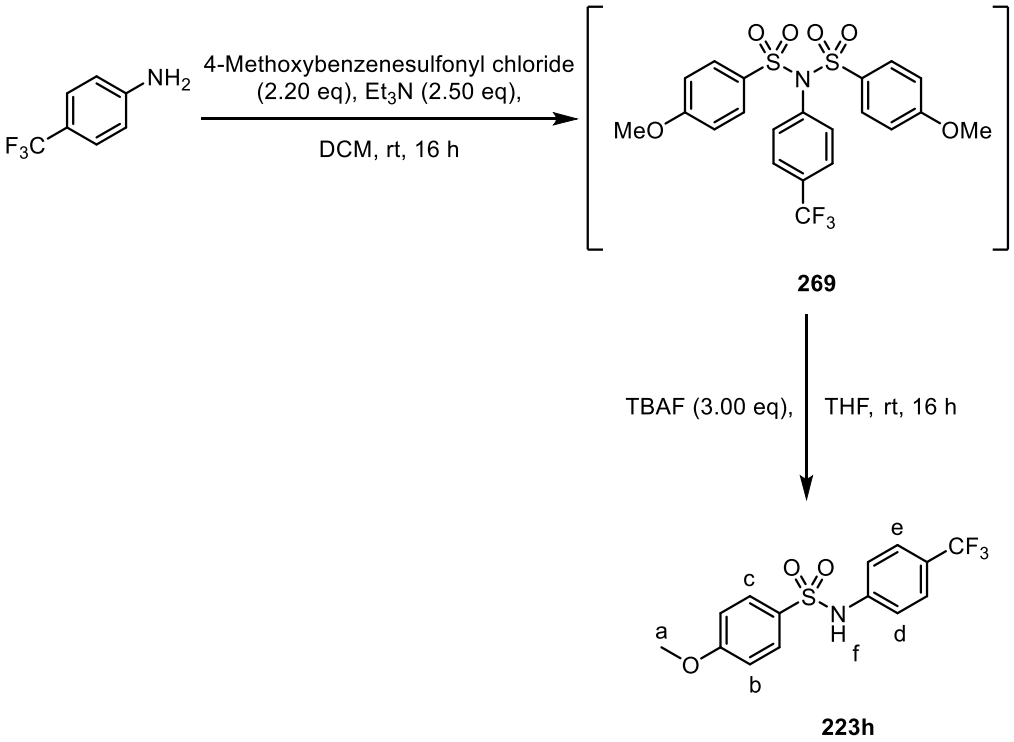

223h

Scheme 8.2

To a 100 mL round-bottom flask was added 4-trifluoromethylaniline (0.75 g, 4.65 mmol, 1.00 eq), triethylamine (1.6 mL, 11.6 mml, 2.50 eq) and DCM (15 mL). To this was added 4-methoxybenzenesulfonyl chloride (2.10 g, 10.2 mmol, 2.20 eq). The reaction was stirred at room temperature for 16 h. The reaction mixture was diluted with DCM (100 mL), transferred to a separating funnel and washed with 2 M NaOH (100 mL). The organic layer was dried over sodium sulfate, filtered and concentrated *in vacuo*. The resulting white solid was dissolved in THF (10 mL), under inert atmosphere and a 1 M solution of TBAF in THF (14.0 mL, 14.0 mmol, 3.00 eq) was added. The reaction was stirred at room temperature for 16 h. The solvent was removed in vacuo, and the residue dissolved in DCM (100 mL). The organic solution was washed with water (100 mL), dried over sodium sulfate, filtered and concentrated *in vacuo*. The crude product was purified by column chromatography, eluting with 50% DCM in petroleum ether, affording 4-methoxy-*N*-(4-(trifluoromethyl)phenyl)benzenesulfonamide **223h** (1.22 g, 3.69 mmol, 79% yield) as a white solid.

Melting Point: 116-118 °C.

IR (neat, cm^{-1}): 3296, 3238, 1614, 1593, 1573, 1517, 1496, 1463, 1400, 1321, 1300, 1265, 1226, 1149, 1114.

^{1}H NMR (400 MHz, $CDCl_3$): δ 7.78-7.73 (m, 2H, H^d), 7.47 (d, *J* = 8.5 Hz, 2H, H^b), 7.15 (d, *J* = 8.5 Hz, 2H, H^c), 7.00 (bs, 1H, H^f), 6.93-6.88 (m, 2H, H^e), 3.82 (s, 3H, H^a).

^{13}C NMR (101 MHz, $CDCl_3$) δ 157.8, 141.9, 134.0 (q, $^{2}J_{FC}$ = 33.5 Hz), 127.5, 127.3, 125.6, 125.2, 122.7 (q, $^{1}J_{FC}$ = 270.6 Hz), 114.1, 54.9.

^{19}F NMR (376 MHz, $CDCl_3$): δ -62.3 (s).

HRMS: m/z calculated for =$[M]^+$ $C_{14}H_{12}F_3NO_3S$ =311.0490; found: 311.0493.

N-(4-Methoxyphenyl)-4-(trifluoromethyl)benzenesulfonamide **223i**[175]

Prepared according to *General Procedure H*, with 4-methoxyaniline (1.00 g, 8.12 mmol) and 4-(trifluoromethyl)benzenesulfonyl chloride (1.99 g, 8.12 mmol). Purified by column chromatography, eluting with 50% DCM in petroleum ether, isolated as a white solid (0.98 g, 37% yield).

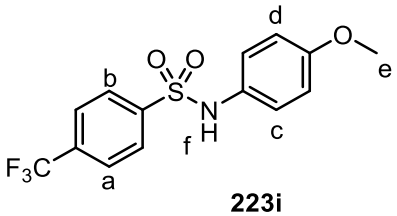

223i

Melting Point: 141-142 °C (lit:[175] 141-143 °C)

IR (neat, cm^{-1}): 3246, 1506, 1402, 1394, 1336, 1323, 1249, 1157, 1128.

^{1}H NMR (400 MHz, $CDCl_3$): δ 7.78 (d, *J* = 8.2 Hz, 2H, H^b), 7.68 (d, *J* = 8.2 Hz, 2H, H^a), 6.98 (m, 2H, H^c), 6.74 (m, 2H, H^d), 6.24 (bs, 1H, H^f), 3.76 (s, 3H, H^e).

^{13}C NMR (101 MHz, $CDCl_3$) δ 163.0, 136.6, 129.5, 128.9, 126.1, 126.0 (q, $^{2}J_{FC}$ = 33.1 Hz), 123.4 (q, $^{1}J_{FC}$ = 271.9 Hz), 119.0, 114.0, 55.1.

^{19}F NMR (376 MHz, $CDCl_3$): δ -63.2 (s).

HRMS: m/z calculated for $[M+Na]^+$ $C_{14}H_{12}F_3NO_3SNa$: 354.0382; found: 354.0381.

N,N-Dimethyl-(p-methoxybenzene)sulfonamide **223j**[164]

Prepared according to *General Procedure H*, with a 40% solution of dimethylamine (1.10 mL, 7.25 mmol) and 4-methoxybenzenesulfonyl chloride (1.65 g, 7.98 mmol). Purified by column

chromatography, eluting with 50% DCM in petroleum ether, isolated as a white solid (1.51 g, 97% yield).

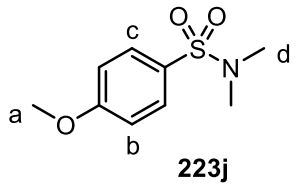

223j

Melting Point: 70-71 °C (lit:[166] 71-72 °C)

IR (neat, cm^{-1}): 2968, 1591, 1573, 1496, 1454, 1328, 1300, 1251, 1145.

^{1}H NMR (400 MHz, $CDCl_3$): δ 7.70 (d, *J* = 8.9 Hz, 2H, H^c), 6.98 (d, *J* = 8.9 Hz, 2H, H^b), 3.86 (s, 3H, H^a), 2.66 (s, 6H, H^d).

^{13}C NMR (101 MHz, $CDCl_3$) δ 162.9, 129.9, 127.2, 114.2, 55.6, 37.9.

N,N-Dimethyl-(p-trifluoromethylbenzene)sulfonamide **223k**[164]

Prepared according to *General Procedure H*, with a 40% solution of dimethylamine (0.78 mL, 6.13 mmol) and 4-(trifluoromethyl)benzenesulfonyl chloride (1.65 g, 6.74 mmol). Purified by column chromatography, eluting with 50% DCM in petroleum ether, isolated as a white solid (1.52 g, 98% yield).

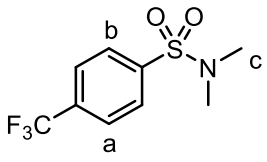

223k

Melting Point: 81-82 °C (li:t[176] 81-82 °C)

IR (neat, cm^{-1}): 2968, 1456, 1406, 1336, 1323, 1313, 1296, 1145, 1109, 1091.

^{1}H NMR (400 MHz, $CDCl_3$): δ 7.89 (d, *J* = 8.5 Hz, 2H, H^b), 7.80 (d, *J* = 8.5 Hz, 2H, H^a), 2.74 (s, 6H, H^c).

^{13}C NMR (101 MHz, $CDCl_3$) δ 139.5, 134.5 (q, $^{2}J_{FC}$ = 33.1 Hz), 128.3, 126.3 (q, $^{3}J_{FC}$ = 4.0 Hz), 123.5 (q, $^{1}J_{FC}$ = 271.3 Hz), 37.8.

^{19}F NMR (376 MHz, $CDCl_3$): δ -63.1 (s).

N-isopropyl-4-methyl-N-(p-tolyl)benzenesulfonamide **223l**

To a 50 mL round-bottom flask was added 4-methyl-*N*-(*p*-tolyl)benzenesulfonamide **223g** (0.50 g, 1.91 mmol, 1.00 eq) and potassium carbonate (0.535 g, 3.83 mmol, 2.00 eq). The mixture was suspended in DMF (6.0 mL) and 2-iodopropane (0.30 mL, 2.87 mmol, 1.50 eq) was added. The reaction was stirred at room temperature overnight. The reaction was diluted with water (300 mL) and extracted into DCM (3 x 50 mL). The organic layer was dried over sodium sulfate, filtered and concentrated *in vacuo*. The residue was purified by column chromatography, eluting with 30% EtOAc in petroleum ether, affording *N-iso*-propyl-4-methyl-*N*-(*p*-tolyl)benzenesulfonamide **223l** (0.575 g, 1.89 mmol, 99% yield) as a white solid.

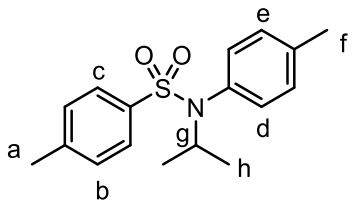

223l

Melting Point: 108-110 °C

IR (neat, cm^{-1}): 2991, 1508, 1336, 1238, 1165, 1157.

^{1}H NMR (400 MHz, $CDCl_3$): δ 7.61 (d, *J* = 8.5 Hz, 2H, H^c), 7.23 (d, *J* = 8.5 Hz, 2H, H^b), 7.10 (d, *J* = 8.6 Hz, 2H, H^e), 6.90 (d, *J* =8.5 Hz, 2H, H^d), 4.56 (sep, *J* = 7.0 Hz, 1H, H^g), 2.40 (s, 3H, H^a), 2.33 (s, 3H, H^f), 1.01 (d, *J* = 7.0 Hz, 6H, H^h).

^{13}C NMR (101 MHz, $CDCl_3$) δ 142.8, 138.8, 138.5, 132.2, 132.1, 129.4, 129.3, 127.4, 51.0, 22.0, 21.5, 21.1.

HRMS: m/z calculated for = $[M+H]^+$ $C_{17}H_{22}NO_2S$: 304.1371; found: 304.1373.

N-Tosyl-1,2,3,4-tetrahydroquinoline **223m**[177]

Prepared according to *General Procedure H*, with 1,2,3,4-tetrahydroquinoline (1.50 mL, 10.6 mmol) and *p*-toluenesulfonyl chloride (2.23 g, 11.7 mmol). Purified by column chromatography, eluting with 50% DCM in petroleum ether, isolated as a white solid (1.73 g, 57% yield).

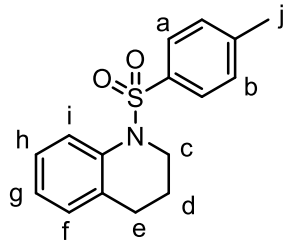

223m

Melting Point: 76-78 °C (lit:[177] 77-79°C)

IR (neat, cm^{-1}): 2908, 1487, 1354, 1338, 1307, 1159.

^{1}H NMR (400 MHz, $CDCl_3$): δ 7.77 (d, *J* = 8.0 Hz, 1H, H^i), 7.46 (d, *J* = 8.0 Hz, 2H, H^a), 7.19-7.13 (m, 3H, H^b + H^g), 7.05 (t, *J* = 7.5 Hz, $^4J_{HH}$ = 1.2 Hz, 1H, H^h), 6.98 (d, *J* = 7.9 Hz, 1H, H^f), 3.81-3.76 (m, 2H, H^c), 2.45-2.39 (m, 2H, H^e), 2.36 (s, 3H, H^j), 1.67-1.58 (m, 2H, H^d).

^{13}C NMR (101 MHz, $CDCl_3$) δ 143.4, 136.9, 136.8, 130.6, 129.5, 129.0, 127.1, 126.5, 124.9, 124.8, 46.5, 26.6, 21.6, 21.5.

N-Mesyl-1,2,3,4-tetrahydroquinoline **223n**[177]

To a flame-dried 100 mL round-bottom flask was added 1,2,3,4-tetrahydroquinone (1.50 mL, 10.6 mmol, 1.00 eq) and THF (30.0 mL). The solution was cooled to 0 °C and a 60% dispersion of sodium hydride in mineral oil (0.509 g, 12.7 mmol, 1.20 eq) was added. The reaction was stirred at 0 °C for 0.5 h. Methanesulfonyl chloride (1.30 mL, 12.8 mmol, 1.50 eq) was added, and the reaction stirred at room temperature overnight. The suspension was concentrated *in vacuo*, and the residue dissolved in DCM (100 mL). The organic solution was washed with 2 M HCl (100 mL), dried over sodium sulfate, filtered, and concentrated *in vacuo*. The crude product was purified by column chromatography, eluting with 30% DCM in petroleum ether, affording *N*-mesyl-1,2,3,4-tertahydroquinoline **223n** (1.61 g, 7.63 mmol, 72% yield) as a pale-yellow oil, which solidified on standing.

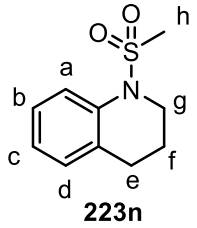

223n

Melting Point: (lit:[178] 58-59 °C)

IR (neat, cm^{-1}): 3016, 2931, 1489, 1361, 1332, 1319, 1168, 1149.

^{1}H NMR (400 MHz, $CDCl_3$): δ 7.68 (d, *J* = 8.5 Hz, 1H, H^a), 7.19-7.02 (m, 3H, H^b + H^c + H^d), 3.83 (m, 2H, H^g), 2.88 (s, 3H. H^h), 2.86-2.81 (m, 2H, H^e), 2.03-1.95 (m, 2H, H^f).

^{13}C NMR (101 MHz, $CDCl_3$) δ 137.0, 129.8, 129.3, 126.9, 124.6, 122.7, 46.5, 38.7, 27.1, 22.3.

N-Tosylpiperidine **223o**[179]

Prepared according to *General Procedure H*, with piperidine (2.00 mL, 30.3 mmol) and *p*-toluenesulfonyl chloride (6.90 g, 36.4 mmol). Purified by column chromatography, eluting with 50% DCM in petroleum ether, isolated as a white solid (7.40 g, quantitative yield).

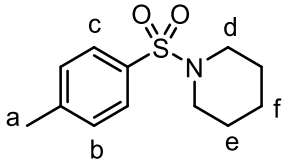

223o

Melting Point: 98-100 °C (lit:[179] 99-100 °C)

IR (neat, cm^{-1}): 2924, 1450, 1354, 1336, 1273, 1161.

^{1}H NMR (400 MHz, $CDCl_3$): δ7.64 (d, *J* = 8.3 Hz, 2H, H^c), 7.32 (d, *J* = 8.3 Hz, 2H, H^b), 3.00-2.94 (m, 4H, H^d), 2.44 (s, 3H, H^a), 1.68-1.59 (m, 4H, H^e), 1.45-1.38 (m, 2H, H^f).

^{13}C NMR (101 MHz, $CDCl_3$) δ 143.2, 133.4, 129.5, 127.7, 46.9, 25.2, 23.5, 21.5.

N-Tosylpyrazole **223p**[171]

Prepared according to *General Procedure H*, with pyrazole (1.00 g, 14.7 mmol) and *p*-toluenesulfonyl chloride (3.10 g, 16.2 mmol). Purified by column chromatography, eluting with 50% DCM in petroleum ether, isolated as a white solid (2.45 g, 75% yield).

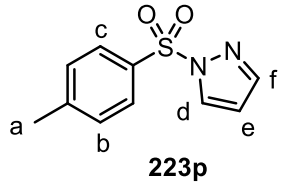

223p

Melting Point: 145-146 °C

IR (neat, cm^{-1}): 3128, 1591, 152, 1409, 1396, 1369, 1357, 1284, 1168, 1155.

^{1}H NMR (400 MHz, CDCl$_3$): δ 8.09 (d, *J* = 2.9 Hz, 1H, H^{d}), 7.88 (d, *J* = 8.0 Hz, 2H, H^{c}), 7.70 (d, *J* = 1.7 Hz, 1H, H^{f}), 7.1 (d, *J* = 8.0 Hz, 2H, H^{b}), 6.37 (dd, *J* = 2.9 Hz, *J* = 1.7 Hz, 1H, H^{e}), 2.40 (s, 3H, H^{a}).

^{13}C NMR (101 MHz, CDCl$_3$) δ 145.9, 145.2, 134.1, 131.1, 130.0, 128.1, 108.7, 21.7.

N-Tosylimidazole **223q**[171]

Prepared according to *General Procedure H*, with imidazole (1.00 g, 14.7 mmol) and *p*-toluenesulfonyl chloride (3.10 g, 16.2 mmol). Purified by column chromatography, eluting with 50% DCM in petroleum ether, isolated as a white solid (3.22 g, 99% yield).

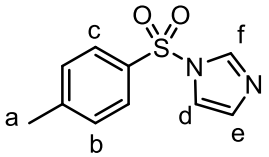

223q

Melting Point: 77-80 °C (lit:[180] 78-80 °C)

IR (neat, cm^{-1}): 1595, 1444, 1367, 1359, 1259, 1186, 1166, 1126.

^{1}H NMR (400 MHz, CDCl$_3$): δ 7.97 (t, $^{4}J_{HH}$ = $^{4}J_{HH}$ = 1.0 Hz, 1H, H^{f}), 7.79 (d, *J* = 8.4 Hz, 2H, H^{c}), 7.32 (d, *J* = 8.4 Hz, 2H, H^{b}), 7.25 (t, *J* = 1.5 Hz, $^{4}J_{HH}$ = 1.0 Hz, 1H, H^{d}), 7.04 (t, *J* = 1.6 Hz, $^{4}J_{HH}$ = 1.0 Hz, 1H, H^{e}), 2.40 (s, 3H, H^{a}).

^{13}C NMR (101 MHz, CDCl$_3$) δ 146.3, 136.6, 134.9, 131.4, 130.4, 127.3, 117.4, 21.7.

N-Tosylindole **223r**[181]

To a 50 mL round-bottom flask was added indole (1.00 g, .8.53 mmol, 1.00 eq) and tetra-n-butylammonium hydrogen sulfate (0.203 g, 0.597 mmol, 0.07 eq), and toluene (14.0 mL). To this mixture was added a solution of potassium hydroxide in water (50% wt, 4.52 mL, 85.3 mmol, 10.0 eq), followed by *p*-toluenesulfonyl chloride (2.11 g, 11.1 mmol, 1.30 eq). The reaction was stirred at room temperature for 4 h, at which point it was diluted with water (150 mL) and extracted into EtOAc (3 x 50 mL). The organic layer was dried over sodium sulfate, filtered and concentrated *in vacuo*. The crude product was purified by column chromatography, 0-50% EtOAc in petroleum ether, affording *N*-tosylindole **223r** (2.17 g, 8.00 mmol, 94% yield) as a white solid, which was stored at -30 °C.

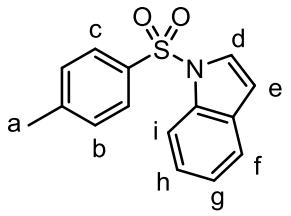

223r

Melting Point: 78-80 °C lit:[181] 78-80 °C)

IR (neat, cm^{-1}): 1593, 1460, 1377, 1190, 1172, 1149.

^{1}H NMR (400 MHz, $CDCl_3$): δ 7.97 (dd, J = 8.3 Hz, $^{4}J_{HH}$ = 0.7 Hz, 1H H^{i}), 7.74 (d, J = 8.6 Hz, 2H, H^{c}), 7.54 (d, J = 3.7 Hz, 1H, H^{d}), 7.50 (ddd, J = 8.0 Hz, $^{4}J_{HH}$ = 1.0 Hz, $^{4}J_{HH}$ = 0.7 Hz, 1H, H^{f}), 7.28 (ddd, J = 8.4 Hz, J = 7.6 Hz, $^{4}J_{HH}$ = 1.1 Hz, 1H, H^{g}), 7.22-7.16 (m, 3H, H^{b} + H^{h}), 6.63 (dd, J = 4.0 Hz, $^{4}J_{HH}$ = 0.7 Hz, 1H, H^{e}) 2.32 (s, 3H, H^{a}).

^{13}C NMR (101 MHz, $CDCl_3$) δ 144.9, 135.4, 134.8, 130.7, 129.8, 126.8, 126.3, 124.5, 123.2, 121.3, 113.5, 109.0, 21.5.

N-Methyl-4-nitrobenzenesulfonamide **223s**[182]

Prepared according to *General Procedure H*, with a 33% solution of methylamine in ethanol (0.62 mL, 4.96 mmol) and *p*-toluenesulfonyl chloride (1.00 g, 4.51 mmol). Purified by column chromatography, eluting with 0-100% DCM in petroleum ether. The resulting solid was then recrystallised from boiling Et_2O, affording *N*-methyl-4-nitrobenzenesulfonamide **223s** as a white solid (0.702 g, 72% yield).

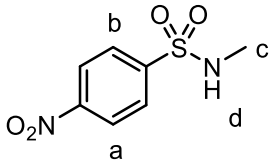

223s

Melting Point: 105-107 °C (lit:[182] 105-106 °C)

IR (neat, cm^{-1}): 3298, 3111, 1604, 1529, 1350, 1319, 1303, 1290, 1159.

^{1}H NMR (400 MHz, $CDCl_3$): δ 8.39 (d, *J* = 9.0 Hz, 2H, H^a), 8.07 (d, *J* = 9.0 Hz, 2H, H^b), 4.84 (bs, 1H, H^d), 2.76 (d, *J* = 5.0 Hz, 3H, H^c).

^{13}C NMR (101 MHz, $CDCl_3$) δ 150.2, 144.9, 128.5, 124.4, 29.3.

Towards Methyl 4-(N,N-dimethylsulfamoyl)benzoate **223t**

Methyl-4-(*N*,*N*-dimethylsulfamoyl)benzoate **223t** was synthesised *via* the benzylic oxidation of *p*-toluenesulfonamide **69**, followed by esterification with thionyl chloride, and methylation with methyl iodide, as shown in **Scheme 8.3**.

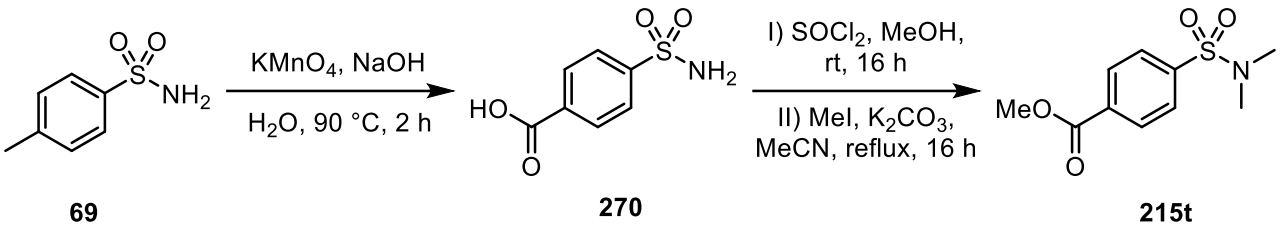

Scheme 8.3

4-Sulfamoylbenzoic Acid **266**[183]

To a 250 mL round-bottom flask was added *p*-toluenesulfonamide **69** (2.00 g, 11.7 mmol, 1.00 eq) and water (30 mL). To this suspension was added NaOH (2.34 g, 58.4 mmol, 5.00 eq), followed by the portionwise addition of $KMnO_4$ (2.40 g, 15.2 mmol, 1.30 eq). The reaction was heated to 90 °C and stirred for 2 h. The reaction was cooled to room temperature and filtered, washing the filter cake with minimal amounts of water. The colourless filtrate was then acidified with 6 M HCl, and the resulting precipitate filtered. The filter cake was washed with water and then dried under high vacuum to afford 4-sulfamoylbenzoic acid **270** (1.81 g, 9.00 mmol, 77% yield) as a white solid.

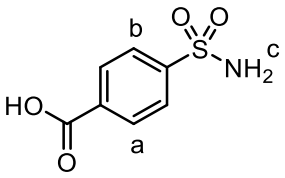

266

Melting Point: 273-274 °C (lit[183]: 276-277 °C)

IR (neat, cm^{-1}): 3356, 3255, 1685, 1560, 1427, 1338, 1317, 1284.

^{1}H NMR (400 MHz, DMSO-d$_6$): δ 8.10 (d, *J* = 8.6 Hz, 2H, H^a), 7.93 (d, *J* = 8.6 Hz, 2H, H^b), 7.52 (bs, 2H, H^c).

^{13}C NMR (101 MHz, DMSO-d_6) δ 166.2, 147.7, 133.5, 130.0, 125.9.

HRMS (Positive ESI): m/z calculated for $[M-H]^+$ $C_7H_6O_4NS$: 200.0023; found: 200.0027.

Methyl 4-(N,N-dimethylsulfamoyl)benzoate **223t**

To a 100 mL round-bottom flask was added 4-sulfamoylbenzoic acid **270** (0.800 g, 3.97 mmol, 1.00 eq) and methanol (15.0 mL). To this was added $SOCl_2$ (0.30 mL, 4.37 mmol, 1.10 eq) and the reaction stirred at room temperature for 16 h. The volatiles were then removed *in vacuo*. In order to fully remove any volatiles, the residue was re-dissolved in methanol and concentrated, and this cycle repeated another two times. The residue was then dissolved in MeCN (30.0 mL). To the solution was added potassium carbonate (1.65 g, 11.9 mmol, 3.00 eq) and methyl iodide (0.74 mL, 11.9 mmol, 3.00 eq). The reaction mixture was heated to reflux and stirred for 16 h. The suspension was cooled to room temperature and filtered. The filtrate was concentrated in vacuo and the crude product was purified by column chromatography, eluting with 50% EtOAc in petroleum ether. Methyl 4-(*N*,*N*-dimethylsulfamoyl)benzoate **223t** (0.860 g, 3.79 mmol, 95% yield) was isolated as a white solid.

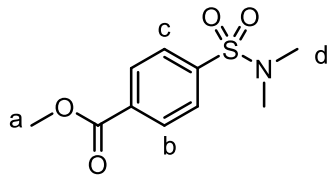

223t

Melting Point: 130-132 °C.

IR (neat, cm^{-1}): 3022, 2960, 1716, 1433, 1336, 1286, 1161, 1111

^{1}H NMR (400 MHz, $CDCl_3$): δ 8.18 (d, *J* = 8.5 Hz, 2H, H^b), 7.83 (d, *J* = 8.5 Hz, 2H, H^c), 3.95 (s, 3H, H^a), 2.72 (s, 6H, H^d).

NOSEY (400 MHz, $CDCl_3$):

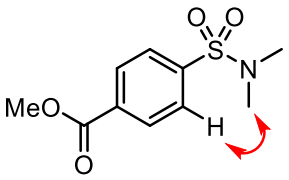

223t

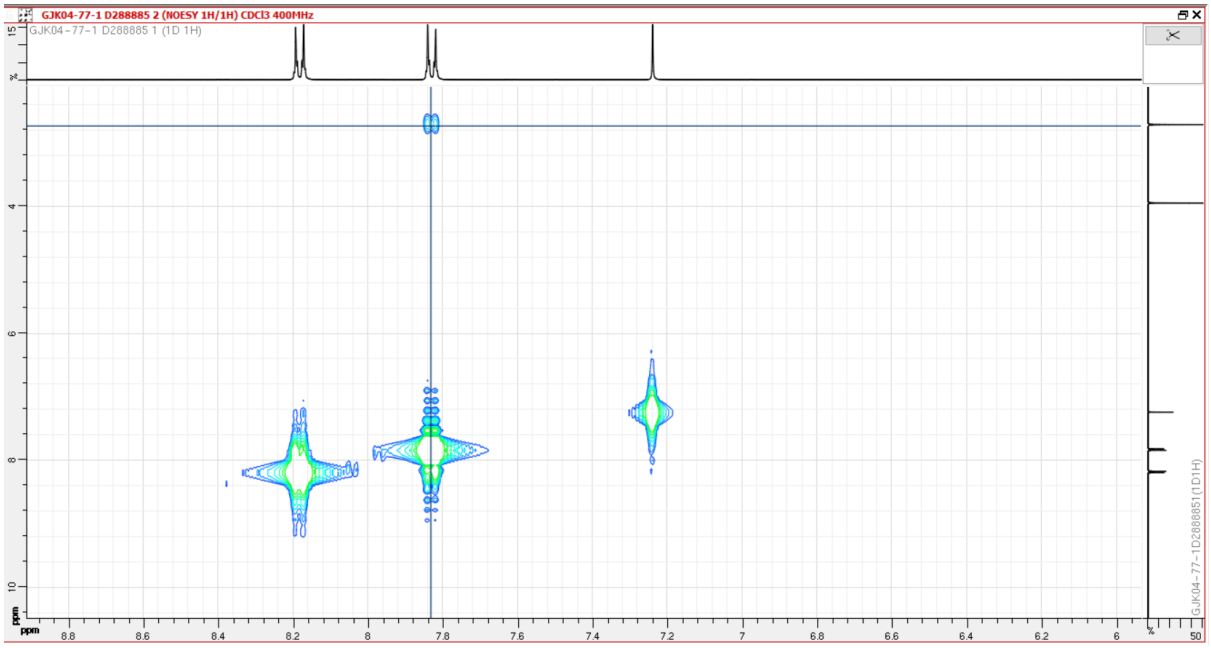

^{13}C NMR (101 MHz, $CDCl_3$) δ 165.7, 139.7, 133.9, 130.2, 127.7, 52.6, 37.8.

HRMS (Positive ESI): m/z calculated for $[M+H]^+$ $C_{10}H_{14}NO_4S$: 244.0638; found: 244.0637.

Towards N-(4-(N,N-dimethylsulfamoyl)phenyl)acetamide **223u**

The synthesis of *N*-(4-(*N*,*N*-dimethylsulfamoyl)phenyl)acetamide **223u** was performed as shown in **Scheme 8.4**. Sulfalinamide **271** could be acetylated using acetyl chloride and potassium carbonate to yield *N*-(4-sulfamoylphenyl)acetamide **272**. This could then be methylated by refluxing with methyl iodide in MeCN to afford *N*-(4-(*N*,*N*-dimethylsulfamoyl)phenyl)acetamide **223u**.

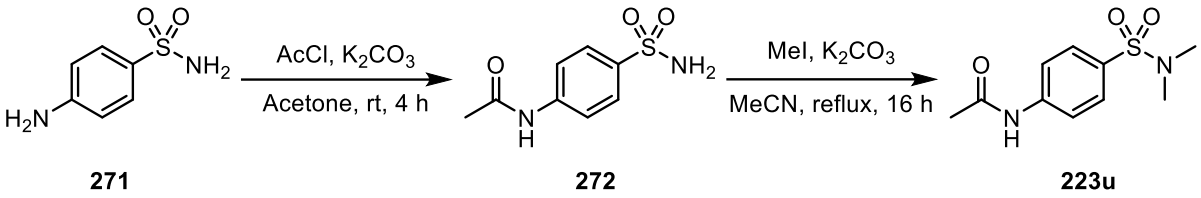

Scheme 8.4

N-(4-sulfamoylphenyl)acetamide **272**[184]

To a 250 mL round-bottom flask was added sulfalinamide **271** (2.00 g, 11.6 mmol, 1.00 eq) and potassium carbonate (9.60 g, 69.6 mmol, 6.00 eq). The mixture was suspended in acetone (40.0 mL) and acetyl chloride (4.96 mL, 69.6 mmol, 6.00 eq) was added. The reaction was stirred at reflux for 16 h. The suspension was cooled to room temperature and filtered. The filtrate was concentrated in vacuo. The crude product was purified by column chromatography, eluting with 0-100% EtOAc in petroleum ether, affording *N*-(4-sulfamoylphenyl)acetamide **272** (1.37 g, 6.39 mmol, 55% yield) as a white solid.

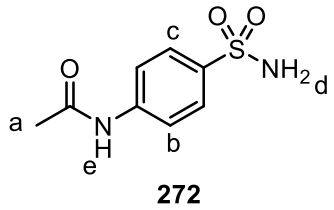

272

Melting Point: 221-224 °C (lit:[184] 223-224 °C)

IR (neat, cm^{-1}): 3302, 3255, 3118, 3061, 1670, 1591, 1533, 1404, 1373, 1315, 1316, 1265, 1159, 1145.

^{1}H NMR (400 MHz, DMSO-d$_6$): δ 10.3 (s, 1H, H^e), 7.77-7.69 (m, 4H, H^c + H^d), 7.22 (s, 2H, H^d), 2.08 (s, 3H, H^a).

^{13}C NMR (101 MHz, DMSO-d$_6$) δ 168.9, 142.2, 138.1, 126.7, 118.4, 24.1.

HRMS (Positive ESI): m/z calculated for $[M+H]^+$ $C_8H_{11}O_3N_2S$: 215.0485; found: 215.0486.

N-(4-(N,N-dimethylsulfamoyl)phenyl)acetamide **223u**

To a 100 mL round-bottom flask was added *N*-(4-sulfamoylphenyl)acetamide **272** (0.513 g, 2.39 mmol, 1.00 eq) and potassium carbonate (1.16 g, 8.38 mmol, 3.50 eq). The mixture was suspended in MeCN (25.0 mL) and methyl iodide (0.45 mL, 7.17 mmol, 3.00 eq) was added. The reaction was heated to reflux for 16 h. The suspension was cooled to room temperature and filtered. The filtrate was concentrated in vacuo, and the crude product purified by column chromatography, eluting with 30-50% EtOAc in petroleum ether. *N*-(4-(*N*,*N*-Dimethylsulfamoyl)phenyl)acetamide **223u** (0.493 g, 2.03 mmol, 85% yield) was isolated as a white solid.

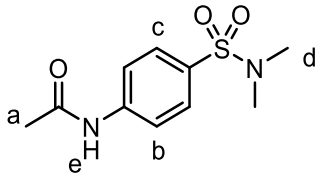

223u

Melting Point: 140-142 °C

IR (neat, cm^{-1}): 3302, 3255, 3118, 3061, 1670, 1591, 1533, 1404, 1373, 1315, 1265, 1159, 1145.

^{1}H NMR (400 MHz, DMSO-d$_6$): δ 10.35 (bs, 1H, H^e), 7.82 (d, *J* = 8.0 Hz, 2H, H^b), 7.67 (d, *J* = 8.0 Hz, 2H, H^c), 2.57 (s, 3H, H^a), 2.09 (s, 6H, H^d).

NOSEY (400 MHz, DMSO-d$_6$):

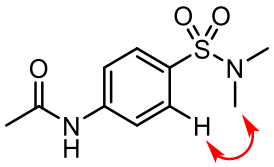

223u

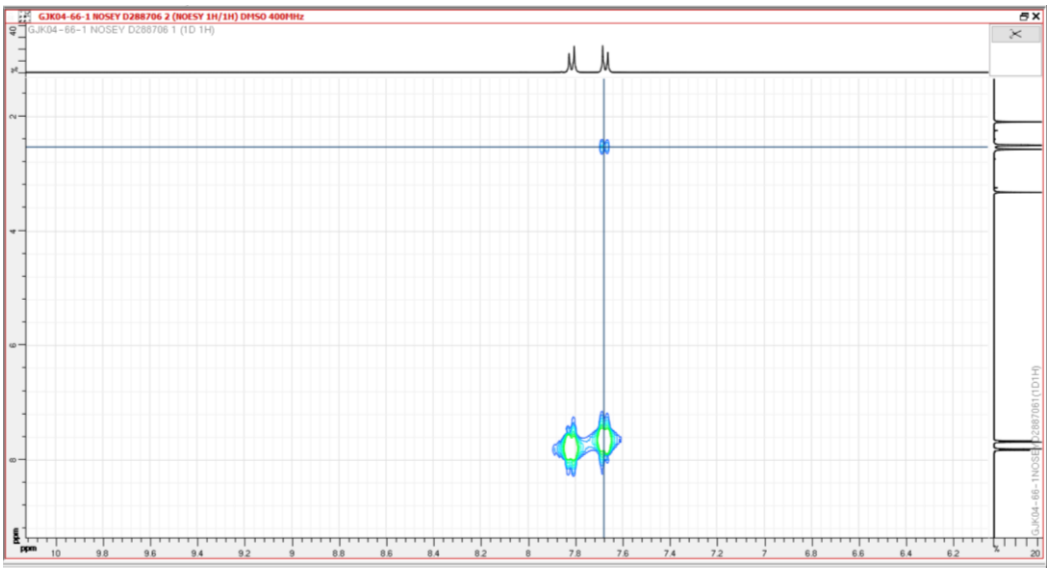

^{13}C NMR (101 MHz, DMSO-d$_6$) δ 169.0, 143.3, 128.7, 128.1, 118.6, 37.6, 24.1.

HRMS: m/z calculated for $[M+H]^+$ $C_{10}H_{15}N_2O_3S$ = 243.0803. Found: 243.0806.

*8.13.3 N-Substituted Sulfonamide Labelling Substrate Scope (**Scheme 4.8**)*

All reactions were run as described in *General Procedure I* (unless stated otherwise). Data are reported as: (a) amount of substrate, and (b) Incorporation.

N-Methyl-p-toluenesulfonamide **127**

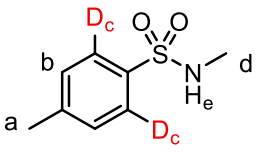

d-127

^{1}H NMR (400 MHz, $CDCl_3$): δ 7.73 (d, *J* = 8.1 Hz, 2H. H^c), 7.30 (d, *J* = 8.1 Hz, 2H, H^d), 4.34 (bs, 1H, H^e), 2.63 (s, 3H, H^d), 2.41 (s, 3H, H^a).

Labelling expected against signal at δ 7.73 ppm, measured against signal at δ 2.41 ppm.

Run 1

(a) 91% Incorporation

Run 2

(a)88% Incorporation

Run 3

(a)89% Incorporation

Average Incorporation = 89%

N-Methyl-m-toluenesulfonamide **223a**

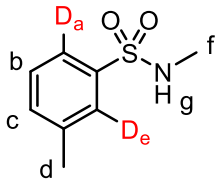

d-223a

^{1}H NMR (400 MHz, $CDCl_3$): δ 7.67-7.61 (m, 2H, H^a + H^e), 7.42-7.34 (m, 2H, H^b + H^c), 4.39 (bs, 1H, H^g), 2.64 (s, 3H, H^f), 2.41 (s, 3H, H^d).

Labelling expected against signal at δ 7.67-7.61 ppm, measured against signal at δ 2.41 ppm.

Run 1

(a) 39.8 mg, (b) 95% (Average across both positions)

Run 2

(a) 39.8 mg, (b) 93% (Average across both positions)

Run 3

(a) 39.8 mg, (b) 95% (Average across both positions)

Average Incorporation = 94% (Average across both positions)

N-Methyl-o-toluenesulfonamide **223b**

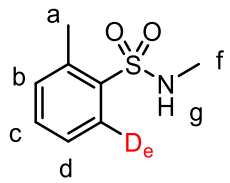

d-223b

^{1}H NMR (400 MHz, $CDCl_3$): δ7.97-7.92 (m, 1H, H^e), 7.47-7.41 (m, 1H, H^d), 7.34-7.28 (m, 2H, H^b +H^c), 4.43 (bs, 1H, H^g) 2.64-2.60 (m, 6H, H^a + H^f).

Labelling expected against signal at δ 7.97-7.92 ppm, measured against signal at δ 2.64-2.60 ppm.

Run 1

(a) 39.8 mg, (b) 76%

Run 2

(a) 39.8 mg, (b) 80%

Run 3

(a) 39.8 mg, (b) 84%

Average Incorporation = 80% (Average across both positions)

N-Cyclopropyl-p-toluenesulfonamide ***223c***

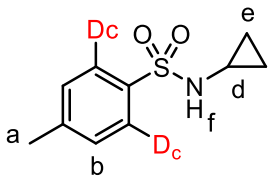

d-223c

^{1}H NMR (400 MHz, $CDCl_3$): δ 7.77 (d, *J* = 8.3 Hz, 2H, H^{c}), 7.30 (d, *J* = 8.3 Hz, 2H, H^{b}), 4.74 (bs, 1H, H^{f}), 2.42 (s, 3H, H^{a}), 2.22 (sep, *J* = 3.3 Hz, 1H, H^{d}), 0.62-0.54 (m, 4H, H^{e}).

Labelling expected against signal at δ 7.77 ppm, measured against signal at δ 2.42 ppm.

Run 1

(a) 45.4 mg, (b) 86%

Run 2

(a) 45.4 mg, (b) 83%

Run 3

(a) 45.4 mg, (b) 85%

Average Incorporation = 85%

N-tert-Butyl-p-toluenesulfonamide ***223d***

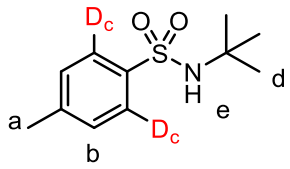

d-223d

^{1}H NMR (400 MHz, $CDCl_3$): δ 7.76 (d, *J* = 8.4 Hz, 2H, H^c), 7.25 (d, *J* = 8.4 Hz, 2H, H^b), 4.71 (bs, 1H, H^e), 2.39 (s, 3H, H^a), 1.19 (s, 9H, H^d).

Labelling expected against signal at δ 7.76 ppm, measured against signal at δ 1.19 ppm.

Run 1

(a) 48.9 mg, (b) 98%

Run 2

(a) 48.9 mg, (b) 97%

Run 3

(a) 48.9 mg, (b) 94%

Average Incorporation = 96%

N-Methylnapthalene-1-sulfonamide **223e**

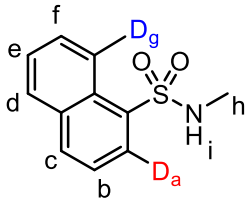

d-223e

^{1}H NMR (400 MHz, $CDCl_3$): δ 8.68 (d, *J* = 8.5 Hz, 1H, H^g), 8.30 (dd, *J* = 7.4 Hz, $^4J_{HH}$ = 1.0 Hz, 1H, H^a), 8.11 (d, *J* = 7.9 Hz, 1H, H^c), 7.99 (d, *J* = 8.1 Hz, 1H, H^d), 7.73-7.56 (m, 3H, H^b + H^e + H^f), 4.55 (bs, 1H, H^i), 2.62 (d, *J* = 5.5 Hz, 3H, H^h).

Labelling expected against signal at δ 8.68 ppm and δ 8.30 ppm, measured against signal at δ 2.62 ppm.

Run 1

(a) 47.6 mg, (b) D_a = 97%, D_g = 55%

Run 2

(a) 47.6 mg, (b) D_a = 97%, D_g = 47%

Run 3

(a) 47.6 mg, (b) D_a = 96%, D_g = 47%

Average Incorporation = D_a = 97%, D_g = 50%

N-Benzyl-p-toluenesulfonamide **223f**

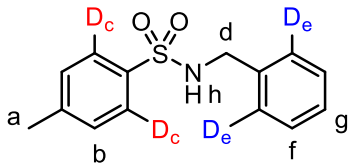

d-223f

^{1}H NMR (400 MHz, $CDCl_3$): δ 7.75 (d, *J* = 8.0 Hz, 2H, H^c), 7.31-7.24 (m, 5H, H^b + H^g + H^f), 7.18 (d, *J* = 8.0 Hz, 2H, H^e), 4.54 (bs, 1H, H^h), 4.11 (d, *J* = 6.2 Hz, 2H, H^d), 2.42 (s, 3H, H^a).

Labelling expected against signal at δ 7.75 ppm and δ 7.18 ppm, measured against signal at δ 2.42 ppm.

Run 1

(a) 56.2 mg, (b) D_c = 82%, D_e = 88%

Run 2

(a) 56.2 mg, (b) D_c = 79%, D_e = 85%

Run 3

(a) 56.2 mg, (b) D_c = 83%, D_e = 87%

Average Incorporation = D_c = 81%, D_e = 87%

4-Methyl-N-(p-tolyl)benzenesulfonamide **223g**

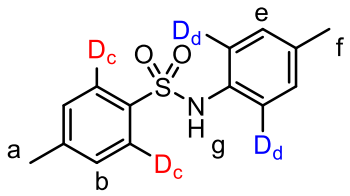

d-223g

^{1}H NMR (400 MHz, $CDCl_3$): δ 7.60 (d, *J* = 8.1 Hz, 2H, H^c), 7.19 (d, *J* = 8.1 Hz, 2H, H^b), 7.01 (d, *J* = 8.5 Hz, 2H, H^c), 6.92 (d, *J* = 8.5 Hz, 2H, H^d), 6.41 (bs, 1H, H^g), 2.36 (s, 3H, H^a), 2.25 (s, 3H, H^f).

Labelling expected against signal at δ 7.60 ppm and δ 6.92 ppm, measured against signal at δ 2.25 ppm.

Run 1 *(General Procedure J)*

(a) 56.2 mg, (b) D_c = 94%, D_d = 88%

Run 2 *(General Procedure J)*

(a) 56.2 mg, (b) D_c = 93%, D_d = 88%

Run 3 *(General Procedure J)*

(a) 56.2 mg, (b) D_c = 95%, D_d = 93%

Average Incorporation = D_c = 94%, D_d = 90%

4-Methoxy-N-(4-(trifluoromethyl)phenyl)benzenesulfonamide **223h**

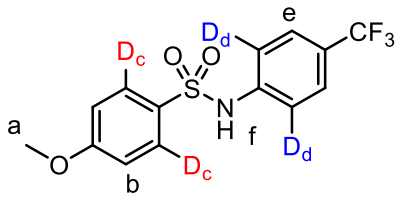

d-223h

^{1}H NMR (400 MHz, $CDCl_3$): δ 7.78-7.73 (m, 2H, H^d), 7.47 (d, *J* = 8.5 Hz, 2H, H^b), 7.15 (d, *J* = 8.5 Hz, 2H, H^c), 7.00 (bs, 1H, H^f), 6.93-6.88 (m, 2H, H^e), 3.82 (s, 3H, H^a).

Labelling expected against signal at δ 7.78-7.73 ppm and δ 7.15 ppm, measured against signal at δ 3.82 ppm.

Run 1

(a) 71.2 mg, (b) D_c = 82%, D_d = 33%

Run 2

(a) 71.2 mg, (b) D_c = 84%, D_d = 35%

Run 3

(a) 71.2 mg, (b) D_c = 86%, D_d = 38%

Average Incorporation = D_c = 83%, D_d = 35%

N-(4-Methoxyphenyl)-4-(trifluoromethyl)benzenesulfonamide **223i**

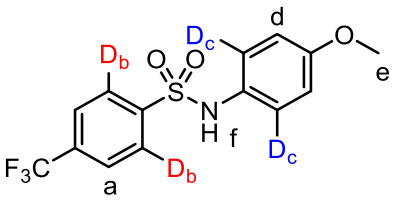

d-223i

^{1}H NMR (400 MHz, $CDCl_3$): δ 7.78 (d, *J* = 8.2 Hz, 2H, H^b), 7.68 (d, *J* = 8.2 Hz, 2H, H^a), 6.98 (m, 2H, H^c), 6.74 (m, 2H, H^d), 6.24 (bs, 1H, H^f), 3.76 (s, 3H, H^e).

Labelling expected against signal at δ 7.78 ppm and δ 6.98 ppm, measured against signal at δ 3.76 ppm.

Run 1 *(General Procedure J)*

(a) 71.2 mg, (b) D_b = 80%, D_c = 82%

Run 2 *(General Procedure J)*

(a) 71.2 mg, (b) D_b = 81%, D_c = 84%

Run 3 *(General Procedure J)*

(a) 71.2 mg, (b) D_b = 85%, D_c = 88%

Average Incorporation = D_b = 82%, D_c = 85%

*8.13.4 N,N-Disubstituted Sulfonamide Labelling (**Scheme 4.9**)*

All reactions were run as described in *General Procedure B* (unless stated otherwise). Data are reported as: (a) amount of substrate, and (b) Incorporation.

N,N-Dimethyl-(p-methoxybenzene)sulfonamide **223j**

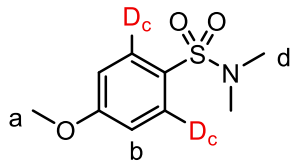

d-223j

^{1}H NMR (400 MHz, $CDCl_3$): δ 7.70 (d, *J* = 8.9 Hz, 2H, H^c), 6.98 (d, *J* = 8.9 Hz, 2H, H^b), 3.86 (s, 3H, H^a), 2.66 (s, 6H, H^d).

Labelling expected against signal at δ 7.70 ppm, measured against signal at δ 2.66 ppm.

Run 1

(a) 46.3 mg, (b) 90%,

Run 2

(a) 46.3 mg, (b) 96%

Run 3

(a) 46.3 mg, (b) 90%

Average Incorporation = 93%

N,N-Dimethyl-(p-trifluoromethylbenzene)sulfonamide **223k**

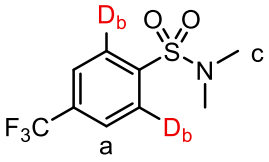

d-223k

^{1}H NMR (400 MHz, $CDCl_3$): δ 7.89 (d, *J* = 8.5 Hz, 2H, H^b), 7.80 (d, *J* = 8.5 Hz, 2H, H^a), 2.74 (s, 6H, H^c).

Labelling expected against signal at δ 7.89 ppm, measured against signal at δ 2.74 ppm.

Run 1 *(General Procedure J)*

(a) 54.4 mg, (b) 70%,

Run 2 *(General Procedure J)*

(a) 54.4 mg, (b) 72%

Run 3 *(General Procedure J)*

(a) 54.4 mg, (b) 77%

Average Incorporation = 73%

N-isopropyl-4-methyl-N-(p-tolyl)benzenesulfonamide **223l**

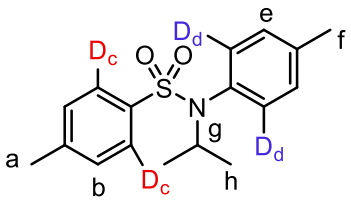

d-223l

^{1}H NMR (400 MHz, $CDCl_3$): δ 7.61 (d, *J* = 8.5 Hz, 2H, H^c), 7.23 (d, *J* = 8.5 Hz, 2H, H^b), 7.10 (d, *J* = 8.6 Hz, 2H, H^e), 6.90 (d, *J* =8.5 Hz, 2H, H^d), 4.56 (sep, *J* = 7.0 Hz, 1H, H^g), 2.40 (s, 3H, H^a), 2.33 (s, 3H, H^f), 1.01 (d, *J* = 7.0 Hz, 6H, H^h).

Labelling expected against signal at δ 7.61 ppm and δ 6.90 ppm, measured against signal at δ 2.33 ppm.

Run 1

(a) 65.2 mg, (b) D_c = 96%, D_d = 93%

Run 2

(a) 65.2 mg, (b) D_c = 97%, D_d = 96%

Run 3

(a) 65.2 mg, (b) D_c = 97%, D_d = 96%

Average Incorporation = D_c =97 %, D_d = 95%

N-Tosyl-1,2,3,4-tetrahydroquinoline **223m**

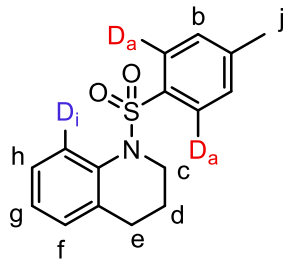

d-223m

^{1}H NMR (400 MHz, $CDCl_3$): δ 7.77 (d, *J* = 8.0 Hz, 1H, H^i), 7.46 (d, *J* = 8.0 Hz, 2H, H^a), 7.19-7.13 (m, 3H, H^b + H^g), 7.05 (t, *J* = 7.5 Hz, $^4J_{HH}$ = 1.2 Hz, 1H, H^h), 6.98 (d, *J* = 7.9 Hz, 1H, H^f), 3.81-3.76 (m, 2H, H^c), 2.45-2.39 (m, 2H, H^e), 2.36 (s, 3H, H^j), 1.67-1.58 (m, 2H, H^d).

Labelling expected against signal at δ 7.77 ppm and δ 7.46 ppm, measured against signal at δ 2.36 ppm.

Run 1

(a) 61.8 mg, (b) D_a = 97%, D_i = 83%

Run 2

(a) 61.8 mg, (b) D_a = 97%, D_i = 88%

Run 3

(a) 61.8 mg, (b) D_a = 96%, D_i = 75%

Average Incorporation = D_a = 97%, D_i = 82%

N-Mesyl-1,2,3,4-tetrahydroquinoline **223n**

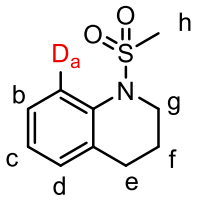

d-223n

^{1}H NMR (400 MHz, $CDCl_3$): δ 7.68 (d, *J* = 8.5 Hz, 1H, H^a), 7.19-7.02 (m, 3H, H^b + H^c + H^d), 3.83 (m, 2H, H^g), 2.88 (s, 3H. H^h), 2.86-2.81 (m, 2H, H^e), 2.03-1.95 (m, 2H, H^f).

Labelling expected against signal at δ 7.68 ppm, measured against signal at δ 2.88 ppm.

Run 1

(a) 45.4 mg, (b) 97%

Run 2

(a) 45.4 mg, (b) 99%

Run 3

(a) 45.4 mg, (b) 99%

Average Incorporation = 98%

N-Tosylpiperidine **223o**

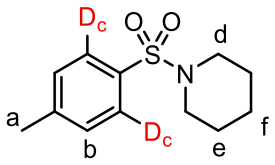

223o

^{1}H NMR (400 MHz, $CDCl_3$): δ7.64 (d, *J* = 8.3 Hz, 2H, H^c), 7.32 (d, *J* = 8.3 Hz, 2H, H^b), 3.00-2.94 (m, 4H, H^d), 2.44 (s, 3H, H^a), 1.68-1.59 (m, 4H, H^e), 1.45-1.38 (m, 2H, H^f).

Labelling expected against signal at δ 7.64 ppm, measured against signal at δ 2.44 ppm.

Run 1

(a) 51.5 mg, (b) 88%

Run 2

(a) 51.5 mg, (b) 90%

Run 3

(a) 51.5 mg, (b) 95%

Average Incorporation = 91%

N-Tosylpyrazole **223p**

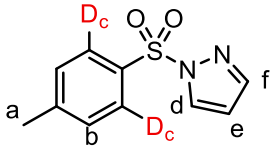

d-223p

^{1}H NMR (400 MHz, $CDCl_3$): δ 8.09 (d, *J* = 2.9 Hz, 1H, H^d), 7.88 (d, *J* = 8.0 Hz, 2H, H^c), 7.70 (d, *J* = 1.7 Hz, 1H, H^f), 7.1 (d, *J* = 8.0 Hz, 2H, H^b), 6.37 (dd, *J* = 2.9 Hz, *J* = 1.7 Hz, 1H, H^e), 2.40 (s, 3H, H^a).

Labelling expected against signal at δ 7.88 ppm, measured against signal at δ 2.40 ppm.

Run 1

(a) 47.8 mg, (b) 90%

Run 2

(a) 47.8 mg, (b) 82%

Run 3

(a) 47.8 mg, (b) 81%

Average Incorporation = 84%

N-Tosylimidazole **223q**

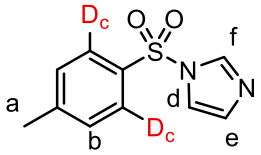

d-223q

^{1}H NMR (400 MHz, $CDCl_3$): δ 7.97 (t, $^4J_{HH}$ = $^4J_{HH}$ = 1.0 Hz, 1H, H^f), 7.79 (d, *J* = 8.4 Hz, 2H, H^c), 7.32 (d, *J* = 8.4 Hz, 2H, H^b), 7.25 (t, *J* = 1.5 Hz, $^4J_{HH}$ = 1.0 Hz, 1H, H^d), 7.04 (t, *J* = 1.6 Hz, $^4J_{HH}$ = 1.0 Hz, 1H, H^e), 2.40 (s, 3H, H^a).

Labelling expected against signal at δ 7.79 ppm, measured against signal at δ 2.40 ppm.

Run 1

(a) 47.8 mg, (b) 0%

Run 2

(a) 47.8 mg, (b) 0%

Run 3

(a) 47.8 mg, (b) 0%

Average Incorporation = 0%

N-Tosylindole **223r**

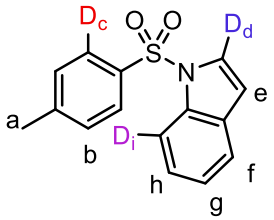

d-223r

^{1}H NMR (400 MHz, $CDCl_3$): δ 7.97 (dd, *J* = 8.3 Hz, $^{4}J_{HH}$ = 0.7 Hz, 1H H^{i}), 7.74 (d, *J* = 8.6 Hz, 2H, H^{c}), 7.54 (d, *J* = 3.7 Hz, 1H, H^{d}), 7.50 (ddd, *J* = 8.0 Hz, $^{4}J_{HH}$ = 1.0 Hz, $^{4}J_{HH}$ = 0.7 Hz, 1H, H^{f}), 7.28 (ddd, *J* = 8.4 Hz, *J* = 7.6 Hz, $^{4}J_{HH}$ = 1.1 Hz, 1H, H^{g}), 7.22-7.16 (m, 3H, H^{b} + H^{h}), 6.63 (dd, *J* = 4.0 Hz, $^{4}J_{HH}$ = 0.7 Hz, 1H, H^{e}) 2.32 (s, 3H, H^{a}).

Labelling expected against signal at δ 7.97 ppm, δ 7.74 ppm, and δ 7.54 ppm, measured against signal at δ 2.32 ppm.

Run 1

(a) 58.3 mg, (b) D_c =14%, D_d = 96%, D_i = 93%

Run 2

(a) 58.3 mg, (b) D_c = 13%, D_d = 91%, D_i = 97%

Run 3

(a) 58.3 mg, (b) D_c = 13%, D_d = 89%, D_i = 96%

Average Incorporation = D_c = 13%, D_d = 91%, D_i = 96%

*8.13.5 Investigation of Competing Directing Groups in Sulfonamide Labelling (**Scheme 4.10**)*

All reactions were run as described in *General Procedure I* (unless stated otherwise). Data are reported as: (a) amount of substrate, and (b) Incorporation.

N-Methyl-4-nitrobenzenesulfonamide **223s**

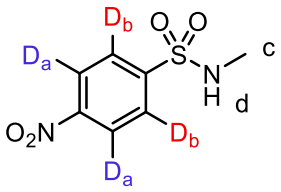

d-223s

^{1}H NMR (400 MHz, $CDCl_3$): δ 8.39 (d, *J* = 9.0 Hz, 2H, H^a), 8.07 (d, *J* = 9.0 Hz, 2H, H^b), 4.84 (bs, 1H, H^d), 2.76 (d, *J* = 5.0 Hz, 3H, H^c).

Labelling expected against signal at δ 8.39 ppm and δ 8.07 ppm, measured against signal at δ 2.76 ppm.

Run 1 *(General Procedure J)*

(a) 46.5 mg, (b) D_b =89%, D_a = 88%,

Run 2 *(General Procedure J)*

(a) 46.5 mg, (b) D_b = 88%, D_a = 87%,

Run 3 *(General Procedure J)*

(a) 46.5 mg, (b) D_b = 87%, D_a = 87%,

Average Incorporation = D_b = 88%, D_a = 87%,

Methyl 4-(N,N-dimethylsulfamoyl)benzoate **223t**

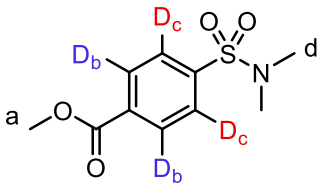

d-223s

^{1}H NMR (400 MHz, $CDCl_3$): δ 8.18 (d, *J* = 8.5 Hz, 2H, H^b), 7.83 (d, *J* = 8.5 Hz, 2H, H^c), 3.95 (s, 3H, H^a), 2.72 (s, 6H, H^d).

Labelling expected against signal at δ 8.18 ppm and δ 7.83 ppm, measured against signal at δ 2.72 ppm.

Run 1

(a) 52.3 mg, (b) D_c = 60%, D_b = 94%

Run 2

(a) 52.3 mg, (b) D_c = 58%, D_b = 93%

Run 3

(a) 52.3 mg, (b) D_c = 50%, D_b = 92%,

Average Incorporation = D_c = 56%, D_b = 93%,

N-(4-(N,N-dimethylsulfamoyl)phenyl)acetamide **223u**

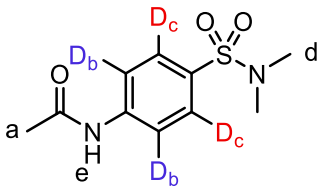

d-223u

^{1}H NMR (400 MHz, DMSO-d$_6$): δ 10.35 (bs, 1H, H^e), 7.82 (d, *J* = 8.0 Hz, 2H, H^b), 7.67 (d, *J* = 8.0 Hz, 2H, H^c), 2.57 (s, 3H, H^a), 2.09 (s, 6H, H^d).

Labelling expected against signal at δ 7.82 ppm and δ 7.67 ppm, measured against signal at δ 2.57 ppm.

Run 1

(a) 52.1 mg, (b) D_c = 8%, D_b = 77%

Run 2

(a) 52.1 mg, (b) D_c = %6, D_b = 82%

Run 3

(a) 52.1 mg, (b) D_c = 3%, D_b = 76%

Average Incorporation = D_c = 6%, D_b = 78%

*8.13.6 Investigating Selectivity at Reduced Catalyst Loading (**Scheme 4.10**)*

To a three-necked 100 mL round-bottom flask, fitted with two stopcocks, was added 4-methyl-*N*-(*p*-tolyl)benzenesulfonamide **223g** (56.2 mg, 0.215 mmol, 1.00 eq) and complex **218** (3.20 mg, 0.00215 mmol, 1 mol%). The mixture was dissolved in chlorobenzene (2.5 mL) and the flask placed in a heating block, pre-set to 25 °C. The atmosphere in the flask was exchanged

via three vacuum/D_2 cycles, with the system then being isolated upon the third influx of deuterium. The reaction mixture was then stirred at 25 °C for 16 h, unless stated otherwise. The reaction mixture was then loaded directly onto a silica column, the chlorobenzene eluted with petroleum ether, and the deuterated product eluted with Et_2O and concentrated *in vacuo*. The level of deuteration was then calculated as described in *General Procedure D*. Experiment carried out as single run.

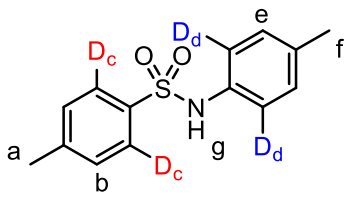

d-223g

^{1}H NMR (400 MHz, $CDCl_3$): δ 7.60 (d, *J* = 8.1 Hz, 2H, H^c), 7.19 (d, *J* = 8.1 Hz, 2H, H^b), 7.01 (d, *J* = 8.5 Hz, 2H, H^c), 6.92 (d, *J* = 8.5 Hz, 2H, H^d), 6.41 (bs, 1H, H^g), 2.36 (s, 3H, H^a), 2.25 (s, 3H, H^f).

Labelling expected against signal at δ 7.60 ppm and δ 6.92 ppm, measured against signal at δ 2.25 ppm.

Run 1

(a) 56.2 mg, (b) D_c = 47%, D_d = 45%

8.14 Applying an NHC-Py Type Catalyst in the HIE of Other Pharmaceutically Relevant Sulfur Based Groups

8.14.1 Sulfoximine Synthesis

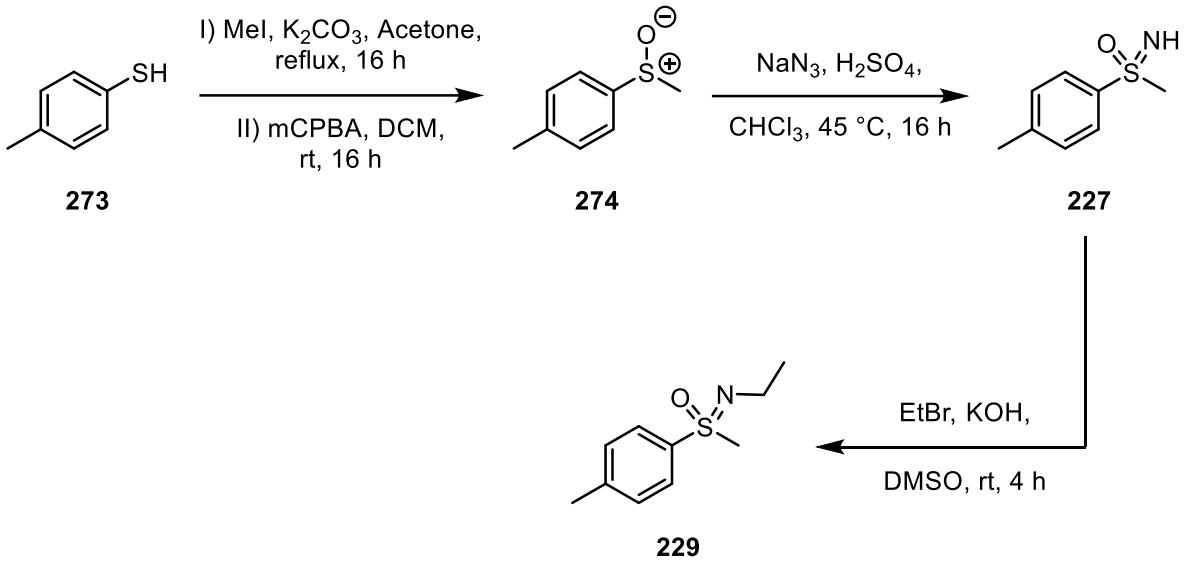

Scheme 8.5

1-Methyl-4-(methylsulfinyl)benzene **270**[185]

A 500 mL round-bottom flask was charged with 4-methylthiophenol **273** (2.66 g, 21.4 mmol, 1.00 eq), potassium carbonate (4.34 g, 32.1 mmol, 1.50 eq) and acetone (60.0 mL). To this was added methyl iodide (1.73 mL, 27.8 mmol, 1.30 eq), and the reaction refluxed for 16 h. The reaction mixture was cooled to room temperature and filtered. The filtrate was concentrated *in vacuo* to yield the methylated product. This was immediately redissolved in DCM (60.0 mL) and the solution cooled to 0 °C. To this was added *m*CPBA (4.80 g, 27.8 mmol, 1.30 eq), portionwise. The reaction was stirred at room temperature overnight, at which point it was transferred to a separating funnel. The mixture was washed once with a saturated solution of aqueous sodium bicarbonate. The organic layer was dried over sodium sulfate, filtered, and concentrated *in vacuo*. The residue was purified by column chromatography, eluting with 10%

MeOH/DCM. 1-Methyl-4-(methylsulfinyl)benzene **274** (2.72 g, 17.6 mmol, 82% yield) was afforded as a white solid.

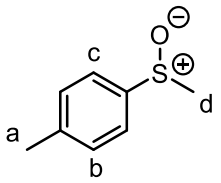

274

Melting Point: 51-52 °C (lit:[185] 52-54 °C).

IR (neat, cm^{-1}): 3462, 3041, 2916, 1597, 1494, 1409, 1085, 1035, 1014.

^{1}H NMR (400 MHz, $CDCl_3$): δ 7.52 (d, *J* = 8.0 Hz, 2H, H^c), 7.31 (d, *J* = 8.0 Hz, 2H, H^b), 2.68 (s, 3H, H^d), 2.40 (s, 3H, H^a).

^{13}C NMR (101 MHz, $CDCl_3$) δ 142.3, 141.4, 130.0, 123.5, 43.9, 21.3.

Imino(methyl)(p-tolyl)-λ^6-sulfanone **227**[186]

To a 250 mL round-bottom flask was added **274** (2.50 g, 16.2 mmol, 1.00 eq), sodium azide (3.16 g, 48.6 mmol, 3.00 eq) and chloroform (55.0 mL). This suspension was cooled to 0 °C, and 98% sulfuric acid (4.52 mL, 84.2 mmol, 5.20 eq) was added, slowly. The reaction mixture was then heated to 45 °C for 16 h. The suspension was cooled to 0 °C and a 2 M solution of aqueous sodium hydroxide (200 mL) was added and the mixture transferred to a separating funnel. Once separated, the aqueous layer was washed a further two times with chloroform. The basic aqueous layer was then discarded. The organic phases were combined and washed three times with 2 M aqueous hydrochloric acid and discarded. The acidic aqueous layer was washed with a further two amounts of chloroform, which were also discarded. The acidic aqueous solution was basified with solid sodium bicarbonate. The resulting suspension was

extracted three times with chloroform. The organic layers were combined, dried over sodium sulfate, filtered, and concentrated *in vacuo*. The residue was purified by column chromatography, eluting with 50% EtOAc/petroleum ether. Imino(methyl)(*p*-tolyl)-λ^6-sulfanone **227** (2.15g, 12.7 mmol, 78% yield).

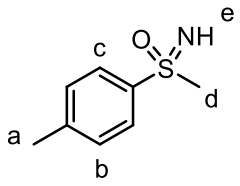

227

Melting Point: 66-68 °C (lit:[186] 69-70 °C)

IR (neat, cm^{-1}): 3415, 3277, 2924, 1595, 1492, 1408, 1317, 1217, 1093, 1024.

^{1}H NMR (400 MHz, CDCl$_3$): δ 7.87 (d, *J* = 8.4 Hz, 2H, H^c), 8.32 (d, *J* = 8.4 Hz, 2H, H^b), 3.07 (s, 3H, H^d), 2.61 (bs, 1H, H^e), 2.42 (s, 3H, H^a).

^{13}C NMR (101 MHz, CDCl$_3$) δ 144.0, 140.8, 130.0, 127.9, 46.5, 21.6.

(Ethylimino)(methyl)(p-tolyl)-λ^6-sulfanone **229**[187]

To a flame-dried Schlenk tube was added **227** (0.800 g, 4.72 mmol, 1.00 eq) and KOH (0.531 g, 9.45 mmol, 2.00 eq). The mixture was dissolved in DMSO (5.0 mL) and ethyl bromide (0.52 mL, 7.08 mmol, 1.50 eq) was added. The reaction was stirred at room temperature for 4 h. The reaction mixture was diluted with water (100 mL) and extracted three times into DCM. The organic layers were combined, dried over sodium sulfate, filtered, and concentrated *in vacuo*. The compound was purified by column chromatography, eluting with 30% acetone/petroleum ether. (Ethylimino)(methyl)(*p*-tolyl)-λ^6-sulfanone **229** (0.856 g, 4.34 mmol, 92% yield) as a colourless oil.

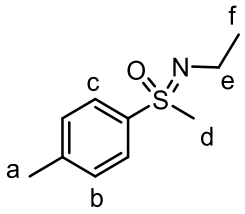

229

IR (neat, cm^{-1}): 2966, 2924, 2864, 1595, 1317, 1290, 1224, 1139, 1116, 1089.

^{1}H NMR (400 MHz, $CDCl_3$): δ 7.76 (d, *J* = 8.1 Hz, 2H, H^c), 7.33 (d, *J* = 8.1 Hz, 2H, H^b), 3.04 (s, 3H, H^d), 3.03-2.94 (m, 1H, H^e), 2.88-2.77 (m, 1H, H^e), 2.42 (s, 3H, H^a), 1.16 (t, *J* = 7.4 Hz, 3H, H^f).

^{13}C NMR (101 MHz, $CDCl_3$) δ 143.4, 136.4, 129.9, 128.5, 45.1, 38.3, 21.3, 18.1.

8.14.2 Sulfoximine Labelling with an NHC-Py Type Catalyst

All reactions were run as described in *General Procedure I*. Data are reported as: (a) amount of substrate, and (b) Incorporation.

Imino(methyl)(p-tolyl)-λ^6-sulfanone **227** (**Scheme 4.14**)

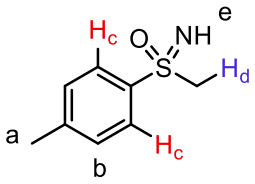

d-227

^{1}H NMR (400 MHz, $CDCl_3$): δ 7.87 (d, *J* = 8.4 Hz, 2H, H^c), 8.32 (d, *J* = 8.4 Hz, 2H, H^b), 3.07 (s, 3H, H^d), 2.61 (bs, 1H, H^e), 2.42 (s, 3H, H^a).

Labelling expected against signal at δ 7.87 ppm, and δ 3.07 ppm, measured against signal at δ 2.42 ppm.

Run 1

(a) 35.7 mg, (b) D_c = 73%, D_d = 0%

Run 2

(a) 35.7 mg, (b) D_c = 75%, D_d = 0%

Run 3

(a) 35.7 mg, (b) D_c = 71%, D_d = 0%

Average Incorporation = D_c = 73%, D_d = 0%

(Ethylimino)(methyl)(p-tolyl)-λ^6-sulfanone **221** (**Scheme 4.15**)

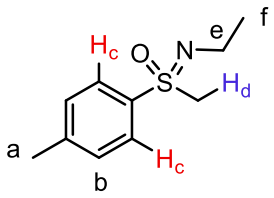

d-221

^{1}H NMR (400 MHz, $CDCl_3$): δ 7.76 (d, *J* = 8.1 Hz, 2H, H^c), 7.33 (d, *J* = 8.1 Hz, 2H, H^b), 3.04 (s, 3H, H^d), 3.03-2.94 (m, 1H, H^e), 2.88-2.77 (m, 1H, H^e), 2.42 (s, 3H, H^a), 1.16 (t, *J* = 7.4 Hz, 3H, H^f).

Labelling expected against signal at δ 7.76 ppm, and δ 3.04 ppm, measured against signal at δ 2.42 ppm.

Run 1

(a) 42.4 mg, (b) D_c = 97%, D_d = 15%

Run 2

(a) 42.2 mg, (b) D_c = 97%, D_d = 8%

Average Incorporation = D_c = 97%, D_d = 12%

(Ethylimino)(methyl)(p-tolyl)-λ^6-sulfanone **229** *Rate Study* (**Figure 4.13**)

A flame-dried, two-neck 250 mL round-bottom flask fitted with a stopcock was placed under an inert atmosphere. The flask was charged with **229** (212 mg, 1.08 mmol, 1 eq) and complex **218** (79.9 mg, 0.0538 mmol, 5 mol%). The mixture was dissolved in chlorobenzene (25.0 mL) and the flask was placed in an heating block preheated to 25 °C. The atmosphere was exchanged *via* two vacuum/D_2 cycles and the timer started. Aliquots of 0.3 mL were withdrawn at each time point and injected into a vial containing acetonitrile (0.5 mL). Each solution was then concentrated *in vacuo* and the residues analysed by ^{1}H NMR spectroscopy. The incorporations were calculated as described in *General Procedure D*. The data are presented in **Table 8.8**.

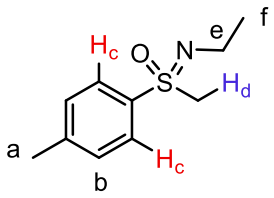

d-229

^{1}H NMR (400 MHz, $CDCl_3$): δ 7.76 (d, *J* = 8.1 Hz, 2H, H^c), 7.33 (d, *J* = 8.1 Hz, 2H, H^b), 3.04 (s, 3H, H^d), 3.03-2.94 (m, 1H, H^e), 2.88-2.77 (m, 1H, H^e), 2.42 (s, 3H, H^a), 1.16 (t, *J* = 7.4 Hz, 3H, H^f).

Labelling expected against signal at δ 7.76 ppm, and δ 3.04 ppm, measured against signal at δ 2.42 ppm.

Table 8.8

Entry	Time (mins)	%D_c	%D_d
1	5	5	3
2	10	9	7
3	15	8	5
4	20	9	5
5	30	9	4
6	40	23	4
7	60	49	3
8	90	77	4
9	120	88	5
10	180	94	4
11	240	96	5
12	360	96	5
13	480	96	5
14	540	96	6
15	1080	97	6

8.14.3 Sulfoximine Labelling with a Monodentate NHC/Phosphine Type Catalyst

Imino(methyl)(p-tolyl)-λ^6-sulfanone **227** (**Scheme 4.16**)

To a 100 mL round-bottom flask, fitted with two stopcocks, was added **227** (35.7 mg, 0.215 mmol, 1.00 eq) and complex **75** (18.7 mg, 0.108 mmol, 5 mol%). The mixture was dissolved in DCM (2.5 mL). The solution was cooled to -78 °C, and the atmosphere in the flask was

exchanged with three vacuum/D_2 cycles, with the system being isolated upon the third influx of deuterium. The flask was immediately placed in a heating block, pre-set to 25 °C. The reaction was stirred at 25 °C for 16 h. The reaction mixture was concentrated *in vacuo*. The extent of deuteration was assessed by ^{1}H NMR. The incorporations were calculated as described in *General Procedure D*.

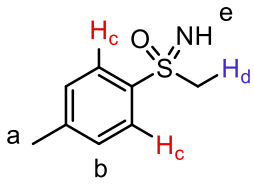

d-227

^{1}H NMR (400 MHz, $CDCl_3$): δ 7.87 (d, *J* = 8.4 Hz, 2H, H^c), 8.32 (d, *J* = 8.4 Hz, 2H, H^b), 3.07 (s, 3H, H^d), 2.61 (bs, 1H, H^e), 2.42 (s, 3H, H^a).

Labelling expected against signal at δ 7.87 ppm, and δ 3.07 ppm, measured against signal at δ 2.42 ppm.

Run 1

(a) D_c = 96%, D_d = 22%

Run 2

(a) D_c = 96%, D_d = 20%

Run 3

(a) D_c = 85%, D_d = 29%

Average Incorporation = D_c = 93%, D_d = 24%

(Ethylimino)(methyl)(p-tolyl)-λ^6-sulfanone **229**

To a 100 mL round-bottom flask, fitted with two stopcocks, was added **229** (42.4 mg, 0.215 mmol, 1.00 eq) and complex **75** (18.7 mg, 0.108 mmol, 5 mol%). The mixture was dissolved in DCM (2.5 mL). The solution was cooled to -78 °C, and the atmosphere in the flask was exchanged with three vacuum/D_2 cycles, with the system being isolated upon the third influx of deuterium. The flask was immediately placed in a heating block, pre-set to 25 °C. The reaction was stirred at 25 °C for 16 h. The reaction mixture was concentrated *in vacuo*. The extent of deuteration was assessed by ^{1}H NMR. The incorporations were calculated as described in *General Procedure D*.

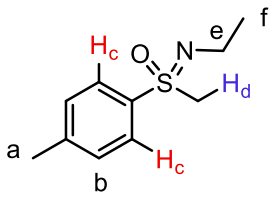

d-229

^{1}H NMR (400 MHz, $CDCl_3$): δ 7.76 (d, *J* = 8.1 Hz, 2H, H^c), 7.33 (d, *J* = 8.1 Hz, 2H, H^b), 3.04 (s, 3H, H^d), 3.03-2.94 (m, 1H, H^e), 2.88-2.77 (m, 1H, H^e), 2.42 (s, 3H, H^a), 1.16 (t, *J* = 7.4 Hz, 3H, H^f).

Labelling expected against signal at δ 7.76 ppm, and δ 3.04 ppm, measured against signal at δ 2.42 ppm.

Run 1

(a) D_c = 92%, D_d = 53%

Run 2

(a) D_c = 96%, D_d = 48%

Run 3

(a) D_c = 95%, D_d = 53%

Average Incorporation = D_c = 94%, D_d = 51%

8.15 Investigating Ether Directed Labelling

8.15.1 Substrate Synthesis

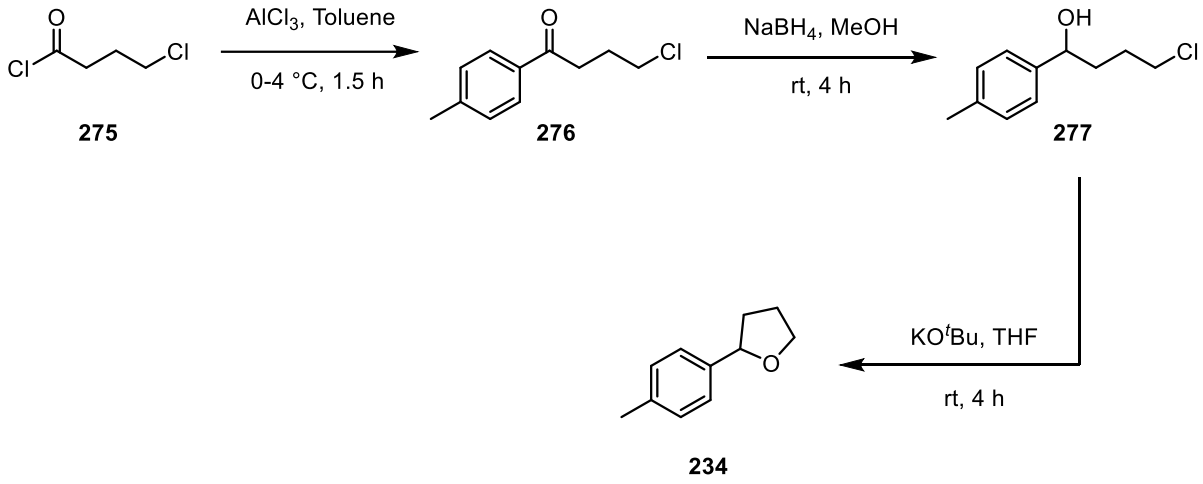

Scheme 8.6

4-Chloro-1-(p-tolyl)butan-1-one **276**[188]

To a flame-dried, 3-necked, 250 mL round-bottom flask, equipped with an internal thermometer, was added anhydrous aluminium chloride (10.0 g, 74.0 mmol, 1.00 eq) and dry toluene (75.0 mL). The flask was cooled to 0 °C using an ice bath. In a separate flame-dried, 2-necked 50 mL round-bottom flask was added 4-chlorobutyryl chloride **275** (8.40 mL, 74.0 mmol, 1.00 eq) and dry toluene (20.0 mL). This solution was added, dropwise, into the suspension of aluminium chloride, being careful not to let the temperature raise above 4 °C. Once the addition was complete, the reaction was stirred at 1-2 °C for a further 1.5 h. At this point, the reaction mixture was poured into 250 mL of ice/water, and subsequently diluted with

100 mL of a 2 M aqueous hydrochloric acid solution, to dissolve the resulting aluminium salts. The mixture was transferred to a separating funnel, and the acidic aqueous layer washed three times with toluene. The organic layers were combined, and washed with three amounts of a saturated solution of aqueous sodium bicarbonate. The organic layer was collected, dried over sodium sulfate, filtered, and concentrated *in vacuo*. 4-Chloro-1-(*p*-tolyl)butan-1-one **276** (14.5 g, 73.7 mmol, 99.6% yield) isolated as a colourless oil. The residue was taken on without any further purification.

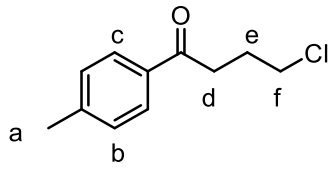

276

IR (neat, cm^{-1}): 2953, 2868, 258, 1512, 1442, 1305, 1178, 1060.

^{1}H NMR (400 MHz, $CDCl_3$): δ 7.66 (d, *J* = 8.2 Hz, 2H, H^c), 7.25 (d, *J* = 8.2 Hz, 2H, H^b), 3.66 (t, *J* = 6.3 Hz, 2H, H^d), 3.13 (t, *J* = 7.0 Hz, 2H, H^f), 2.40 (s, 3H, H^a), 2.21 (p, *J* = 6.6 Hz, 2 H, H^e).

^{13}C NMR (101 MHz, $CDCl_3$) δ 198.5, 144.0, 134.3, 129.3, 128.2, 44.7, 35.2, 26.9, 21.6.

4-Chloro-1-(p-tolyl)butan-1-ol **277**[189]

To a 500 mL round-bottom flask was added **276** (8.00 g, 40.0 mmol, 1.00 eq) and methanol (130 mL). This was cooled to 0 °C and sodium borohydride (2.31 g, 60.0 mmol, 1.50 eq) was added, portionwise. The reaction was stirred at room temperature for 4 h. The mixture was quenched with a solution of 2 M aqueous hydrochloric acid (50 mL), and the majority of the methanol removed *in vacuo*. The mixture was further diluted with water (250 mL) and extracted three times with ethyl acetate. The organic layers were combined, dried over sodium

sulfate, filtered, and concentrated *in vacuo*. The residue was purified by column chromatography, eluting with 50% DCM in petroleum ether. 4-Chloro-1-(*p*-tolyl)butan-1-ol **277** (4.29 g, 21.6 mmol, 54% yield) isolated as a colourless liquid.

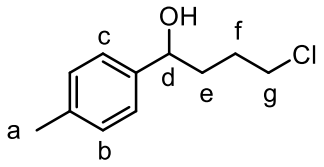

277

IR (neat, cm^{-1}): 2960, 2922, 2341, 1680, 1606, 1446, 1408, 1363, 1319, 1228, 1180.

^{1}H NMR (400 MHz, $CDCl_3$): δ 7.22 (d, *J* = 7.8 Hz, 2H, H^c), 7.15 (d, *J* = 7.8 Hz, 2H, H^b), 4.66 (t, *J* = 6.6 Hz, 1H, H^d), 3.58-3.49 (m, 2H, H^g), 2.33 (s, 3H, H^a) 1.95-1.67 (m, 4H, H^e + H^f).

^{13}C NMR (101 MHz, $CDCl_3$) δ 141.4, 137.5, 129.3, 125.8, 73.8, 45.0, 36.1, 29.0, 21.4.

HRMS: m/z calculated for $[M-H]^+$ $C_{11}H_{14}ClO$: 197.0733; found 197.0732.

2-(p-Tolyl)tetrahydrofuran **234**[190]

To a flame-dried, 3-necked, 250 mL round-bottom flask was added **274** (2.00 g, 10.0 mmol, 1.00 eq) and potassium *tert*-butoxide (2.46 g, 20.0 mmol, 2.00 eq). To the mixture was added dry THF (100 mL) and the reaction stirred at room temperature for 4 h. The reaction mixture was concentrated in vacuo, and equal amounts of diethyl ether and water added. The mixture was separated, and the aqueous layer washed twice with further amounts of diethyl ether. The organic layers were combined, dried over sodium sulfate, filtered, and concentrated *in vacuo*. The residue was purified by column chromatography, eluting with 0-10% diethyl ether/petroleum ether. 2-(*p*-Tolyl)tetrahydrofuran **234** (1.63 g, 10.0 mmol, quantitative yield) was isolated as a colourless liquid.

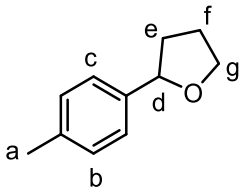

226

IR (neat, cm^{-1}): In Progress.

^{1}H NMR (400 MHz, CDCl$_3$): δ 7.21 (d, *J* = 8.0 Hz, 2H, H^{c}), 7.12 (d, *J* = 8.0 Hz, 2H, H^{b}), 4.84 (t, *J* = 7.2 Hz, 1H, H^{d}), 4.07 (ddd, $^{2}J_{HH}$ = 8.1 Hz, *J* = 7.8 Hz, *J* = 6.3 Hz, 1H, H^{g}), 3.90 (ddd, $^{2}J_{HH}$ = 8.1 Hz, *J* = 7.8 Hz, *J* = 6.3 Hz, 1H, H^{g}), 2.32 (s, 3H, H^{a}), 2.31-2.23 (m, 1H, H^{f}), 2.05-1.92 (m, 2H, H^{e}), 1.82-1.73 (m, 1H, H^{f}).

^{13}C NMR (101 MHz, CDCl$_3$) δ.140.6, 136.9, 129.2, 125.8, 80.8, 68.8, 34.8, 26.2, 21.3.

1-Methoxy-4-(methoxymethyl)benzene **235a**[191]

To a flame-dried, 3-necked, 250 mL round-bottom flask was added *p*-methoxybenzyl alcohol (1.40 mL, 10.0 mmol, 1.00 eq) and dry THF (30.0 mL). The solution was cooled to 0 °C and 60% sodium hydride (0.523 g, 13.0 mmol 1.30 eq) was added. The reaction was stirred at 0 °C for 0.5 h. Methyl iodide (0.93 mL, 15.0 mmol, 1.50 eq) was added, and the reaction stirred at room temperature for 2 h. The reaction was concentrated *in vacuo*, and equal amounts of diethyl ether and water were added. The layers were separated, and the aqueous layer washed twice with further amounts of diethyl ether. The organic layers were combined, dried over sodium sulfate, filtered, and concentrated *in vacuo*. The residue was purified by column chromatography, eluting with 5% diethyl ether/petroleum ether. 1-Methoxy-4-(methoxymethyl)benzene **235a** (1.20 g, 7.88 mmol, 79% yield) isolated as a colourless liquid.

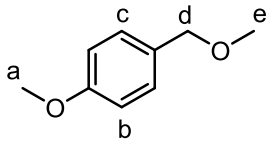

235a

IR (neat, cm^{-1}): 2981, 2931, 2835, 1610, 1510, 1463, 1381, 1300, 1244, 1172, 1089.

^{1}H NMR (400 MHz, $CDCl_3$): δ 7.24 (d, *J* = 8.7 Hz, 2H, H^c), 6.87 (d, *J* = 8.7 Hz, 2H, H^b), 4.37 (s, 2H, H^d), 3.79 (s, 3H, H^a), 3.34 (s, 3H, H^e).

^{13}C NMR (101 MHz, $CDCl_3$) δ 159.2, 130.2, 129.2, 113.6, 74.2, 57.6, 55.0.

1-(1-Methoxyethyl)-4-methylbenzene **235b**[192]

To a flame-dried, 3-necked, 250 mL round-bottom flask was added 1-(*p*-tolyl)ethan-1-ol (1.50 mL, 11.2 mmol, 1.00 eq) and dry THF (20.0 mL). The solution was cooled to 0 °C and 60% sodium hydride (0.490 g, 12.3 mmol 1.10 eq) was added. The reaction was stirred at 0 °C for 1 h. Methyl iodide (0.84 mL, 13.5 mmol, 1.20 eq) was added, and the reaction stirred at room temperature for 4 h. The reaction was concentrated *in vacuo*, and equal amounts of diethyl ether and water were added. The layers were separated, and the aqueous layer washed twice with further amounts of diethyl ether. The organic layers were combined, dried over sodium sulfate, filtered, and concentrated *in vacuo*. The residue was purified by column chromatography, eluting with 5% diethyl ether/petroleum ether. 1-(1-Methoxyethyl)-4-methylbenzene **235b** (1.21 g, 8.05 mmol, 72% yield) isolated as a colourless liquid.

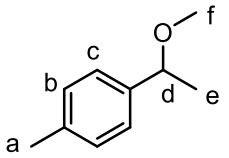

235b

IR (neat, cm^{-1}): 2976, 2926, 2818, 1514, 1448, 1369, 1219, 1209, 1107, 1083.

^{1}H NMR (400 MHz, $CDCl_3$): δ 7.18 (d, *J* = 8.0 Hz, 2H, H^c), 7.14 (d, *J* = 8.0 Hz, 2H, H^b), 4.24 (q, *J* = 6.4 Hz, 1H, H^d), 3.19 (s, 3H, H^f), 2.33 (s, 3H, H^a), 1.41 (d, *J* = 6.4 Hz, 3H, H^e).

^{13}C NMR (101 MHz, $CDCl_3$) δ 140.6, 137.0, 129.1, 126.2, 79.5, 56.2, 23.9, 21.1.

HRMS (Positive ESI): m/z calculated for $[M]^+$ $C_9H_{11}O$: 135.0810; found: 135.0808.

(2-Methoxypropan-2-yl)benzene **235c**[193]

To a flame-dried, 3-necked, 100 mL round-bottom flask was added 2-phenylpropan-2-ol (1.00 g, 7.34 mmol, 1.00 eq) and dry THF (15.0 mL). The solution was cooled to 0 °C and 60% sodium hydride (0.352 g, 8.81 mmol 1.20 eq) was added. The reaction was stirred at 0 °C for 1 h. Methyl iodide (0.59 mL, 9.54 mmol, 1.30 eq) was added, and the reaction stirred at room temperature for 16 h. The reaction was concentrated *in vacuo*, and equal amounts of diethyl ether and water were added. The layers were separated, and the aqueous layer washed twice with further amounts of diethyl ether. The organic layers were combined, dried over sodium sulfate, filtered, and concentrated *in vacuo*. The residue was purified by column chromatography, eluting with 10% diethyl ether/petroleum ether. (2-Methoxypropan-2-yl)benzene **235c** (0.989 g, 6.58 mmol, 90% yield) isolated as a colourless liquid.

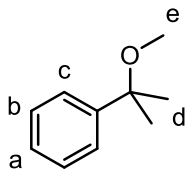

235c

IR (neat, cm^{-1}): 3061, 2978, 2933, 2823, 1492, 1446, 1377, 1361, 1259, 1170, 1070.

^{1}H NMR (400 MHz, $CDCl_3$): δ 7.41-7.37 (m, 2H, H^c), 7.35-7.30 (m, 2H, H^b), 7.26-7.20 (m, 1H, H^a), 3.06 (s, 3H, H^e), 1.52 (s, 6H, H^d).

^{13}C NMR (101 MHz, $CDCl_3$) δ 146.0, 128.3, 126.9, 125.8, 76.8, 50.6, 28.0.

HRMS: No fragment ions yet observed.

1-Methoxy-1,2,3,4-tetrahydronaphthalene **235d**[194]

To a flame-dried, 3-necked, 100 mL round-bottom flask was added tetrahydronaphthol (075 mL, 5.51 mmol, 1.00 eq) and dry THF (20.0 mL). The solution was cooled to 0 °C and 60% sodium hydride (0.242 g, 6.07 mmol, 1.10 eq) was added. The reaction was stirred at 0 °C for 0.5 h. Methyl iodide (0.45 mL, 7.17 mmol, 1.30 eq) was added, and the reaction stirred at room temperature for 5 h. The reaction was concentrated *in vacuo*, and equal amounts of diethyl ether and water were added. The layers were separated, and the aqueous layer washed twice with further amounts of diethyl ether. The organic layers were combined, dried over sodium sulfate, filtered, and concentrated *in vacuo*. The residue was purified by column chromatography, eluting with 10% diethyl ether/petroleum ether. 1-Methoxy-1,2,3,4-tetrahydronaphthalene **235d** (0.821 g, 5.07 mmol, 92% yield) isolated as a colourless liquid.

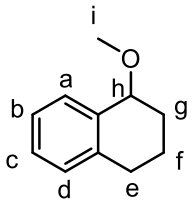

235d

IR (neat, cm^{-1}): 2935, 2816, 1681, 1600, 1454, 1284, 1257, 1083.

^{1}H NMR (400 MHz, $CDCl_3$): δ 7.36-7.31 (m, 1H, H^a), 7.19-7.14 (m, 2H, H^b + H^c), 7.10-7.05 (m, 1H, H^d), 4.30 (t, *J* = 4.8 Hz, 1H, H^h), 3.42 (s, 3H, H^i), 2.87-2.77 (m, 1H, H^g), 2.75-2.65 (m, 1H, H^g), 2.07-1.83 (m, 3H, H^e + H^f), 1.78-1.67 (m, 1H, H^f).

^{13}C NMR (101 MHz, $CDCl_3$) δ 129.5, 129.1, 127.7, 127.4, 126.8, 125.8, 77.0, 56.3, 29.3, 27.6, 18.8.

5-Methoxy-6,7,8,9-tetrahydro-5H-benzo[7]annulene **235e**

To 100 mL round-bottom flask was added benzosuberone (2.00 mL, 13.3 mmol, 1.00 eq) and ethanol (13.0 mL). The mixture was cooled to 0 °C, and sodium borohydride (0.531 g, 14.0 mmol, 1.05 eq) was added in one portion. The reaction was stirred at room temperature for 4 h. The reaction was quenched with a 2 M solution of aqueous hydrochloric acid (100 mL). The mixture was transferred to a separatory funnel and washed three times with diethyl ether. The organic layers were combined, dried over sodium sulfate, filtered, and concentrated *in vacuo*. The residue was transferred to a 3-necked 250 mL round-bottom flask and put under inert atmosphere with 5 vacuum/argon cycles. To this was added dry THF (30 mL), and the resulting solution cooled to 0 °C. To the chilled solution was added 60% sodium hydride (0.692 g, 17.3 mmol, 1.30 eq) and the reaction stirred at 0 °C for 2 h. Methyl iodide (1.24 mL, 20.0 mmol,1.50 eq) was added and the reaction stirred at room temperature for 16 h. The reaction was diluted

with water (200 mL) and extracted three times into diethyl ether. The organic layers were combined, dried over sodium sulfate, filtered, and concentrated *in vacuo*. The residue was purified by column chromatography, eluting with 5% diethyl ether/petroleum ether. *5*-Methoxy-6,7,8,9-tetrahydro-5H-benzo[7]annulene **235e** (1.33 g, 7.55 mmol, 57% yield) was isolated as a colourless liquid.

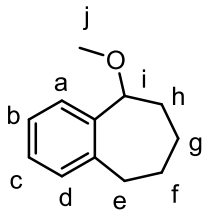

235e

IR (neat, cm^{-1}): 2920, 2850, 2818, 1444, 1112, 1085.

^{1}H NMR (400 MHz, $CDCl_3$): δ 7.31-7.28 (m, 1H, H^a),7.22-7.15 (m, 2H, H^b + H^c), 7.14-7.10 (m, 1H, H^d), 4.36-4.31 (m, 1H, H^i), 3.34 (s, 3H, H^j), 3.08-2.96 (m, 1H, H^h), 2.74-2.63 (m, 1H, H^h), 2.14-2.02 (m, 1H, alkyl CH), 1.97-1.85 (m, 2H, alkyl CH_2), 1.81-1.71 (m, 1H, alkyl CH), 1.70-1.60 (m, 2H, alkyl CH_2).

^{13}C NMR (101 MHz, $CDCl_3$) δ 142.1, 141.7, 129.7, 127.3, 127.0, 125.9, 84.0, 56.9, 35.6, 33.8, 28.2, 27.2.

HRM: m/z calculated for $[M\text{-}OMe]^+$ $C_{11}H_{13}^+$: 145.1012; found: 145.1002.

1-(Benzyloxy)-4-methoxybenzene **235f**[195]

To a 100 mL round-bottom flask was added 4-methoxyphenol (1.00 g, 9.24 mmol, 1.00 eq), potassium carbonate (7.92 g, 13.9 mmol, 1.50 eq), and acetonitrile (30.0 mL). To this was added benzyl bromide (1.30 mL, 11.1 mmol, 1.20 eq), and the suspension stirred at reflux for 16 h. The reaction was cooled to room temperature and filtered. The filtrate was concentrated

in vacuo, and the residue purified by column chromatography, eluting with 30% diethyl ether/petroleum ether. 1-(Benzyloxy)-4-methoxybenzene **235f** (1.97 g, 9.24 mmol quantitative yield) was isolated as a white solid.

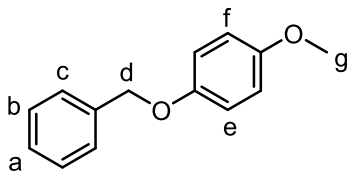

235f

Melting Point: 75-77 °C (lit:[195] 75-77 °C)

IR (neat, cm^{-1}): 2995, 2833, 1504, 1439, 1290, 1222, 1111, 1034, 1009.

^{1}H NMR (400 MHz, $CDCl_3$): δ 7.44-7.39 (m, 2H, H^c) 7.38-7.33 (m, 2H, H^b), 7.32-7.27 (m, 1H, H^a), 6.90 (d, *J* = 9.0 Hz, 2H, H^e), 6.81 (d, *J* = 9.0 Hz, 2H, H^f), 5.00 (s, 2H, H^d), 3.75 (s, 3H, H^g).

^{13}C NMR (101 MHz, $CDCl_3$) δ 154.2, 153.2, 137.5, 128.7, 128.0, 127.7, 116.1, 114.8, 70.9, 55.9.

1-Chloro-4-(2-methoxyethyl)benzene **235g**[196]

To a flame-dried, 3-necked, 100 mL round-bottom flask was added 2-(4-chlorophenyl)ethan-1-ol (1.50 mL, 9.57 mmol, 1.00 eq) and dry THF (20.0 mL). The solution was cooled to 0 °C and 60% sodium hydride (0.420 g, 10.5 mmol, 1.10 eq) was added. The reaction was stirred at 0 °C for 0.5 h. Methyl iodide (070 mL, 11.5 mmol, 1.20 eq) was added, and the reaction stirred at room temperature for 16 h. The reaction was concentrated *in vacuo*, and equal amounts of diethyl ether and water were added. The layers were separated, and the aqueous layer washed twice with further amounts of diethyl ether. The organic layers were combined, dried over

sodium sulfate, filtered, and concentrated *in vacuo*. The residue was purified by column chromatography, eluting with 20% diethyl ether/petroleum ether. 1-Chloro-4-(2-methoxyethyl)benzene **235g** (1.58 g, 9.26 mmol, 97 % yield) isolated as a colourless oil.

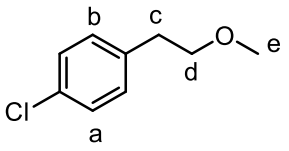

235g

IR (neat, cm^{-1}): 2924, 2868, 1490, 1112, 1089.

^{1}H NMR (400 MHz, CDCl$_3$): δ 7.24 (d, *J* = 8.4 Hz, 2H, H^{b}), 7.13 (d, *J* = 8.5 Hz, 2H, H^{a}), 3.56 (t, *J* = 7.0 Hz, 2H, H^{d}), 3.33 (s, 3H, H^{e}), 2.83 (t, *J* = 7.0 Hz, 2H, H^{c}).

^{13}C NMR (101 MHz, CDCl$_3$) δ 137.7, 131.9, 130.2, 128.4, 73.3, 58.6, 35.6.

(Benzyloxy)tri-iso-propylsilane **235i**[197]

To a flame-dried 250 mL round-bottom flask was added benzyl alcohol (3.00 mL, 26.7 mmol, 1.00 eq), triethylamine (3.60 mL, 40.0 mmol, 1.50 eq), and THF (30.0 mL). The solution was cooled to 0 °C and TIPSCl (7.5 mL, 34.7 mmol, 1.30 eq). The reaction was stirred at room temperature for 16 h. The solution was concentrated *in vacuo*, and equal amounts of diethyl ether and water were added. The layers were separated, and the aqueous layer washed twice with further amounts of diethyl ether. The organic layers were combined, dried over sodium sulfate, filtered, and concentrated *in vacuo*. The residue was purified by column chromatography, eluting with 2% diethyl ether/petroleum ether. (Benzyloxy)tri-*iso*-propylsilane **235i** (6.85 g, 25.9 mmol, 97% yield) was isolated as a colourless liquid.

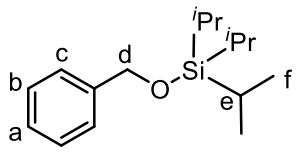

227i

IR (neat, cm^{-1}): 2943, 2866, 2358, 1462, 1384, 1012, 993.

^{1}H NMR (400 MHz, $CDCl_3$): δ 7.38-7.35 (m, 2H, H^c), 7.35-7.32 (m, 2H, H^b), 7.31-7.25 (m, 1H, H^a), 4.69 (s, 2H, H^d), 1.26 (m, 3H, H^e), 1.11-1.06 (m, 18H, H^f).

^{13}C NMR (101 MHz, $CDCl_3$) δ 141.1, 128.7, 127.1, 125.9, 65.3, 17.9, 12.6.

*8.15.2 Ether Directed Labelling – Optimisation (**Table 5.1**)*

To a three-necked 100 mL round-bottom flask, fitted with two stopcocks, was added 2-(*p*-tolyl)tetrahydrofuran **234** (34.9 mg, 0.215 mmol, 1.00 eq) and complex **175**. The mixture was dissolved in chlorobenzene or MTBE (2.5 mL) and the flask placed in a heating block, pre-set to 25 °C. The atmosphere in the flask was exchanged *via* three vacuum/D_2 cycles, with the system then being isolated upon the third influx of deuterium. The reaction mixture was then stirred at 25 °C for the time specified. The reaction mixture was then loaded directly onto a silica column, the chlorobenzene eluted with petroleum ether, and the deuterated product eluted with Et_2O and concentrated *in vacuo*. The level of deuteration was then calculated as described in *General Procedure D*. Data are reported as: (a) amount of catalyst, and (b) incorporation.

2-(p-Tolyl)tetrahydrofuran **234**

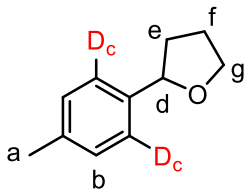

d-234

^{1}H NMR (400 MHz, $CDCl_3$): δ 7.21 (d, *J* = 8.0 Hz, 2H, H^c), 7.12 (d, *J* = 8.0 Hz, 2H, H^b), 4.84 (t, *J* = 7.2 Hz, 1H, H^d), 4.07 (ddd, $^2J_{HH}$ = 8.1 Hz, *J* = 7.8 Hz, *J* = 6.3 Hz, 1H, H^g), 3.90 (ddd, $^2J_{HH}$ = 8.1 Hz, *J* = 7.8 Hz, *J* = 6.3 Hz, 1H, H^g), 2.32 (s, 3H, H^a), 2.31-2.23 (m, 1H, H^f), 2.05-1.92 (m, 2H, H^e), 1.82-1.73 (m, 1H, H^f).

Labelling expected against signal at δ 7.21 ppm, measured against signal at 2.32 ppm.

5 mol% 175, 16 h, Chlorobenzene, Entry 1

Run 1

(a) 18.0 mg, (b) 95%

Run 2

(a) 18.0 mg, (b) 97%

Run 3

(a) 18.0 mg, (b) 97%

Average Incorporation = 96%

5 mol% 175, 1 h, Chlorobenzene, Entry 2

Run 1

(a) 18.0 mg, (b) 93%

Run 2

(a) 18.0 mg, (b) 95%

Run 3

(a) 18.0 mg, (b) 95%

Average Incorporation = 94%

2.5 mol% 175, 1 h, Chlorobenzene, Entry 3

Run 1

(a) 9.0 mg, (b) 88%

Run 2

(a) 9.0 mg, (b) 91%

Average Incorporation = 90%

5 mol% 175, 1 h, MTBE, Entry 4

Run 1

(a) 18.0 mg, (b) 31%

Run 2

(a) 18.0 mg, (b) 28%

Average Incorporation = 30%

*8.15.3 Ether Labelling – Substrate Scope (**Scheme 5.2**)*

All reactions were run as described in *General Procedure K* (unless stated otherwise). Data are reported as: (a) amount of substrate, and (b) Incorporation.

1-Methoxy-4-(methoxymethyl)benzene **235a**

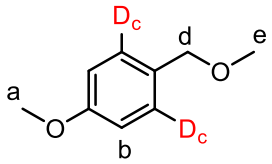

d-235a

^{1}H NMR (400 MHz, $CDCl_3$): δ 7.24 (d, *J* = 8.7 Hz, 2H, H^c), 6.87 (d, *J* = 8.7 Hz, 2H, H^b), 4.37 (s, 2H, H^d), 3.79 (s, 3H, H^a), 3.34 (s, 3H, H^e).

Labelling expected against signal at δ 7.24 ppm, measured against signal at δ 3.79 ppm.

Run 1

(a) 32.7 mg, (b) 97%

Run 2

(a) 32.7 mg, (b) 96%

Run 3

(a) 32.7 mg, (b) 92%

Average Incorporation = 95%

1-(1-Methoxyethyl)-4-methylbenzene **235b**

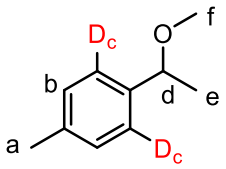

d-235b

^{1}H NMR (400 MHz, $CDCl_3$): δ 7.18 (d, *J* = 8.0 Hz, 2H, H^c), 7.14 (d, *J* = 8.0 Hz, 2H, H^b), 4.24 (q, *J* = 6.4 Hz, 1H, H^d), 3.19 (s, 3H, H^f), 2.33 (s, 3H, H^a), 1.41 (d, *J* = 6.4 Hz, 3H, H^e).

Labelling expected against signal at δ 7.18 ppm, measured against signal at δ 2.33 ppm.

Run 1

(a) 29.3 mg, (b) 92%

Run 2

(a) 29.3 mg, (b) 91%

Run 3

(a) 29.3 mg, (b) 92%

Average Incorporation = 92%

(2-Methoxypropan-2-yl)benzene **235c**

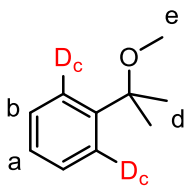

d-235c

^{1}H NMR (400 MHz, $CDCl_3$): δ 7.41-7.37 (m, 2H, H^c), 7.35-7.30 (m, 2H, H^b), 7.26-7.20 (m, 1H, H^a), 3.06 (s, 3H, H^e), 1.52 (s, 6H, H^d).

Labelling expected against signal at δ 7.41-7.37 ppm, measured against signal at δ 3.06 ppm.

Run 1

(a) 81.8 mg, (b) 0%

Run 2

(a) 81.8 mg, (b) 0%

Run 3

(a) 81.8 mg, (b) 0%

Average Incorporation = 0%

1-Methoxy-1,2,3,4-tetrahydronaphthalene **235d**

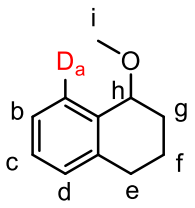

d-235d

^{1}H NMR (400 MHz, $CDCl_3$): δ 7.36-7.31 (m, 1H, H^a), 7.19-7.14 (m, 2H, H^b + H^c), 7.10-7.05 (m, 1H, H^d), 4.30 (t, *J* = 4.8 Hz, 1H, H^h), 3.42 (s, 3H, H^i), 2.87-2.77 (m, 1H, H^g), 2.75-2.65 (m, 1H, H^g), 2.07-1.83 (m, 3H, H^e + H^f), 1.78-1.67 (m, 1H, H^f).

Labelling expected against signal at δ 7.36-7.31 ppm, measured against signal at δ 3.42 ppm.

Run 1

(a) 34.9 mg, (b) 66%

Run 2

(a) 34.9 mg, (b) 61%

Run 3

(a) 34.9 mg, (b) 71%

Average Incorporation = 66%

5-Methoxy-6,7,8,9-tetrahydro-5H-benzo[7]annulene **235e**

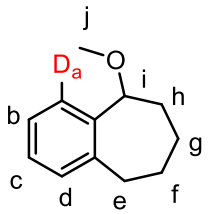

d-235e

^{1}H NMR (400 MHz, $CDCl_3$): δ 7.31-7.28 (m, 1H, H^a),7.22-7.15 (m, 2H, H^b + H^c), 7.14-7.10 (m, 1H, H^d), 4.36-4.31 (m, 1H, H^i), 3.34 (s, 3H, H^j), 3.08-2.96 (m, 1H, H^h), 2.74-2.63 (m, 1H, H^h), 2.14-2.02 (m, 1H, alkyl CH), 1.97-1.85 (m, 2H, alkyl CH_2), 1.81-1.71 (m, 1H, alkyl CH), 1.70-1.60 (m, 2H, alkyl CH_2).

Labelling expected against signal at δ 7.31-7.28 ppm, measured against signal at δ 3.34 ppm.

Run 1

(a) 37.9 mg, (b) 79%

Run 2

(a) 37.9 mg, (b) 76%

Run 3

(a) 37.9 mg, (b) 83%

Average Incorporation = 79%

1-(benzyloxy)-4-methoxybenzene **235f**

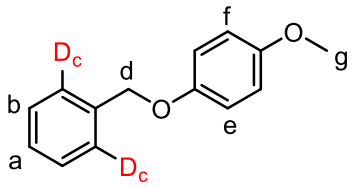

d-235f

^{1}H NMR (400 MHz, $CDCl_3$): δ 7.44-7.39 (m, 2H, H^c) 7.38-7.33 (m, 2H, H^b), 7.32-7.27 (m, 1H, H^a), 6.90 (d, *J* = 9.0 Hz, 2H, H^e), 6.81 (d, *J* = 9.0 Hz, 2H, H^f), 5.00 (s, 2H, H^d), 3.75 (s, 3H, H^g).

Labelling expected against signal at δ 7.44-7.39 ppm, measured against signal at δ 3.75 ppm.

Run 1

(a) 46.1 mg, (b) 72%

Run 2

(a) 46.1 mg, (b) 71%

Run 3

(a) 46.1 mg, (b) 73%

Average Incorporation = 72%

1-Chloro-4-(2-methoxyethyl)benzene **235g**

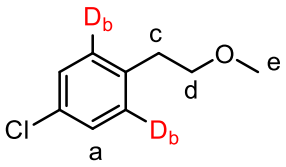

d-235g

^{1}H NMR (400 MHz, $CDCl_3$): δ 7.24 (d, *J* = 8.4 Hz, 2H, H^b), 7.13 (d, *J* = 8.5 Hz, 2H, H^a), 3.56 (t, *J* = 7.0 Hz, 2H, H^d), 3.33 (s, 3H, H^e), 2.83 (t, *J* = 7.0 Hz, 2H, H^c).

Labelling expected against signal at δ 7.24 ppm, measured against signal at δ 3.33 ppm.

Run 1

(a) 36.7 mg, (b) 44%

Run 2

(a) 36.7 mg, (b) 48%

Run 3

(a) 36.7 mg, (b) 46%

Average Incorporation = 46%

Benzyl alcohol **235h**

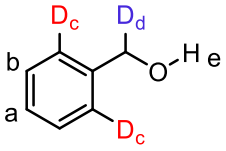

d-235h

^{1}H NMR (400 MHz, d$_6$-Acetone): δ 7.39-7.33 (m, 2H, H^c), 7.32-7.28 (m, 2H, H^b), 7.25-7.20 (m, 1H, H^a), 4.63 (d, *J* = 5.9 Hz, 2H, H^d), 4.13 (t, *J* = 5.9 Hz, 1H, H^e). [198]

Labelling expected against signal at δ 7.39-7.33 ppm and at δ 4.63 ppm, measured against signal at δ 7.25-7.20 ppm.

Run 1

(a) 23.3 mg, (b) D_c = >95%, D_d = 24%

Run 2

(a) 23.3 mg, (b) D_c = >95%, D_d = 20%

Run 3

(a) 23.3 mg, (b) D_c = >95%, D_d = 21%

Average Incorporation = D_c = >95%, D_d = 22%

(Benzyloxy)triisopropylsilane **235i**

During the labelling of **235i**, the silyl protecting group was removed, affording only benzyl alcohol:

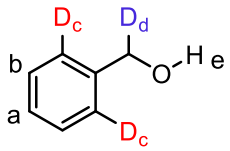

d-235h (from **235i**)

^{1}H NMR (400 MHz, d$_6$-Acetone): δ 7.39-7.33 (m, 2H, H^c), 7.32-7.28 (m, 2H, H^b), 7.25-1.20 (m, 1H, H^a), 4.63 (d, *J* = 5.9 Hz, 2H, H^d), 4.13 (t, *J* = 5.9 Hz, 1H, H^e).

Labelling expected against signal at δ 7.39-7.33 ppm and at δ 4.63 ppm, measured against signal at δ 7.25-7.20 ppm.

Run 1

(a) 56.9 mg, (b) D_c = 66%, D_d = 0%

Run 2

(a) 56.9 mg, (b) D_c = 64%, D_d = 0%

Run 3

(a) 56.9 mg, (b) D_c = 68%, D_d = 0%

Average Incorporation = D_c = 66%, D_d = 0%

1-(p-Tolyl)ethan-1-ol **235j**[199]

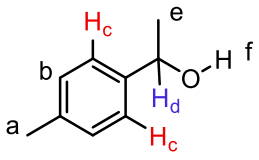

d-235j

^{1}H NMR (400 MHz, $CDCl_3$): δ 7.25 (d, *J* = 8.0 Hz, 2H, H^c), 7.14 (d, *J* = 8.0 Hz, 2H, H^b), 4.85 (q, *J* = 6.5 Hz, 1H, H^d), 2.33 (s, 3H, H^a), 1.67 (bs, 1H, H^f), 1.47 (d, *J* = 6.5 Hz, 3H, H^e).

Labelling expected against signal at δ 7.25 ppm, measured against signal at δ 2.33 ppm.

Run 1

(a) 29.3 mg, (b) D_c = >95%, D_d = 17%

Run 2

(a) 29.3 mg, (b) D_c = >95%, D_d = 15%

Average Incorporation = D_c = >95%, D_d = 16%

8.16 Synthesis of Natural Product-like Substrates

*8.16.1 Towards (±)-Eudesmine (**Scheme 5.7**)*

Ferulic Acid **245**[200]

To a 250 mL round-bottom flask was added vanillin **246** (20.0 g, 131 mmol, 1.00 eq), malonic acid (17.1 g, 164 mmol, 1.25 eq), and pyridine (50.0 mL). The suspension was stirred and piperidine (1.28 mL, 13.1 mmol, 0.10 eq) was added. The mixture was then stirred at 80 °C for 24 h. The reaction was cooled to room temperature and poured into 600 mL of a 6 M solution of aqueous hydrochloric acid, with ice, and left to stand overnight. The resulting precipitate was filtered, washed with copious amounts of water and small amounts of DCM. Ferulic acid **245** (16.3 g, 83.9 mmol, 64% yield) was isolated as an off-white solid.

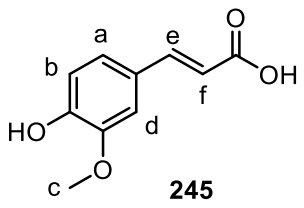

245

Melting Point: 171-173 °C (lit:[200] 171-173 °C)

IR (neat, cm^{-1}): 3429, 2935, 1662, 1418, 1597, 1512, 1431, 1323, 1267, 1201.

^{1}H NMR (400 MHz, d$_6$-DMSO): δ 6.79 (d, *J* = 16.0 Hz, 1H, H^e), 6.37 (d, $^4J_{HH}$ = 1.8 Hz, 1H, H^d), 6.26 (dd, *J* = 8.0 Hz, $^4J_{HH}$ = 1.8 Hz, 1H, H^a), 6.00 (d, *J* = 8.0 Hz, 1H, H^b), 5.50 (d, *J* = 16.0 Hz, 1H, H^f), 3.09 (s, 3H, H^c).

^{13}C NMR (101 MHz, d_6-DMSO) δ 168.1, 149.2, 148.0, 144.6, 125.9, 122.9, 115.8, 115.7, 111.3, 55.8.

Methyl Ferulate **244**[201]

To a 250 mL round-bottom flask was added ferulic acid **245** (8.00 g, 41.2 mmol, 1.00 eq) and methanol (80.0 mL). The suspension was cooled to 0 °C and acetyl chloride (4.41 mL, 61.8 mmol, 1.50 eq) was added. The reaction was then stirred at room temperature for 16 h. The reaction was quenched by portionwise addition of sodium bicarbonate (6.92 g, 82.4 mmol, 2.00 eq) and the resulting suspension filtered. The filtrate was concentrated *in vacuo* and the residue purified by column chromatography, eluting with 30% ethyl acetate/petroleum ether. Methyl ferulate **244** (8.58 g, 41.2 mmol, quantitative yield) was isolated as a colourless oil.

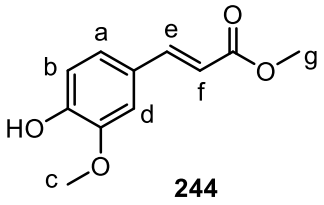

244

IR (neat, cm^{-1}): 3462, 3221, 2922, 2362, 1595, 1514, 1274, 1259, 1220, 1093, 1012.

^{1}H NMR (400 MHz, $CDCl_3$): δ 7.60 (d, J = 16.0 Hz, 1H, H^f), 7.05 (dd, J = 8.0 Hz, $^4J_{HH}$ = 2.0 Hz, 1H, H^a), 7.01 (d, $^4J_{HH}$ = 2.0 Hz, 1H, H^4), 6.90 (d, *J* = 8.0 Hz, 1H, H^b), 6.27 (d, *J* = 16.0 Hz, H^e), 3.91 (s, 3H, H^c), 3.78 (s, 3H, H^g).

^{13}C NMR (101 MHz, $CDCl_3$) δ 168.2, 148.3, 147.2, 145.4, 127.3, 123.4, 115.5, 115.2, 109.8, 56.3, 52.0.

Coniferyl Alcohol **243**[202]

To a 1 L, 3-necked, round-bottom flask, equipped with an internal thermometer, was added methyl ferulate **244** (13.0 g, 62.4 mmol, 1.00 eq) and dry toluene (300 mL). The solution was cooled to 0 °C and DIBAL (25% wt. in hexane, 152 mL, 187 mmol, 3.00 eq) was added, slowly. Once complete, the reaction was stirred at room temperature for 1 h. The reaction mixture was then cooled to 0 °C and quenched with ethanol (30.0 mL). The majority of the solvent was removed *in vacuo*. To the resulting gum was added water (500 mL) and ethyl acetate (200 mL) and the mixture transferred to a separating funnel. The layers were separated, and the aqueous layer washed a further three times with ethyl acetate. The organic layers were combined, dried over sodium sulfate, filtered, and concentrated *in vacuo*. The residue was purified by column chromatography, eluting with 50% ethyl acetate/petroleum either. Coniferyl alcohol **243** (9.78g, 54.3 mmol, 87% yield) was isolated as a pale-yellow solid.

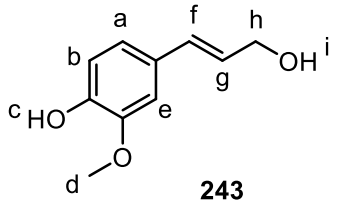

243

Melting Point: 73-75 °C (lit:[202] 74-75 °C).

IR (neat, cm^{-1}): 3460, 3236, 2850, 1593, 1514, 1255, 1220, 1083.

^{1}H NMR (400 MHz, $CDCl_3$): δ 6.93-6.82 (m, 3H, H^a + H^b + H^e), 6.52 (d, *J* = 16.0 Hz, 1H, H^f), 6.20 (dt, *J* = 16.0 Hz, *J* = 5.8 Hz, 1H, H^g), 5.62 (bs, 1H, H^c), 4.28 (d, *J* = 5.8 Hz, 2H, H^h), 3.89 (s, 3H, H^d), 3.47 (bs, 1H, H^i).

^{13}C NMR (101 MHz, $CDCl_3$) δ 146.9, 145.8, 131.5, 129.5, 126.3, 120.5, 114.7, 108.6, 64.0, 56.1.

(±)-Pinoresinol & Dehydrodiconiferyl Alcohol **247**[203,204] ***(Table 5.2)***

To a 5 L round-bottom flask was added water. To this was added a 0.2 M solution of coniferyl alcohol **243** (1.00 eq) in acetone, with vigorous stirring. To this mixture was added a 1 M solution of iron chloride hexahydrate (1.10 eq) in water and the reaction stirred vigorously at room temperature for 1 h. The reaction mixture was transferred directly to a separating funnel and washed with ethyl acetate (6 x 500 mL). The organic layers were combined, dried over sodium sulfate, filtered, and concentrated *in vacuo*. The residue was purified by column chromatography, eluting with 0-50% acetone/petroleum ether. (±)-Pinoresinol was isolated as a pale yellow gum. Dehydrodiconiferyl alcohol **247**, when isolated, was afforded as an off-white solid. Data are presented as: (a) amount of water, (b) amount of acetone, (c) amount of coniferyl alcohol **243**, (d), amount of water for $FeCl_3 \bullet H_2O$ solution (e) amount of $FeCl_3 \bullet H_2O$, (f) yield of (±)-pinoresinol, and (g) dehydrodiconiferyl alcohol **247**.

Run 1 (Table 5.2, Entry 1)

(a) 500 mL, (b) 50 mL, (c) 1.80 g, 9.98 mmol, (d) 11 mL, (e) 2.98 g, 11.0 mmol, (f) 0.411 g, 1.15 mmol, 23% yield. (g) Not isolated.

Run 2 (Table 5.2, Entry 2)

(a) 0.50 L mL, (b) 125 mL, (c) 4.49 g, 24.9 mmol, (d) 25 mL, (e) 7.40 g, 27.4 mmol, (f) 0.759 g, 2.12 mmol, 17% yield. (g) 0.803 g, 2.24 mmol, 18% yield.

Run 1 (Table 5.2, Entry 3)

(a) 3.0 L, (b) 300 mL, (c) 11.5 g, 61.9 mmol, (d) 70 mL, (e) 184 g, 68.0 mmol, (f) 2.33 g, 6.50 mmol, 21% yield. (g) Not isolated.

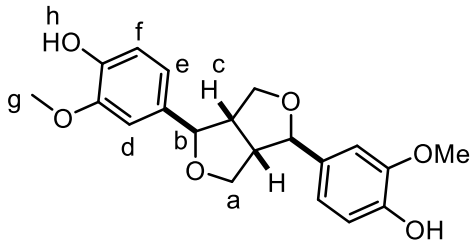

(±)-Pinoresinol

IR (neat, cm^{-1}): 3385, 2935, 2866, 1602, 1512, 1429, 1363, 1267, 1029.

^{1}H NMR (400 MHz, $CDCl_3$): δ 6.91-6.84 (m, 4H, H^d + H^f), 6.80 (dd, J = 8.0 Hz, $^{4}J_{HH}$ = 2.0 Hz, 2H, H^e), 5.56 (s, 2H, H^h), 4.72 (d, J = 4.1 Hz, 2H, H^b), 4.27-4.19 (m, 2H, H^a), 3.89 (s, 6H, H^g), 3.88-3.84 (m, 2H, H^a), 3.12-3.04 (m, 2H, H^c).

^{13}C NMR (101 MHz, D_6-DMSO) δ 147.6, 146.0, 132.4, 118.7, 115.2, 110.5, 85.3, 71.0, 55.7, 53.7.

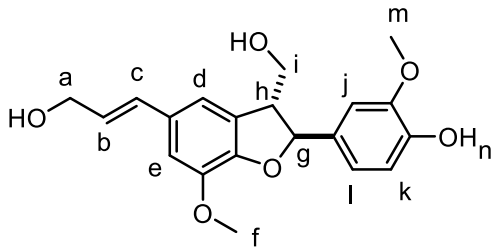

247

Melting Point: 138-140 °C (lit:[205] 140-141 °C)

IR (neat, cm^{-1}): 2933, 2835, 1589, 1514, 142, 1365, 1309, 1251, 1236, 1159, 1136, 1078.

^{1}H NMR (400 MHz, $CDCl_3$): δ 6.92-6.84 (m, 5H, H^d + H^e + H^j + H^l + H^k), 5.55 (d, J = 16.0 Hz, 1H, H^c), 6.23 (dt, J = 16.0 Hz, J = 6.0 Hz, 1H, H^b), 5.60-5.54 (m, 3H, H^a + H^n), 4.32-4.26 (m, 2H, H^i), 4.00-3.93 (m, 1H, H^g), 3.89 (s, 3H, H^m), 3.85 (s, 3H, H^f), 3.61 (q, J = 6.0 Hz, 1H, H^h).

^{13}C NMR (101 MHz, d_6-DMSO) δ 147.5, 147.2, 146.4, 143.7, 132.4, 130.5, 129.5, 129.0, 128.0, 118.6, 115.3, 115.0, 110.4, 87.2, 63.0, 62.7, 61.7, 55.7, 55.6, 53.0.

(±)-Eudesmin[206,207] ***(Scheme 5.8)***

To a 100 mL round-bottom flask was added (±)-Pinoresinol (0.400 g, 1.11 mmol, 1.00 eq), potassium carbonate (0.231 g, 16.7 mmol, 1.50 eq) acetone (50.0 mL). To this was added methyl iodide (1.38 mL, 22.2 mmol, 20.0 eq), and the reaction stirred at reflux for 48 h. The reaction mixture was cooled to room temperature and filtered. The filtrate was concentrated *in vacuo*, and residue purified by column chromatography, eluting with 50% acetone/petroleum ether. (±)-Eudesmin (0.356 g, 0.921 mmol, 83% yield) isolated as a colourless gum.

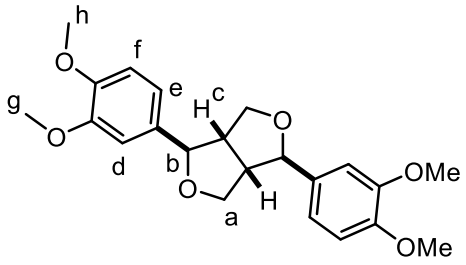

(±)-Eudesmin

IR (neat, cm^{-1}): 2933, 2835, 1589, 1514, 1442, 1365, 1309, 1251, 1236, 1159, 1136, 1078.

^{1}H NMR (400 MHz, $CDCl_3$): δ 5.91-6.80 (m, 6H, H^d + H^e + H^f), 4.74 (d, *J* = 3.8 Hz, 2H, H^b), 4.24-2.22 (m, 2H, H^a) 3.92-3.84 (m, 14 H, H^a + H^g + H^h), 3.13-3.07 (m, 2H, H^c).

^{13}C NMR (101 MHz, $CDCl_3$) δ 149.5, 148.9, 133.8, 118.4, 111.3, 109.4, 86.0, 71.9, 56.2, 55.9, 54.4

*8.16.2 Towards (±)-Cedrusin Methyl Ether (**Scheme 5.9** + **Scheme 5.10**)*

Attempted Hydrogenation of Dehydrodiconiferyl Alcohol **247**

To a 50 mL round-bottom flask was added *Dehydrodiconiferyl Alcohol* **247** (230 mg, 0.64 mmol, 1.00 eq) and Pd/C (10% wt., 68.1 mg, 0.064 mmol 10 mol%). The mixture was suspended in methanol (13.0 mL). The atmosphere in the flask was exchanged *via* three vacuum/hydrogen cycles, with the system then being left open to the hydrogen balloon. The reaction was stirred at room temperature for 1 h, at which point it was filtered through Celite. The filtrate was concentrated *in vacuo*, however no discernible products, or starting material, could be identified by TLC or ^{1}H NMR spectroscopic analysis.

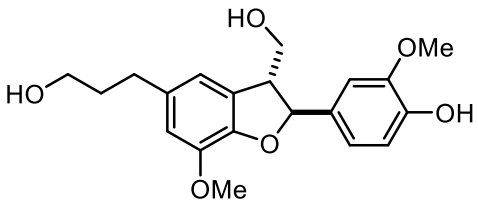

(±)-Cedrusin methyl ether

Dehydrodiferulate Dimethyl Ester **248**[208]

To a flame-dried, 3-necked, 250 mL round-bottom flask was added methyl ferulate **244** (1.00 eq). To this was added dry acetone (0.2 M w.r.t. SM) and dry toluene (0.3 M w.r.t SM). The flask was covered with tin foil to protect from light, and silver oxide (0.50 eq) added. The reaction was stirred at room temperature for 24 h, at which point it was filtered through Celite, washing with ethyl acetate. The filtrated was concentrated *in vacuo*. The residue was suspended in boiling methanol and the insoluble orange solid allowed to settle, before the solution was decanted. The methanol was removed in vacuo, and the residue purified by column chromatography, eluting with 30% ethyl acetate/petroleum ether. Dehydrodiferulate dimethyl

ester **248** isolated as a white solid. Data are presented as (a) amount of methyl ferulate, (b) amount of acetone, (c) amount of toluene, (d) amount of silver oxide, and (e) yield.

Run 1

(a) 2.30 g, 11.1 mmol, (b) 55.0 mL, (c) 37.0 mL, (d) 1.28 g, 5.55 mmol, (e) 0.307 mg, 0.72 mmol, 13% yield.

Run 2

(a) 6.00 g, 28.8 mmol, (b) 140 mL, (c) 95.0 mL, (d) 3.33 g, 14.4 mmol, (e) 1.80 g, 4.34 mmol, 30% yield.

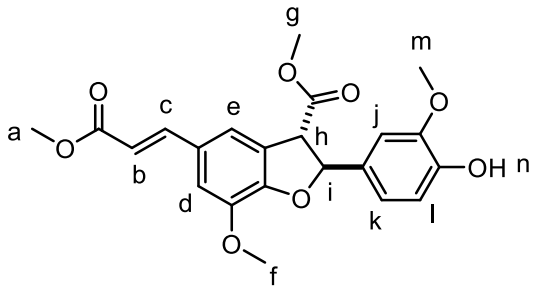

248

Melting Point: 151-152 °C (lit:[209] 155 °C)

IR (neat, cm^{-1}): 3385, 1739, 1728, 1519, 1489, 1263, 1161, 1139, 987.

^{1}H NMR (400 MHz, $CDCl_3$): δ 7.63 (d, J = 15.8 Hz, 1H, H^c), 7.17 (s, 1H, H^d), 7.00 (s, 1H, H^e), 6.91-6.84 (m, 3H, H^j + H^k + H^l), 6.30 (d, *J* = 15.8 Hz, 1H, H^b), 6.09 (d, *J* = 8.0 Hz, 1H, H^h), 5.64 (s, 1H, H^n), 4.32 (d, *J* = 8.0 Hz, 1H, H^i), 3.90 (s, 3H, CH_3), 3.86 (s, 3H, CH_3), 3.81 (s, 3H, CH_3), 3.78 (s, 3H, CH_3).

^{13}C NMR (101 MHz, $CDCl_3$) δ 170.8, 166.9, 149.4, 147.7, 147.1, 144.7, 144.3, 129.7, 128.1, 126.2, 119.3, 118.2, 115.4, 115.3, 112.7, 110.8, 98.2, 55.9, 55.7, 54.1, 52.6, 51.3.

(±)-Cedrusin Methyl Ether[210,211]

To a 50 mL round-bottom flask was added dehydrodiferulate dimethyl ester **248** (1.00 eq), Pd/C (10% wt., 2 mol%) and methanol (0.3M w.r.t. SM). The atmosphere in the flask was exchanged *via* three vacuum/hydrogen cycles, with the system then being left open to the hydrogen balloon. The reaction was at room temperature for 1 h, at which point it was filtered through Celite. The filtrate was concentrated *in vacuo*, and the residue transferred to a 100 mL round-bottom flask. To flask was put under inert atmosphere with 3 vacuum/argon cycles, and dry THF (0.2M w.r.t SM) was added. The solution was cooled to 0 °C and lithium aluminium hydride (4.00 eq) was added. The reaction was stirred at 0 °C for 1 h and quenched with a 2 M aqueous hydrochloric acid solution. The mixture was transferred to a separatory funnel and separated. The aqueous layer was washed twice with ethyl acetate. The organic layers were combined, dried over sodium sulfate, filtered, and concentrated in vacuo. The residue was purified by column chromatography, eluting with 75-100% ethyl acetate/petroleum ether. (±)-Cedrusin methyl ether was isolated as a colourless oil. Data are presented as (a) amount of **248**, (b) amount of Pd/C, (c) volume of methanol, (d) volume of THF, (e) amount of lithium aluminium hydride, and (f) yield.

Run 1

(a) 0.320 g, 0.77 mmol, (b) 0.016 g, 0.0015 mmol, (c) 3.0 mL (d) 4.0 mL, (e) 0.117 g, 3.08 mmol, (f) 0.184 g, 0.51 mmol, 66% yield.

Run 2

(a) 1.00 g, 2.41 mmol, (b) 0.051 g, 0.048 mmol, (c) 8.0 mL, (d)12.0 mL, (e) 0.361 g, 9.64 mmol, (f) 0.715 g, 1.98 mmol, 82% yield.

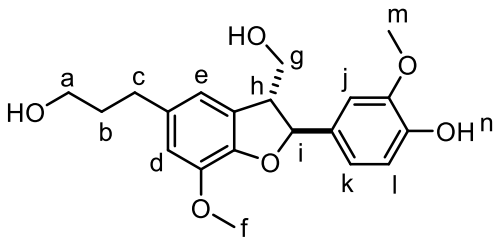

(±)-Cedrusin methyl ether

IR (neat, cm^{-1}): 3309, 2941, 2833, 1612, 1462, 1274, 1211, 1024.

^{1}H NMR (400 MHz, $CDCl_3$): δ 6.94-6.81 (m, 3H, H^j + H^k + H^l), 6.67-6.63 (m, 2H, H^d + H^e), 5.65 (s, 1H, H^n), 5.52 (d, *J* = 7.5 Hz, 1H, H^i), 3.98-3.90 (m, 1H, H^h), 3.86 (s, 3H, H^f), 3.84 (s, 3H, H^m), 3.67 (t, *J* = 6.5 Hz, 2H, H^a), 3.58 (q, 1H, H^h), 2.64 (t, *J* = 7.5 Hz, 2H, H^g), 1.91-1.82 (m, 2H, H^c), 1.27-1.16 (m, 2H, H^b).

^{13}C NMR (101 MHz, $CDCl_3$) δ 147.6, 146.3, 145.6, 143.4, 135.1, 132.6, 129.1, 118.5, 116.5, 115.3, 112.5, 110.4, 86.9, 63.1, 60.3, 55.7, 55.3, 48.6, 34.8, 31.6.

*8.16.3 Towards (±)-Medicarpin (**Scheme 5.11**)*

3-(2,4-Dimethoxyphenyl)-7-hydroxy-4H-chromen-4-one **251**[212]

To a flame-dried, 3-necked, 250 mL round-bottom flask was added 2,4-dimethoxyphenyl acetic acid **250** (1.00 eq) and resorcinol (1.00 eq). To this was added BF_3•OEt_2 (neat, 3.3 M w.r.t. SM), and the mixture transferred to a pre-set heating block at 100 °C for 10 minutes, stirring vigorously. The reaction was then cooled to 0 °C and DMF (0.7 M w.r.t. SM) was added, before the reaction was stirred at 55 °C for 20 minutes. To this was added methane sulfonyl chloride (7.00 eq) and the reaction stirred at 80 °C for 4 h, before being poured into ice water. The mixture was washed three times with ethyl acetate. The organic phases were collected, dried over sodium sulfate, filtered, and concentrated in vacuo. The residue was purified by column chromatography, eluting with 0-5% methanol/chloroform, followed by

trituration with ethyl acetate. 3-(2,4-Dimethoxyphenyl)-7-hydroxy-4H-chromen-4-one **251** was isolated as an off-white solid. Data are presented as (a) amount of added 2,4-dimethoxyphenyl acetic acid (b) amount of resorcinol, (c) volume of BF_3•OEt_2, (d) volume of DMF, (e) amount of methane sulfonic acid, and (f) yield

Run 1

(a) 5.00 g, 25.5 mmol, (b) 2.81 g, 25.5 mol, (c) 8.0 mL, (d) 36.0 mL, (e) 13.8 mL, 178 mmol, (f) 1.86 g, 6.22 mmol, 24% yield.

Run 2

(a) 6.58 g, 33.5 mmol, (b) 3.69 g, 33.5 mmol, (c) 11.0 mL, (d) 48.0 mL, (e) 18.2 mL, 235 mmol, (f) 2.50 g, 8.38 mmol, 25% yield.

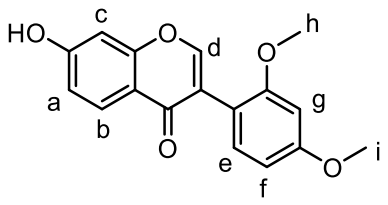

251

Melting Point: 238-240 °C (lit:[212] 238-240 °C).

IR (neat, cm^{-1}): 3197, 1625, 1610, 1583, 1570, 1504, 1269, 1236, 1157.

^{1}H NMR (400 MHz, D_6-DMSO): δ 8.10 (s, 1H, H^d), 7.90 (d, *J* = 8.5 Hz, 1H, H^b), 7.12 (d, *J* = 8.5 Hz, 1H, H^a), 6.91 (d, *J* = 8.0 Hz, 1H, H^e), 6.84 (s, 1H, H^c), 6.62 (d, $^4J_{HH}$ = 2.5 Hz, 1H, H^g), 6.56 (dd, *J* = 8.0 Hz, $^4J_{HH}$ = 2.5 Hz, 1H, H^f), 3.79 (s, 3H, H^h), 3.70 (s, 3H, H^i).

^{13}C NMR (101 MHz, D_6-DMSO) δ 174.4, 162.4, 160.7, 158.4, 157.5, 153.9, 132.0, 127.1, 121.6, 116.6, 115.0, 113.5, 104.6, 102.2, 98.6, 55.5, 55.3.

7-hydroxy-3-(2-hydroxy-4-methoxyphenyl)-4H-chromen-4-one **252**[212]

To a flame-dried 250 mL round-bottom flask was added 3-(2,4-dimethoxyphenyl)-7-hydroxy-4H-chromen-4-one **251** (1.00 eq), and dry acetonitrile (0.2 M w.r.t.SM). The solution was cooled to 0 °C and anhydrous aluminium chloride (30.0 eq) was added, portionwise. The dark suspension was stirred at reflux for 16 h, at which point it was poured into ice water. The mixture was transferred to a separating funnel, and washed three times with chloroform. The organic layers were combined, dried over sodium sulfate, filtered, and concentrated *in vacuo*. The residue was purified by column chromatography, eluting with 2% methanol/chloroform. 7-Hydroxy-3-(2-hydroxy-4-methoxyphenyl)-4H-chromen-4-one **252** was isolated as an off-white solid. Data are presented as (a) amount of **251**, (b) volume of acetonitrile, (c) amount of aluminium chloride, and (d) yield.

Run 1

(a) 1.14 g, 3.82 mmol, (b) 20.0 mL, (c) 15.5 g, 116 mmol, (d) 0.944 g, 3.32 mmol, 87% yield.

Run 2

(a) 2.00 g, 6.70 mmol, (b) 34.0 mL, (c) 26.8 g, 201 mmol, (d) 1.70 g, 5.98 mmol, 89% yield.

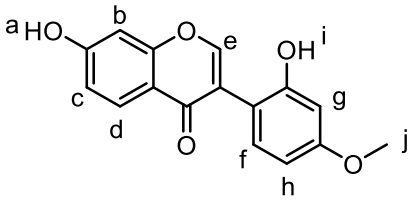

244

Melting Point: 210-212 °C (lit:[212] 212-215 °C).

IR (neat, cm^{-1}): 3317, 1624, 1570, 1502, 1355, 1269, 1236, 1159, 1136.

^{1}H NMR (400 MHz, $CDCl_3$): δ 10.7 (bs, 1H, H^a), 9.44 (bs, 1H, H^i), 8.17, (s, 1H, H^e), 7.94 (d, J = 8.8 Hz, 1H, H^d), 7.10 (d, J = 7.9 Hz, 1H, H^f), 6.93 (dd, J = 8.8 Hz, $^{4}J_{HH}$ = 2.5 Hz, 1H, H^c), 6.87 (d, $^{4}J_{HH}$ = 2.5 Hz, 1H, H^b), 6.48-6.41 (m, 2H, H^h + H^g), 3.73 (s, 3H, H^j).

^{13}C NMR (101 MHz, $CDCl_3$) δ 175.1, 162.5, 160.2, 157.5, 156.5, 154.5, 132.2, 127.2, 121.5, 116.6, 115.1, 111.9, 104.5, 102.1, 101.6, 55.0.

(±)-Medicarpin

To a 100 mL round-bottom flask was added 7-hydroxy-3-(2-hydroxy-4-methoxyphenyl)-4H-chromen-4-one **252** (1.00 eq) and ethanol (0.2 M w.r.t. SM). The solution was cooled to 0 °C and sodium borohydride (7.00 eq) was added. The reaction was stirred at room temperature for 24 h, and quenched with a 2 M solution of aqueous hydrochloric acid. The mixture was transferred to a separation funnel and washed three times with ethyl acetate. The organic layers were combined, dried over sodium sulfate, filtered, and concentrated *in vacuo*. The residue was purified by column chromatography, eluting with 75-100% chloroform/petroleum ether. (±)-Medicarpin was isolated as a white solid. Data are presented as (a) amount of **252**, (b) volume of ethanol, (c) amount of sodium borohydride, and (d) yield.

Run 1

(a) 0.900 g, 3.17 mmol, (b) 16.0 mL, (c) 0.839 g, 22.2 mmol, (d) 0.547 g, 2.02 mmol, 64% yield.

Run 2

(a) 1.50 g, 5.28 mmol, (b) 26.0 mL, (c) 1.40 g, 37.0 mmol, (d) 0.964 g, 3.57 mmol, 68% yield.

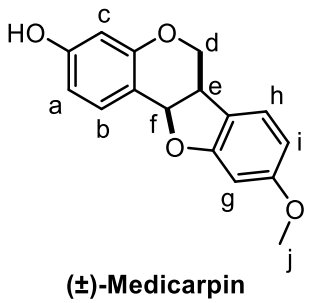

(±)-Medicarpin

Melting Point: 193-195 °C (lit:[212] 194-195 °C).

IR (neat, cm^{-1}): 3367, 2360, 1618, 1591, 1492, 1448, 1286, 1153, 1114, 1083.

^{1}H NMR (400 MHz, D$_4$-Methanol): δ 7.29 (d, *J* = 8.3 Hz, 1H, H^{c}), 7.17 (d, *J* = 8.3 Hz, 1H, H^{h}), 6.49 (dd, J = 8.3 Hz, $^{4}J_{HH}$ = 2.5 Hz, 1H, H^{b}), 6.45 (dd, *J* = 8.3 Hz, $^{4}J_{HH}$ = 2.5 Hz, 1H, H^{i}), 6.38 (d, *J* = 2.5 Hz, 1H, H^{a}), 6.31 (d, *J* = 2.5 Hz, 1H, H^{g}), 5.49 (m, 1H, H^{f}), 4.26-4.17 (m, 1H, H^{f}), 3.74 (s, 3H, H^{j}), 3.57-3.47 (m, 2H, H^{d}).

^{13}C NMR (101 MHz, D$_6$-DMSO) δ 160.5, 160.3, 158.7, 156.3, 132.1, 125.1, 119.4, 111.2, 109.7, 105.9, 102.9, 96.3, 78.1, 65.9, 55.3, 38.9.

8.16.4 Attempts at Labelling Natural Product-Like Molecules

*Attempts Towards Deuterium Labelled (±)-Eudesmin (**Table 5.3**)*

All reactions were run as described in *General Procedure L*. Data are presented as (a) amount of (±)-Eudesmin, (b) amount of catalyst (c) solvent volume (d) temperature (e) Incorporation (f) (±)-Eudesmin : by-product ratio.

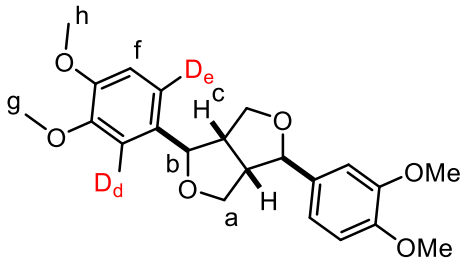

(±)-d-Eudesmin

^{1}H NMR (400 MHz, $CDCl_3$): δ 5.91-6.80 (m, 6H, H^d + H^e + H^f), 4.74 (d, *J* = 3.8 Hz, 2H, H^b), .4.24-2.22 (m, 2H, H^a) 3.92-3.84 (m, 14 H, H^a + H^g + H^h), 3.13-3.07 (m, 2H, H^c).

Labelling expected against signal at δ 5.91-6.80 ppm, measured against signal at δ 3.13-3.07 ppm.

Table 5.3 Entry 1

(a) 77.1 mg (b) 18.0 mg (c) 2.50 mL (d) 25 °C (e) >95% (f) 1.70 : 1.00

Table 5.3 Entry 2

(a) 38.5 mg (b) 9.0 mg (c) 12.0 mL (d) 25 °C (e) >95% (f) 3.55 : 1.00

Table 5.3 Entry 3

(a) 38.5 mg (b) 9.0 mg (c) 12.0 mL (d) -10 °C (e) >95% (f) 3.55 : 1.00

*Attempts Towards Deuterium Labelled (±)-Cedrusin Methyl Ether (**Scheme 5.12** + **Table 5.4**)*

To a three-necked 100 mL round-bottom flask, fitted with two stopcocks, was added (±)-cedrusin methyl ether (38.7 mg, 0.108 mmol, 1.00 eq) and complex **175** (9.0 mg, 0.0054 mmol, 5 mol%). The mixture was dissolved in chlorobenzene (2.5 mL). The atmosphere in the flask was exchanged *via* three vacuum/D_2 cycles, with the system then being isolated upon the third influx of deuterium. The flask was immediately placed in a heating block, pre-set to the

specified temperature. The reaction mixture was then stirred at the stated temperature for the specified time. The reaction mixture was then loaded directly onto a silica column and the chlorobenzene eluted with petroleum ether. The catalyst residues were removed by one column volume of DCM, and the deuterated product eluted with ethyl acetate and concentrated *in vacuo*. The level of deuteration was then calculated as described in *General Procedure D*. Data are presented as (a) temperature (b) time (c) result.

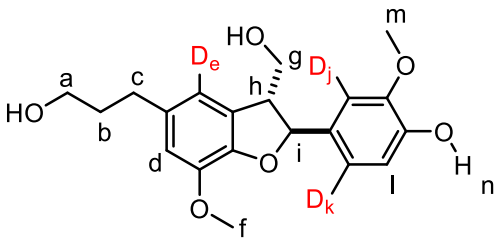

(±)-d-Cedrusin methyl ether

^{1}H NMR (400 MHz, $CDCl_3$): δ 6.94-6.81 (m, 3H, H^j + H^k + H^l), 6.67-6.63 (m, 2H, H^d + H^e), 5.65 (s, 1H, H^n), 5.52 (d, *J* = 7.5 Hz, 1H, H^i), 3.98-3.90 (m, 1H, H^h), 3.86 (s, 3H, H^f), 3.84 (s, 3H, H^m), 3.67 (t, *J* = 6.5 Hz, 2H, H^a), 3.58 (q, 1H, H^h), 2.64 (t, *J* = 7.5 Hz, 2H, H^g), 1.91-1.82 (m, 2H, H^c), 1.27-1.16 (m, 2H, H^b).

Labelling expected against signal at δ 6.94-6.81 ppm and δ 6.67-6.63, measured against signal at δ 3.84 ppm.

Scheme 5.12

(a) 25 °C (b) 16 h (c) No incorporation observed

Table 5.4 Entry 1

(a) 90 °C (b) 16 h (c) Complete Degradation

Table 5.4 Entry 2

(a) 50 °C (b) 16 h (c) Complete Degradation

Table 5.4 Entry 3

(a) 50 °C (b) 1 h (c) D_e = 25%

*Attempts Towards Deuterium Labelled (±)-Medicarpin (**Table 5.5**)*

To a three-necked 100 mL round-bottom flask, fitted with two stopcocks, was added (±)-medicarpin (58.1 mg, 0.215 mmol, 1.00 eq) and complex **175** (18.0 mg, 0.108 mmol, 5 mol%). The mixture was dissolved in specified solvent or solvent mixture (2.5 mL). The atmosphere in the flask was exchanged *via* three vacuum/D_2 cycles, with the system then being isolated upon the third influx of deuterium. The flask was immediately placed in a heating block, pre-set to the specified temperature. The reaction mixture was then stirred at the stated temperature for the specified time. The reaction mixture was then concentrated *in vacuo*. The catalyst residues were removed by triturating with diethyl ether. The level of deuteration was then calculated as described in *General Procedure D*. Data are presented as (a) solvent system (b) temperature (c) time (d) result.

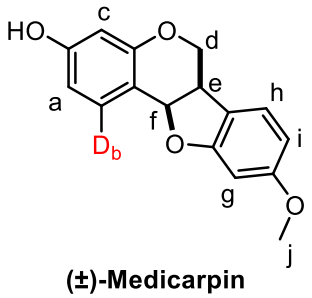

(±)-Medicarpin

^{1}H NMR (400 MHz, D_4-Methanol): δ 7.29 (d, *J* = 8.3 Hz, 1H, H^c), 7.17 (d, *J* = 8.3 Hz, 1H, H^h), 6.49 (dd, J = 8.3 Hz, $^4J_{HH}$ = 2.5 Hz, 1H, H^b), 6.45 (dd, *J* = 8.3 Hz, $^4J_{HH}$ = 2.5 Hz, 1H, H^i), 6.38 (d, *J* = 2.5 Hz, 1H, H^a), 6.31 (d, *J* = 2.5 Hz, 1H, H^g), 5.49 (m, 1H, H^f), 4.26-4.17 (m, 1H, H^f), 3.74 (s, 3H, H^j), 3.57-3.47 (m, 2H, H^d).

Labelling expected against signal at δ 7.29 ppm, measured against signal at δ 3.74 ppm.

Table 5.5 Entry 1

(a) Chlorobenzene (b) 25 °C (c) 16 h (d) No Incorporation

Table 5.5 Entry 2

(a) 20% *tert*-Butanol in chlorobenzene (b) 25 °C (c) 16 h (d) No Incorporation

Table 5.5 Entry 3

(a) 2-Methyl tetrahydrofuran (b) 25 °C (c) 1 h (d) No Incorporation

Table 5.5 Entry 4

(a) 2-Methyl tetrahydrofuran (b) 60 °C (c) 16 h (d) Complete Degradation

Table 5.5 Entry 5

(a) 2-Methyl tetrahydrofuran (b) 60 °C (c) 1 h (d) Complete Degradation

8.17 General Computational Details

Gaussian 09 quantum chemistry program package was used to perform all relevant Density Functional Theory (DFT) calculations discussed in the manuscript. Structures were optimised using the M06L functional (hybrid meta-GGA exchange correlation), and 6-31G(d) basis set for all main group atoms. The Ir centre was described using the Stuttgart RSC effective core potential and associated basis set. Coordinates and additional computational details are supplied in the appendix.

8.18 Counterpoise Method for Binding Energy Calculations

Counterpoise method for binding energy calculation requires optimised structures of the free complex (**A**), free substrate (**B**) and the catalyst-substrate complex (**AB**), shown in **Scheme 8.7**.

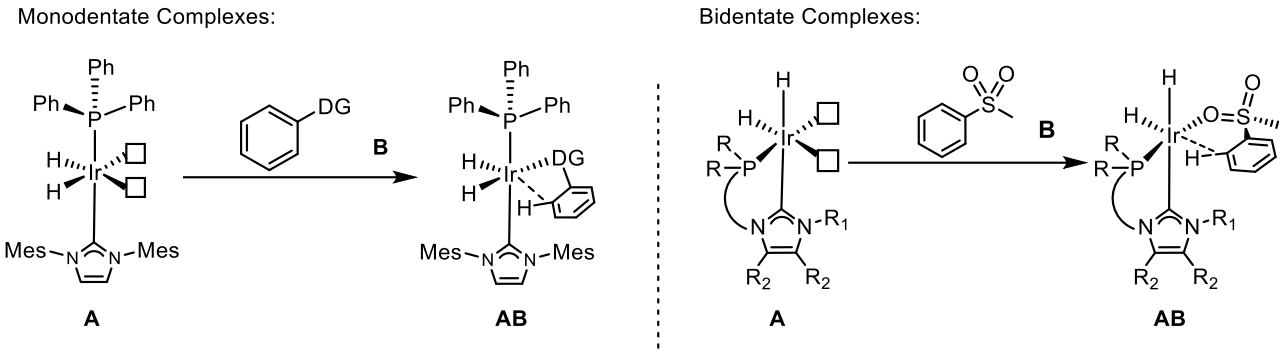

Scheme 8.7

The electronic energy for each of these structures was then used in Equation **2**, in order to deliver the binding energy (ΔE_{Bind}) discussed in the manuscript.

$$\Delta E_{Bind} = \left[E_{AB}^{\alpha\beta}(AB) - E_{AB}^{\alpha\beta}(A) - E_{AB}^{\alpha\beta}(B)\right] + \left[\left(E_{AB}^{\alpha}(A) - E_{A}^{\alpha}(A)\right) + \left(E_{AB}^{\beta}(B) - E_{B}^{\beta}(B)\right)\right] \quad \mathbf{2}$$

Key: $E_{geometry}^{basis\ set}(structure)$

Equation **2** can be simplified into terms describing the counterpoise corrected interaction energy (E_{int}) and the sum of distortion energies (E_{dist}), as shown in Equation **3**.

$$\Delta E_{Bind} = E_{int} + E_{dist} \quad \mathbf{3}$$

A full account of the individual electronic energies as calculated in Gaussian 09 are reported in the appendix.

8.19 Solid Angle Analysis using SolidG

Solid angle measurements, as well as the derived values, were made using the program SolidG. Structures were first optimised using DFT calculations *via* Gaussian 09, as described in the general computational details section. In order to investigate the solid angle properties of the full catalyst/substrate combination, the hydride ligands were removed, and the remaining coordinates input directly into the SolidG software. Similarly, in order to obtain decomposed

values for the catalyst fragments, the relevant moiety was also removed. This is broadly summarised for the NHC-P system in **Scheme 8.8**. Visual representation of the solid angle analysis was performed on the accompanying SolidAngleGL software. The solid angle associated with the substrate molecule is coloured in red, while that of the ligand motif is coloured in blue. The granularity was set to 900 for all images shown.

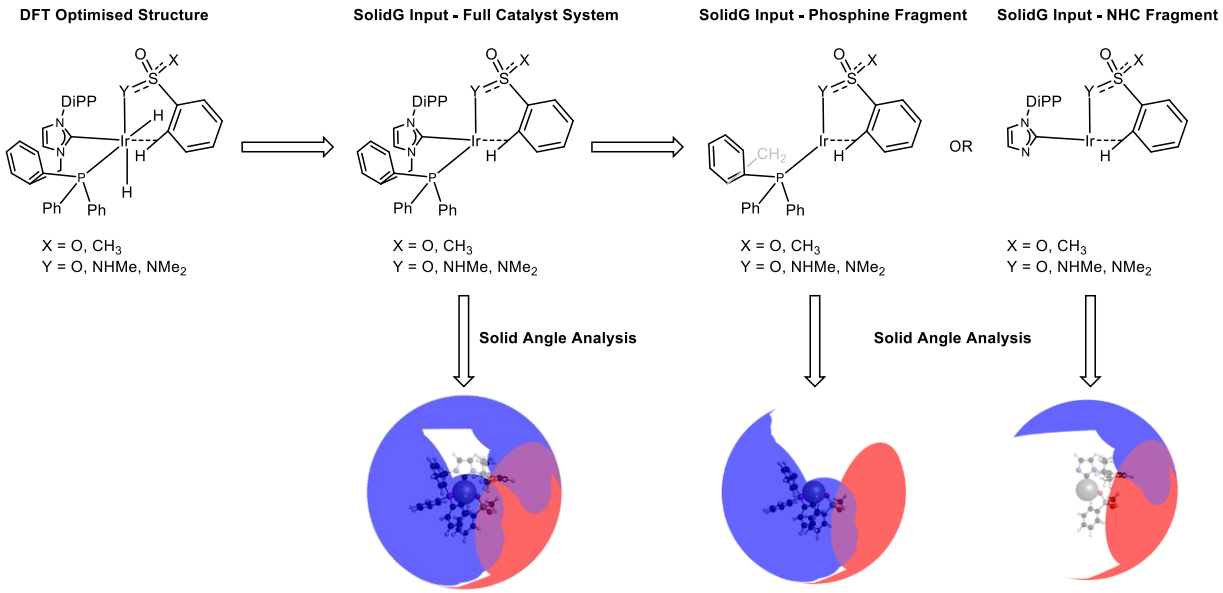

Scheme 8.8

The output from the SolidG software, along with the coordinates used, can be found in the appendix section.

9. References

[1] Mullard, A. 2013 FDA drug approvals. *Nat. Rev. Drug Discov.* **2013**, *13*, 85-89.
[2] Waring, M. J.; J., Arrowsmith; A. R., Leach; P. D., Mandrell, S.; Owen, R. M.; Pairaudeau, G.; Pennie, W. D.; Picket, S. D.; Wang, J.; Wallace, O.; Weir, A. An analysis of the attrition of drug candidates from four major pharmaceutical companies. *Nat. Rev. Drug Discov.* **2015**, *14*, 475-486.
[3] Mullard, A. New drugs cost US42.6 billion to develop. *Nat. Rev. Drug Discov.* **2014**, *13*, 877-877.
[4] DiMasi, J. A.; Grabowski, H. G.; Hansen, R. W. Innovation in the pharmaceutical industry: New estimates of R&D costs. *J. Health Econ.* **2016**, *47*, 20-33.
[5] Turner, M. J. The current state of drug discovery and what it might take to improve drug discover outcomes and approval successes. *Drug Discov. Today* **2015**, *20*, 917-919.
[6] Hay, M.; Thomas, D. W.; Craighead, J. L.; Economides, C.; Rosenthal, J. Clinical development success rates for investigational drugs. *Nat. Biotechnol*. **2014**, *32*, 40-51.
[7] European Federation of Pharmaceutical Industries and Associations. *Industry in Figures*, **2018**.
[8] Tetko, I. V.; Bruneau, P.; Mewes, H-W.; Rohrer, D. C.; Poda, G. I. Can we estimate the accuracy of ADME-Tox predictions? *Drug Discov. Today*, **2006**, *11*, 700-707.
[9] Lipinski, C. A.; Lombardo, F.; Dominy, B. W.; Feeney, P. J. Experimental and computational approaches to estimate solubility and permeability in drug discovery and development settings. *Adv. Drug. Deliv. Rev.* **2001**, *46*, 3-26.
[10] Wager, T. T.; Chandrasekaran, R. Y.; Hou, X.; Troutman, M. D.; Verhoest, P. R.; Villalobos, A.; Will, Y. Defining desirable central nervous system drug space through the alignment of molecular properties, *in vitro* ADME, and safety attributes. *ACS Chem. Neurosci.* **2010**, *1*, 420-434.
[11] Wager, T. T.; Hou, X.; Verhoest, P. R.; Villalobos. Central nervous system multiparameter optimization desirability: Application in drug discovery. *ACS Chem. Neurosci.* **2016**, *7*, 767-775.
[12] Atzrodt, J.; Derdau, V.; Kerr, W. J.; Reid, M. Deuterium- and tritium-labelled compounds: Applications in life sciences. *Angew. Chem. Int. Ed.* **2018**, *57*, 1758-1784.
[13] Werstiuk, N. H.; Kadai, T. Acid-catalyzed exchange at 250 °C; a simple and quantitative method for the replacement of aromatic protons by deuterium. *Can. J. Chem*. **1973**, *51*, 1485-1486.
[14] Werstiuk, N. H.; Kadai, T. The high temperature and dilute acid (HTDA) procedure as a general method of replacing aromatic hydrogen by deuterium. *Can. J. Chem*. **1974**, *52*, 2169-2171.
[15] Werstiuk, N. H.; Timmins, G. Hydrogen-deuterium exchange and rearrangement of polycyclic aromatic hydrocarbons in dilute acid medium at elevated temperatures. *J. Can. Chem*. **1981**, *59*, 3218-3219.
[16] Shibasaki, H.; Furuta, T.; Kasuya, Y. Preparation of multiply deuterium-labelled cortisol. *Steroids*, **1992**, *57*, 13-17.
[17] Yamamoto, M.; Oshima, K.; Matsubara, S. Platinum(IV) oxide catalyzed H—D exchange reactions in arylsilanes. *Org. Lett.* **2004**, *6*, 5015-5017.
[18] Baram P.S.; Corey, E. J. A short synthetic route to (+)-austamide, (+)-deoxyisoaustamide, and (+)-hydrati=oaustamide from a common precursor by a novel palladium-mediated indole – Dihydroindoloazocine cyclisation. *J. Am. Chem. Soc.* **2002**, *124*, 7904-7905.
[19] Hutchison, A. J.; Kishi, Y. Stereospecific total synthesis of dl-austamide. *J. Am. Chem. Soc.* **1979**, *101*, 6786-6788.
[20] Gröll, B.; Schnürch, M.; Mihovilovic, M. D. Selective Ru(0)-catalyzed deuteration of electron-rich and elecron-poor nitrogen containing heterocycles. *J. Org. Chem.* **2012**, *77*, 4432-4437.
[21] Yu, R. P.; Hesk, D.; Rivera, N.; Pelczer, I.; Chirik, P. J. Iron-catalyzed tritiation of pharmaceuticals, *Nature*, **2016**, *529*, 195-199.
[22] Palmer, W. N.; Chirik, P.; J. Cobalt-catalyzed stereoretentive hydrogen isotope exchange of C(sp3)—H bonds. *ACS Catal.* **2017**, *7*, 5674-5678.
[23] Lockley, W. J. S. Regioselective deuterium labelling of aromatic acids, amides and amines using groups VIII metal catalysts. *J. Label. Compd. Radiopharm.* **1984**, *21*, 45-57.
[24] Hesk, D.; Jones, J .R.; Lockley, W. J. S. Regiospecific deuteration and tritiation of various drugs using a homogeneous rhodium trichloride catalyst. *J. Pharma. Sci.* **1991**, *80*, 887-890.
[25] Salter, R. The development and use of iridium(I) phosphine systems for ortho-directed hydrogen-isotope exchange. *J. Label. Compd. Radiopharm.* **2010**, *53*, 654-657.
[26] Atzrodt, J.; Derdau, V.; Kerr, W. J.; Reid, M. C—H functionalisation for hydrogen isotope exchange. *Angew. Chem. Int. Ed.* **2018**, *57*, 3022-3047.
[27] Crabtree, R. H.; Felkin, H.; Morris, G. E. Cationic diolefin complexes as alkene hydrogenation catalysts and the isolation of some related hydrido complexes. *J. Organomet. Chem*. **1977**, *141*, 205-215.

[28] Hesk, D.; Das, P. R.; Evans, D. Deuteration of acetanilites and other substituted aromatics using [Ir(COD)(Cy_3P)(Py)]PF_6 as catalyst. *J. Label. Compd. Radiopharm.* **1995**, *36*, 497-502.
[29] Ellames, G. J.; Gibson, J. S.; Herbert, J. M.; McNeill, A. H. The scope and limitations of deuteration mediated by Crabtree's catalyst. *Tetrahedron* **2001**, *57*, 9487-9497.
[30] Brown, J. A.; Irvine, S.; Kennedy, A. R.; Kerr, W. J.; Andersson, S.; Nilsson, G. N. Highly active iridium(I) complexes for catalytic hydrogen isotope exchange. *Chem. Commun.* **2008**, 1115-1117.
[31] Brown, J. A.; Cochrane, A. R.; Irvine, S.; Kerr, W. J.; Mondal, B.; Parkinson, J. A.; Paterson, L. C.; Reid, M.; Tuttle, T.; Andersson, S.; Nilsson, A. N.The synthesis of highly active iridium(I) complexes and their application in catalytic hydrogen isotope exchange. *Adv. Synth. Catal.* **2014**, *356*, 3551-3562.
[32] Devlin, J.; Kerr, W. J.; Lindsay, D. M.; McCabe, T. J. D.; Reid, M.; Tuttle, T. Iridium-catalysed ortho-directed deuterium labelling of aromatic esters - An experimental and theoretical study on directing group chemoselectivity. *Molecules*, **2015**, *20*, 11676-11698.
[33] Atzrodt, J.; Derdau, V.; Kerr, W. J.; Reid, M.; Rojahn, P.; Weck. R. Expended applicability of iridium(I) NHC/Phosphine catalysts in hydrogen isotope exchange processes with pharmaceutically-relevant heterocycles. *Tetrahedron* **2015**, *71*, 1924-1929.
[34] Kerr, W. J.; Mudd, R. J.; Paterson, L. C.; Brown, J. A. Iridium(I)-catalyzed regioselective C—H activation and hydrogen isotope exchange of non-aromatic unsaturated functionality. *Chem Eur. J.* **2014**, *20*, 14604-14607.
[35] Simonsson, R.; Stenhagen, Gunnar, Ericsson, C.; Elmore, C. S. Synthesis of ximelagatran, melagatran, hydroxymelagatran, and ethylmelagatran in H-3 labelled form. *J. Label. Compd. Radiopharm.* **2013**, *56*, 334-337.
[36] Allen, P. A.; Bragg, R. A.; Caffrey, M.; Ericsson, C.; Hickey, M. J.; Kingston, L. P.; Elmore, C. S. The synthesis of a tritium, carbon-14, and stable isotope-labelled cathepsin C inhibitors. *J. Label. Compd. Radiopharm.* **2017**, *60* 124-129.
[37] Elmore, C. S.; Hall, J. E.; Ye, X.; Hey, J. R. Synthesis of two isotopically labelled 5-HT_{1B} antagonists. *J. Label. Compd. Radiopharm.* **2007**, *50*, 412-413.
[38] Lindelöf, A.; Ericsson, C.; Simonsson, R.; Nilsson, G.; Grönberg, G.; Elmore, C. S. Synthesis of [^{3}H] and [$^2H_6$]AZD6642, an inhibitor of 5-lipoxygenase activating protein (FLAP). *J. Label. Compd. Radiopharm.* **2016**, *59*, 340-345.
[39] Modvig, A.; Andersen, T. L.; Taaning, R. H.; Lindhardt, A. T.; Skrydstrup, T. Two-chamber hydrogen generation and application: Access to pressurized deuterium gas. *J. Org. Chem.* **2014**, *79*, 5861-5868.
[40] Flinker, M.; Yin, H.; Juhl, R. W.; Eikeland, E. Z.; Overgaard, J.; Nielsen, D. U.; Skrydstrup, T. Efficient water reduction with sp^3-sp^3 diboron(4) compounds: Application to hydrogenations, H-D exchange reactions, and carbonyl reductions. *Angew. Chem. Int. Ed.* **2017**, *56*, 15910-15915.
[41] Cochrane, A. R,; Idziak, C.; Kerr, W. J.; Mondal, B.; Paterson, L. C.; Tuttle, T.; Andersson, S.; Nilsson, G. N. Anion effects to deliver enhanced iridium catalysts for hydrogen isotope exchange processes. *Org. Biomol. Chem.* **2014**, *12*, 3598-3603.
[42] Kennedy, A. R.; Kerr, W. J.; Moir, R.; Reid, M. Anion effects to deliver enhanced iridium catalysts for hydrogen isotope exchange processes, *Org. Biomol. Chem*. **2014**, *12*, 7927-7931.
[43] Kerr, W. J.; Mudd, R. J.; Owens, P. K.; Reid, M.; Brown, J. A.; Campos, S. Hydrogen isotope exchange with highly active iridium(I) NHC/phosphine complexes: a comparative counterion study. *J. Label. Compd. Radiopharm.* **2016**, *59*, 601-603.
[44] Kerr, W. J.; Lindsay, D. M.; Reid, M.; Atzrodt, J.; Derdau, J.; Rojahn, P.; Weck, R. Iridium-catalyzed *ortho*-H/D and -H/T exchange under basic conditions: C—H activation of unprotected tetrazoles. *Chem. Commun*. **2016**, *52*, 6669-6672.
[45] Kerr, W. J.; Reid, M.; Tuttle, T. Iridium catalyzed C—H activation and deuteration of primary sulfonamides: An experimental and computational study. *ACS Catal*. **2015**, *5*, 402-410.
[46] Kerr, W. J.; Reid, M.; Tuttle, T. Iridium-catalyzed formyl-selective deuteration of aldehydes. *Angew. Chem. Int. Ed.* **2017**, *56*, 7808-7812.
[47] Kerr, W. J.; Lindsay, D. M.; Owens, P. K.; Reid, M.; Tuttle, T.; Campos, S. Site-selective deuteration of *N*-heterocycles *via* iridium-catalyzed hydrogen isotope exchange. *ACS Catal.* **2017**, *7*, 7182-7186.
[48] Kerr, W. J.; Mudd, R. J.; Reid, M.; Atzrodt, J.; Derdau, V. Iridium-catalyzed Csp^3—H activation for mild and selective hydrogen isotope exchange. *ACS Catal*. **2018**, *8*, 10895-10900.
[49] Valero, M.; Weck, W.; Güssregen, S.; Atzrodt, J.; Derdau, V. Highly selective directed iridium-catalyzed hydrogen isotope exchange reactions of aliphatic amides. *Angew. Chem. Int. Ed.* **2018**, *57*, 8159-8163.
[50] Parmentier, M.; Hartung, T.; Pfaltz, A.; Muri, D. Iridium-catalyzed H/D exchange: Ligand complexes with improved efficiency and scope. *Chem. Eur. J.* **2014**, *20*, 11496-11504.
[51] Powell, M. T.; Hou, D-R.; Perry, M. C.; Cui, X.; Burgess, K. Chiral imidazolylidene ligands for asymmetric hydrogenation of aryl alkenes. *J. Am. Chem. Soc*. **2001**, *123*, 8878-8879.
[52] Burhop, A.; Weck, R.; Atzrodt, J.; Derdau, V. Hydrogen-isotope exchange (HIE) reactions of secondary and tertiary sulfonamides and sulfonylureas with iridium(I) catalysts. *Eur. J. Org. Chem.* **2017**, 1418-1424.

[53] Burhop, A.; Prohaska, R.; Weck, R.; Atzrodt, J.; Derdau, V. Burgess iridium(I)-catalyst for selective hydrogen isotope exchange. *J. Label. Compd. Radiopharm.* **2017**, *60*, 343-348.
[54] Jess, K.; Derdau, V.; Weck, R.; Atzrodt, J.; Freytag, M.; Jones, P. G.; Tamm, M. Hydrogen isotope exchange with iridium(I) complexes supported by phosphine-imidazolin-2-imine P,N ligands. *Adv. Synth. Catal.* **2017**, *359*, 629-638.
[55] Valero, M.; Burhop, A.; Jess, K.; Weck, R.; Tamm, M.; Atzrodt, J.; Derdau, V. Evaluation of a P,N-ligated iridium(I) catalyst in hydrogen isotope exchange reactions of aryl and heteroaryl compounds. *J. Label. Compd. Radiopharm.* **2018**, *61*, 380-385.
[56] Hartwig, J. Organotransition metal chemistry: From bonding to catalysis; University Science Books, Berkley, 2010.
[57] Tolman, C. A. Electron donor-acceptor properties of phosphorus ligands. Substituent additivity. *J. Am. Chem. Soc.* **1970**, *92*, 2953-2956.
[58] Tolman, C. A. Steric effects of phosphorus ligands in organometallic chemistry and homogeneous catalysis. *Chem. Rev.* **1977**, *77*, 313-348.
[59] Bilbrey, J. A.; Kazez, A. H.; Locklin, J.; Allen, W. D. Exact ligand cone angles. *J. Comput. Chem.* **2013**, *34*, 1189-1197.
[60] Arduengo III, A. J.; Harlow, R. L.; Kline, M. A stable crystalline carbene. *J. Am. Chem. Soc.* **1991**, *113*, 361-363.
[61] Kelly III, R. A.; Clavier, H.; Guidice, S.; Scott, N. M.; Stevens, E. D.; Bordner, J.; Samardjiev, I.; Hoff, C. D.; Cavallo, L.; Nolan, S. P. Determination of *N*-heterocyclic carbene (NHC) steric and electronic parameters using the [(NHC)Ir$(CO)_2$Cl] system. *Organomet.* **2008**, *27*, 202-210.
[62] Huynh, H. V. Electronic properties of N-heterocyclic carbenes and their experimental determination. *Chem. Rev.* **2018**, *118*, 9457-9492.
[63] (a) **Values for SIMes**: (I) Wolf, S.; Plenio, H. Synthesis of (NHC)Rh(cod)Cl and (NHC)RhCl$(CO)_2$ Complexes - Translation of the Rh- into the Ir- Scale for the Electronic Properties of NHC Ligands. *J. Organomet. Chem.* **2009**, *694*, 1487−1492. (II) Iglesias, M.; Beetstra, D. J.; Kariuki, B.; Cavell, K. J.; Dervisi, A.; Fallis, I. A. Synthesis and Structural Features of Rhodium Complexes of Expanded Ring *N*-Heterocyclic Carbenes. *Eur. J. Inorg. Chem.* **2009**, 1913−1919. (III) Türkmen, H.; Çetinkaya, B. N-Heterocyclic Carbene Complexes of Rh(I) and Electronic Effects on Catalysts for 1,2-Addition of Phenylboronic Acid to Aldehydes. *Appl. Organomet. Chem.* **2011**, *25*, 226−232.(IV) Türkmen, H.; Çetinkaya, B. 1,3-Diarylimidazolidin-2-Ylidene (NHC) Complexes of Pd(II): Electronic Effects on Cross-Coupling Reactions and Thermal Decompositions. *J. Organomet. Chem.* **2006**, *691*, 3749−3759. (b) **Values for 6-Mes**: (I) Iglesias, M.; Beetstra, D. J.; Kariuki, B.; Cavell, K. J.; Dervisi, A.; Fallis, I. A. Synthesis and Structural Features of Rhodium Complexes of Expanded Ring *N*-Heterocyclic Carbenes. *Eur. J. Inorg. Chem.* **2009**, 1913−1919. (II) César, V.; Lugan, N.; Lavigne, G. Electronic Tuning of a Carbene Center *via* Remote Chemical Induction, and Relevant Effects in Catalysis. *Chem. Eur. J.* **2010**, *16*, 11432−11442. (c) **Values for IPr and SIPr**: Dorta, R.; Stevens, E. D.; Hoff, C. D.; Nolan, S. P. Stable, Three-Coordinate Ni$(CO)_2$(NHC) (NHC = N-Heterocyclic Carbene) Complexes Enabling the Determination of Ni-NHC Bond Energies. *J. Am. Chem. Soc.* **2003**, *125*, 10490−10491. (d) **Value for IMes^{Br}**: Urbina-Blanco, C. A.; Bantreil, X.; Clavier, H.; Slawin, A. M. Z.; Nolan, S. P. Backbone Tuning in Indenylidene-Ruthenium Complexes Bearing an Unsaturated *N*-Heterocyclic Carbene. Beilstein *J. Org. Chem.* **2010**, *6*, 1120−1126. (e) **Value for Me$_2$-pery**: Verlinden, K.; Ganter, C. Converting a Perimidine Derivative to a Cationic *N*-Heterocyclic Carbene. *J. Organomet. Chem.* **2014**, *750*, 23−29. (f) **Values for CAAC^{Cy} and CAAC^{Menthyl}**: Paul, U. S. D.; Radius, U. Synthesis and Reactivity of Cyclic (Alkyl)(amino)carbene Stabilized Nickel Carbonyl Complexes. *Organometallics* **2017**, *36*, 1398−1407.
[64] Huynh, H. V.; Han, Y.; Jothibasu, R.; Yang, J. A. ^{13}C NMR spectroscopic determination of ligand donor strengths using *N*-heterocyclic carbene complexes of palladium(II). *Organometallics* **2009**, *28*, 5395-5404.
[65] Teng, Q.; Huynh, H. V. A unified ligand electronic parameter based on ^{13}C NMR spectroscopy of *N*-heterocyclic carbene complexes. *Dalton Trans.* **2017**, *46*, 614-627.
[66] (a) **Values for SIBn, IBn, Bn$_2$-bimy, Bn$_2$-tazy, IMesBn, and IMes:** Huynh, H. V.; Han, Y.; Jothibasu, R.; Yang, J. A. ^{13}C NMR Spectroscopic Determination of Ligand Donor Strengths Using *N*-Heterocyclic Carbene Complexes of Palladium(II). *Organometallics* **2009**, *28*, 5395−5404. (b) **Values for trz15 and trz21**: Wright, J. R.; Young, P. C.; Lucas, N. T.; Lee, A.; Crowley, J. D. Gold(I) and Palladium(II) Complexes of 1,3,4-Trisubstituted 1,2,3-Triazol-5-Ylidene "Click" Carbenes: Systematic Study of the Electronic and Steric Influence on Catalytic Activity. *Organometallics* **2013**, *32*, 7065−7076. (c) **Value for trz19**: Yuan, D.; Huynh, H. V. 1,2,3-Triazolin-5-Ylidenes: Synthesis of Hetero-Bis(carbene) Pd(II) Complexes, Determination of Donor Strengths, and Catalysis. *Organometallics* **2012**, *31*, 405−412.
[67] Liske, A.; Verlinden, K.; Buhl, H.; Schaper, K.; Ganter, C. Determining the π-acceptor properties of *N*-heterocyclic carbenes by measuring the ^{77}Se NMR chemical shifts of their selenium adducts. *Organometallics* **2013**, *32*, 5269-5272.

[68] Vummaleti, A. V. C.; Nelson, D. J.; Poater, A.; Gómez-Suárez, A.; Cordes, D. B.; Slawin, A. M. Z.; Nolan, S. P.; Cavallo, L. *Chem. Sci.* **2015**, *6*, 1895-1904.
[69] Cheng, G-J.; Zhang, X.; Chung, L. W.; Xu, L.; Wu, Y-D. *J. Am. Chem. Soc.* **2015**, *137*, 1706-1725.
[70] Plata, R. E.; Singleton, D. A case study of the mechanism of alcohol-mediated Morita Baylis-Hillman reactions. The importance of experimental observations. *J. Am. Chem. Soc.* **2015**, *137*, 3811-3826.
[71] Houk, K. N.; Cheong, P. H-Y. Computational prediction of small-molecule catalysts. *Nature*, **2008**, *455*, 309-313.
[72] Poree, C.; Schonenbeck, F. A holy grail in chemistry: Computational catalyst design: Feasible or fiction? *Acc. Chem. Res.* **2017**, *50*, 605-608.
[73] Reid, J. P.; Sigman, M. S. Comparing quantitative prediction methods for the discovery of small-molecule chiral catalysts. *Nat. Rev. Chem.* **2018**, *2*, 290-305.
[74] Reid, M. On the design and further applications of iridium(I) complexes in hydrogen isotope exchange processes. PhD Thesis, University of Strathclyde, 2015.
[75] Boys, S. F.; Bernardi, F. The calculation of small molecular interactions by the differences of separate total energies. Some procedures with reduced errors. *Mol. Phys.* **1970**, *19*, 553-566.
[76] Wang, A-E.; Xi, J-H.; Wang, L-X. ; Zhour, Q-L. Triaryl phosphine-functionalised N-heterocyclic carbene ligands for Heck reaction. *Tetrahedron* **2005**, *61*, 259-266.
[77] Chan, A.; Scheidt, K. A. Highly stereoselective formal [3+3] cycloaddition of enals and azomethine imines catalyzed by N-heterocyclic carbenes. *J. Am. Chem. Soc.* **2007**, *129*, 5334-5335.
[78] Crabtree. R. H. The organometallic chemistry of the transition metals, 4th ed.; Wiley-VCH Verlag GmbH & Co. KGaA, 2005.
[79] Poater, A.; Cosenza, B.; Correa, A.; Giudice, S.; Ragone, F.; Scarano, V.; Cavallow, L. SambVca,: A web application for the calculation of the buried volume of *N*-heterocyclic carbene ligands. *Eur. J. Inorg. Chem.* **2009**, 1759-1766.
[80] Scott, J. S.; Bowker, S. S.; Brocklehurst, K. J.; Brown, H. S.; Clarke, D. S.; Easter, A.; Ertan, A.; Goldberg, K.; Hudson, J. A.; Kavanagh, S.; Laber, D.; Leach, A. G.; Macfaul, P. A.; Martin, E. A.; McKerrecher, D.; Schofield, P.; Svensson, P. H.; Teague, J. Circumventing seizure activity in a series of G protein coupled receptor 119 (GPR119) agonists. *J. Med. Chem.* **2014**, *57*, 8984-8989
[81] Vanjari, R.; Guntreddi, T.; Singh, K. N. Palladium-catalyzed site-selective C—H functionalisation of weakly coordinating sulfonamides: Synthesis of biaryl sulfonamides.*Chem. Asian J.* **2016**, *11*, 696-699.
[82] Cheng, G.; Wang, P.; Yu, J-Q. *meta*-C—H arylation and alkylation of benzylsulfonamide enables by a palladium(II)/isoquinoline catalyst. *Angew. Chem. Int. Ed.* **2017**, *56*, 8183-8186.
[83] Dai, H-X.; Stepan, A. F.; Plummer, M. S.; Zhang, Y-H.; Yu, J-Q. Divergent C—H functionalisations directed by sulfonamide pharmacophores: Late-stage diversification as a tool for drug discovery. *J. Am. Chem. Soc.* **2011**, *113*, 7222-7228.
[84] Pham, M. V.; Ye, B.; Cramer, N. Access to sulfams by rhodium(III)-catalyzed directed C—H activation. *Angew. Chem. Int. Ed.* **2012**, *51*, 10610-10614.
[85] Thrimurtulu, N.; Nallagonda, R.; Volla, C. M. R. Cobalt-catalyzed aryl C—H activation and highly regioselective intermolecular annulation of sulfonamides with allenes. *Chem. Commun.* **2017**, *53*, 1872-1875.
[86] Kerr, W. J.; Knox, G. J.; Reid, M.; Tuttle, T. Rational Catalyst Design in C—activation: A case study in intramolecular directing group selectivity in iridium catalysis. Paper submitted.
[87] Guzei, I. A.; Wendt, M. An improved method for the computation of ligand steric effects based on solid angles. *Dalton Trans.* **2006**, 3991-3999.
[88] R. Fraser, C. G. C. E. van Sittert, R. H. van Rooyen, M. Landman. Ynthesis and structural investigation of mono- and dimetallic *N*-heterocyclic carbene complexes of groups VII transition metals. *J. Organomet. Chem.* **2017**, *835*, 60-69.
[89] A. H. Christian Z. L. Niemeyer, M. S. Sigman, D. F. Toste. Uncovering subtle ligands effects of phosphines using gold(I) catalysis. *ACS Catal.* **2017**, *7*, 3973-3978.
[90] J. Wang, Z. Su, N. Yang, C. Hu. Mechanistic study of the asymmetric carbonyl-ene reaction between alkyl enol ethers and Isatin catalyzed by the *N,N'*-dioxide-$Mg(OTf)_2$ complex. *J. Org. Chem.* **2016**, *81*, 6444-6456.
[91] Z. L. Neimeyer, A. Milo, D. P. Hickey, M. S. Sigman. Paramaterization of phosphine ligands reveals mechanistic pathways and predicts reaction outcomes. *Nat. Chem.* **2016**, *8*, 610-617.
[92] M. N. Magubane, G. S. Nyamato, S. O. Ojwach, O. Q. Munro, Structural, kinetic, and DFT studies of the of the transfer hydrogenation of ketones mediated by (pyrazole)pyridine iron(II) and nickel(II) complexes. *RSC Adv.* **2016**, *6*, 65205-65221.
[93] C. Chen, S. M. Bellows, P. L. Holland. Tuning steric and electronic effects in transition-metal ß-diketiminate complexes. *Dalton Trans.* **2015**, *44*, 16654-16670
[94] Zhao, S.; Gensch, T.; Murray, B.; Niemeyer, Z. L.; Sigman, M. S.; Biscoe, M. R. Enantiodivergent Pd-catalyzed C—C bond formation enabled through ligand paramaterization. *Science* **2018**, *362*, 670-674

[95] Ruddleston, A. J.; Mewis, R. E.; Green, G. R.; Whitwood, A. C.; Duckett, S. B. Catalytic transfer of magnetism using a neutral iridium phenoxide complex. *Organometallics* **2015**, *34*, 2997-3006.
[96] Liang, Q.; Song, D. Reactivity of Fe and Ru complexes of picolyl-substituted *N*-heterocyclic carbene ligand: Diverse coordination modes and small molecule binding. *J. Inorg. Chem.* **2017**, *56*, 11956-11970.
[97] Lücking, U. Sulfoximines: A neglected opportunity in medicinal chemistry. *Angew. Chem. Int. Ed*. **2013**, *52*, 9399-9408.
[98] Sirvent, J. A.; Lücking, U. Novel pieces for the emerging picture of sulfoximines in drug discovery: Synthesis and evaluation of sulfoximine analogues of marketerd drugs and advances clinical candidates. *Chem. Med. Chem.* **2017**, *12*, 587-501.
[99] Hendriks, C. M. M.; Hartkamp, J.; Wiezorek, S.; Steinkamp, A-D.; Rossetti, G.; Lüscher, B.; Bolm, C. Sulfoximines as ATR knhibitors: Analogs of VE-821. *Bioorg. Med. Chem. Lett.* **2017**, 2659-2662.
[100] Lücking, U.; Jautelat, R.; Krüger, M.; Brumby, T.; Lienau, P.; Schäfer, M.; Briem, H.; Schulze, J; Hillisch, A.; Reichel, A.; Wengner, A. M.; Siemeister, G. The Lab Oddity Prevails: Discovery of Pan-CDK Inhibitor (R)-S-Cyclopropyl-S-(4-{[4-{[(1R,2R)-2-hydroxy-1-methylpropyl]oxy}-5-(trifluoromethyl)pyrimidin-2-yl]amino}phenyl)sulfoximide (BAY 1000394) for the Treatment of Cancer. *Chem. Med. Chem.* **2013**, *8*, 1067-1085.
[101] Satzinger, G. Drug discovery and commercial exploitation. *Drug News Perspect.* **2001**, *14*, 197-207.
[102] Foote, K. M.; Nissink, J. W. M.; McGuire, T.; Turner, P.; Giuchard, S.; Yates, J. W. T.; Lau, A.; Blades, K.; Heathcote, D.; Odedra, R.; Wilkinson, G.; Wilson, Z.; Wood, C. M.; Jewsbury, P. J. Discovery and Characterization of AZD6738, a Potent Inhibitor of Ataxia Telangiectasia Mutated and Rad3 Related (ATR) Kinase with Application as an Anticancer Agent. *J. Med. Chem.* **2018**, *61*, 9899-9907.
[103] Fernández, J.; Alonso, J. M.; Andrés, J. I.; Cid, J. M.; Díaz, A.; Iturrino, L.; Gil, P.; Megens, A.; Sipido, V. K.; Trabanco, A. A. Discovery of new tetracyclic tetrahydrofuran derivatives as potential broad-spectrum psycotropic agents. *J. Med. Chem.* **2005**, *48*, 1709-1712.
[104] Stover, C. K.; Warrener, P.; VanDevanter, D. R.; Sherman, D. R.; Arain, T. M.; Langhorne, M. H.; Anderson, S. W.; Towell, J. A.; Yuan, Y.; McMurray, D. N.; Kreiswirth, B. N.; Barry, C. E.; Baker, W. R. A small molecule nitroimidazopyran drug candidate for the treatment of tuberculosis. *Nature* **2000**, *405*, 962–966.
[105] Biftu, T.; Sinha-Roy, R.; Chen, P.; Qian, X.; Feng, D.; Keuthe, J. T.; Scapin, G.; Gao, Y. D.; Yan, Y.; Krueger, D.; Bak, A.; Eiermann, G. He, J.; Cox, J.; Hicks, J.; Lyons, K.; He, H.; Salituro, G.; Tong, S.; Patel, S.; Doss, G.; Petrov, A.; Wu, J.; Xu, S. S.; Sewall, C.; Zhang, X.; Xhang, B.; Thornberry, N. A.; Weber, A. E. Omarigliptin (MK-3102): A novel long-acting DPP-4 inhibitor for once-weekly treatment of type 2 diabetes. *J. Med. Chem.* **2014**, *57*, 3205-3212.
[106] Battersby, A. S. Applications of tritium labelling for the exploration of biochemical mechanisms. *Acc. Chem Res.* **1972**, *5*, 148-154.
[107] Filer, C. N. Morphinan alkaloids labelled with tritium: Synthesis and applications. *J. Label. Compd. Radiopharm.* **2013**, *56*, 639-648.
[108] Filer, C. N. Tritium-labelled alkaloids: Synthesis and applications. *J. Label. Compd. Radiopharm.* **2017**, *60*, 96-109.
[109] Filer, C. N. Iboetnic acid: On the mechanism of its conversion to [^{3}H] muscimol. *J. Radioanal. Nucl. Chem.* **2018**, *318*, 2033-2038.
[110] Stitch, S. R.; Toumba, J. K.; Groen, M. B.; Funke, C. W.; Leemhius, J.; Vink, J.; Woods, G, F. Excretion, isolation and structure of a new phenolic constituent of female urine. *Nature* **1980**, *287*, 738-740.
[111] Setchell, K. D. R.; Lawson, A. M.; Mitchel, F. L.; Adlercreutz, H.; Kirk, D. N.; Axelson, M. Lignans in man and in animal species, *Nature* **1980**, *287*, 740-742.
[112] Saleem, M.; Kim, H. J.; Ali, M. S.; Lee, Y. S. An update on bioactive plant lignans. *Nat. Prod. Rep.* **2005**, *22*, 696-716.
[113] Gautam, R.; Jachak, S. M. Recent developments in anti-inflammatory natural products. *Med. Res. Rev.* **2009**, *29*, 767-820.
[114] Pan, J-Y.; Chen, S-L.; Yang, M-H.; Wu, J.; Sinklonen, J.; Zou, K. An update on liganans: Natural products and synthesis. *Nat. Prod. Rep.* **2009**, *26*, 1251-1292.
[115] Setchell, K. D. R.; Lawson, A. M.; McLaughlin, L. M.; Patel, S.; Axelson, M. Measurement of enterolactone and enterodiol, the first mammalian lignans, using stable isotope dilution and gas chromatography mass spectrometry. *Biomed. Mass Spec.* **1983**, *10*, 227-235.
[116] Wähälä, K.; Rasku, S. Synthesis of D_4-genistein, a stable deutero-labelled isoflavone, by a perdeuteration-selective dedeuteration approach. *Tet. Lett.* **1997**, *38*, 7287-7290.
[117] Leppälä, E. Pohjoispää, M.; Koskimies, J.; Wähälä, K. Synthesis of new deuterium-labelled linanolactones. *J. Label. Compd. Radiopharm.* **2008**, *51*, 407-412.
[118] Biavatti, M.W.; Vieira, P.C.; da Silva, M.F.; Fernandes, J.B.; Degani, A.L.; Cass, Q.B.; Schefer; A.B.; Ferreira, A.G. Separation and NMR studies on lignans of Raulinoa echinata. *Phytochem. Anal.* **2001**, *12*, 64–68.
[119] Vuckovic, I.; Trajkovic, V.; Macura, S.; Tesevic, V.; Janackovic, P.; Milosavljevic, S. A

novel cytotoxic lignan from Seseli annuum L. *Phytother. Res.* **2007**, *21*, 790–792.
[120] Céspedes, C.L.; Ávila, J.G.; Garcia, A.M.; Becerra, J.; Flores, C.; Aqueveque, P.; Bittner, M.; Hoeneisen, M.; Martinez, M.; Silva, M. Antifungal and antibacterial activities of Araucaria araucana (Mol.) K. Koch heartwood lignans. *Z. Naturforsch. [C]* **2006**, *61*, 35–43.
[121] Cantrell, C.L.; Schrader, K.K.; Mamonov, L.K.; Sitpaeva, G.T.; Kustova, T.S.; Dunbar, C.; Wedge, D.E. Isolation and identification of antifungal and antialgal alkaloids from Haplophyllum sieversii. *J. Agric. Food Chem.* **2005**, *53*, 7741–7748.
[122] Chae, S.H.; Kim, P.S.; Cho, J.Y.; Park, J.S.; Lee, J.H.; Yoo, E.S.; Baik, K.U.; Lee, J.S.; Park, M.H. Isolation and identification of inhibitory compounds on TNF-alpha production from Magnolia fargesii. *Arch. Pharm. Res.* **1998**, *21*, 67–69.
[123] Raimundo, J. M.; Trindade, A. P. F.; Velozo, L. S.; M.; Kaplan, M. A. C.; Sudo, R. T; Zapata-Sudo, G. The lignan eudesmin extracted from piper truncatum included vascular relaxation *via* activation of endothelial histamine H_1 receptors. *Eur. J. Pharmacol.* **2009**, *606*, 150-154.
[124] Deyama, T.; Ikawa, T.; Kitagawan, S.; Nishibe, S. The constituents of *Eucommia olmoies* OLIV. V. Isolation of Dihydroxydehydrodiconiferyl Alcohol Isomers and Phenolic Compounds. *Chem. Pharm. Bull.* **1987**, *35*, 1785-1789.
[125] Kim, K. H.; Moon, E.; Choi, S. U.; Kim, S. Y.; Lee, K. R. Biological evaluation of phenolic constituents from the trunk of *berberis koreana*. *Bioorg. Med. Chem. Lett.* **2001**, *21*, 2270-2273.
[126] Kim, C. S.; Kwon, O. W. Kim, S. Y.; Lee, K. R. Bioactive lignans from the trunk of *abies holophylla*. *J. Nat. Prod.* **2013**, *76*, 2131-2135.
[127] Goda, Y.; Kiuchi, F.; Shibuya, M.; Sankawa, U. Inhibitors of prostaglandin biosynthesis from *Dalbergia odorifera. Chem. Pharm. Bull.* **1992**, *42*, 2452-2457.
[128] Strange, R. N.; Ingham, J. L.; Cole, D. L.; Cavill, M. E.; Edwards, C.; Cooksey, C. J.; Garrattd, P. J. Isolation of the phytoalexin medicarpin from leaflets of *Arachis hypogaea* and related species of the tribe *Aeschynomeneae*. *Z. Naturforsch. [C]* **1985**, *40*, 313-316.
[129] Paiva, N. L.; Edwards, R.; Sun, Y.; Hrazdina, G.; Dixon, R. A. Stress responses in alfalfa (*Medicago satvia* L.) 11. Molecular cloning and expression of alfalfa isoflavone reductase, a key enzyme of isoflavonoid phytoalexin biosynthesis. *Plant Mol. Bio*.**1991**, *17*, 653-667.
[130] Xia, W.; Luo, P.; Heu, P.; Ding, P.; Li, C.; Xu, J.; Zhou, H.; Gu, Q. Discovery of a New Pterocarpan-Type Antineuroinflammatory Compound from *Sophora tonkinensis* through Suppression of the TLR4/NFκB/MAPK signalling Pathway with PU.1 as a Potentential target. ACS Neurosci, ASAP.
[131] Awale, S.; Shrestha, S. P.; Tezuka, Y.; Ueda, J-Y.; Matsushige, K.; Kadota. Neoflavonoids and related constituents from *Nepalese Propolis* and their nitric oxide production inhibitory activity *S. J. Nat. Prod.* **2005**, *68*, 858-864.
[132] Lancefield, C. S.; Westwood, N. J. The synthesis and analysis of advanced lignin model polymers. *Green Chem.* **2015**, *17*, 4980-4990.
[133] Apers, S.; Paper, D.; Bürgermeister, J.; Baronikova, S.; Dyck, S. V.; Lemiére, G.; Vlientinck, A.; Pieters, L. Antiangionenic activity of synthetic dihydrobenzofuran lignands. *J. Nat. Prod.* **2002**, *65*, 718-720.
[134] Goel, A.; Kumar, A.; Hemberger, Y.; Raghuvanshi, A.; Jeet, R.; Tiwari, G.; Knauer, M.; Kureel, J.; Singh, A. K.; Gautam, A.; Trivedi, R.; Singh, D.; Bringmann, G. Synthesis, optical resolution, absolute configuration, and osteogenic activity of cis-pterocarpans. *Org. Biomol. Chem.* **2012**, *10*, 9583-9592.
[135] Armarego, W. L. F.; Perrin, D. D. *Purification of Laboratory Chemicals*, 4th ed., Butterworth Heinemann, **1998**
[136] Zhao, Y.; Gilbertson, S. R. Synthesis of proline-based *N*-heterocyclic carbene ligands. *Org. Lett.* **2014**, *16*, 1033-1035.
[137] Schroeder, K.; Enthaler, S.; Bitterlich, B.; Schulz, T.; Spannenberg, A.; Tse, M. K.; Junge, K.; Beller, M. Design of and mechanistic studies on a biomimetic iron-imidazole catalyst system for epoxidation of olefins with hydrogen peroxide. *Chem. Eur. J.* **2009**, *15*, 5471-5481.
[138] Augurusa, A.; Mehta, M.; Perez, M.; Zhu, J.; Stephan, D. W. Catalytic reduction of amides to amines by electrophilic phosphonium cations *via* FLP hydrosilylation. *Chem. Commun.* **2016**, *52*, 12195-12198.
[139] Wang, A.-E.; Xie, J.-H.; Wang, L-X.; Zhou, Q.-L. Triaryl phosphine-functionalized *N*-heterocyclic carbene ligands for Heck reaction. *Tetrahedron*, **2005**, *61*, 259-266.
[140] Rauchfuss, T. B.; Patino, F. T.; Roundhill, D. M. Platinum metal complexes of amine- and ether-substituted phosphines. *Inorg. Chem.* **1975**, *14*, 652-656.
[141] Kuriyama, M.; Hamaguchi, N.; Yano, G.; Tsukuda, K.; Sato, K.; Onomura, O.; Deuterodechlorination of aryl/heteroaryl chlorides by palladium/unsymmetrical NHC systems. *J. Org. Chem.* **2016**, *81*, 8934-8946.
[142] Kumar, M. R.; Park, K.; Lee, S. Synthesis of amido-N-imidazolium salts and their applications as ligands in Suzuki-Miyaura reactions: Coupling of hetero-aromatic halides and the synthesis of milrinone and irbesartan. *Adv. Synth. Catal.* **2010**, *352*, 3255-3266.
[143] Wolf, J.; Labande, A.; Daran, J.-C.; Poli, R. Nickel(II) complexes with bifunctional phosphine-imidazolium ligands and their catalytic activity in the Kumada-Corriu coupling reaction. *J. Organomet. Chem.* **2006**, 433-443.

[144] Wolf J.; Labande, A.; Daran, J.; Poli, R.; Reactivity of phosphane-imidazolium salts towards $[Ir(COD)Cl]_2$: Preparation of new hydroiridium(III) complexes bearing abnormal carbenes. *Eur. J. Inorg. Chem.* **2008**, 3024-3030.

[145] Lutz, M.; Wenzler, M.; Likhotvorik, I. An efficient oxidation of sulfides to sulfones with urea-hydrogen peroxide in the presence of phthalic anhydride in ethyl acetate. *Synthesis* **2018**, *2018*, 2231-2234.

[146] Bhadra, S.; Dzik, W. I.; Gooßen, L. L. J.; Synthesis of aryl ethers from aromatic carboxylic acids. *Synthesis (Germany)*, **2013**, *45*, 2387-2390

[147] Shavnya, A.; Coffey, S. B.; Smith, A. C.; Mascitti, V. Palladium catalyzed sulfination of aryl and heteroaryl halides: Direct access to sulfones and sulfonamides. *Org. Lett.* **2013**, *15*, 6226-6229.

[148] Heppenstall, S.; Smiles, S. Aromatic hydroxy-sulfones. *J. Chem. Soc.* **1938**, 899-902.

[149] Zhu, W.; Wa, D. Synthesis of aryl sulfones *via* L-proline-promoted CuI-catalyzed coupling reaction of aryl halides with sulfinic acid salts. *J. Org. Chem.* **2005**, *70*, 2696-2700.

[150] Hanson, P.; Hendricks, R. A. A. J.; Smith, J. R. L. An investigation by means of correlation analysis into the mechanisms of oxidation of aryl methyl sulfides and sulfoxides by dimethyloxirane in various solvents. *Org. Biomol. Chem.* **2008**, *6*, 745-761.

[151] Todd, S. A comparison of the activating effect of the sulfone group with that of the nitro group. *J. Am. Chem. Soc.* **1934**, *56*, 1382-1382.

[152] Shen, C.; Xu, J.; Yu, W.; Zhang, P. A highly active and easily recoverable chitosan@copper catalyst for the C-S coupling and its application in the synthesis of zolimidine. *Green Chem.* **2014**, *16*, 3007-3012.

[153] Liu, J.; Jiangmeng, B-B. Oxidation of aromatic amines into nitroarenes with *m*-CPBA. *Tett. Lett.* **2014**, *55*, 1581-1584.

[154] Zhao, J.; Niu, S.; Jiang, X.; Jiang, Y.; Zhang, X.; Sun, T.; Ma, D. A class of amide ligands enable Cu-catalyzed coupling of (hetero)aryl halides with sulfinic acid salts under mild conditions. *J. Org. Chem.* **2018**, *83*, 6589-6598.

[155] Bulakowska, A.; Konieczny, M. T. Synthesis of vinyl sulfones by ring opening of 4,4-dioxo-2,3-dihydrobenzo[b][1,4]oxathiines and their *in situ* reactions with nucleophilic or electrophilic reagents. *J. Heterocycl. Chem.* **2015**, *2*, 440-444

[156] Margraf, N.; Manolikakies, G. One-pot synthesis of aryl sulfones from organometallic reagents and iodonium salts. *J. Org. Chem.* **2015**, *80*, 2580-2600

[157] Zhang, X-S.; Zhu, Q-L.; Zhang, Y-F.; Li, Y-B.; Shi, Z-J. Controllable mono/dialkenylation of benzyl thioethers through Ru-catalyzed aryl C-H activation. *Chem. Eur. J.* **2013**, *19*, 11898-11903.

[158] Fu, Y.; Zhu, W.; Zhao, X.; Huegel, H.; Wu, Z.; Su, Y.; Du, Z.; Haung, D.; Hu, Y. CuI catalyzed sulfonylation of organozinc reagents with sulfonyl halides. *Org. Biomol. Chem.* **2014**, *12*, 4295-4299.

[159] Chakravarthy, R. D.; Ramkumar, V.; Chand, D. K. A molybdenum based metallomicellar catalyst for controlled and selective sulfoxidation reactions in aqueous medium. *Green Chem.* **2014**, *16*, 2190-2196.

[160] Takahasi, T.; Sakuraba, A.; Hirohashi T.; Shibata, T.; M. Hirose, M.; Haga Y.; Nonoshita, K.; Kanno, T.; Ito, J.; Iwaasa, H.; Kanatani, A.; Fukami, T.; Sato, N. Novel potent neuropeptide Y Y5receptor agonists:Synthesis and structure-activity relationships of phenylpiperazine derivatives. *Bioorg. Med. Chem.* **2006**, *14*, 7501-7511.

[161] Fu, Y.; Xu, Q-S.; Li ,Q-Z.; Du, Z.; Wang, K-H.; Huang, D.; Hu, Y. Efficient synthesis of aliphatic sulfones by Mg mediated coupling reactions of sulfonyl chloride and aliphatic halides. *Org. Biomol. Chem*. **2017**, *15*, 2841-2845.

[162] Scott, J. S.; Bowker, S. S.; Brocklehurst, K. J.; Brown, H. S.; Clarke, D. S.; Easter, A.; Ertan, A.; Goldberg, K.; Hudson, J. A.; Kavanagh, S.; Laber, D.; Leach, A. G.; Macfaul, P. A.; Martin, E. A.; McKerrecher, D.; Schofield, P.; Svensson, P. H.; Teague, J. Circumventing seizure activity in a series of G protein coupled receptor 119 (GPR119) agonists. *J. Med. Chem.* **2014**, *57*, 8984-8989

[163] Laha, J. K.; Sharma, S.; Dayal, N. Palladium-catalyzed regio- and chemoselective reactions of 2-bromobenzyl bromides: Expanding the scope for the synthesis of biaryls fused to a seven-membered sultam. *Eur. J. Org. Chem.* **2015**, 7885-7891.

[164] Haung, X.; Wang, J.; Ni, Z.; Pan, Y. Copper-mediated S-N formation *via* an oxygen-activated radical process: A new synthesis method for sulfonamides. *Chem. Commun.* **2014**, *50*, 4582-4584.

[165] Ding, R.; He, Y.; Wang, X.; Xu, J.; Chen, Y.; Feng, M.; Qi, C. Treatment of alcohols with tosyl chloride does not always lead to the formation of tosylates. *Molecules* **2011**, *16*, 5665-5673.

[166] Malik, S.; Nadir, U. K.; Pandey, P. S. Microwave-assisted efficient methylation of alkyl and areresulfonamides with trimethylsulfoxonium iodide and KOH. *Synth. Commun.* **2008**, *38*, 3074-3081.

[167] Tang, Z.; Otten, E.; Reek, J. N. H.; Vlugt, J. I. van der, Bruin, B. de. Dynamic, ligand reactivity in a rhodium pincer complex. *Chem. Eur. J.* **2015**, *21*, 12683-12693.

[168] Li, F.; Xie, J.; Shan, H.; Sun, C.; Chen, L. General and efficient method for direct *N*-monomethylation of aromatic primary amines with methanol. *RSC Adv.* **2012**, *2*, 8645-8652.

[169] Sarkar, D.; Ghosh, M. K.; Rout, N. PTAB mediated open air synthesis of sulfonamides, thiosulfonates and symmetrical disulfanes. *Tet. Lett.* **2018**, *59*, 2360-2364.

[170] O'Sullivan, S.; Doni, E.; Tuttle, T.; Murphy, J. A. Metal-free reductive cleavage of C-N and S-N bonds by photoactivated electron transfer from a neutral organic donor. *Angew. Chem. Int. Ed.* **2013**, *216*, 484-488.
[171] Buathongjan, C.; Beukeaw, D.; Yotphan, S. Iodine—catalyzed oxidative amination of sodium sulfinates: A convenient approach to the synthesis of sulfonamides under mild conditions. *Eur. J. Org. Chem.* **2015**, 1575-1582.
[172] Shi, W.; Bai, C-M.; Zhu, K.; Cui, D-M.; Zhang, C. Bronsted acid-assisted N-alkylation of sulfonamides using ethers as the alkylation reagent. *Tetrahedron* **2014**, *70*, 434-438.
[173] Hopkins, M. D.; Brandeburg, Z. C.; Hanson, A. J.; Lamar, A. A. Visible-light, iodine-promoted formation of *N*-sulfonyl imines and *N*-alkylsulfonamides from aldehydes and hypervalent iodine reagents. *Molecules* **2018**, *23*, 1838.
[174] Lee, D.; Chang, S. Direct C-H amidation of benzoic acids to introduce *meta*- and *para*-amino groups by tandem decarbonylation. *Chem. Eur. J.* **2015**, *21*, 5364-5368.
[175] Pan, C.; Cheng, J.; Wu, H.; Ding, J.; Liu, M. $Cu(OAc)_2$-catalyzed *N*-arylation of sulfonamides with arylboronic acids or trimethoxy(phenyl)silane. *Synth. Commun.* **2009**, *39*, 2082-2092.
[176] DeBergh, J. R.; Niljianskul, N.; Buchwald, S. L. Synthesis of aryl sulfonamides *via* palladium-catalyzed chlorosulfonylation of aryl boronic acids. *J. Am. Chem. Soc*. **2013**, *135*, 10638-10641.
[177] Yan, C-S.; Peng, Y.; Xu, X-B.; Wang, Y-W. Nickel-mediated inter- and intramolecular reductive cross-coupling of unactivated alkyl bromides and aryl iodides at room temperature. *Chem. Eur. J.* **2012**, *18*, 6039-6048.
[178] Smith, C. J.; Tsang, M. W. S.; Holmes, A. B.; Danheiser, R. L.; Tester, J. W. Palladium catalysed aryl amination reactions in supercritical carbon dioxide. *Org. Biomol. Chem.* **2005**, *3*, 3767-3781.
[179] Zhang, W.; Luo, M. Iron-catalyzed synthesis of arylsulfinates through radical coupling reaction. *Chem. Commun*. **2016**, *52*, 2980-2983.
[180] Griffiths-Jones, C. M.; Knight, D. W. *Tetrahedron*, **2011**, *44*, 8515-8528.
[181] Sayyad, M.; Nanaji, Y.; Ghorai, M. A synthetic route to 2-alkyl indoles via thiophenol-mediated ring-opening of *N*-tosylaziridines followed by copper powder-mediated C-N cyclization/aromatization. *J. Org. Chem.* **2015**, *80*, 12659-12667.
[182] Lawrence, H. R.; Kazi, A.; Luo, Y.; Kending, R.; Ge, Y.; Jain, S.; Daniel, K.; Santiago, D.; Guida, W. C.; Sebti, S. M. Synthesis and biological evaluation of napthoquinone analogs as a novel class of proteasome inhibitors. *Bioorg. Med. Chem.* **2010**, *18*, 5576-5592.
[183] R. Gaspari, C. Rechlin, A. Heine, G. Bottegoni, W. Rocchia, D. Schwarz, J. Bomke, H-D. Gerber, G. Klebe, A. Cavalli. Kinetic and structural insights into the mechanism of binding of sulfonamides to human carbonic anhydrase by computational and experimental studies. *J. Med. Chem.* **2016**, *59*, 4245-4256.
[184] F. Wang, H. Liu, H. Fu, Y. Jiang, Y. Zhao. Highly efficient iron(II) chloride/*N*-bromosuccinimidee-mediated synthesis of imides and acylsulfonamides. *Adv. Synth. Catal.* **2009**, *351*, 246-252.
[185] Imada, Y.; Tonomura, I.; Komiya, N.; Naota. Aerobic oxidation of sulfides with a vitamin B_{12}-derived organocatalyst. *Synlett.* **2013**, *24*, 1679-1682.
[186] Zenzola, M.; Doran, R.; Luisi, R.; Bull, J. A. Synthesis of sulfoximine carbamates by rhodium-catalyzed nitrene transfer of carbamates to sulfoxides. *J. Org. Chem.* **2015**, *80*, 6391-6399.
[187] Teng, F.; Cheng, J.; Jin-Tao, Y. Copper-catalyzed N-methylation/ethylation of sulfoximines. *Org. Biomol. Chem.* **2015**, *13*, 9934-9937.
[188] Huang, F-Q.; Xie, J.; Sun, J-G.; Wangm Y-W.; Dong, X.; Qi, L-W.; Zhang, B. Regioselective synthesis of carbonyl-containing alkyl chlorides *via* silver-catalyzed ring-opening chlorination of cycloalkanols. *Org. Lett.* **2016**, *18*, 684-687.
[189] Yu, F.; Zhou, J-N.; Zhang, X-C.; Sui, Y-Z.; Wu, F-F.; Xie, L-J.; Chan, A. S. C. Copper(II)-catalyzed hydrosilylation of ketones using chiral dipyridylphosphane ligands: Highly enantioselective synthesis of valuable alcohols. *Chem. Eur. J.* **2011**, *50*, 14234-14240.
[190] Shields, B. J.; Doyle, A. G. Direct $C(sp^3)$-H cross coupling enabled by catalytic generation of chloride radicals. *J. Am. Chem. Soc.* **2016**, *138*, 12719-12722.
[191] Bakos, M.; Gyömore, A.; Domján, A.; Soós, T. *Angew. Chem. Int. Ed.* **2017**, *129*, 5301-5305.
[192] Ke F.; Li, Z.; Xiang, H.; Zhou, X. Catalytic Hydroalkoxylation of alkenes by iron(III) catalyst. *Tett. Lett.* **2011**, *52*, 318-320.
[193] Matsumoto, S.; Naito, M.; Oseki, T.; Akazome, M.; Otani, Y. Selective reaction of benzyl alcohols with HI gas: iodination, reduction, and indane ring formations. *Tetrahedron* **2017**, *73*, 7254-7259.
[194] Lee, S. H.; Kim, I. S.; Li, Q. R.; Dong, G. R.; Jong, L. S.; Jung, Y. H.Stereoselective amination of chiral benzylic ethers using chlorosulfonyl isocyanate: Total synthesis of (+)-setraline. *J. Org. Chem.* **2011**, *76*, 10011-10019.
[195] Velasco, R.; Feberero, C.; Sanz, R. α-lithiated aryl benyl ethers: inhibition of [1,2]-wittig rearrangement and application to the synthesis of benzo[b]furan derivatives. *Org. Lett.* **2015**, *17*, 4416-4419.
[196] Guptill, D. M.; Davies, H. M. L. 2,2,2-trichloroethl aryldiazoacetates as robust reagents for the enantioselective C-H functionalisation of methyl ethers. *J. Am. Chem. Soc.* **2014**, *136*, 17718-17721.

[197] Yoshimura, F.; Saito, H.; Abe, T.; Tanino, K. Nucleophilic addition of alkane nitriles to aldehydes *via N*-silyl ketene imines generated *in situ*. *Synlett.* **2017**, *28*, 1816-1820.
[198] Wu, J.; Zeng, H.; Cheng, J.; Zheng, S.; Golen, J. A.; Manke, D. R.; Zhang, G. Cobalt(II) coordination polymer as a precatalyst for selective hydroboration of aldehydes, ketones, and imines. *J. Org. Chem.* **2018**, *83*, 942-9448.
[199] Gao, L.; Kojima, K.; Nagashima, H. *Tetrahedron* **2015**, *71*, 6414-6423.
[200] Jarrige, L.; Blanchard, F.; Masson, G. Enantioselective organocatalytic intramolecular aza-Diels-Alder reaction. *Angew. Chem. Int. Ed.* **2017**, *129*, 10709-10712.
[201] Schmidt, B.; Wolf, F. Synthesis of phenylpropanoids via Matsuda-Heck coupling of arene diazonium salts. *J. Org. Chem.* **2017**, *82*, 4386-4395.
[202] Konrádová, D.; Kozubíková, H.; Doležal, Pospíšil, J. Microwave-assisted synthesis of phenylpropanoids and coumarins, Total synthesis of osthol. *Eur. J. Org. Chem.* **2017**, 5204-5213.
[203] Kerratou, M.; Redouane-Salah, A.; Léon, F.; Brouard, I.; Mosset, P.; Menad, A.; Ameddah, S.; Benyache, S.; Bermejo, J.; Benayache, F. Secondary metabolites and antioxidant activity of *limonium duriusculum* (de girard) kuntze extracts. *Asian J. Chem.* **2016**, *28*, 2695-2700.
[204] Lou, L-L.; Yao, G-D.; Wang, J.; Zhao, W-Y.; Wang, X-B.; Huang, X-X.; Song, S-J. Enantiomeric neolignands from *piscrasma quassioides* exhibit distinctive cytotoxicity on hepatic carcinoma cells through ROS generation of apoptosis induction. *Bioorg. Med. Chem. Lett.* **2018**, *28*, 1263-1268.
[205] Karim, A.; Noor, A. T.; Malik, A. Structure of barlericin, the neolignan diglycoside from *Barleria acanthiodes*. *J. Asian Nat. Prod. Res.* **2010**, *12*, 714-718.
[206] Cantrell, C. L.; Schrader, K. K.; Mamonov, L. K.; Sitpaeva, G. T.; Dunbar, C.; Wedge, D. E. Isolation and identification of antifunal and antialgal alkaloids from *Haplophyllum sieversii*. *J. Agric. Food Chem.* **2005**, *53*, 7741-7748.
[207] Korea Research Institute of Bioscience and Biotechnology; Oh, S-R; Anh, K. S.; Lee, S. U.; Ryu, H. W.; Kim, D.-Y.; Lee, H. K.; Kwon, O.-K.; Kim, J. H.; Lee, H.-J.; Shin, I.-S.. Pharmaceutical Composition for preventing and treating chronic obstructive lung disease containing, as active ingredient, *Magnloiae flos* extact, fraction, or active fraction thereof. EP3295947, **2018**, A2
[208] Snyder, S. A.; Kontes, F. Exploration into neolignan biosynthesis: Concise total syntheses of helicterin B, helisorin, and helisterculin A from a common intermediate. *J. Am. Chem. Soc.* **2009**, *131*, 1745-1752.
[209] Constantin, M-A.; Conrad, J.; Beifuss, U. Laccase-catalyzsed oxidative coupling of vanillidene derivatives. *Green Chem*. **2012**, *14*, 2375-2379.
[210] Liu, Y.; Rose, K. N.; DaSilva, N. A.; Johnson, S.; L.; Seeram, N. P. Isolation, identification, and biological evaluation of phenolic compounds from a traditional American confectionary, maple sugar. *J. Agric. Food, Chem.* **2017**, *65*, 4289-4295.
[211] Xiong, L-Y.; Song, H-J.; Li, L.; Chuang, Z. Chemical constituents of *Miscanthus floridulus*. *Chem. Nat. Compd.* 2015, 51, 552-553
[212] Goel, A.; Kumar, A.; Hemberger, Y.; Raghuvanshi, A.; Jeet, R.; Tiwari, G.; Knauer, M.; Kureel, J.; Singh, A.; J.; Gautam, A.; Trivedi, R; Singh, D.; Bringmann, G. Synthesis, optical resolution, absolute configuration, and osteogenic activity of *cis*-pterocarpins. *Org. Biomol. Chem.* **2012**, *10*, 9583-9592.